

**AN INVESTIGATION OF THE EFFECTS OF HAEM
ON THE ACTIVITY OF RAT ARTERIAL LARGE-
CONDUCTANCE Ca^{2+} -ACTIVATED K^+ (BK_{Ca})
CHANNELS**

Thesis submitted for the degree of
Doctor of Philosophy
at the University of Leicester

by

Oluwamodupe Oluwaseyi Ayeni BSc (Hons)
Department of Molecular and Cell Biology
University of Leicester

January 2019

ABSTRACT

An investigation of the effects of haem on the activity of rat arterial large-conductance Ca²⁺-activated K⁺ (BK_{Ca}) channels.

By Oluwamodupe O. Ayeni

Local Ca²⁺ release in smooth muscle cells (SMCs) activates large-conductance Ca²⁺-activated K⁺ (BK_{Ca}) channels resulting in spontaneous transient outward currents (STOCs) which counteract vasoconstriction. Evidence shows that haem regulates a variety of ion channels, including BK_{Ca} channels. However, little is known about the mechanism of action of haem and its degradation products on BK_{Ca} channels. Earlier studies, mostly on inside-out patches, show that haem and CO (a haem degradation product) inhibit and stimulate BK_{Ca} channel activity respectively. Thus, it is hypothesised that the haem interaction with BK_{Ca} channels is involved in the vasospasm that occurs during haemolytic diseases. This study focuses primarily on the effects of haem and CO on whole-cell BK_{Ca} currents.

SMCs were isolated from the mesenteric artery of male Wistar rats. Single and whole-cell BK_{Ca} channel currents were recorded using inside-out, outside-out, ruptured and perforated patch recordings as appropriate. As in earlier studies, intracellular haem or CO application to BK_{Ca} channels in inside-out patches inhibited and stimulated channel activity, respectively. However, extracellular haem enhanced whole-cell BK_{Ca} currents. Based on the hypothesis that the stimulatory effect of haem resulted from CO generated from HO-mediated haem degradation, it was surprising that extracellular haem enhanced whole-cell BK_{Ca} currents in cells pre-treated with the HO-inhibitor, zinc protoporphyrin-IX (ZnPP-IX). Extracellular haem also enhanced single BK_{Ca} channel activity in outside-out patches.

This is the first study to report a haem mediated CO-independent stimulation of STOCs. The discrepancy between the effects of haem in inside-out patches and intact cells suggest that intracellular components play a key role in the haem-mediated stimulatory effect on STOCs. Nevertheless, the outside-out and ruptured patch results indicate that haem could enhance channel activity independent of intracellular components. In conclusion, this study shows that haem may act as a feedback regulator to counteract the vasospasm that occurs during haemolytic diseases.

ACKNOWLEDGEMENTS

I will begin by thanking the Almighty God for His blessings upon my life which has made it possible for me to be where I am today.

My PhD journey has truly been an exciting and enjoyable experience and I am immensely grateful to my wonderful supervisors, Dr Noel Davies (a.k.a “dad labordy”) and Dr Nina Storey for their invaluable advice and support prior to and throughout the duration of my project. I thank the British Heart Foundation (BHF) for awarding me the PhD studentship and the University of Leicester for providing the facilities and training required for the project.

Special thanks to Prof. Emma Raven for making her laboratory readily available for my spectrophotometric studies and Dr Sofia Kapetanaki for providing the technical support. I am also grateful to Dr Kees Stratsman for training me in the use of the University’s imaging facility, which provided me with the technical skills to perform my imaging studies. I indeed appreciate Dr Richard Rainbow and Prof. John Challiss who played key roles in organising the animal culling required for my study. I thank Dr Gary Willars, Dr Mark Burton, Dr Lory Francescut, Dr Rawan Khuwaileh and members of the Rainbow lab for their various contributions to my project. I am also grateful to my project committee members; Dr Ralf Schmid and Dr John Mitcheson for their advice and contributions to my project.

Finally, I thank my amazing family and lovely friends for all their love, support and prayers throughout my study.

TABLE OF CONTENTS

| | |
|--|-------|
| ABSTRACT | i |
| ACKNOWLEDGEMENTS | ii |
| TABLE OF CONTENTS..... | iii |
| LIST OF TABLES | xi |
| LIST OF FIGURES | xii |
| ABBREVIATIONS | xviii |
| Chapter 1 INTRODUCTION | 1 |
| 1.1 Blood vessels | 2 |
| 1.1.1 Structure of blood vessels | 2 |
| 1.1.2 Types of blood vessels..... | 3 |
| 1.1.3 Regulation of blood vessel diameter | 4 |
| 1.2 Vascular smooth muscle cells | 5 |
| 1.2.1 Mechanisms of calcium (Ca ²⁺) handling in vascular SMCs | 5 |
| 1.2.1.1 Cytosolic Ca ²⁺ mobilisation pathways..... | 5 |
| 1.2.1.1.1 Voltage-gated Ca ²⁺ channels (VGCC)..... | 6 |
| 1.2.1.1.2 Non-selective cation channels (NSCC) | 6 |
| 1.2.1.1.3 Store-operated Ca ²⁺ entry (SOCE) | 7 |
| 1.2.1.1.4 Ca ²⁺ -induced Ca ²⁺ release (CICR) | 7 |
| 1.2.1.1.5 Ca ²⁺ release from intracellular stores via IP ₃ receptors | 7 |
| 1.2.1.2 Ca ²⁺ removal pathways | 8 |
| 1.2.1.2.1 Re-uptake into intracellular stores..... | 8 |
| 1.2.1.2.2 Extrusion into the extracellular space | 8 |
| 1.2.2 Vascular SMC excitation-contraction coupling | 9 |
| 1.2.3 Regulation of vascular SMC membrane potential (V _m)..... | 11 |
| 1.2.3.1 Ca ²⁺ channels..... | 11 |
| 1.2.3.2 Cl ⁻ channels..... | 12 |
| 1.2.3.3 Na ⁺ channels..... | 13 |
| 1.2.3.4 K ⁺ channels | 14 |
| 1.2.3.4.1 K _v channels..... | 14 |
| 1.2.3.4.2 K _{ATP} channels | 15 |
| 1.2.3.4.3 K _{ir} channels..... | 15 |
| 1.2.4 BK _{Ca} channels..... | 16 |
| 1.2.4.1 Function of BK _{Ca} channels | 16 |
| 1.2.4.2 Structure of BK _{Ca} channels | 17 |

| | | |
|-------------|--|----|
| 1.2.4.3 | BK _{Ca} channel gating..... | 19 |
| 1.2.4.3.1 | Voltage-dependent gating | 20 |
| 1.2.4.3.2 | Ligand-dependent gating | 21 |
| 1.2.4.3.2.1 | Ca ²⁺ -dependent gating | 21 |
| 1.2.4.3.2.2 | Mg ²⁺ -dependent gating..... | 23 |
| 1.2.4.4 | Modulation of BK _{Ca} channel activity by endogenous molecules..... | 24 |
| 1.2.4.4.1 | H ⁺ | 24 |
| 1.2.4.4.2 | Lipids | 24 |
| 1.2.4.4.3 | ROS..... | 25 |
| 1.2.4.4.4 | Kinases | 25 |
| 1.3 | Haem | 26 |
| 1.3.1 | Structure and function of haem | 26 |
| 1.3.2 | Role of free haem in pathophysiology | 27 |
| 1.3.3 | Haem homeostasis..... | 28 |
| 1.3.3.1 | Haem Synthesis | 28 |
| 1.3.3.2 | Haem Degradation | 29 |
| 1.3.3.2.1 | Enzymatic degradation of haem | 30 |
| 1.3.3.2.2 | Haem degradation products | 31 |
| 1.3.3.3 | Haem Transport | 33 |
| 1.3.3.3.1 | Receptor-mediated endocytosis..... | 33 |
| 1.3.3.3.2 | Haem exporters | 33 |
| 1.3.3.3.3 | Haem importers | 35 |
| 1.3.3.3.4 | Haem carriers..... | 36 |
| 1.3.3.3.5 | Passive diffusion..... | 37 |
| 1.3.4 | Haem and CO regulation of ion channels | 38 |
| 1.3.4.1 | Na ⁺ channels..... | 38 |
| 1.3.4.2 | Ca ²⁺ channels..... | 38 |
| 1.3.4.3 | K ⁺ channels | 39 |
| 1.3.5 | Haem and CO regulation of BK _{Ca} channels..... | 40 |
| 1.3.5.1 | Haem regulation of BK _{Ca} channel activity | 40 |
| 1.3.5.2 | CO regulation of BK _{Ca} channel activity | 41 |
| 1.4 | Aims of this study..... | 45 |
| Chapter 2 | METHODS..... | 46 |
| 2.1 | Smooth muscle cell isolation..... | 47 |
| 2.2 | Chemicals and Materials | 47 |
| 2.3 | Preparation of solutions..... | 48 |

| | | |
|-------------|---|----|
| 2.3.1.1 | Haem solution | 48 |
| 2.3.1.2 | CO gas solution..... | 48 |
| 2.3.1.3 | CORM-3 solution | 49 |
| 2.4 | Electrophysiology | 49 |
| 2.4.1 | Patch clamp technique..... | 49 |
| 2.4.2 | Superfusion systems | 52 |
| 2.4.3 | Micropipette fabrication and polishing | 52 |
| 2.4.4 | Giga seal formation | 53 |
| 2.4.5 | Recording BK _{Ca} currents | 53 |
| 2.4.5.1 | Single channel current recording | 53 |
| 2.4.5.1.1 | Inside-out patch configuration | 53 |
| 2.4.5.1.2 | Outside-out patch configuration..... | 55 |
| 2.4.5.2 | Whole-cell current recording | 55 |
| 2.4.5.2.1 | Ruptured patch configuration..... | 56 |
| 2.4.5.2.2 | Perforated patch configuration | 57 |
| 2.5 | Data Acquisition | 59 |
| 2.6 | Data Analysis | 59 |
| 2.6.1 | Single-channel current analysis..... | 59 |
| 2.6.1.1 | Measurement of unitary current amplitude..... | 59 |
| 2.6.1.2 | Measurement of open probability (Popen) | 60 |
| 2.6.1.3 | Measurement of the channel's open and closed times..... | 61 |
| 2.6.2 | Whole-cell current analysis..... | 62 |
| 2.6.2.1 | STOC detection and analysis | 62 |
| 2.6.2.2 | Measurement of pulsed BK _{Ca} current size | 67 |
| 2.6.3 | Statistics | 67 |
| 2.7 | Absorption spectrophotometry | 68 |
| 2.7.1 | Haem assays..... | 68 |
| 2.7.1.1 | Measurement of haem concentration..... | 68 |
| 2.7.1.2 | Effects of pH on haem | 70 |
| 2.7.1.3 | Effects of reducing agents on haem..... | 72 |
| 2.7.1.3.1 | Natural-occurring reducing agents | 75 |
| 2.7.1.3.1.1 | Glutathione and haem | 75 |
| 2.7.1.3.1.2 | Ascorbic acid and haem | 81 |
| 2.7.1.3.2 | Synthetic reducing agents..... | 83 |
| 2.7.1.3.2.1 | DTE and haem | 83 |
| 2.7.1.3.2.2 | DTT and haem | 84 |

| | | |
|-------------|---|-----|
| 2.7.1.3.2.3 | TCEP and haem | 86 |
| 2.7.1.3.2.4 | Na ₂ S ₂ O ₄ and haem..... | 88 |
| 2.7.1.3.3 | Summary/conclusion from the reducing agent study | 89 |
| 2.7.2 | Carbon monoxide (CO) assays..... | 91 |
| 2.7.2.1 | Deoxymyoglobin carbonylation assays with CO gas | 91 |
| 2.7.2.1.1 | Interaction of CO gas with ferrous myoglobin (Fe ²⁺ -Mb) | 92 |
| 2.7.2.1.2 | CO was present in freshly prepared CO gas solution..... | 93 |
| 2.7.2.1.3 | CO was present in CO gas solution exposed to air | 94 |
| 2.7.2.1.4 | CO was present in CO gas solution exposed to air for over 4 hours..... | 95 |
| 2.7.2.1.5 | CO was present in sealed “Aged” CO gas solution..... | 96 |
| 2.7.2.1.6 | Summary/conclusion from CO gas solution experiments | 97 |
| 2.7.2.2 | Deoxymyoglobin carbonylation assays with CORM-3 | 98 |
| 2.7.2.2.1 | Investigation of CO release from CORM-3..... | 99 |
| 2.7.2.2.1.1 | CO was released from anaerobically prepared CORM-3 solution | 99 |
| 2.7.2.2.1.2 | Time-resolved studies with anaerobic CORM-3 solution | 100 |
| 2.7.2.2.1.3 | CO was released from aerobically prepared CORM-3 solution | 101 |
| 2.7.2.2.1.4 | Time-resolved studies with aerobic CORM-3 solution | 102 |
| 2.7.2.2.1.5 | Summary/conclusion from CORM-3 solution experiments | 103 |
| 2.7.2.2.3 | Synthesis of inactive CORM-3 (iCORM-3) | 104 |
| 2.7.2.2.3.1 | N ₂ -bubbled fresh CORM-3 solution | 104 |
| 2.7.2.2.3.2 | “Aged” CORM-3 solution | 105 |
| 2.7.2.2.3.3 | N ₂ -bubbled “Aged” CORM-3 solution | 106 |
| 2.7.2.2.3.4 | Summary/conclusion from CORM-3 inactivation experiments | 107 |
| 2.7.3 | Zinc protoporphyrin IX (ZnPP-IX) assays | 107 |
| 2.7.3.1 | Light and dark assays with ZnPP-IX..... | 109 |
| 2.7.3.2 | Conclusion from ZnPP-IX study | 111 |
| 2.8 | Confocal microscopy | 112 |
| 2.8.1 | Detection of Ca ²⁺ spark events..... | 112 |
| 2.8.2 | Quantification of Ca ²⁺ spark frequency..... | 113 |
| Chapter 3 | THE EFFECTS OF HAEM AND CO ON SINGLE BK _{Ca} CHANNEL ACTIVITY | 115 |
| 3.1 | Introduction | 116 |
| 3.2 | Characterisation of single BK _{Ca} channel activity..... | 116 |
| 3.2.1 | Investigation of the i-V relationship of the channel | 116 |
| 3.2.2 | Channel Popen increased with membrane depolarisation and a rise in [Ca ²⁺] _i | 118 |
| 3.2.3 | External TEA ⁺ reduced the amplitude of single BK _{Ca} channel currents..... | 120 |
| 3.3 | Effects of haem on single BK _{Ca} channel activity | 122 |

| | | |
|-----------|--|-----|
| 3.3.1 | Intracellular haem application inhibited single BK _{Ca} channel activity..... | 122 |
| 3.3.2 | The haem-mediated inhibition of BK _{Ca} channel activity was affected by intracellular pH (pH _i) | 126 |
| 3.4 | Effects of CO and CORM-3 on single BK _{Ca} channel activity | 128 |
| 3.4.1 | Effects of intracellular CO gas application on BK _{Ca} channel activity | 128 |
| 3.4.2 | Intracellular application of CORM-3 enhanced BK _{Ca} channel activity..... | 132 |
| 3.5 | Intracellular application of biliverdin inhibited BK _{Ca} channel activity..... | 137 |
| 3.6 | Intracellular application of ZnPP-IX had no effect on BK _{Ca} channel activity | 139 |
| 3.7 | Discussion..... | 141 |
| 3.7.1 | Characterisation of single BK _{Ca} channel activity..... | 141 |
| 3.7.2 | Effects of haem on single BK _{Ca} channel activity | 141 |
| 3.7.3 | Effects of CO on single BK _{Ca} channel activity..... | 142 |
| 3.7.4 | Effects of biliverdin on single BK _{Ca} channel activity | 144 |
| 3.7.5 | Effects of ZnPP-IX on single BK _{Ca} channel activity | 144 |
| 3.8 | Summary | 144 |
| Chapter 4 | THE EFFECTS OF HAEM AND CO ON STOCs..... | 145 |
| 4.1 | Introduction | 146 |
| 4.2 | Characterisation of STOCs..... | 146 |
| 4.2.1 | STOCs were sensitive to changes in external Ca ²⁺ concentration, [Ca ²⁺] _o | 147 |
| 4.2.2 | STOCs were voltage sensitive..... | 149 |
| 4.2.3 | Effects of K ⁺ channel blockers on STOCs | 151 |
| 4.2.3.1 | External TEA ⁺ inhibited STOCs..... | 151 |
| 4.2.3.2 | STOCs were blocked by external application of penitrem A..... | 152 |
| 4.2.4 | STOCs were abolished by the inhibition of Ca ²⁺ release and depletion of intracellular Ca ²⁺ from Ca ²⁺ stores..... | 154 |
| 4.2.4.1 | STOCs were abolished by intracellular application of ryanodine | 154 |
| 4.2.4.2 | Extracellular application of caffeine abolished STOCs..... | 155 |
| 4.3 | Effects of haem on STOCs | 157 |
| 4.3.1 | Extracellular haem application enhanced STOC amplitude but not STOC frequency | 157 |
| 4.3.2 | Low and high extracellular haem concentrations enhanced STOC frequency but not STOC amplitude | 162 |
| 4.3.3 | External haem enhanced STOC amplitude at less depolarised V _m | 166 |
| 4.4 | Effects of haem on STOCs after inhibition of endogenous CO production..... | 170 |
| 4.4.1 | Extracellular application of ZnPP-IX had no effect on STOCs..... | 170 |
| 4.4.2 | STOC amplitude and frequency decreased in ZnPP-IX pre-treated cells | 172 |

| | | |
|-----------|--|-----|
| 4.4.3 | Extracellular haem application enhanced STOC amplitude and frequency in ZnPP-IX pre-treated cells..... | 174 |
| 4.5 | Effects of extracellular CO application on STOCs..... | 177 |
| 4.5.1 | Extracellular CO gas application only increased STOC frequency..... | 177 |
| 4.5.2 | Extracellular application of CORM-3 only increased STOC frequency | 179 |
| 4.5.3 | Summary of the effects of CO on STOCs | 182 |
| 4.5.4 | Extracellular CORM-3 application had no effect on STOC amplitude and frequency in ZnPP-IX pre-treated cells..... | 182 |
| 4.6 | Effects of haem and CO on STOCs after caveolae disruption | 186 |
| 4.6.1 | STOC amplitude was reduced in mβCD pre-treated cells | 187 |
| 4.6.2 | External haem enhanced STOC frequency in mβCD pre-treated cells but had no effect on STOC amplitude | 189 |
| 4.6.3 | Extracellular application of CORM-3 did not affect STOC amplitude or frequency in mβCD pre-treated cells | 192 |
| 4.7 | Extracellular application of haem did not influence Ca ²⁺ spark frequency..... | 196 |
| 4.8 | Effects of haem localization on STOCs | 199 |
| 4.8.1 | Intracellular haem application had no modulatory effect on STOCs..... | 199 |
| 4.8.2 | Simultaneous intracellular and extracellular haem application enhanced STOC frequency but not STOC amplitude..... | 203 |
| 4.9 | Discussion..... | 207 |
| 4.9.1 | Characterisation of STOCs..... | 207 |
| 4.9.2 | Effects of haem on STOCs | 207 |
| 4.9.3 | Effects of haem on STOCs after inhibition of endogenous CO production via cell pre-incubation with ZnPP-IX | 208 |
| 4.9.4 | Effects of extracellular CO on STOCs..... | 209 |
| 4.9.5 | Effects of haem and CO on STOCs after caveolae disruption via cell pre-incubation with mβCD | 211 |
| 4.9.6 | Haem and Ca ²⁺ spark frequency..... | 212 |
| 4.9.7 | Effects of the location of haem application on STOCs | 212 |
| Chapter 5 | THE EFFECTS OF HAEM AND CO ON VOLTAGE PULSE-INDUCED BK _{Ca} CURRENTS | 214 |
| 5.1 | Introduction | 215 |
| 5.2 | Characterisation of voltage pulsed BK _{Ca} currents using BK _{Ca} channel blockers..... | 216 |
| 5.2.1 | Pulsed currents were inhibited by external TEA ⁺ | 216 |
| 5.2.2 | Extracellular application of the selective BK _{Ca} channel blocker, penitrem A, inhibited voltage pulsed currents | 217 |
| 5.2.3 | Investigation of the stability of pulsed BK _{Ca} current over time..... | 218 |
| 5.3 | Effects of haem on voltage pulsed BK _{Ca} currents..... | 219 |
| 5.3.1 | Extracellular haem application enhanced pulsed currents..... | 219 |

| | | |
|---------|--|-----|
| 5.3.2 | The stimulatory effect of haem on pulsed currents was inhibited during co-application with penitrem A | 224 |
| 5.4 | Investigation of the mechanism of haem-mediated stimulation of voltage pulsed BK _{Ca} currents | 226 |
| 5.4.1 | Is Ca ²⁺ entry via L-type Ca ²⁺ channels involved in the stimulatory effect of haem on pulsed BK _{Ca} current | 226 |
| 5.4.1.1 | Extracellular application of Cd ²⁺ inhibited pulsed BK _{Ca} current..... | 226 |
| 5.4.1.2 | The stimulatory effect of extracellular haem on pulsed BK _{Ca} currents was not abolished during co-application with Cd ²⁺ | 228 |
| 5.4.2 | Is endogenous CO involved in the stimulatory effect of haem on voltage pulsed BK _{Ca} current..... | 230 |
| 5.4.2.1 | Voltage pulse-induced BK _{Ca} current was unaltered by extracellular application of ZnPP-IX..... | 230 |
| 5.4.2.2 | Voltage pulsed BK _{Ca} current was higher in ZnPP-IX pre-treated cells compared with untreated cells | 232 |
| 5.4.2.3 | Extracellular application of haem enhanced pulsed BK _{Ca} current in ZnPP-IX pre-treated cells..... | 233 |
| 5.5 | Effects of CO on voltage pulsed BK _{Ca} current | 235 |
| 5.5.1 | Extracellular application of CO gas or CORM-3 did not produce significant effects on pulsed BK _{Ca} current | 235 |
| 5.5.2 | Does intracellular Ca ²⁺ concentration, [Ca ²⁺] _i , modulate the effect of CO on pulsed BK _{Ca} currents..... | 240 |
| 5.5.2.1 | Investigation of the stability of whole-cell voltage pulsed BK _{Ca} current in higher [Ca ²⁺] _i , 300 nM..... | 240 |
| 5.5.2.2 | Extracellular application of CO gas or CORM-3 in 300 nM [Ca ²⁺] _i had no significant effect on pulsed BK _{Ca} current | 244 |
| 5.6 | Effects of extracellular haem or CO application on single BK _{Ca} channels in outside-out patches..... | 247 |
| 5.6.1 | Extracellular haem application enhanced single BK _{Ca} channel activity in outside-out patches..... | 247 |
| 5.6.1.1 | The stimulatory effect of extracellular haem on single BK _{Ca} channel activity was abolished in the presence a BK _{Ca} channel blocker, penitrem A..... | 250 |
| 5.6.2 | Extracellular CO gas application did not alter single BK _{Ca} channel activity in outside-out patches | 252 |
| 5.6.3 | Extracellular application of CORM-3 had no effect on single BK _{Ca} channels in outside-out patches | 254 |
| 5.7 | Discussion..... | 258 |
| 5.7.1 | Characterisation of voltage pulsed BK _{Ca} currents | 258 |
| 5.7.2 | Effects of haem on voltage pulsed BK _{Ca} currents | 258 |
| 5.7.3 | Effects of CO on voltage pulsed BK _{Ca} currents | 259 |

| | | |
|------------|---|-----|
| 5.7.4 | Effects of extracellular application of haem or CO on single BK _{Ca} channels in outside-out patches | 260 |
| Chapter 6 | GENERAL DISCUSSION..... | 262 |
| 6.1 | The biological context of my study | 263 |
| 6.2 | Intracellular acidic pH slows the rate of haem-mediated channel inhibition without affecting its potency..... | 263 |
| 6.3 | Externally applied haem enhanced STOC amplitude and voltage pulsed whole-cell BK _{Ca} currents via a CO-independent mechanism..... | 264 |
| 6.4 | The stimulatory effects of haem on whole-cell BK _{Ca} channel activity does not require Ca ²⁺ sparks..... | 266 |
| 6.5 | Haem signalling to BK _{Ca} channels could occur within but not be limited to caveolae 266 | |
| 6.6 | The location of haem application might influence its effect on whole-cell BK _{Ca} channel activity | 267 |
| 6.7 | Limitations of this study..... | 268 |
| 6.8 | Future work..... | 271 |
| 6.8.1 | Mutagenesis studies could be used to further confirm the number and location of haem binding sites on BK _{Ca} channels..... | 271 |
| 6.8.2 | Inhibition of haem synthesis can be used to investigate the modulatory effect of endogenous haem on STOCs. | 271 |
| 6.8.3 | Investigate whether the stimulatory effects of haem might have occurred via cGMP-dependent and -independent mechanisms | 272 |
| 6.8.4 | Investigate whether intracellular pH influences the effects of haem on whole-cell BK _{Ca} channel activity | 272 |
| 6.8.5 | Investigate whether haem, CO and NO interact to regulate whole-cell BK _{Ca} channel activity | 273 |
| 6.9 | Conclusion..... | 274 |
| REFERENCES | | 275 |

LIST OF TABLES

| | |
|---|-----|
| Table 2.1: Pipette and bath solutions used for inside-out patch recordings..... | 54 |
| Table 2.2: Pipette and bath solutions used for outside-out patch and whole-cell recordings... | 55 |
| Table 2.3: Reducing agents and their reduction potentials. | 74 |
| Table 4.1: Summary of the effects of haem and CO on STOCs under different experimental conditions..... | 206 |
| Table 5.1: Summary of the effects of haem and CO on voltage pulsed whole-cell BK _{Ca} currents under the different experimental conditions. | 257 |
| Table 6.1: Summary of the key findings from this study. | 269 |

LIST OF FIGURES

| | |
|---|----|
| Figure 1.1: Structure of a blood vessel wall. | 3 |
| Figure 1.2: Ca ²⁺ handling in vascular SMCs. | 9 |
| Figure 1.3: Regulation of vascular SMC excitation-contraction coupling. | 11 |
| Figure 1.4: Structure of BK _{Ca} channel subunits | 18 |
| Figure 1.5: BK _{Ca} channel activation is influenced by the interaction between the allosteric modulators, Ca ²⁺ and voltage..... | 23 |
| Figure 1.6: Structure of haem | 27 |
| Figure 1.7: Haem synthesis and degradation..... | 29 |
| Figure 1.8: Haem metabolism requires O ₂ and a reducing agent. | 30 |
| Figure 1.9: Haem transport. | 37 |
| Figure 1.10: Historical evidence of the mechanism of interaction of haem and CO with BK _{Ca} channels. | 44 |
| Figure 2.1: Series resistance error in whole-cell recordings. | 51 |
| Figure 2.2: Schematic diagrams of excised patch configurations. | 54 |
| Figure 2.3: Schematic diagrams of whole-cell patch configurations. | 56 |
| Figure 2.4: Example traces illustrating the process of smooth muscle cell membrane perforation by amphotericin B in the pipette solution..... | 58 |
| Figure 2.5: Measurement of unitary current amplitude..... | 60 |
| Figure 2.6: Example images showing the process of individual STOC detection in whole-cell records. | 63 |
| Figure 2.7: Analysis of STOC amplitude. | 65 |
| Figure 2.8: Analysis of STOC frequency..... | 66 |
| Figure 2.9: Analysis of pulsed BK _{Ca} currents..... | 67 |
| Figure 2.10: UV-visible absorption spectrum of haem. | 69 |
| Figure 2.11: Structures of hemin in aqueous solution..... | 70 |
| Figure 2.12: UV-visible absorption spectra of haem in aqueous media at pH 6.7, 7.2 and 8.7.. | 72 |
| Figure 2.13: Chemical structure of different reducing agents..... | 74 |
| Figure 2.14: UV-visible absorption spectra of distilled water (dH ₂ O) and reducing agents prepared in bath solution. | 75 |
| Figure 2.15: Representative UV-visible absorption spectra of haem showing its degradation over time in the presence and absence of GSH (2 mM). | 77 |
| Figure 2.16: Representative UV-visible absorption spectra showing haem degradation over time. | 77 |

| | |
|---|-----|
| Figure 2.17: Representative UV-visible absorption spectra of haem showing its degradation over time in lower GSH concentration (50 μ M)..... | 78 |
| Figure 2.18: Representative UV-visible absorption spectra of haem showing its degradation over time in the presence of GSSG (2 mM). | 79 |
| Figure 2.19: Representative UV-visible absorption spectra of haem showing its degradation over time in the presence of GSH (2 mM), under anaerobic conditions. | 80 |
| Figure 2.20: Representative UV-visible absorption spectra of haem showing its degradation over time in the presence of ascorbate (2 mM) under aerobic conditions. | 82 |
| Figure 2.21: Representative UV-visible absorption spectra of haem showing its degradation over time in the presence of ascorbate (2 mM) under anaerobic conditions. | 82 |
| Figure 2.22: Representative UV-visible absorption spectra of haem showing its degradation over time in the presence of DTE (2 mM). | 84 |
| Figure 2.23: Representative UV-visible absorption spectra of haem showing its degradation over time in the presence of DTT (2 mM). | 85 |
| Figure 2.24: Representative UV-visible absorption spectra of haem in the presence of TCEP (2 mM). | 87 |
| Figure 2.25: Representative UV-visible absorption spectra of haem in the presence of $\text{Na}_2\text{S}_2\text{O}_4$ | 89 |
| Figure 2.26: Kinetics of haem degradation in the absence and presence of natural and artificial reducing agents. | 90 |
| Figure 2.27: UV-visible absorption spectra showing the formation of myoglobin-CO complex, $\text{Mb}(\text{Fe}^{2+})\text{CO}$, by direct bubbling of CO gas into ferric myoglobin, $\text{Mb}(\text{Fe}^{3+})$, solution. | 93 |
| Figure 2.28: UV-visible absorption spectra showing the formation of myoglobin-CO complex, $\text{Mb}(\text{Fe}^{2+})\text{CO}$, using freshly bubbled CO gas solution. | 94 |
| Figure 2.29: UV-visible absorption spectra showing the formation myoglobin-CO complex, $\text{Mb}(\text{Fe}^{2+})\text{CO}$, using CO gas solution that had been exposed to air. | 95 |
| Figure 2.31: UV-visible absorption spectra of $\text{Mb}(\text{Fe}^{2+})\text{CO}$ solution produced using CO gas solution that had been exposed to air for over 4 hours. | 96 |
| Figure 2.30: UV-visible absorption spectra showing the formation of myoglobin-CO complex, $\text{Mb}(\text{Fe}^{2+})\text{CO}$, using “aged” CO solution. | 97 |
| Figure 2.32: Molecular structure of CORM-3. | 99 |
| Figure 2.33: UV-visible absorption spectra of anaerobically prepared CORM-3 and ferrous myoglobin, $\text{Mb}(\text{Fe}^{2+})$ | 100 |
| Figure 2.34: Kinetic study of CO release from anaerobically prepared CORM-3 solution. | 101 |

| | |
|--|-----|
| Figure 2.35: UV-visible absorption spectra of aerobically prepared CORM-3 solution. | 102 |
| Figure 2.36: Kinetic study of CO release from aerobically prepared stock CORM-3 solution. . | 103 |
| Figure 2.37: UV-visible absorption spectra of N ₂ -bubbled CORM-3 solution. | 105 |
| Figure 2.38: UV-visible absorption spectra of “aged” CORM-3 solution. | 106 |
| Figure 2.39: UV-visible absorption spectra of N ₂ -bubbled “aged” CORM-3 solution. | 107 |
| Figure 2.40: Molecular structures of PP-IX and ZnPP-IX. | 108 |
| Figure 2.41: Absorption spectra of PP-IX with a strong Soret peak at 405 nm and 4 Q-bands between 500 and 630 nm | 109 |
| Figure 2.42: Spectral measurements of ZnPP-IX in light and dark conditions. | 111 |
| Figure 2.43: Analysis window on WinFlour software showing the selection of a region of interest (ROI) at a position of high fluorescent intensity in a smooth muscle cell. | 114 |
| Figure 3.1: Current-voltage (i-V) relationship of BK _{Ca} channels. | 117 |
| Figure 3.2: Effects of [Ca ²⁺] _i on single BK _{Ca} channel activity..... | 119 |
| Figure 3.3: Effects of membrane potential on single BK _{Ca} channel activity..... | 119 |
| Figure 3.4: Effects of extracellular TEA ⁺ application on single BK _{Ca} channel activity..... | 121 |
| Figure 3.5: Effects of intracellular haem application on BK _{Ca} channel Popen. | 123 |
| Figure 3.6: Effects of intracellular haem application on the open duration of single BK _{Ca} channels. | 125 |
| Figure 3.7: Effects of intracellular pH on the modulatory effect of haem on single BK _{Ca} channel activity..... | 127 |
| Figure 3.8: Effects of intracellular CO gas application on single BK _{Ca} channel activity..... | 129 |
| Figure 3.9: Effects of intracellular CO gas application on single BK _{Ca} channel activity in high [Ca ²⁺] _i | 131 |
| Figure 3.10: Effects of intracellular CORM-3 application on single BK _{Ca} channel activity. | 133 |
| Figure 3.11: Effects of intracellular iCORM-3 application on single BK _{Ca} channel activity. | 134 |
| Figure 3.12: Effects of intracellular application of CORM-3 on BK _{Ca} channels exposed to high [Ca ²⁺] _i | 136 |
| Figure 3.13: Effects of intracellular application of biliverdin on single BK _{Ca} channel activity... | 138 |
| Figure 3.14: Effects of intracellular application of ZnPP-IX on single BK _{Ca} channel activity. | 140 |
| Figure 4.1: Effects of external Ca ²⁺ concentration on STOCs. | 148 |
| Figure 4.2: Effects of changes in membrane potential (V _m) on STOCs. | 149 |
| Figure 4.3: STOCs are influenced by changes in membrane potential (V _m)..... | 150 |
| Figure 4.4: Effects of external TEA ⁺ on STOCs..... | 152 |
| Figure 4.5: Effects of penitrem A on STOCs. | 153 |

| | |
|--|-----|
| Figure 4.6: Effects of intracellular application of ryanodine via the pipette solution on STOCs. | 155 |
| Figure 4.7: Effects of caffeine on STOCs. | 156 |
| Figure 4.8: Effects of extracellular haem application on STOCs, using perforated patch configuration. | 158 |
| Figure 4.9: Effects of extracellular haem application on STOCs, using ruptured patch configuration. | 160 |
| Figure 4.10: Effects of extracellular haem application on STOCs. | 161 |
| Figure 4.11: Effects of low extracellular haem concentration on STOCs. | 163 |
| Figure 4.12: Effects of high extracellular haem concentration on STOCs. | 165 |
| Figure 4.13: Effects of different extracellular haem concentrations on STOCs. | 166 |
| Figure 4.14: Effects of V_m on STOCs under control (haem-free) conditions. | 167 |
| Figure 4.15: Effects of extracellular haem application on STOCs at less depolarised potential. | 169 |
| Figure 4.16: Effects of extracellular application of ZnPP-IX on STOCs. | 171 |
| Figure 4.17: Effects of ZnPP-IX pre-treatment of cells on STOCs. | 173 |
| Figure 4.18: Effects of haem on STOCs after cell pre-treatment with ZnPP-IX. | 175 |
| Figure 4.19: Comparison between the effects of haem on STOCs in ZnPP-IX-treated and untreated cells. | 176 |
| Figure 4.20: Effects of extracellular application of CO gas on STOCs. | 178 |
| Figure 4.21: Effects of extracellular application of CORM-3 on STOCs. | 180 |
| Figure 4.22: Effects of extracellular application of iCORM-3 on STOCs. | 181 |
| Figure 4.23: Summary of the effects of CO on STOCs. | 182 |
| Figure 4.24: Effects CORM-3 on STOCs following cell pre-treatment with ZnPP-IX. | 184 |
| Figure 4.25: Comparison between the effects of CORM-3 on STOCs in the presence and absence of ZnPP-IX. | 185 |
| Figure 4.26: Effects of m β CD (1 to 5 mM) pre-treatment of cells on STOCs. | 188 |
| Figure 4.27: Effects of haem on STOCs after cell pre-treatment with m β CD. | 190 |
| Figure 4.28: Comparison between the effects of haem on STOCs recorded from m β CD pre- treated and untreated cells. | 191 |
| Figure 4.29: Effects of CORM-3 on STOCs after cell pre-treatment with m β CD. | 193 |
| Figure 4.30: Effects of iCORM-3 on STOCs after cell pre-treatment with m β CD. | 194 |
| Figure 4.31: Comparison between the effects of CORM-3/iCORM-3 on STOCs recorded from m β CD pre-treated and untreated cells. | 195 |

| | |
|--|-----|
| Figure 4.32: Observation of Ca ²⁺ sparks in a SMC under control (haem-free) conditions..... | 197 |
| Figure 4.33: Observation of Ca ²⁺ sparks in the presence of extracellular haem (5 µM)..... | 198 |
| Figure 4.34: Effects of haem (5 µM) on Ca ²⁺ spark frequency in mesenteric artery SMCs..... | 199 |
| Figure 4.35: Recording of STOCs in the absence of haem. | 201 |
| Figure 4.36: Effects of intracellular haem (added via the pipette solution) on STOCs. | 201 |
| Figure 4.37: Comparison of STOCs under control conditions and in the presence of intracellular haem (haem _i). | 202 |
| Figure 4.38: Effects of simultaneous application of intracellular and extracellular haem on STOCs. | 204 |
| Figure 4.39: Effects of intracellular haem (haem _i) versus extracellular and intracellular haem (haem _{i+o}) on STOCs. | 205 |
| Figure 5.1: Effects of extracellular TEA ⁺ application on voltage pulsed whole-cell currents. ... | 217 |
| Figure 5.2: Effects of extracellular application of penitrem A on voltage pulsed whole-cell currents. | 218 |
| Figure 5.3: Stability of voltage pulsed whole-cell BK _{Ca} currents measured using the ruptured patch technique. | 219 |
| Figure 5.4: Effects of extracellular haem application on pulsed whole-cell BK _{Ca} current. | 221 |
| Figure 5.5: Effects of prolonged extracellular haem application on pulsed whole-cell BK _{Ca} current..... | 223 |
| Figure 5.6: Effects of extracellular haem application on pulsed whole-cell current in the presence of a BK _{Ca} channel blocker. | 225 |
| Figure 5.7: Effects of extracellular application of Cd ²⁺ on pulsed whole-cell BK _{Ca} current..... | 227 |
| Figure 5.8: Effects of extracellular haem application on pulsed whole-cell BK _{Ca} current in the presence of the L-type Ca ²⁺ channel blocker, Cd ²⁺ | 229 |
| Figure 5.9: Effects of extracellular application of ZnPP-IX on pulsed whole-cell BK _{Ca} current. | 231 |
| Figure 5.10: Comparison between BK _{Ca} current density in ZnPP-IX pre-treated and untreated (control) cells..... | 232 |
| Figure 5.11: Effects of extracellular haem application on pulsed whole-cell BK _{Ca} current recorded from ZnPP-IX pre-treated cells. | 234 |
| Figure 5.12: Effects of extracellular application of CORM-3 on pulsed whole-cell BK _{Ca} currents. | 236 |
| Figure 5.13: Effects of extracellular application of iCORM-3 on pulsed whole-cell BK _{Ca} currents. | 237 |

| | |
|---|-----|
| Figure 5.14: Effects of extracellular application of CO gas on pulsed whole-cell BK _{Ca} currents. | 239 |
| Figure 5.15: Comparison between the stability of BK _{Ca} currents in different [Ca ²⁺] _i . | 241 |
| Figure 5.16: Effects of Ca ²⁺ chelators on single BK _{Ca} channel activity. | 243 |
| Figure 5.17: Effects of extracellular CORM-3 application on pulsed whole-cell BK _{Ca} currents in 300 nM [Ca ²⁺] _i | 245 |
| Figure 5.18: Effects of extracellular CO gas application on pulsed whole-cell BK _{Ca} currents in 300 nM [Ca ²⁺] _i | 246 |
| Figure 5.19: Effects of extracellular haem application on single BK _{Ca} channel activity. | 249 |
| Figure 5.20: Effects of extracellular haem application on single BK _{Ca} channel activity in the presence of the BK _{Ca} channel blocker, penitrem A. | 251 |
| Figure 5.21: Effects of extracellular CO gas application on single BK _{Ca} channel activity. | 253 |
| Figure 5.22: Effects of extracellular CORM-3 application on single BK _{Ca} channel activity..... | 255 |
| Figure 5.23: Effects of extracellular iCORM-3 application on single BK _{Ca} channel activity..... | 256 |
| Figure 6.1: Schematic diagram showing the proposed mechanisms of action of haem on SMC BK _{Ca} channel activity, based on results from the present study. | 270 |

ABBREVIATIONS

| <u>Abbreviation</u> | <u>Meaning</u> |
|-------------------------------|--|
| ATP | adenosine triphosphate |
| BAPTA | 1,2-bis(o-aminophenoxy) ethane-N, N, N', N'-tetraacetic acid |
| CICR | Ca ²⁺ -induced Ca ²⁺ release |
| cGMP | cyclic guanosine monophosphate |
| CO | carbon monoxide |
| CORM | carbon monoxide releasing molecule |
| CORM-2 | tricarbonyldichlororuthenium (II) dimer or [Ru(CO ₃)Cl ₂] ₂ |
| CORM-3 | tricarbonylchloro(glycinato)ruthenium (II) or Ru(CO) ₃ Cl(glycinate) |
| CTD | cytosolic terminal domain |
| DMSO | dimethyl sulphoxide |
| EGTA | ethylene glycol-bis(β-aminoethyl ether)-N,N,N',N'-tetraacetic acid) |
| ER | endoplasmic reticulum |
| Fe ²⁺ -Mb | ferrous myoglobin |
| Fe ³⁺ -Mb | ferric myoglobin |
| HBP | haem binding protein |
| HEDTA | N-(2-hydroxyethyl) ethylenediamine triacetic acid |
| HLL | haem-L-lysinate |
| H ₂ O ₂ | hydrogen peroxide |
| HO | haem oxygenase |
| iCORM-3 | inactivated CORM-3 |
| LTCC | L-type Ca ²⁺ channel |
| mβCD | methyl β-cyclodextrin |
| mot | mean open time |
| NADPH | nicotinamide adenine dinucleotide phosphate |
| NO | nitric oxide |
| NOS | nitric oxide synthase |

| | |
|------------------|---|
| PGD | pore gate domain |
| PKA | cAMP-dependent protein kinase |
| PKC | protein kinase C |
| PKG | cGMP-dependent protein kinase |
| Popen | open probability |
| PP-IX | protoporphyrin-IX |
| RCK | regulator of conductance for K ⁺ |
| RyR | ryanodine receptor |
| sGC | soluble guanylate cyclase |
| SMC | smooth muscle cell |
| SR | sarcoplasmic reticulum |
| STOC | spontaneous transient outward current |
| TEA ⁺ | tetraethylammonium ion |
| TTCC | T-type Ca ²⁺ channel |
| VGCC | voltage-gated Ca ²⁺ channel |
| V _m | membrane potential |
| VSD | voltage sensor domain |
| ZnPP-IX | zinc protoporphyrin-IX |

Chapter 1 INTRODUCTION

1.1 Blood vessels

The cardiovascular system comprises of the heart and blood vessels; the heart pumps blood which is transported around the body via a variety of blood vessels. The unique structure of blood vessels facilitates their role in blood transportation.

This section discusses the structure and types of blood vessels, as well as the contributions from different endogenous signalling molecules and pathways to the regulation of vascular tone.

1.1.1 Structure of blood vessels

The walls of some blood vessels comprise of 3 layers; tunica intima, tunica media and tunica adventitia (Figure 1.1). The tunica intima consists of endothelial cells and a thin layer of connective tissues. The endothelial cells form the lumen of the blood vessel, so they are directly in contact with blood. A layer of elastic sheet called the internal elastic lamina exists between the tunica intima and tunica media. Myoendothelial junctions in the internal elastic lamina allow for cross communication between endothelial and smooth muscle cells (SMCs) contained in the tunica media. The tunica media also contains elastin and collagen. The contractile state of the SMCs affects the diameter of blood vessels; with SMC contraction and relaxation producing smaller and wider diameters respectively. Therefore, the contractile state of the SMCs plays a crucial role in the regulation of vascular tone and blood pressure. Elastin and collagen influence the flexibility of blood vessels. After the tunica media is another layer of elastic sheet called the external elastic lamina. The external elastic lamina separates the tunica media from the tunica adventitia. The tunica adventitia functions to loosely connect the blood vessel to the surrounding tissue. Thus, it mainly comprises of connective tissue. This layer can also contain small blood vessels, nociceptive nerve fibres and sympathetic nerve fibre endings called varicosities, which release noradrenaline and adenosine triphosphate (ATP) from synaptic vesicles.

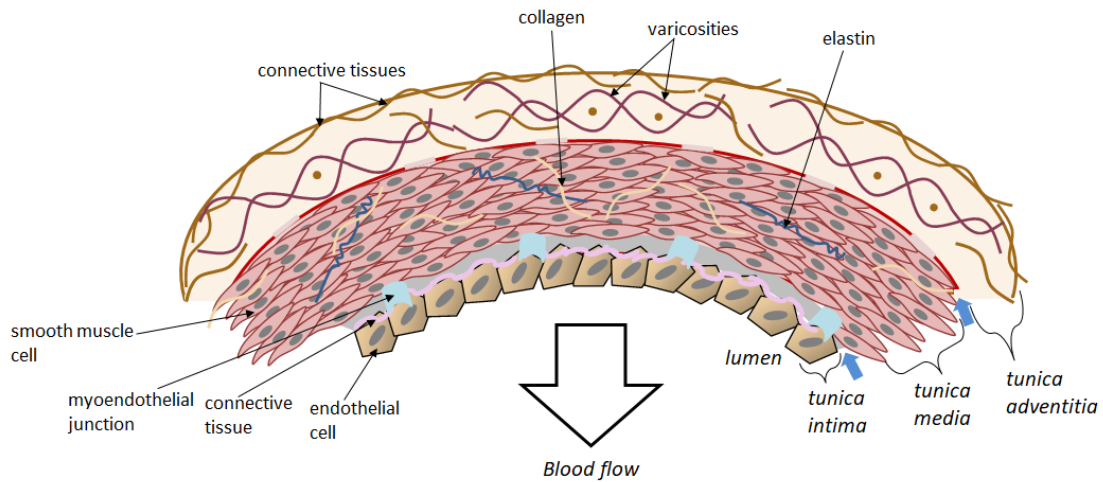


Figure 1.1: Structure of a blood vessel wall. The schematic diagram shows the 3 different layers in a blood vessel wall; tunica intima, tunica media and tunica adventitia. The different layers are separated by layers of elastic sheet called internal and external elastic laminae, indicated by the blue arrows.

1.1.2 Types of blood vessels

Blood vessels can be categorised into different functional groups, including elastic arteries, conduit arteries, exchange vessels and capacitance vessels.

Elastic arteries

These are vessels which have walls comprising of elastin and collagen, examples include the aorta and iliac arteries. Elastin enables the wall of the arteries to expand temporarily during systole to accommodate the ejected blood. The mechanical energy stored in elastin is also involved in the maintenance of arterial pressure during diastole. Collagen functions to regulate arterial diameter by reducing overextension of the arteries with increase in blood pressure.

Conduit arteries

Conduit arteries are branches from elastic arteries. Examples include cerebral and coronary arteries. The tunica media of these vessels contain more SMCs than that of the elastic arteries. Their adventitia layer is also richly innervated by sympathetic nerve fibres. These arteries supply blood to smaller feed arteries which in turn feed into arterioles, also referred to as resistance arteries due to their large resistance to blood flow.

Exchange vessels

This includes capillaries and microvessels that exist immediately upstream and downstream of the capillaries (such as postcapillary venules). Capillaries have only a single layer of endothelial cells which are closely associated with highly branched cells, called pericytes. Pericytes are believed to be involved in regulating the permeability of capillaries, as fewer pericytes results in leaky capillaries. The high resistance of capillaries to blood flow and the large cross-sectional area of capillary beds reduces blood velocity. This promotes efficient delivery of nutrients and removal of metabolites from body tissues, by red blood cells.

Capacitance vessels

Capacitance vessels have a thinner layer of SMCs, they include veins and venules. They are referred to as capacitance vessels because their large number and size enables them to contain two-thirds of the circulating blood at any given time. Furthermore, some veins possess semilunar valves to prevent the backflow of blood, due to gravity.

1.1.3 Regulation of blood vessel diameter

Vascular tone refers to the tension exerted by vascular SMCs that line the wall of blood vessels. Changes in vascular tone is controlled by the contractile state of vascular SMCs, which is influenced by a combination of factors including intrinsic factors (such as metabolites and endogenous signalling molecules), extrinsic factors (controlled by the autonomic nervous system) and the activity of ion channels expressed in the membrane of the cells. The regulation of vascular SMC contractility by the activity of ion channels expressed in their plasma membrane will be discussed in section 1.2.3.

Vasoconstriction

Vasoconstriction is defined as a decrease in size of a blood vessel lumen. Myogenic autoregulation is an intrinsic mechanism via which vascular SMCs regulate their contractile state. The process is triggered by an increase in intraluminal pressure, which temporarily stretches the SMCs in arterial walls causing them to contract, thereby inducing vasoconstriction. The tonic discharge of noradrenaline from sympathetic varicosities can also induce vasoconstriction via the binding of noradrenaline to α -

adrenergic receptors expressed in vascular SMCs. Other endogenous vasoconstrictive molecules include endothelins and angiotensin II.

Vasodilation

Vasodilation is the increase in the size of the blood vessel lumen. The intrinsic factors involved in vasodilation include low O₂ levels and high level of metabolites released from tissues such as; CO₂, protons (H⁺) and potassium (K⁺). Endogenous signalling molecules including histamine, nitric oxide (NO) and adenosine also contribute to vasodilation. Adrenaline also contributes to vasodilation by acting on β₂-adrenergic receptors which are predominantly expressed in blood vessels of the heart, liver and skeletal muscle. The atrial natriuretic peptide released from overstretched atrial cells also contributes to vasodilation by altering sodium (Na⁺) and water excretion from the kidneys. Unlike the tonic contribution of sympathetic nerves to vasoconstriction, parasympathetic vasodilator nerves are not tonically active. Acetylcholine released from parasympathetic postganglionic terminals produces vasodilation by acting on muscarinic, M₃, receptors expressed in endothelial cells. Activated M₃ receptors stimulate NO production which encourages vasodilation.

1.2 Vascular smooth muscle cells

1.2.1 Mechanisms of calcium (Ca²⁺) handling in vascular SMCs

Ca²⁺ is an important signalling molecule which plays a key role in vascular SMC contraction. Therefore, vascular SMCs tightly control intracellular Ca²⁺ concentration, [Ca²⁺]_i, via a variety of mechanisms which regulate Ca²⁺ entry and removal from the cytosol, as shown in Figure 1.2.

1.2.1.1 Cytosolic Ca²⁺ mobilisation pathways

Cytosolic Ca²⁺ increases can occur due to either influx from the extracellular space, via voltage-gated Ca²⁺ channels (VGCC), non-selective cation channels (NSCCs), store operated Ca²⁺ entry (SOCE) or release from intracellular stores (via Ca²⁺-induced Ca²⁺ release and IP₃ receptors).

1.2.1.1.1 Voltage-gated Ca²⁺ channels (VGCC)

L-type Ca²⁺ channels (LTCCs) and T-type Ca²⁺ channels (TTCCs) are types of VGCCs which have been characterised in SMCs (Benham *et al.*, 1987; Yatani *et al.*, 1987; Loirand *et al.*, 1989; Smirnov & Aaronson, 1992a). L-type Ca²⁺ channels (LTCCs) are abundantly expressed in vascular SMCs. LTCC activation plays a major role in Ca²⁺ influx into SMCs with minor contributions from T-type channels (TTCC). This is because unlike LTCCs, TTCCs are activated at negative potentials, - 55 mV to - 50 mV, and display rapid inactivation at more positive membrane potentials (V_m), \sim - 40 mV (Yatani *et al.*, 1987; Ganitkevich & Isenberg, 1990).

1.2.1.1.2 Non-selective cation channels (NSCC)

The NSCCs expressed in vascular SMCs include second messenger-operated (SMOCs) and stretch-activated cation (SAC) channels. These channels are permeable to both Ca²⁺ and Na⁺. The membrane depolarization induced by Na⁺ conductance can also promote Ca²⁺ entry via LTCCs.

Second messenger-operated channels (SMOC)

These include members of the transient receptor potential C (TRPC) subfamily. TRPC3 and TRPC6 are activated by diacylglycerol (DAG) which is synthesised by coupling of α_1 -adrenoceptor activation to G_{q/11} pathway (Boulay *et al.*, 1997; Hofmann *et al.*, 1999). The activated TRPC3 and TRPC6 channels are permeable to both Na⁺ and Ca²⁺ (Hofmann *et al.*, 1999). Membrane depolarization evoked by Na⁺ entry enhances Ca²⁺ influx via LTCC (Soboloff *et al.*, 2005).

Ligand-gated cation channels (LGCC)

P2X receptors are non-selective cation-conducting channels which are activated by the binding of ATP to an extracellular site on the channel (Coddou *et al.*, 2011). Studies from knock-out mice indicate that P2X₁ receptors are the predominant isoform expressed in smooth muscle cells (Hill-Eubanks *et al.*, 2011).

Stretch-activated cation channels (SAC)

Evidence from electrophysiology studies indicates the existence of stretch-activated non-selective cation channels in vascular SMC membrane (Davis *et al.*, 1992a; Davis *et al.*, 1992b; Setoguchi *et al.*, 1997). These channels were activated by membrane stretch

and found to conduct Na^+ , Ca^{2+} and K^+ . The mechanical sensitivity of SAC channels suggests their involvement in myogenic autoregulation.

1.2.1.1.3 Store-operated Ca^{2+} entry (SOCE)

SOCE is a term used to define the process whereby Ca^{2+} depletion from intracellular stores promotes Ca^{2+} entry into SMCs (Parekh & Putney, 2005). Stromal interaction molecule (STIM) proteins expressed in the endoplasmic reticulum (ER) membrane act as Ca^{2+} sensors. Thus, a decrease in ER Ca^{2+} content induces aggregation of the STIM proteins, thereby enabling them to couple to Orai proteins located in the plasma membrane (Liou *et al.*, 2005; Zhang *et al.*, 2005; Luik *et al.*, 2006). This results in the activation of the Orai proteins which promotes Ca^{2+} entry into the cell.

1.2.1.1.4 Ca^{2+} -induced Ca^{2+} release (CICR)

CICR is another mechanism of Ca^{2+} entry into the cytosol. It is a process whereby Ca^{2+} entry into the cytosol, through plasmalemmal Ca^{2+} channels, promotes Ca^{2+} release from intracellular stores which further increases $[\text{Ca}^{2+}]_i$. The sarcoplasmic reticulum (SR) membrane expresses Ca^{2+} -gated channels called ryanodine sensitive Ca^{2+} -release channels (RyRs).

Three RyR isoforms have been identified in mammals; RyR1 to RyR3 (Zucchi & RoncaTestoni, 1997). The open-state probability (Popen) of RyRs is regulated by cytoplasmic and intraluminal Ca^{2+} (Endo, 1975; Nelson & Nelson, 1990; Ching *et al.*, 2000). The coordinated opening of several (RyRs) results in the generation of “ Ca^{2+} sparks” which are local transient increases in $[\text{Ca}^{2+}]_i$ (Cheng *et al.*, 1993).

1.2.1.1.5 Ca^{2+} release from intracellular stores via IP_3 receptors

Inositol 1,4,5-trisphosphate receptor (IP_3R) are also located on the SR membrane. There are 3 known subtypes of IP_3Rs ; $\text{IP}_3\text{R1}$, $\text{IP}_3\text{R2}$ and $\text{IP}_3\text{R3}$ (Newton *et al.*, 1994; Tasker *et al.*, 1999). IP_3R activation is regulated by IP_3 and Ca^{2+} . IP_3 , produced by the activation of $\text{G}_{q/11}$ -coupled GPCRs, binds to IP_3Rs . This enhances channel gating thereby promoting Ca^{2+} release into the cytosol. Low $[\text{Ca}^{2+}]_i$ (< 300 nM) also potentiates IP_3R activation but micromolar $[\text{Ca}^{2+}]_i$ acts as negative feedback regulators (Hirata *et al.*, 1984; Iino, 1990). Unlike RyRs, IP_3R activation results in the generation of “ Ca^{2+} puffs” which are also transient Ca^{2+} release events but distinct from Ca^{2+} sparks in their kinetics, magnitude and spatial spread (Yao & Parker, 1994; Callamaras & Parker, 2000). Ca^{2+} puffs can

initiate the generation of Ca^{2+} waves, described as the propagation of oscillations in $[\text{Ca}^{2+}]_i$ from an initial site to the rest of the cell (Iino *et al.*, 1994; Boittin *et al.*, 2000). Ca^{2+} puffs trigger Ca^{2+} waves via cascading Ca^{2+} events whereby Ca^{2+} release from an IP_3R promotes activation of neighbouring IP_3Rs (Bootman & Berridge, 1996; Thomas *et al.*, 1998).

1.2.1.2 Ca^{2+} removal pathways

The removal of Ca^{2+} from the cytosol is a rapid process. It involves transporting Ca^{2+} into intracellular stores or extrusion into the extracellular space.

1.2.1.2.1 Re-uptake into intracellular stores

Ca^{2+} re-uptake into the SR or ER is mediated by the sarco-/endoplasmic reticulum Ca^{2+} -ATPase pump (SERCA) which is located on the SR/ER membrane. SERCA is inhibited by phospholamban (PLB), a transmembrane protein located on the SR/ER (Inui *et al.*, 1986; Suzuki & Wang, 1986). The phosphorylation of PLB by protein kinase A (PKA) or Ca^{2+} -calmodulin dependent kinase promotes the dissociation of PLB, thereby reversing its inhibitory effect on SERCA (Tada *et al.*, 1974; Tada *et al.*, 1983; Kranias, 1985). This increases the Ca^{2+} sensitivity of SERCA which results in higher SR Ca^{2+} load. The SR can store up to 10 to 15 mM of Ca^{2+} (Sanders, 2001). This is due to the presence of Ca^{2+} buffers, calsequestrin and calreticulin, in the SR which increase its storage capacity by binding to Ca^{2+} (Milner *et al.*, 1992; Raeymaekers *et al.*, 1993).

Mitochondria also act as intracellular Ca^{2+} stores. Proton (H^+) extrusion during the electron transport chain creates a negative mitochondrial V_m (Sanders, 2001). This produces a strong electrochemical gradient for Ca^{2+} entry into the mitochondria. Nevertheless, the involvement of the mitochondria in Ca^{2+} re-uptake mainly occurs at high $[\text{Ca}^{2+}]_i$. This is because the mitochondrial Ca^{2+} uniporter has a low Ca^{2+} affinity with half-maximal transport (K_d) ranging from 1 μM to 189 μM (Gunter & Pfeiffer, 1990).

1.2.1.2.2 Extrusion into the extracellular space

Ca^{2+} ATPases are also expressed on the plasma membrane of SMCs; PMCA. Ca^{2+} extrusion via PMCA is an active process which requires ATP because of the steep gradient for Ca^{2+} entry. PMCA are activated by the binding of calmodulin to their

carboxyl terminus (James *et al.*, 1988; Enyedi *et al.*, 1989). Alternatively, autoinhibition of PMCA can be removed by PKA or protein kinase C (PKC) -mediated phosphorylation either close to or within the calmodulin binding site (Enyedi *et al.*, 1996; Baggaley *et al.*, 2007). Such phosphorylation can interfere with calmodulin binding (Enyedi *et al.*, 1997). $\text{Na}^+/\text{Ca}^{2+}$ exchangers located in the plasma membrane of SMCs are also involved in the rapid removal of Ca^{2+} from the cytosol (Ashida & Blaustein, 1987). Unlike PMCA, the extrusion of Ca^{2+} via the forward mode of $\text{Na}^+/\text{Ca}^{2+}$ exchanger is not an active process, as it is driven by the energy derived from the electrochemical gradient of Na^+ .

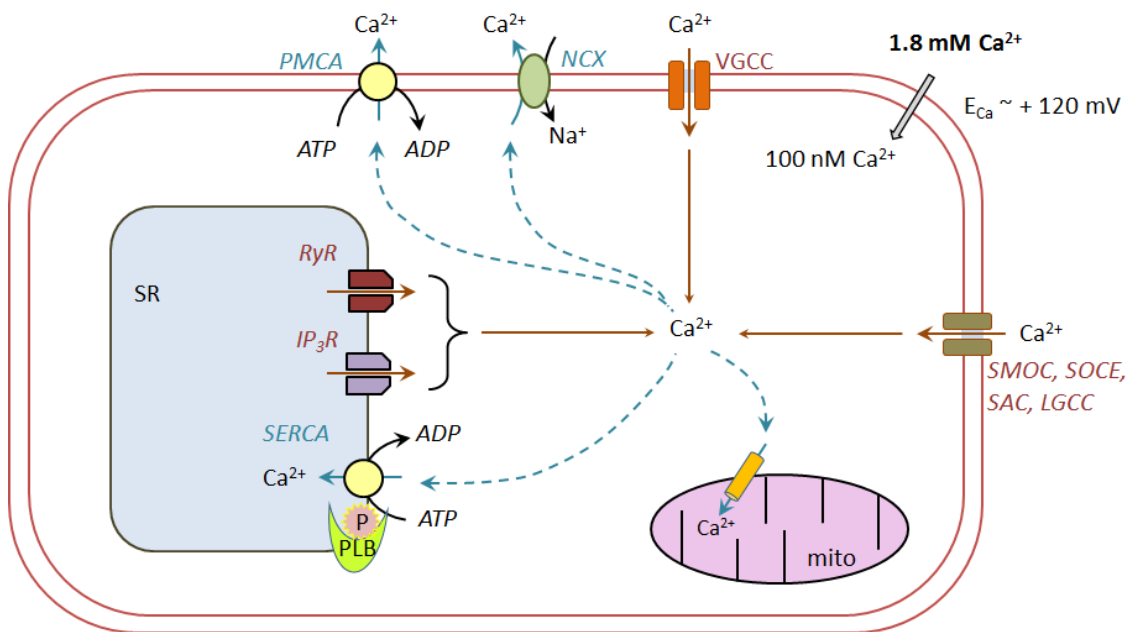


Figure 1.2: Ca^{2+} handling in vascular SMCs. Schematic diagram shows a summary of the Ca^{2+} entry and exit pathways which work together to tightly regulate intracellular Ca^{2+} concentration in vascular SMCs.

1.2.2 Vascular SMC excitation-contraction coupling

Contraction

Vascular SMC contraction is a graded and highly controlled process. It is triggered by a rise in $[\text{Ca}^{2+}]_i$ and regulated by different mechanisms and regulatory proteins (such as caldesmon and calponin) as explained below.

Depolarization of vascular SMC membrane activates LTCC. This results in Ca^{2+} influx which promotes CICR from the SR, as discussed in section 1.2.1.1.3. The rise in $[\text{Ca}^{2+}]_i$

results in the formation of Ca^{2+} -calmodulin complexes (Figure 1.3). The Ca^{2+} -calmodulin complex activates myosin light chain kinase (MLCK), a serine/threonine kinase (Murphy, 1982). Activated MLCK phosphorylates myosin regulatory light chain (MLC), a component of the myosin head, at serine (Ser) 19 (Kamm & Stull, 1985; Stull *et al.*, 1998; Kamm & Stull, 2001). This activates myosin ATPase activity which promotes the binding of actin to MLC and crossbridge cycling. Tension is generated by the rotation of the myosin head. Unlike striated muscles, SMCs can maintain tension at a constant length with low ATP consumption. This is achieved via a “Latch” mechanism in which cross bridges are maintained for longer resulting in less ATP consumption (Siegman *et al.*, 1976).

Crossbridge cycling is regulated by caldesmon and calponin which are proteins bound to actin. Caldesmon directly inhibits myosin ATPase activity by binding to myosin (Sobue *et al.*, 1982; Bryan, 1990; Wang *et al.*, 1991). The interaction of caldesmon with myosin is regulated by Ca^{2+} -calmodulin whereas phosphorylation of caldesmon on Ser789 by extracellular-signal-regulated kinase (ERK) regulates its interaction with actin (Hemric *et al.*, 1993; Patchell *et al.*, 2002). Furthermore, phosphorylation of calponin on Ser175 by PKC and calmodulin kinase II removes its ability to bind actin and relieves its inhibitory effect on myosin ATPase activity (Winder & Walsh, 1990; Winder *et al.*, 1993).

Relaxation

Relaxation of vascular SMCs is triggered by a cascade of events starting with a decrease in $[\text{Ca}^{2+}]_i$, via mechanisms explained in section 1.2.1.2. The decrease in $[\text{Ca}^{2+}]_i$ results in the dissociation of Ca^{2+} from calmodulin and MLCK inactivation which allows the intrinsic activity of myosin light chain phosphatase (MLCP) to dominate. MLCP contributes to the inhibition of crossbridge formation by dephosphorylating MLC (Hartshorne *et al.*, 2004), as shown in Figure 1.3.

MLCP can also be inactivated by kinases. This promotes Ca^{2+} sensitization of the contractile machinery, thus, even though Ca^{2+} -calmodulin complex formation is low and MLCP activity is inhibited, tonic contraction can still occur. The kinases involved in MLCP inactivation are RhoA kinase and PKC (Figure 1.3). RhoA kinase is activated downstream of $G_{12/13}$ -protein coupled receptors. Phosphorylation of MLCP by RhoA kinase inhibits its activity (Shin *et al.*, 2002; Ito *et al.*, 2003; Grassie *et al.*, 2012). On the other hand, PKC

activated downstream of G_q -protein coupled receptors promotes the activation of CPI-17, which inhibits MLCP activity (Kitazawa *et al.*, 2000; Niiro *et al.*, 2003).

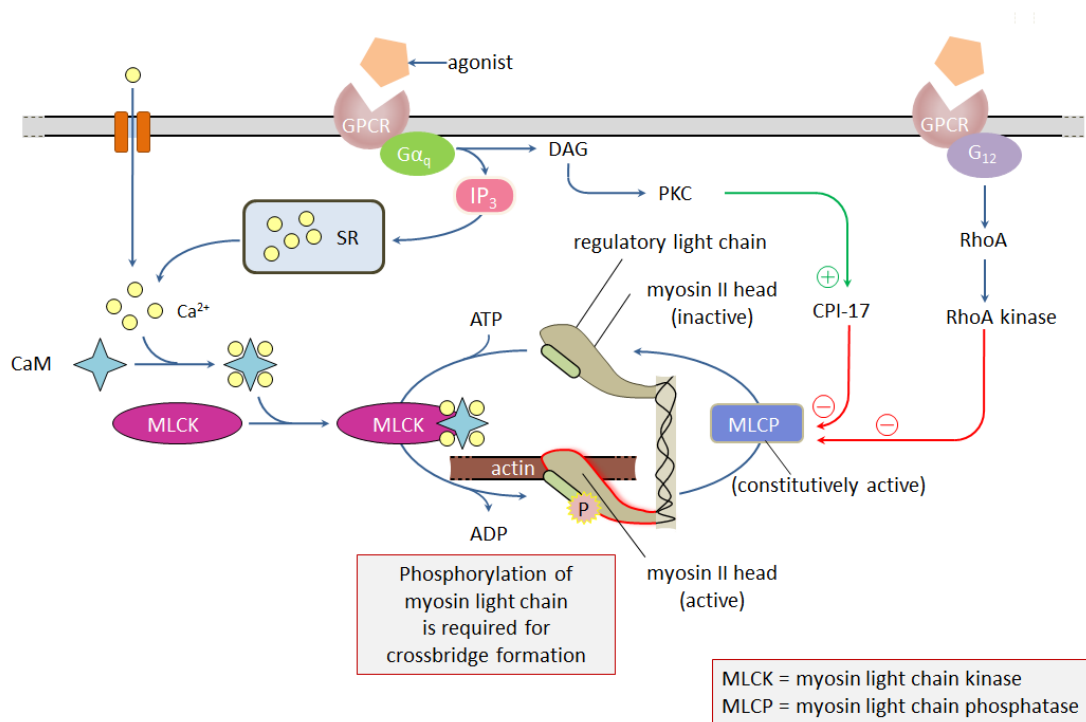


Figure 1.3: Regulation of vascular SMC excitation-contraction coupling. The schematic diagram shows the different proteins and signalling pathways involved in regulating vascular SMC contraction and relaxation.

1.2.3 Regulation of vascular SMC membrane potential (V_m)

The V_m of vascular SMCs has direct effects on their contractile state which in turn influences vascular tone and blood pressure. Thus, vascular SMC V_m is tightly regulated by a variety of ion channels expressed in their membrane. These include Ca^{2+} , chloride (Cl^-), Na^+ and K^+ channels. The different subtypes, structure, mechanism of activation, regulation and function of these channels will be discussed in turn.

1.2.3.1 Ca^{2+} channels

There are two main types of voltage-gated Ca^{2+} channels expressed in vascular SMCs, LTCC and TTCCs (Bean *et al.*, 1986; Benham *et al.*, 1987; Ball *et al.*, 2009). These channels are comprised of a pore-forming α_1 -subunit which has four homologous domains, each

consisting of six transmembrane segments with intracellular amino- (N) and carboxyl- (C) termini. LTCCs are also associated with modulatory auxiliary $\alpha_2\delta$, β and γ subunits (Catterall, 2011; Dolphin, 2013). TTCCs are activated at negative potentials with fast inactivation kinetics at positive potentials (c.f. section 1.2.1.1.1). They are characterised by their small conductance and transient current. On the other hand, LTCCs are activated at more depolarised potentials (~ -30 mV) with slow inactivation kinetics, from ~ 0 mV to 10 mV (Bean *et al.*, 1986; Yatani *et al.*, 1987; Ganitkevich & Isenberg, 1990). They have a larger conductance and long-lasting current. LTCCs are also targets of signalling cascades involving protein kinases (Keef *et al.*, 2001). The PKC-mediated enhancement of LTCC activity has been proposed to be involved in the basal and persistent activity of the channel (Santana *et al.*, 2008; Nieves-Cintrón *et al.*, 2008; Weiss & Dascal, 2015). Conversely, cGMP-dependent protein kinase (PKG) mediates inhibitory effects on LTCC activity whereas the effects of PKA is controversial, as different studies have reported activation, inhibition and no effect (Keef *et al.*, 2001).

LTCCs channels play an important role in the regulation of vascular tone. This is due to their involvement in excitation-contraction coupling as detailed in section 1.2.1.1.3. LTCCs are also principal mediators of myogenic tone (Nelson *et al.*, 1990; Knot & Nelson, 1998; Amberg & Navedo, 2013). TTCCs have also been implicated in depolarization-induced vasoconstriction and Ca^{2+} influx in rat mesenteric arterioles (Gustafsson *et al.*, 2001; Jensen *et al.*, 2004).

1.2.3.2 Cl^- channels

Vascular SMCs have a high $[\text{Cl}^-]_i$ ranging from ~ 40 to 70 mM (Hirst & Edwards, 1989). This results from the combined activity of $\text{Cl}^-/\text{HCO}_3^-$ anion exchangers and $\text{Na}^+/\text{K}^+/\text{Cl}^-$ co-transporters in SMCs (Bulley & Jaggar, 2014).

Vascular SMCs express at least 2 types of Cl^- channels; Ca^{2+} -activated (Cl_{Ca}) and volume-sensitive Cl^- channels (Cl_{vs}) (Large & Wang, 1996; Nelson *et al.*, 1997). Cl_{Ca} channels are activated by the Ca^{2+} sparks produced from the opening of RyRs located on the SR (Pacaud *et al.*, 1992; Klockner, 1993; Lamb *et al.*, 1994; Yuan, 1997). The activation of these channels results in Cl^- efflux which are recorded as spontaneous transient inward currents, STICs, (Hogg *et al.*, 1994). STICs produce membrane depolarization which

result in LTCC activation and Ca^{2+} influx, thereby promoting contraction (Large & Wang, 1996). Therefore, Cl_{Ca} are involved in the regulation of the V_m and contractility of SMCs.

A combination of electrophysiology and molecular techniques provided evidence for the expression of Cl_{Vs} channels in vascular SMCs (Yamazaki *et al.*, 1998). It has been proposed that these channels are activated by the mechanical stretch induced by a rise in intravascular pressure (Nelson *et al.*, 1997). Therefore, Cl_{Vs} channels can be involved in the regulation of myogenic tone and resting V_m .

1.2.3.3 Na^+ channels

Tetrodotoxin-sensitive rapidly inactivating voltage-gated Na^+ (Na_v) channels have been identified in cultured human and freshly-isolated rabbit pulmonary artery and freshly-isolated mice mesenteric artery SMCs (Okabe *et al.*, 1988; James *et al.*, 1995; Platoshyn *et al.*, 2005; Berra-Romani *et al.*, 2005). These channels were reported to be activated at potentials positive to -30 mV or -40 mV, with maximum activation occurring at -10 mV (Okabe *et al.*, 1988; James *et al.*, 1995; Meguro *et al.*, 2009). The presence of Na_v channels in vascular SMCs has been controversial as they have been reported to be unexpressed in native human aortic SMCs (Meguro *et al.*, 2009).

There are at least nine known isoforms of Na_v channels; $\text{Na}_v1.1$ to $\text{Na}_v1.9$, which have been classified based on their different characteristics including rate of inactivation and tetrodotoxin sensitivity (Goldin, 2001; Catterall *et al.*, 2003). Each Na_v channel consists of a single pore-forming α -subunit with four domains, each comprising of six transmembrane segments (Marban *et al.*, 1998). However, at present only 3 of the 11 known α -subunit genes; *SCN5A*, *SCN6A*, *SCN7A*, have been identified in vascular SMCs (Platoshyn *et al.*, 2005). The α -subunits can also be expressed with auxiliary β -subunits (Catterall *et al.*, 2003). The function of Na_v channels in the vasculature is unclear. However, it has been proposed that Na^+ influx through Na_v channels causes the $\text{Na}^+/\text{Ca}^{2+}$ exchanger to work in reverse mode and the resulting rise in Ca^{2+} activates Cl_{Ca} channels leading to membrane depolarisation (Saleh *et al.*, 2005; Fort *et al.*, 2009; Ho *et al.*, 2013). Nevertheless, since Na^+ currents were recorded in cultured human aortic SMCs but not in native cells, Meguro *et al.*, 2009 suggested that Na_v channels might not be involved in the regulation of vascular SMC membrane potential under normal physiological conditions.

1.2.3.4 K⁺ channels

K⁺ channels play a major role in maintaining the resting V_m of SMCs. This is because in their resting state, SMCs have a high K⁺ permeability (Salkoff *et al.*, 2006). However, the resting V_m of SMCs is not at the equilibrium potential for K⁺, E_K , instead in arterial and arteriolar SMCs it ranges from -40 mV to -55 mV *in vivo* and -60 mV to -75 mV *in vitro* (Neild & Keef, 1985; Hirst & Edwards, 1989). This results from the permeability of the membrane to other ions. For instance, the unusually high intracellular Cl⁻ concentration in SMCs (see section 1.2.3.2) promotes the efflux of Cl⁻; E_{Cl} of SMCs is relatively positive between -20 mV to -30 mV (Casteels *et al.*, 1977).

Four distinct types of K⁺ channels have been identified in vascular SMC membrane. They include voltage-gated (K_v), Ca²⁺-activated (K_{Ca}), inward-rectifier (K_{ir}) and ATP-sensitive (K_{ATP}) K⁺ channels. This project mainly focuses on a subtype of the K_{Ca} channel referred to as the large-conductance Ca²⁺-activated K⁺ (BK_{Ca}) channel. BK_{Ca} channels will be discussed in section 1.2.4.

1.2.3.4.1 K_v channels

K_v channels are voltage-gated channels which are activated by membrane depolarisation (substantial activation occurs at \sim -30 mV) and inactivated by sustained depolarisation (Nelson & Quayle, 1995). They are formed by the tetrameric assembly of pore-forming α -subunits. Each α -subunit consists of six transmembrane domains with cytoplasmic N- and C-termini. The α -subunits can also be co-expressed with auxiliary β -subunits (Sewing *et al.*, 1996; Yu *et al.*, 1996; Leicher *et al.*, 1998).

There are at least 12 known subfamilies of K_v channels; K_v1 to K_v12 (Gutman *et al.*, 2005). These channels display different voltage-dependent activation and inactivation kinetics. The membrane expression and activity of K_v channels can be regulated by protein kinases (Jonas & Kaczmarek, 1996). For instance, vascular SMC delayed rectifier currents have been shown to be inhibited and stimulated by PKC and PKA, respectively (Aiello *et al.*, 1996; Aiello *et al.*, 1998).

The activation of K_v channels in vascular SMCs limits membrane depolarisation and contributes to the regulation of resting V_m (Nelson & Quayle, 1995; Cheong *et al.*, 2001a; Cheong *et al.*, 2001b).

1.2.3.4.2 K_{ATP} channels

K_{ATP} channels are expressed in a variety of cells, including SMCs (Standen *et al.*, 1989). They exist as hetero-octameric channels comprised of four pore-forming K^+ conducting Kir6.0 subunits, which are members of the K_{ir} subfamily, and four regulatory sulphonylurea receptor (SUR) subunits, which are members of the ATP-binding cassette (ABC) protein family. In the vertebrate genome there are 2 Kir6 genes (*Kir6.1* and *Kir6.2*) and 2 SUR genes, *SUR1* and *SUR2* (*SUR2* has 2 splice variants; *SUR2A* and *SUR2B*) with subunit composition varying between cells (Aguilar-Bryan & Bryan, 1999). For instance, Kir6.1/Kir6.2 and SUR2B are found in SMCs.

K_{ATP} channels are activated by adenosine diphosphate (ADP), which interacts with the SUR subunit, and inhibited by ATP, which binds to specific ATP-binding sites on the Kir subunit (Nichols, 2006). Therefore, K_{ATP} channels can be involved in regulating the resting V_m of vascular SMCs particularly during periods of metabolic stress (Samaha *et al.*, 1992; Quayle & Standen, 1994). K_{ATP} channel activity is also regulated by protein kinases. For instance, phosphorylation of serine and threonine residues on Kir6.1 and SUR2B subunits by PKA and PKG results in channel activation whereas PKC activity promotes channel inhibition (Quayle *et al.*, 1994; Nelson & Quayle, 1995; Quinn *et al.*, 2004).

1.2.3.4.3 K_{ir} channels

K_{ir} channels are so-called because they conduct large inward currents at V_m negative to E_K but small outward current at potentials positive to E_K (Quayle *et al.*, 1997). The inward rectification results from voltage-dependent block of the channels by Mg^{2+} and polyamines, such as spermine and spermidine, as explained below.

Functional K_{ir} channels exist as tetrameric complexes of pore-forming α -subunits (Yang *et al.*, 1995). Each α -subunit comprises of 2 transmembrane domains with cytoplasmic N- and C-termini (Kubo *et al.*, 1993). There are at least seven known K_{ir} channel subfamilies; $K_{ir}1.0$ to $K_{ir}7.0$. Some subfamilies display strong inward rectification whilst others have weak or intermediate rectification. The difference between weak and strong inward rectifiers is partly influenced by the amino acid residue at position 172 of the second transmembrane domain of the channels (Quayle *et al.*, 1997). Weak inward rectifiers have a neutral asparagine residue whereas strong inward rectifiers, such as

K_{ir}2.0 and K_{ir}3.0 subfamilies, have a negatively charged aspartic acid residue (Quayle *et al.*, 1997; Hibino *et al.*, 2010). Furthermore, Mg²⁺-mediated channel block mainly accounts for the rectification in weak inward rectifiers, whereas both Mg²⁺ and polyamines are responsible for the rectification in strong inward rectifiers (Matsuda *et al.*, 1987; Ishihara *et al.*, 1989; Fakler *et al.*, 1994; Ficker *et al.*, 1994; Lopatin *et al.*, 1994; Yamada & Kurachi, 1995; Fakler *et al.*, 1995). In addition, phosphorylation of ROMK1, a type of K_{ir} channel, by PKC has been shown to increase its cell surface expression (Lin *et al.*, 2002).

K_{ir} 2.1 has been reported to be the predominant K_{ir} isoform in vascular SMCs (Bradley *et al.*, 1999). These channels play crucial roles in the regulation of resting V_m due to their large conductance at hyperpolarised potentials (Edwards *et al.*, 1988; Edwards & Hirst, 1988). In addition, during periods of high metabolic activity K_{ir} channels can act as K⁺ sensors. This is because inward rectification shifts with external K⁺ concentration (Quayle *et al.*, 1993), thus, encouraging membrane hyperpolarisation and vasodilation which results in increased blood flow to the tissues.

1.2.4 BK_{Ca} channels

1.2.4.1 Function of BK_{Ca} channels

BK_{Ca} channels belong to a family of Ca²⁺-activated K⁺ channels which includes the intermediate (IK) and small-conductance (SK) channels (Vergara *et al.*, 1998). BK_{Ca} channels are ubiquitously expressed in mammalian tissues. They are expressed most abundantly in the brain and smooth-muscle containing organs but are absent in ventricular cardiomyocytes (Wu & Marx, 2010). They are characterised by their large single channel conductance of ~ 250 pS, from which the name “BK_{Ca} or Big K_{Ca}” is derived. BK_{Ca} channels are also referred to as Maxi-K, K_{Ca}1.1 or Slo1 channels. They are activated by depolarisation and a rise in [Ca²⁺]_i. Thus, BK_{Ca} channels act as negative feedback regulators to counteract the vasoconstriction induced by calcium entry (Brayden & Nelson, 1992).

1.2.4.2 Structure of BK_{Ca} channels

α -subunit

Functional BK_{Ca} channels exist as tetramers formed from the assembly of four pore-forming α -subunits encoded by the *Slo1* or *KCNMA1* gene in humans (Shen *et al.*, 1994; Kyle & Braun, 2014). This gene was first identified in a *Drosophila slowpoke* mutant in which Ca²⁺-activated K⁺ current was abolished from their flight muscles (Elkins *et al.*, 1986; Atkinson *et al.*, 1991). The human homologue of the *Slo1* gene was subsequently cloned and isolated from human brain cDNA library and foetal muscle cDNA, respectively (Dworetzky *et al.*, 1994; Pallanck & Ganetzky, 1994).

Each α -subunit comprises of seven transmembrane segments (S0 to S6) and extracellular N- and intracellular C-termini (Figure 1.4). The extracellular N-terminus results from the existence of the extra S0 segment, which is absent from K_V channels. Nevertheless, the S1 to S6 segments are homologous to those of K_V channels.

The α -subunit can be divided into three structural domains, the voltage sensor domain (VSD), the pore gate domain (PGD) and the cytosolic terminal domain (CTD). The VSD is formed by the S1 to S4 segments whereas the S5, S6 segments and the p-loop between them form the PGD. The diameter of the ion conduction pore is similar to those of other K⁺ channels with a narrow selectivity filter of 0.9 Å (in the open conformation) which contains the signatory V-G-Y-G motif (Tao *et al.*, 2017). The CTD consists of two homologous “regulator of conductance for K⁺” (RCK) domains; RCK1 and RCK2, which are connected by an ~100 amino acid residue linker (Yang *et al.*, 2015). The CTD is connected to the PGD via a 20 amino acid residue linker between the S6 segment and RCK1 domain, S6-RCK1 linker. The RCK1 domain contains a low-affinity Ca²⁺ binding site whereas the RCK2 domain contains a string of aspartic acid residues known as the “Ca²⁺ bowl” which provides a high-affinity Ca²⁺ binding site (Schreiber & Salkoff, 1997; Bian *et al.*, 2001; Bao *et al.*, 2004).

A gating ring is formed by the assembly of the four sets of RCK1/2 dimers from the four α -subunits (Jiang *et al.*, 2002). The crystal structure of the Ca²⁺ bound and unbound structures of the human Slo1 gating ring has been resolved to 3 Å (Yuan *et al.*, 2010). In addition, recent studies have now presented a cryo-electron microscopy structure of full length *Aplysia californica* Slo1 channel resolved to 3.5 Å (Tao *et al.*, 2017).

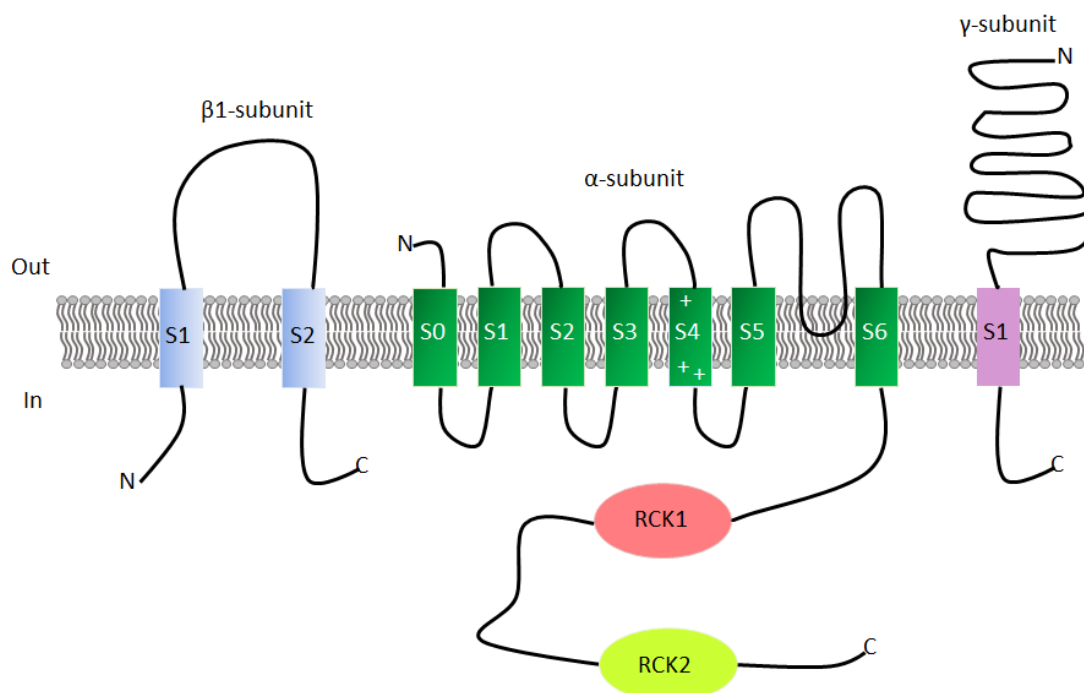


Figure 1.4: Structure of BK_{Ca} channel subunits. Functional BK_{Ca} channels are formed by the tetrameric assembly of the α -subunits. The α -subunits can be co-expressed with auxiliary β - and γ subunits which modulate the channel's properties.

β -subunit

β -subunits are auxiliary subunits which can co-assemble with the α -subunits of native BK_{Ca} channels (McManus *et al.*, 1995). There are at least four types of β -subunits in mammals; β 1 to β 4 subunits (Wallner *et al.*, 1999; Behrens *et al.*, 2000; Brenner *et al.*, 2000; Uebele *et al.*, 2000). These subunits have been shown to influence BK_{Ca} channel properties including Ca²⁺ and voltage sensitivity, activation and inactivation kinetics and pharmacology (Brenner *et al.*, 2000; Behrens *et al.*, 2000; Meera *et al.*, 2000; Orio *et al.*, 2002; Zeng *et al.*, 2003; Ha *et al.*, 2004; Wang & Brenner, 2006; Wang *et al.*, 2006a). The β 1-subunit is most abundantly expressed in SMCs (Knaus *et al.*, 1994b; Jiang *et al.*, 1999; Brenner *et al.*, 2000) whereas β 2- and β 3-subunits are abundantly expressed in the brain (Behrens *et al.*, 2000; Brenner *et al.*, 2000; Uebele *et al.*, 2000). β 4-subunits which are distantly related to the other β -subunits are predominantly expressed in neurons (Behrens *et al.*, 2000; Brenner *et al.*, 2000). Each α -subunit can exist in a 1:1 stoichiometry with β -subunits, nevertheless, individual BK_{Ca} channels can exist with < 4 β -subunits (Knaus *et al.*, 1994a; Wang *et al.*, 2002).

β 1-subunits comprise of two transmembrane domains with a large extracellular loop and intracellular N- and C-termini (Figure 1.4). The N-terminal tail of the α -subunit has been shown to be essential for the interaction of β 1 subunits (Morrow *et al.*, 2006). β 1 subunits increase the Ca^{2+} sensitivity and slow the activation and deactivation kinetics of BK_{Ca} channels (Bao & Cox, 2005; Orio & Latorre, 2005). It has also been reported that key amino acid residues; Tyr74, Ser104, Tyr105, Ile106, contained in the extracellular loop of the β 1-subunit influence channel opening, by interacting with the activation gate and voltage sensor located on the α -subunit (Gruslova *et al.*, 2012).

γ -subunit

The γ -subunit has a single transmembrane domain with a large extracellular N-terminus which consists of leucine-rich repeat motifs and an intracellular C-terminus, as shown in Figure 1.4 (Yan & Aldrich, 2010; Yan & Aldrich, 2012).

There are at least 4 known members of the γ -subunit family; LRRC26, 38, 52 and 55. Although, knowledge about the stoichiometry of interaction between γ - and α -subunits is limited. The γ -subunits have been shown to induce a negative shift of ~ 20 to 140 mV in the voltage-dependence of channel activation (Yan & Aldrich, 2010; Yan & Aldrich, 2012). This results in an increase in BK_{Ca} channel activation at physiological resting conditions, characterised by low $[\text{Ca}^{2+}]_i$ and hyperpolarised potentials. Interestingly, evidence from electrophysiology experiments performed on recombinant channels showed that a single BK_{Ca} channel can simultaneously co-assemble with β - and γ -subunits, with both auxiliary subunits independently regulating channel function (Gonzalez-Perez *et al.*, 2015).

1.2.4.3 BK_{Ca} channel gating

Ion channel gating involves two major steps; 1) stimulus sensing by a sensor domain and 2) coupling of the stimuli to the activation gate (Cui, 2009). The opening and closing of the ion conduction gate of BK_{Ca} channels is influenced by voltage, Ca^{2+} and Mg^{2+} . Voltage sensors and Ca^{2+} and Mg^{2+} binding sites have been identified in BK_{Ca} channels. The coupling mechanism of these 3 stimuli to BK_{Ca} channel activation will be discussed below.

1.2.4.3.1 Voltage-dependent gating

Voltage-sensing

In the absence of Ca^{2+} , BK_{Ca} channels can be maximally activated by membrane depolarization (Cui *et al.*, 1997; Stefani *et al.*, 1997; Horrigan & Aldrich, 1999; Horrigan *et al.*, 1999; Talukder & Aldrich, 2000). The VSD of BK_{Ca} channels traverses the membrane electric field, thus, membrane depolarisation displaces the charged residues in the VSD. The movement of these residues in the transmembrane electric field induces a gating current (Yusaf *et al.*, 1996).

The VSD of BK_{Ca} channels resembles that of K_v channels as it comprises the S1 to S4 segments. However, only 1 of the 3 arginine (Arg) residues in the S4 segment of BK_{Ca} channels, Arg213, contributes to the gating charge whereas all 4 Arg residues in the S4 segment of Shaker channels (a type of K_v channel) contribute to their gating charge (Aggarwal & MacKinnon, 1996; Gandhi & Isacoff, 2002; Ma *et al.*, 2006). Other residues that contribute to voltage-sensing in BK_{Ca} channels are Asp153 & Arg167 in the S2 segment and Asp186 in S3 segment (Ma *et al.*, 2006).

Coupling of the VSD to the pore gate domain

Voltage-dependent activation of BK_{Ca} channels occurs via electromechanical coupling between the VSD and the pore gate domain. Movement of the gating charge across the membrane electric field induces a conformational change, outward movement of S4 segment, in the VSD. This pulls the S4 to S5 linker which interacts with the S6 segment thereby resulting in the opening of the pore gate (Lu *et al.*, 2002; Tristani-Firouzi *et al.*, 2002; Long *et al.*, 2005; Chowdhury & Chanda, 2012; Tao *et al.*, 2017). Mutagenesis studies confirmed that interactions between the S4 to S5 linker and the C-terminal of the S6 segment can directly couple the VSD to the pore gate domain (Lu *et al.*, 2002). Nevertheless, activation of the VSD is not required for the opening of the pore gate domain. This is evident from the fact that at hyperpolarised potentials and in the absence of Ca^{2+} , BK_{Ca} channels open, albeit infrequently and briefly (Horrigan & Aldrich, 2002a). Thus, the VSD activation merely facilitates the opening of BK_{Ca} channel pore gate.

The VSD can also be indirectly coupled to the pore gate domain via Ca^{2+} binding. This is evident from the fact that the coupling strength between the VSD and pore gate domain was reduced by truncation of the CTD (Zhang *et al.*, 2017). Furthermore, Ca^{2+} binding shifts the conductance-voltage curve to more negative potentials, as shown in Figure 1.5 (Horrigan & Aldrich, 2002b).

1.2.4.3.2 Ligand-dependent gating

1.2.4.3.2.1 Ca^{2+} -dependent gating

Ca^{2+} sensing

Ca^{2+} sparks which result from the opening of RyRs on the SR (see section 1.2.1.1.3) can increase local, $\sim 1\%$ of cell volume, $[\text{Ca}^{2+}]_i$ up to $4\ \mu\text{M} - 30\ \mu\text{M}$ (Perez *et al.*, 2001). This can result in the activation of several or few BK_{Ca} channels, depending on their proximity to the spark site (Fay, 1995). The activation of BK_{Ca} channels by Ca^{2+} sparks produce spontaneous transient outward currents (STOCs) that hyperpolarise SMC membrane, thereby inhibiting L-type Ca^{2+} channel activity and Ca^{2+} entry. Evidence for the coupling of Ca^{2+} sparks to STOCs includes the fact that both events occur simultaneously and originate on or near the cell surface (Nelson *et al.*, 1995). In addition, STOCs are inhibited by BK_{Ca} channel blockers (TEA^+ and iberiotoxin) and pharmacological agents that disrupt Ca^{2+} release from internal stores, such as ryanodine and thapsigargin (Nelson *et al.*, 1995). Ca^{2+} sparks can also contribute to global increase in $[\text{Ca}^{2+}]_i$ thereby promoting contraction, nevertheless, the negative feedback dominates (Jaggar *et al.*, 2000). Therefore, Ca^{2+} sparks are mostly involved in SMC relaxation.

Coupling between the Ca^{2+} binding domains and the pore gate domain

The Ca^{2+} -mediated activation of BK_{Ca} channels occurs via chemomechanical coupling of the CTD to the pore gate domain (Yang *et al.*, 2015). This involves the binding of Ca^{2+} to the RCK1 and RCK2 domains which tilts the RCK1 N-lobe, thereby exerting a force on the RCK1-S6 linker which directly opens the channel pore (Hite *et al.*, 2017). Hill analyses indicate that single BK_{Ca} channels can bind from 2 to 6 Ca^{2+} ions (Cui *et al.*, 1997; Bian *et al.*, 2001; Niu & Magleby, 2002).

Furthermore, Ca^{2+} can indirectly activate BK_{Ca} channels by facilitating the coupling of the VSD to channel pore opening. This results from the existence of a non-covalent protein-protein interface between the RCK1 N-lobes and the S4 to S5 linker, which connects the VSD to the channel's pore. This allows Ca^{2+} binding to produce an outward displacement of the voltage sensors and S5 helices leading to the channel pore opening (Hite *et al.*, 2017). This explains why BK_{Ca} channels can be activated at less positive potentials in high $[\text{Ca}^{2+}]_i$, as illustrated in Figure 1.5.

Conversely, activation of the voltage sensors can increase the Ca^{2+} affinity of BK_{Ca} channels. This is because membrane depolarisation favours the open conformation of the RCK1 N-lobe which enhances Ca^{2+} binding, thereby increasing the Ca^{2+} affinity of the binding sites (Hite *et al.*, 2017). Thus, at more depolarised V_m lower $[\text{Ca}^{2+}]_i$ is required for channel activation. Nevertheless, even though the Ca^{2+} and voltage sensors can work synergistically to activate BK_{Ca} channels, both allosteric modulators can also activate the channel independently (Horrigan & Aldrich, 2002b; Budelli *et al.*, 2013).

Kinetic models have been used to show that depolarization and intracellular Ca^{2+} activate BK_{Ca} channels by primarily destabilizing the closed state of the channel (Geng & Magleby, 2014). A 10-state two-tiered model (comprising of 5 closed states on the upper tier and 5 open state on the lower tier) and a 50-state two-tiered model (comprising of 25 closed states on the upper tier and 25 open states on the lower tier) have previously been described. The information about the gating kinetics was further improved by the addition of flicker states to the 10-state and 50-state models (Geng & Magleby, 2014).

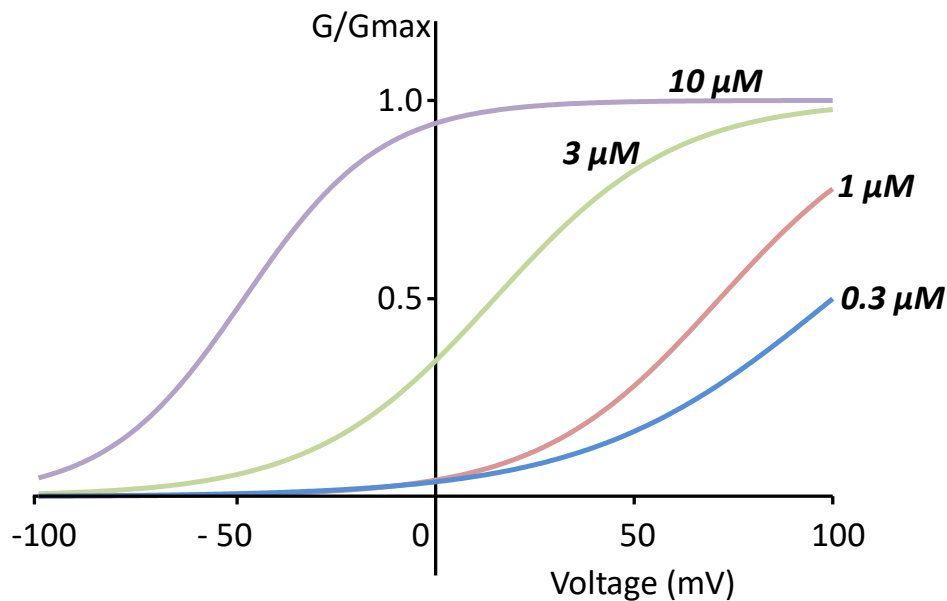


Figure 1.5: BK_{Ca} channel activation is influenced by the interaction between the allosteric modulators, Ca²⁺ and voltage. The different [Ca²⁺]_i are denoted in bold italics. As [Ca²⁺]_i increases, the voltage sensitivity of BK_{Ca} channels shift to more negative potentials. Conversely, at more positive potentials, low [Ca²⁺]_i is sufficient to activate the channels. Graphs have been adapted from (Lippiat *et al.*, 2003).

1.2.4.3.2.2 Mg²⁺-dependent gating

Mg²⁺ has been shown to activate BK_{Ca} channels in both zero and saturating [Ca²⁺]_i. This showed that both divalent ions activate BK_{Ca} channels via independent pathways (Shi & Cui, 2001). In addition, at negative voltages, when voltage sensors are in a resting state, Mg²⁺ did not produce a measurable effect on channel activation (Yang *et al.*, 2007; Horrigan & Ma, 2008). For instance, 10 mM Mg²⁺ had no effect on channel Popen at extreme negative potentials (≤ 100 mV) but the application of 2 μM [Ca²⁺]_i under the same conditions increased channel Popen by 15-fold (Horrigan & Ma, 2008). This indicates that the mechanism of action by Mg²⁺ is distinct from that of Ca²⁺, as the effects of Mg²⁺ appear to be voltage-dependent whereas Ca²⁺ can mediate voltage-independent effects. Chimeric studies confirmed that the Mg²⁺ binding site was at a different location to the high affinity Ca²⁺ bowl (Shi & Cui, 2001).

Furthermore, evidence from mutagenesis studies showed that the Mg²⁺ binding site exists at the interface between the VSD and the N-lobe of the RCK1 domain (Yang *et al.*, 2007; Yang *et al.*, 2008; Yang *et al.*, 2013). It is formed by Glu374 and Glu399 in RCK1

domain and key amino acid residues from the VSD; Asp99 in the S0 to S1 linker and Asn172 in the S2 to S3 linker (Shi *et al.*, 2002; Yang *et al.*, 2007; Yang *et al.*, 2008).

1.2.4.4 Modulation of BK_{Ca} channel activity by endogenous molecules

BK_{Ca} channels have been shown to be regulated by a variety of endogenous signalling molecules including protons (H⁺), haem, carbon monoxide (CO), lipids, reactive oxygen species (ROS) and kinases. The influence of haem and CO on BK_{Ca} channel activity is discussed in section 1.3.5.

1.2.4.4.1 H⁺

Intracellular H⁺ levels can increase during high cell metabolism and ischemia. Low pH has been shown to induce a negative shift in the conductance-voltage curve of recombinant human Slo1 channels in the absence of Ca²⁺ and Mg²⁺ (Avdonin *et al.*, 2003; Hou *et al.*, 2008b). This effect was reportedly absent in the presence of high concentrations of Ca²⁺ and Mg²⁺.

Nevertheless, the influence of H⁺ on BK_{Ca} channel activity has been controversial, as some studies have reported inhibition (Kume *et al.*, 1990; Peers & Green, 1991; Church *et al.*, 1998) whereas others have shown activation (Hayabuchi *et al.*, 1998; Avdonin *et al.*, 2003; Hou *et al.*, 2008b). The proposed mechanism of activation involves electrostatic interaction between protonated His365 and His394 residues, located in the RCK1 domain, and the negatively charged Asp367 in the RCK2 domain (Avdonin *et al.*, 2003; Hou *et al.*, 2008b). In addition, as all 3 amino acid residues are involved in the Ca²⁺ sensing of BK_{Ca} channels, H⁺ was proposed to promote the opening of the channel pore by acting as a Ca²⁺ mimetic (Xia *et al.*, 2002; Hou *et al.*, 2008b; Hou *et al.*, 2009).

1.2.4.4.2 Lipids

BK_{Ca} channel activity can be modulated by membrane lipids including phosphatidylinositol (4,5)-bisphosphate (PIP₂) and cholesterol. PIP₂ has been shown to enhance the Ca²⁺-dependent activation of BK_{Ca} channels via electrostatic interactions with Lys392 and Arg393 located in the N-lobe of the RCK1 domain (Vaithianathan *et al.*, 2008; Tang *et al.*, 2014).

On the other hand, cholesterol has been shown to inhibit BK_{Ca} channel activity (Bolotina *et al.*, 1989; Dopico *et al.*, 2012). Direct and indirect mechanisms of inhibition have been proposed (Bukiya *et al.*, 2011; Dopico *et al.*, 2012; Singh *et al.*, 2012). The indirect mechanism results from the insertion of cholesterol into the plasma membrane which induces a conformational change of the BK_{Ca} channel protein. Conversely, the direct mechanism involves hydrophobic interactions of cholesterol with BK_{Ca} channels via cholesterol recognition/interaction amino acid consensus (CRAC) motifs located in the CTD of the channels (Singh *et al.*, 2012).

1.2.4.4.3 ROS

Low concentrations of ROS are generated during normal cell physiology, as they are involved in normal cell signalling (Hensley *et al.*, 2000). Hydrogen peroxide (H₂O₂) is a ROS which acts as a physiological oxidant.

Intracellular application of H₂O₂ inhibited recombinant BK_{Ca} channel activity (DiChiara & Reinhart, 1997; Soto *et al.*, 2002; Tang *et al.*, 2004). The proposed mechanism of inhibition by H₂O₂ involves the disruption of the Ca²⁺-dependent activation of BK_{Ca} channels via oxidation of Cys911 in the RCK2 domain (Tang *et al.*, 2004). H₂O₂ has also been reported to stimulate BK_{Ca} channel activity (Barlow & White, 1998; Bychkov *et al.*, 1999). The H₂O₂-mediated stimulation of recombinant endothelial human Slo1 channels was shown to involve NO production, which occurs downstream of sGC/cGMP pathway (Dong *et al.*, 2008). Other studies have suggested that PTEN (phosphatase and tensin homolog deleted on chromosome 10), a tumour suppressor, might be involved in the stimulatory effect of H₂O₂ on BK_{Ca} channel activity (Liu *et al.*, 2009).

1.2.4.4.4 Kinases

BK_{Ca} channels can be modulated via phosphorylation mediated by protein kinases (including PKA, PKG and PKC) and c-Src tyrosine kinase. The phosphorylation sites of BK_{Ca} channels are mainly found in the carboxyl terminus (Toro *et al.*, 1998).

PKA and PKG have been shown to enhance BK_{Ca} channel activity in vascular SMCs (Kume *et al.*, 1989; Robertson *et al.*, 1993; Kume *et al.*, 1994; Meera *et al.*, 1995). Mutagenesis studies identified the possible phosphorylation sites of PKA (Ser869) and PKG (Ser691, Ser855, Ser873, Ser1072 and Ser1112) on the α -subunit of BK_{Ca} channels (Nara *et al.*, 1998; Fukao *et al.*, 1999; Nara *et al.*, 2000; Kyle *et al.*, 2013). PKA and PKG mediated

channel phosphorylation promotes channel activation by altering channel kinetics and shifting the voltage-dependence to more negative potentials (Schubert & Nelson, 2001). However, these effects have been shown to be reversed by protein phosphatase-mediated dephosphorylation (Kume *et al.*, 1989; Peng *et al.*, 1996). Interestingly, the activity of protein phosphatase 2A (PP2A) was reported to be essential for PKG-mediated channel activation, as the catalytic subunit of PP2A appeared to mimic the stimulatory effect of PKG (Zhou *et al.*, 1996). In contrast, PKC has been reported to mediate inhibitory effects on vascular SMC BK_{Ca} channel activity (Minami *et al.*, 1993; Schubert *et al.*, 1999; Taguchi *et al.*, 2000). The proposed phosphorylation sites of PKC include Ser695 and Ser1151. Interestingly, phosphorylation at Ser1151 abolished PKA-mediated channel activation whereas phosphorylation at Ser 695 abolished both PKA & PKG-mediated channel activation.

BK_{Ca} channel activity can also be modulated by tyrosine (Tyr) phosphorylation. The co-expression of c-Src with BK_{Ca} channels in human embryonic kidney 293 (HEK293) cells produced phosphorylation at Tyr766 located in the C-terminal domain of the channel (Ling *et al.*, 2000). This enhanced BK_{Ca} channel activity by increasing the Ca²⁺-sensitivity of the channel. This is corroborated by the fact that the stimulatory effect of c-Src was abolished in the absence of Ca²⁺ but observed when free cytosolic Ca²⁺ was > 4 μM.

1.3 Haem

1.3.1 Structure and function of haem

Haem is an essential physiological molecule found in aerobic cells (Ponka, 1999). It is an iron-protoporphyrin complex, with the central iron atom either existing in a reduced ferrous (Fe²⁺) or oxidised ferric (Fe³⁺) state (Figure 1.6). Ferric haem is often referred to as hemin. However, for simplicity, throughout this thesis the term haem will be used for both states, unless otherwise stated.

Three major haem pools exist in mammalian tissues; haem bound to proteins, unbound or 'free' haem (released from degraded hemoproteins) and newly synthesized haem (released from the mitochondria) (Foresti *et al.*, 2004a). The existence of haem as a prosthetic group in hemoproteins (such as haemoglobin, cytochrome, and nitric oxide

synthase) enables haem to participate in a variety of biological processes including oxygen transport, respiration and drug metabolism.

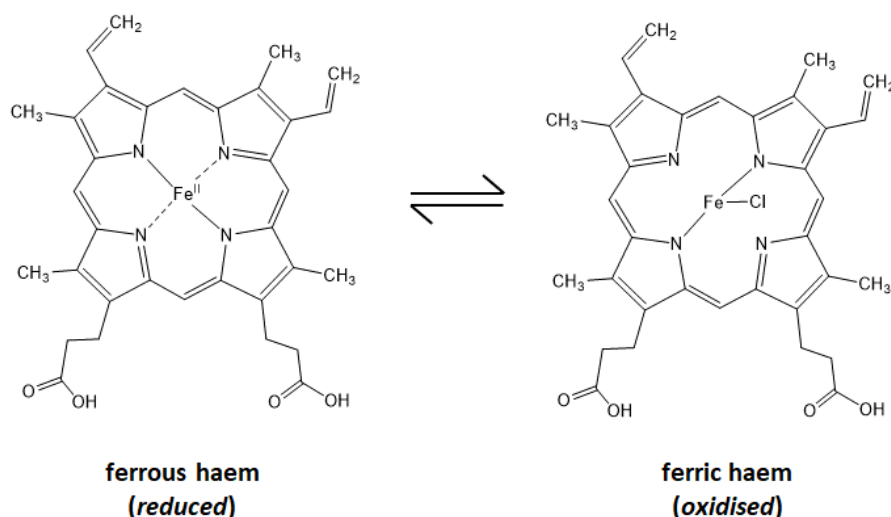


Figure 1.6: Structure of haem. Haem is a metalloporphyrin, comprised of a protoporphyrin ring and an iron centre which can be reversibly oxidised.

1.3.2 Role of free haem in pathophysiology

Several haemolytic diseases, such as sickle cell anaemia, malaria and haemorrhagic stroke, are associated with severe haemolysis which can lead to a build-up of extracellular free haem. For instance, during sickle cell anaemia, the fragility of sickle cells encourages haemolysis which raises intravascular haemoglobin and free haem concentrations (Wagener *et al.*, 2001). The hemin content in the hemolysate of sickle cell anaemia patients (0.4 to 0.75 $\mu\text{mol/L}$) was shown to be 3 to 5-fold higher than in normal individuals, 0.1 to 0.15 $\mu\text{mol/L}$ (Liu *et al.*, 1988). Furthermore, during malaria, *Plasmodium*-infected red blood cells burst to release haemoglobin and haem. The extracellular haem levels of children with severe malaria on hospital admission was measured as 4 to 22 μM (Elphinstone *et al.*, 2016). In addition, the vascular haemorrhage that occurs during haemorrhagic stroke can lead to the surprising extracellular accumulation of up to 10 mM haem from haematomas (Robinson *et al.*, 2009).

The lipophilic nature of haem means that extracellular haem overload can increase intracellular free haem pool (Chiabrando *et al.*, 2014). Free haem is cytotoxic as it

catalyses oxidative stress which promotes protein aggregation, lipid peroxidation and DNA damage, leading to tissue and organ damage (Kumar & Bandyopadhyay, 2005). In addition, free haem can act as a pro-inflammatory agent by activating neutrophil responses. This is demonstrated by the expression of the chemokine, interleukin-8, by human neutrophils exposed to 3 μM hemin (Graca-Souza *et al.*, 2002). Free haem can also encourage further haemolysis via a colloid-osmotic mechanism (Chou & Fitch, 1981). This results from the intercalation of haem in the plasma membrane of red blood cells which alters the cation gradient of the cell, thereby encouraging a massive loss of K^+ from the cells. This promotes the entry of water due to the presence of haemoglobin and other molecules in the cells. The cell subsequently swells and bursts.

Due to the cytotoxic effects of free haem, different mechanisms exist to regulate intracellular and extracellular haem levels. I will only focus on the regulation of intracellular haem concentration, $[\text{haem}]_i$; which occurs via its synthesis, degradation and transport, as detailed below.

1.3.3 Haem homeostasis

1.3.3.1 Haem Synthesis

Haem biosynthesis is an eight-step enzymatic process which occurs in the mitochondria and cytoplasm (Hou *et al.*, 2006). The first step which involves the condensation of glycine and succinyl coenzyme A to 5-aminolevulinate (ALA) occurs in the mitochondria (Figure 1.7). This process is catalysed by 5-aminolevulinate synthase (ALAS). There are at least 2 isozymes for ALAS; ALAS1 and ALAS2, which exist in non-erythroid and erythroid cells, respectively (Furuyama *et al.*, 2007; Khan & Quigley, 2011).

ALA is subsequently transported into the cytoplasm where it is transformed, by the catalytic activity of 4 different enzymes, to coproporphyrinogen III (CPgenIII). CPgenIII is transported back into the mitochondria where a further 2-step enzymatic process converts it to protoporphyrin-IX (PP-IX). In the final step of haem synthesis, ferrochelatase catalyses the insertion of Fe^{2+} , rather than Fe^{3+} , into the PP-IX ring (Camadro & Labbe, 1982). However, under conditions of low Fe^{2+} , Zn^{2+} could be inserted.

The newly synthesised haem is then transported into the cytoplasm where it is either degraded, as discussed in section 1.3.3.2, inserted into apo-hemoproteins or exists free. Interestingly, haem also provides a negative feedback for its synthesis by repressing the activity of ALAS1, but not ALAS2. The proposed mechanisms for ALAS1 repression includes; reduction of transcription and translation of ALAS gene, mRNA destabilization and inhibition of transport of the precursor protein into the mitochondria (Yamauchi *et al.*, 1980; Yamamoto *et al.*, 1982; Yamamoto *et al.*, 1983; Hamilton *et al.*, 1991).

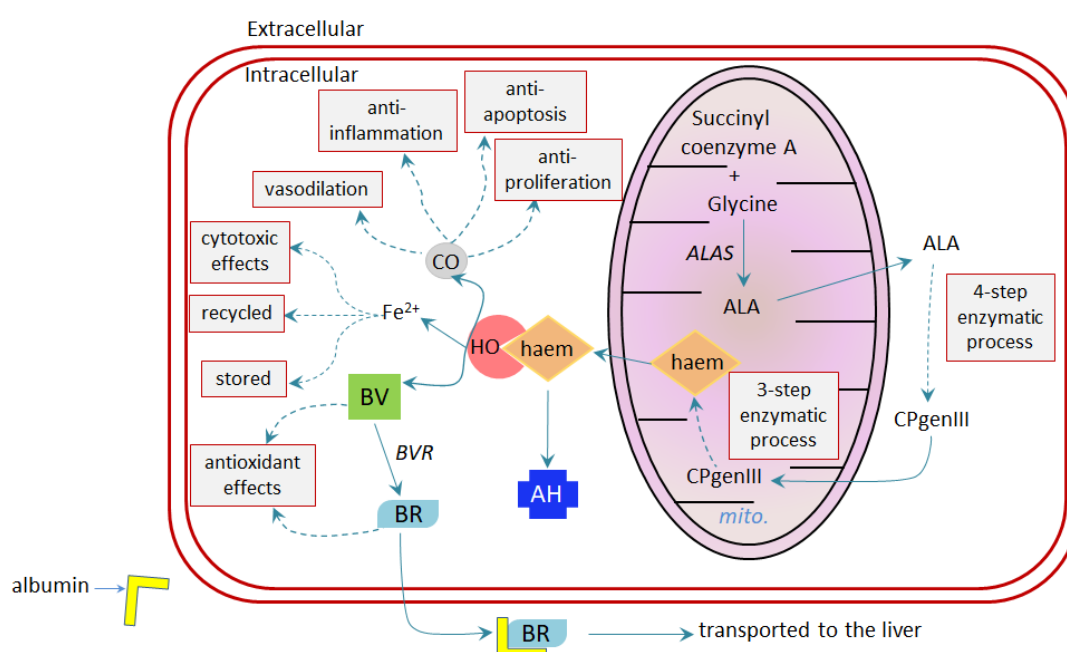


Figure 1.7: Haem synthesis and degradation. Haem synthesis occurs via an eight-step enzymatic process in the mitochondria and cytoplasm, with 5-aminolevulinate synthase (ALAS) serving as the rate-limiting enzyme. Free haem can be inserted into an apo-hemoprotein (AH) or degraded by cytosolic enzymes, called haem oxygenase (HO), to carbon monoxide (CO), Fe²⁺ and biliverdin (BV). Biliverdin is further degraded to bilirubin (BR) by biliverdin reductase (BVR), another cytosolic enzyme. The haem degradation products participate in a variety of cell signalling pathways.

1.3.3.2 Haem Degradation

Haem degradation primarily occurs via an enzymatic process (Maines, 1997). The mechanism of haem degradation, as well as the functions of the primary haem degradation products will be discussed in turn.

1.3.3.2.1 Enzymatic degradation of haem

Intracellular haem is primarily degraded by haem oxygenase (HO) enzymes (Tenhunen *et al.*, 1969; Tenhunen, 1972). HO cleaves haem at the α -methene carbon in an O_2 -dependent manner, which requires the activity of nicotinamide adenine dinucleotide phosphate (NADPH)-cytochrome P450 reductase (Khan & Quigley, 2011), see Figure 1.8. This results in the formation of CO, biliverdin and Fe^{2+} (Maines, 1988). Biliverdin is rapidly converted to bilirubin by the cytosolic enzyme, biliverdin reductase (BVR) (Kutty & Maines, 1981). Unbound bilirubin is unstable and spontaneously oxidised to biliverdin by H_2O_2 (Foresti *et al.*, 2004a; Iwamori *et al.*, 2015). Bilirubin oxidation can also result in the formation of pyrrole fragments and propentdyopent adducts (Bonnett & Ioannou, 1987; Kranc *et al.*, 2000). However, bilirubin in the blood is bound to albumin (Ryter *et al.*, 2006).

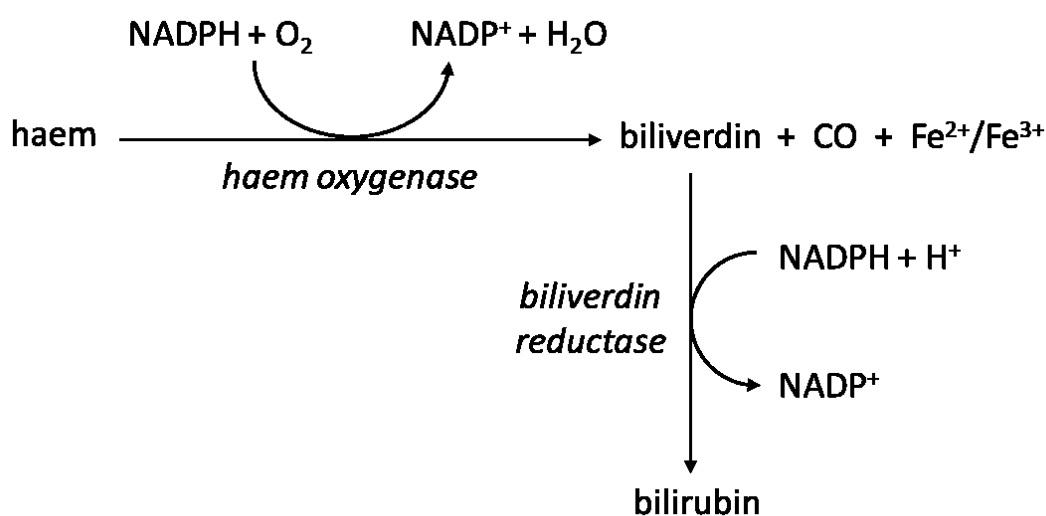


Figure 1.8: Haem metabolism requires O_2 and a reducing agent. Haem degradation is primarily catalysed by haem oxygenase enzymes. This process requires the activity of the reducing agent, NADPH.

There are at least 3 isoforms of HO enzymes; HO-1, HO-2 and HO-3 (Shibahara *et al.*, 1985; Maines *et al.*, 1986; McCoubrey *et al.*, 1997b). HO-1 and HO-2 are the main catabolic isozymes. They are derived from different genes and have different molecular and biochemical properties but similar haem degradative function (Cruse & Maines,

1988). In contrast, HO-3 is encoded by a pseudogene derived from HO-2 (McCoubrey *et al.*, 1997b; Scapagnini *et al.*, 2002; Hayashi *et al.*, 2004). It is expressed in many tissues including brain, liver and kidney but its enzymatic activity is negligible (McCoubrey *et al.*, 1997b).

HO-1 is a stress-inducible protein with a molecular weight of 32 kDa, which is highly expressed in the liver and spleen. Its expression is induced by a variety of stimuli including heavy metals, oxidative stress and hypoxia (Maines, 1988). Haem also induces HO-1 expression thereby promoting its own degradation (Yoshida *et al.*, 1988). HO-1 is mainly located on the membrane of smooth ER (Shibahara *et al.*, 1985; Ishikawa *et al.*, 1991). However, evidence from immunocytochemical and electron microscopy studies showed that HO-1 can also be compartmentalized to the plasma membrane and nucleus (Nguyen & Dennery, 2002; Kim, 2004; Ma *et al.*, 2004; Li Volti *et al.*, 2004).

In contrast, HO-2 is a non-inducible enzyme which is highly expressed in the brain and testes (Trakshel *et al.*, 1986). HO-2 is ~ 20 amino acids longer than HO-1 and has a molecular weight of 36 kDa. Nevertheless, HO-1 and HO-2 both have a hydrophobic carboxyl terminus which enables them to be membrane bound (Shibahara *et al.*, 1985; Yoshida *et al.*, 1988). Unlike HO-1, HO-2 is classed as a hemoprotein because of its functional domains referred to as haem regulatory motifs (HRMs) which form additional haem binding sites, separate from the haem catalytic domain of the enzyme (McCoubrey *et al.*, 1997a). There are two main HRMs at the N-terminal of HO-2, they comprise of conserved Cys-Pro motifs (Yi & Ragsdale, 2007). The HRMs have been proposed to act as thiol-disulfide redox switches which respond to the redox state of the cell. The reduced thiolate state binds haem 14-fold more tightly than the oxidised disulfide state (Yi *et al.*, 2010).

1.3.3.2.2 Haem degradation products

Carbon monoxide (CO)

Haem degradation by HO accounts for over 80 % of the CO produced in humans (Mann & Motterlini, 2007). The remaining fraction of CO is generated by HO-independent

processes including peroxidation of lipid bilayers, photo-oxidation and auto-oxidation of organic molecules (Abraham & Kappas, 2008).

CO can mediate both detrimental and beneficial effects. For instance, haemoglobin binds CO with high affinity (200 times more than oxygen, O₂) (Wagener *et al.*, 2003). This results in the formation of carboxyhaemoglobin which promotes O₂ starvation of tissues, leading to death (Johnson *et al.*, 1999). Nevertheless, CO acts as an important endogenous signalling molecule, mediating a variety of beneficial effects including vasodilatory, anti-inflammatory and anti-apoptotic effects. The vasodilatory effects of CO occur via cGMP-dependent and -independent pathways (Morita *et al.*, 1995; Maines, 1997). The cGMP-independent pathway involves BK_{Ca} channel activation. Furthermore, the CO-mediated activation of p38 mitogen-activated protein kinase signalling pathway inhibits proinflammatory genes, promotes anti-inflammatory cytokine production and inhibits apoptosis (Brouard *et al.*, 2000; Otterbein *et al.*, 2000; Song *et al.*, 2003). CO also inhibits vascular SMC proliferation and platelet aggregation which limit the progression of atherosclerosis (Brune & Ullrich, 1987; Togane *et al.*, 2000).

Biliverdin and Bilirubin

Biliverdin and bilirubin are potent antioxidants as they can scavenge free radicals and ROS (Stocker *et al.*, 1987b; Stocker *et al.*, 1987a; Neuzil & Stocker, 1993). Biliverdin has also been shown to inhibit HO activity supposedly by interacting with the haem binding site of the enzyme, thereby preventing haem binding and degradation (Kutty & Maines, 1984). Furthermore, high concentrations of bilirubin can promote irreversible damage to cells and tissues, and low levels of serum bilirubin can be an important risk factor for coronary artery disease (Hopkins *et al.*, 1996; Foresti *et al.*, 2004a). Exogenous bilirubin application has also been shown to mediate cytoprotective effects against oxidative stress induced by ROS (Foresti *et al.*, 1999; Clark *et al.*, 2000; Baranano *et al.*, 2002; Sedlak & Snyder, 2004). In addition, bilirubin inhibits the activity of NADPH oxidase and PKC which are both involved in angiotensin-II induced vascular injury (Sano *et al.*, 1985; Kwak *et al.*, 1991; Rajagopalan *et al.*, 1996).

Iron (Fe²⁺)

The Fe²⁺ produced from haem degradation can either be recycled, stored or mediate cytotoxic effects, such as oxidative stress. Fe²⁺ is recycled and used for the synthesis of new haemoglobin molecules (Sassa, 2006). It can also be sequestered by ferritin which binds intracellular Fe²⁺ with low affinity (Kumar & Bandyopadhyay, 2005; Abraham & Kappas, 2008). Interestingly, the iron released from HO activity can also enhance ferritin synthesis (Eisenstein *et al.*, 1991). However, Fe²⁺ reacts with H₂O₂ in a process called Fenton reaction which leads to the formation of cytotoxic free radicals (Wagener *et al.*, 2003). Fe²⁺ can also integrate in the plasma membrane where it facilitates oxidation of cell membrane constituents, leading to plasma membrane injury and possibly cell death and tissue damage (Valko *et al.*, 2005).

1.3.3.3 Haem Transport

Over the years, different modes of cellular haem transport have been proposed. These include; receptor-mediated endocytosis, membrane-bound haem importers and exporters, haem carriers and passive diffusion.

1.3.3.3.1 Receptor-mediated endocytosis

In 1979, the discovery of a haem binding protein (HBP) on the intestinal microvillus of pigs and humans led to the proposal of haem receptor-mediated endocytosis (Grasbeck *et al.*, 1979). The HBP was later characterised as a protein receptor on the membrane of the intestinal microvillus (Tenhunen *et al.*, 1980; Grasbeck *et al.*, 1982). Further studies showed that the HBP was also expressed in erythroleukemia cells which internalise haem intact (Galbraith *et al.*, 1985; Majuri, 1989). Haem endocytosis appeared to be an active process since ATP was required (Vaghefi *et al.*, 2000; Worthington *et al.*, 2001).

1.3.3.3.2 Haem exporters

There are two known haem exporters; FLVCR1 (Feline Leukaemia Virus, subgroup C, Receptor 1) and ABCG2 (ATP-binding cassette, sub-family G, member 2), see Figure 1.9.

FLVCR1

FLVCR1 is a member of the cell surface receptor for feline leukemia virus, subgroup C (Tailor *et al.*, 1999; Quigley *et al.*, 2000; Chiabrando *et al.*, 2012). *In vivo* studies performed on mice indicated the existence of two FLVCR1 isoforms; FLVCR1a and FLVCR1b (Chiabrando *et al.*, 2012).

There is limited information about the subcellular localization of endogenous FLVCR1a. This is due to lack of specific antibodies that can target FLVCR1a. So far, FLVCR1a has been reported to be localised on the membrane of hepatocytes where it supposedly exports haem into the bloodstream (Vinchi *et al.*, 2014). Earlier evidence from quantitative fluorescent microscopy, performed with zinc mesoporphyrin (ZnMP), a fluorescent haem analog, and ⁵⁵Fe-heme confirmed that FLVCR1a can export cytoplasmic haem (Quigley *et al.*, 2004). The involvement of FLVCR1a in haem export was further demonstrated by the slight decrease in haem content in heterologous cells overexpressing FLVCR1a (Quigley *et al.*, 2004). Conversely, suppression of FLVCR1a in mice hepatocytes resulted in an accumulation of haem and iron in the liver (Vinchi *et al.*, 2014). On the other hand, FLVCR1b was found to be expressed in the mitochondrial membrane, where it plays the important role of exporting newly synthesised haem into the cytosol for incorporation into apo-hemoproteins (Chiabrando *et al.*, 2012).

ABCG2

ABCG2 is also known as BRCP (breast cancer resistance protein). It is a member of the ABC transport family which was found to be responsible for the drug resistance in breast cancer cells (Doyle *et al.*, 1998). ABCG2 was serendipitously discovered as a haem exporter due to the accumulation of pheophorbide (a PP-IX analog and chlorophyll degradation product) in ABCG2 null mice that had been fed a modified diet containing chlorophyll (Jonker *et al.*, 2002).

ABCG2 is localised on the apical membrane of duodenal enterocytes where it is suggested to be involved in exporting excess haem and PP-IX from the enterocyte to the lumen (Latunde-Dada *et al.*, 2006). ABCG2 has also been found in other tissues including renal proximal tubules and placenta (Doyle & Ross, 2003). However, ABCG2 is a non-specific haem exporter, as it can transport other substrates such as food metabolites and antibiotics (Chiabrando *et al.*, 2014). Thus, the role of ABCG2 in haem export under physiological and pathophysiological conditions is unclear.

1.3.3.3.3 Haem importers

The haem importers that have been characterised to date include; HRG (haem responsive genes), FLVCR2 (Feline Leukaemia Virus, subgroup C, Receptor 2) and HCP1 (haem carrier protein 1), see Figure 1.9.

HRG

The haem responsive genes that have been implicated in haem transport are *hrg-1* and *hrg-4*. The knockdown of *Caenorhabditis elegans hrg-1* gene (Cehrg1) surprisingly increased ZnMP uptake rather than abolish it (Rajagopal *et al.*, 2008). The human ortholog (hHRG1) is highly expressed in the brain, kidney, heart and skeletal muscle (Rajagopal *et al.*, 2008). Both proteins were also found localized in endosomes and lysosomes of HEK293 cells (Rajagopal *et al.*, 2008). In addition, *in vivo* studies performed with mice confirmed the expression of HRG1 in macrophages (White *et al.*, 2013). Haem transport from the phagolysosomal compartment was abolished upon depletion of *hrg1* from mouse macrophages. In addition, yeast and zebrafish studies revealed that missense polymorphisms in hHRG1 can also remove haem transport (White *et al.*, 2013). In contrast to results from Cehrg1 studies, the knockdown of Cehrg4 removed ZnMP uptake. This clearly indicates that HRG-4 is a haem importer. Further evidence from localization studies indicate that HRG-4 is a plasma membrane-associated protein unlike HRG-1 (Rajagopal *et al.*, 2008). However, mammalian orthologs of *hrg-4* are yet to be characterised.

FLVCR2

FLVCR2 shares ~ 60 % homology with FLVCR1. FLVCR1 and FLVCR2 belong to the solute carrier family 49 (SLC49) of haem transporters which are members of the major facilitator superfamily (MFS) (Pao *et al.*, 1998; Khan & Quigley, 2013). In humans, FLVCR2 mRNA was found in several tissues including the brain and liver (Duffy *et al.*, 2010). However, due to the lack of specific antibodies, there is limited information about the localisation of FLVCR2.

Evidence for the role of FLVCR2 in haem import is presented by the fact that ZnMP uptake was enhanced in human cells that overexpressed FLVCR2. There was also an increased uptake of ⁵⁵Fe-heme in *Xenopus* oocytes expressing human FLVCR2 (Duffy *et al.*

al., 2010). However, yeast studies did not demonstrate a role for FLVCR2 in haem transport (Yuan *et al.*, 2012). This discrepancy could arise from differences in expression systems.

HCP1

HCP1, also known as proton-coupled folate transporter (PCFT), belongs to the solute carrier family 46 (SLC46) which are members of the MFS. HCP1 was initially identified as a haem importer but further studies indicate that it also acts as a folate transporter (Shayeghi *et al.*, 2005; Qiu *et al.*, 2006). In addition, the results from binding assays suggest that folate is the primary physiological substrate for HCP1, since HCP1 has a greater affinity for folate, $K_m = 1 \mu\text{M}$, than haem, $K_m > 100 \mu\text{M}$ (Laftah *et al.*, 2009; Yuasa *et al.*, 2009).

HCP1 was detected in several human tissues, including liver, kidney and placenta (Qiu *et al.*, 2006). Thus, the expression of HCP1 in the liver and duodenum has been proposed to be important for haem uptake from the plasma or gut lumen (Shayeghi *et al.*, 2005). Evidence for the involvement of HCP1 in haem transport was presented by the fact that *Xenopus* oocytes injected with HCP1 cDNA showed an increase in ^{55}Fe -heme uptake compared with controls (Shayeghi *et al.*, 2005). This was shown to be a pH-independent but temperature dependent process. However, transfection of HCP1 small interference RNA (siRNA) in Chinese hamster ovary (CHO) cells did not reduce haem uptake (Shayeghi *et al.*, 2005). This discrepancy supposedly indicates that other haem acquisition pathways apart from HCP1 existed on the CHO cells.

In addition, HCP1 has also been found to be expressed in the endosome of human macrophages, where it is suggested to be involved in the export of haemoglobin-derived haem from the endosome to the cytosol (Schaer *et al.*, 2008).

1.3.3.3.4 Haem carriers

Haem carriers, such as haem binding protein 23 (HBP 23), bind haem and transport it to its degradation site.

HBP 23 is a physiological protein which has a high affinity for haem. It also reduces haem toxicity by forming a complex with it. HBP 23 is highly expressed in the liver where it is

proposed to play a role in intracellular haem transport (Muller-Eberhard & Vincent, 1985; Immenschuh *et al.*, 1995).

1.3.3.3.5 Passive diffusion

The lipophilic properties of haem and its ability to interact with membrane phospholipids allows it to be transported across the plasma membrane via facilitated passive diffusion (Light & Olson, 1990).

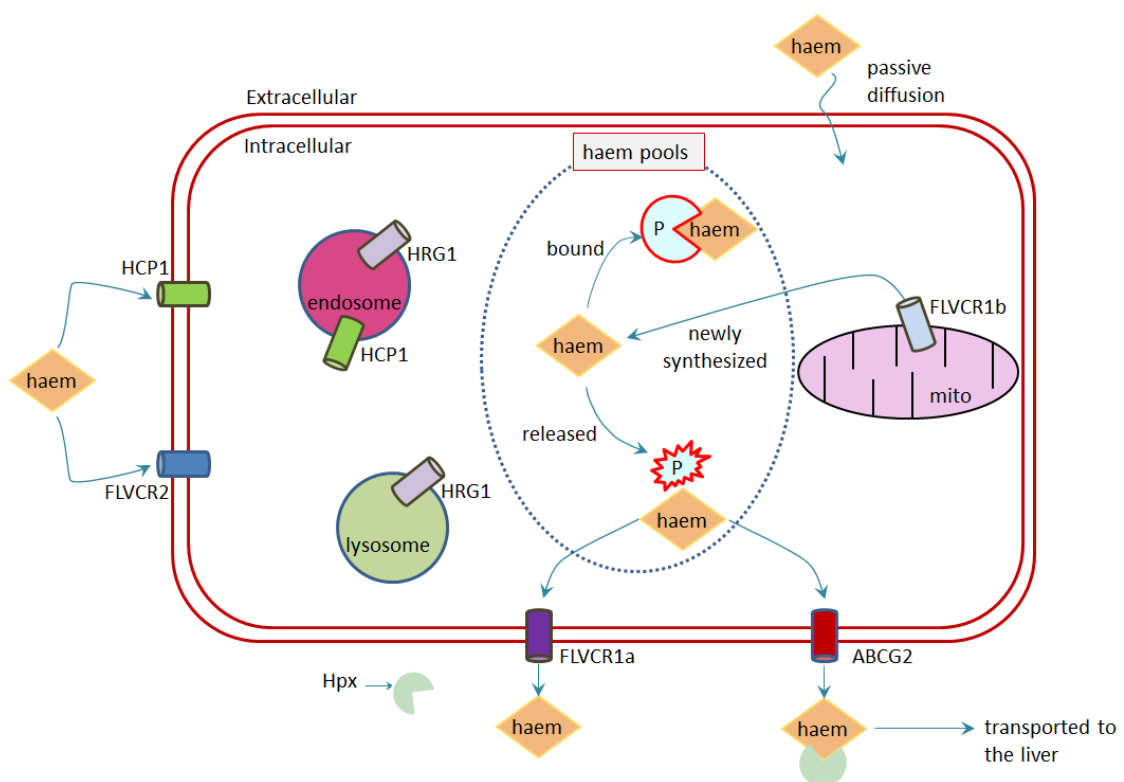


Figure 1.9: Haem transport. Haem pool can comprise of haem released from the mitochondria (post-synthesis), haem bound to hemoproteins (with “P” representing any hemoprotein) and haem released from degraded hemoproteins. There is limited knowledge about the haem transporters that exist in cells. So far, evidence presented indicates that FLVCR1a and ABCG2 exist as plasma membrane haem exporters whereas HRG1, HCP1 and FLVCR1b could act as haem exporters in organelles. In addition, HCP1 and FLVCR2 have been characterised as plasma membrane haem importers. The lipophilic nature of haem also enables it to diffuse freely across the plasma membrane. Extracellular haem could also be conjugated to hemopexin (Hpx) and transported to the liver for degradation by the reticuloendothelial system (RES).

1.3.4 Haem and CO regulation of ion channels

Haem and CO have been shown to modulate the activity of a variety of ion channels, including Na⁺, Ca²⁺ and K⁺ channels. Notably, most studies show that the effects of both molecules result from their interaction with the cytoplasmic side of the channels. However, their exact mechanism of action is mostly unclear.

1.3.4.1 Na⁺ channels

Intracellular application of haem and tricarbonyldichlororuthenium (II) dimer (CORM-2) to epithelial Na⁺ channels (ENaCs) in inside-out patches isolated from cultured M1 (mouse kidney cortical collecting duct) cells inhibited and stimulated the channel activity, respectively (Wang *et al.*, 2009). The inhibitory effect of haem was reversed under normoxic conditions in the presence of NADPH. Thus, CO generated from HO-mediated haem degradation was proposed to enhance channel activity.

Nevertheless, the mechanism of action of CO and haem on ENaC activity is generally unclear. Wang *et al.*, 2009 hypothesised that ENaC and HO might colocalise in caveolae, allowing localised regulation of channel activity by CO. However, evidence of colocalization of ENaC and HO was not presented. It was also proposed that haem might modulate channel activity by binding to an unknown haem binding domain or to proteins in close-association with ENaC, such as HO or caveolin-1. Information derived from mutagenesis studies might elucidate possible haem binding sites on the channel. Wang *et al.*, 2009 also performed experiments with NADPH, a reducing agent, under aerobic conditions. Thus, it is likely that the reducing ability of NADPH was compromised, such that the reversal of haem inhibition might not have been due to HO-mediated CO production.

1.3.4.2 Ca²⁺ channels

To date, no evidence has been presented for the interaction of haem with VGCC. On the other hand, CO has been shown to modulate the activity of LTCCs. However, this has been somewhat controversial, as CO has been shown to inhibit LTCC activity in cardiac tissue (Uemura *et al.*, 2005; Scragg *et al.*, 2008) but enhance its activity in SMCs (Lim *et al.*, 2005).

Scragg *et al.*, 2008 showed that extracellular application of CO gas and CORM-2 to native and recombinant LTCCs expressed in intact cells produced inhibitory effects. The inhibitory effect of CO was prevented by a mitochondria-specific antioxidant, MitoQ₁₀ methanesulfonate, whereas its control, decyl-TPP bromide, was without effect. Furthermore, mutagenesis studies showed that the CO sensitivity of the channels was influenced by 3 cysteine residues; Cys1789, Cys1790 and Cys1810, in the cytoplasmic domain of the channel. It was concluded that CO inhibited cardiac LTCC by upregulating mitochondrial ROS synthesis which facilitates the redox modulation of key Cys residues, in the cytoplasmic tail of LTCC. In contrast, LTCCs expressed in human jejunal SMCs were activated by CO (Lim *et al.*, 2005). Channel activation was shown to occur via a NO-dependent mechanism which involves PKA rather than PKG. The discrepancy between the effects of CO in cardiac and SMC tissue could indicate that CO mediates tissue-specific effect. This suggests that different signalling pathways are more active in different cells.

In addition, extracellular application of CORM-2 inhibited all 3 isoforms of TTCC, Ca_v3.1, Ca_v3.2 and Ca_v3.3, expressed in intact HEK293 cells (Boycott *et al.*, 2013). The mechanism of CO-mediated inhibition of Ca_v3.2 channel activity was shown to involve the disruption of a thioredoxin-mediated redox modulation of the channel. However, the mechanisms for CO-mediated inhibition of Ca_v 3.1 and Ca_v3.3 is unknown.

1.3.4.3 K⁺ channels

K_v channels

Intracellular application of haem impairs the N-type inactivation of K_v1.4 channels in inside-out membrane patches isolated from *Xenopus* oocytes expressing these channels (Sahoo *et al.*, 2013). The proposed mechanism of action results from haem binding to the CXXH motif in the N-terminal of the channel. This interaction is assumed to alter the flexibility of the N-terminal thereby preventing the ball peptide from reaching and blocking the ion conduction pore.

On the other hand, application of CORM-2 or CO gas to native and recombinant K_v2.1 channel expressed in intact cells reversibly inhibited channel activity (Dallas *et al.*, 2011). The mechanism of action of CO was reported to involve mitochondrial reactive oxygen species (ROS) and PKG activity. This is because pre-treatment of cells with antioxidants

and the PKG inhibitor, Rp-cGMPs, suppressed CO-mediated inhibition of channel activity.

K_{ATP} channels

Intracellular application of haem enhanced the activity of native and recombinant K_{ATP} channels expressed in inside-out patches isolated from ventricular cardiomyocytes and HEK 293 cells (Burton *et al.*, 2016). Spectroscopic and mutagenesis studies confirmed that haem interacts with the channel by binding to a CXXHXH motif, located between the first transmembrane domain and the first nucleotide binding domain, in the cytoplasmic domain of the SUR2A subunit. However, the mechanism via which haem binding promotes channel activation is unclear.

Recently, CO has been shown to stimulate recombinant K_{ATP} channel activity via a haem-dependent mechanism (Kapetanaki *et al.*, 2018). This is because CO application to haem bound channels enhanced the stimulatory effect of haem whereas CO application in the absence of haem did not increase channel activity. Spectroscopic studies were used to confirm further the interaction between haem and CO.

1.3.5 Haem and CO regulation of BK_{Ca} channels

1.3.5.1 Haem regulation of BK_{Ca} channel activity

BK_{Ca} channels have been classified as hemoproteins (a group of proteins which have haem as a cofactor) due to the existence of the highly conserved c-type cytochrome CXXCH sequence motif located in the linker segment between the RCK1 and RCK2 domains, with X representing any amino acid, see Figure 1.10 (Tang *et al.*, 2003; Allen *et al.*, 2003). In c-type cytochrome proteins, CXXCH motif forms a haem binding domain. The histidine residue in this sequence motif interacts with the iron-centre of haem protoporphyrin ring, two thioether bonds are also formed between the thiol groups of the cysteine residues and the vinyl groups of haem (Allen *et al.*, 2003). These interactions covalently attach haem to the polypeptide chain of c-type cytochromes.

Intracellular application of haem to recombinant, human Slo1 and cbv1 (cloned rat cerebral artery SMC Slo1) and native, rat hippocampal neurons and cerebral arteries, BK_{Ca} channels inhibited channel activity (Tang *et al.*, 2003; Jaggar *et al.*, 2005; Horrigan

et al., 2005). Mutagenesis studies confirmed that haem mediates its inhibitory effect by interacting with the CXXCH motif. Intracellular haem application to brain mitochondrial BK_{Ca} channels, also inhibited channel activity (Augustynek *et al.*, 2014). Interestingly, extracellular application of haem-L-lysinate (HLL), a HO substrate, to intact cerebral arteriolar SMCs enhanced STOC amplitude and frequency (Jaggar *et al.*, 2002). So far, the proposed mechanism of haem inhibition is that haem binding to the CXXCH motif results in expansion of the S6-RCK1 linker, thereby weakening the allosteric coupling of the voltage and calcium sensors to channel activation (Horrigan *et al.*, 2005).

Most studies performed experiments on isolated patches, thus, the effects of haem on STOCs could not be examined. Furthermore, Jaggar *et al.* (2002) proposed that HLL stimulated STOCs via CO released from HO-mediated HLL degradation. However, their study was not performed with haem and no other study has investigated the effects of haem on STOCs. The influence of intracellular factors, particularly cellular redox state, on the modulatory effect of haem is unclear. In addition, the number of haem molecules required for channel inhibition or the number of functional haem binding sites on BK_{Ca} channels is not known. Furthermore, haem studies have mostly been performed with brain tissues or cell lines expressing BK_{Ca} α -subunits with hardly any study on visceral tissues. Thus, the possibility of tissue-specific effects of haem has not been explored.

1.3.5.2 CO regulation of BK_{Ca} channel activity

Intracellular application of CO (via CO gas or CORMs) has been shown to stimulate native and recombinant BK_{Ca} channels in inside-out patches (Wang *et al.*, 1997b; Wang & Wu, 1997; Dong *et al.*, 2007). Several mechanisms of CO-mediated activation have been proposed which can be divided into haem-dependent and haem-independent effects. There is much controversy around both mechanisms, hence the mechanism of action of CO on BK_{Ca} channel activity is still unclear.

To the best of my knowledge, Jaggar *et al.*, 2005 is the only study that presented evidence for a haem-dependent CO effect on BK_{Ca} channel activity. Mutagenesis studies performed by Jaggar *et al.*, 2005 showed that the -CH residues in the CXXCH motif were essential for haem and CO interaction with BK_{Ca} channels. Mutation of the -CH residues abolished the inhibitory and stimulatory effects of haem and CO on BK_{Ca} channel activity,

respectively. However, other studies have reported that single (His616Arg) and double (Cys615Ser:His616Arg) mutations of the CXXCH motif abolished the haem-mediated inhibition of channel activity but had no effect on the CO activation of channel activity (Hou *et al.*, 2008a; Williams *et al.*, 2008). Furthermore, consistent with the fact that CO binds to only ferrous iron, Fe²⁺ (Boczkowski *et al.*, 2006), Jaggar *et al.*, 2005 showed that CO reverses the inhibitory effect of haem but not hemin (the ferric form of haem). However, Hou *et al.*, 2008 observed that CO still mediated its stimulatory effect in the presence of the oxidising agent, H₂O₂.

Several haem-independent mechanisms have been proposed (see Figure 1.10). For instance, CO has been suggested to interact with extracellular histidine residues supposedly by forming hydrogen bonds with the imidazole group of the histidine residues (Wang & Wu, 1997; Wu *et al.*, 2002). Evidence from mutagenesis studies by Hou *et al.*, 2008 led to the proposal that CO-mediated stimulation occurs via its direct interaction with Asp367, His365 and His394 located in the RCK1 domain. This is because mutation of the 3 amino acid residues abolished the stimulatory effect of CO with no effect on the inhibitory action of haem. However, later work performed by Telezhkin *et al.*, 2011, showed that the double mutation, His365Arg and His394Arg, increased the CO sensitivity of BK_{Ca} channels. The discrepancy between results from both studies could arise from the fact that Hou *et al.*, 2008 performed their experiments in the virtual absence of Ca²⁺ but Telezhkin *et al.*, 2011 worked with 300 nM [Ca²⁺]_i. Furthermore, Hou *et al.*, 2008 suggested that CO acts as a Ca²⁺ mimetic but Williams *et al.*, 2008 showed that CO enhanced BK_{Ca} channel activity in saturating [Ca²⁺]_i. Also, Telezhkin *et al.*, 2011 showed that CORM-2 produced no effect on channel activity in the absence of Ca²⁺.

Chimeric studies, performed with the human Slo1 core and the S9 to S10 segments of the mSlo3 C-terminal, indicated that a motif in the C-terminal tail of BK_{Ca} channel α -subunit was essential for the CO-mediated effect (Williams *et al.*, 2008). Consistent with this observation, mutating Cys911 in the C-terminal tail influenced BK_{Ca} channel's CO sensitivity (Telezhkin *et al.*, 2011). Therefore, based on previous evidence that Asp367, His365 and His394, located in the RCK1 domain, influenced BK_{Ca} channel CO sensitivity, it was proposed that Cys911 and the 3 amino acid residues coordinate a metallocluster to which CO binds (Telezhkin *et al.*, 2011). The idea of a metallocluster is in line with

reports from bacterial studies which showed haem independent interaction of CO with metalloclustered active sites in bacterial enzymes; iron-only hydrogenases and CO-dehydrogenase II (Lemon & Peters, 1999; Nicolet *et al.*, 2002; Boer *et al.*, 2014). Although, such metalloclustered sites are yet to be characterised in mammalian proteins.

The evidence presented so far shows that the mechanism of action of CO on BK_{Ca} channel activity is still unclear. Also, the hypothesis about the direct interaction of CO with amino acids on BK_{Ca} channels is chemically implausible (Leffler *et al.*, 2011). This leaves the uncharacterised metallocluster and haem-dependent mechanism as plausible mechanisms of action of CO. Nevertheless, cytoplasmic factors could also contribute to the interaction of CO with BK_{Ca} channels.

Whole-cell studies performed on SMCs isolated from cerebral arteriole showed that CO enhanced STOC amplitude and frequency (Jaggar *et al.*, 2002). The proposed mechanism of action involved enhancing the coupling between Ca²⁺ sparks and BK_{Ca} channels. To the best of my knowledge no other study has examined the effects of CO on STOCs. Further studies performed on recombinant and native BK_{Ca} channels, expressed in intact HEK293 cells and newborn pig cerebral arteriole SMCs, respectively, showed that CO enhanced whole-cell BK_{Ca} channel activity by increasing the Ca²⁺ sensitivity of the channels (Xi *et al.*, 2004). However, STOCs were not recorded in this study; thus, there is limited knowledge about the effects of CO on STOCs.

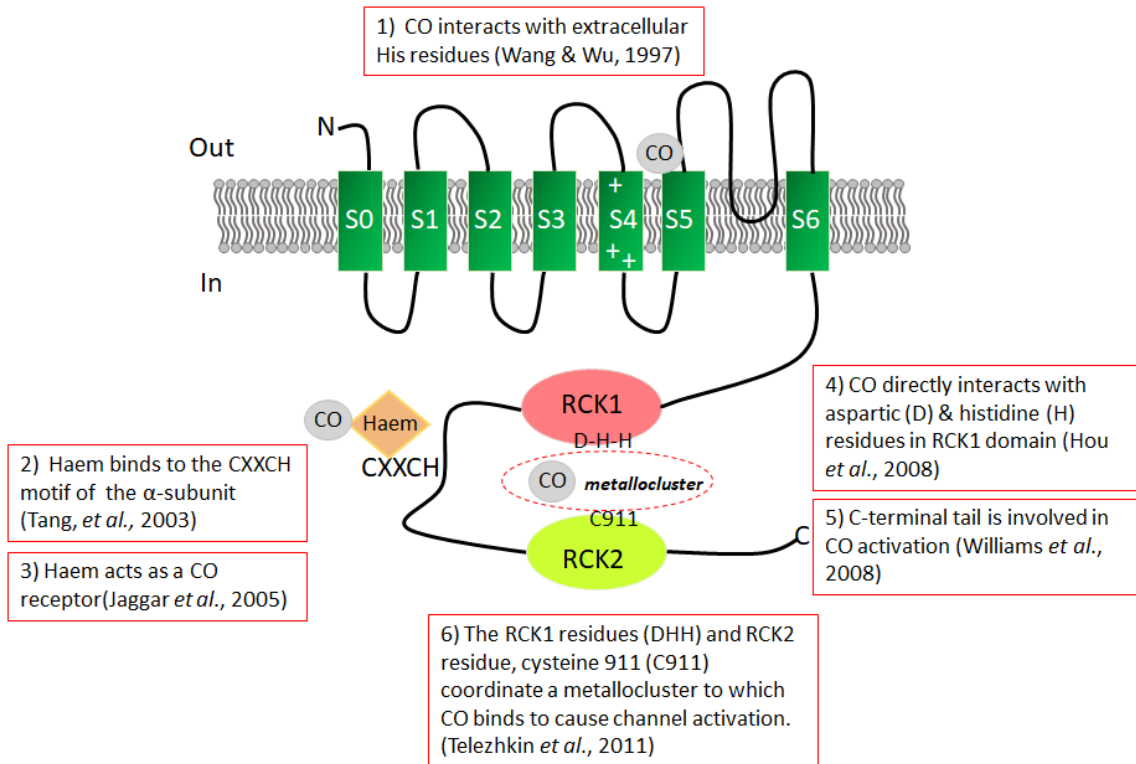


Figure 1.10: Historical evidence of the mechanism of interaction of haem and CO with BK_{Ca} channels. The schematic diagram summarises the experimental evidence presented to date. Haem and CO have been reported to mediate inhibitory and stimulatory effects respectively, but their mechanism of action is poorly understood.

1.4 Aims of this study

The mechanism by which haem and CO interact to modify BK_{Ca} channel activity is poorly understood. The evidence presented so far indicates that both molecules play important roles in regulating these channels in arterial SMCs.

To gain a better understanding of haem and CO regulation of BK_{Ca} channels, this project aims to: (1) investigate the effects of haem and CO on whole-cell BK_{Ca} currents (by recording STOCs and voltage-pulsed whole-cell BK_{Ca} currents) and on single BK_{Ca} channel activity; (2) investigate the influence of key intracellular components such as pH, Ca²⁺ and endogenous CO, on such interaction; (3) Examine whether haem signalling to BK_{Ca} channels occurs within a functional complex. Therefore, my research is designed to further elucidate the role of haem in ion channel regulation, particularly focusing on arterial SMC BK_{Ca} channels.

My experiments were performed on BK_{Ca} channels of mesenteric artery SMCs. Single BK_{Ca} channel activity was recorded using inside-out and outside-out patches whereas the perforated and ruptured patch techniques were used for recording whole-cell BK_{Ca} channel activity.

Chapter 2 METHODS

2.1 Smooth muscle cell isolation

The mesenteric artery was isolated from freshly culled male Wistar rats. Rats were culled by stunning followed by cervical dislocation in accordance with the Home Office regulations. The isolated artery was placed in Ca^{2+} -free solution comprising (mM) 5.4 KCl, 137 NaCl, 0.44 Na_2HPO_4 , 0.42 NaH_2PO_4 , 10 HEPES, 4 glucose, 6 mannitol and 1 MgCl_2 . This was done to avoid stimulating Ca^{2+} entry through stretch-activated Ca^{2+} channels during the removal of protective fatty layers and residual blood from the isolated artery to ensure optimal digestion. Digestive enzymes were prepared in bovine serum albumin (BSA) solution which had been pre-incubated at 37°C for ~ 60 minutes. BSA solution, 0.9 mg/ml, was made by adding BSA powder to 0.1 mM Ca^{2+} solution comprising (mM) 5.4 KCl, 137 NaCl, 0.44 Na_2HPO_4 , 0.42 NaH_2PO_4 , 10 HEPES, 4 glucose, 6 mannitol, 1 MgCl_2 and 0.1 CaCl_2 . The 0.1 mM Ca^{2+} -containing solution was used instead of Ca^{2+} -free solution because the enzymes need some Ca^{2+} to function properly. Also, a certain amount of Ca^{2+} is required for cell survival. Smooth muscle cells were isolated via a two-step digestion of the artery. All enzymatic solutions were prepared with the BSA solution. The first enzymatic digestion was carried out by placing the artery in 1.2 mg/ml papain and 1.1 mg/ml dithioerythritol (DTE), for 31 minutes. The digested artery (which appeared feathery) was placed in a second enzymatic solution containing 1.2 mg/ml collagenase and 1.2 mg/ml hyaluronidase, for 13 minutes. After the second digestion, the artery was washed once with BSA solution and thrice with 0.1 mM Ca^{2+} -containing solution. The artery was then transferred into a fresh vial of 0.1 mM Ca^{2+} -containing solution. A wide-bore pipette was used to release cells by triturating several times until the solution appeared cloudy. The new cell-suspension solution was stored on ice to slow down cell metabolism, thereby prolong cell viability.

2.2 Chemicals and Materials

All reagents used for electrophysiology and chemical experiments were purchased from Sigma Aldrich (Dorset, United Kingdom) with the exception of collagenase from Worthington Biochemical Corporation (Lakewood, New Jersey), TCEP (tris(2-

carboxyethyl)phosphine) from Melford laboratories Ltd (Ipswich, United Kingdom), amphotericin B from Apollo Scientific Ltd (Stockport, United Kingdom), ryanodine from SantaCruz Biotechnology Inc (Dallas, Texas) and CO gas from CK Gas Products Limited (Leicester, United Kingdom). Fire polished capillary tubes used for micropipette fabrication were purchased from Warner Instruments (Hamden, Connecticut) and Harvard Apparatus Ltd (Cambridge, United Kingdom). Glass bottom petri dishes and fluorescent indicator (Fluo 4-AM) used for imaging studies were purchased from Thermo Scientific (Rochester, New York) and Molecular Probes (Eugene, Oregon), respectively.

2.3 Preparation of solutions

2.3.1.1 Haem solution

Haem is a difficult molecule to work with because of its strong tendency to adsorb onto different materials including glass and plastic (de Villiers *et al.*, 2007; Asher *et al.*, 2009). Therefore, it was important to design an effective method for preparing haem solutions of known concentrations.

Hemin was first dissolved in 9 % v/v of 0.1M NaOH solution (as haem is only soluble in alkaline aqueous solutions) and 91 % v/v of 0.05M HEPES was added to make the stock solution. The stock solution was vortexed and centrifuged a few times to remove undissolved haem. The solution was then wrapped in foil and placed on ice to slow down haem degradation. The procedure used for measuring haem concentration in solution is described in section 2.7.1.1.

2.3.1.2 CO gas solution

CO gas stock solution was always prepared by a 5-minute bubbling of CO gas from a compressed cylinder into 5 to 10 ml of the required electrophysiology bath solution, contained in a sealed vessel. This procedure was always performed in a fume cupboard. The stock solution was subsequently diluted to a final concentration that was used for experiments. The details of how the presence of CO gas in solution was confirmed is described in section 2.7.2.1.

2.3.1.3 CORM-3 solution

CORM-3 stock solution was always prepared by adding distilled water to CORM-3 powder (30 % w/v). Dilutions were then made to the required concentration that was used for experiments. The method of confirmation of CO gas release from CORM-3 is detailed in section 2.7.2.2.

2.4 Electrophysiology

2.4.1 Patch clamp technique

The patch clamp technique was pioneered by Neher and Sakmann in 1976 and refined further by Hamill *et al.* in 1981. The aim of patch clamp recording is to electrically isolate a patch of membrane and record current flowing through ion channels in the isolated patch. This requires the use of a microelectrode which comprises of a micropipette and silver chloride (Ag/AgCl) electrode. The pipette is filled with a suitable electrolyte such that the flow of electrons (e^-), generated and consumed by the redox (reduction and oxidation) reactions on the electrode as shown in equations 2.1, 2.2 and 2.3, produces a detectable electric current (Berman & Awayda, 2013).

Equation 2.1 (*Cathode half-reaction*): $2AgCl + 2e^- \rightleftharpoons 2Ag + 2Cl^-$

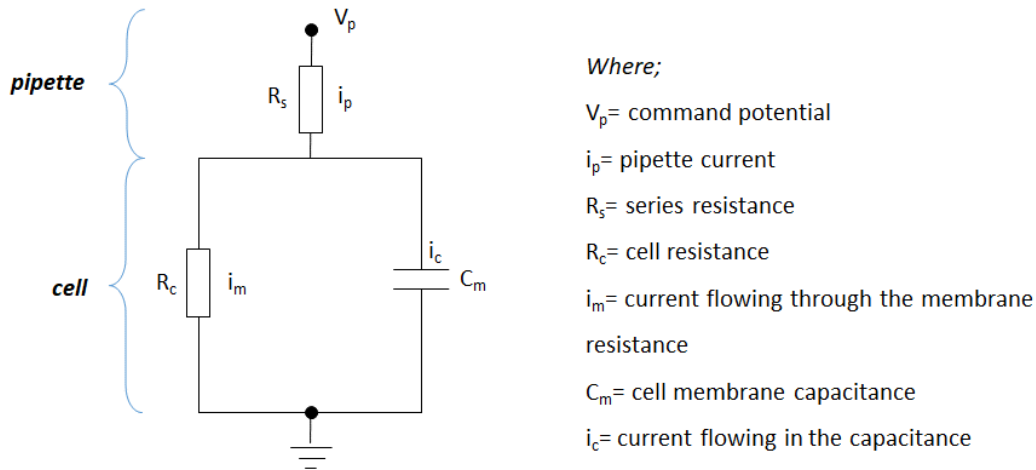
Equation 2.2 (*Anode half reaction*): $H_2 \rightleftharpoons 2H^+ + 2e^-$

Equation 2.3 (*Combined equation*): $2AgCl + H_2 \rightleftharpoons 2Ag + 2HCl$

In this study, the patch clamp technique was used under the voltage clamp mode. This allowed the membrane potential to be held steady at a desired potential whilst recording changes in channel current. A patch clamp amplifier converts the pipette currents to voltage signals. An analogue-to-digital (AD) converter then converts the voltage signals to digital signals which are sampled by a computer. Noise can arise from the seal conductance and recording system, but a high signal-to-noise ratio is maintained via a high resistance seal (giga seal) and the use of low-pass filters which eliminate high-frequency signals at the pipette tip. In addition, background noise that

arise from nearby surfaces including the micromanipulators and microscope can be reduced by grounding.

Nevertheless, during whole-cell recording, series access resistance, which occurs between the pipette electrode and cell interior as shown in Figure 2.1, can be an issue. This is because the pipette current, which flows between the pipette and the cell, produces a voltage error ($i_p R_s$) that is equal to the difference between the pipette potential and cell potential. High series resistance interferes with the accuracy of whole-cell recordings, as it restricts the flow of capacitive charging currents when a voltage step is applied to the microelectrode (Penner, 1995). Therefore, it is important for series-resistance to be compensated for. This involves calculating the voltage error arising from the estimated series resistance, so that the appropriate amount of correction is made to the command potential that is administered to the pipette (Sigworth, 1995). However, only a proportion (~ 75 %) of the error is corrected because further attempts to increase the compensation could result in oscillation of the clamp circuitry.



$$\text{True cell potential} = V_p - i_p R_s$$

Figure 2.1: Series resistance error in whole-cell recordings. Series resistance is introduced by the pipette tip. It is so-called because the pipette resistance is in series with the cell membrane. Current flow through the pipette produces a voltage error that must be compensated to record the true cell potential; the difference between the command potential and the voltage error introduced by series resistance.

Cell capacitance can also contribute to voltage errors during whole-cell recordings. This is because some of the pipette current is used to charge the cell capacitance. Cell capacitance is compensated for using the slow and fast capacitance compensation potentiometers on the amplifier. These work by injecting current into the pipette via a positive feedback circuit which compensates for the current lost through membrane capacitance (Halliwell *et al.*, 1994).

The different components of the electrophysiology set-up used in the present study, and specific details of how channel activity was measured in intact cells and excised membrane patches, are described below.

2.4.2 Superfusion systems

During single channel experiments, excised patches were placed in the common outflow of a multi-reservoir gravity-fed superfusion system made with high-performance liquid chromatography (HPLC) tubing. This enabled the exposure of the cytoplasmic side of the membrane to different solutions. HPLC tubing was used to reduce haem adhesion to the walls of the tube.

In contrast, for whole-cell experiments, cells were superfused in the bath chamber using a peristaltic pump. A dead space time of 2.1 minutes was calculated using the non-selective and quick acting BK_{Ca} channel blocker, tetraethylammonium ion (TEA^+) as demonstrated in chapter 4, section 4.2.3.1.

2.4.3 Micropipette fabrication and polishing

Fire-polished glass capillary tubes were used for fabricating micropipettes. Vertical or horizontal pullers were used to achieve this process. Both pullers work by passing large currents through a tungsten filament which heats and melts the glass. The vertical puller, (Narishige Scientific Instrument Lab., model PC-10: Tokyo, Japan) employs a two-step mechanism, during which the capillary glass is thinned by heating and split into two micropipettes by gravitational pull. The heat level of the second pull determines the diameter of the micropipette tip; with high and low heat levels producing small and large micropipette tips, respectively. The horizontal puller (Sutter Instrument Company, model P-97: Novato, California) employs a 'velocity sensing' mechanism to pull the glass. This works by heating up the glass until it is drawn and reaches a set velocity, at which point the heat is turned off and cooling air is applied to the glass. This heating and cooling process were repeated in a multi-loop fashion until the glass was separated to form two micropipettes.

Once the micropipettes were fabricated, they were polished using a pipette microforge (Narishige Scientific Instrument Lab., model MF-83: Tokyo, Japan). Heat polishing the pipette tip smooths the edges and removes debris from it, thereby enhancing the rate of successful and stable seal formations. The microforge works by using a platinum wire

as a heat source with an air stream directed at the wire such that a steep temperature gradient is created near it.

2.4.4 Giga seal formation

A giga seal is achieved by applying gentle suction to a pipette attached to a cell. This encourages the membrane to seal around the circumference of the electrode tip. Giga seal formation can be sudden or gradual. It is required to obtain satisfactory patch clamp records because it enhances the resolution of single channel current via the reduction of noise levels that could arise from thermal agitation of electrical charges (Aidley & Stanfield, 1996). The tightness of the giga seal also prevents the flooding of the cytosol with bath solution constituents. It also prevents the flow of leak currents between the pipette and reference electrode.

2.4.5 Recording BK_{Ca} currents

2.4.5.1 Single channel current recording

Single channel studies were used to examine the direct effect of haem and other molecules on single BK_{Ca} channel activity. Two different excised patch techniques, inside-out and outside-out, were employed for single BK_{Ca} channel studies. Drug applications to the intracellular and extracellular side of single BK_{Ca} channels was performed using the inside-out and outside-out patch techniques, respectively. All recordings were made at room temperature (22 – 25°C).

2.4.5.1.1 Inside-out patch configuration

Heat polished microelectrodes with typical resistance of 7 to 10 MΩ were brought into contact with intact cells. Once a giga-seal was obtained the electrode was pulled away leading to excision of the membrane patch in an inside-out configuration (Figure 2.2). Excised patches were then placed in the perfusion system (c.f. section 2.4.2). The composition of pipette and bath solutions used for the inside-out patch experiments are shown in Table 2.1.

A major caveat of this technique is the absence of many intracellular components because of membrane excision. Also, the formation of vesicular patches due to membrane re-seal after patch excision can prevent the recording of channel current.

| bath solution (pH 7.2) | | pipette solution (pH 7.4) | |
|------------------------|------------|---------------------------|------------|
| reagent/ion | conc. (mM) | reagent/ion | conc. (mM) |
| K ⁺ | 140 | Na ⁺ | 135 |
| HEPES | 10 | K ⁺ | 5 |
| EGTA | 5 | HEPES | 10 |
| HEDTA | 5 | Mg ²⁺ | 1 |
| Ca ²⁺ | variable | Ca ²⁺ | 0.1 |

Table 2.1: Pipette and bath solutions used for inside-out patch recordings.

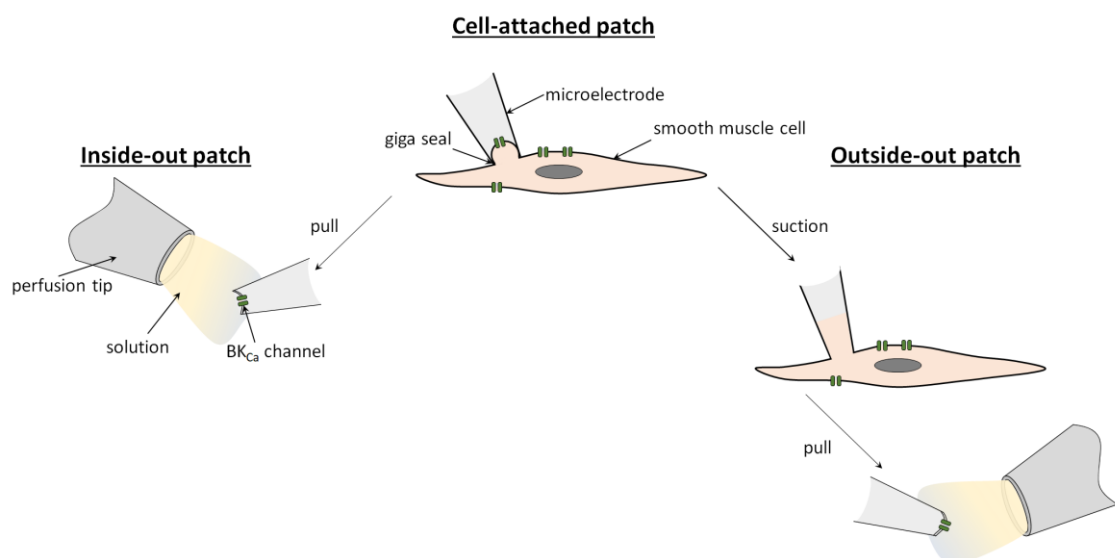


Figure 2.2: Schematic diagrams of excised patch configurations. The inside-out and outside-out patch techniques expose the intracellular and extracellular side of channels, respectively.

2.4.5.1.2 Outside-out patch configuration

This technique was used for the direct application of substances to the extracellular side of BK_{Ca} channels. The range of resistances of the electrodes used for this technique was 3 to 8 MΩ. This time, after achievement of a giga seal, additional suction was applied to rupture the plasma membrane (Figure 2.2). The pipette was then pulled away slowly from the cell thereby exposing the extracellular surface to the bath solution. The constituents of pipette and bath solutions used are shown in Table 2.2. A limitation of this technique, as with inside-out patches, is that some intracellular components are lost with patch excision. Furthermore, the transition from the whole-cell to the outside-out mode can be hindered if cells are not fully adhered to the bath chamber.

| bath solution (pH 7.4) | | pipette solution (pH 7.2) | |
|------------------------|------------|---------------------------|--------------------|
| reagent/ion | conc. (mM) | reagent/ion | conc. (mM) |
| K ⁺ | 5 | K ⁺ | 140 |
| Na ⁺ | 135 | Na ⁺ | 2 |
| Mg ²⁺ | 1 | Mg ²⁺ | 1 |
| Ca ²⁺ | 1 | Ca ²⁺ | 0.36 (100 nM free) |
| HEPES | 10 | HEPES | 10 |
| glucose | 4 | ATP | 1 |
| mannitol | 6 | EGTA | 1 |

Table 2.2: Pipette and bath solutions used for outside-out patch and whole-cell recordings.

2.4.5.2 Whole-cell current recording

Whole-cell recordings were achieved using two types of patch clamp configurations; ruptured and perforated patch. The ruptured patch technique was used when experiments required the addition of membrane impermeable substances to the

cytoplasm. On the other hand, the perforated patch technique was useful for maintaining the cytoplasmic conditions as physiological as possible thereby overcoming the typical current rundown seen with ruptured patches. All experiments were performed at room temperature (22 – 25°C).

2.4.5.2.1 Ruptured patch configuration

STOCs were examined using the ruptured patch configuration. The constituents of the pipette and bath solutions were the same as those used for outside-out patches (Table 2.2). Micropipettes of resistances 3 to 4 MΩ were used to aid rupture of the membrane by applying strong suction (Figure 2.3). This made the pipette solution continuous with the cytosol and provided a low resistance access. This technique was also used to examine voltage-pulsed whole-cell BK_{Ca} currents. Ryanodine application via the pipette solution inhibited the activity of ryanodine sensitive Ca²⁺-release channels (RyRs) in the sarcoplasmic reticulum, thereby eliminating STOCs.

A major caveat of using the ruptured patch technique is the dialysis of the cytosol with the pipette solution, which could remove key intracellular signalling components.

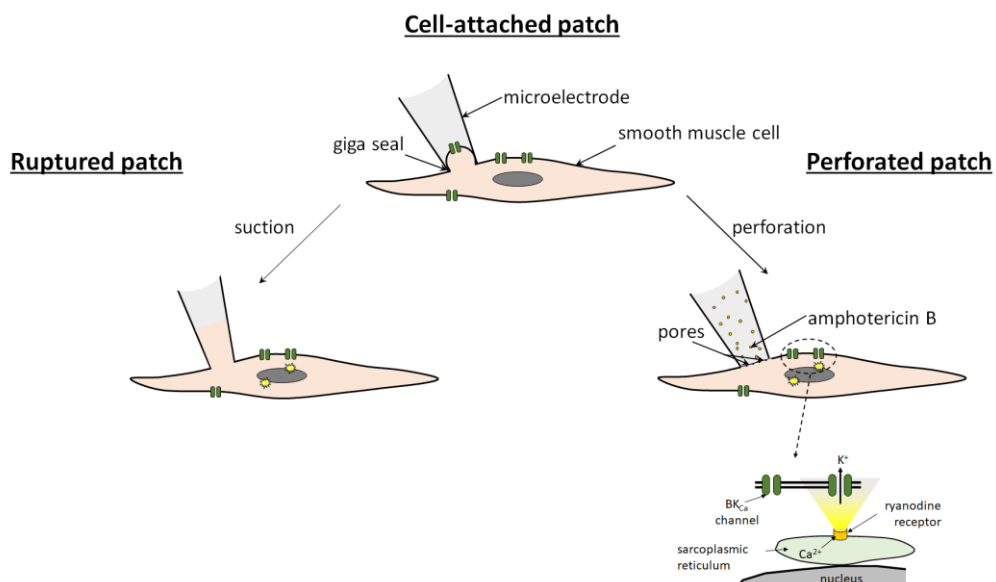


Figure 2.3: Schematic diagrams of whole-cell patch configurations.

2.4.5.2.2 Perforated patch configuration

This technique differs from the ruptured whole-cell technique because instead of membrane rupture via application of suction, polyene antibiotics (amphotericin B or nystatin) are used to create low-resistance pores in the membrane. This prevents the dialysis of intracellular components thereby overcoming the issue of current rundown.

Amphotericin B was used in the present study. As with other polyene antibiotics, amphotericin B has a large polyhydroxylic lactone ring with one side of the lactone ring comprising of hydrophilic groups and the other side hydrophobic groups. This property enables polyene antibiotics to act as amphipathic molecules. The amphotericin B molecules assemble to form barrel-shaped pores in the plasma membrane. Each pore is ~ 2.8 nm long and 0.8 nm wide with small access resistance (3 to 10 M Ω) and conductance in the pS range (Sarantopoulos, 2007). Only certain molecules, including monovalent ions (with higher cation permeability) and water, can pass through the pores.

The constituents of the pipette and bath solutions used for ruptured patch studies were also used for perforated patch studies, except that ATP was excluded from the pipette solution and amphotericin B was added to it (Table 2.2). Exclusion of ATP was due to its inability to traverse the polyene pores (Lippiat, 2008). Amphotericin B stock solution (60 mg/ml) was prepared by dissolving amphotericin B powder with DMSO (dimethyl sulphoxide) as previously reported (Rae *et al.*, 1991). The solution was vortexed and sonicated. Final dilutions (0.48 mg/ml) were made using the pipette solution, with final DMSO concentration of 0.8 % v/v. Stock solutions were stored at - 20 °C and used within 48 hours. Pipette resistance was typically between 2 to 3 M Ω . To limit the interference of amphotericin B with giga seal formation, the pipette tip was half-filled with amphotericin B-free pipette solution before back-filling the pipette shank with amphotericin B-containing pipette solution. The pipette was then brought into contact with a cell and slight suction was applied to achieve a giga seal. Suction was removed during the process of membrane perforation. The gradual increase in capacitance spikes indicated the decrease in access resistance resulting from the formation of pores in the membrane (Figure 2.4). Sharper spikes typically occurred between 20 to 50 minutes indicating good electrical access between the cell and patch pipette. Series-resistance

was then compensated and whole-cell capacitance was adjusted. The average whole-cell capacitance was 17.6 ± 2.7 pF with series resistance of 13.3 ± 1.2 M Ω .

The caveats of this technique include the long wait to obtain low resistance access to the cell via membrane perforation and the inability to apply large molecules such as ryanodine to the cytosol via the pipette solution.

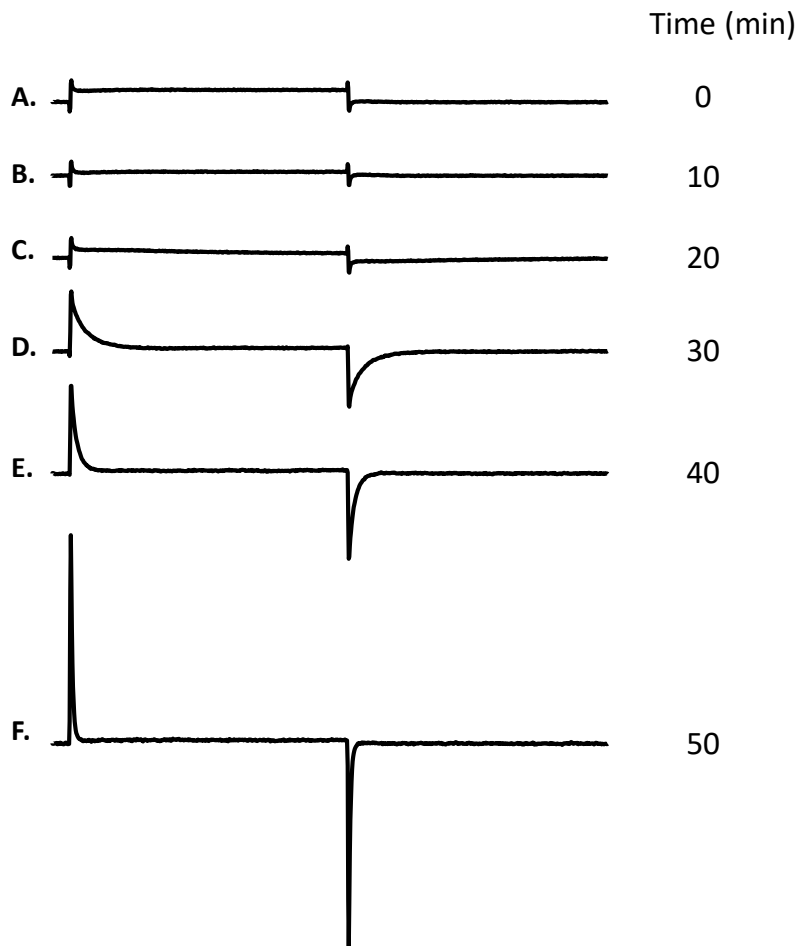


Figure 2.4: Example traces illustrating the process of smooth muscle cell membrane perforation by amphotericin B in the pipette solution. Time (in minutes) after giga seal formation is indicated on the right side of each trace. Traces A & B Show high resistance (giga seal) formation between the patch pipette and the cell membrane. Traces C, D & E show increases in whole-cell capacitance transients as access resistance decreases over time. Trace F shows large amplitude capacitance transients which indicate low access resistance of the patch. This signifies good electrical access between the pipette and the cell. Experiments are usually commenced at this point.

2.5 Data Acquisition

In the present study, analogue signals were observed by connecting an Axopatch 200A amplifier to an oscilloscope. The amplifier was also connected to an analogue-to-digital (AD) converter, Digidata 1440A interface, controlled by pClamp (v.10) software. This enabled the recording of data on a computer. Inside-out patch and STOC data were acquired using a gap-free mode whilst outside-out patch and pulsed whole-cell currents were obtained with episodic stimulations. Single channel and whole-cell signals were digitized at 10 kHz and 5 kHz, respectively. High frequency noise was reduced by filtering signals at 2 kHz using a lowpass Bessel filter.

2.6 Data Analysis

2.6.1 Single-channel current analysis

2.6.1.1 Measurement of unitary current amplitude

The data points from each current trace were sorted into bins and plotted as histograms. Each individual peak represented either open levels, corresponding to the number of active channels in the patch, or the closed level (see Figure 2.5). All peaks were fitted with Gaussian distributions. The area under each peak is proportional to the length of time spent at that level.

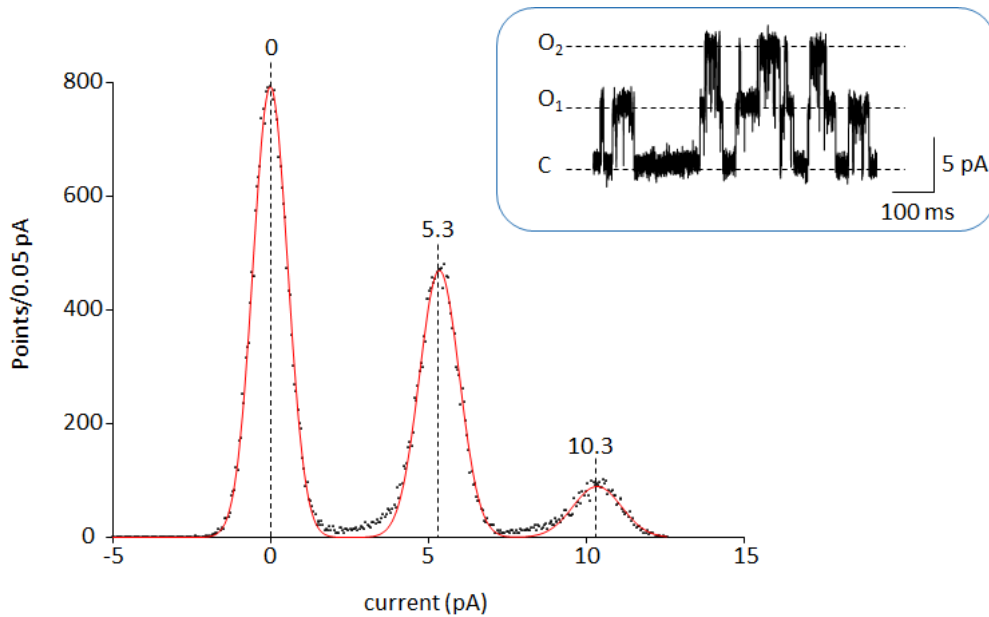


Figure 2.5: Measurement of unitary current amplitude. Amplitude histograms were generated by plotting the points per bin width (0.05 pA) against the current amplitude (in pA). The inset shows the current trace for the amplitude histograms. The closed level (C) was fitted with one peak, with current size of 0 pA. The open levels (O_1 and O_2) were fitted with two peaks, with current sizes of 5.3 pA and 10.3 pA, respectively.

2.6.1.2 Measurement of open probability (P_{open})

The open probability (P_{open}) of a channel measures the likelihood of the channel being open at a given time. A 50 % threshold was set for the open level such that only data points that exceed the threshold are counted as open events. For patches that contained > 1 active channel, a threshold was set for each open level. Thus, channel P_{open} was calculated as a proportion of the number of open channels in a patch and the total recording duration, as shown in Equation 2.4.

Equation 2.4 (open probability):

$$P_{open} = \left(\sum_{j=1}^N t_{jj} \right) \div TN$$

Where t_j = time spent at current level corresponding to $j = 0, 1, 2 \dots N$ channels, T = total recording duration.

2.6.1.3 Measurement of the channel's open and closed times

Open events were detected when current level crossed a threshold set at 50 % of the fully open amplitude. Baseline current was defined at the level of channel closure.

The dwell-times of open and closed channel events display stochastic variability. In this study, the dwell-times were sorted into 25 bins per log unit using the method detailed by Sigworth & Sine, 1987. The dwell-time histograms are displayed as square-root of the ordinate axis against a logarithmic time axis. The square root ordinate ensures that the scatter in bins is constant whereas logarithmic time axis allows events of widely different duration to be viewed in the same graph (Sigworth & Sine, 1987). The open and closed time distributions were fitted to the probability density function shown in Equation 2.5 using the maximum-likelihood method. The number of exponential components reflects the number of open and closed states. Open distributions were typically fitted with 2 components whereas closed time distributions were fitted with at least 4 components.

Equation 2.5 (*probability density function*):

$$f(t) = \sum_{j=1}^n \left(\frac{a_j}{\tau_j} \right) \exp\left(\frac{-t}{\tau_j} \right)$$

Where; n = number of summed exponentials; a_j and τ_j represent the area and time constant, respectively, of component j .

A minimum time resolution of 100 μ s was always imposed on the data. This determined the minimum duration for an event to be classed as open. It also made it easier to correct the mean open time (mot) for missed closed events. Brief closed events can be missed due to filtering, thereby resulting in inaccurate information about the duration of open events. Missed events were corrected by first automatically fitting closed and open event histograms with an exponential function, which provided information about the mot. The mot was then multiplied by the proportion of detected closed events to obtain the corrected mots.

2.6.2 Whole-cell current analysis

2.6.2.1 STOC detection and analysis

The analysis and detection of STOCs was coded using an in-house software, Tracan.

STOC Detection

STOC detection can be complicated by STOCs appearing on a fluctuating baseline. This limits the use of a conventional threshold detection algorithm. This limitation was overcome by developing a detection process based on slope detection as shown in Figure 2.6.

STOCs are rapid upward deflections in whole-cell current. STOC detection was initiated by smoothing the raw current trace by calculating the running average of A_{width} successive data points (Figure 2.6). Potential STOCs were identified by measuring the slope between successive pairs of points S_{width} apart on the smoothed trace; if the slope remained above a set threshold for a duration greater than T_{width} , it was identified as a potential STOC with the beginning of the STOC taken as the initial time of crossing the threshold (see Figure 2.6).

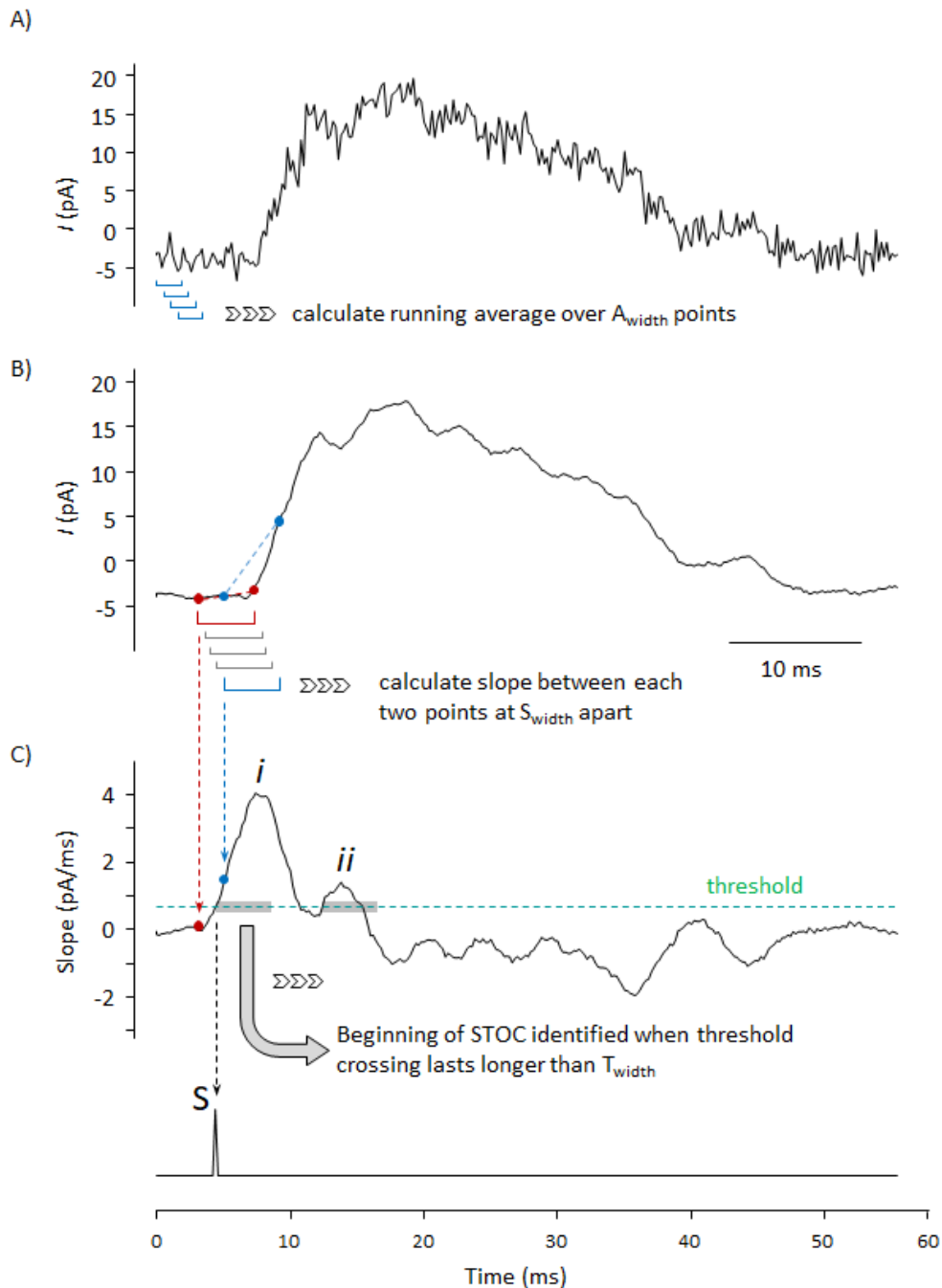


Figure 2.6: Example images showing the process of individual STOC detection in whole-cell records. Image A shows a section of an original recording. Calculating the running average of 11 successive (A_{width}) points smoothed the original trace to that seen in trace B. The slope of pairs of successive points, 21 points (S_{width}) apart in trace B, illustrated by the pair of red and blue points, was used to obtain trace C. Potential STOCs were identified if the value of the slope in trace C exceeded a threshold set at 0.65 pA/ms and had a duration \geq the threshold width (T_{width}) which was set at 21 points, indicated by the shaded region. Slope i in trace C is classed as a transient, indicated by the spike, S , whereas, slopes that reach the threshold but are $< T_{width}$ are ignored, like slope ii .

STOC Analysis

For analysis purposes each detected STOC was aligned, with the baseline set to zero, and placed in an individual record; each record (see Figure 2.7A) was added to a file. The number of records in a file corresponded to the number of STOCs detected.

Once potential STOCs were detected and aligned, an amplitude threshold was set so that transients with an amplitude ≥ 15 pA were accepted as STOCs, as performed by a previous study (Bayguinov *et al.*, 2001). This threshold was set because a STOC was defined as the simultaneous opening of 3 or more BK_{Ca} channels, with the assumption that each single BK_{Ca} channel opening at -30 mV produced current amplitude of ~ 5 pA. However, the threshold of ≥ 10 pA was used when recordings were made at -50 mV, where STOC amplitude was usually low.

STOC amplitude was the peak outward current measured within 75 ms of the beginning of the STOC (Figure 2.7). Cumulative STOC amplitude histograms were plotted as the proportion of STOCs with amplitude $> x$ -value (Figure 2.7B). STOC frequency was calculated by measuring the gaps between detected STOCs (Figure 2.8A). This information was reflected in STOC frequency distribution histograms which were fitted with a single-component exponential function (Figure 2.8B).

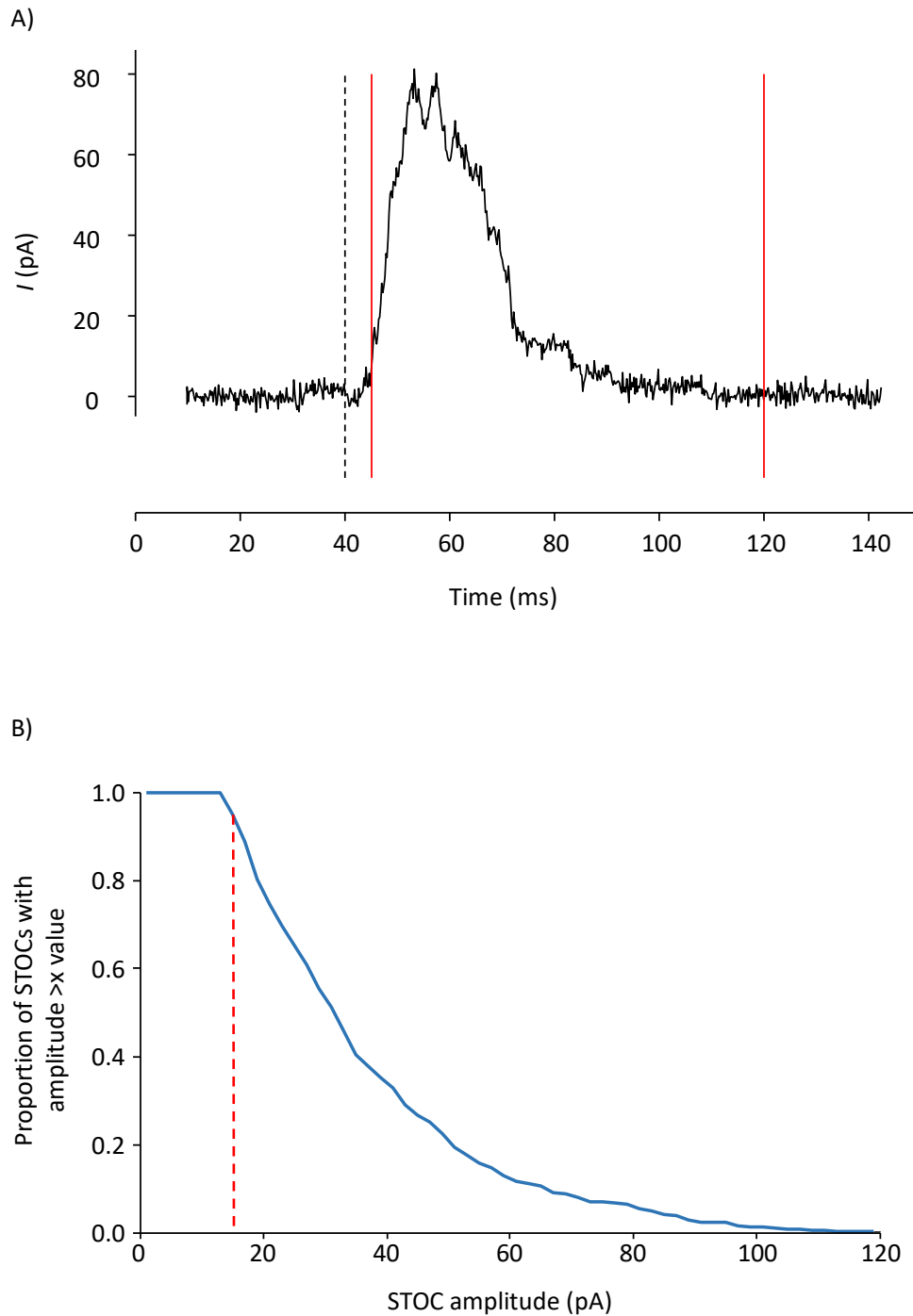


Figure 2.7: Analysis of STOC amplitude. STOC amplitude was calculated for each individual record as the difference between the peak and baseline current. A) Example trace shows that each STOC was aligned to start at 40 ms, (indicated by the dashed line) and STOC amplitude was measured within 75 ms of the beginning of each STOC (indicated by the red lines). B) Example of a cumulative STOC amplitude histogram showing the distribution of STOC amplitudes in a recording. The y-axis is expressed as the proportion of STOCs with amplitude greater than the corresponding STOC amplitude value on the x-axis. The dashed line shows that STOCs with amplitude < 15 pA was ignored.

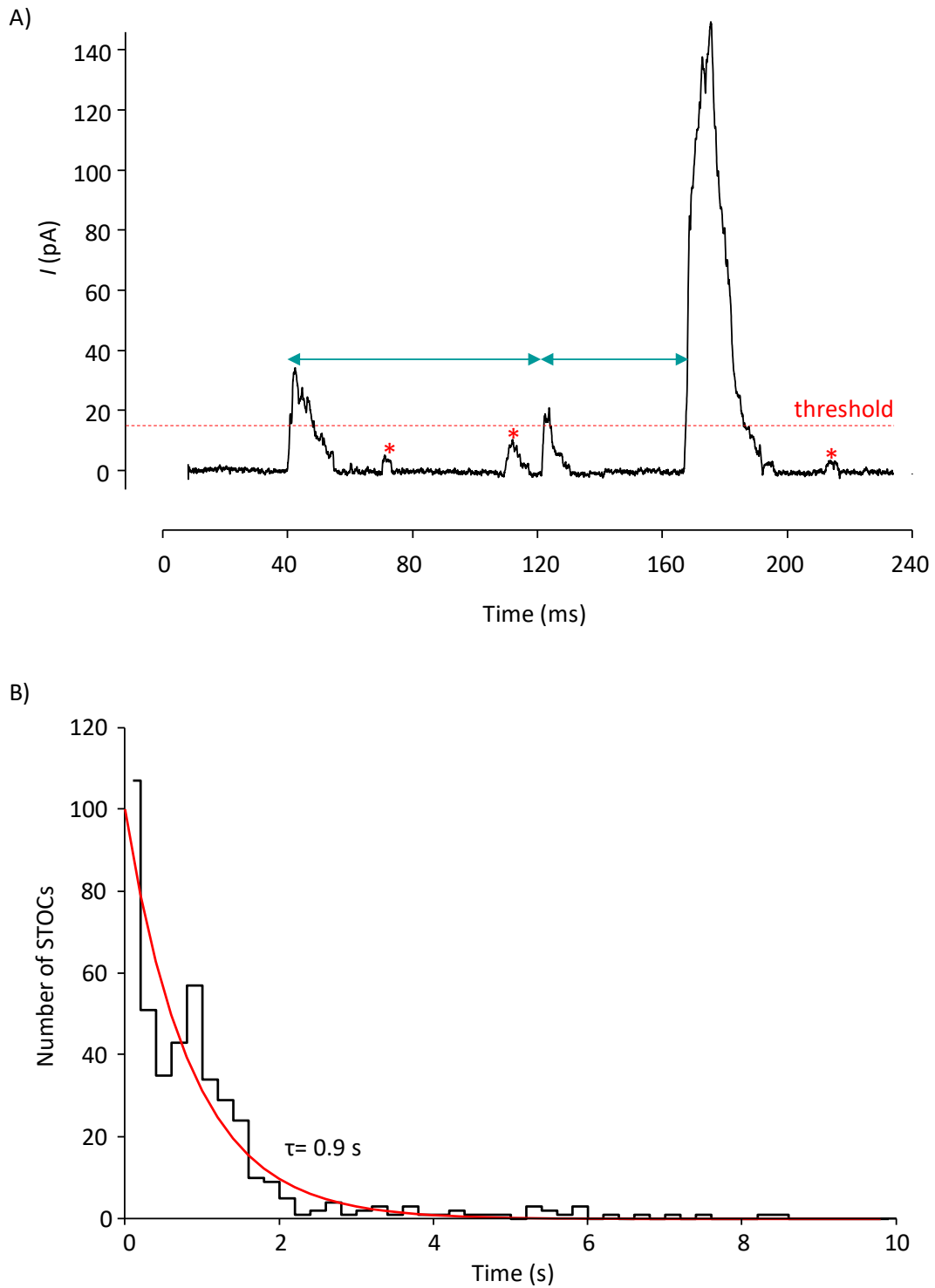


Figure 2.8: Analysis of STOC frequency. A) STOC frequency was calculated as the time between each detected STOC, indicated by the double-head arrows. The dashed line shows that only transients with amplitude ≥ 15 pA were counted as STOCs, thus, the starred transients were ignored. B) Example of STOC frequency distribution histogram showing the distribution of STOC frequency in a recording. The histogram was fitted using an exponential function (red line).

2.6.2.2 Measurement of pulsed BK_{Ca} current size

BK_{Ca} currents were induced by applying 200 ms of depolarising pulses to + 60 mV every 2 s from a holding potential of - 20 mV. The ensemble average of 50 pulses was calculated and the instantaneous component subtracted from the total current leaving the time-dependent component which was analysed (Figure 2.9).

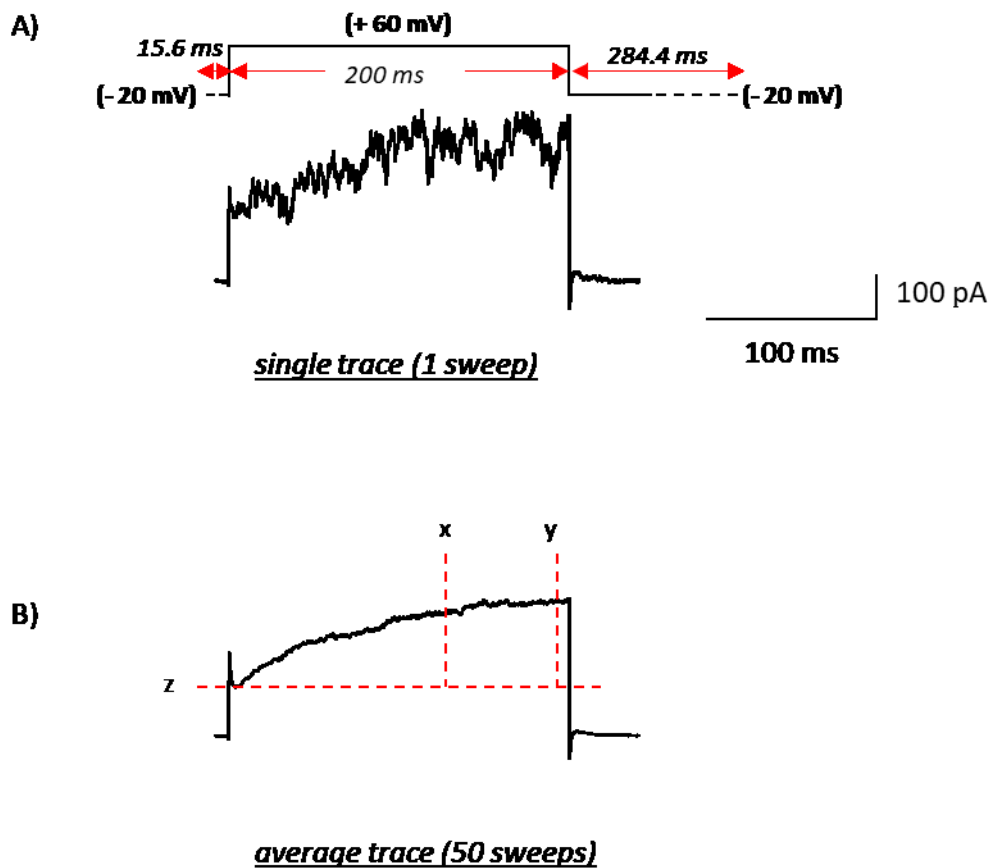


Figure 2.9: Analysis of pulsed BK_{Ca} currents. A) Example trace showing whole-cell BK_{Ca} current induced by a depolarization from - 20 mV to + 60 mV. B) Example ensemble average whole-cell BK_{Ca} current from 50 sweeps. Mean current was calculated between x and y, current at z was subtracted to give the time-dependent amplitude.

2.6.3 Statistics

All data are expressed as mean \pm standard error of the mean (SEM). Unpaired or ratio paired Student's t-tests and one-way analysis of variance (ANOVA) followed by Tukey multiple comparisons tests were performed as appropriate using GraphPad Prism 7 software. Statistical significance was accepted at $p \leq 0.05$.

2.7 Absorption spectrophotometry

Absorption spectrophotometry is a technique used to measure the absorbance and transmission of light by a chemical substance. A beam of light, which is passed through the sample solution, gets absorbed by the chemical compounds in the solution and subsequently transmitted at a specific wavelength.

UV-visible spectrophotometers, which have a light source with wavelength within the ultraviolet and visible range (200 to 700 nm), were used for all spectrophotometric experiments in the current study. Spectrophotometric measurements were made at room temperature either under aerobic conditions using a Perkin Lamda 40 UV-Visible spectrophotometer or anaerobic (glovebox) conditions using a JASCO V630 spectrophotometer.

2.7.1 Haem assays

Here, the procedure for measuring haem concentration in solution is described. In addition, the effects of different experimental conditions such as pH change or presence of reducing agents on haem structure was also investigated, to determine whether alterations in these conditions could influence electrophysiological results.

2.7.1.1 Measurement of haem concentration

Haem concentration in the stock solution was always calculated retrospectively using spectral measurements from diluted stock solutions. This is because the stock solution was too concentrated to be used. The absorption spectrum of haem had a bell-shaped profile with a broad Soret peak at 385 nm (Figure 2.10). Haem absorbance was measured at 385 nm with an extinction coefficient (ϵ) of $58.44 \text{ mM}^{-1}\text{cm}^{-1}$ (Dawson *et al.*, 1975). The Beer-Lambert law (Equation 2.6), which postulates that the concentration of a molecule in solution is directly proportional to its measured absorbance, was used to calculate haem concentration in the diluted stock solution. The haem concentration in the diluted solution was subsequently used to calculate the haem concentration in the stock solution. The stock solution was then used to prepare the final haem solution that was used for experiments.

Equation 2.6 (Beer-Lambert Law):

$$A = l \cdot \epsilon \cdot c$$

Where A = absorbance, l = length of the light path, ϵ = extinction coefficient of the molecule, c = concentration of the solution

The broad peak observed in the haem spectrum (Figure 2.10) suggests that the haem solution used for electrophysiology experiments contained dimeric haem species. This is consistent with the fact that neutral pH solutions were used in this study and haem has been reported to easily form dimers in neutral/basic conditions (Crespo *et al.*, 2010). In addition, monomeric species of haem are known to produce sharper Soret peaks (Asher *et al.*, 2009). Nevertheless, the type of dimeric structure that exists in aqueous solution is still under debate. Some studies suggest that haem exists as a μ -oxo dimer, formed by the association of two ferric haem molecules via an oxygen atom bound to their central Fe^{3+} atom (Asher *et al.*, 2009), see Figure 2.11. Others have suggested a π - π dimer, formed by the association of two ferric haem molecules via π - π interactions (de Villiers *et al.*, 2007), see Figure 2.11.

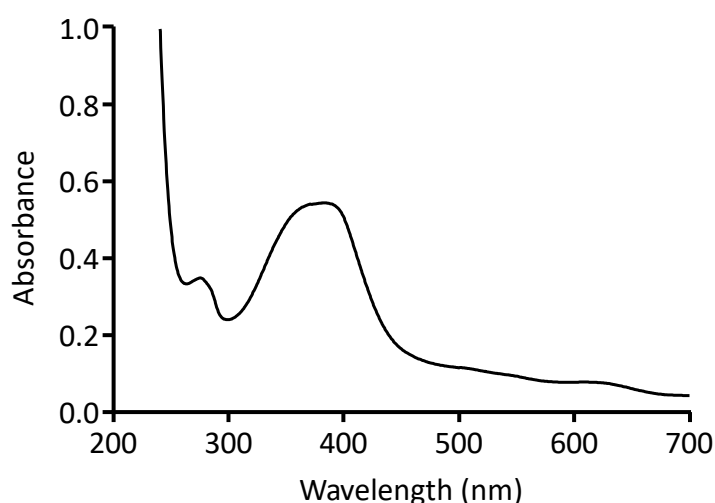


Figure 2.10: UV-visible absorption spectrum of haem. Spectral measurements were made in 0.05 M HEPES solution (pH 7.2). Haem concentration in the cuvette was 9.3 μM , using $\epsilon_{385} = 58.44 \text{ mM}^{-1}\text{cm}^{-1}$ (Dawson *et al.*, 1975).

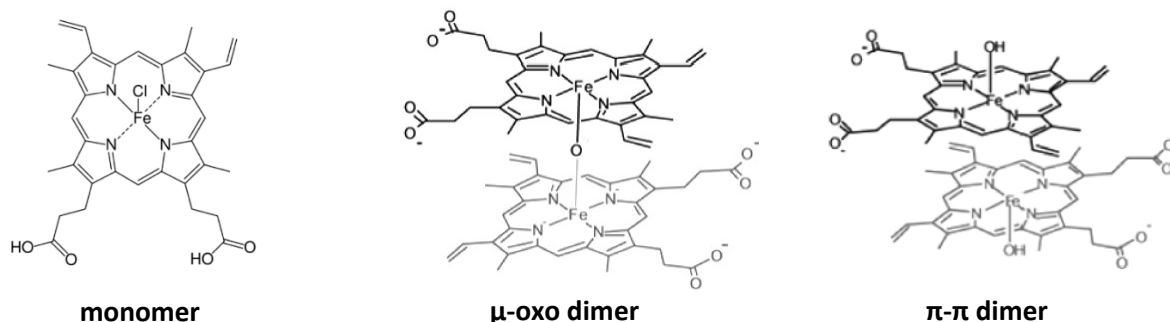


Figure 2.11: Structures of hemin in aqueous solution. Hemin can exist as a monomeric or dimeric (μ -oxo dimer and π - π dimer) species.

2.7.1.2 Effects of pH on haem

i) Effects of pH on haem structure in aqueous solution

Haem structure in aqueous solution has been reported to be influenced by pH and the salt concentration of the solution (de Villiers *et al.*, 2007; Asher *et al.*, 2009). Due to plans to perform electrophysiology experiments with haem at different intracellular pH levels, it was important to examine whether haem structure could be altered by pH changes under the present experimental conditions. Although, it is unclear whether such pH-induced changes in haem structure could interfere with the haem interaction with BK_{Ca} channels. In low pH (pH 2 to 5.5) haem has been reported to exist as a monomer with a high tendency to dimerise in neutral/basic pH conditions (Crespo *et al.*, 2010), c.f. Figure 2.11.

Haem was prepared as detailed previously (see section 2.3.1.1) and the final dilution of stock haem solution for spectrophotometric measurements was prepared in the bath solution used for inside-out patch electrophysiology experiments (see Table 2.1). The pH of the bath solution was set to 6.7, 7.2 and 8.7 to allow the measurement of haem absorbance at acidic, neutral and basic pH levels, respectively. The spectral results showed that at neutral pH, pH 7.2, there was only a single Soret peak at 385 nm, see Figure 2.12. This was inconsistent with observations from a previous study where the Soret band was shown to be resolved to 2 peaks, at 363 nm and 386 nm, in pH 7.0 (Wood *et al.*, 2004). The reason for this discrepancy is unclear, as Wood *et al.* (2004) had also prepared haem in NaOH solution.

In acidic pH, pH 6.7, broadening of the haem absorption spectrum was observed. Q-bands were also seen at 495, 507, 545 and 637 nm. This result is consistent with reports by Wood *et al.* (2004) who also observed a broadening and decrease in the Soret band intensity in acidic pH with Q-bands at similar positions, 495, 517, 550 and 640 nm. At pH 8.7 the absorption spectrum was narrower than seen at pH 6.7, with an additional Q-band at 612 nm (see Figure 2.12). This is consistent with earlier reports where hemin absorbance spectrum was also narrower at basic pH with a distinctive Q-band at 612 nm (Wood *et al.*, 2004; de Villiers *et al.*, 2007; Asher *et al.*, 2009). Furthermore, the expected changes in the Soret band under basic conditions, sharper peak at 386 nm relative to the 363 nm peak, was not observed as there was only a single Soret peak at 385 nm in this study (Wood *et al.*, 2004; de Villiers *et al.*, 2007; Asher *et al.*, 2009).

ii) Implications of the spectral results on my electrophysiology study

In acidic pH, protonation of the carboxyl side chains of haem can occur. This could alter the stacking of haem molecules in solution thereby encouraging the monomeric existence of haem. Also, the electrostatic interaction (e.g. hydrogen bond) between the carboxyl side chains and other charged residues of the protein might be inhibited. Furthermore, the protonation of haem propionate groups can alter haem interaction with proteins via the disruption of hydrophobic (weak) interaction of haem with protein molecules. Therefore, the net effect of haem protonation at low pH will be an unstable protein interaction.

In contrast, at high pH, hydroxide acts as the axial ligand of haem (Kuter *et al.*, 2014). Therefore, the spectral changes seen at alkaline pH might result from the deprotonation of the axial ligand of haem (de Villiers *et al.*, 2007). This could promote a change in haem structure from a π - π dimer to a μ -oxo dimer. This assumption is supported by evidence presented by Egan *et al.* (2009), where rapid transformation of the π - π dimer to μ -oxo dimer was observed in high pH and high salt concentration in aqueous solution.

In conclusion, my results suggest that under the present experimental conditions, the pH changes induced to haem structure are subtle. Therefore, even though changes in intracellular pH might alter haem structure, haem interaction with BK_{Ca} channel under such conditions will predominantly be influenced by the protonation state of key histidine and cysteine residues on the channel protein.

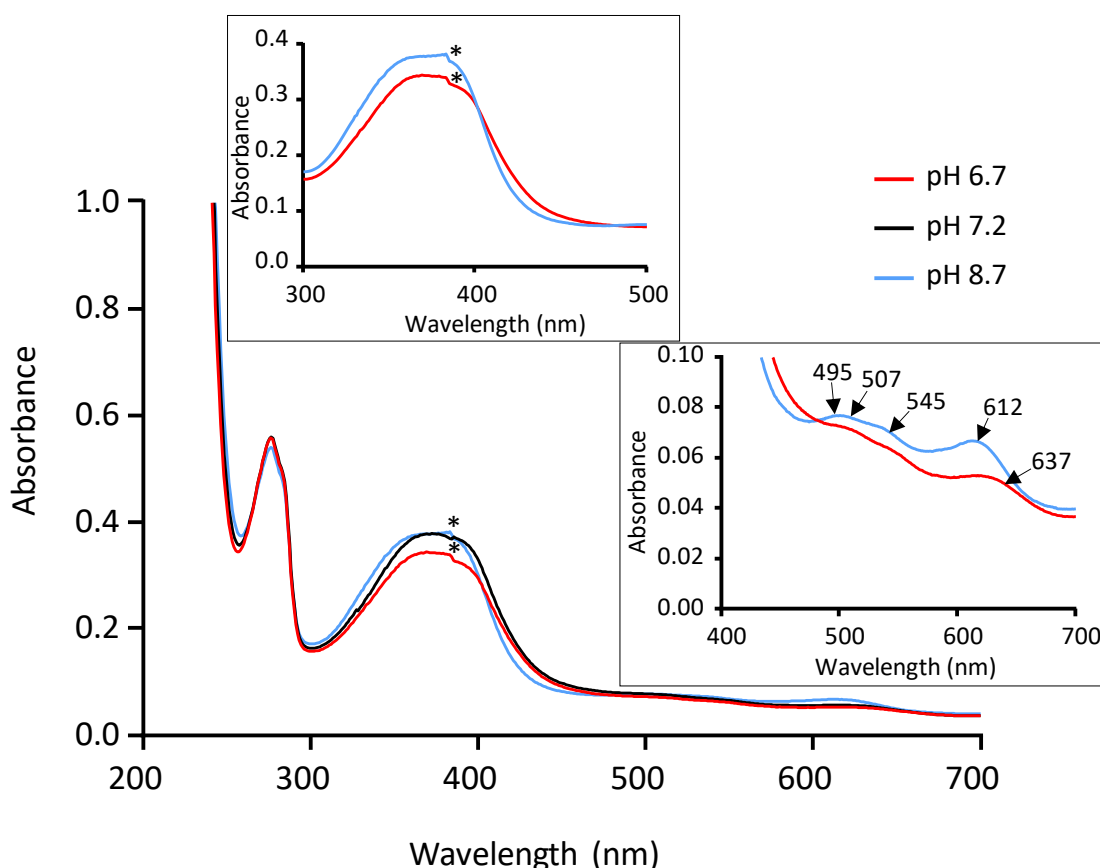


Figure 2.12: UV-visible absorption spectra of haem in aqueous media at pH 6.7, 7.2 and 8.7. Spectral measurements were made in 1 μM Ca^{2+} -containing bath solution used for inside-out patch electrophysiology recordings. Top inset shows spectral changes in the Soret band region. Bottom inset shows spectral changes in the Q-band region. Haem concentration in the cuvette at pH 6.7, 7.2 and 8.7 was 5.6 μM , 6.3 μM and 6.3 μM , respectively, using $\epsilon_{385} = 58.44 \text{ mM}^{-1}\text{cm}^{-1}$. (* indicates technical artefact from the absorption spectrophotometer).

2.7.1.3 Effects of reducing agents on haem

Cells have a dynamic redox environment which can be further altered by intracellular changes like oxidative stress (Ragsdale & Yi, 2011). Therefore, intracellular thiol/disulfide systems such as glutathione and cysteine exist to regulate the redox environment within cells.

Evidence suggest that haem interaction with BK_{Ca} channels can be regulated by a reversible thiol/disulfide redox switch, formed by the two cysteine residues in the highly conserved CXXCH motif located in its haem binding domain (HBD) (Yi *et al.*, 2010). Under

normoxic conditions, the HBD exists in a disulfide state (-SS) but reverts to a thiol state (-RSH) in hypoxic conditions. BK_{Ca} channels have been shown to bind haem more tightly ($K_d = 210$ nM) in the reduced thiolate state than in the oxidised disulfide state (Yi *et al.*, 2010).

There were plans to investigate haem interaction with BK_{Ca} channels and the effects of cellular redox conditions on such interaction using the inside-out and ruptured whole-cell patch techniques, respectively. However, the lack and wash of essential intracellular milieu with the inside-out and ruptured patch techniques respectively, could result in the absence of the thiol/disulfide systems. Therefore, it was necessary to examine whether exogenous reducing agents could be used to perform such electrophysiology experiments. In the past, a range of reducing agents have been used to reduce proteins. These include; glutathione (GSH), ascorbic acid (H₂A), dithioerythritol (DTE), dithiothreitol (DTT), tris(2-carboxyethyl) phosphine (TCEP) and sodium dithionite (Na₂S₂O₄) which have different reducing abilities (see Figure 2.13 and Table 2.3). The suitability of the reducing agents for use in electrophysiology experiments was determined by investigating their ability to reduce heme Fe³⁺-iron. Their ability to reduce protein disulphide bonds or maintain R-SH groups (as reported by other studies) was only discussed and not examined. The bath solution used for inside-out patch recordings (see Table 2.1), containing 0.003 mM CaCl₂ (at pH 7.2), was used to prepare the reducing agents.

This study primarily focuses on changes in the Soret band because reduction of the heme ferric iron is reflected in the π - π^* transitions. In the absence of heme, the reducing agents did not produce absorbance within the Soret band region (300 - 400 nm), except Na₂S₂O₄ which had a characteristic band at 314 nm (Figure 2.14). The absorbance between 250 - 300 nm wavelength in bath solution solvents could indicate the formation of EGTA-Ca²⁺ complex, as previously reported (Tsien, 1980), because this peak was absent in distilled water (dH₂O).

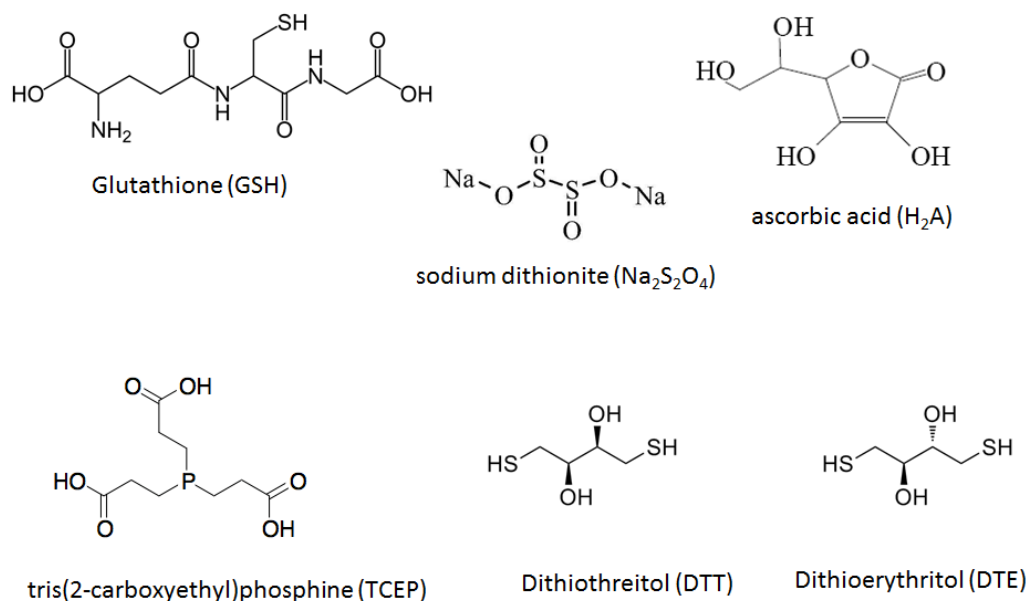


Figure 2.13: Chemical structure of different reducing agents.

| Reducing agent | Reduction potential (volts) |
|-----------------------------------|--|
| H_2A | - 0.066 (Borsook & Keighley, 1933) |
| TCEP | - 0.29 (Dergousova <i>et al.</i> , 2017) |
| DTT | - 0.33 (Cleland, 1964) |
| DTE | - 0.33 (Cleland, 1964) |
| GSH | - 0.35 to + 0.04 (Rost & Rapoport, 1964) |
| $\text{Na}_2\text{S}_2\text{O}_4$ | - 0.66 (Mayhew, 1978) |

Table 2.3: Reducing agents and their reduction potentials. All measurements were made at pH 7. The reducing agents with more negative reduction potentials are stronger than those with more positive potentials.

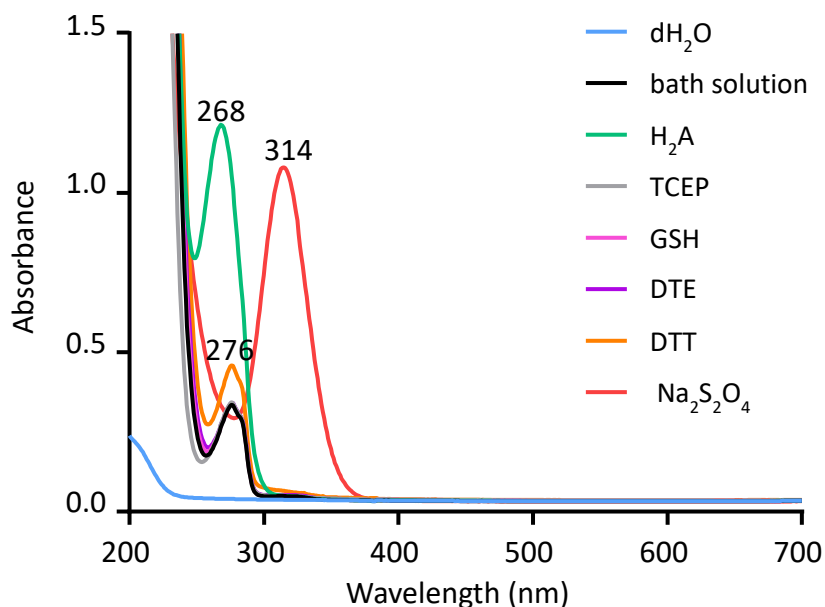


Figure 2.14: UV-visible absorption spectra of distilled water (dH₂O) and reducing agents prepared in bath solution. The concentration of each reducing agent in the cuvette was ~ 2 mM.

2.7.1.3.1 Natural-occurring reducing agents

2.7.1.3.1.1 Glutathione and haem

The first choice of reducing agent was glutathione as it is abundantly expressed in living organisms with intracellular concentrations ranging between 0.5 to 10 mM, depending on the cell type (Maher, 2005; Ji *et al.*, 1992). The ability of GSH to maintain the R-SH group of proteins in a reduced state enables it to play important roles in maintaining the reduced environment in cells (Soh *et al.*, 2001; Dringen, 2000). Most of the glutathione in cells exist in a reduced form (GSH) with the oxidised form (GSSG) kept at low concentrations by GSH regenerating systems (Soh *et al.*, 2001).

Therefore, the physiological properties of GSH made it attractive for use as a reducing agent in the present study. However, GSH has been reported to have a direct degradative effect on haem which is optimal at pH 7 (the pH at which electrophysiology experiments are performed) (Atamna & Ginsburg, 1995; Kumar & Bandyopadhyay, 2005). Different assays were performed to confirm the degradative effect of GSH on haem and the implications it might have on electrophysiology studies.

i) Effects of 2 mM GSH on haem absorbance

Haem was prepared in 2 mM GSH solutions and the time course of haem absorbance was observed using absorption spectroscopy. The absorbance peak of the haem-GSH mixture was sharper than the absorbance peak for only haem (Soret band at 385 nm, extinction coefficient (ϵ) = 58.44 mM⁻¹ cm⁻¹), see Figure 2.15. Furthermore, haem absorbance in the presence of GSH decreased over time and significantly flattened in 2 hours. The decrease in haem absorbance is indicative of haem degradation, as absorbance is directly proportional to concentration (see Equation 2.6, Beer-Lambert law). The kinetics of haem degradation was determined by measuring the absorbance value at 385 nm as a function of time, see inset in Figure 2.15.

The changes observed in the Soret band are similar to the changes that occur in acidic pH, characterised by a narrow Soret band around 363 nm (Crespo *et al.*, 2010). Thus, the addition of GSH may have acidified the solution. Furthermore, the spectral changes could indicate a change in haem structure resulting from the coordination of the thiol (-RSH) group of GSH to the haem iron. These results corroborate with previous findings, as haem degradation was reported to occur in the presence of GSH (Atamna & Ginsburg, 1995). However, GSH might merely be expediting haem degradation via its alteration of the solution pH, as haem also displays a time-dependent degradation (see Figure 2.16). The degradation observed in haem only solutions could have resulted from several factors including, haem adsorption onto the glass surface of the cuvette over time or haem oxidation and photodegradation (Han *et al.*, 2005; de Villiers *et al.*, 2007).

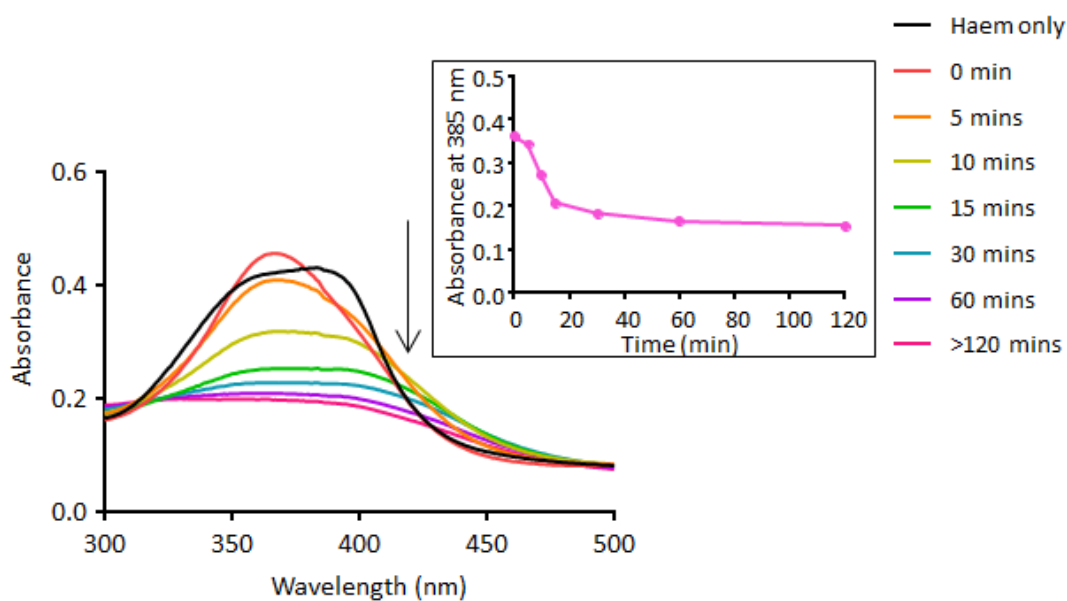


Figure 2.15: Representative UV-visible absorption spectra of haem showing its degradation over time in the presence and absence of GSH (2 mM). All solutions were prepared in 3 μM Ca^{2+} -containing bath solutions at pH 7.2. The absorption spectrum of the initial haem-GSH mixture is shown at “0 min”. The arrow and inset show the time-dependent decrease in haem absorbance. Initial [haem] in the cuvette was $\sim 6 \mu\text{M}$ ($\epsilon_{385} = 58.44 \text{ mM}^{-1}\text{cm}^{-1}$)

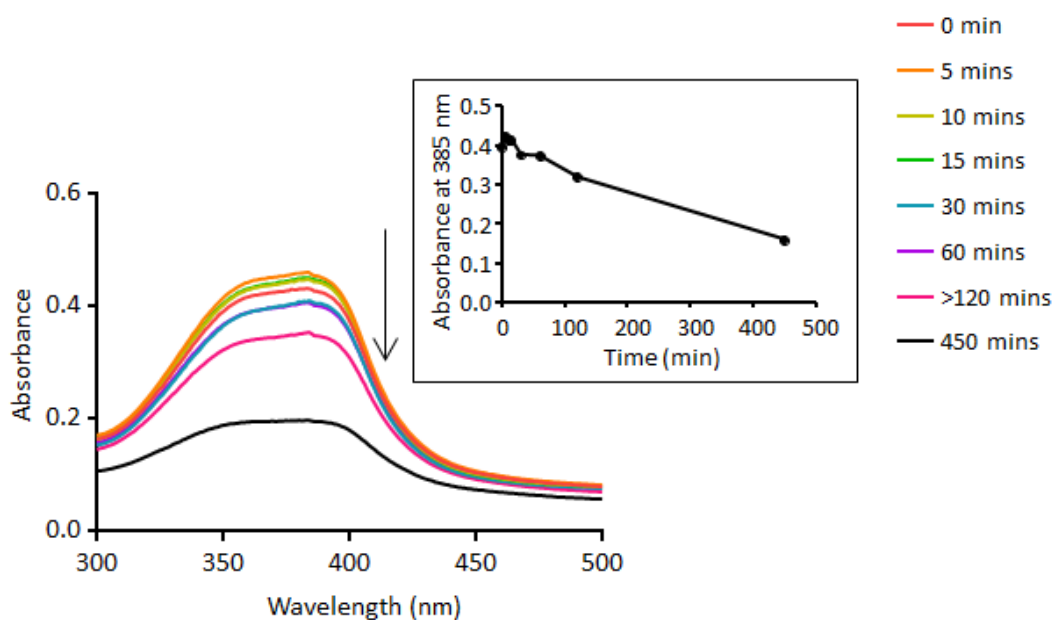


Figure 2.16: Representative UV-visible absorption spectra showing haem degradation over time. Haem solution was prepared in 3 μM Ca^{2+} -free bath solutions at pH 7.2. The arrow and inset show the time-dependent decrease in haem absorbance. Initial [haem] in the cuvette was $\sim 6 \mu\text{M}$.

ii) Effects of 50 μM GSH on haem absorbance

Further investigations were performed to determine whether GSH mediated a concentration-dependent degradative effect on haem. Thus, low concentration, 50 μM , of GSH was used. The results show that in 50 μM GSH, haem degradation occurs relatively slower and is less compared with observations made in 2 mM GSH (Figure 2.17).

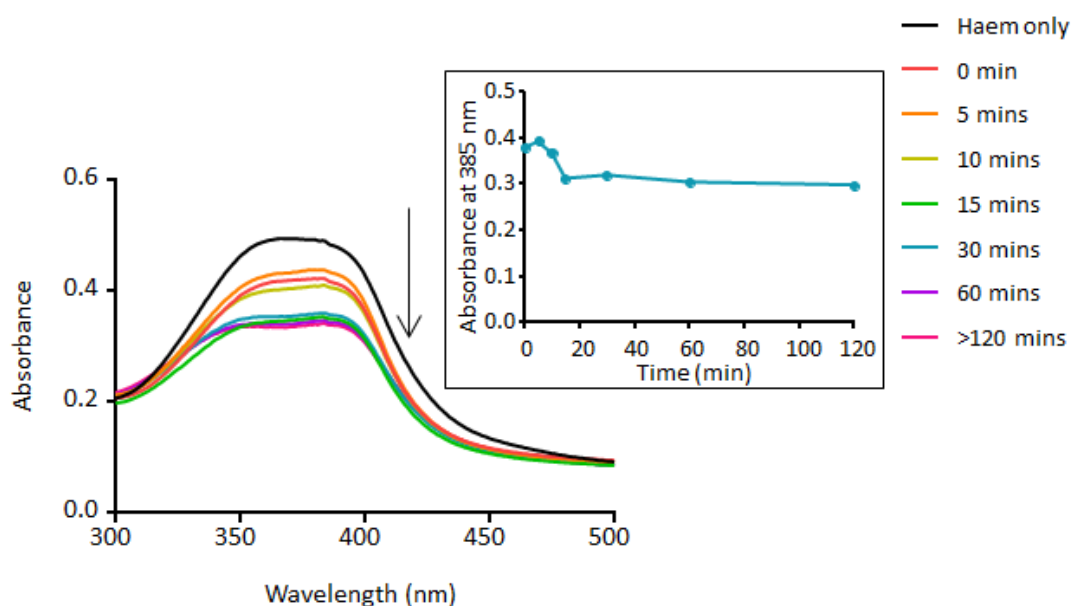


Figure 2.17: Representative UV-visible absorption spectra of haem showing its degradation over time in lower GSH concentration (50 μM). GSH was prepared in 3 μM Ca^{2+} -free bath solutions at pH 7.2. The absorption spectrum of the initial haem-GSH mixture is shown at “0 min”. The arrow and inset show the time-dependent decrease in haem absorbance. Initial [haem] in the cuvette was $\sim 6 \mu\text{M}$.

iii) Effects of oxidised glutathione (GSSG) on haem absorbance

The role of the glutathione redox state in its haem-mediated degradation was also explored. Experiments were performed using oxidised glutathione (GSSG). The results show a shift in the Soret band from 385 nm to ~ 363 nm which typically occurs in acidic pH (Wood *et al.*, 2004). Furthermore, haem degradation was delayed and the decrease in absorbance was only evident after 30 minutes of preparing the haem-GSSG solution (Figure 2.18).

The stability of haem absorbance within the first 30 minutes of spectral measurements could have resulted from a less acidic pH in GSSG compared with GSH. Thus, it is possible that the alteration of haem structure in GSSG solution would have been less severe than in GSH. Nevertheless, it is unclear why haem absorbance in GSSG solution decreased with time. Perhaps, this could be attributable to the natural degradation of haem.

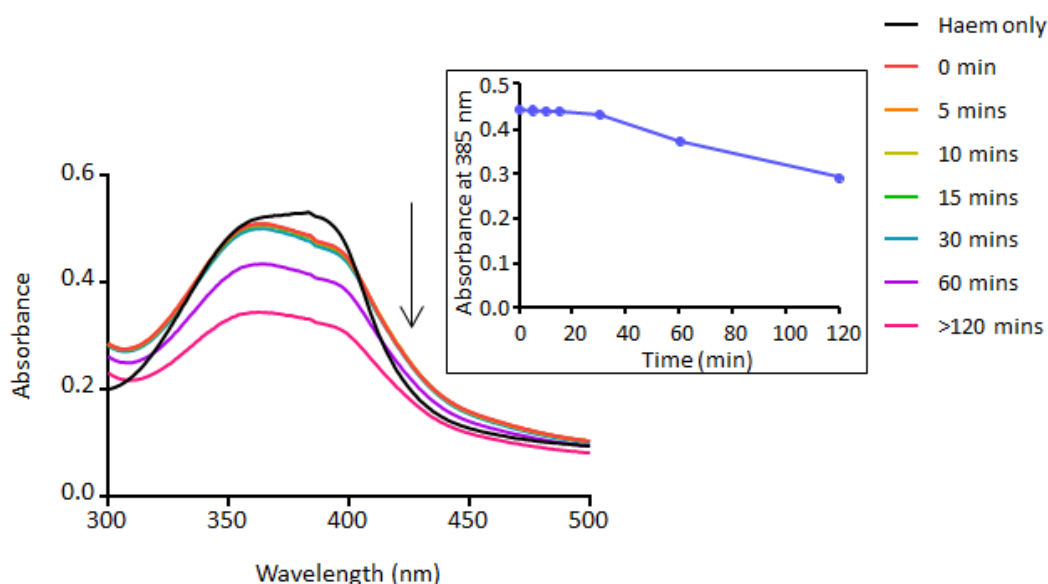


Figure 2.18: Representative UV-visible absorption spectra of haem showing its degradation over time in the presence of GSSG (2 mM). GSSG was prepared in 3 μM Ca^{2+} -free bath solutions at pH 7.2. The absorption spectrum of the initial haem-GSSG mixture is shown at “0 min”, The arrow and inset show the time-dependent decrease in haem absorbance. Initial [haem] in the cuvette was $\sim 7 \mu\text{M}$.

iv) Effects of 2 mM GSH on haem absorbance under anaerobic conditions

Electrophysiology experiments are performed under aerobic conditions because cells require oxygen (O_2) for survival. Thus, the oxygen-dependence of GSH-mediated haem degradation was explored by performing experiments with GSH (2 mM) under anaerobic conditions created by a glove box.

For these set of experiments, the GSH (2 mM) solution was bubbled with nitrogen (N_2) gas and de-gassed for ~ 2 hours in a glove box, to remove O_2 from the solution. Haem was then added to the de-gassed solution. Time-course experiments were subsequently performed as previously shown. The results (Figure 2.19) were identical to those seen with GSH and haem under aerobic conditions (see Figure 2.15), as a shaper Soret peak

was observed. In addition, haem degradation was also evident albeit slower than observed under aerobic conditions (see Figures 2.15). This suggests that the GSH-induced degradation of haem is oxygen-independent but might be accelerated by oxygen.

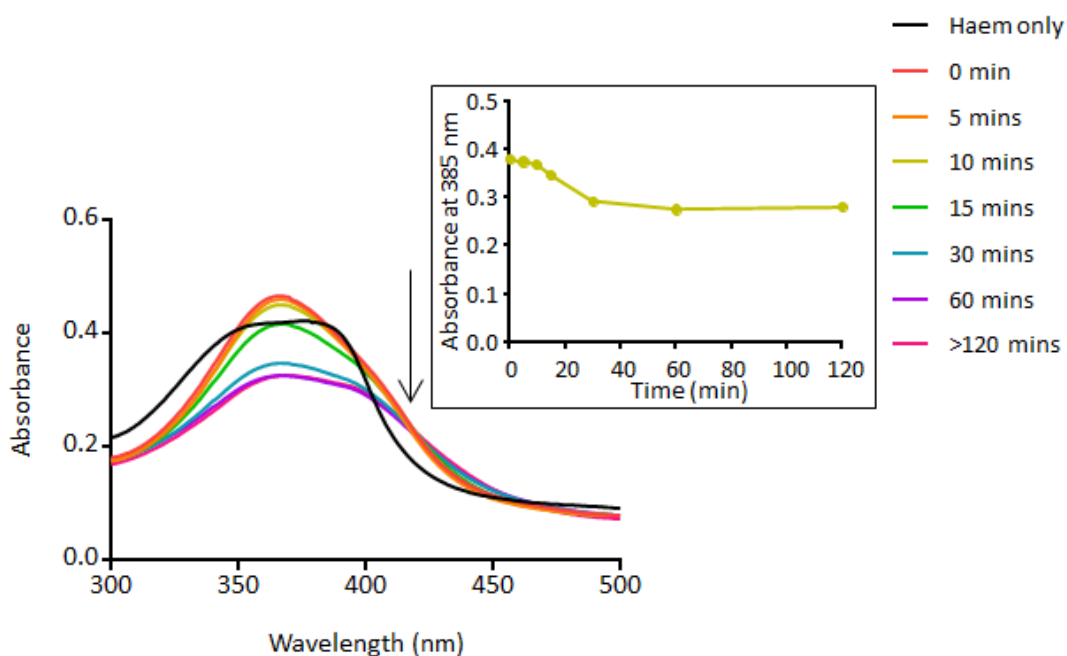


Figure 2.19: Representative UV-visible absorption spectra of haem showing its degradation over time in the presence of GSH (2 mM), under anaerobic conditions. GSH was prepared in 3 μM Ca^{2+} -free bath solutions at pH 7.2, under anaerobic conditions. The absorption spectrum of the initial haem-GSH mixture is shown by the “0 min” spectrum. The “haem only” spectrum was generated under aerobic conditions. The arrow and inset show the time-dependent decrease in haem absorbance. Initial [haem] in the cuvette was $\sim 6 \mu\text{M}$.

v) Summary of the effects of glutathione on haem absorbance

In summary, spectroscopic results indicate that GSH can only be used in electrophysiology experiments involving haem provided that the experiments are completed within 5 to 10 minutes after the preparation of the haem-GSH solution, but this time frame is impractical. Also, the degradative effect of GSH on haem could complicate result interpretation as there would be some uncertainty about whether results are due to haem or its degradation products. The identity of the degradation products was not further explored as it is beyond the scope of the current study. Nevertheless, GSH might still be useful for reducing BK_{Ca} channel disulfide bonds as it

has previously been reported to be useful for the reduction of disulfide bonds (Linke & Jakob, 2003; Cumming *et al.*, 2004; Chakravarthi *et al.*, 2006).

2.7.1.3.1.2 Ascorbic acid and haem

L-ascorbic acid (H_2A) was the next choice of reducing agent as it also exists as a physiological reductant in plants and animals. H_2A readily dismutates into ascorbate (AH^-) which is the dominant form of the reductant at physiological pH (Du *et al.*, 2012).

Ascorbate plays a crucial role in maintaining iron in the ferrous (Fe^{2+}) state (Englard & Seifter, 1986). This has been demonstrated by its ability to reduce ferrylmyoglobin, a powerful pro-oxidant, via the reduction of its haem iron (Giulivi & Cadenas, 1993). Furthermore, ascorbate has a lower redox potential, - 0.066 V (see Table 2.3) than the redox pair Fe^{3+}/Fe^{2+} , + 0.77V (Straub *et al.*, 2001). Therefore, ascorbate should theoretically be able to reduce ferric (Fe^{3+}) haem to ferrous (Fe^{2+}) haem in the present study.

i) Effects of 2 mM ascorbate on haem absorbance under aerobic and anaerobic conditions

The concentration of ascorbate, 2 mM, used for assays was significantly higher than physiological levels (40 - 80 μM) in the plasma of healthy humans (Du *et al.*, 2012). Nevertheless, in the presence of ascorbate, under aerobic and anaerobic conditions, there was no indication of ferric haem reduction (Figures 2.20 & 2.21). However, haem appeared to degrade over time in the presence of ascorbate under aerobic conditions (Figure 2.20).

The inability of ascorbate to reduce ferric haem under the present conditions could result from several factors, including the oxidation of ascorbate under aerobic conditions which could impinge on its reducing ability (Du *et al.*, 2012). However, this does not account for its inability to reduce haem under anaerobic conditions albeit degradation was less evident (Figure 2.21). Ascorbate is a mild reducing agent (c.f. Table 2.3), thus, a mediator (such as methylene blue or hexamine ruthenium) might be required to enhance its reducing ability under the present experimental conditions.

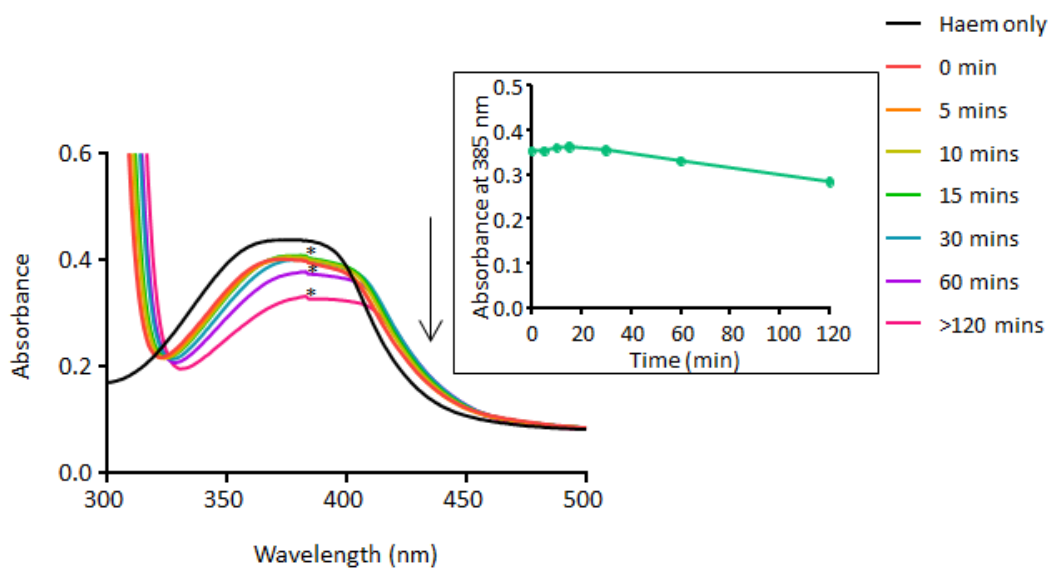


Figure 2.20: Representative UV-visible absorption spectra of haem showing its degradation over time in the presence of ascorbate (2 mM) under aerobic conditions. Ascorbate solution was prepared in 3 μM Ca^{2+} -containing bath solutions at pH 7.2. The absorption spectrum of the initial haem-ascorbate mixture is shown by the “0 min” spectrum. The arrow and inset show the time-dependent decrease in haem absorbance. Initial [haem] in the cuvette was $\sim 6 \mu\text{M}$. (* indicates technical artefact from the absorption spectrometer).

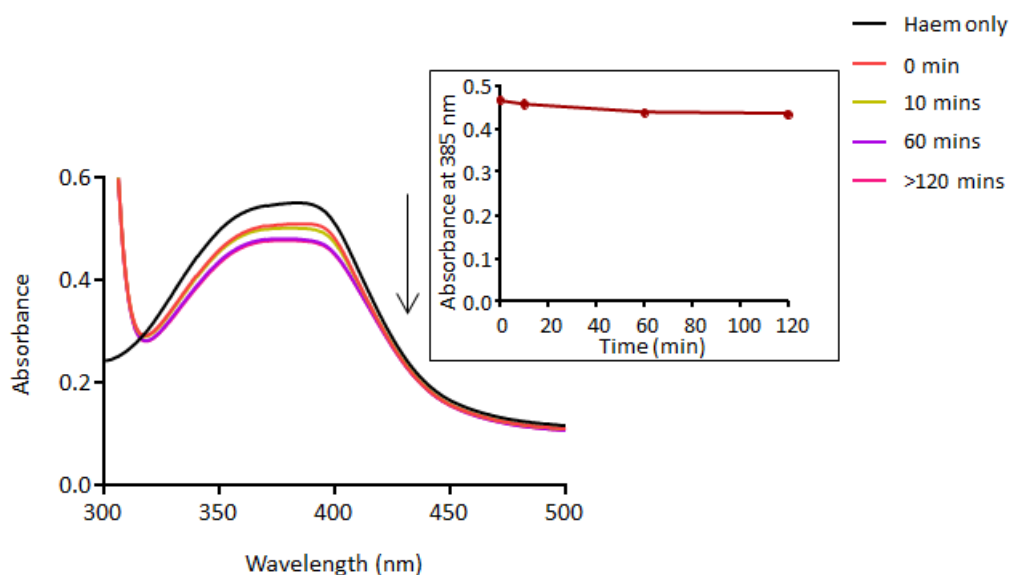


Figure 2.21: Representative UV-visible absorption spectra of haem showing its degradation over time in the presence of ascorbate (2 mM) under anaerobic conditions. Ascorbate solution was prepared in 3 μM Ca^{2+} -containing bath solutions at pH 7.2. The absorption spectrum of the initial haem-ascorbate mixture is shown by the “0 min” spectrum. The “haem only” spectrum was generated under aerobic conditions. The arrow and inset show the time-dependent decrease in haem absorbance. Initial [haem] in the cuvette was $\sim 8 \mu\text{M}$.

ii) Summary of the effects of ascorbate on haem absorbance

In summary, the spectroscopic results indicate that ascorbate might be unsuitable for the reduction of haem in the present study. Although, haem degradation observed in the presence of ascorbate was negligible compared with results from GSH studies. Ascorbate could still be useful for the reduction of BK_{Ca} channel disulfide bonds, as previous studies have demonstrated its ability to reduce protein disulfides (Landino *et al.*, 2006; Giustarini *et al.*, 2008).

2.7.1.3.2 Synthetic reducing agents

So far, the spectral results demonstrate that natural reducing agents have a degradative effect on haem with intense degradation observed in GSH. Also, the naturally-occurring reductants do not appear to reduce ferric haem, as the distinctive red-shift of the Soret band which indicates haem reduction was not observed. Therefore, attention shifted to the use of artificial reductants.

2.7.1.3.2.1 DTE and haem

Dithioerythritol (DTE), an isomer of dithiothreitol (DTT), is a thiol reductant which has been shown to be useful for reducing disulfide bonds in proteins (Santarino *et al.*, 2012; Cleland, 1964).

i) Effects of 2 mM DTE on haem absorbance

In the presence of DTE (2 mM), haem absorbance rapidly decreased such that after 2 hours haem concentration in solution was in trace amounts (Figure 2.22). A sharper Soret band around 363 nm which can occur in acidic pH was also noticed (Wood *et al.*, 2004). Like observations made in the presence of GSH, the Soret band change suggests protonation of haem molecules. This might have occurred via the interaction of the DTE thiol (-RSH) group with the central haem iron. The pH reduction induced by DTE might have increased the rate of haem degradation. In addition, a group has reported that the dithiol groups of DTE can readily undergo oxidation thereby making DTE unstable (Domkin & Chabes, 2014). Therefore, autooxidation of the dithiol groups of DTE might have also occurred such that DTE was unable to reduce haem.

ii) Summary of the effects of 2 mM DTE on haem absorbance

In summary, the results suggest that DTE cannot be used as a reductant in electrophysiology experiments because in its presence the amount of haem available to perform experiments is significantly less. However, the results from previous studies suggest that DTE might be useful for reducing BK_{Ca} channel disulfide bonds (Cleland, 1964; Cline *et al.*, 2004).

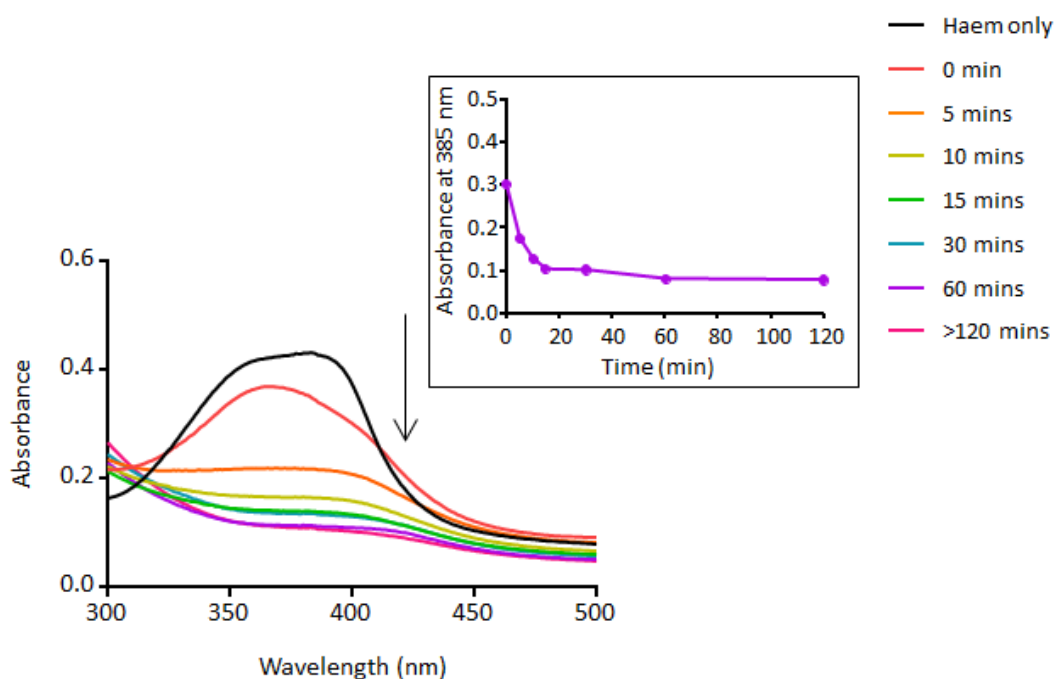


Figure 2.22: Representative UV-visible absorption spectra of haem showing its degradation over time in the presence of DTE (2 mM). DTE solution was prepared in 3 μM Ca^{2+} -containing bath solutions at pH 7.2. The absorption spectrum of the initial haem-DTE mixture is shown by the “0 min” spectrum. The arrow and inset show the time-dependent decrease in haem absorbance. Initial [haem] in the cuvette was $\sim 7 \mu\text{M}$.

2.7.1.3.2.2 DTT and haem

DTT is a thiol reductant that is commonly used to reduce disulfide bonds in proteins (Getz *et al.*, 1999; Berman & Awayda, 2013; Cleland, 1964). Solutions of reduced DTT are more stable to air oxidation than glutathione solutions (Cleland, 1964). Interestingly, DTT has been reported to chelate ferrous iron (Fe^{2+}) (Franco *et al.*, 1995). Nevertheless, its suitability for use in the reduction of Fe^{3+} -haem in the present study was examined.

i) Effects of 2 mM DTT on haem absorbance

In the presence of DTT (2 mM) a sharper Soret band around 363 nm and rapid decline in haem absorbance over time were observed (Figure 2.23). This was similar to observations from the DTE assay.

Therefore, as with DTE, the results indicate that DTT is unsuitable for use in electrophysiology experiments involving haem, due to its rapid degradative effect on haem. There is presently no evidence of the reduction of ferric haem iron (Fe^{3+}) by DTT, even though a previous study reportedly used it to reduce haem (Jaggar *et al.*, 2005). Nevertheless, DTT has been used to reduce the cysteine residues in the haem regulatory motif (HRM) of wild-type haem oxygenase-2 (HO-2) (Yi & Ragsdale, 2007). This suggests that DTT might be useful for reducing BK_{Ca} channel disulfide bonds in the present study, but its use is limited because of its degradative effect on haem.

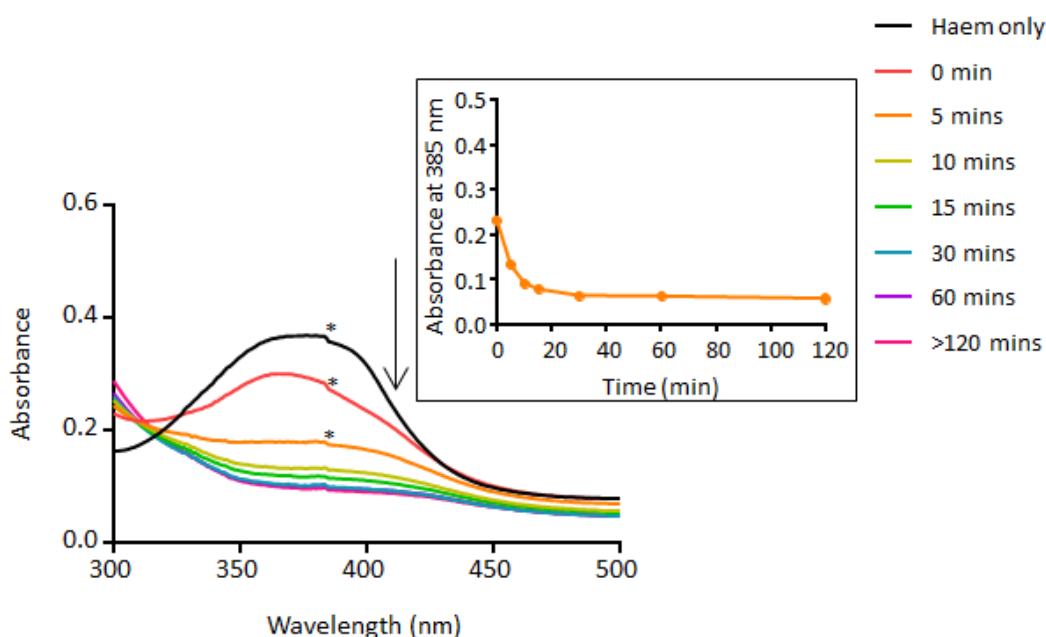


Figure 2.23: Representative UV-visible absorption spectra of haem showing its degradation over time in the presence of DTT (2 mM). DTT solution was prepared in $1 \mu\text{M}$ Ca^{2+} -containing bath solutions at pH 7.2. The absorption spectrum of the initial haem-DTT mixture is shown by the “0 min” spectrum. The arrow and inset show the time-dependent decrease in haem absorbance. Initial [haem] in the cuvette was $\sim 6 \mu\text{M}$. (* indicates technical artefact from the absorption spectrometer).

2.7.1.3.2.3 TCEP and haem

TCEP, a water-soluble phosphine with a high selectivity for reducing disulfide bonds, is often used for the maintenance of free sulfhydryl (R-SH) groups in proteins (Burns *et al.*, 1991; Liu *et al.*, 2010; van den Akker *et al.*, 2011). It is mostly preferred over other reducing agents due to the advantages it offers including its ability to effectively and irreversibly reduce disulfide bonds (Getz *et al.*, 1999; Winther & Thorpe, 2014), its high stability in aqueous solutions (Tzanavaras *et al.*, 2012) and ability to work effectively over a wide pH range, 1.5 to 8.5 (Getz *et al.*, 1999). However, the stability of TCEP can be negatively affected by the presence of phosphates and metal chelators, such as EGTA, which catalyse TCEP oxidation (Getz *et al.*, 1999).

i) Effects of 2 mM TCEP on haem absorbance

In the presence of TCEP (2 mM) the Soret band appeared to split into multiple peaks with absorbance barely decreasing over time (Figure 2.24). This suggests that TCEP produced negligible degradative effect on haem. However, TCEP may have altered the structure of haem because splitting of the Soret band has been reported to be a unique characteristic of hyperporphyrin spectrum (Sono *et al.*, 1984). Bisthiolation of ferric haem has been reported to result in a hyperporphyrin spectrum but this is unlikely to be the case with TCEP, since it is not a thiol reducing agent. Thus, the reason for the hyperporphyrin spectrum in the presence of TCEP is unclear.

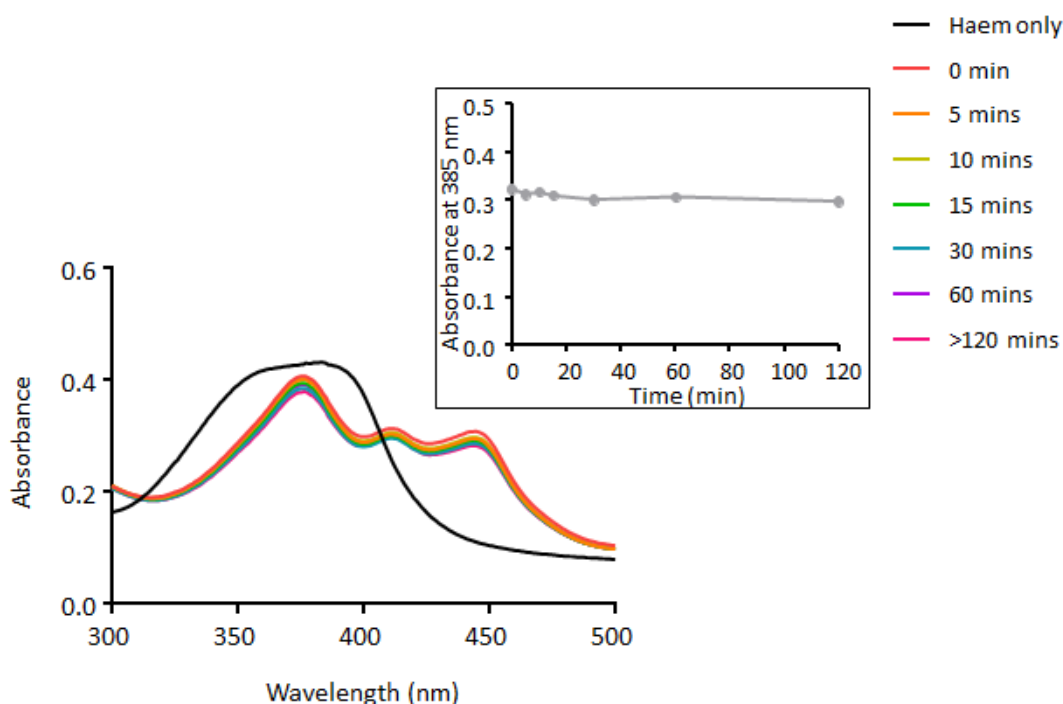


Figure 2.24: Representative UV-visible absorption spectra of haem in the presence of TCEP (2 mM). TCEP solution was prepared in 3 μM Ca^{2+} -containing bath solutions at pH 7.2. The absorption spectrum of the initial haem-TCEP mixture is shown by the “0 min” spectrum. The Soret band was split into distinct peaks in the presence of TCEP. The inset shows the time-dependent decrease in haem absorbance. Initial [haem] in the cuvette was $\sim 7 \mu\text{M}$.

TCEP is known to be useful for irreversibly reducing disulfide bonds (Getz *et al.*, 1999). This suggests that it can also be used to irreversibly reduce BK_{Ca} channels. However, the over-exposure (hours to weeks) of cysteine-containing proteins (such as BK_{Ca} channels) to TCEP could lead to protein cleavage by a side reaction, via an unidentified mechanism (Liu *et al.*, 2010).

ii) Summary of the effects of TCEP on haem absorbance

Spectroscopic results suggest that TCEP might not be a suitable reductant for use in electrophysiology experiments as its effect on haem is not clearly understood. In addition, there is a high possibility that TCEP will be unstable under electrophysiology conditions since EGTA is used as a metal chelator in electrophysiology solutions. However, TCEP might still be useful for reducing BK_{Ca} channel disulfide bonds provided its interaction with the protein channel does not prevent haem binding.

2.7.1.3.2.4 Na₂S₂O₄ and haem

Na₂S₂O₄ is a well-known reducing agent that has often been used to reduce ferric haem (Tang *et al.*, 2003; Jaggar *et al.*, 2005; Sahoo *et al.*, 2013). Na₂S₂O₄ has also been reported to be useful for the reduction of disulfide bonds in proteins (Lundbald, 2014). Therefore, it seemed plausible to speculate that Na₂S₂O₄ might be useful for performing a dual role (reducing ferric haem and BK_{Ca} channel disulfide bonds) during electrophysiology experiments. Na₂S₂O₄ is a strong reducing agent which reacts rapidly with oxygen to become oxidised. Therefore, Na₂S₂O₄ solution was prepared under anaerobic conditions. Time course experiments were commenced under anaerobic conditions but completed in aerobic conditions.

i) Effects of Na₂S₂O₄ on haem absorbance

When haem was added to 2 mM Na₂S₂O₄ solution, two distinct peaks were observed, the peak at 314 nm represented Na₂S₂O₄ absorbance whilst the Soret band at 385 nm represented haem absorbance. Interestingly, a shoulder peak was also noticed at ~ 410 nm (Figure 2.25). The spectral results show that haem degradation is negligible in the presence of Na₂S₂O₄ but it is unclear whether the shoulder peak at 410 nm indicates a haem reduction. This is because Na₂S₂O₄ depletion occurred over time, shown by the loss of the 314 nm absorbance peak in Figure 2.25; thus, oxygen ligation to ferrous iron could also account for the change in the haem absorption spectra.

ii) Summary/conclusion of the effects of Na₂S₂O₄ on haem absorbance

Spectroscopic results from Na₂S₂O₄ assays look promising as it suggests that Na₂S₂O₄ reduces haem with negligible degradative effect. However, Na₂S₂O₄ would be unsuitable for use in electrophysiology study as experiments are usually performed under aerobic conditions and Na₂S₂O₄ degradation appears to be accelerated by O₂. Furthermore, it is possible that the strong reducing ability of Na₂S₂O₄ (which enables it to reduce other membrane proteins) might complicate the interpretation of electrophysiology results.

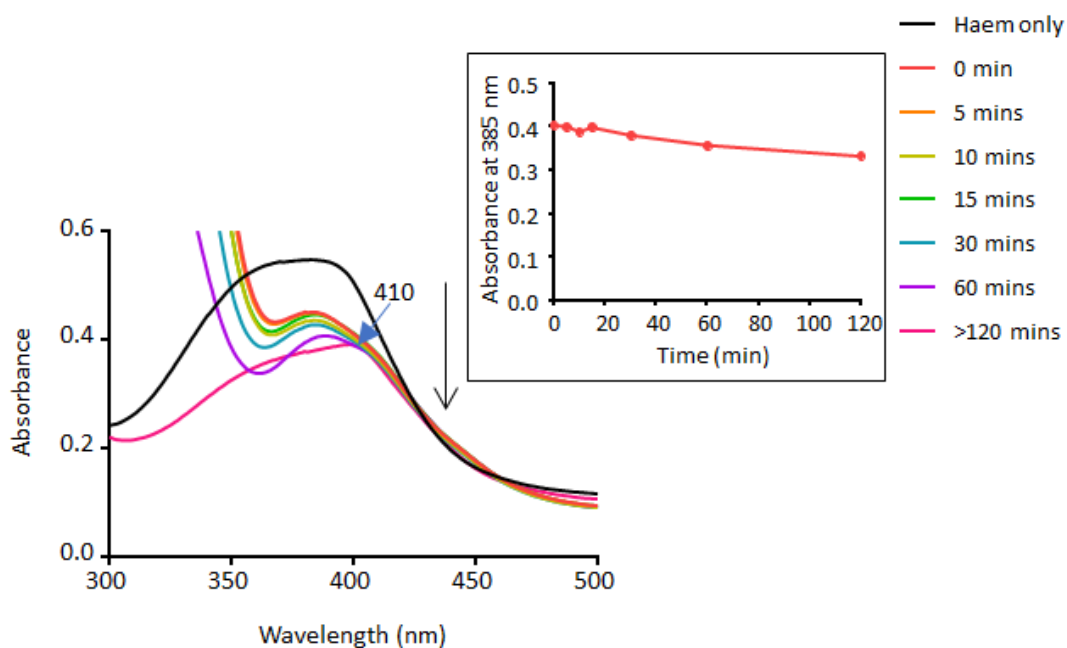


Figure 2.25: Representative UV-visible absorption spectra of haem in the presence of $\text{Na}_2\text{S}_2\text{O}_4$. $\text{Na}_2\text{S}_2\text{O}_4$ solution was prepared in $3 \mu\text{M}$ Ca^{2+} -containing bath solutions at pH 7.2. The absorption spectrum of the initial haem- $\text{Na}_2\text{S}_2\text{O}_4$ mixture is shown by the “0 min” spectrum. $\text{Na}_2\text{S}_2\text{O}_4$ addition resulted in a shoulder peak at 410 nm (indicated with the blue arrow). The absorption peak produced by $\text{Na}_2\text{S}_2\text{O}_4$ at 314 nm has been truncated for simplicity. The black arrow and inset show the time-dependent decrease in haem absorbance. Initial [haem] in the cuvette was $\sim 9 \mu\text{M}$.

2.7.1.3.3 Summary/conclusion from the reducing agent study

The cumulative graph (Figure 2.26) can be used to make direct comparison between the kinetics of haem degradation in the absence and presence of the different reducing agents. TCEP data have been excluded as its effect on haem is unique and obscure.

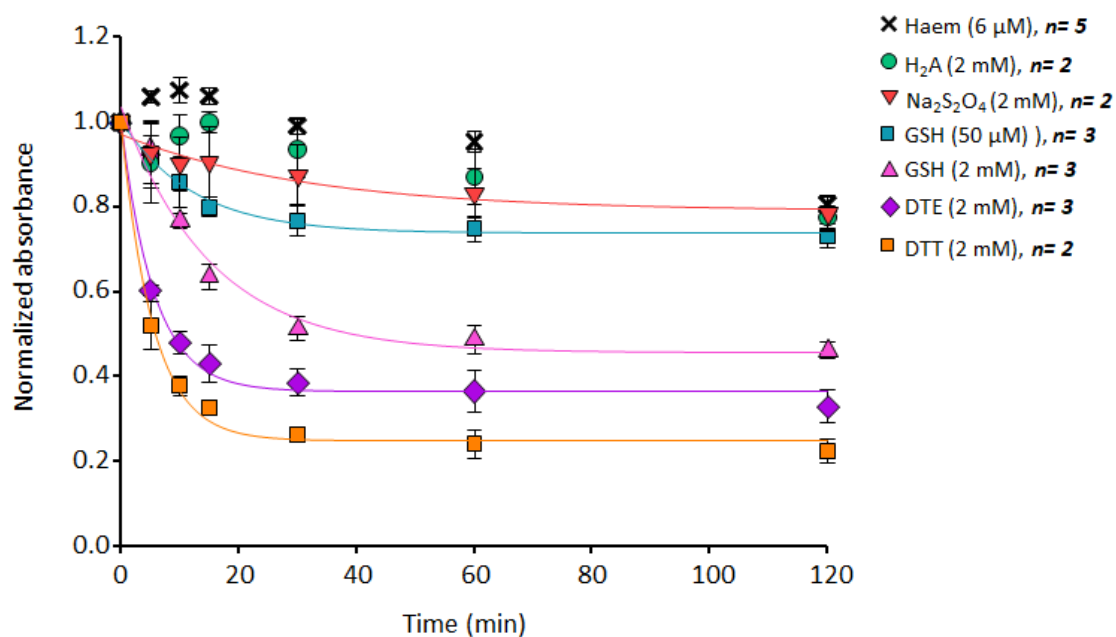


Figure 2.26: Kinetics of haem degradation in the absence and presence of natural and artificial reducing agents. Haem absorbance was measured at 385 nm (extinction coefficient = $58.44 \text{ mM}^{-1} \text{ cm}^{-1}$). Time course experiments were performed with the different reducing agents. Thus, the absorbance (y-axis) was normalized to the absorbance value from the initial haem + reducing agent mixture recorded at time point “0” minute. The half-life ($t_{1/2}$) of haem decay in $\text{Na}_2\text{S}_2\text{O}_4$, GSH (50 μM), GSH (2 mM), DTE and DTT solutions are (in minutes), 32, 12, 11, 6 and 5, respectively. The number of experimental repeats is shown in bold italics, next to name and quantity of reducing agent that was used.

In conclusion, most of the reductants used in the present study, appear to degrade rather than reduce haem. There was profound haem degradation in the presence of GSH, DTE and DTT, but such degradative effect was negligible or absent in H_2A , TCEP and $\text{Na}_2\text{S}_2\text{O}_4$ solutions. Therefore, results suggest that H_2A , TCEP and $\text{Na}_2\text{S}_2\text{O}_4$ could be useful for reducing the BK_{Ca} channel disulfide bonds in electrophysiology experiments involving haem, but this would need to be characterised. Furthermore, the natural reductant, GSH, could also be used to maintain the R-SH group of BK_{Ca} channels, provided low concentrations are used and the pH of the solution is closely monitored. This is because results from experiments with the thiol compounds (GSH, DTE and DTT) suggest that the pH change induced by these agents could be responsible for the accelerated haem degradation that was observed in their presence.

2.7.2 Carbon monoxide (CO) assays

Over the years, CO has been shown to regulate the activity of several ion channels including BK_{Ca} channels (Peers *et al.*, 2015). Earlier studies have investigated the effects of CO on BK_{Ca} channel activity using either CO gas or CO releasing molecules (CORMs) (Wang & Wu, 1997; Williams *et al.*, 2004; Jaggar *et al.*, 2005; Williams *et al.*, 2008; Hou *et al.*, 2008a). The results have consistently shown that CO mediates stimulatory effects on channel activity, but the mechanism of action remains unclear.

There are a variety of methods for measuring CO release in solution such as gas chromatography using a gas detector, fluorescent probes by exploiting the binding affinity of CO for the hemoprotein and, deoxymyoglobin carbonylation assay by exploiting the binding affinity of CO for myoglobin, Mb, (Vreman *et al.*, 2011; McLean *et al.*, 2012; Yuan *et al.*, 2013).

Deoxymyoglobin carbonylation assay is the most common test used to quantify CO release in solution (McLean *et al.*, 2012). This technique works by exploiting the high affinity of CO for myoglobin because CO binds to Mb 30 times more strongly than O₂ (Antonini & Brunori, 1971). This assay was used in the current study to;

- 1) Confirm the presence of CO in solution that has been bubbled with CO gas.
- 2) Examine CO release from CORM-3 solution and measure the kinetics of release.
- 3) Design protocols to generate inactivated CORM-3 (iCORM-3)

Experiments were performed using horse heart ferric myoglobin (Fe³⁺-Mb) powder which was first dissolved in 50 mM HEPES buffer (pH 7.2) and then diluted using whole-cell recording bath solution containing (in mM) 135 NaCl, 140 KCl, 10 HEPES, 1 MgCl₂, 1 CaCl₂, 4 glucose, 6 mannitol at pH 7.4, see Table 2.2.

2.7.2.1 Deoxymyoglobin carbonylation assays with CO gas

The aim of performing assays with CO gas was to confirm the presence of CO in bath solution that had been bubbled with CO gas. Furthermore, because electrophysiology experiments are performed under aerobic conditions, it was important to investigate whether air-exposure of CO solution could promote CO depletion from the solution.

Also, since the preparation process for electrophysiology studies is time-consuming, it was also important to investigate whether CO solution that had been prepared but left sealed for hours could still contain CO gas for use in electrophysiology studies.

CO binds exclusively to Fe^{2+} (Boczkowski *et al.*, 2006), so the first step in performing deoxymyoglobin carbonylation assays involved the reduction of ferric myoglobin (Fe^{3+} -Mb). Fe^{3+} -Mb was typically reduced using sodium dithionite ($\text{Na}_2\text{S}_2\text{O}_4$) as previously reported (Motterlini *et al.*, 2002; Atkin *et al.*, 2011). Estimates of CO concentration was made, based on the assumption that 1 μl of CO gas solution contains 30 ng of CO gas (Wang *et al.*, 1997a; Wang & Wu, 1997). Therefore, the amount of CO in freshly prepared CO gas solution was ~ 1 mM, consistent with previous report (Olson *et al.*, 2003).

2.7.2.1.1 Interaction of CO gas with ferrous myoglobin (Fe^{2+} -Mb)

The direct interaction of CO with Fe^{2+} -Mb had to be confirmed prior to performing different assays with CO gas solution. Bath solution which had been de-gassed (bubbled with N_2 gas to remove dissolved O_2) was used to prepare Fe^{3+} -Mb stock solution. This solution was transferred into a glovebox where the reduction of Fe^{3+} -Mb to Fe^{2+} -Mb was to be performed, using $\text{Na}_2\text{S}_2\text{O}_4$.

Final dilution (~ 200 -fold) of the Fe^{3+} -Mb solution was made in a cuvette. This solution contained 0.15 μM of Fe^{3+} -Mb, extinction coefficient (ϵ) of $12.9 \text{ mM}^{-1} \text{ cm}^{-1}$ at 555 nm (Antonini & Brunori, 1971). Consistent with reports by Antonini & Brunori (1971), Fe^{3+} -Mb solution had a Soret band at 409 nm, Spectrum I, see Figure 2.27. Subsequent addition of $\text{Na}_2\text{S}_2\text{O}_4$ (0.5% v/v) resulted in a red-shift of the Soret band from 409 nm (Spectrum I) to 435nm (Spectrum II), see Figure 2.27. This was accompanied by the appearance of a single peak in the Q-band region at 560 nm. These observations indicate the reduction of Fe^{3+} -Mb to Fe^{2+} -Mb as previously documented by Antonini & Brunori (1971).

The Fe^{2+} -Mb solution contained in the cuvette was sealed and removed from the glovebox. Authentic CO gas was then directly bubbled into the Fe^{2+} -Mb solution for ~ 5 seconds. This resulted in a blue-shift in the Soret band from 435 nm (Spectrum II) to 425 nm (Spectrum III), see Figure 2.27. The sharp peak at 425 nm (Spectrum III) suggests that all free Fe^{2+} -Mb in the solution had become CO-bound. Furthermore, in line with

previous report, the single peak in the Q-band region (at 560 nm) was split to double peaks, at 540 nm and 580 nm (Antonini & Brunori, 1971).

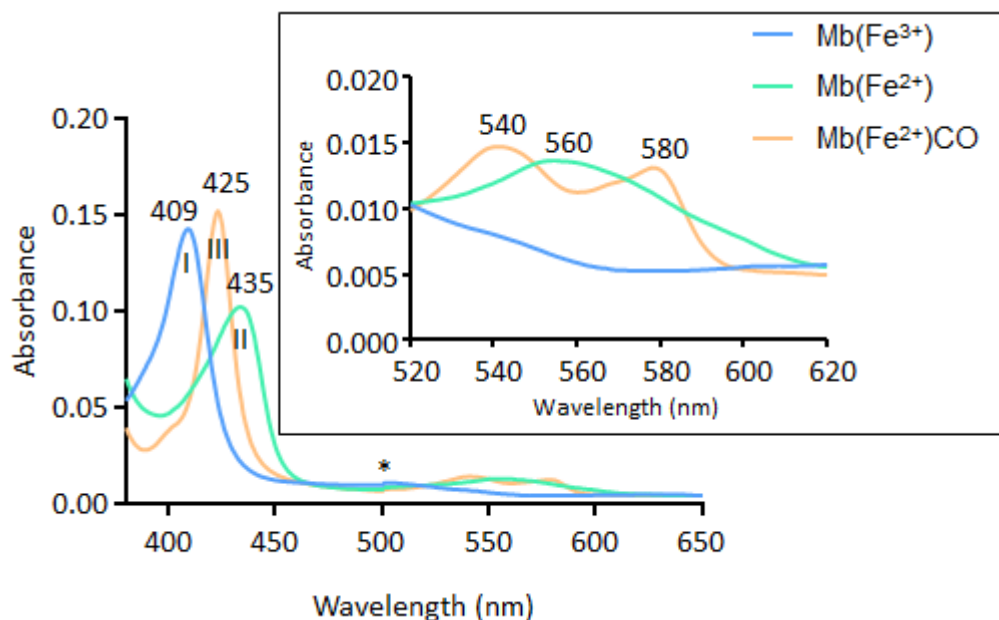


Figure 2.27: UV-visible absorption spectra showing the formation of myoglobin-CO complex, $\text{Mb}(\text{Fe}^{2+})\text{CO}$, by direct bubbling of CO gas into ferric myoglobin, $\text{Mb}(\text{Fe}^{3+})$, solution. $\text{Mb}(\text{Fe}^{3+})$ in Spectrum I, was reduced to ferrous myoglobin, $\text{Mb}(\text{Fe}^{2+})$ in Spectrum II, via the addition of 0.5 % v/v sodium dithionite ($\text{Na}_2\text{S}_2\text{O}_4$). The direct bubbling of CO gas to the $\text{Mb}(\text{Fe}^{2+})$ solution resulted in the formation of $\text{Mb}(\text{Fe}^{2+})\text{CO}$ complex in Spectrum III. Inset shows spectral changes in the Q-band region. The concentration of $\text{Mb}(\text{Fe}^{2+})$ in the cuvette = $0.15 \mu\text{M}$ ($\epsilon_{555} = 12.9 \text{ mM}^{-1}\text{cm}^{-1}$) (Antonini & Brunori, 1971). (* indicates technical artefact from the absorption spectrophotometer).

2.7.2.1.2 CO was present in freshly prepared CO gas solution

For this experiment, CO gas solution was prepared separately as opposed to directly bubbling CO gas into the Fe^{2+} -Mb solution. Fe^{3+} -Mb solution was prepared and reduced as previously explained in section 2.7.2.1.1.

The CO gas solution was prepared by bubbling CO gas into 10 ml of degassed bath solution for 5 minutes. The solution was then transferred into a glove box via a sealed vial. Addition of the CO solution to freshly prepared Fe^{2+} -Mb solution (1% v/v) resulted in a blue-shift of the Soret band from 435 nm (Spectrum II) to 425 nm (Spectrum III). This was accompanied by concomitant changes in the Q-band region from a single peak

at 560 nm (Spectrum II) to double peaks at 540 nm and 580 nm (Spectrum III), see Figure 2.28. These changes are indicative of the formation of Fe^{2+} -Mb-CO complex, consistent with observations from section 2.7.2.1.1.

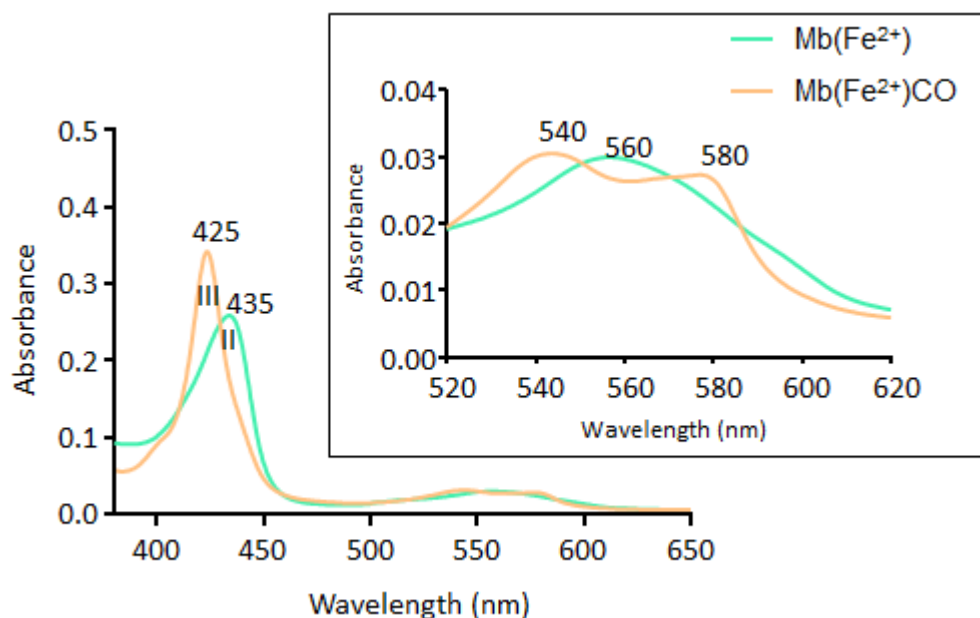


Figure 2.28: UV-visible absorption spectra showing the formation of myoglobin-CO complex, $\text{Mb}(\text{Fe}^{2+})\text{CO}$, using freshly bubbled CO gas solution. Addition of CO gas to $\text{Mb}(\text{Fe}^{2+})$, resulted in a blue-shift (from Spectrum II to III) of the Soret band and appearance of double peaks in the Q-band region (shown in inset).

2.7.2.1.3 CO was present in CO gas solution exposed to air

CO gas solution was prepared as previously mentioned (see section 2.3.1.2 in Methods chapter). The CO solution was then exposed to air for ~ 1 hour prior to its addition to freshly prepared Fe^{2+} -Mb solution (1% v/v). This resulted in a blue-shift of the Soret band from 435 nm (Spectrum II) to 425 nm (Spectrum III) with peaks at 540 nm and 580 nm in the Q-band region, see Figure 2.29.

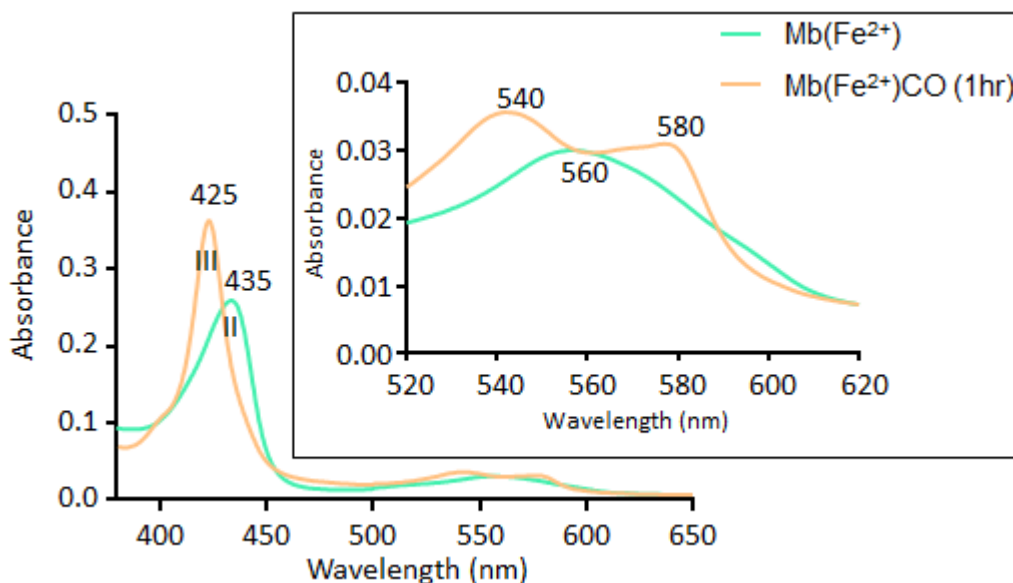


Figure 2.29: UV-visible absorption spectra showing the formation myoglobin-CO complex, $\text{Mb}(\text{Fe}^{2+})\text{CO}$, using CO gas solution that had been exposed to air. Addition of CO gas solution (exposed to air 1 hour post-preparation) to $\text{Mb}(\text{Fe}^{2+})$ resulted in a blue-shift (from Spectrum II to III) of the Soret band and appearance of double peaks in the Q-band region (shown in inset).

2.7.2.1.4 CO was present in CO gas solution exposed to air for over 4 hours

CO solution which had been prepared and left exposed to air for > 4 hours post-preparation, was added to freshly prepared Fe^{2+} -Mb solution (1% v/v). The absorbance intensity of the resulting $\text{Mb}(\text{Fe}^{2+})\text{CO}$ solution was very low (Figure 2.31). Also, the blue-shift of the Soret band from 435 nm (Spectrum II) to 425 nm (Spectrum III) or the twin peaks at 540 nm and 580 nm in the Q-band region was not pronounced. The results indicate that the CO gas was present in the solution but at low concentrations. The low concentration could result from the fact that measurements were made using a diluted (30 μM) CO gas solution rather than the stock CO gas solution. The diluted solution was used to determine whether the actual solution used for experiments contained haem after 4 hours of exposure.

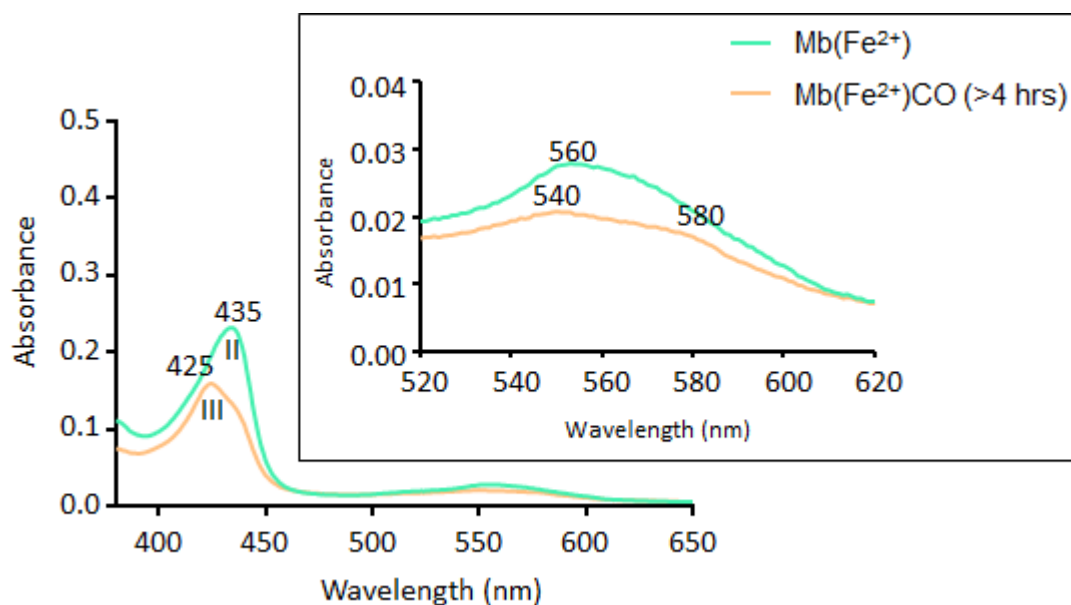


Figure 2.31: UV-visible absorption spectra of Mb(Fe²⁺)CO solution produced using CO gas solution that had been exposed to air for over 4 hours. Addition of the CO gas solution (prepared and exposed to air > 4 hours post-preparation) to Mb(Fe²⁺) resulted in a slight blue-shift (from Spectrum II to III) of the Soret band and the appearance of double peaks in the Q-band region (shown in inset).

2.7.2.1.5 CO was present in sealed “Aged” CO gas solution

CO solution which had been left sealed ~ 4 days post-preparation, was added to freshly prepared Fe²⁺-Mb solution (1% v/v). This still resulted in a blue-shift of the Soret band from 435 nm (Spectrum II) to 425 nm (Spectrum III) and appearance of the characteristic double peaks at 540 nm and 580 nm in the Q-band region, see Figure 2.30.

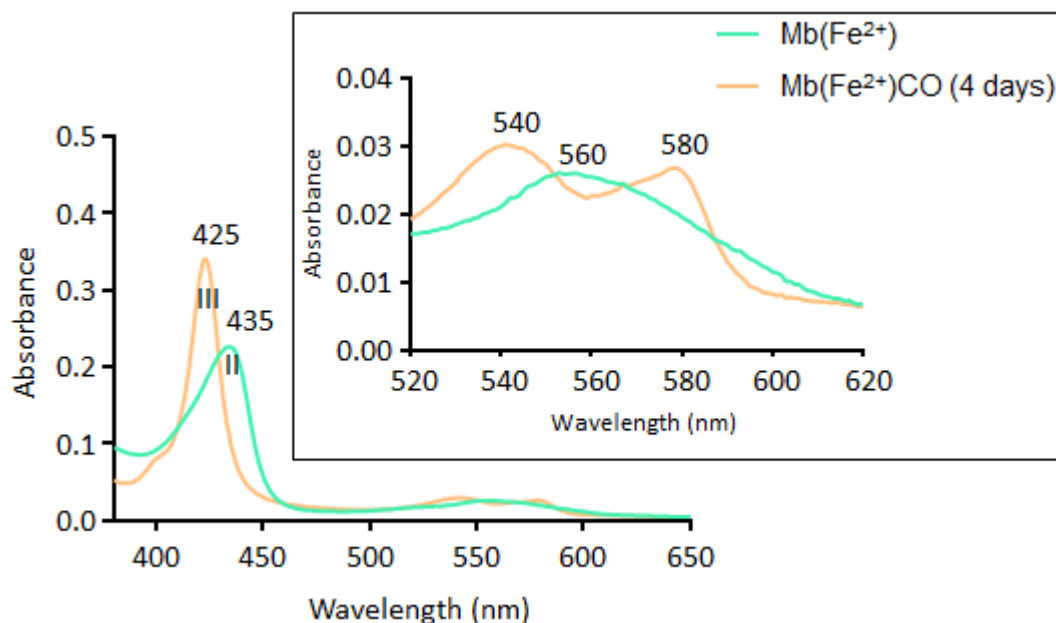


Figure 2.30: UV-visible absorption spectra showing the formation of myoglobin-CO complex, $\text{Mb}(\text{Fe}^{2+})\text{CO}$, using “aged” CO solution. Addition of the CO gas solution (prepared and left sealed 4 days post-preparation) to $\text{Mb}(\text{Fe}^{2+})$ resulted in a blue-shift (from Spectrum II to III) of the Soret band and appearance of double peaks in the Q-band region (shown in inset).

2.7.2.1.6 Summary/conclusion from CO gas solution experiments

The spectral results show that CO gas solution, prepared in the present study, will contain enough CO to perform electrophysiology experiments. Nevertheless, minimal exposure of the CO solution to air (post-preparation) is paramount to limit CO depletion from the solution. The minimal exposure can easily be achieved with whole-cell patch technique, as solutions can be synthesised when needed, but the excised patch technique does not afford such flexibility. This is because solutions must be mounted in advance prior to the excision of a good patch, which could be delayed depending on the cell preparation. These results will have to be taken into consideration during the interpretation of excised patch data.

2.7.2.2 Deoxymyoglobin carbonylation assays with CORM-3

Metal carbonyl complexes called CO-releasing molecules (CORMs) are formed from the coordination of carbonyls to transition metals such as nickel, iron or cobalt (Herrmann, 1990). They have different solubilities and can be activated by a variety of stimuli (Romao *et al.*, 2012). In addition, CORMs have been shown to be involved in a variety of roles such as anti-inflammatory, anti-bacterial, cardioprotective and vasorelaxing effects (Clark *et al.*, 2003; Motterlini *et al.*, 2012; Alshehri *et al.*, 2013).

The water-soluble metal carbonyl, tricarbonylchloro(glycinato)ruthenium (II), Ru(CO)₃Cl(glycinate) or CORM-3 was used in this study (Figure 2.32). CORM-3 has attracted a lot of interest due to its therapeutic benefits in clinical studies (Chaves-Ferreira *et al.*, 2015). An earlier study has shown that CORM-3 can relax pre-contracted isolated rat aortic rings via the generation of cGMP and K⁺ channel activation (Foresti *et al.*, 2004b). CORM-3 rapidly releases CO in aqueous solutions via a ligand-exchange mechanism, thus, loss of CO is induced by the coordination of labile ligands in solution to the central transition metal (Johnson *et al.*, 2007; Schatzschneider, 2015). It has been reported that 1 mole of CO is rapidly released per mole of CORM-3 in aqueous solution at pH 7.4, with a half-life of 98 hours in distilled water at 37°C (Clark *et al.*, 2003; Schatzschneider, 2015).

The aims of this experiment are to;

- a) confirm CO release from CORM-3 using deoxymyoglobin carbonylation assay.
- b) determine the best method for generating inactivated CORM-3 (iCORM-3) for use as a negative control in electrophysiology experiments.

Deoxymyoglobin carbonylation assay has previously been used to investigate CO release from CORMs (Motterlini *et al.*, 2002; Smith *et al.*, 2011b; Atkin *et al.*, 2011; McLean *et al.*, 2012). Nevertheless, it was important to re-perform this experiment due to differences in experimental systems. Whole-cell recording bath solution containing (in mM), 135 NaCl, 140 KCl, 10 HEPES, 1 MgCl₂, 1 CaCl₂, 4 glucose, 6 mannitol at pH 7.4 was used as a buffer (c.f. Table 2.2). This solution was de-gassed, to remove dissolved O₂, by bubbling with N₂ gas. All experiments were performed at room temperature.

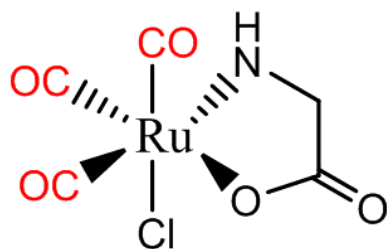


Figure 2.32: Molecular structure of CORM-3.

2.7.2.2.1 Investigation of CO release from CORM-3

The aim of performing these set of experiments was to confirm CO release from CORM-3. Furthermore, since electrophysiology experiments are normally performed under aerobic conditions, CO release under such condition and under anaerobic conditions was also studied. This was done to investigate whether optimal release of CO from CORM-3 can be influenced by the experimental environment. CORM-3 solutions were prepared aerobically and anaerobically, outside and inside a glove box, respectively. The kinetics of CO release from CORM-3 was also examined under both conditions.

2.7.2.2.1.1 CO was released from anaerobically prepared CORM-3 solution

Stock Fe^{3+} -Mb solution was prepared using de-gassed buffer. Final dilution (~ 200 -fold) was made in a cuvette. Fe^{2+} -Mb solution was subsequently prepared using 0.2 % v/v $\text{Na}_2\text{S}_2\text{O}_4$ rather than 0.5 % v/v (used for the CO gas assay). This is because excess $\text{Na}_2\text{S}_2\text{O}_4$ has been reported to increase the rate and amount of CO released from CORM-3, ~ 0.25 mole of CO per mole of CORM-3, compared with observations made in GSH and cysteine-containing solutions, 0.16 mole and 0.09 mole per mole of CORM-3, respectively (McLean *et al.*, 2012). The proposed mechanism of the $\text{Na}_2\text{S}_2\text{O}_4$ effect is via the interaction of the sulphite species from $\text{Na}_2\text{S}_2\text{O}_4$ with the ruthenium centre of CORM-3, thereby competing with CO.

Anaerobic CORM-3 stock solution was prepared in the glovebox by adding distilled water to CORM-3 powder (30 % w/v). Addition of this CORM-3 solution to freshly synthesized Fe^{2+} -Mb solution (0.14 % v/v) resulted in a blue-shift of the Soret band from 435 nm (Spectrum II) to 425 nm (Spectrum III) and appearance of peaks at 540 nm and 580 nm in the Q-band region of Spectrum III, see Figure 2.33. In contrast with the sharp Soret

bands observed with Spectrum III in the CO gas assays (see Section 2.7.2.1), the Soret band of Spectrum III was broad with a noticeable shoulder peak at 437 nm (Figure 2.33). This suggests that there was still some unbound Fe^{2+} -Mb in the solution.

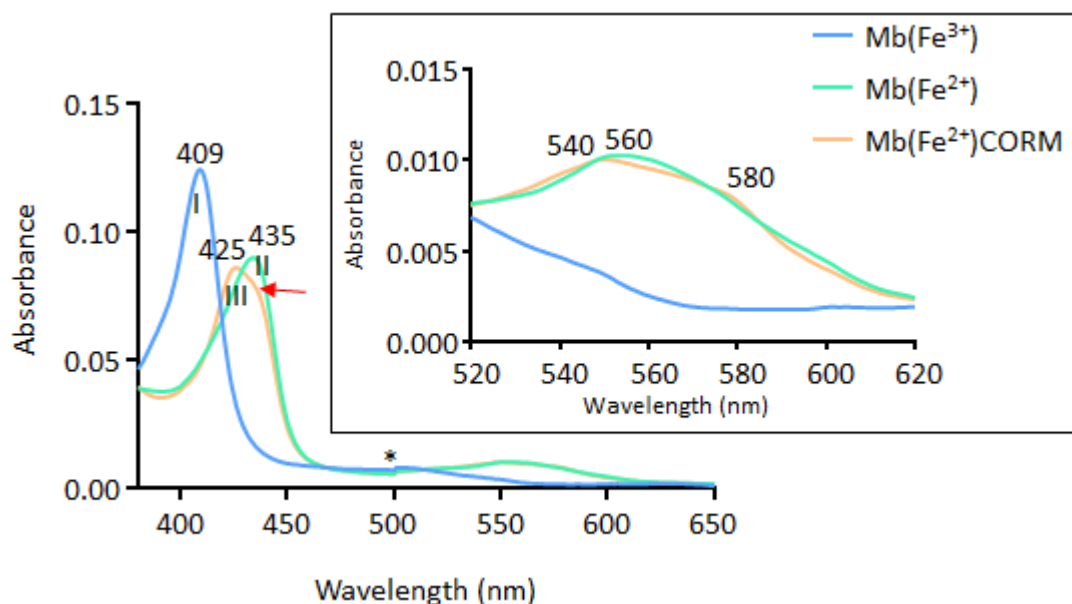


Figure 2.33: UV-visible absorption spectra of anaerobically prepared CORM-3 and ferrous myoglobin, Mb (Fe^{2+}). Ferric Mb solution, Mb (Fe^{3+}), was reduced (from Spectrum I to Spectrum II) by addition of $\text{Na}_2\text{S}_2\text{O}_4$ (0.2% v/v). Addition of CORM-3 to Mb (Fe^{2+}) solution resulted in a blue-shift of the Soret band, from Spectrum II to III with changes in the Q-band region (shown in inset). The arrow (Spectrum III) indicates the shoulder peak at 437 nm. The concentration of Mb(Fe^{2+}) in the cuvette = $0.21 \mu\text{M}$, $\epsilon_{555} = 12.9 \text{ mM}^{-1}\text{cm}^{-1}$. (* indicates technical artefact from the absorption spectrophotometer).

2.7.2.2.1.2 Time-resolved studies with anaerobic CORM-3 solution

The rate of CO release in anaerobically prepared CORM-3 solution was measured. This was achieved by always adding CORM-3 solution to freshly prepared Fe^{2+} -Mb solution (0.14 % v/v) at each of the different time points shown in Figure 2.34. At the 90-minute time point (i.e. 90 minutes post-preparation of the anaerobic stock CORM-3 solution) there was a blue-shift in the Soret band from 435 nm (Spectrum II) to 425 nm (Spectrum III) with concomitant appearance of peaks at 560 nm and 580 nm in the Q-band region (Spectrum III), see Figure 2.34. The shoulder peak at 437 nm was also observed. However, at 60, 120, 180 and 240-minute time points, addition of CORM-3 to the Fe^{2+} -Mb solution did not result in a blue-shift of the Soret bands (Figure 2.34). This indicates

that maximal release of CO from anaerobically prepared CORM-3 solution occurred between 60 to 120 minutes.

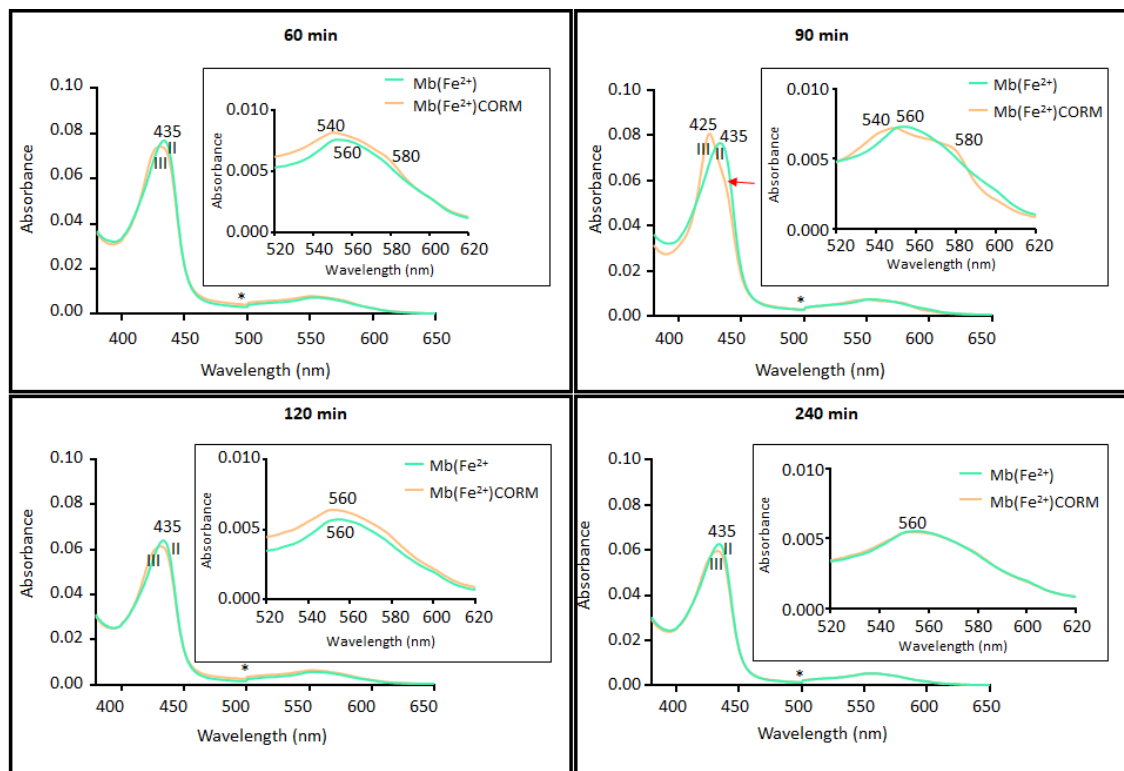


Figure 2.34: Kinetic study of CO release from anaerobically prepared CORM-3 solution. CORM-3 solution was added to freshly prepared Mb(Fe²⁺) at different time points (Spectrum III). A blue-shift in the Soret band (from Spectrum II to III) after CORM-3 addition, which indicates formation of Mb(Fe²⁺)CORM complex, was only noticed at the 90-minute time point. The arrow indicates a shoulder peak at 437 nm. Insets shows changes observed in the Q-band region. (* indicates technical artefact from the absorption spectrophotometer).

2.7.2.2.1.3 CO was released from aerobically prepared CORM-3 solution

Aerobic stock CORM-3 solution was prepared outside the glovebox by adding distilled water to CORM-3 powder (30% w/v). The solution was sealed in a glass vial and transferred into the glovebox. Therefore, the CORM-3 solution-containing O₂ was not in contact with the anaerobic environment of the glove box. Fe³⁺-Mb solution was reduced to Fe²⁺-Mb solution by addition of 0.2% v/v Na₂S₂O₄ as indicated by the red-shift from 409 nm (Spectrum I) to 435 nm (Spectrum II), see Figure 2.35. The CORM-3 solution was then added to the Fe²⁺-Mb solution using a gas-tight syringe (0.07% v/v) at 30 minutes

post-preparation of the CORM-3 solution. This resulted in a blue-shift of the Soret band from 435 nm (Spectrum II) to 425 nm (Spectrum III), Figure 2.35. The shoulder peak of the Soret band in Spectrum III and the low absorbance intensity indicates that not all the free Fe^{2+} -Mb have formed complexes with the CO released from CORM-3.

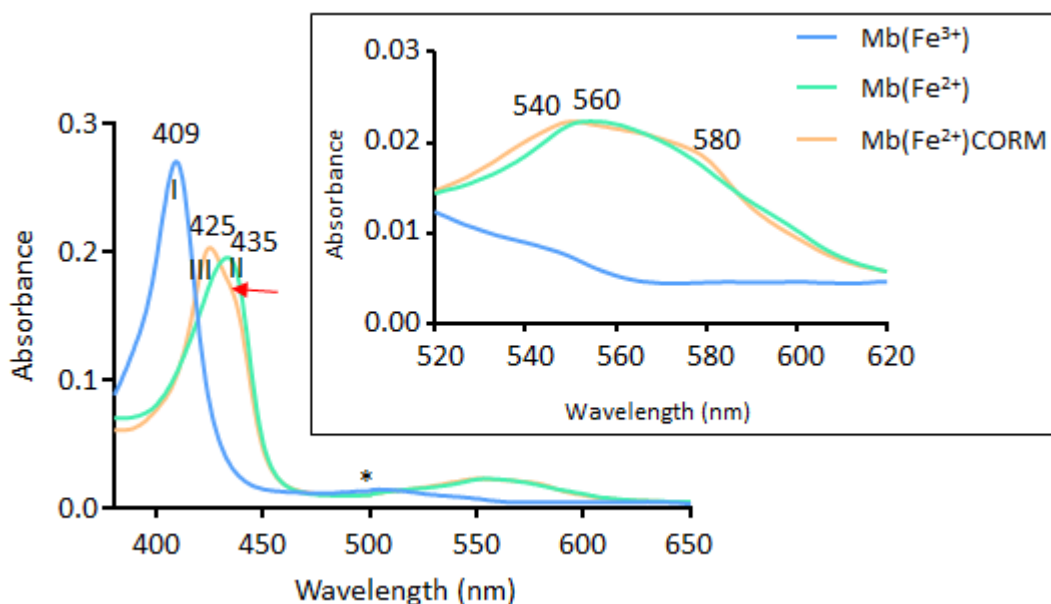


Figure 2.35: UV-visible absorption spectra of aerobically prepared CORM-3 solution. Ferric Mb, Mb (Fe^{3+}), was reduced (from Spectrum I to Spectrum II) by addition of $\text{Na}_2\text{S}_2\text{O}_4$ (0.2% v/v). Addition of CORM-3 (30 minutes post-preparation) resulted in a blue-shift (from Spectrum II to Spectrum III) with changes in the Q-band region (shown in inset). Arrow indicates shoulder peak at 437 nm. The concentration of Mb(Fe^{2+}) in the cuvette = $0.4 \mu\text{M}$ ($\epsilon_{555} = 12.9 \text{ mM}^{-1}\text{cm}^{-1}$). (* indicates technical artefact from the absorption spectrometer).

2.7.2.2.1.4 Time-resolved studies with aerobic CORM-3 solution

A kinetic study (identical to the anaerobic experiments) was performed using the aerobically prepared CORM-3 solution. This was done to determine whether the rate of CO release from CORM-3 was influenced by O_2 .

Fe^{2+} -Mb solution was freshly prepared at each time-point measurement. Aerobic stock CORM-3 solution was added to each freshly prepared Fe^{2+} -Mb using an air-tight syringe, as explained in section 2.7.2.2.1.3. This procedure was repeated at different time points over a period of 4 hours (Figure 2.36). Each addition of the aerobic CORM-3 to freshly prepared Fe^{2+} -Mb always resulted in a blue-shift of the Soret band from 435 nm (Spectrum II) to 425 nm (Spectrum III) and appearance of peaks at 560 nm and 580 nm

in the Q-band region of Spectrum III, see Figure 2.36. In comparison with anaerobic assays (Figure 2.34), the Soret peaks of Spectrum III were always very sharp with higher absorbance than Spectrum II (Figure 2.36). This indicates that CO was still being released from aerobically prepared CORM-3 solution even at 240 minutes post-preparation of the CORM-3 solution. However, a shoulder peak was always present on Spectrum III of each time point, excluding the 90-minute time point. The results also indicate that optimal CO release from aerobic CORM-3 solution occurred between 60 to 120 minutes. However, unlike the anaerobic CORM-3 solution, CO was always present in the aerobic CORM-3 solution at the different time-points, as indicated by the intense absorbance peaks at 425 nm.

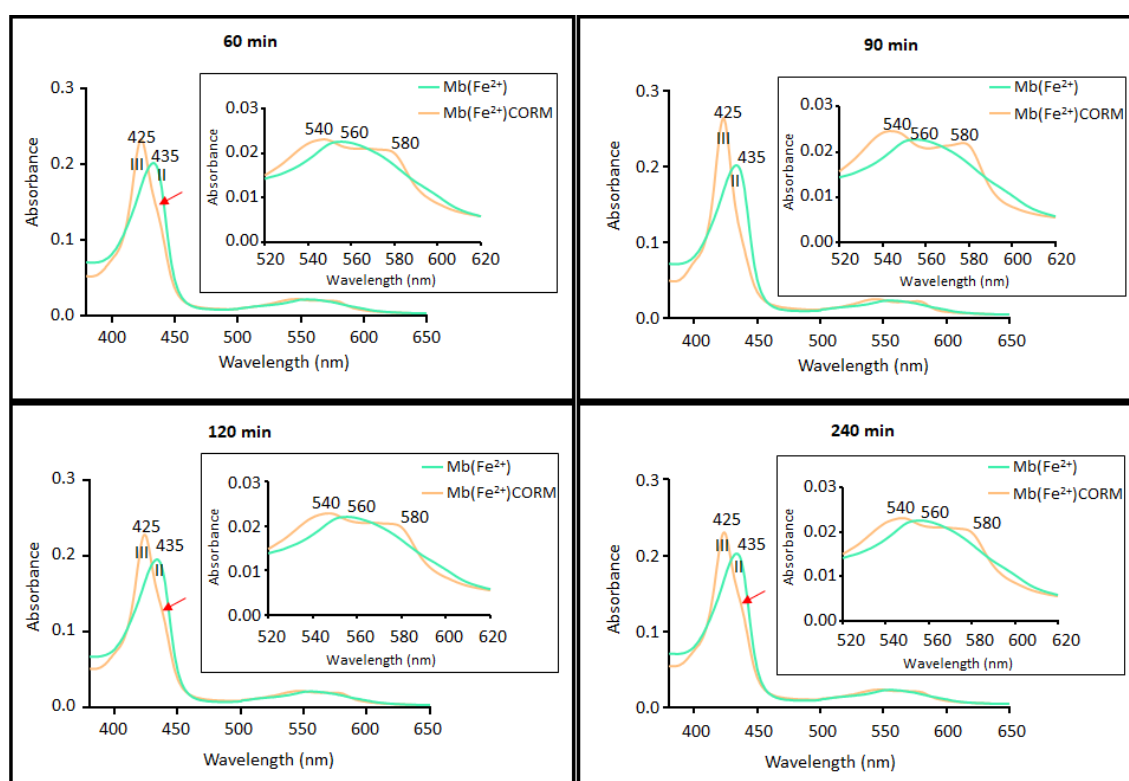


Figure 2.36: Kinetic study of CO release from aerobically prepared stock CORM-3 solution. Stock CORM-3 solution was added at different time points to freshly prepared Mb(Fe²⁺). This always produced a blue-shift in the Soret band (from Spectrum II to III) with spectral changes in the Q-band region (shown in insets). Arrows indicates shoulder peaks at 437 nm.

2.7.2.2.1.5 Summary/conclusion from CORM-3 solution experiments

CO is released from both aerobically and anaerobically prepared CORM-3 solutions. However, the CO release rate from anaerobically prepared CORM-3 solution appears to

be slow compared with aerobically prepared CORM-3 solution. In addition, aerobically prepared CORM-3 solutions release CO continually up to 4 hours post-preparation of the stock CORM-3 solution, with maximal release occurring between 60 to 120 minutes. Therefore, the spectral results suggest that O₂ might play an important role in the CO release rate from CORM-3. Thus, since CO release from CORM-3 appears to be enhanced under aerobic conditions and electrophysiology studies are typically performed in aerobic environments, CORM-3 is suitable for use as a CO donor in the present study.

2.7.2.3 Synthesis of inactive CORM-3 (iCORM-3)

Previous studies have reported that CORM-3 can be inactivated by overnight incubation of freshly prepared CORM-3 solution in a suitable buffer at room temperature (Motterlini *et al.*, 2003; Foresti *et al.*, 2004b). Others have reported inactivation of CORM-3 by bubbling with N₂ gas (McLean *et al.*, 2012; Alshehri *et al.*, 2013). Therefore, the most effective protocol for the preparation of inactivated CORM-3 (iCORM-3) for use in my electrophysiology studies was investigated.

2.7.2.3.1 N₂-bubbled fresh CORM-3 solution

Fresh CORM-3 stock solution (30 % w/v) was prepared outside the glove box and immediately bubbled with N₂ gas for 10 minutes. This solution was transferred into a glovebox. Fe²⁺-Mb solution was prepared as previously explained in section 2.7.2.2.1.1. Addition of the N₂-bubbled CORM-3 solution to the Fe²⁺-Mb solution (0.14 % v/v) at different time points (0 and 50 minutes) did not result in a shift in the Soret band to 425 nm or a split of the single peak at 560 nm (see Figure 2.37). This suggests that there was no formation of Fe²⁺-Mb-CO complex. However, this method of generating iCORM-3 is not cost effective, since CORM-3 solution must be freshly prepared each time before iCORM-3 can be produced. Therefore, another protocol was investigated.

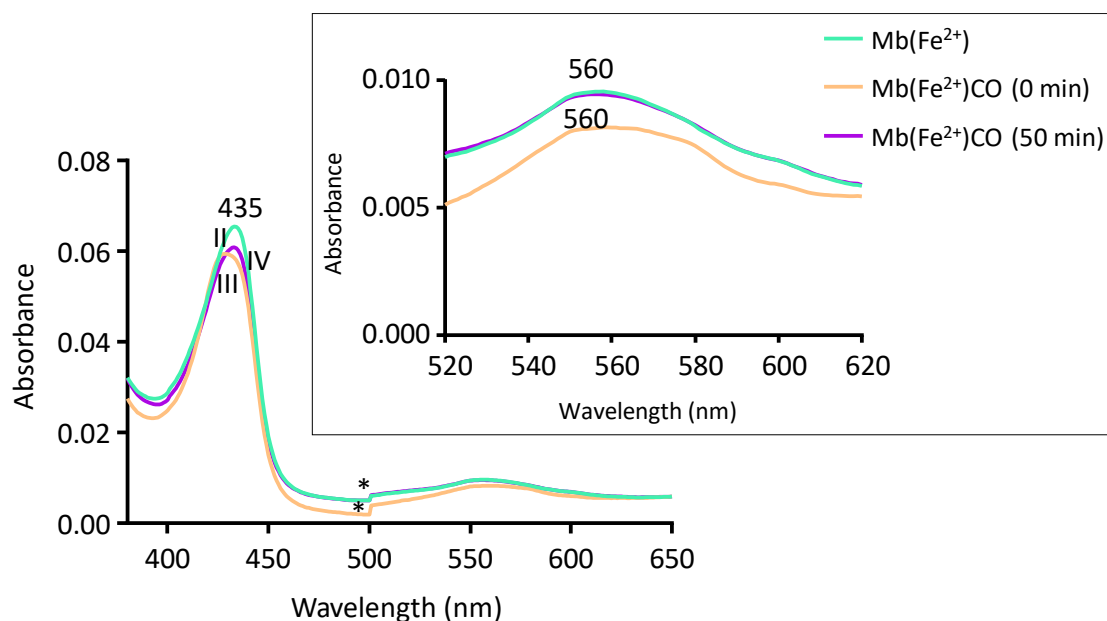


Figure 2.37: UV-visible absorption spectra of N₂-bubbled CORM-3 solution. Addition of N₂-bubbled CORM-3 solution to Mb (Fe²⁺) solution did not produce any change in Mb (Fe²⁺) spectrum (Spectrum II) at 0 minutes (Spectrum III) and 50 minutes (Spectrum IV) time points. There were no spectral changes in the Q-band region (shown in the inset). (* indicates technical artefact from the absorption spectrometer).

2.7.2.3.2 “Aged” CORM-3 solution

CORM-3 has been reported to have a half-life of 98 hours in distilled water at 37°C (Schatzschneider, 2015). Therefore, fresh CORM-3 stock solution (30% w/v) was prepared aerobically in distilled water and left at room temperature for 4 days. This solution was sealed in an air-tight vial and transferred into a glove box. Addition of the aged CORM-3 solution to freshly prepared Fe²⁺-Mb solution (0.14% v/v) produced a blue-shift, from 435 nm (Spectrum II) to 425 nm (Spectrum III) with a broad shoulder around 437 nm (Figure 2.38). However, absorbance intensity was low. These results indicate the formation of Fe²⁺-Mb-CO complex with some unbound Fe²⁺-Mb, as the broad shoulder is indicative of the presence of additional species.

CO was surprisingly present in the 4-day old CORM-3 solution, albeit in low amounts. Therefore, this cost-effective protocol needed be improved by ensuring complete elimination of CO from the solution.

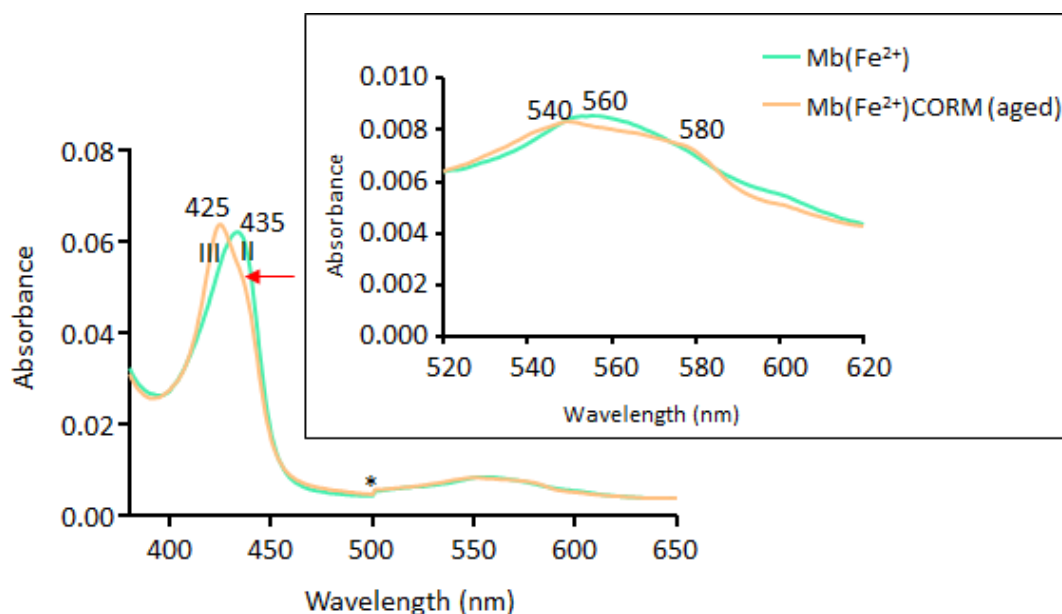


Figure 2.38: UV-visible absorption spectra of “aged” CORM-3 solution. CORM-3 solution was prepared under aerobic conditions and left sealed at room temperature for 4 days. Addition of the CORM-3 solution to Mb(Fe²⁺) solution resulted in a blue-shift of the Soret band (Spectrum II to III) and spectral changes in the Q-band region (shown in inset). Arrow indicates shoulder peak at ~ 437 nm. (* indicates technical artefact from the absorption spectrometer).

2.7.2.3.3 N₂-bubbled “Aged” CORM-3 solution

An “Aged” (4-day old) CORM-3 solution was bubbled with N₂ gas for 10 minutes. This solution was then sealed in a glass vial and transferred into the glove box. The N₂ bubbled “Aged” CORM-3 solution was added to freshly prepared Fe²⁺-Mb solution using an air-tight syringe. This resulted in no change in the absorption spectra of Fe²⁺-Mb which signified the absence of CO in solution (Figure 2.39).

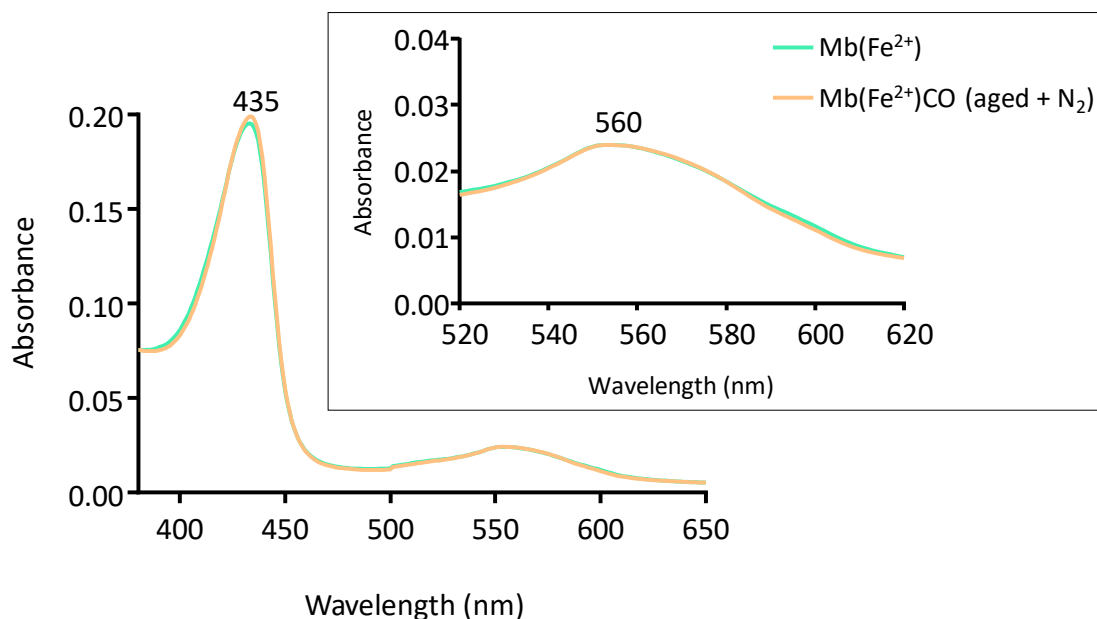


Figure 2.39: UV-visible absorption spectra of N₂-bubbled “aged” CORM-3 solution. CORM-3 solution was prepared under aerobic conditions and left at room temperature for 4 days. The “aged” CORM-3 solution was bubbled in N₂ gas prior to addition to Mb (Fe²⁺) solution. No change was observed in the absorption spectra of Mb (Fe²⁺).

2.7.2.3.4 Summary/conclusion from CORM-3 inactivation experiments

Spectroscopic results showed that “aged” CORM-3 solution still contained some residual CO whereas N₂-bubbled “fresh” and “aged” CORM-3 solutions were completely CO-free. Therefore, bubbling “aged” CORM-3 solution with N₂ gas is the most economic and efficient protocol for the generation of iCORM-3 for use in my electrophysiology studies.

2.7.3 Zinc protoporphyrin IX (ZnPP-IX) assays

Zinc protoporphyrin IX (ZnPP-IX) is a type of metalloporphyrin formed in trace amounts during haem biosynthesis but ZnPP-IX synthesis is enhanced during periods of iron deficiency via the chelation of zinc (Zn) to the porphyrin ring by ferrochelatase (Labbe *et al.*, 1999). ZnPP-IX structure differs from that of protoporphyrin IX (PP-IX) as the two hydrogen atoms of the amide side group of protoporphyrin IX (PP-IX) are replaced with Zn (Figure 2.40).

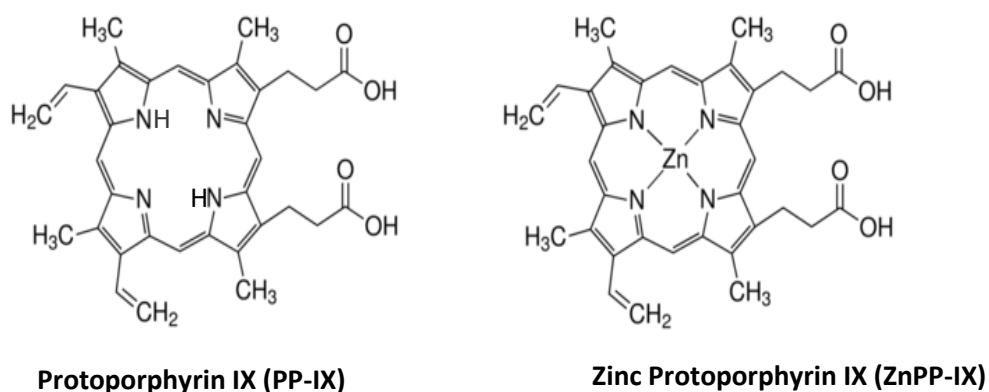


Figure 2.40: Molecular structures of PP-IX and ZnPP-IX.

Metalloporphyrins have been proposed to competitively inhibit haem oxygenase (HO) enzymes (Yoshinaga *et al.*, 1982; Serfass & Burstyn, 1998). This proposal originated from the 1974 discovery, where ZnPP-IX although being an endogenous metabolite was observed to be unsusceptible to oxidation by haem oxygenase (HO) enzymes (Frydman *et al.*, 1981). ZnPP-IX has since been used in a variety of studies to inhibit HO activity (Maines, 1988; Christodoulides *et al.*, 1995; Grundemar & Ny, 1997; Nowis *et al.*, 2008). Nevertheless, the use of ZnPP-IX at concentrations $> 0.5 \mu\text{M}$ has been shown to mediate non-selective effects such as inhibition of soluble guanylate cyclase (sGC) activity and stimulation of nitric oxide synthase (NOS) activity (Serfass & Burstyn, 1998; Chakder *et al.*, 1996). However, ZnPP-IX at $< 50 \mu\text{M}$ and $10 \mu\text{M}$ has been shown to have no inhibitory effect on vascular endothelial cell NOS and sGC activity respectively (Zakhary *et al.*, 1996).

ZnPP-IX, like other metalloporphyrins, is lipophilic, soluble in alkaline aqueous solution or basic organic solvents (Labbe *et al.*, 1999). However, ZnPP-IX is photosensitive which can result in its inactivation upon exposure to light (Grundemar & Ny, 1997). The PP-IX spectrum is well known, thus, it was used as a reference for the ZnPP-IX spectrum (see Figure 2.41).

The aim of this experiment was to investigate the photosensitivity and stability of ZnPP-IX for use in electrophysiology studies; thus, light and dark assays were performed. The light assays were used to investigate the degree of light-sensitivity of ZnPP-IX to determine whether extra measures need to be taken to prevent or minimise ZnPP-IX

inactivation, especially during the preparation of ZnPP-IX solutions. Dark assays were also performed to confirm whether the molecule was more stable in the dark. ZnPP-IX solutions were prepared using 50 mM HEPES solution. All experiments were performed at room temperature.

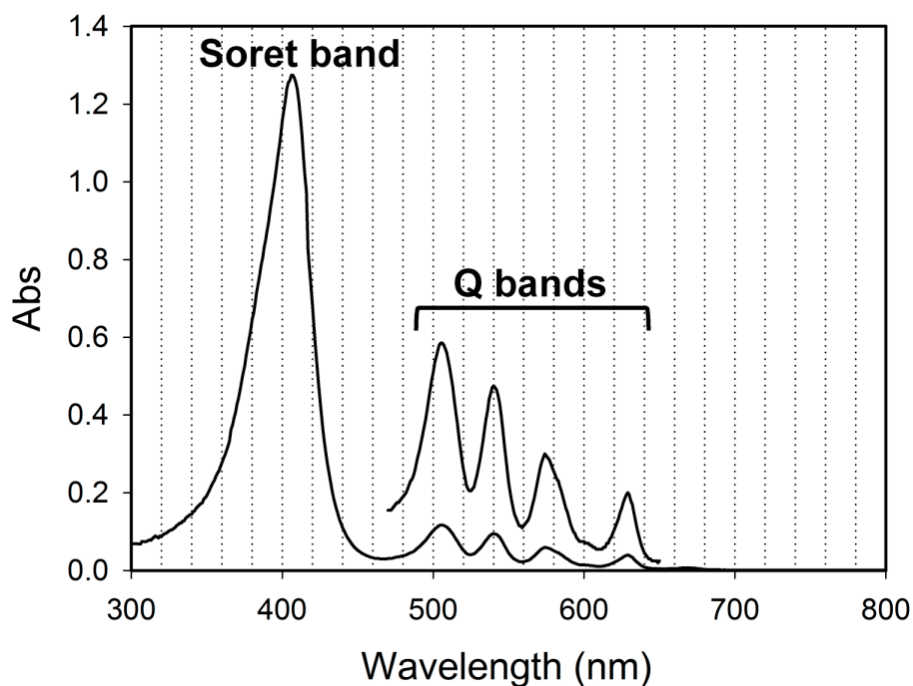


Figure 2.41: Absorption spectra of PP-IX with a strong Soret peak at 405 nm and 4 Q-bands between 500 and 630 nm (Sawamura *et al.*, 2015).

2.7.3.1 Light and dark assays with ZnPP-IX

ZnPP-IX stock solution (0.2 % w/v) was prepared under near dark conditions by dissolving ZnPP-IX powder with 0.1 M NaOH and 50 mM HEPES solutions. The stock solution was wrapped in aluminium foil to shield it from light. Spectral measurements were made at different time points using a diluted (6-fold dilution) stock solution. The light assay was performed by exposing the cuvette-containing ZnPP-IX to laboratory light between spectral measurements, whereas during the dark assay the cuvette was shielded from light.

The absorption spectra of ZnPP-IX in the light and dark assays was similar to that of PP-IX with a Soret peak at 356 nm and 4 peaks in the Q-band region at 535 nm, 563 nm, 590 nm and 644 nm (Figure 2.42). Compared with the PP-IX spectrum (Figure 2.41), ZnPP-IX appeared to have a broader Soret peak with the 4 peaks in the Q-band region slightly red-shifted (Figure 2.42). The broad Soret peaks might have resulted from the type of buffer used in this study. This is because spectral results of PP-IX from a previous study in which organic solvents were used showed a sharper Soret band (Marcelli *et al.*, 2013). Furthermore, the slight red-shift noticed between the PP-IX and ZnPP-IX absorption bands might be due to the central Zn atom in ZnPP-IX (Figure 2.40). However, it is unclear why the absorption peak at 563 nm was less defined in the ZnPP-IX spectrum compared with the PP-IX spectrum.

The results evidently showed that ZnPP-IX degradation is accelerated in light compared with dark conditions. This is because absorbance intensity rapidly decreased over time in the light assay (Figure 2.42B).

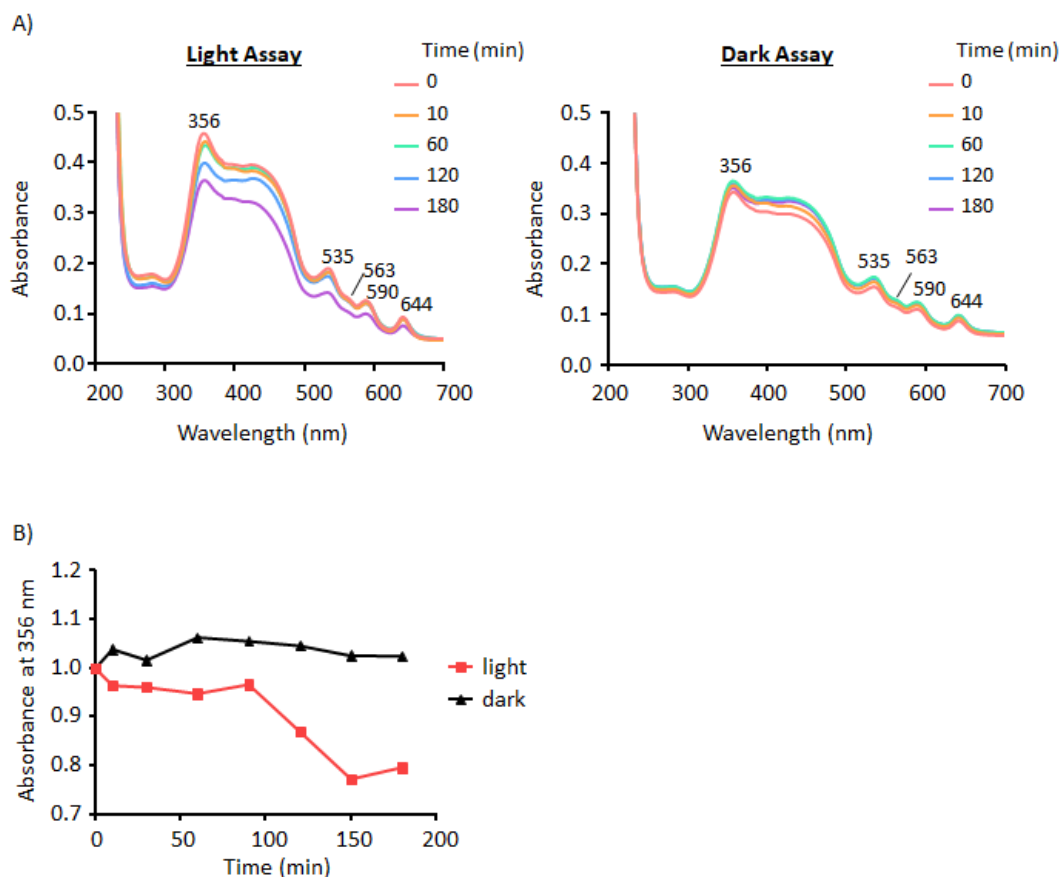


Figure 2.42: Spectral measurements of ZnPP-IX in light and dark conditions. In both assays, spectral measurements were made at different time points, 5 distinct peaks were observed at (nm) 356, 535, 563, 590 and 644. A) UV-visible absorption spectra of light-exposed and dark-incubated ZnPP-IX solutions. B) Kinetics of ZnPP-IX degradation observed under dark and light conditions at 356 nm. Absorbance was normalized to the 0 min time point measurement.

2.7.3.2 Conclusion from ZnPP-IX study

These results confirm that ZnPP-IX is more stable in the dark. Therefore, it would be beneficial to shield ZnPP-IX solutions from light during electrophysiology studies.

2.8 Confocal microscopy

Confocal microscopy is a technique used to obtain high resolution non-invasive optical slices from biological specimens. The system works by scanning a laser beam across a sample whilst collecting the transmitted light through a pin hole aperture. This pin hole produces the confocality by rejecting out-of-focus light emitted by the rest of the sample.

In this study, confocal microscopy was used to observe Ca^{2+} spark frequency in the presence and absence of haem. Ca^{2+} sparks are localised transient Ca^{2+} release events with a rise time of ~ 20 ms and decay time of ~ 50 ms (Nelson *et al.*, 1995; Arnaudeau *et al.*, 1996; Perez *et al.*, 1999). Therefore, wide-field imaging system was preferred to avoid missing Ca^{2+} spark events. As with electrophysiology studies, all imaging experiments were performed at room temperature.

2.8.1 Detection of Ca^{2+} spark events

Cells were isolated using the protocol detailed in section 2.1. A non-ratiometric fluorescein-based membrane permeable fluorescent indicator, Fluo-4 AM, was used to observe fluorescent changes in cytosolic free Ca^{2+} of SMCs. In addition, the fungal steroid metabolite, wortmannin, was used to inhibit SMC contraction to improve image quality.

Stock solutions of Fluo-4 AM (1.1 % w/v) and wortmannin (0.4 % w/v) were prepared in DMSO. Cells were incubated in eppendorf tubes, containing Fluo-4 AM (10 μM) and wortmannin (10 μM) for 40 minutes, on a rocker at room temperature. The eppendorf tubes were wrapped in foil to protect the photosensitive fluorescent dye from degradation. After dye loading, 43 % v/v cells were directly transferred (without washing) per glass bottom petri dish which already contained bath solution (see Table 2.2). Thus, cells were imaged in solution containing a final DMSO concentration of ~ 0.04 % v/v. My plans to record Ca^{2+} sparks at the same V_m used for electrophysiology recordings (-30 mV), by increasing the external K^+ concentration, $[\text{K}^+]_o$, in the bath solution to 40 mM, proved abortive. This was because cells were stressed under that condition and had a low survival rate. This might have resulted from Ca^{2+} overloading of

cells promoted by a sustained membrane depolarisation induced by the high $[K^+]_o$. Therefore, imaging was performed at the resting V_m of the cells, by using bath solution containing 5 mM $[K^+]_o$.

Smooth muscle cells were imaged with the VisiTech HAWK confocal laser scanning microscope and a 60x oil immersion objective (CFI Plan Apo VC 60x oil/1.4 DIC N2 - WD = 0.13 mm) attached to a Nikon4 microscope illuminated with a solid-state laser diode (SSLD) filtered at 488 nm. This used a fast scanning system comprising of a 2D array scanner with a scan rate of 360 Hz. Images were acquired at 10 frames s^{-1} (100 ms exposure) with 200 images $cell^{-1}$ (under control conditions) and 400 images $cell^{-1}$ (after haem application). Data were collected by a 16-bit Hamamatsu C11440 -22CU Flash 4.0 V2 cCMOS camera and saved in the *.ome.tiff file format by the VisiTech acquisition software VoxCell Scan v8.03.0.2. The equipment lacked a superfusion system; thus, haem was applied using a gilson pipette. This inevitably produced some cell detachment which made it difficult to re-image the 'control' cells.

The caveat of using a non-ratiometric indicator such as poor indicator loading was minimised by diluting the loaded cells rather than washing them. Furthermore, the issue of dye compartmentalization and photobleaching were avoided by loading cells at room temperature and using a fast scanning system, respectively. However, a major limitation of the present study was the lack of a combination system which impeded the simultaneous execution of imaging and electrophysiology experiments.

2.8.2 Quantification of Ca^{2+} spark frequency

Fluorescent images were analysed using two software packages; WinFluor: Fluorescence Image Capture & Analysis Program V4.0.1 and Tracan (an in-house software).

The initial image processing of *.ome.tiff files was performed using WinFluor (see Figure 2.43). This was achieved by drawing a region of interest (ROI) at a Ca^{2+} spark site. Time course analysis of the ROI was performed where upward deflections indicated changes in fluorescent intensity resulting from a rise in $[Ca^{2+}]_i$ (Figure 2.43). Ca^{2+} sparks were displayed as sharp peaks with slow decay times whereas Ca^{2+} waves appeared as broad

peaks. Data from time course analysis graphs were imported into Tracan to allow for accurate quantification of Ca^{2+} spark frequency.

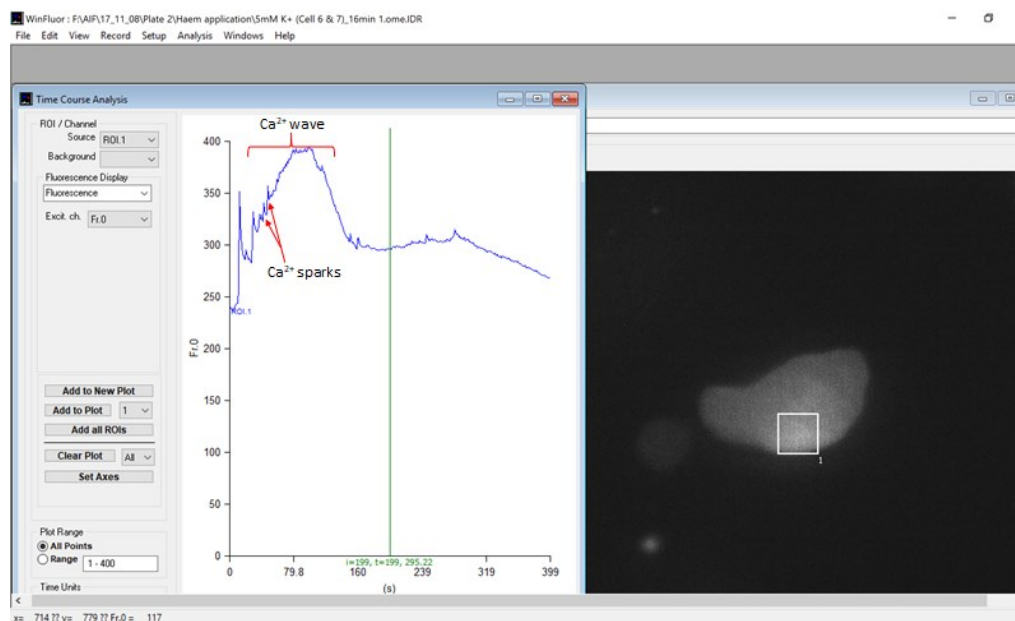


Figure 2.43: Analysis window on WinFluor software showing the selection of a region of interest (ROI) at a position of high fluorescent intensity in a smooth muscle cell. The corresponding time course analysis of the ROI is shown on the left-hand panel. Sharp and broad peaks indicate Ca^{2+} spark and Ca^{2+} waves, respectively.

In Tracan, the raw trace of F/F_0 was differentiated to identify slopes, as they indicate Ca^{2+} spark events. Each file had a unique threshold such that only slopes that exceeded the threshold value were accepted. This was useful for eliminating random slopes that occurred due to undulating baseline. It also ensured that the Ca^{2+} sparks that occurred on Ca^{2+} waves were detected whilst discounting the wave. Finally, an automated calculation of the sum of positive deflections that exceeded the threshold was performed. However, the $[\text{Ca}^{2+}]$ per Ca^{2+} spark could not be quantified using the area under each Ca^{2+} spark event, because of the use of a non-ratiometric Ca^{2+} indicator.

**Chapter 3 THE EFFECTS OF HAEM AND CO ON SINGLE
BK_{Ca} CHANNEL ACTIVITY**

3.1 Introduction

Tang *et al.* (2003) showed that intracellular haem inhibited both recombinant and native BK_{Ca} channels. In contrast, CO has been reported to stimulate native and recombinant BK_{Ca} channels (Wang *et al.*, 1997b; Wang & Wu, 1997; Jaggar *et al.*, 2005; Hou *et al.*, 2008a; Williams *et al.*, 2008; Telezhkin *et al.*, 2011).

The effects of haem and CO were re-examined in this study (using native BK_{Ca} channels in inside-out patches isolated from rat mesenteric artery SMCs) because the complex interaction of haem and CO with BK_{Ca} channels is still poorly understood. For instance, ferric and ferrous haem have been shown to modulate BK_{Ca} channel activity (Jaggar *et al.*, 2005). However, CO has been proposed to influence channel activity via its interaction with channel bound haem, provided the haem was in its ferrous state. To the best of my knowledge this is the first study to examine the effects of other intracellular factors, such as pH, on the haem interaction with BK_{Ca} channels. Furthermore, since this study was performed on mesenteric artery SMC BK_{Ca} channels, it also provides information about whether haem and CO mediate tissue-specific effects.

The membrane density of BK_{Ca} channels has been estimated to be in the range of 1,000 to 10,000/cell (Nelson & Quayle, 1995). This high density was reflected in my recordings, where many patches contained several channels. Nevertheless, the presence of BK_{Ca} channels in inside-out patches was still investigated by measuring the single channel current-voltage (i-V) relationship and the channel's sensitivity to [Ca²⁺]_i, voltage, and sub-millimolar concentration of tetraethylammonium ion, TEA⁺ (which is known to block BK_{Ca} channels).

3.2 Characterisation of single BK_{Ca} channel activity

3.2.1 Investigation of the i-V relationship of the channel

The i-V relationship of a channel can be useful for obtaining certain information about the channel's properties, including its conductance. This approach was used to determine whether BK_{Ca} channels were in the inside-out patches isolated from rat mesenteric artery SMCs.

Membrane patches were excised into a bath solution containing $1 \mu\text{M}$ free Ca^{2+} . Channel activity was recorded at V_m ranging from 0 to +70 mV, in 10 mV increments. Single-channel current (i) increased with V_m (V) such that every 10 mV of depolarisation evoked ~ 2 pA increase in current amplitude (see Figure 3.1). The slope of conductance, measured at +50 mV and +20 mV, was 210 pS. This value is close to the previously reported range of 250 to 300 pS measured in symmetrical K^+ (Barrett *et al.*, 1982; Singer & Walsh, 1984).

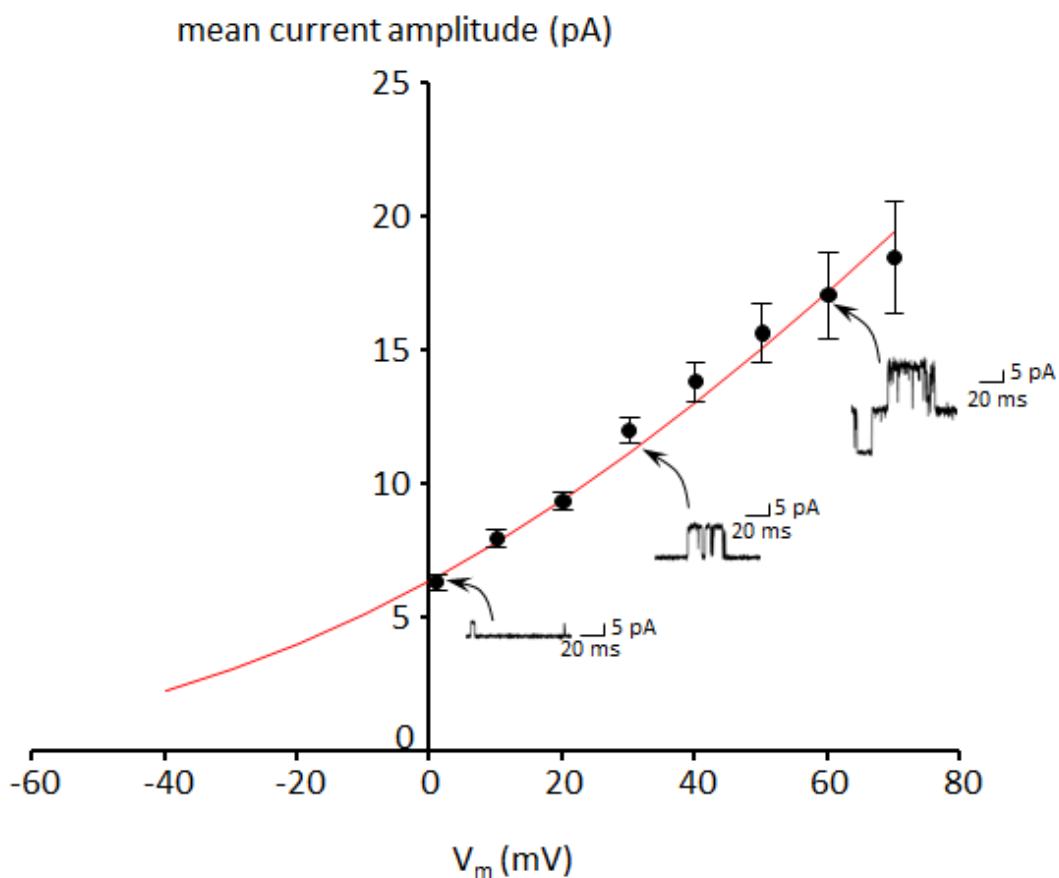


Figure 3.1: Current-voltage (i-V) relationship of BK_{Ca} channels. The membrane potential of different patches was held at different potentials, 0 to +70 mV. Example traces show channel activity at 0 mV, +30 mV and +60 mV. Error bars show SEM, $n=3$. The i-V curve was fitted with the sum of least squares. Inside-out patch configuration was used for recordings. $[\text{Ca}^{2+}]_i = 1 \mu\text{M}$; $[\text{K}^+]_i = 140 \text{ mM}$; $[\text{K}^+]_o = 5 \text{ mM}$.

3.2.2 Channel Popen increased with membrane depolarisation and a rise in $[Ca^{2+}]_i$

BK_{Ca} channels are activated by membrane depolarisation and a rise in $[Ca^{2+}]_i$. Therefore, the presence of BK_{Ca} channels in inside-out patches was also investigated by monitoring channel activity whilst changing $[Ca^{2+}]_i$ and V_m .

The Ca^{2+} sensitivity of channels was investigated by holding V_m at + 30 mV whilst applying different $[Ca^{2+}]_i$, 0.1 μ M, 1 μ M, 3 μ M and 10 μ M. Channel activity was observed to increase with a rise in $[Ca^{2+}]_i$ (Figure 3.2). For instance, mean channel activity was ~ 10 times higher in 10 μ M $[Ca^{2+}]_i$ than in 3 μ M $[Ca^{2+}]_i$, 0.60 ± 0.08 pA and 0.06 ± 0.01 pA, respectively ($n= 4$ for 10 μ M $[Ca^{2+}]_i$ and $n= 5$ for 3 μ M $[Ca^{2+}]_i$, $p \leq 0.001$; Figures 3.2 and 3.3). This result is in line with previous report where recombinant BK_{Ca} channel activity recorded from inside-out patches was also shown to increase with a rise in $[Ca^{2+}]_i$ (Barrett *et al.*, 1982).

Next, V_m was held at a less depolarised potential of 0 mV, whilst applying the same $[Ca^{2+}]_i$. Graphs of Popen against $[Ca^{2+}]_i$ were plotted for the results obtained at 0 mV and + 30 mV. My results show that in $[Ca^{2+}]_i > 1 \mu$ M, channel activation at + 30 mV was higher than at 0 mV (Figure 3.3). The increase in channel Popen with a rise in $[Ca^{2+}]_i$ and membrane depolarisation is consistent with reports from earlier studies performed on inside-out patches isolated from cultured hamster and rat cells (Barrett *et al.*, 1982; Jackson & Blair, 1998).

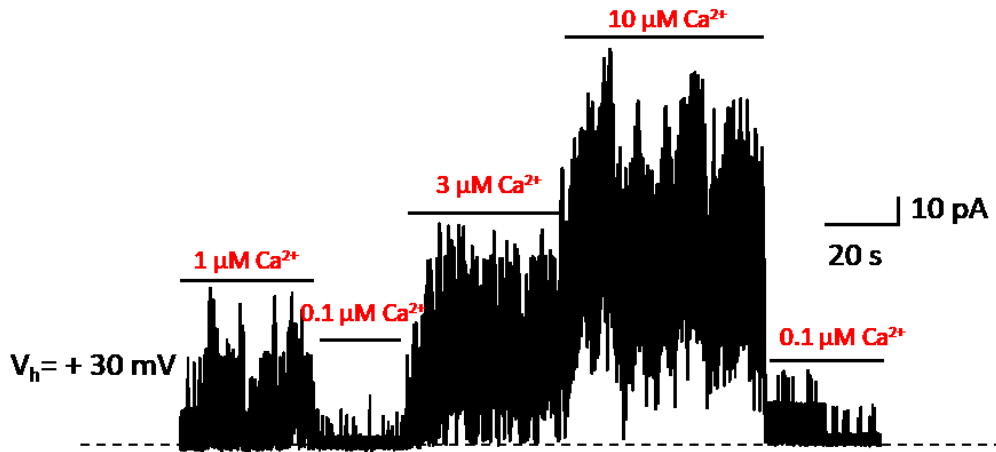


Figure 3.2: Effects of $[Ca^{2+}]_i$ on single BK_{Ca} channel activity. Example trace shows changes in channel activity in response to changes in $[Ca^{2+}]_i$, 0.1 μM , 1 μM , 3 μM and 10 μM . The recording was made using inside-out patch configuration. Membrane potential (V_m) was held at +30 mV. $[K^+]_i = 140$ mM; $[K^+]_o = 5$ mM.

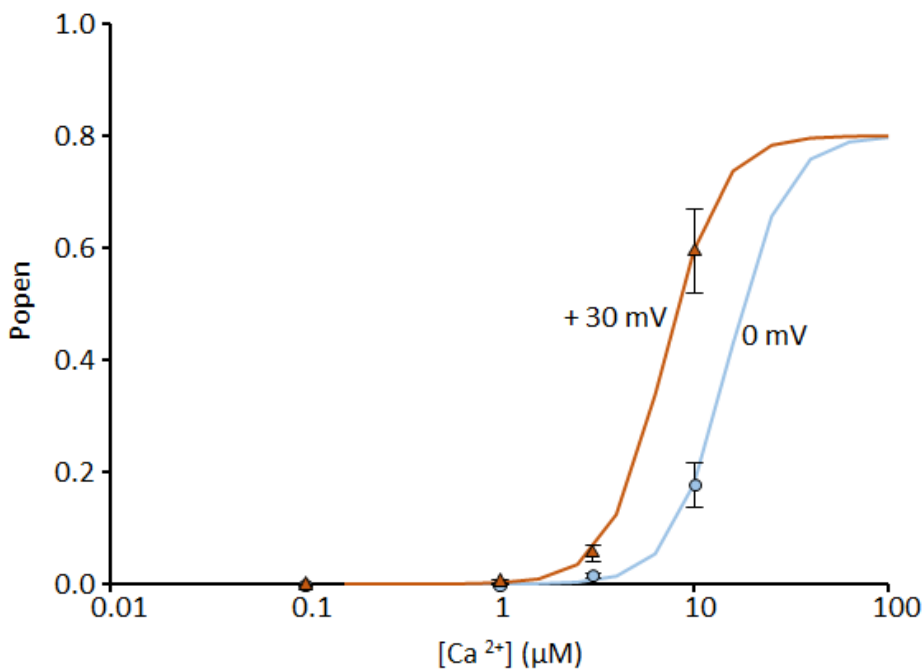


Figure 3.3: Effects of membrane potential on single BK_{Ca} channel activity. Graphs show changes in channel P_{open} in response to changes in membrane potential in different $[Ca^{2+}]_i$, 0.1 μM , 1 μM , 3 μM and 10 μM . Curves were fitted to the equation; $P_{open} = \frac{P_{max} [Ca^{2+}]^x}{[Ca^{2+}]^x + EC_{50}^x}$, where; x (Hill Coefficient)= 3, P_{max} (maximum P_{open})= 0.8 and EC_{50} (amount of Ca^{2+} required to produce half-activation of channels) at +30 mV= 7 μM and EC_{50} at 0 mV= 15 μM . Error bars show SEM, n= 5 (at 0 mV) and n= 4 to 5 (at +30 mV). All recordings were performed with inside-out patch configuration. $[K^+]_i = 140$ mM; $[K^+]_o = 5$ mM.

3.2.3 External TEA⁺ reduced the amplitude of single BK_{Ca} channel currents

TEA⁺ is a non-selective blocker of K⁺ channels. External TEA⁺ (0.2 mM) was shown to induce a half-block of BK_{Ca} channels at 0 mV and + 50 mV (Langton *et al.*, 1991; Brayden & Nelson, 1992). Identical concentration was used in the present study to confirm the presence of BK_{Ca} channels in the excised patches.

Recordings were made with V_m held at + 50 mV. TEA⁺ (0.2 mM) was applied to the extracellular side of BK_{Ca} channels via the pipette solution. Therefore, a separate patch, which had not been exposed to TEA⁺, was used for the control recording. My results are in line with earlier reports (Langton *et al.*, 1991; Brayden & Nelson, 1992), as external TEA⁺ (0.2 mM) reduced unitary current from 12.7 pA to 8.4 pA, see Figure 3.4. In addition, broadening of the “open level” peak, which represents a “flickery block” induced by TEA⁺, was observed (Figure 3.4).

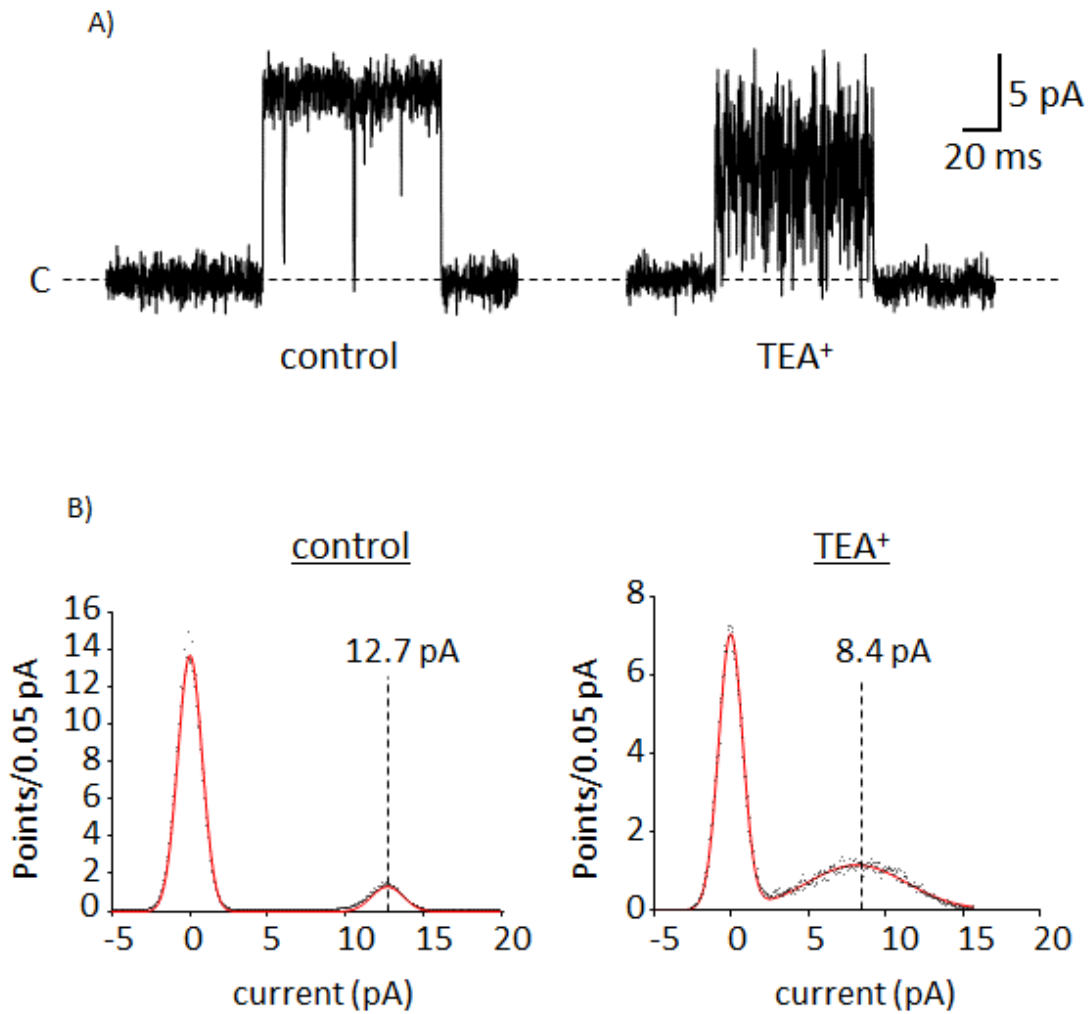


Figure 3.4: Effects of extracellular TEA⁺ application on single BK_{Ca} channel activity. A) Example traces showing channel activity in control, 1 μM $[\text{Ca}^{2+}]_i$, and with extracellular TEA⁺ (200 μM). Channel closed level is indicated by 'C'. B) Amplitude histograms of traces shown in A (above). The peaks were fitted with Gaussian curves. Mean unitary current was reduced from 12.7 pA (in control) to 8.4 pA with TEA⁺ in the pipette solution. Recordings were performed with inside-out patch configuration. V_m was held at +50 mV. $[\text{Ca}^{2+}]_i = 1 \mu\text{M}$; $[\text{K}^+]_i = 140 \text{ mM}$; $[\text{K}^+]_o = 5 \text{ mM}$.

3.3 Effects of haem on single BK_{Ca} channel activity

3.3.1 Intracellular haem application inhibited single BK_{Ca} channel activity

Haem has been reported to inhibit native and recombinant BK_{Ca} channel activity (Tang *et al.*, 2003; Jaggar *et al.*, 2005; Horrigan *et al.*, 2005). Therefore, the effects of haem under the present experimental conditions was also examined. Intracellular free haem concentration is predicted to be $\sim \leq 100$ nM (Smith *et al.*, 2011a; Khan & Quigley, 2011). Thus, my experiments were performed with 100 nM haem.

Recordings were made with V_m held at + 30 mV. Prior to the commencement of experiments, the Ca²⁺ sensitivity of the channels in inside-out patches was examined by alternating the perfusion of the intracellular side of the channels with 100 nM and 3 μ M Ca²⁺ solutions. This procedure was repeated throughout this study prior to performing experiments. Experiments were performed by first running control recordings, for ~ 5 minutes, by perfusing channels with the bath solution used to prepare the reagent. In this case, 3 μ M [Ca²⁺]_i was used to perform control recordings. Haem (100 nM) was then applied for ~ 5 minutes and washed.

Channel Popen was analysed 160 ± 40 s after haem application. My results showed that haem induced a mean relative inhibition of 99.6 ± 0.2 % in channel Popen, from 0.25 ± 0.07 to 0.0014 ± 0.0012 ($n = 7$, $p < 0.001$; Figure 3.5). These results are consistent with the findings from previous studies, where intracellular haem application was shown to reversibly inhibit the activity of native and recombinant BK_{Ca} channels (Tang *et al.*, 2003; Jaggar *et al.*, 2005; Horrigan *et al.*, 2005). The kinetics of haem inhibition and channel recovery was also measured by analysing channel Popen in sections of 10 second duration (Figure 3.5A). The graphs were normalized to the Popen measured under control conditions. The time constant (τ) of haem-mediated inhibition and channel recovery was 20.5 s and 39.8 s, respectively, although the delay in channel recovery produced an unusual fit of the 'wash' graph (Figure 3.5A). Noticeably, the kinetics of haem-mediated inhibition was close to the reported range of $\tau = 22$ s and 24 s (Tang *et al.*, 2003; Horrigan *et al.*, 2005).

The effects of haem on the mean open time (mot) of channels was also measured. To account for the variability in the number of open channel events detected between patches, mot was weighted. Weighting was performed by dividing the number of open events in each patch by the total number of open events measured in all patches. Such that the average mot was the sum of each weighted mot. Weighted variance was also calculated using Equation 4. The weighted variance was then used to calculate weighted standard deviation and weighted standard error of the mean (SEM).

My results showed that haem reduced the weighted mot of channels from 9.5 ± 0.4 ms to 3.6 ± 0.4 ms ($n=5$, $p < 0.0001$; Figure 3.6). This is in line with the reports from Horrigan *et al.*, 2005, where haem was shown to reduce the mot of recombinant BK_{Ca} channels at a depolarised potential, $V_m = +170$ mV.

Equation 4:
$$\sigma^2 = \frac{\sum(x_i - \bar{x}_w)^2 w_i}{N-1}$$

Where; w_i = weight for the i th patch and N = total number of open events.

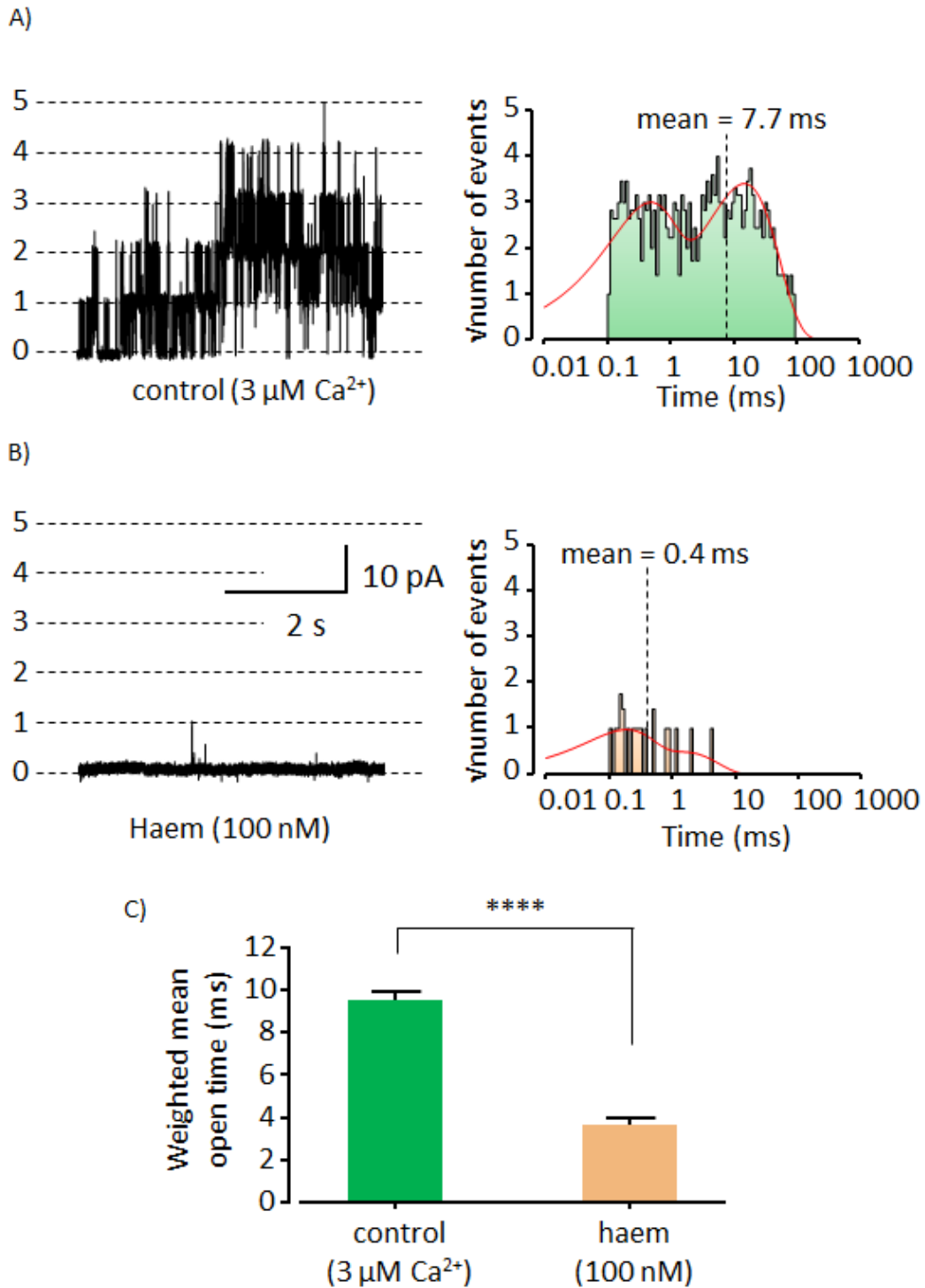


Figure 3.6: Effects of intracellular haem application on the open duration of single BK_{Ca} channels. Example traces with their corresponding event detection histograms show channel activity in A) control, $3 \mu\text{M} [\text{Ca}^{2+}]_i$; 535 open events detected, and B) Haem (100 nM); 21 open events detected. C) Histograms show weighted corrected mean open times of BK_{Ca} channels in the presence and absence of haem (100 nM). Recordings in the presence of haem were analysed ~ 160 seconds after haem application. Unpaired t-test was used for statistical analysis, **** $p < 0.0001$. Error bars show SEM, $n = 5$. Inside-out patch configuration was used for recording. V_m was held at +30 mV. $[\text{Ca}^{2+}]_i = 3 \mu\text{M}$; $[\text{K}^+]_i = 140 \text{ mM}$; $[\text{K}^+]_o = 5 \text{ mM}$.

3.3.2 The haem-mediated inhibition of BK_{Ca} channel activity was affected by intracellular pH (pH_i)

Intracellular pH (pH_i) in vascular SMCs is typically around 7.1 but fluctuations can occur due to cell metabolism or during pathophysiology (Smith *et al.*, 1998). For instance, during hypoxia, pH_i can drop from 7 to 6.4 (Avdonin *et al.*, 2003).

The effects of H⁺ on BK_{Ca} channel activity is controversial, as some studies have shown stimulatory effects (Hayabuchi *et al.*, 1998; Avdonin *et al.*, 2003; Hou *et al.*, 2008b) whilst others reported inhibitory effects (Kume *et al.*, 1990; Peers & Green, 1991; Church *et al.*, 1998; Liu *et al.*, 1999). I hypothesised that protonation of the imidazole side chains of the His residue within the CXXCH motif can interfere with haem binding to the channel. This was tested by applying haem to BK_{Ca} channels at pH_i 6.7 and comparing the results to observations already made at pH_i 7.2 (see section 3.3.1).

Experiments were performed with the same haem concentration (100 nM) that was used for pH 7.2 experiments, but here control experiments were performed at pH 6.7. Data was analysed 154 ± 34 s after haem application. The results showed that at pH 6.7, haem produced a mean relative inhibition of 99.8 ± 0.1 % in channel Popen, from 0.36 ± 0.07 to 0.0005 ± 0.0002 (n=7, p< 0.0001; Figure 3.7A). This was similar to the amount of haem-mediated inhibition, 99.6 ± 0.2 %, observed at pH 7.2. However, the time course of haem inhibition at pH_i 6.7 was slower, τ= 89 s, compared with observations at pH_i 7.2, τ= 20.5 s (n= 7 at pH_i 6.7, and n= 4 at pH_i 7.2, p< 0.05; Figure 3.7B). This suggests that the inhibitory effect of haem was slower in acidic intracellular pH. Also, in pH_i 6.7 weighted mot was reduced from 3.08 ± 0.23 ms to 1.52 ± 0.19 ms (n= 3, p> 0.05; graph not shown) but this was statistically not significant. To the best of my knowledge, this is the first study to examine the effects of pH_i on the haem-mediated inhibition of BK_{Ca} channel activity.

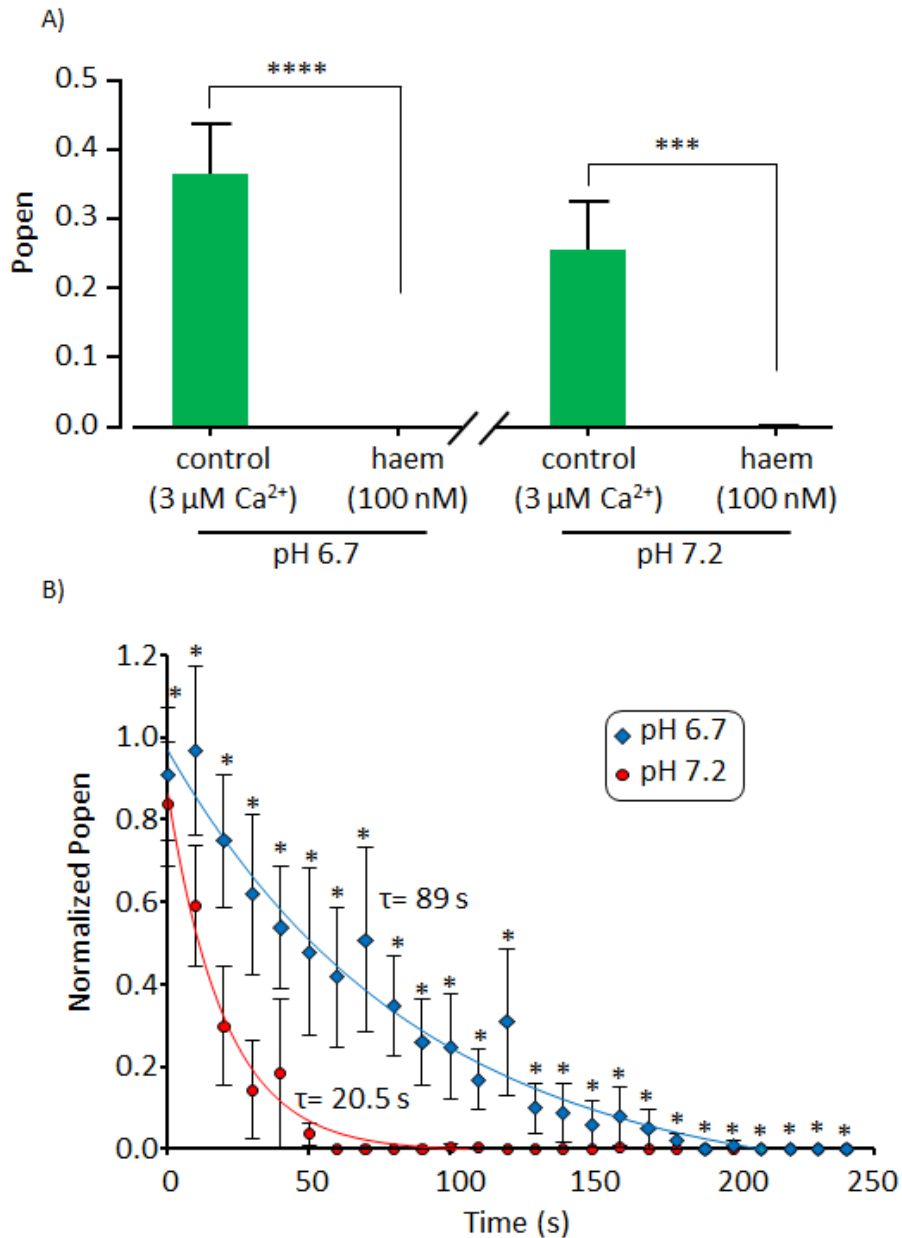


Figure 3.7: Effects of intracellular pH on the modulatory effect of haem on single BK_{Ca} channel activity. Popen analysis in the presence of haem at pH_i 6.7 and 7.2 was performed ~ 154 seconds and ~ 160 seconds after haem application, respectively. A) Histograms show channel Popen in the presence and absence of haem (100 nM) at pH_i 7.2 (obtained from Figure 3.5) and pH_i 6.7. Paired and unpaired t-tests were used for comparison within and between both pH conditions, respectively, $*** p \leq 0.001$ and $**** p \leq 0.0001$. Results from unpaired t-tests are not shown as they were non-significant. Error bars show SEM, $n = 7$. B) Graphs show the time course of haem (100 nM) inhibition in pH_i 7.2 (same as in Figure 3.5) and pH_i 6.7. These graphs were generated from 10 seconds analysis of channel Popen, with the 0 second time points representing the onset of haem application. The graphs were normalized to control values (Popen in the absence of haem). Unpaired t-test was used for statistical analysis, $* p \leq 0.05$. Error bars show SEM, $n = 7$ (for pH 6.7) and 4 (for pH 7.2). Inside-out patch configuration was used for all recordings. V_m was held at +30 mV. $[\text{Ca}^{2+}]_i = 3 \mu\text{M}$; $[\text{K}^+]_i = 140 \text{ mM}$; $[\text{K}^+]_o = 5 \text{ mM}$.

3.4 Effects of CO and CORM-3 on single BK_{Ca} channel activity

3.4.1 Effects of intracellular CO gas application on BK_{Ca} channel activity

CO gas has been shown to stimulate BK_{Ca} channels in a variety of tissues (Wang *et al.*, 1997b; Wang & Wu, 1997; Wu *et al.*, 2002; Jaggar *et al.*, 2005). The mechanism of action of CO has been proposed to be haem-dependent and -independent. I chose to examine the effects of CO in the absence of haem, to investigate whether CO mediates haem-independent effects on mesenteric SMC BK_{Ca} channels. Experiments were performed with 30 μ M CO gas solution because this concentration has been shown to stimulate BK_{Ca} channel activity (Wang & Wu, 1997; Wu *et al.*, 2002). Saturated CO gas solution was prepared as described in the Methods section 2.3.1.2. This solution was then diluted to make the 30 μ M CO gas solution.

Intracellular application of CO gas (30 μ M), for 5 minutes, to BK_{Ca} channels exposed to 300 nM [Ca²⁺]_i increased mean relative channel activity by $66 \pm 1.2\%$, from 0.01 ± 0.009 to 0.02 ± 0.01 ($n=3$, $p>0.05$; Figure 3.8), but this effect was not significant. Also, channel stimulation was only observed in 2 out of the 3 patches. Furthermore, CO gas did not significantly increase weighted mot, from 3.5 ± 0.74 ms to 4.8 ± 0.42 ms ($n=3$, $p>0.05$; Figure 3.8).

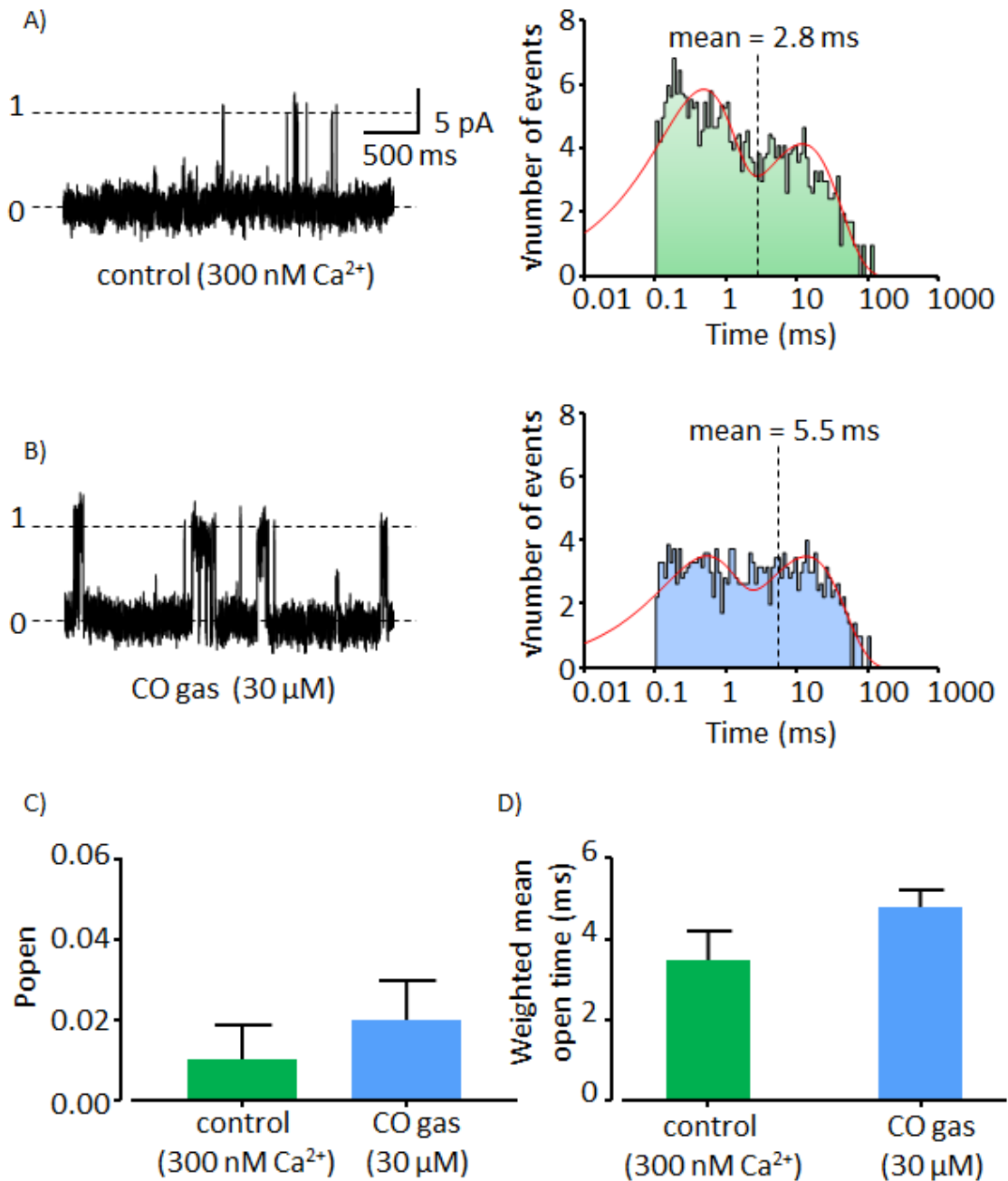


Figure 3.8: Effects of intracellular CO gas application on single BK_{Ca} channel activity. Example traces with their corresponding event detection histograms showing channel activity in A) control, 300 nM [Ca²⁺]_i; 1290 open events detected, and B) CO gas (30 μM) solution; 637 open events detected. Histograms show C) channel Popen and D) weighted mean open time in the presence and absence of CO gas (30 μM). Paired and unpaired t-tests were used for statistical analysis of results in C) and D), respectively. Results were non-significant as $p > 0.05$. Error bars show SEM, $n = 3$. Recordings were performed with inside-out patch configuration. V_m was held at +30 mV. [Ca²⁺]_i = 300 nM; [K⁺]_i = 140 mM; [K⁺]_o = 5 mM.

The effects of CO on BK_{Ca} channel activity have been shown to be abolished in saturating [Ca²⁺]_i supposedly because CO acts as a Ca²⁺ mimetic (Hou *et al.*, 2008a). Therefore, my experiments were also performed in high [Ca²⁺]_i, 3 μM, to investigate whether [Ca²⁺]_i does interfere with the CO-mediated effects on BK_{Ca} channel activity. Intracellular application of CO gas (30 μM) in 3 μM [Ca²⁺]_i decreased mean relative channel activity to 84 ± 0.09 %, from 0.32 ± 0.06 to 0.28 ± 0.08 (n= 3, p> 0.05; Figure 3.9) but this effect was not significant. Furthermore, due to the high number of active channels in 3 μM [Ca²⁺]_i, analysis of open durations could not be performed.

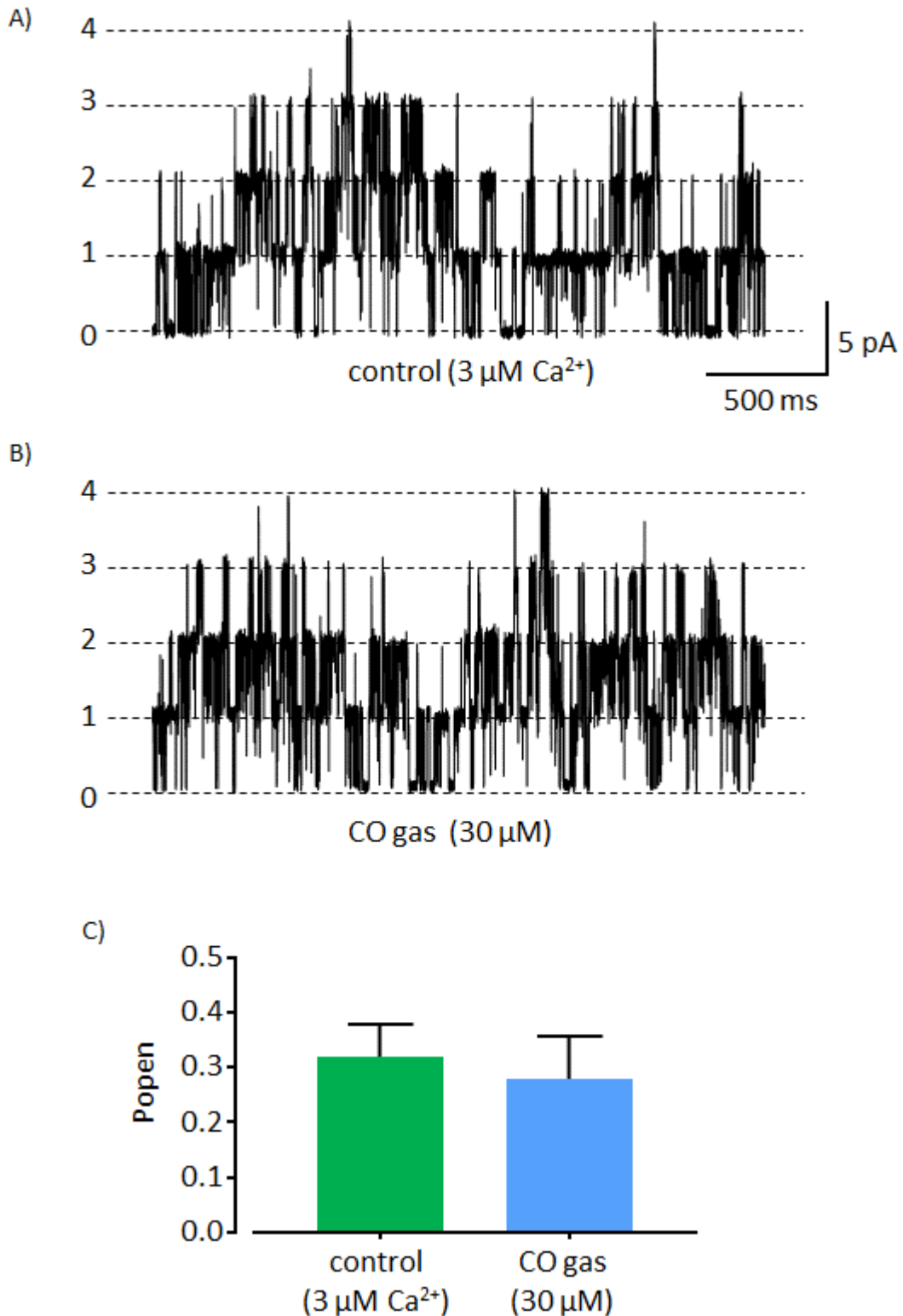


Figure 3.9: Effects of intracellular CO gas application on single BK_{Ca} channel activity in high $[\text{Ca}^{2+}]_{\text{i}}$. Example traces showing channel activity in A) control, 3 μM $[\text{Ca}^{2+}]_{\text{i}}$ and B) CO gas solution (30 μM). C) Histograms show channel Popen in the presence and absence of CO gas (30 μM). Statistical significance was tested using paired t-test, results were non-significant as $p > 0.05$. Error bars show SEM, $n = 3$. Recordings were performed with inside-out patch configuration. V_{m} was held at +30 mV. $[\text{Ca}^{2+}]_{\text{i}} = 3 \mu\text{M}$; $[\text{K}^{+}]_{\text{i}} = 140 \text{ mM}$; $[\text{K}^{+}]_{\text{o}} = 5 \text{ mM}$.

3.4.2 Intracellular application of CORM-3 enhanced BK_{Ca} channel activity

CO gas is relatively expensive and unsafe to use. In addition, diluting a gaseous solution to a required concentration is tricky. Therefore, I turned my attention to the use of CORMs. The preferred CORM was CORM-3 because its water solubility makes it easier to work with. Intracellular application of 30 μM CORM-2 was shown to produce significant enhancement of BK_{Ca} channel activity (Williams *et al.*, 2004; Williams *et al.*, 2008; Telezhkin *et al.*, 2011). Therefore, identical concentration of CORM-3 was used to perform my experiments, as both forms of CORM release CO with fast kinetics (Desmard *et al.*, 2012). Control experiments were also performed using iCORM-3.

Intracellular application of CORM-3 (30 μM) to BK_{Ca} channels, in 300 nM $[\text{Ca}^{2+}]_i$ for 5 minutes, increased mean relative channel Popen to $643 \pm 191\%$, from 0.0007 ± 0.0003 to 0.0074 ± 0.0043 ($n = 7$, $p < 0.01$; Figure 3.10). However, the change in weighted mot, from 3.45 ± 0.14 ms to 4.04 ± 0.25 ms ($n = 7$, $p > 0.05$; Figure 3.10), was non-significant. As expected, the decrease in channel activity, from 0.0017 ± 0.0009 to 0.0009 ± 0.0005 ($n = 5$, $p > 0.05$; Figure 3.11), in the presence of iCORM-3 (30 μM) was non-significant. Also, the effect of iCORM-3 (30 μM) on weighted mot, a decrease from 3.22 ± 0.63 ms to 3.02 ± 0.27 ms ($n = 5$, $p > 0.05$; Figure 3.11), was non-significant.

These results are consistent with previous reports where intracellular application of another CORM, CORM-2 (30 μM), to recombinant BK_{Ca} channels exposed to ~ 300 nM $[\text{Ca}^{2+}]_i$, enhanced channel activity whereas iCORM-2 produced no significant effect (Williams *et al.*, 2004; Williams *et al.*, 2008). Furthermore, the non-significant effect of iCORM-3 is consistent with the lack of CO release from iCORM-3 as previously shown in my deoxymyoglobin carbonylation assays (c.f. Methods section 2.7.2.3).

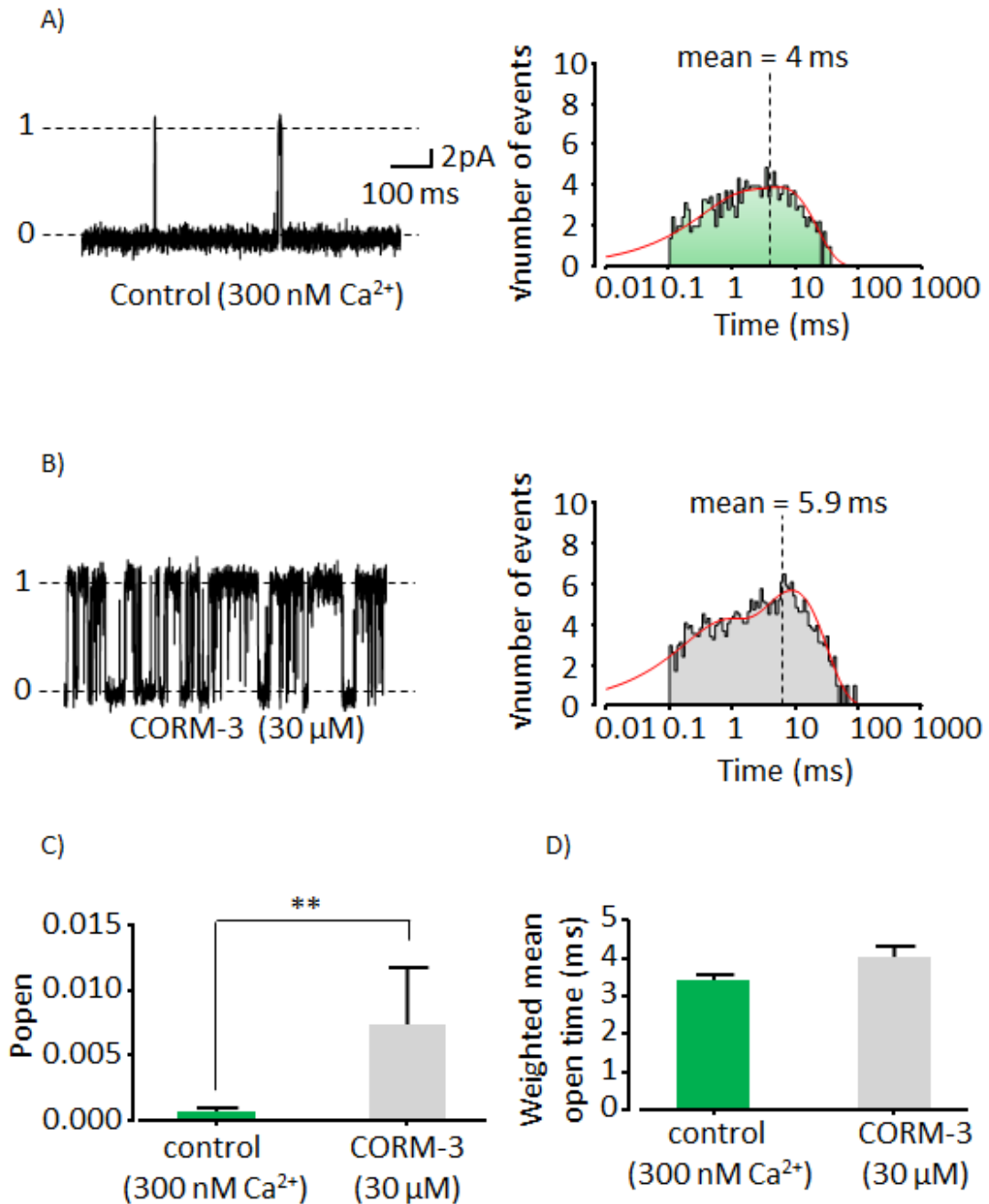


Figure 3.10: Effects of intracellular CORM-3 application on single BK_{Ca} channel activity. Example traces with their corresponding event detection histograms showing channel activity in A) control, 300 nM [Ca²⁺]_i; 515 open events detected, and B) CORM-3 (30 μM); 1286 open events detected. Histograms show C) channel Popen and D) weighted mean open time in the presence and absence of CORM-3 (30 μM). Paired and unpaired t-tests were used for statistical analysis of results in C) and D), respectively. Only significant results are shown ** p < 0.01. Error bars show SEM, n = 7. Recordings were performed with inside-out patch configuration. V_m was held at +30 mV. [Ca²⁺]_i = 300 nM; [K⁺]_i = 140 mM; [K⁺]_o = 5 mM.

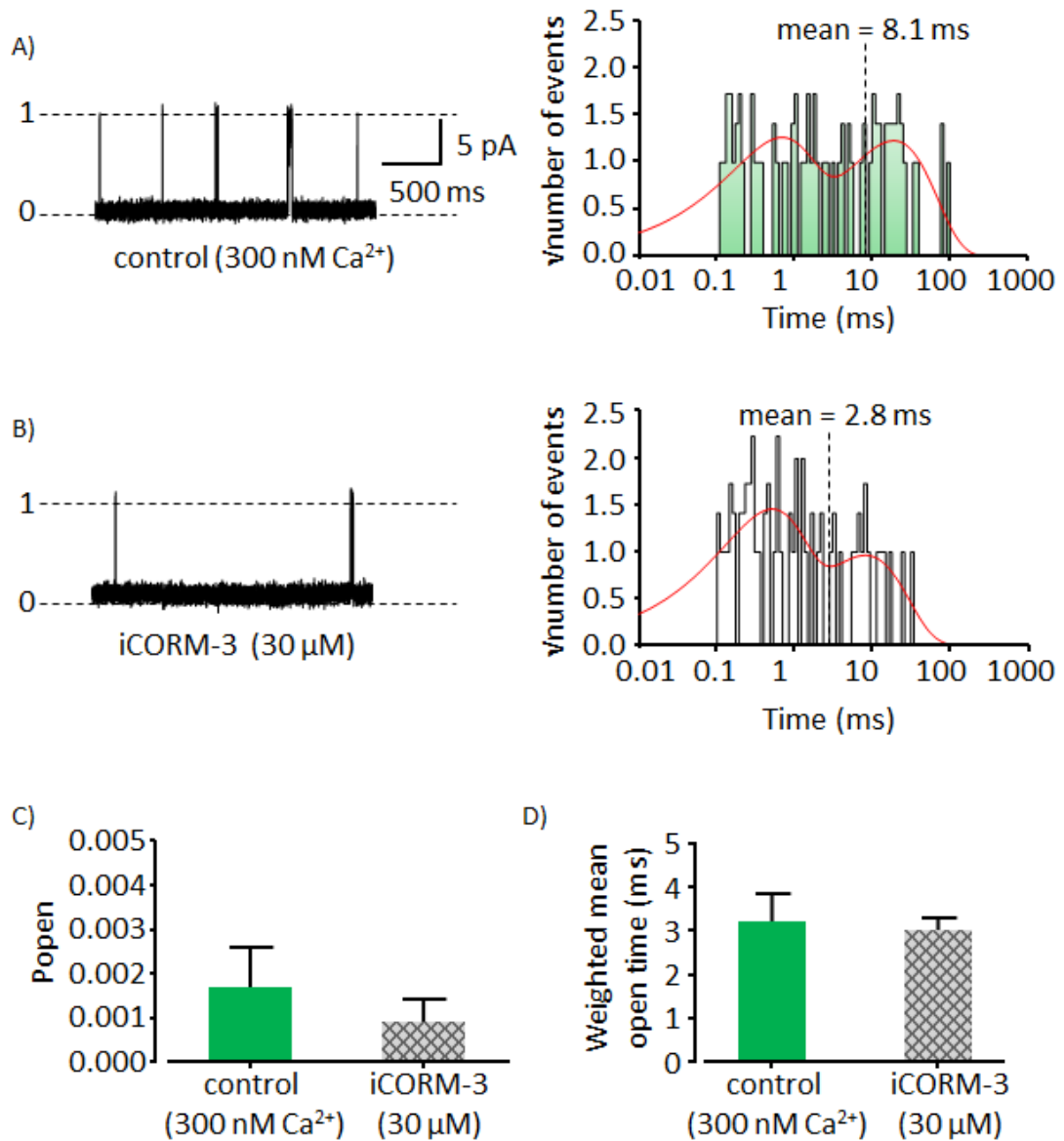


Figure 3.11: Effects of intracellular iCORM-3 application on single BK_{Ca} channel activity. Example traces with their corresponding event detection histograms show channel activity in A) control, 300 nM [Ca²⁺]_i; 80 open events detected, and B) iCORM-3 (30 μM); 75 open events detected. Histograms show C) channel Popen and D) weighted mean open time in the presence and absence of iCORM-3 (30 μM). Paired and unpaired t-tests were used for statistical analysis of results in C) and D), respectively. Results were not significant as $p > 0.05$. Error bars show SEM, $n = 5$. Recording was performed with inside-out patch configuration. V_m was held at +30 mV. [Ca²⁺]_i = 300 nM; [K⁺]_i = 140 mM; [K⁺]_o = 5 mM.

The effects of $[Ca^{2+}]_i$ on the CORM-3-mediated stimulatory effect on BK_{Ca} channel activity was examined via the application of CORM-3 (30 μM) to channels exposed to 3 μM $[Ca^{2+}]_i$. The results showed a mean relative change of 17 ± 0.3 % in channel Popen, from 0.47 ± 0.09 to 0.53 ± 0.12 ($n=3$, $p > 0.05$; Figure 3.12), but this was not significant. Also, as expected, channel activity was high in 3 μM $[Ca^{2+}]_i$ which restricted the generation of weighted event detection histograms. This is because only 1 out of the 3 patches used had a single level of opening that could be used for analysis (see Figure 3.12).

Nevertheless, Williams *et al.* (2008) showed that the stimulatory effect of CORM-2 (30 μM) on recombinant BK_{Ca} channel activity was reduced in higher $[Ca^{2+}]_i$ of 10 and 100 μM . In addition, Hou *et al.* (2008) showed complete abolition of CORM-2 (30 μM)-induced channel activation of recombinant BK_{Ca} channels in 120 μM $[Ca^{2+}]_i$.

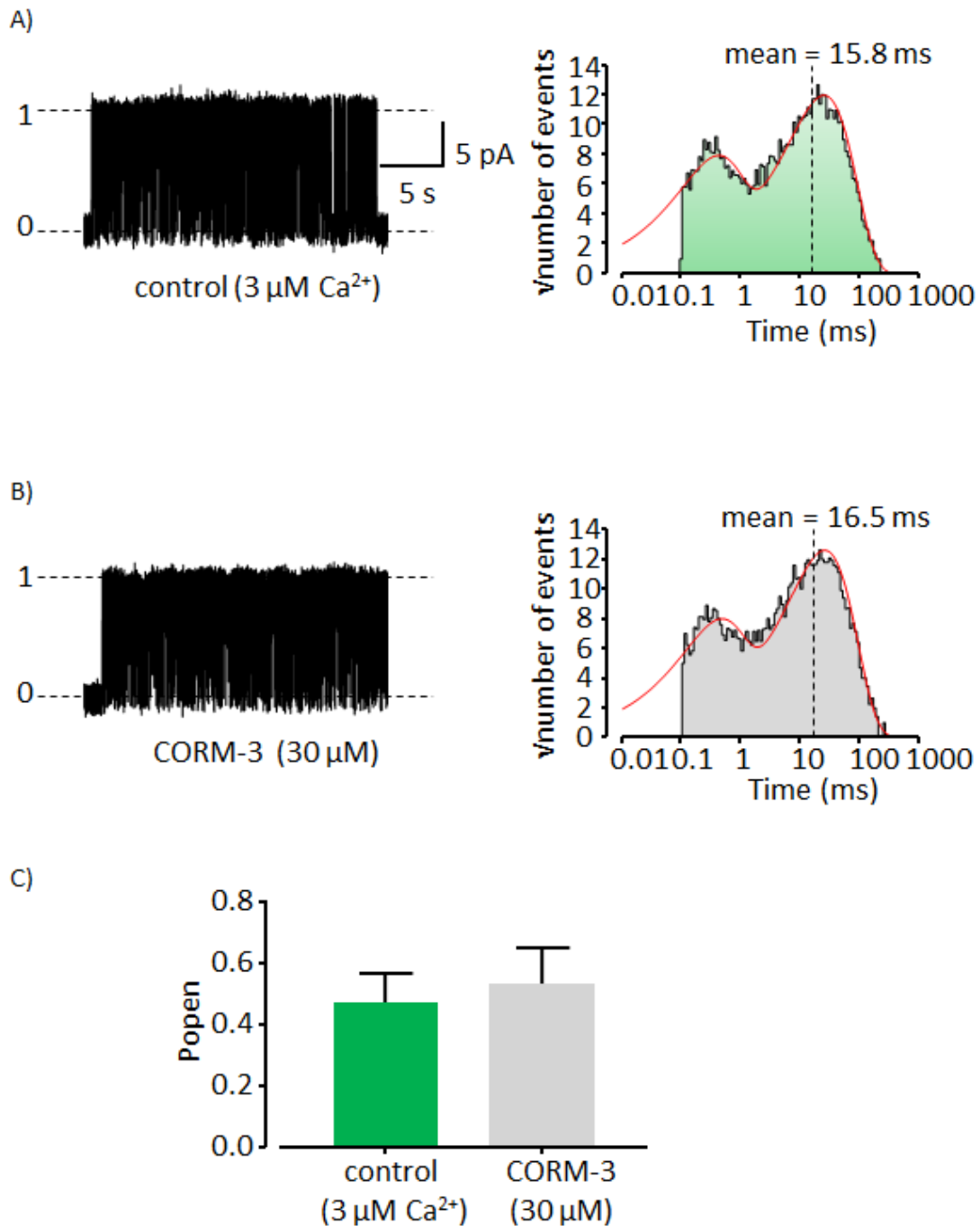


Figure 3.12: Effects of intracellular application of CORM-3 on BK_{Ca} channels exposed to high [Ca²⁺]_i. Example traces with their corresponding event detection histograms show channel activity in A) control, 3 μM [Ca²⁺]_i; 5519 open events detected, and B) CORM-3 (30 μM); 5990 open events detected. C) Histograms show channel Popen in the presence and absence of CORM-3 (30 μM). Paired t-test was used for statistical analysis, results were non-significant as $p > 0.05$. Error bars show SEM, $n=3$. Weighted mean open time histograms were not generated because in 2 out of the 3 patches there was > 1 active BK_{Ca} channel. Recording was performed with inside-out patch configuration. V_m was held at +30 mV. [Ca²⁺]_i = 3 μM; [K⁺]_i = 140 mM; [K⁺]_o = 5 mM.

3.5 Intracellular application of biliverdin inhibited BK_{Ca} channel activity

Like CO, biliverdin is also a primary haem degradation product. Thus, the plan was to investigate whether biliverdin was also involved in the haem regulation of BK_{Ca} channel activity. Experiments were performed with 10 μ M biliverdin because similar concentration has been shown to enhance BK_{Ca} channel activity (Williams *et al.*, 2004). Based on the biliverdin-mediated stimulatory effect reported by Williams *et al.* (2004), my experiments were performed in lower $[Ca^{2+}]_i$, 300 nM. This was done to ensure that channel Popen was not initially at maximum, so that any stimulatory effect induce by biliverdin was measurable.

The results showed that intracellular application of biliverdin (10 μ M), for \sim 5 minutes, decreased mean relative channel Popen to 22.5 ± 9.2 %, from 0.0013 ± 0.0009 to 0.0003 ± 0.0002 (n= 4, p< 0.05; Figure 3.13). Biliverdin also decreased the weighted mot of channels from 1.53 ± 0.27 ms to 0.55 ± 0.07 ms (n= 4, p< 0.05; Figure 3.13). These results were unexpected, as they contradict reports from Williams *et al.* (2004) where intracellular application of biliverdin was shown to produce a 4-fold increase in recombinant BK_{Ca} activity.

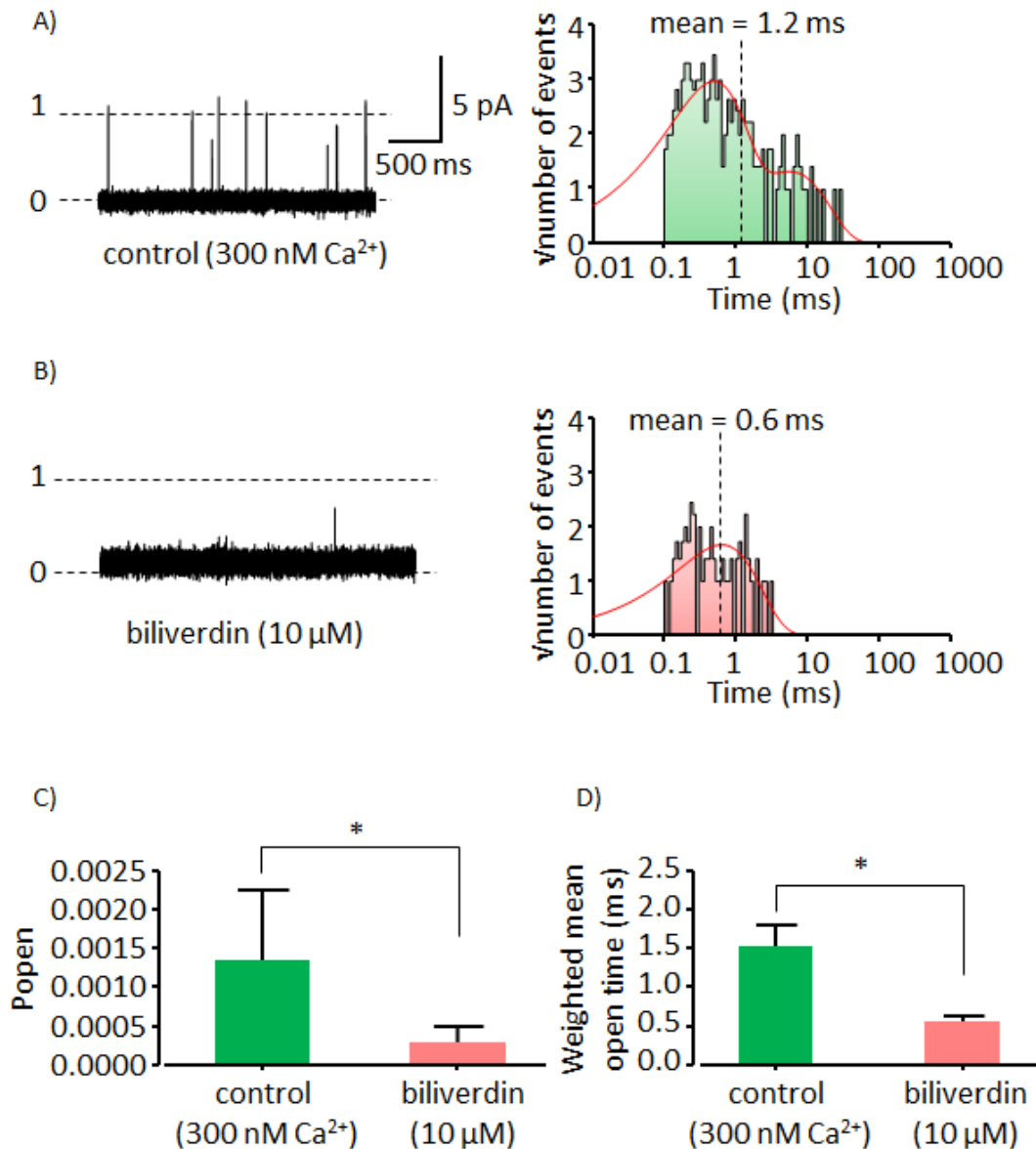


Figure 3.13: Effects of intracellular application of biliverdin on single BK_{Ca} channel activity. Example traces with their corresponding event detection histograms show channel activity in A) control, 300 nM [Ca²⁺]_i; 254 open events detected, and B) biliverdin (10 μM); 71 open events detected. Histograms show C) channel Popen and D) weighted mean open time in the presence and absence of biliverdin (10 μM). Paired and unpaired t-tests were used for statistical analysis of results in C) and D), respectively, * p ≤ 0.05. Error bars show SEM, n = 4. Recordings were performed with inside-out patch configuration. V_m was held at +30 mV. [Ca²⁺]_i = 300 nM; [K⁺]_i = 140 mM; [K⁺]_o = 5 mM.

3.6 Intracellular application of ZnPP-IX had no effect on BK_{Ca} channel activity

Tin and chromium mesoporphyrin have been reported to be the most potent inhibitors of HO activity *in vitro* whereas ZnPP-IX and metal-free metalloporphyrins are least potent (Vreman *et al.*, 1993; Wong *et al.*, 2011). Nevertheless, ZnPP-IX was the preferred HO inhibitor for use in the present study because it is a physiological metalloporphyrin (Labbe *et al.*, 1999). The plan was to use ZnPP-IX to inhibit HO activity in whole-cell studies. Therefore, it was important to examine whether ZnPP-IX also influenced BK_{Ca} channel activity. ZnPP-IX has been reported to inhibit rat tissue HO-1 and HO-2 activity with IC₅₀ 5.45 μ M and 2.65 μ M, respectively (Wong *et al.*, 2011). Thus, I planned to perform whole-cell experiments with 10 μ M ZnPP-IX to ensure complete inhibition of HO activity. Therefore, 10 μ M ZnPP-IX was also used to perform the single channel studies.

These assays were performed in 3 μ M Ca²⁺ solution to induce substantial channel activity. This is because like haem, ZnPP-IX is a metalloporphyrin, so it was expected to produce inhibitory effects. My results showed that a 5-minute intracellular application of ZnPP-IX (10 μ M) to BK_{Ca} channels increased mean relative Popen by 73.5 ± 80.2 %, from 0.25 ± 0.12 to 0.31 ± 0.10 ($n = 4$, $p > 0.05$; Figure 3.14). However, this effect was statistically not significant. Also, the effect of ZnPP-IX on weighted mot, an increase from 13.43 ± 1.0 ms to 16.01 ± 1.48 ms ($n = 4$, $p > 0.05$; Figure 3.14), was non-significant. These results are in line with previous report which showed that intracellular application of ZnPP-IX (125 nM) to recombinant BK_{Ca} channels did not affect channel activity (Tang *et al.*, 2003).

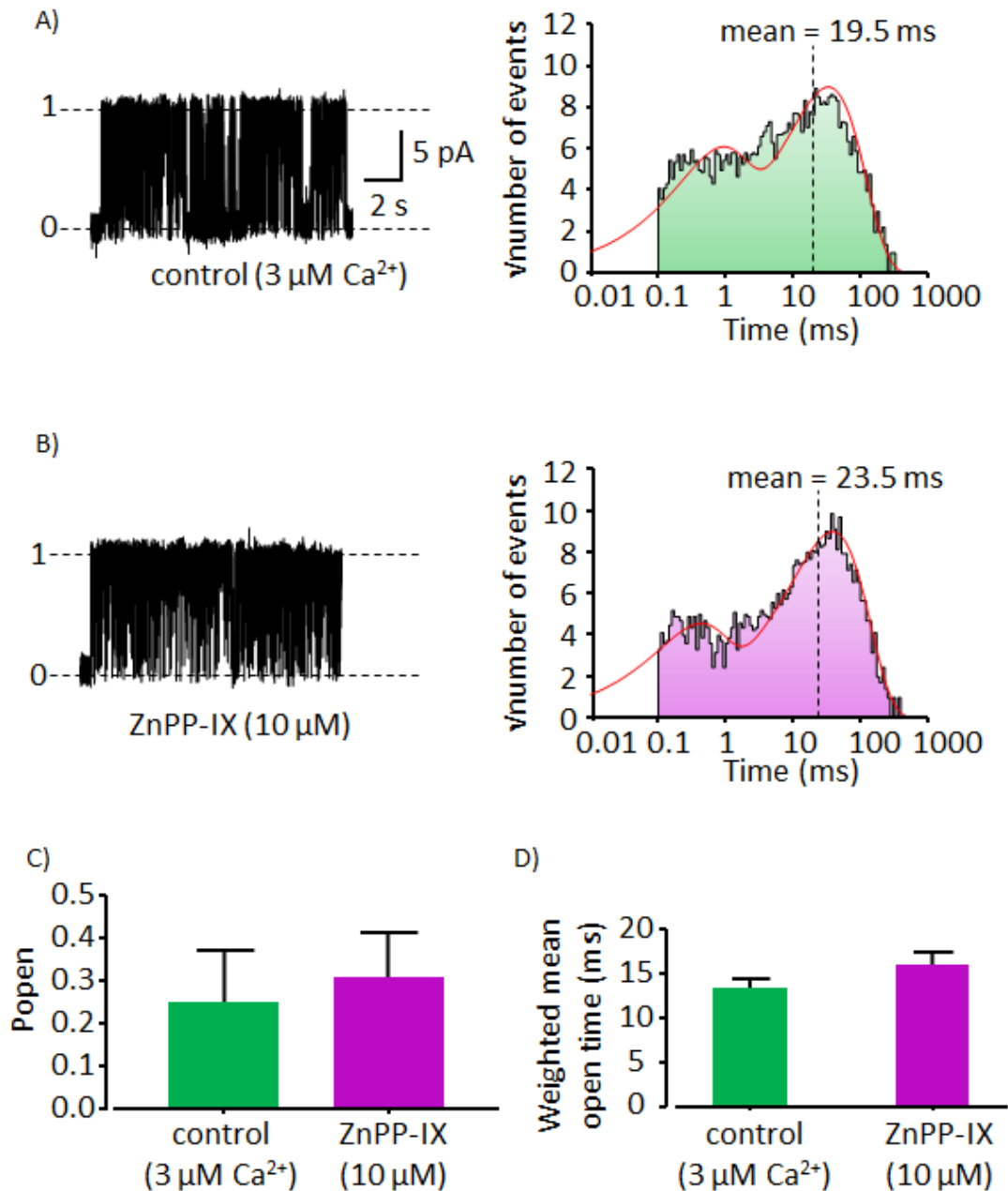


Figure 3.14: Effects of intracellular application of ZnPP-IX on single BK_{Ca} channel activity. Example traces with their corresponding event detection histograms show channel activity in A) control, 3 μM [Ca²⁺]_i; 3201 open events detected, and B) ZnPP-IX (10 μM); 2810 open events detected. The histograms show C) channel Popen and D) weighted mean open time in the presence and absence of ZnPP-IX (10 μM). Paired and unpaired t-tests were used for statistical analysis of the results in C) and D) respectively. Both results were not significant as $p > 0.05$. Error bars show SEM, $n = 4$. Recordings were performed with inside-out patch configuration. V_m was held at +30 mV. [Ca²⁺]_i = 3 μM; [K⁺]_i = 140 mM; [K⁺]_o = 5 mM.

3.7 Discussion

3.7.1 Characterisation of single BK_{Ca} channel activity

The observed channel properties; large single channel conductance (210 pS) and sensitivity to $[Ca^{2+}]_i$, depolarisation and external TEA⁺, are in agreement with the previously reported characteristics of BK_{Ca} channels (Pallotta *et al.*, 1981; Barrett *et al.*, 1982; McManus & Magleby, 1991; Jackson & Blair, 1998). This confirms that the unitary currents recorded here arise from the opening of BK_{Ca} channels.

Notably, the $[Ca^{2+}]_i$ required to activate the channels was less at +30 mV compared with 0 mV. This is consistent with earlier reports where the Ca²⁺ sensitivity of BK_{Ca} channels was shown to increase with depolarisation (Barrett *et al.*, 1982; Jackson & Blair, 1998). Intracellular Ca²⁺ has been proposed to activate BK_{Ca} channels in a cooperative manner produced by the joint effect of the Ca²⁺ sensors on channel gating (Shi & Cui, 2001; Zhang *et al.*, 2001)

The “flickery” block observed in the presence of TEA⁺ results from the rapid kinetics of the blocking and unblocking events which are not fully resolved at the recording frequency of 2 kHz (Langton *et al.*, 1991; Brayden & Nelson, 1992). The proposed mechanism of action of TEA⁺ is via a state-independent block which occurs due to the superficial binding of TEA⁺ to the channel thereby preventing K⁺ entry (Langton *et al.*, 1991).

3.7.2 Effects of haem on single BK_{Ca} channel activity

Previous work using mutagenesis, indicate that the haem-mediated inhibition of BK_{Ca} channel activity occurs because of its interaction with the highly conserved CXXCH motif on the cytoplasmic side of the channels (Tang *et al.*, 2003; Horrigan *et al.*, 2005). The location of the CXXCH motif (on the flexible interface between the RCK domains), enables haem binding to disrupt the gating ring such that it alters the allosteric regulation of the channel by Ca²⁺ and voltage (Horrigan *et al.*, 2005). It should be noted that Tang *et al.* (2003) and Horrigan *et al.* (2005) performed their studies in the virtual absence of Ca²⁺ using recombinant hSlo1 channels which were not co-expressed with β -subunits. However, my study was performed in the presence of Ca²⁺ with native channels which should comprise of $\alpha\beta_1$ subunits. Therefore, since haem still inhibited

BK_{Ca} channel activity under my experimental conditions, consistent with results presented by Tang *et al.* (2003) and Horrigan *et al.* (2005), my results indicate that the modulatory effect of haem on BK_{Ca} channel activity is not influenced by auxiliary subunits or [Ca²⁺]_i. In addition, given that free [haem]_i is estimated to be 100 nM and I and others (Tang *et al.*, 2003; Jaggar *et al.*, 2005; Horrigan *et al.*, 2005) have shown that haem (100 nM) produced channel inhibition, it is surprising that BK_{Ca} channel activity can still be recorded from whole-cell. The reason for this is unclear.

To the best of my knowledge, this is the first study to show that pH_i can influence the haem-mediated inhibition of BK_{Ca} channels. This may be important during pathological conditions, as it has been shown that ischaemia/hypoxia can induce intracellular acidosis and possibly raise haem levels (Tsai *et al.*, 1997; Kintner *et al.*, 2000; Dore, 2002). Since histidine (His) residues have a pK_a of 6.6 ± 1.0, it is apparent that the intracellular His residues of BK_{Ca} channels could have been protonated at pH 6.7 (Grimsley *et al.*, 2009). It is conceivable that the delay in the haem-mediated inhibition of BK_{Ca} channel activity at pH 6.7 might result from either the protonation of the haem molecule (c.f. Methods section 2.7.1.2) or the imidazole side chain of the His 616 in the CXXCH motif. Such modification could have slowed the rate of association between haem and the channel, but the overall block induced by haem at pH_i 6.7 and 7.2 was surprisingly identical.

3.7.3 Effects of CO on single BK_{Ca} channel activity

More experiments are needed in the present study to confirm that intracellular CO gas application enhances BK_{Ca} channel activity. Such results would be in line with previous reports which showed that CO gas enhanced native BK_{Ca} channel activity in the presence of Ca²⁺ (Wang & Wu, 1997; Wu *et al.*, 2002).

Experiments with CORM-3 were performed in different [Ca²⁺]_i but channel activity was too low in 100 nM [Ca²⁺]_i to make any meaningful measurements, so this was not shown. Nevertheless, consistent with previous report (Hou *et al.*, 2008a; Williams *et al.*, 2008), my results suggest that the stimulatory effect of CORM-3 is Ca²⁺-sensitive. This is because CORM-3 produced channel activation in 300 nM [Ca²⁺]_i but no significant effect in 3 μM [Ca²⁺]_i. Furthermore, unlike haem, CORM-3 altered channel Popen with no significant effect on open channel duration. This suggests that CORM-3 might act by shortening mean closed time duration with little effect on mean open time.

Notably, CORM-3 activation was observed without exogenous haem application. Thus, it can be speculated that haem was already bound to the BK_{Ca} channel on the isolated patch, alongside an unknown enzyme which catalyses the reduction of ferric to ferrous haem. Therefore, CO was able to bind to the haem-bound channel to cause channel activation, because the unknown enzyme maintained haem in a ferrous state. However, based on the inhibitory effect of haem reported in this study and by others (Tang *et al.*, 2003; Jaggar *et al.*, 2005; Horrigan *et al.*, 2005), such occurrence is unlikely because channel activity was often observed in freshly isolated patches.

I agree with the haem-independent proposal involving a metallocluster suggested by Telezhkin *et al.* (2011). This metallocluster was proposed to be coordinated to the channel protein by key amino acid residues present on the RCK1/2 domains of the channel protein. Since the stimulatory effect of CO was reported to be low in the absence of Ca²⁺ but completely abolished in saturating Ca²⁺, it is apparent some Ca²⁺ is required for the modulatory effect of CO (Hou *et al.*, 2008a; Telezhkin *et al.*, 2011). Perhaps, Ca²⁺ is essential because of the close interaction between the Ca²⁺ binding sites (RCK1/2) and the metallocluster. So I assume that at low [Ca²⁺]_i, the interaction of CO with Fe²⁺ atoms in the metallocluster indirectly activates the channel by enhancing the binding energy of Ca²⁺. Therefore, the contributions from CO binding to the metallocluster would be redundant because the Ca²⁺ binding is sufficient to cause channel activation. However, *in silico* studies suggest that CO activates BK_{Ca} channels by disrupting highly conserved Fe²⁺ bridges in BK_{Ca} channels (Wang, 2017). In addition, it can be argued that in inside-out patches Fe²⁺ might be oxidised to Fe³⁺. Thus, the CO-mediated activation of channels in inside-out patches could result from other mechanisms besides its binding to metalloclustered sites or Fe²⁺ bridges.

Furthermore, CO has been proposed to activate BK_{Ca} channels by increasing the Ca²⁺-binding sites and enhancing the Ca²⁺-sensitivity of the channels (Wang *et al.*, 1997b; Xi *et al.*, 2004). The proposed mechanism via which CO increases the Ca²⁺-binding sites involves CO binding to specific modulatory sites on BK_{Ca} channels, which alters channel conformation thereby exposing new Ca²⁺-binding sites (Wang *et al.*, 1997b).

3.7.4 Effects of biliverdin on single BK_{Ca} channel activity

The discrepancy between the inhibition of BK_{Ca} channels by biliverdin (10 μM) in this study and the stimulatory effect reported by Williams *et al.* (2004) is unclear. This is because Williams *et al.* (2004) performed experiments using heterologous cells expressing αβ₁ subunits and the native channels used in this study should comprise both subunits. The inhibition produced by haem (100 nM), 99.5 ± 0.34 %, was more than the inhibition induced by biliverdin (10 μM), 77.5 ± 9.20 %, but the mechanism behind the biliverdin-mediated inhibition is unclear.

3.7.5 Effects of ZnPP-IX on single BK_{Ca} channel activity

My experiments did not show any direct effect of ZnPP-IX on single BK_{Ca} channel activity. This makes ZnPP-IX favourable for use as a HO inhibitor in my whole-cell study. Nevertheless, it is plausible that the central Zn²⁺ atom of ZnPP-IX could interact with the His residue in the CXXCH motif of BK_{Ca} channels. However, if such interaction occurred in the present study, it did not significantly affect BK_{Ca} channel activity.

3.8 Summary

The results from my inside-out patch study agree with previous reports because intracellular application of haem and CO inhibits and activates single BK_{Ca} channel activity, respectively. Furthermore, the results show that intracellular factors (such as pH and [Ca²⁺]_i) influence the modulatory effects of haem and CO on BK_{Ca} channel activity; as acidic intracellular pH slowed down the kinetics of haem inhibition without affecting its potency and the stimulatory effect of CO was absent in high (3 μM) and low (100 nM) [Ca²⁺]_i.

The next chapter examines the effects of haem and CO on BK_{Ca} channel STOCs. Based on the results from the inside-out patch study, haem is expected to inhibit STOCs whilst CO is predicted to produce stimulatory effects.

Chapter 4 THE EFFECTS OF HAEM AND CO ON STOCs

4.1 Introduction

Inside-out patch studies provided information about the direct effects of intracellular haem and its degradation products on single BK_{Ca} channel activity. However, taking into consideration that under certain pathological conditions external haem can reach up to 20 μ M (Sawicki *et al.*, 2015), it was important to also assess the effect of haem applied extracellularly. An extensive literature search revealed only one study that examined the effects of CO and heme-L-lysinate (HLL), a HO substrate, on STOCs (Jaggar *et al.*, 2002). Therefore, my data now allows the effects of extracellular haem on STOCs to be examined for the first time. In addition, performing experiments on intact cells where intracellular signalling components are maintained is useful for mimicking physiological conditions more closely.

Based on the hypothesis that haem modulates STOCs via the CO generated from HO-mediated haem degradation, my aim was to elucidate further the mechanism of action of haem by addressing questions such as, could haem signalling to BK_{Ca} channels occur within a signalling complex? Could haem modulate STOCs by influencing Ca²⁺ spark frequency? Could the location of haem (whether intracellular or extracellular) influence its modulatory effect on STOCs? These questions were addressed using both ruptured and perforated patch techniques.

4.2 Characterisation of STOCs

Confirmation of the presence of STOCs and the fact that they are produced by BK_{Ca} channel activation was achieved by examining the effects of; voltage and external Ca²⁺ (BK_{Ca} channel activators), TEA⁺ and penitrem A (BK_{Ca} channel blockers), ryanodine (an inhibitor of Ca²⁺ release from Ca²⁺ stores) and caffeine (a Ca²⁺ store depleting agent) on STOCs. Since these experiments were to confirm the presence of BK_{Ca} channels and mechanism of STOC generation, they were mostly performed just once.

4.2.1 STOCs were sensitive to changes in external Ca^{2+} concentration, $[\text{Ca}^{2+}]_o$

The Ca^{2+} sensitivity of STOCs was examined using 0.1 mM Ca^{2+} and 1 mM Ca^{2+} -containing bath solutions.

The perforated patch technique with membrane potential (V_m) held at -10 mV was used for the experiment. Cells were initially superfused with the 1 mM Ca^{2+} -containing bath solution followed by the 0.1 mM Ca^{2+} solution. Measurements indicate that mean STOC amplitude of the patch-clamped cell increased from 37.4 pA to 47.6 pA with a decrease in $[\text{Ca}^{2+}]_o$ from 1 mM to 0.1 mM $[\text{Ca}^{2+}]_o$, whereas STOC frequency was higher in 1 mM $[\text{Ca}^{2+}]_o$ compared with 0.1 mM $[\text{Ca}^{2+}]_o$, 0.48 Hz and 0.40 Hz, respectively (Figure 4.1). These results are somewhat consistent with those of an earlier study which reported an increase in STOC amplitude and frequency when $[\text{Ca}^{2+}]_o$ was decreased from 2 mM to 1 mM (Bayguinov *et al.*, 2001).

It should be noted that STOC frequency distribution graphs, in this and subsequent experiments, were typically truncated such that longer duration events were not displayed. Thus, the relative areas under each STOC frequency distribution histogram may not necessarily reflect the relative number of STOCs detected. Furthermore, all whole-cell experiments were performed using 1 mM $[\text{Ca}^{2+}]_o$ because it is more physiological. Throughout the rest of the chapter, 1 mM Ca^{2+} -containing bath solution will be referred to as “control solution”.

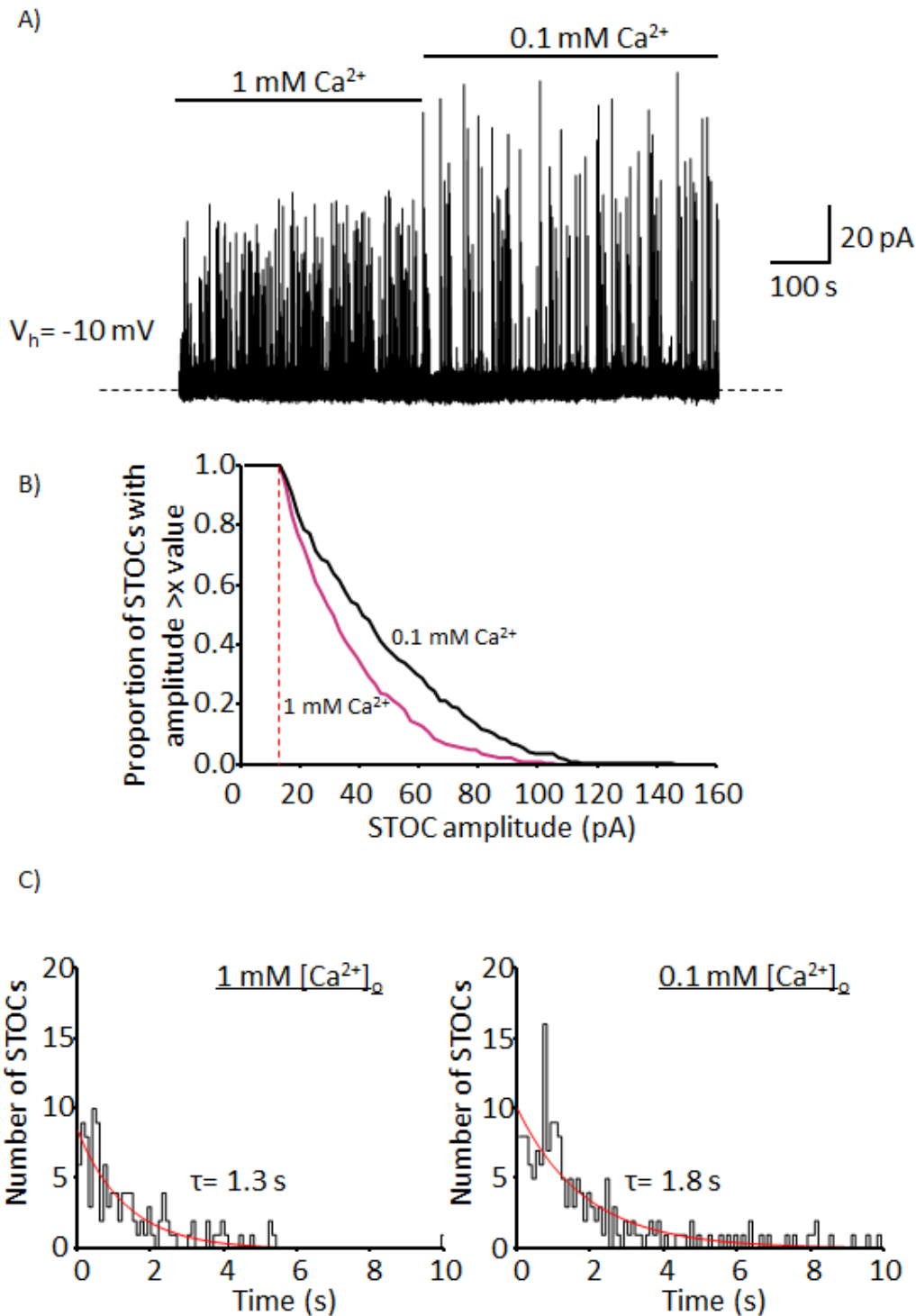


Figure 4.1: Effects of external Ca^{2+} concentration on STOCs. A) Example trace shows the changes in STOCs when $[\text{Ca}^{2+}]_o$ was reduced from 1 mM to 0.1 mM. B) Cumulative histograms, generated from trace A (above), show STOC amplitude before and after reduction of $[\text{Ca}^{2+}]_o$ from 1 mM to 0.1 mM. Dashed line indicates the threshold set (≥ 15 pA) for accepting outward transients as STOCs. C) Histograms show STOC frequency distribution in 1 mM $[\text{Ca}^{2+}]_o$ (recording duration= 161 s, no. of STOCs detected= 118) and 0.1 mM $[\text{Ca}^{2+}]_o$ (recording duration= 508 s, no. of STOCs detected= 204). Recording was performed using perforated patch configuration. V_m was held at -10 mV. $[\text{K}^+]_i = 140$ mM; $[\text{K}^+]_o = 5$ mM.

4.2.2 STOCs were voltage sensitive

The voltage sensitivity of STOCs was investigated using the perforated patch technique. Cells were superfused with control solution whilst changing the V_m from 0 to -50 mV in 10 mV decrements (Figure 4.2). Mean STOC amplitude and frequency decreased as V_m approached the equilibrium potential for K^+ ($E_{K^+} = -84$ mV), see Figure 4.3. These effects of V_m are consistent with those of earlier studies which also showed decreases in STOC amplitude and frequency with hyperpolarisation (Benham *et al.*, 1986; Saunders & Farley, 1991).

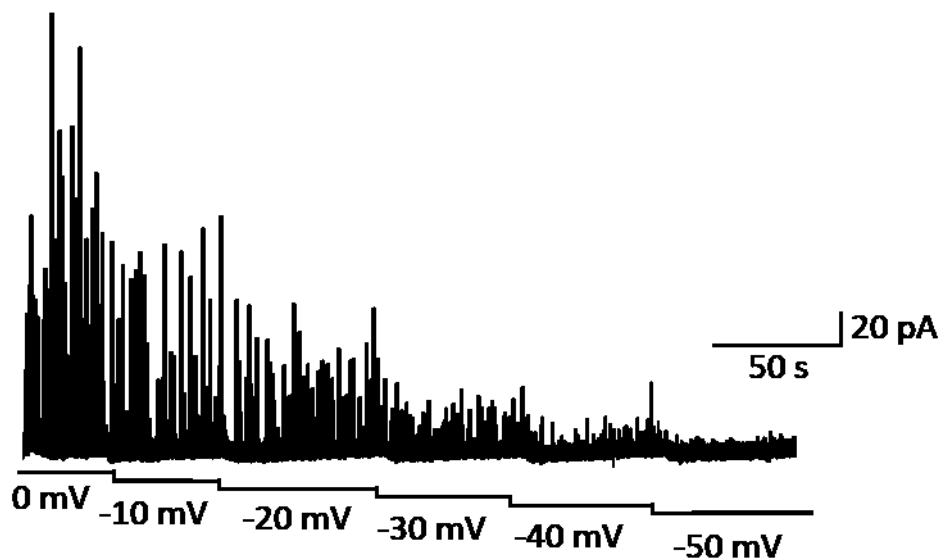


Figure 4.2: Effects of changes in membrane potential (V_m) on STOCs. Example trace shows changes in STOCs in response to a step-wise decrease in V_m from 0 mV to -50 mV. Perforated patch was used for recording. $[K^+]_i = 140$ mM; $[K^+]_o = 5$ mM.

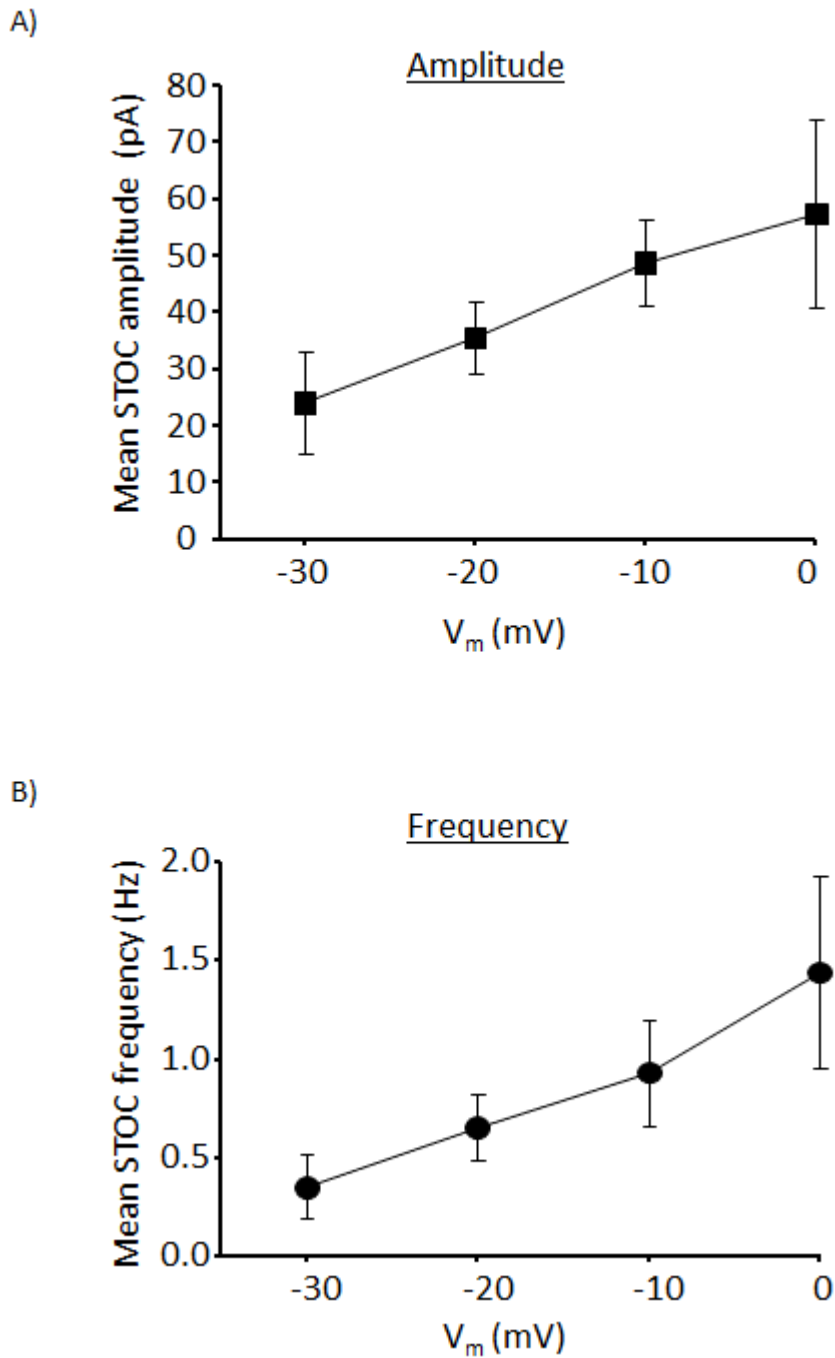


Figure 4.3: STOCs are influenced by changes in membrane potential (V_m). Measurement of A) Mean STOC amplitude and B) Mean STOC frequency during stepwise decrease in V_m from 0 mV to -30 mV. Error bars show SEM, $n=3$. All recordings were performed using perforated patch technique.

4.2.3 Effects of K⁺ channel blockers on STOCs

4.2.3.1 External TEA⁺ inhibited STOCs

My inside-out patch results (see section 3.2.3 in chapter 3) and reports from earlier studies have shown that external TEA⁺ reduces the amplitude of single BK_{Ca} channel current (Benham *et al.*, 1985; Langton *et al.*, 1991). Thus, STOC inhibition induced by external TEA⁺ application to SMCs was expected. External TEA⁺ was also used in the present study to confirm that the STOCs result from BK_{Ca} channel activation. Based on earlier reports that 0.2 mM TEA⁺ produced a half-block of BK_{Ca} channels, my experiment was performed with 3 mM TEA⁺ to completely block the channels (Langton *et al.*, 1991; Brayden & Nelson, 1992).

The perforated patch technique was used and V_m was held at 0 mV. Control solution was then superfused for the first 5 to 7 minutes of recording, with the aim of achieving steady-state recording prior to examining the effects of TEA⁺ on STOCs. Note that the initial superfusion of control solution for 5 to 7 minutes was consistently repeated at the beginning of each experiment throughout this study.

In this experiment, cells were superfused with TEA⁺ (3 mM) for 6 minutes. During the first 2 minutes of superfusion no change was observed in STOC amplitude, but this abruptly decreased after 2 minutes which reflects the superfusion dead-space time. TEA⁺ (3 mM) produced an instantaneous inhibition of STOCs which was reversed 4 minutes after wash (Figure 4.4). The TEA⁺-mediated inhibition of STOCs is consistent with earlier reports where application of external TEA⁺ to rabbit intestinal SMCs blocked STOCs (Ohya *et al.*, 1987; Bolton & Lim, 1989).

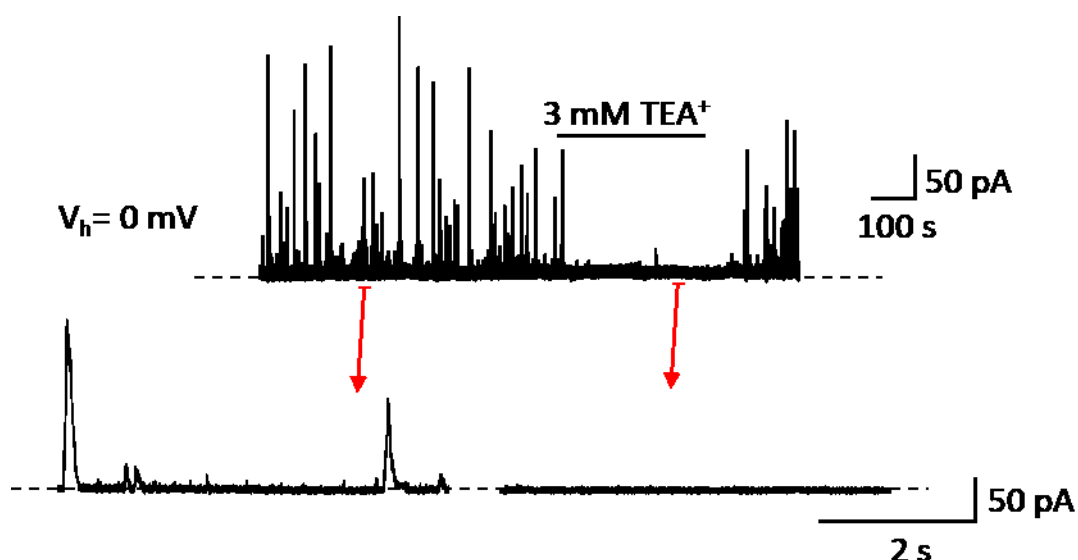


Figure 4.4: Effects of external TEA⁺ on STOCs. Example traces show the effects of extracellular TEA⁺ (3 mM) application on STOCs. Perforated patch was used for recording. V_m was held at 0 mV.

4.2.3.2 STOCs were blocked by external application of penitrem A

Penitrem A is a selective and potent BK_{Ca} channel blocker (Knaus *et al.*, 1994c; Cotton *et al.*, 1997). Intracellular and extracellular applications of penitrem A have been shown to irreversibly block BK_{Ca} channel activity (Knaus *et al.*, 1994c; Asano *et al.*, 2012). Therefore, penitrem A was also used in this study to confirm that STOCs result from BK_{Ca} channel activation. My experiments were performed with 100 nM penitrem A because it has previously been reported that penitrem A inhibited whole-cell BK_{Ca} currents, recorded from heterologous cells expressing $\alpha\beta_1$ subunits, with an IC₅₀ of 64.4 nM (Asano *et al.*, 2012).

The perforated patch technique was used and V_m was held at 0 mV. Extracellular application of penitrem A (100 nM) produced a slow inhibition of STOCs, with no recovery upon wash (Figure 4.5). The irreversibility of the penitrem A-induced inhibition has also been reported in a study performed on recombinant BK_{Ca} channels comprising $\alpha\beta_1$ subunits, where STOCs did not recover from the penitrem A (50 nM and 1 μ M) induced inhibition even after 10 minutes of wash (Asano *et al.*, 2012).

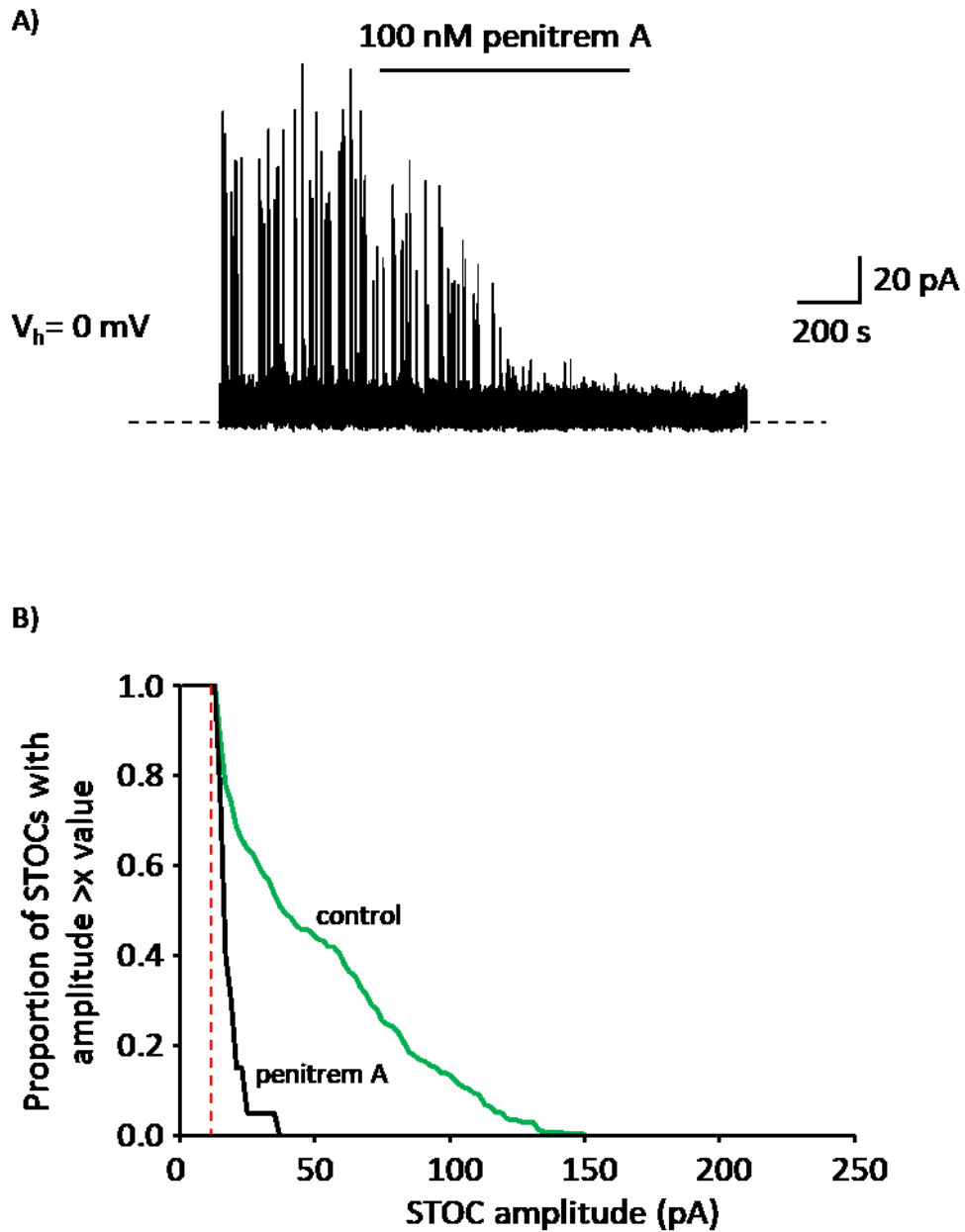


Figure 4.5: Effects of penitrem A on STOCs. A) Example trace shows the effect of extracellular application of penitrem A (100 nM) on STOCs. B) Cumulative histograms, generated from trace A (above), show STOC amplitude in the presence and absence of penitrem A. Perforated patch technique was used for recording. V_m was held at 0 mV.

4.2.4 STOCs were abolished by the inhibition of Ca²⁺ release and depletion of intracellular Ca²⁺ from Ca²⁺ stores

4.2.4.1 STOCs were abolished by intracellular application of ryanodine

Ryanodine is a plant alkaloid which has a high affinity for RyRs (Pessah & Zimanyi, 1991). Sub-micromolar concentrations of ryanodine irreversibly locks RyRs in a sub-conductance state resulting in a gradual depletion of SR Ca²⁺ content (Rousseau *et al.*, 1987). On the other hand, $\geq \mu\text{M}$ concentration of ryanodine inhibits RyRs (Meissner, 1986; Herrmannfrank *et al.*, 1991). The inhibition of RyRs by ryanodine results in the abolition of Ca²⁺ sparks which leads to STOC inhibition. The time course of STOC inhibition has been shown to be concentration dependent with a faster rate observed from 10 μM to 100 μM ryanodine (Bolton & Lim, 1989; Komori & Bolton, 1989).

This experiment was performed with the ruptured patch technique because ryanodine (10 μM) was applied intracellularly via the pipette solution. Thus, recordings were performed immediately after entering the whole-cell configuration. V_m was held at -30 mV and cells were superfused with control solution for the entire duration of the recording. A gradual inhibition and subsequent abolition of STOCs was observed ~ 5 to 7 minutes after entering the whole-cell configuration (Figure 4.6). The effect of ryanodine on STOCs is consistent with previous reports where intracellular application of 0.01 μM to 100 μM ryanodine, via the pipette solution, abolished STOCs in rabbit vein and intestinal SMCs (Bolton & Lim, 1989; Komori & Bolton, 1989).

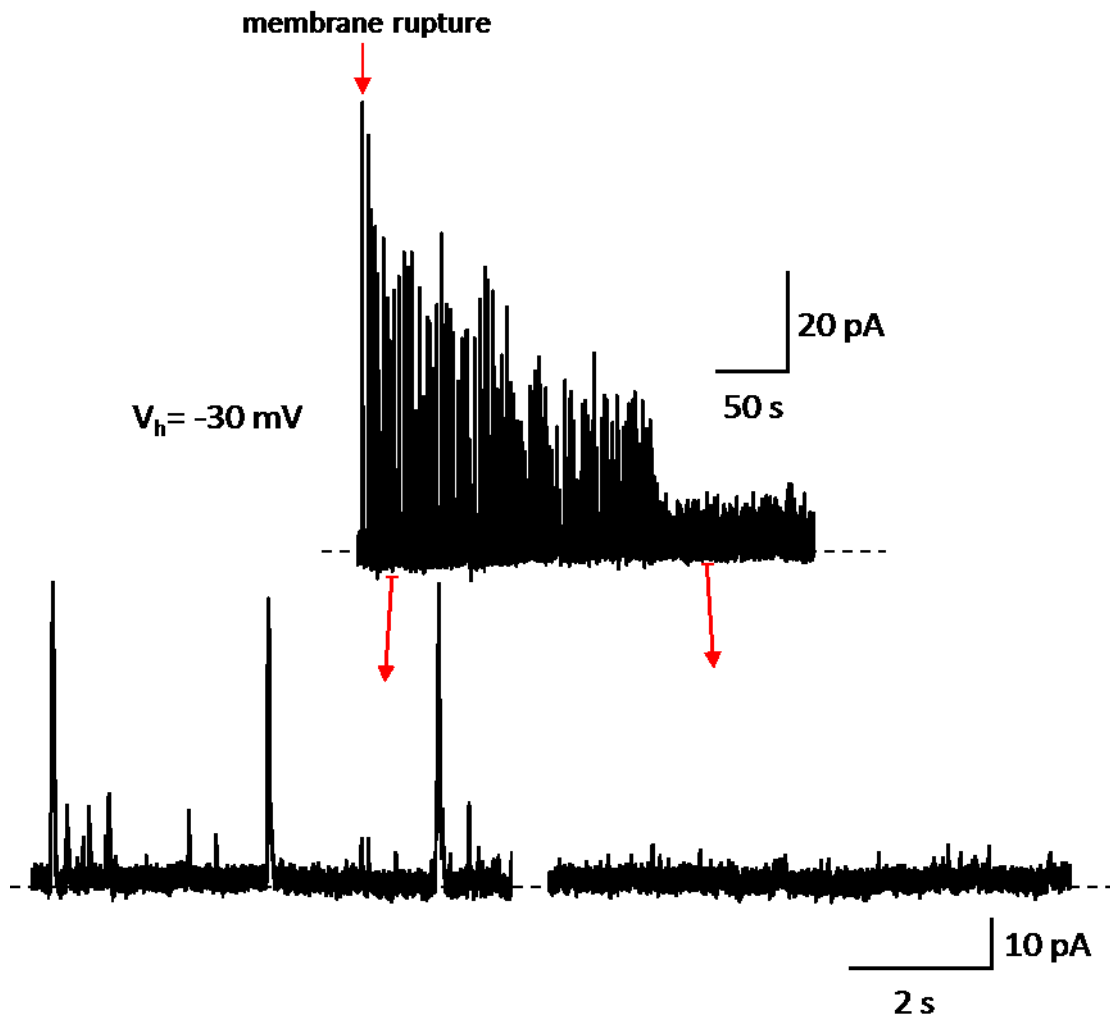


Figure 4.6: Effects of intracellular application of ryanodine via the pipette solution on STOCs. Example traces show the effects of intracellular application of ryanodine (10 μ M) on STOCs. Ruptured patch was used for the recording. V_m was held at -30 mV.

4.2.4.2 Extracellular application of caffeine abolished STOCs

Caffeine increases the Ca^{2+} sensitivity of RyRs thereby promoting CICR from the SR which results in a rapid depletion of intracellular Ca^{2+} stores (Iino *et al.*, 1988; Herrmannfrank *et al.*, 1991). Therefore, in the current study, caffeine was used to confirm that STOCs result from Ca^{2+} release events. Since earlier studies reported STOC inhibition after extracellular application of 5 to 20 mM caffeine, 10 mM caffeine was used in this study (Benham *et al.*, 1986; Bolton & Lim, 1989; Komori & Bolton, 1989).

Perforated patch technique was used, with V_m held at -15 mV. Cells were initially superfused with control solution for ~5 minutes followed by extracellular caffeine (10 mM) application. Caffeine (10 mM) produced a large long-lasting transient outward current followed by complete abolition of STOCs (Figure 4.7). These results are in line with the STOC abolition induced by 5 to 20 mM external caffeine in studies performed with rabbit vein and intestinal SMCs (Benham *et al.*, 1986; Bolton & Lim, 1989; Komori & Bolton, 1989).

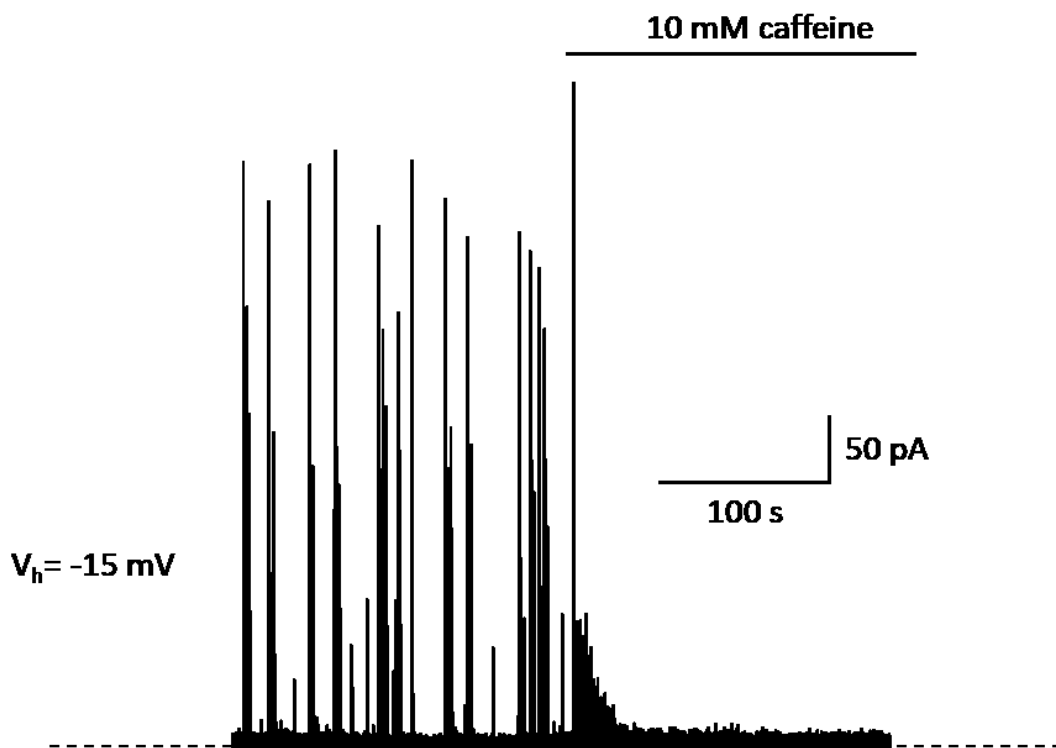


Figure 4.7: Effects of caffeine on STOCs. Example trace shows the effects of extracellular application of caffeine (10 mM) on STOCs. Perforated patch was used for the recording. V_m was held at -15 mV.

4.3 Effects of haem on STOCs

4.3.1 Extracellular haem application enhanced STOC amplitude but not STOC frequency

During haemolysis extracellular haem concentration, $[\text{haem}]_o$, can increase up to 20 μM (Sawicki *et al.*, 2015). It is estimated that 2 to 5 μM of this labile haem gets internalized by the surrounding cells (Gouveia *et al.*, 2017). Therefore, the effects of haem on STOCs under such conditions was examined by exposing intact cells to 5 μM haem.

Recordings were performed using perforated patches with V_m held at -30 mV. Extracellular application of haem (5 μM) for ~ 10 minutes increased mean relative STOC amplitude to 127.1 ± 8.5 % of control, from 37.2 ± 8.2 pA to 46.2 ± 8.4 pA ($p < 0.05$, $n = 4$; Figure 4.8 & 4.10). However, the mean relative change in STOC frequency, 113.5 ± 71.8 %, from 0.35 ± 0.16 Hz to 0.47 ± 0.11 Hz ($p > 0.05$, $n = 4$; Figures 4.8 & 4.10) was non-significant. In contrast, an earlier study reported that extracellular application of HLL (a HO substrate), instead of haem, to BK_{Ca} channels expressed in porcine cerebral arteriole SMCs increased both mean STOC amplitude and frequency (Jaggar *et al.*, 2002).

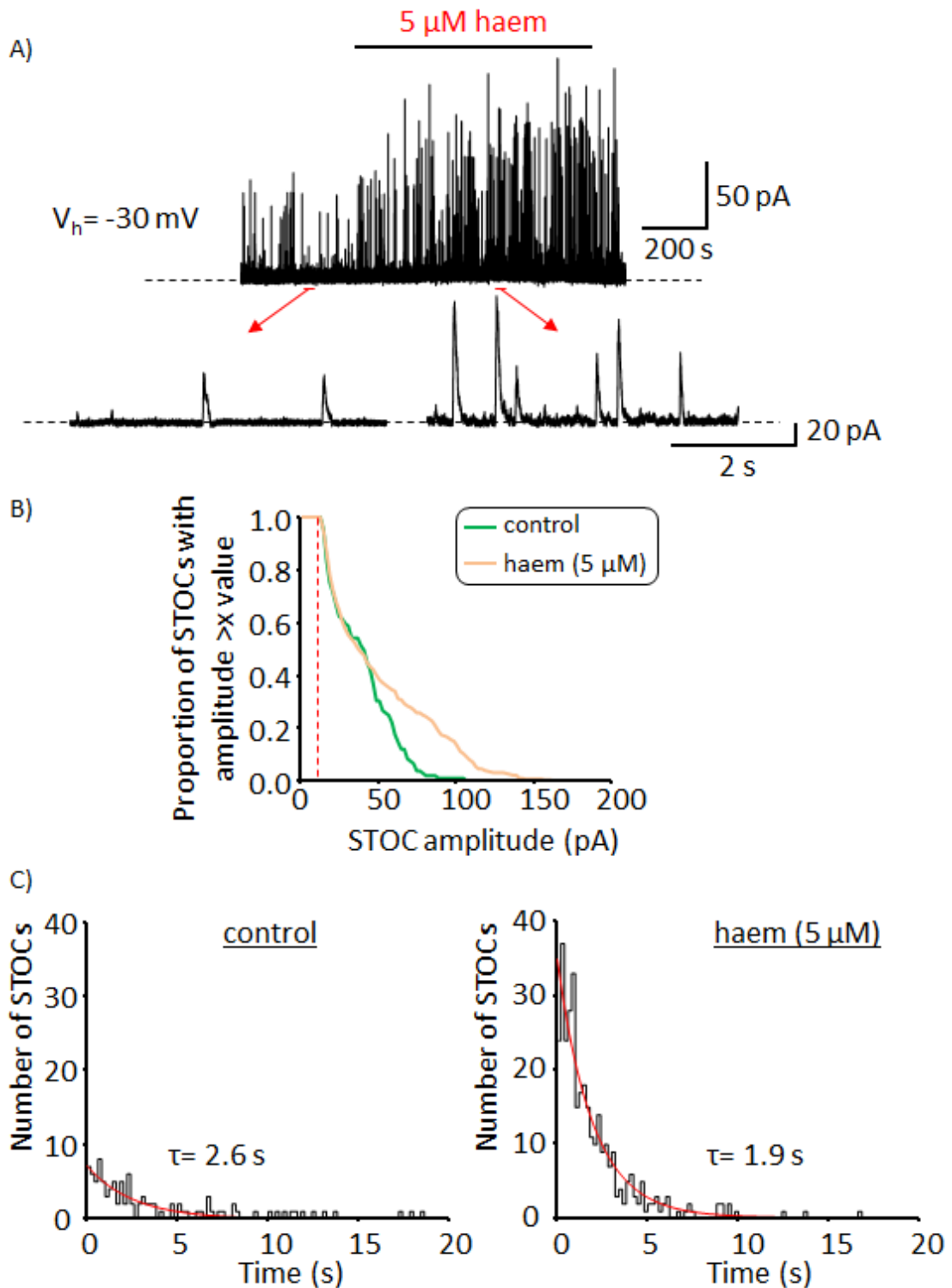


Figure 4.8: Effects of extracellular haem application on STOCs, using perforated patch configuration. A) Example traces show the effects of extracellular haem (5 μM) on STOCs. STOCs were analysed 4 minutes after haem application. B) Cumulative histograms, generated from trace A (above), show STOC amplitude in the presence and absence (control) of haem. C) STOC frequency distribution in control condition (recording duration= 593 s, no. of STOCs detected= 109) and in haem (5 μM) (recording duration= 716 s, no. of STOCs detected= 346). V_m was held at -30 mV. $[\text{K}^+]_i = 140$ mM; $[\text{K}^+]_o = 5$ mM.

Experiments were repeated using ruptured patches, as some future experimental designs required the use of ruptured patches. Extracellular haem (5 μ M) application did not change mean relative STOC amplitude, 100.2 ± 2.2 %, from 27.1 ± 2.5 pA to 28.0 ± 1.6 pA ($p > 0.05$, $n = 4$; Figures 4.9 & 4.10). There was also no significant change in mean relative STOC frequency, 107.9 ± 15.1 %, from 2.17 ± 0.67 Hz to 2.53 ± 0.32 Hz ($p > 0.05$, $n = 4$; Figures 4.9 & 4.10). However, mean STOC frequency was surprisingly higher in ruptured patches compared with perforated patches (Figure 4.10). Nevertheless, the modulatory effects of haem on STOCs was only observed with the perforated patch technique. Experiments were mostly performed with the perforated patch technique since it enhances stable recordings.

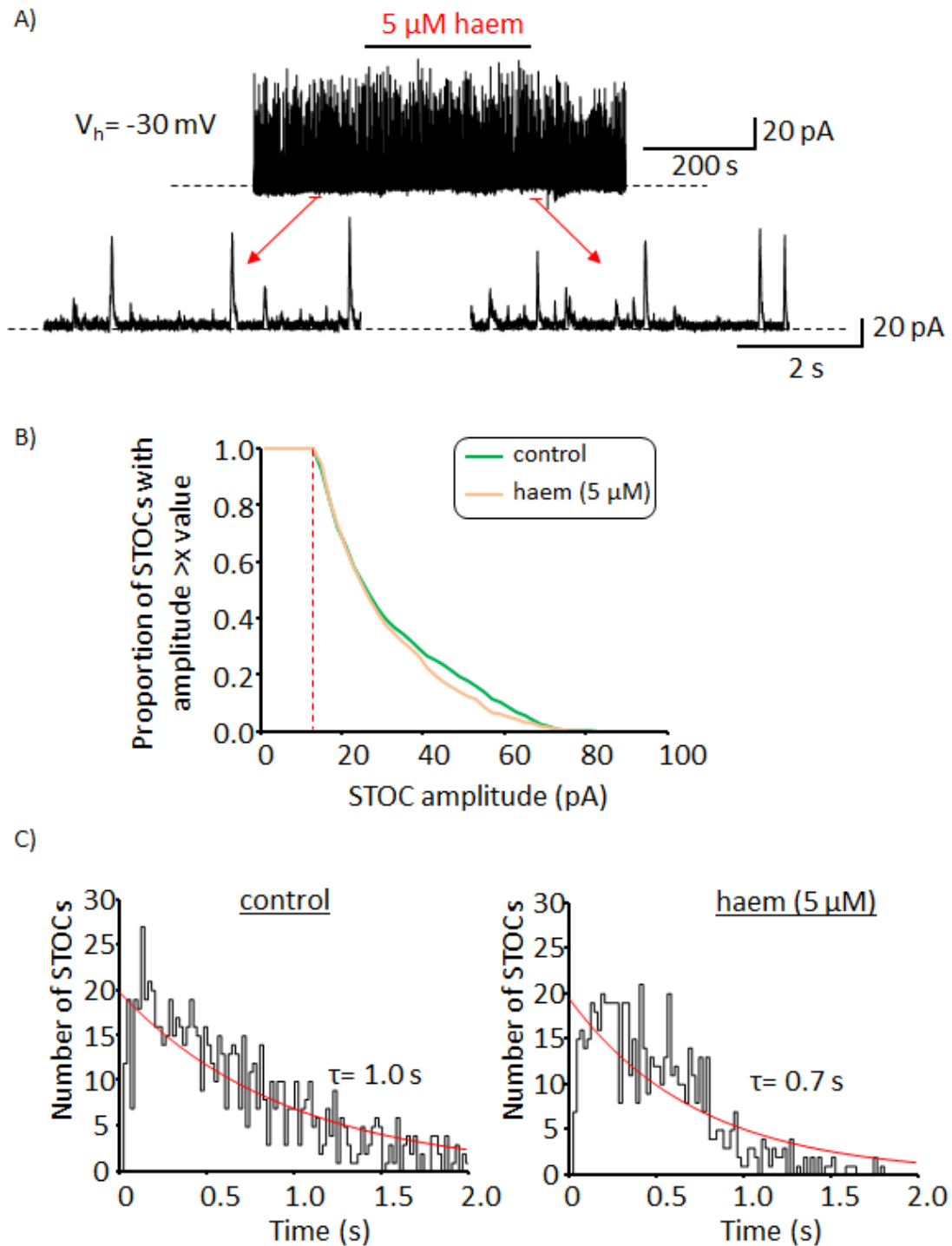


Figure 4.9: Effects of extracellular haem application on STOCs, using ruptured patch configuration. A) Example traces show the effects of extracellular haem ($5 \mu\text{M}$) on STOCs. STOCs were analysed 4 minutes after haem application. B) Cumulative histograms, generated from trace A (above), show STOC amplitude in the presence and absence (control) of haem. C) STOC frequency distribution in control condition (recording duration= 550 s, no. of STOCs detected= 836) and in haem ($5 \mu\text{M}$) (recording duration= 303 s, no. of STOCs detected= 627). Pipette solution contained ATP (1 mM). V_m was held at -30 mV.

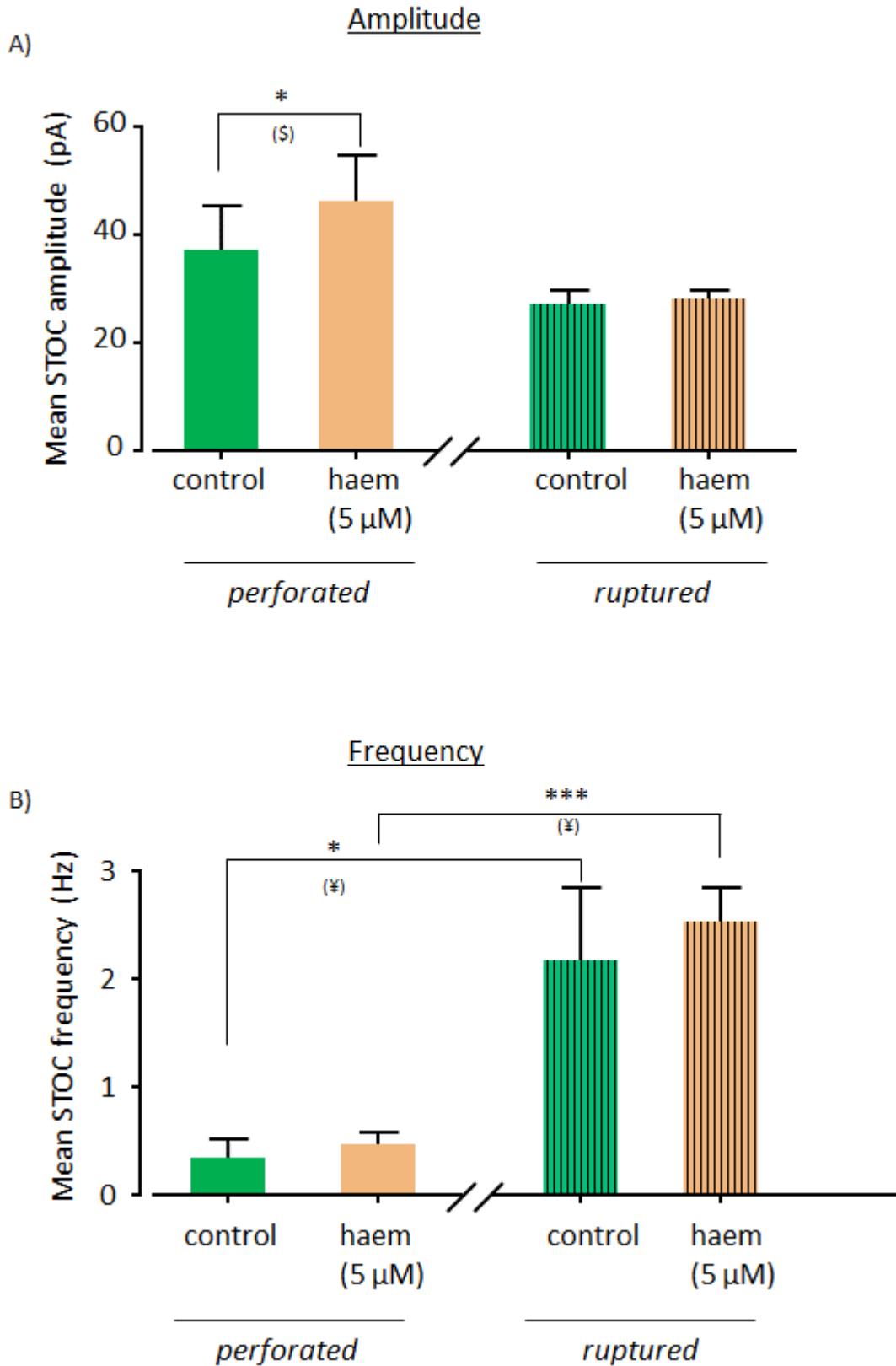


Figure 4.10: Effects of extracellular haem application on STOCs. Recordings were made with perforated and ruptured patch techniques. Unpaired (¥) and ratio paired (\$) t-tests were performed on STOC amplitude and frequency data. Only significant results are indicated, * $p \leq 0.05$, *** $p \leq 0.001$. Error bars show SEM, $n = 4$.

4.3.2 Low and high extracellular haem concentrations enhanced STOC frequency but not STOC amplitude

To investigate whether the effects of extracellular haem on STOCs can be further enhanced, experiments were performed with low and high [haem]_o; 100 nM and 30 μM, respectively.

Perforated patches were used with V_m held at -30 mV. Cells were superfused with control solution, for ~7 minutes before applying haem (100 nM) for 10 minutes followed by a 7-minute application of haem (5 μM). During application of 100 nM [haem]_o mean relative STOC amplitude was increased to 118.2 ± 8.3 % of control, from 28.1 ± 2.7 pA to 33.3 ± 4.4 pA ($p > 0.05$, $n = 6$; Figure 4.11) but this effect was not significant. Nevertheless, haem (100 nM) increased mean relative STOC frequency by 27.2 ± 11 %, from 0.26 ± 0.06 Hz to 0.34 ± 0.08 Hz ($p < 0.05$, $n = 6$; Figure 4.11).

Interestingly, application of 5 μM haem immediately after superfusion of 100 nM haem resulted in 56.2 ± 8.9 % increase of mean relative STOC amplitude, from 28.1 ± 2.7 pA to 44.1 ± 5.7 pA ($p < 0.01$, $n = 5$; Figure 4.11), and 210.5 ± 51.9 % increase in mean relative STOC frequency, from 0.26 ± 0.06 Hz to 0.92 ± 0.28 Hz ($p < 0.01$, $n = 5$; Figure 4.11).

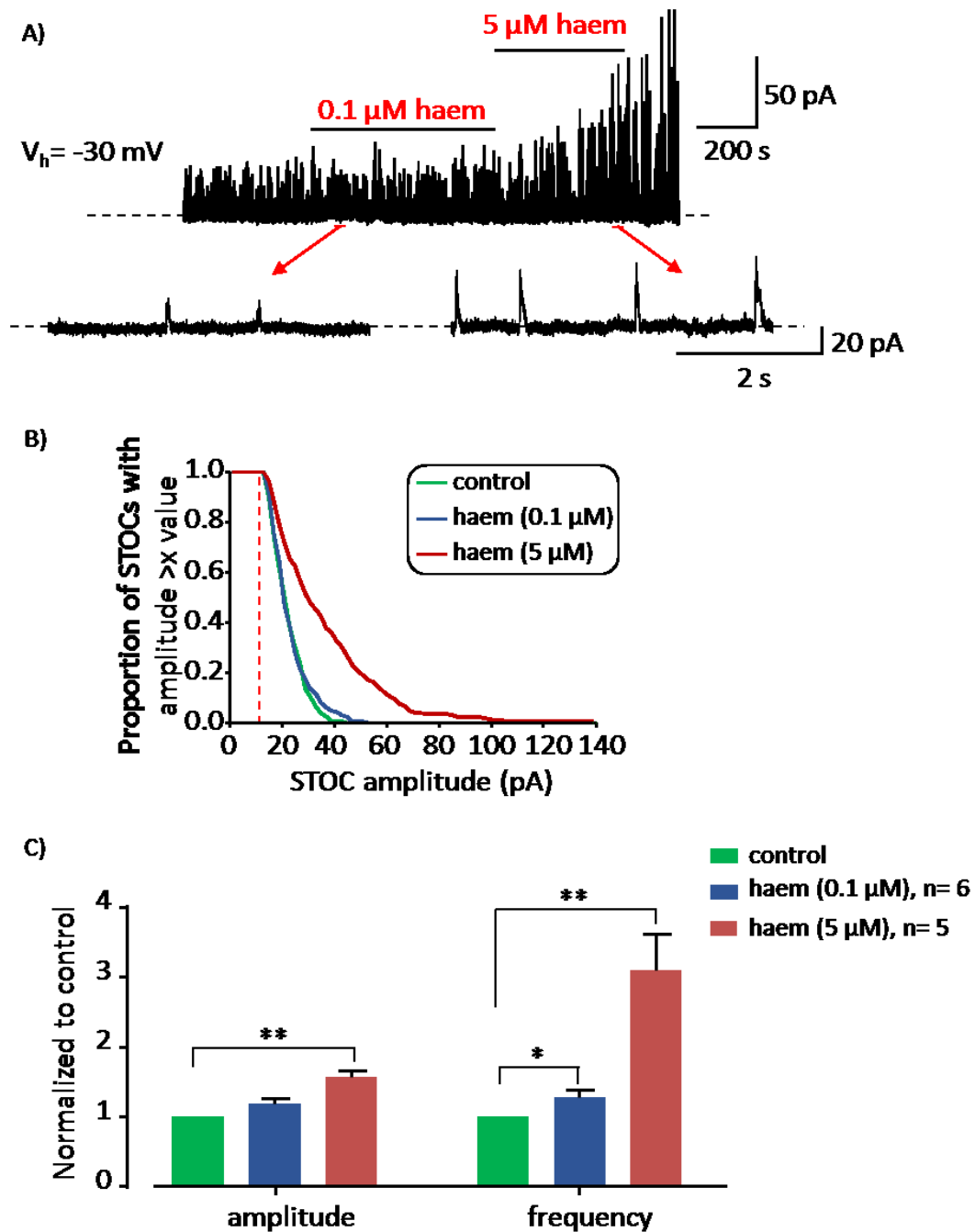


Figure 4.11: Effects of low extracellular haem concentration on STOCs. A) Example traces show the effects of $0.1 \mu\text{M}$ haem followed by $5 \mu\text{M}$ haem application on STOCs. STOCs were analysed 4 minutes after each $[\text{haem}]_o$ application. B) Cumulative histograms, generated from trace A (above), show STOC amplitude in control condition and in $0.1 \mu\text{M}$ and $5 \mu\text{M}$ haem. C) Histograms show effects of $0.1 \mu\text{M}$ and $5 \mu\text{M}$ haem on mean STOC amplitude and frequency. Ratio paired t-tests were performed on raw data. Only significant results are indicated, * $p \leq 0.05$ and ** $p \leq 0.01$. All recordings were performed using perforated patch configuration. V_m was held at -30 mV.

Experiments with 30 μM $[\text{haem}]_o$ were performed separately. Extracellular haem (30 μM) was applied for 10 minutes but the wash stage was barely performed due to frequent loss of seal access towards the end of the recording. Haem (30 μM) did not produce a significant change in STOC amplitude, $34.5 \pm 12.7 \%$, from $28.7 \pm 3.8 \text{ pA}$ to $38.1 \pm 5.4 \text{ pA}$ ($p > 0.05$, $n = 4$; Figures 4.12 & 4.13), even though the increase looks apparent in Figure 4.12. The lack of effect was likely due to the high variability of results, as the stimulatory effect was only profound in 2 out of the 4 cells used for recording. However, haem (30 μM) did increase mean relative STOC frequency to $291.4 \pm 68.1 \%$ of control, from $0.28 \pm 0.08 \text{ Hz}$ to $0.77 \pm 0.22 \text{ Hz}$ ($p < 0.05$, $n = 4$; Figures 4.12 & 13).

Therefore, an increase in mean STOC amplitude was only observed with 5 μM $[\text{haem}]_o$ whereas 100 nM and 30 μM $[\text{haem}]_o$ increased mean STOC frequency, with no effect on mean STOC amplitude (Figure 4.13). Since disruption of patch integrity and decrease in cell survival rate were observed with 30 μM $[\text{haem}]_o$, subsequent experiments were only performed with 5 μM $[\text{haem}]_o$, to still ensure that the amount of haem entering cells is enough to cause a measurable change in STOCs.

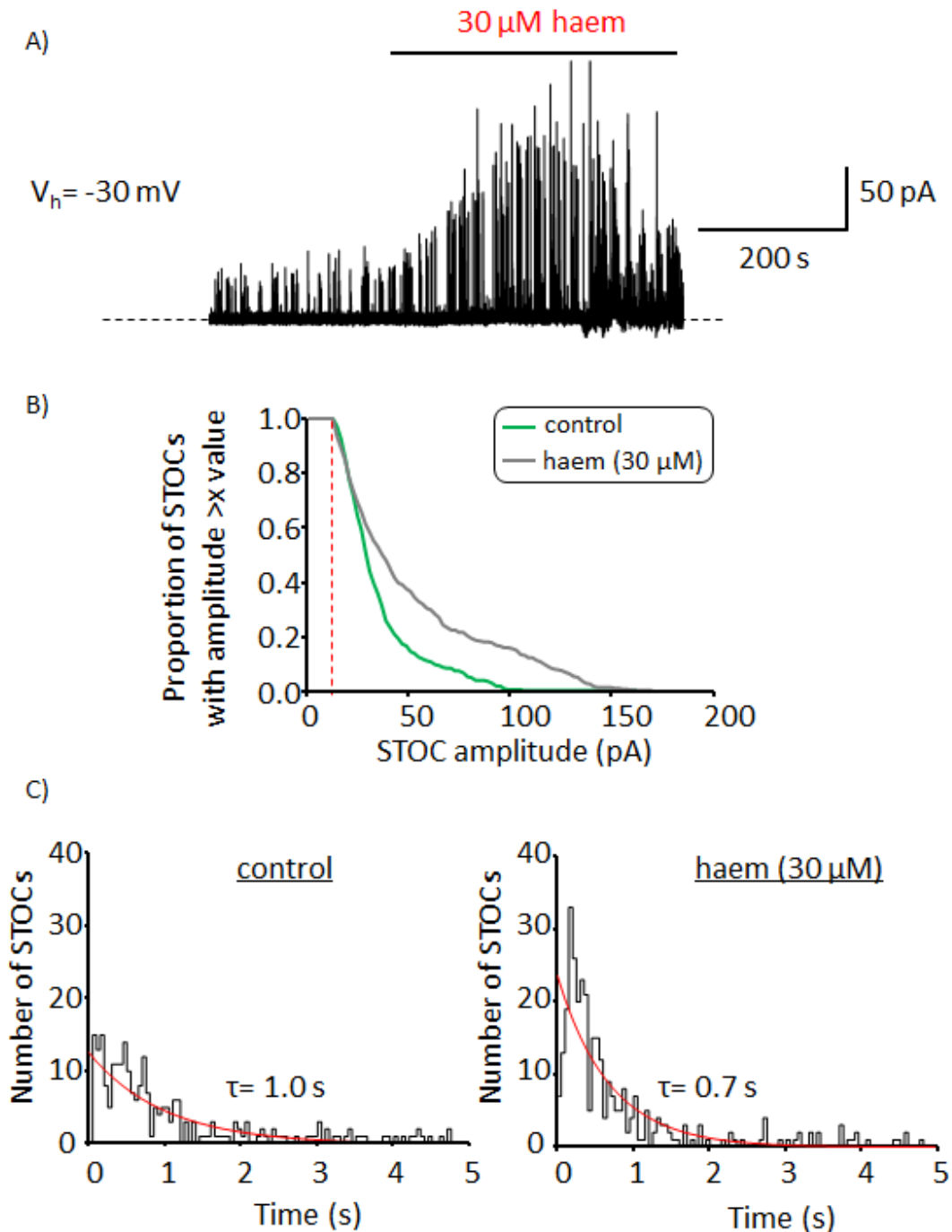


Figure 4.12: Effects of high extracellular haem concentration on STOCs. A) This trace shows the effects of extracellular haem ($30 \mu\text{M}$) on STOCs from one of the 2 cells which had a profound response to haem. STOCs were analysed 4 minutes after haem application. B) Cumulative histograms, generated from trace A (above), show STOC amplitude in the presence and absence (control) of haem ($30 \mu\text{M}$). C) STOC frequency distribution in control condition (recording duration= 666 s, no. of STOCs detected= 296) and in $30 \mu\text{M}$ haem (recording duration= 265 s, no. of STOCs detected= 331). Recording was performed using perforated patch configuration. V_m was held at -30 mV.

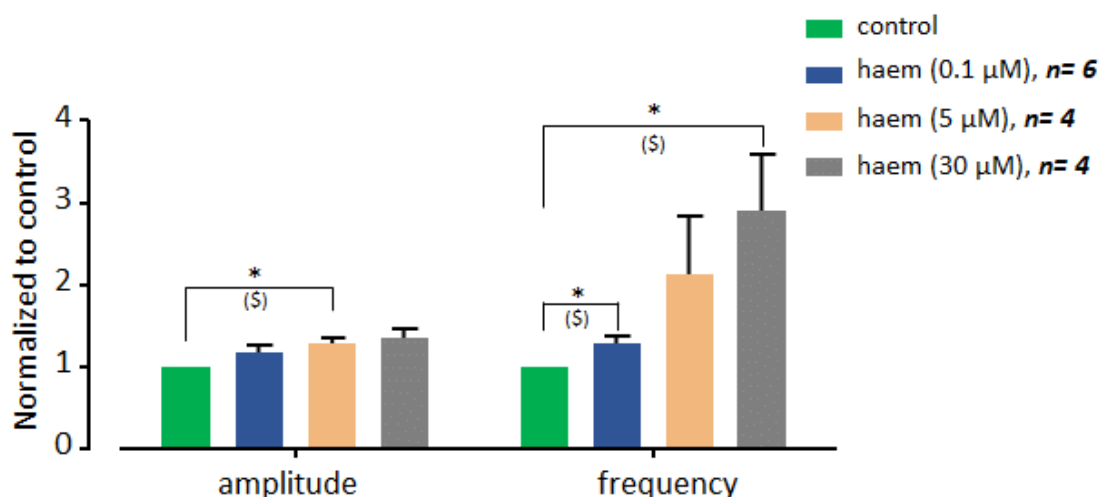


Figure 4.13: Effects of different extracellular haem concentrations on STOCs. Perforated patch technique was used for all recordings. Mean STOC amplitude and frequency were normalized to control conditions. Ratio paired (\$) and unpaired t-tests were performed as appropriate, using raw data. Only significant results are indicated, * $p \leq 0.05$.

4.3.3 External haem enhanced STOC amplitude at less depolarised V_m

A previous study performed on macroscopic patches showed that in zero $[\text{Ca}^{2+}]_i$, haem increased the Popen of BK_{Ca} channels at less depolarised potentials (Horrigan *et al.*, 2005). This suggests that haem enhanced single BK_{Ca} channel activity when the channel Popen was low. Therefore, the plan was to investigate whether the effects of haem on STOCs is enhanced at low channel Popen. This would be achieved by repeating my STOC experiments with V_m held at - 50 mV, although in the presence of Ca^{2+} , as under such condition channel Popen is expected to be less than in the previous experiment performed at - 30 mV (see section 4.3.1 above).

The stability of STOCs during recordings performed at - 50 mV was observed over time. Perforated patches were used with the V_m held at - 50 mV. Cells were then continuously superfused with control solution for ~ 30 minutes. The results obtained were compared with findings from similar experiments performed at a holding potential of - 30 mV. STOCs were analysed in consecutive 5 minutes sections. As expected, based on low BK_{Ca} channel Popen at less depolarised potentials, mean STOC amplitude and frequency were both higher at - 30 mV compared with - 50 mV (Figure 4.14).

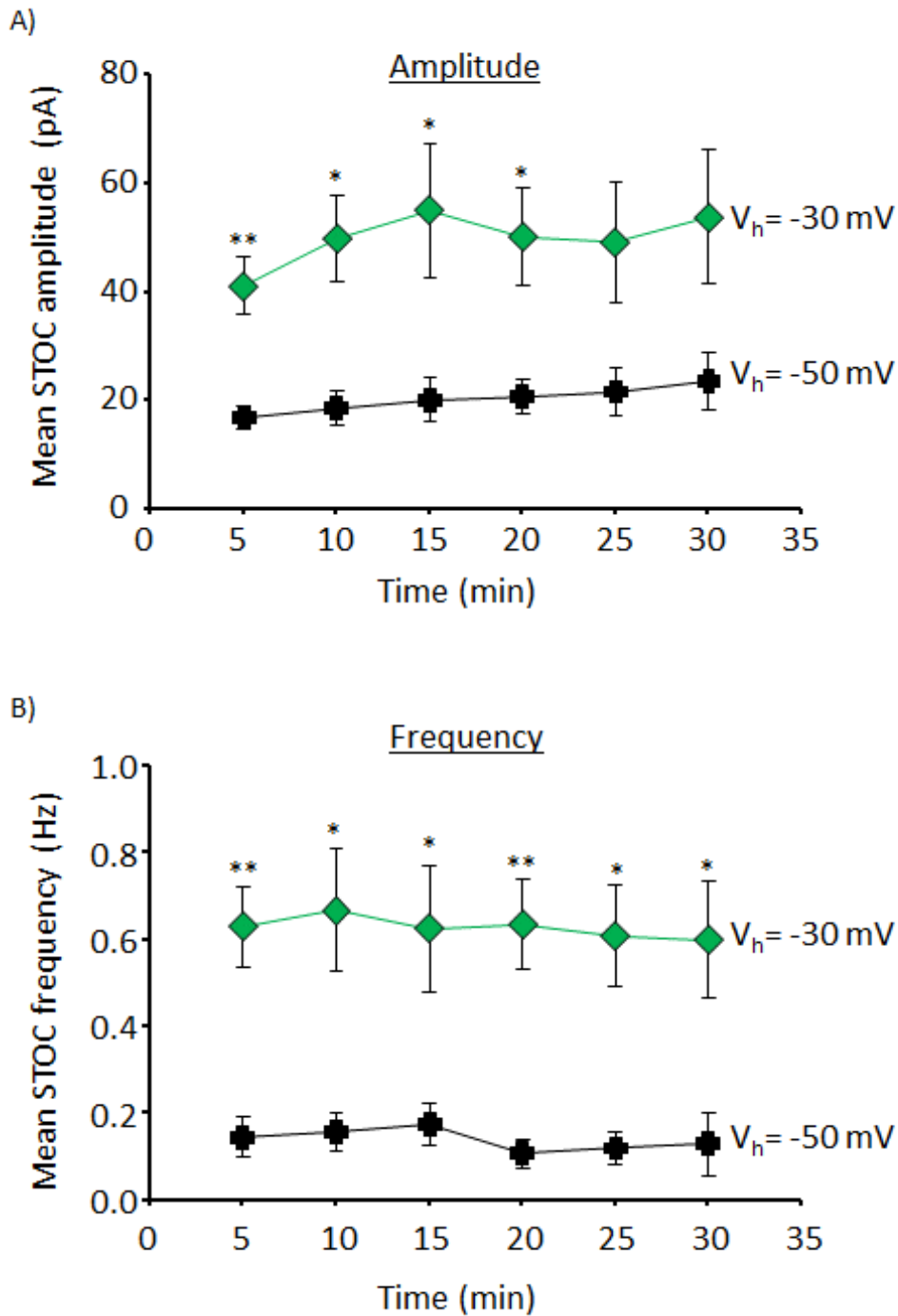


Figure 4.14: Effects of V_m on STOCs under control (haem-free) conditions. Graphs show A) mean STOC amplitude and B) mean STOC frequency under control conditions at holding potentials of -30 mV and -50 mV. The perforated patch configuration was used for all recordings. Unpaired t-tests were performed, * $p \leq 0.05$ and ** $p \leq 0.01$. Error bars show SEM, $n=4$.

Next, the effects of extracellular haem (5 μM) application on STOCs when V_m was held at - 50 mV was examined. Extracellular application of haem (5 μM) for 10 minutes at - 50 mV produced 32.4 ± 9.4 % increase in mean relative STOC amplitude, from 22.1 ± 2.5 pA to 29.8 ± 4.7 pA ($n=5$, $p < 0.05$; Figure 4.15). However, the mean relative change of 12.7 ± 15.2 % in STOC frequency, from 0.27 ± 0.11 Hz to 0.25 ± 0.08 Hz, was not significant ($n=5$, $p > 0.05$; Figure 4.15). These results were compared with the data from the effects of haem when V_m was held at - 30 mV (see section 4.3.1 above). Results from unpaired t-tests showed that there was no significant difference between the effects of haem on STOCs at - 30 mV and - 50 mV (Figure 4.15).

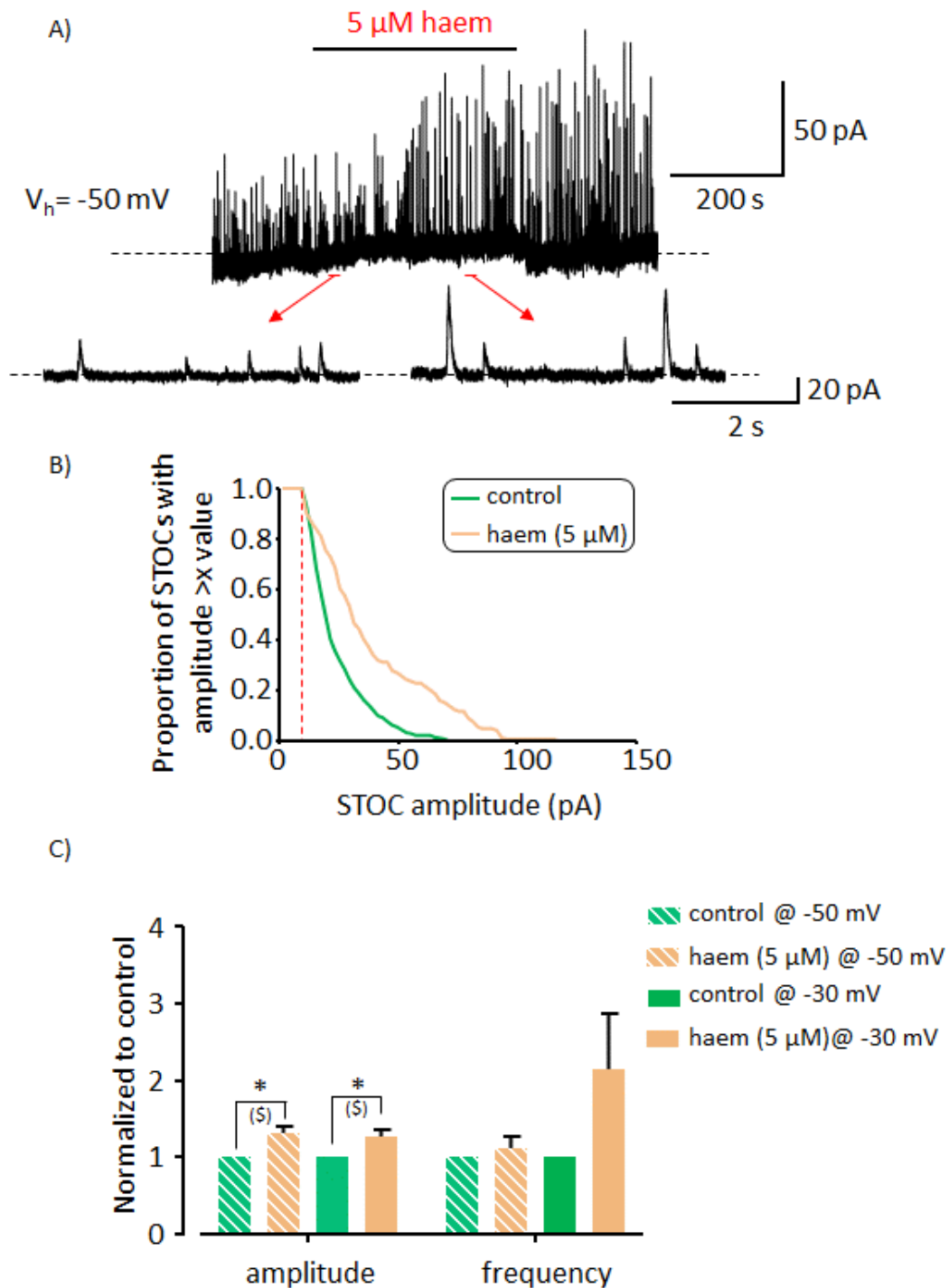


Figure 4.15: Effects of extracellular haem application on STOCs at less depolarised potential.

A) Example traces show the effects of extracellular haem (5 μM) on STOCs at holding potential of -50 mV. STOCs were analysed 4 minutes after haem application. B) Cumulative histograms, generated from trace A (above), show STOC amplitude in the presence and absence (control) of haem (5 μM). C) Histograms show effects of 5 μM haem on mean STOC amplitude and frequency at -30 mV (taken from section 4.3.1) and -50 mV. Ratio paired (\$) and unpaired t-test were performed on raw data. Only significant results are indicated, * $p \leq 0.05$. Error bars show SEM, $n = 4$ (at -30 mV) to 5 (at -50 mV). Perforated patch technique was used for recordings.

4.4 Effects of haem on STOCs after inhibition of endogenous CO production

Free intracellular haem is normally degraded by HO enzymes to CO. Thus, earlier studies performed on cerebral arteriole SMCs proposed that endogenous CO, produced from HO-mediated haem-L-lysinate (HLL) degradation, induced stimulatory effects on STOCs (Jaggar *et al.*, 2002). However, Jaggar *et al.* (2002) performed their study with HLL rather than haem.

In the present study, it is assumed that the extracellularly superfused haem enters the cell either via passive diffusion (due to its lipophilic nature) or haem carriers. Like HLL, the diffused or transported haem is expected to be degraded by HO enzymes to CO. Therefore, the potential role of endogenous CO in the modulatory effect of haem on STOCs was investigated for the first time, by inhibiting HO activity using the non-selective HO inhibitor, zinc protoporphyrin-IX (ZnPP-IX).

4.4.1 Extracellular application of ZnPP-IX had no effect on STOCs

It was important to first investigate whether ZnPP-IX itself influenced STOCs. Experiments were performed using 10 μM ZnPP-IX, as the IC_{50} of HO-1 and HO-2 inhibition in rat tissue has been reported to be 5.45 μM and 2.65 μM , respectively (Wong *et al.*, 2011). The application of high concentration (10 μM) of ZnPP-IX also ensured that enough ZnPP-IX entered the cells during the short incubation period, to cause significant HO inhibition.

Extracellular application of ZnPP-IX (10 μM) for 10 minutes did not change the mean relative STOC amplitude, $99.0 \pm 3.9\%$, from $29.6 \pm 4.2\ \text{pA}$ to $29.6 \pm 4.7\ \text{pA}$ ($p > 0.05$, $n = 7$; Figure 4.16). Mean relative STOC frequency was also not significantly unaltered, $132.5 \pm 17\%$, from $0.49 \pm 0.17\ \text{Hz}$ to $0.64 \pm 0.24\ \text{Hz}$ ($p > 0.05$, $n = 7$; Figure 4.16). Therefore, the lack of effect of ZnPP-IX on STOCs makes it suitable for use as a HO inhibitor in the present study.

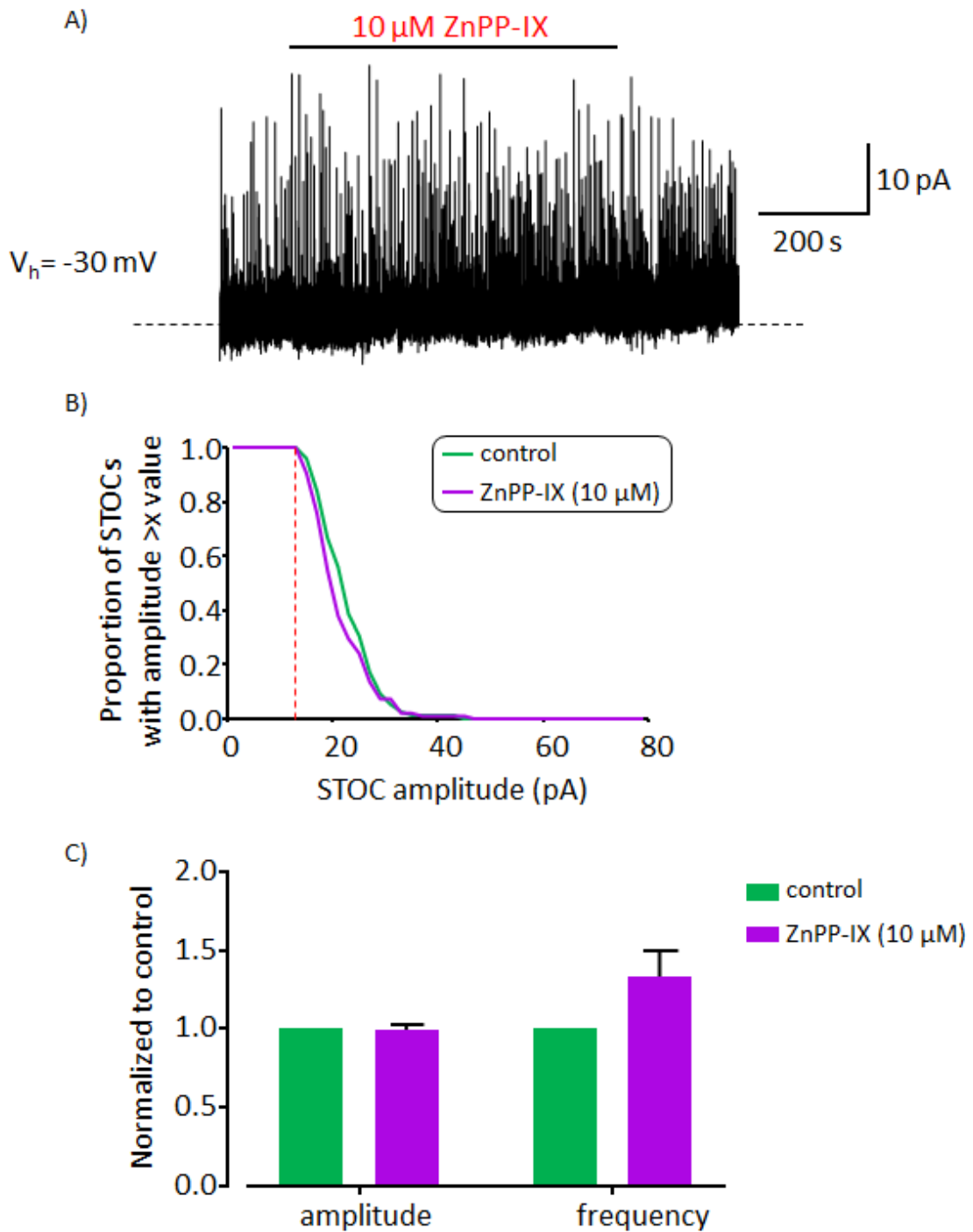


Figure 4.16: Effects of extracellular application of ZnPP-IX on STOCs. A) Example trace shows the effects of extracellular ZnPP-IX ($10 \mu\text{M}$) on STOCs. STOCs were analysed 4 minutes after ZnPP-IX application. B) Cumulative histograms, generated from trace A (above), show STOC amplitude in the presence and absence (control) of ZnPP-IX ($10 \mu\text{M}$). C) Effects of ZnPP-IX ($10 \mu\text{M}$) on STOC amplitude and frequency. Error bars show SEM, $n = 7$. Paired t-test was performed on raw data, results were non-significant as $p > 0.05$. Perforated patch was used for all recordings. V_m was held at -30 mV.

4.4.2 STOC amplitude and frequency decreased in ZnPP-IX pre-treated cells

As the plan was to inhibit endogenous CO production via cell pre-treatment with ZnPP-IX, it was important to examine whether such pre-treatment affects the stability of STOCs over time.

During membrane perforation, which occurred after achieving whole-cell configuration, cells were pre-incubated with ZnPP-IX (10 μ M) in the dark for 30 ± 4 minutes. Pre-incubation was performed in the dark due to the photosensitivity of ZnPP-IX (see section 2.7.3 in Methods chapter). After ZnPP-IX pre-incubation, recordings were commenced during which cells were superfused with control solution for 25 minutes. During 10 to 20 minutes into the recordings, mean STOC amplitude was relatively higher in control cells compared with ZnPP-IX pre-incubated cells ($p \leq 0.05$, $n = 4$; Figure 4.17). Mean STOC frequency was also significantly higher and more stable in control cells compared with ZnPP-IX pre-treated cells ($p \leq 0.05$ and $p \leq 0.01$, $n = 4$; Figure 4.17).

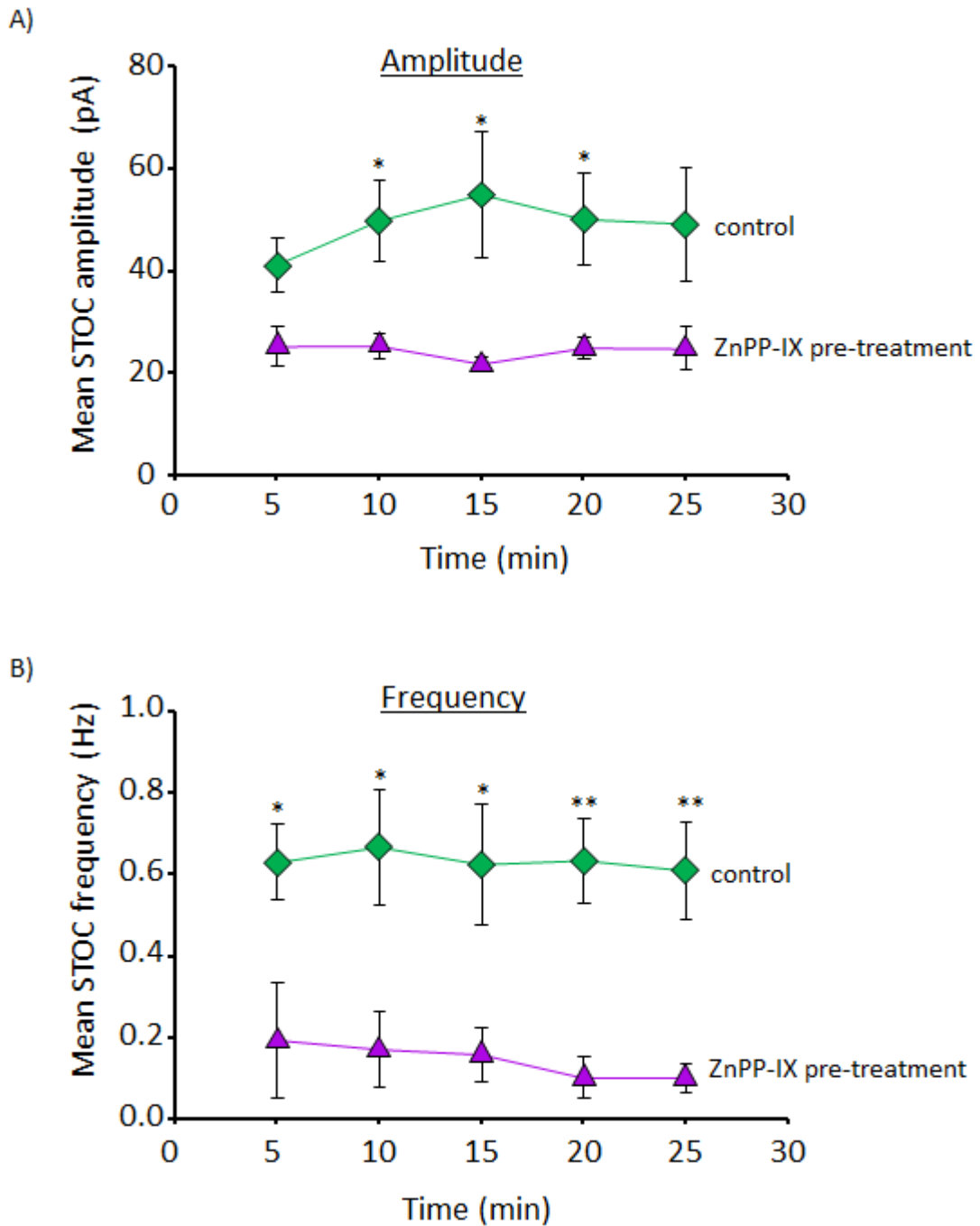


Figure 4.17: Effects of ZnPP-IX pre-treatment of cells on STOCs. A) STOC amplitude and B) STOC frequency recorded from cells with and without (control) ZnPP-IX pre-treatment. Cells were pre-incubated in ZnPP-IX (10 μ M) for \sim 30 minutes. All recordings were performed using the perforated patch technique. V_m was held at -30 mV. Unpaired t-test was performed, * $p \leq 0.05$, ** $p \leq 0.01$. Error bars show SEM, $n = 4$.

4.4.3 Extracellular haem application enhanced STOC amplitude and frequency in ZnPP-IX pre-treated cells

Cells were pre-incubated with ZnPP-IX (10 μ M) for 33 ± 12 minutes, after which excess ZnPP-IX was washed off by perfusing cells with control solution for 7 minutes. Extracellular haem (5 μ M) was then applied for 10 minutes followed by 5 minutes of wash. During extracellular haem (5 μ M) application, mean relative STOC amplitude was increased to 150.3 ± 3.6 % of the initial amplitude recorded from the ZnPP-IX pre-treated cells, from 26.7 ± 1.7 pA to 40.3 ± 3.50 pA ($p < 0.001$, $n = 4$; Figures 4.18 & 4.19). Mean relative STOC frequency was also increased to 236.1 ± 52.4 % of the initial frequency recorded from the ZnPP-IX pre-treated cells, from 0.46 ± 0.15 Hz to 0.87 ± 0.15 Hz ($p < 0.05$, $n = 4$; Figures 4.18 & 4.19). These results contrast with reports from a previous study which showed that the stimulatory effect of extracellular hemin (10 μ M) on cortical collecting duct BK_{Ca} channels, recorded using cell-attached patches, was inhibited by tin mesoporphyrin, SnMP, another HO inhibitor (Wang *et al.*, 2013).

Importantly, my results from one-way ANOVA tests suggests that there was no significant difference between the effects of haem on STOCs generated in ZnPP-IX-treated and untreated cells ($p > 0.05$, $n = 4$, Figure 4.19). Note that data for untreated cells are the same as those in Figure 4.10.

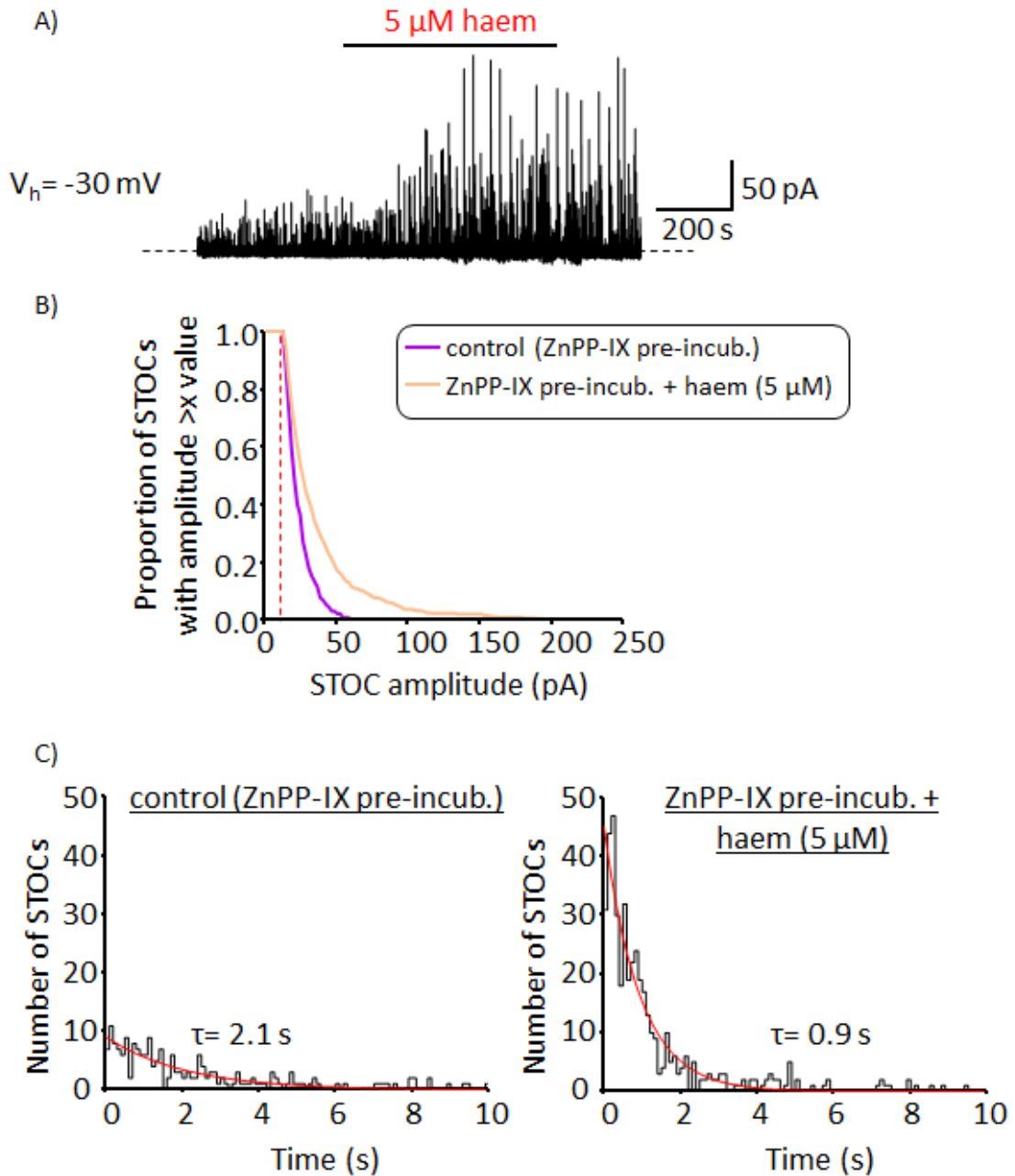


Figure 4.18: Effects of haem on STOCs after cell pre-treatment with ZnPP-IX. A) Example trace shows the effects of extracellular haem ($5 \mu\text{M}$) on STOCs following cell pre-treatment with ZnPP-IX ($10 \mu\text{M}$) for 15 minutes. STOCs were analysed 4 minutes after haem application. B) Cumulative histograms, generated from trace A (above), show STOC amplitude before and after addition of haem to ZnPP-IX ($10 \mu\text{M}$) pre-treated cell. C) STOC frequency distribution after ZnPP-IX pre-treatment (recording duration= 671 s, no. of STOCs detected= 216) and during haem ($5 \mu\text{M}$) application to ZnPP-IX pre-treated cell (recording duration= 569 s, no. of STOCs detected= 474). Perforated patch was used for recording. V_m was held at -30 mV.

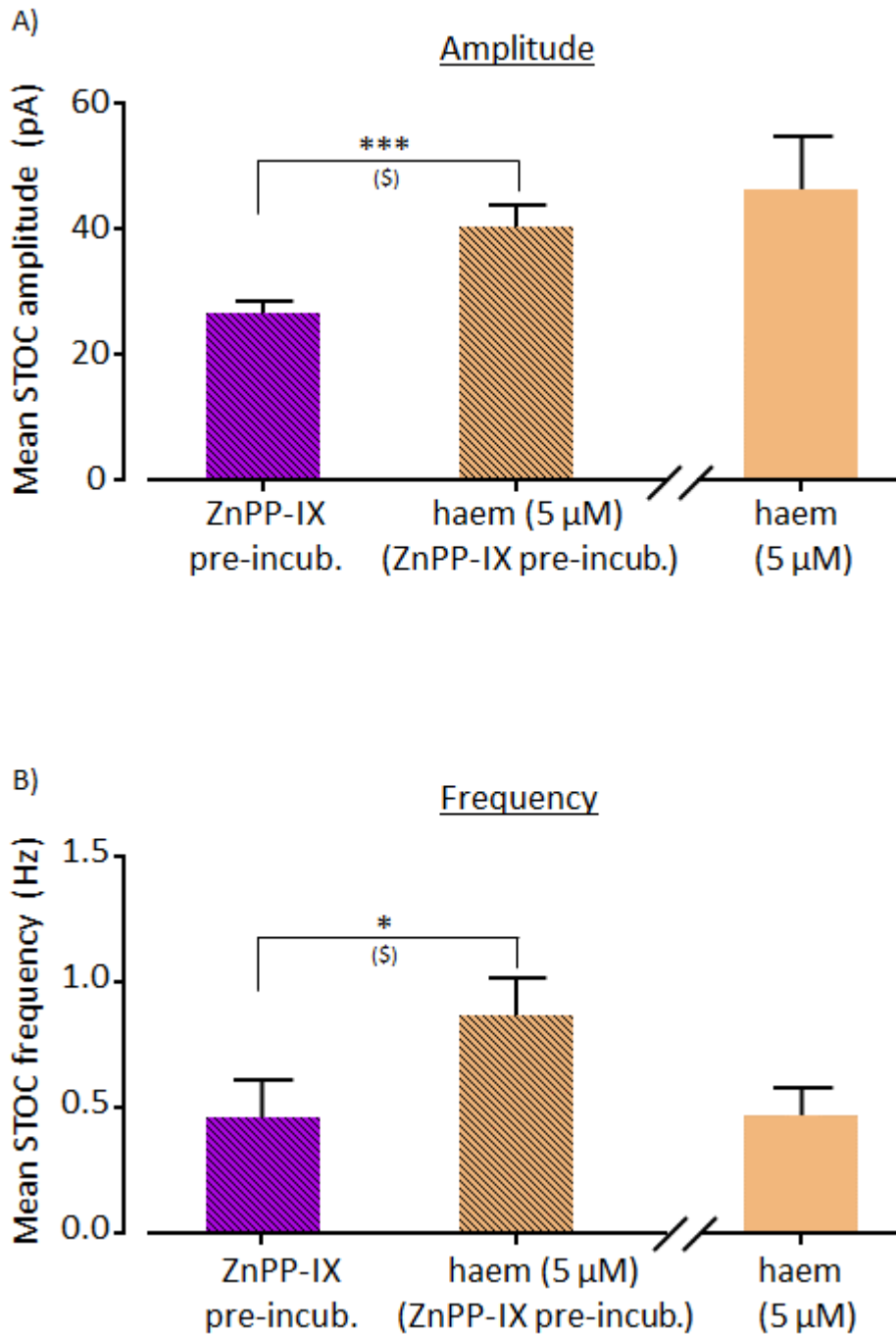


Figure 4.19: Comparison between the effects of haem on STOCs in ZnPP-IX-treated and untreated cells. Histograms show effects of haem (5 μ M) on A) STOC amplitude and B) STOC frequency in ZnPP-IX (10 μ M) pre-incubated cells. A comparison was made with data from untreated cells taken from Fig 4.10 (shown after the break on the x-axes). Error bars show SEM, $n = 4$. Ratio paired t-tests (\$) were performed, * $p \leq 0.05$ and *** $p \leq 0.001$. One-way ANOVA test on amplitude and frequency data was non-significant as $p > 0.05$. All recordings were performed using perforated patch technique.

4.5 Effects of extracellular CO application on STOCs

Intracellular application of CO in earlier studies (Wang *et al.*, 1997b; Wang & Wu, 1997) and the present study (see section 3.4.2 in chapter 3) enhanced single BK_{Ca} channel activity. Therefore, the effects of exogenous CO application on STOCs was also investigated using CO gas or the CO donor, CORM-3.

4.5.1 Extracellular CO gas application only increased STOC frequency

The extracellular application of 100 nM, 10 μ M or 30 μ M CO gas for 10 minutes did not produce significant effects on STOCs. Therefore, cells were superfused with a higher concentration of CO gas, 100 μ M. This evoked a mean relative change of 49.8 ± 12.3 % in mean STOC frequency, from 0.28 ± 0.07 Hz to 0.42 ± 0.09 Hz ($p < 0.01$, $n = 5$; Figure 4.20). However, mean relative STOC amplitude remained unaffected, 108.1 ± 4.5 % of control, from 27.1 ± 2.1 pA to 28.1 ± 2.8 pA ($p > 0.05$, $n = 7$; Figure 4.20).

These results contrast with previous report where the extracellular application of low concentration of gaseous CO (100 nM) increased mean STOC amplitude and frequency in porcine cerebral artery SMCs (Jaggar *et al.*, 2002).

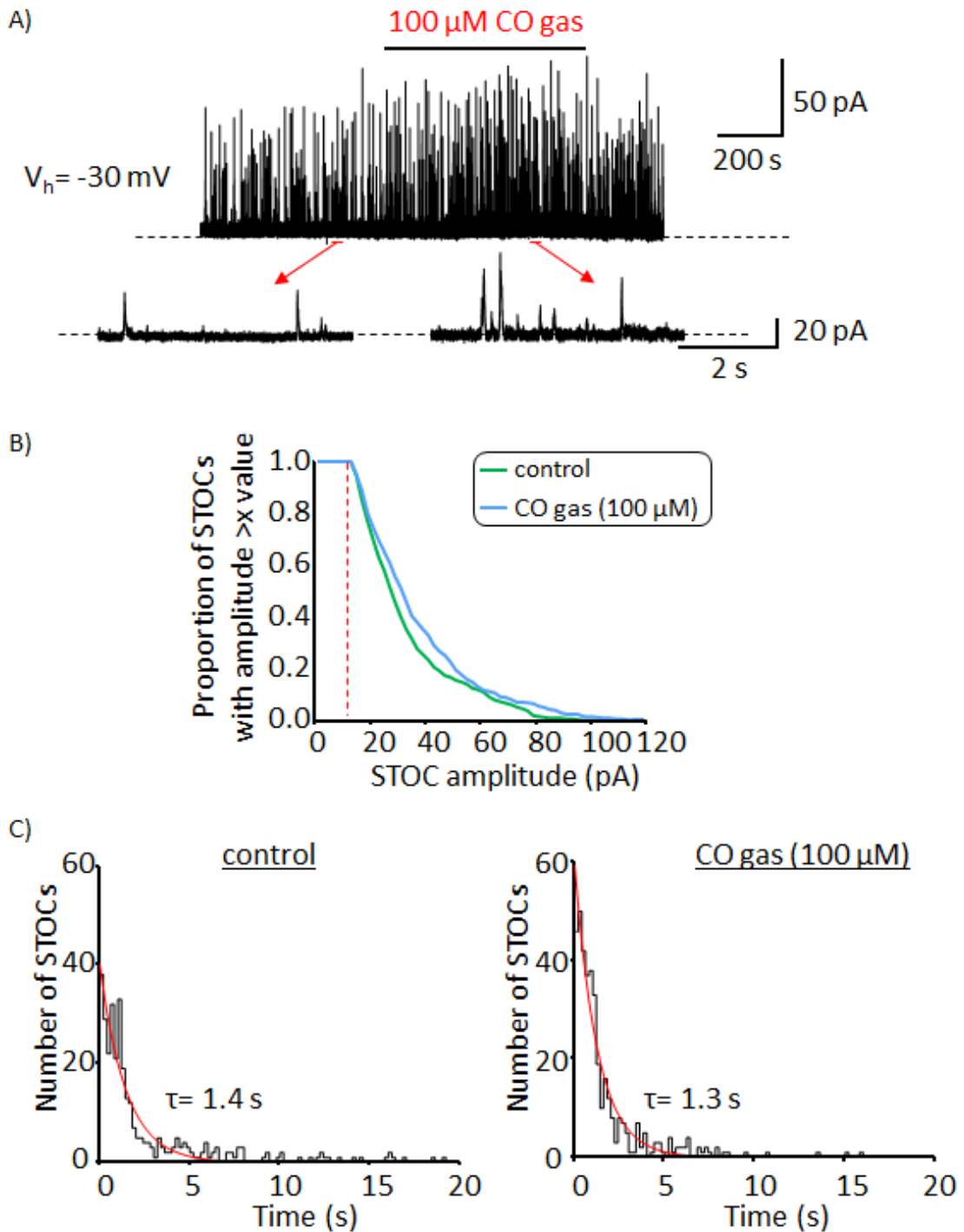


Figure 4.20: Effects of extracellular application of CO gas on STOCs. A) Example traces show the effects of extracellular CO gas (100 μM) application on STOCs. STOCs were analysed 4 minutes after CO gas application. B) Cumulative histograms, generated from trace A (above), show STOC amplitude in the presence and absence (control) of CO gas (100 μM). C) STOC frequency distribution in control condition (recording duration= 863 s, no. of STOCs detected= 329) and in CO gas (100 μM) (record duration = 620 s, no. of STOCs detected= 385). Perforated patch was used for recording. V_m was held at -30 mV.

4.5.2 Extracellular application of CORM-3 only increased STOC frequency

Experiments were also performed with CORM-3, since it increased single BK_{Ca} channel activity when applied to inside-out patches (section 3.4.2 in chapter 3).

Extracellular application of CORM-3 (30 μ M) for 10 minutes, increased mean relative STOC frequency to 232.5 ± 48.3 % of control, from 0.31 ± 0.12 Hz to 0.59 ± 0.21 Hz ($p < 0.01$, $n = 5$; Figure 4.21). Nevertheless, there was no effect on mean relative STOC amplitude, 100.9 ± 5.7 %, from 33.3 ± 5.6 pA to 33.0 ± 5.3 pA ($p > 0.05$, $n = 5$; Figure 4.21).

Furthermore, as expected application of 30 μ M iCORM-3 (inactive CORM-3) did not significantly change mean relative STOC amplitude, 83.7 ± 8.1 %, from 33.8 ± 6.4 pA to 26.8 ± 4.1 pA ($p > 0.05$, $n = 5$; Figure 4.22) or mean relative STOC frequency, 85.7 ± 20 %, from 0.56 ± 0.17 Hz to 0.54 ± 0.22 Hz ($p > 0.05$, $n = 5$; Figure 4.22).

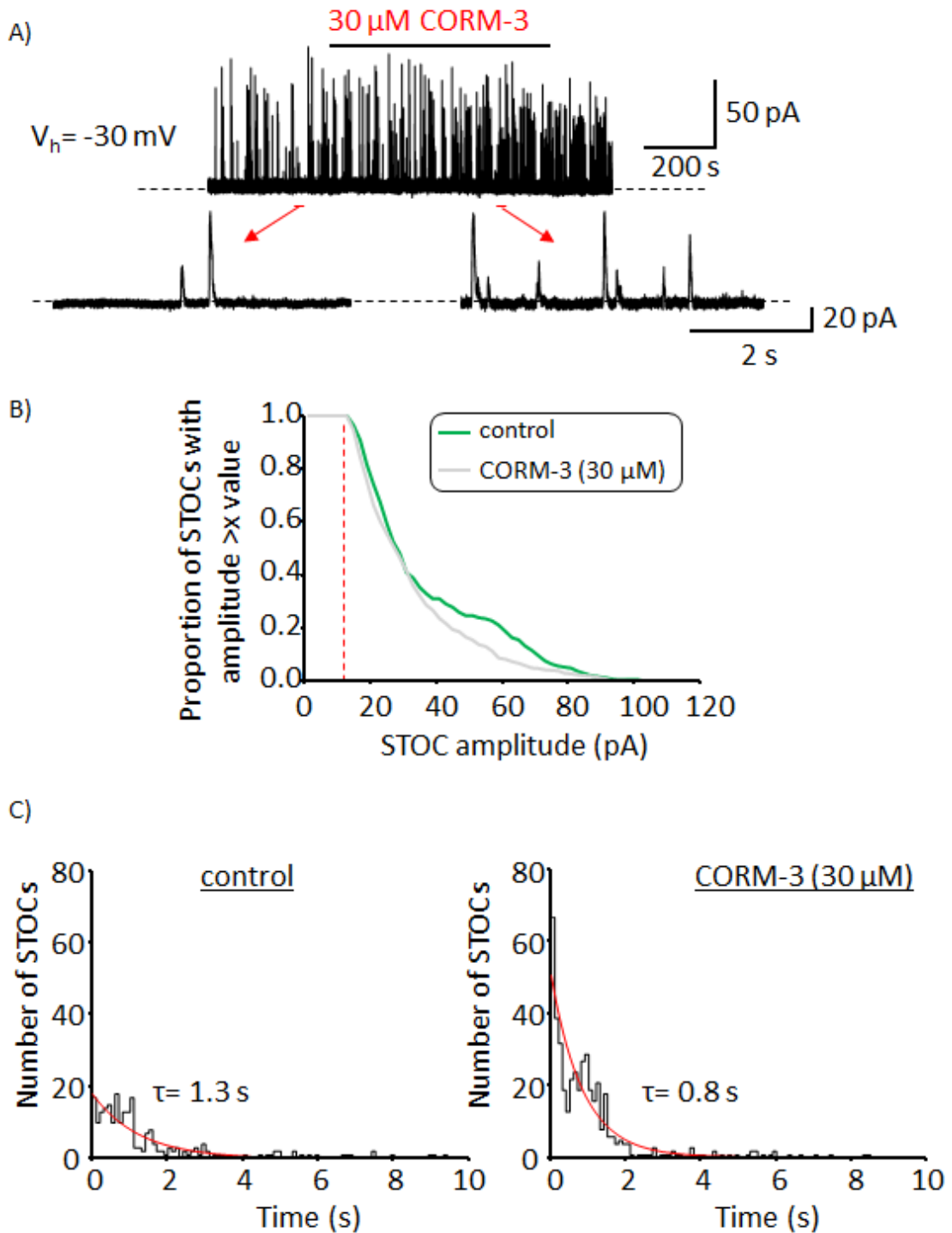


Figure 4.21: Effects of extracellular application of CORM-3 on STOCs. A) Example traces show the effects of extracellular CORM-3 (30 μM) application on STOCs. STOCs were analysed 4 minutes after CORM-3 application. B) Cumulative histograms, generated from trace A (above), show STOC amplitude in the presence and absence (control) of CORM-3 (30 μM). C) STOC frequency distribution in control condition (recording duration= 671 s, no. of STOCs detected= 255) and in the presence of CORM-3 (30 μM) (recording duration= 611 s, no. of STOCs detected= 461). Perforated patch was used for recording. V_m was held at -30 mV.

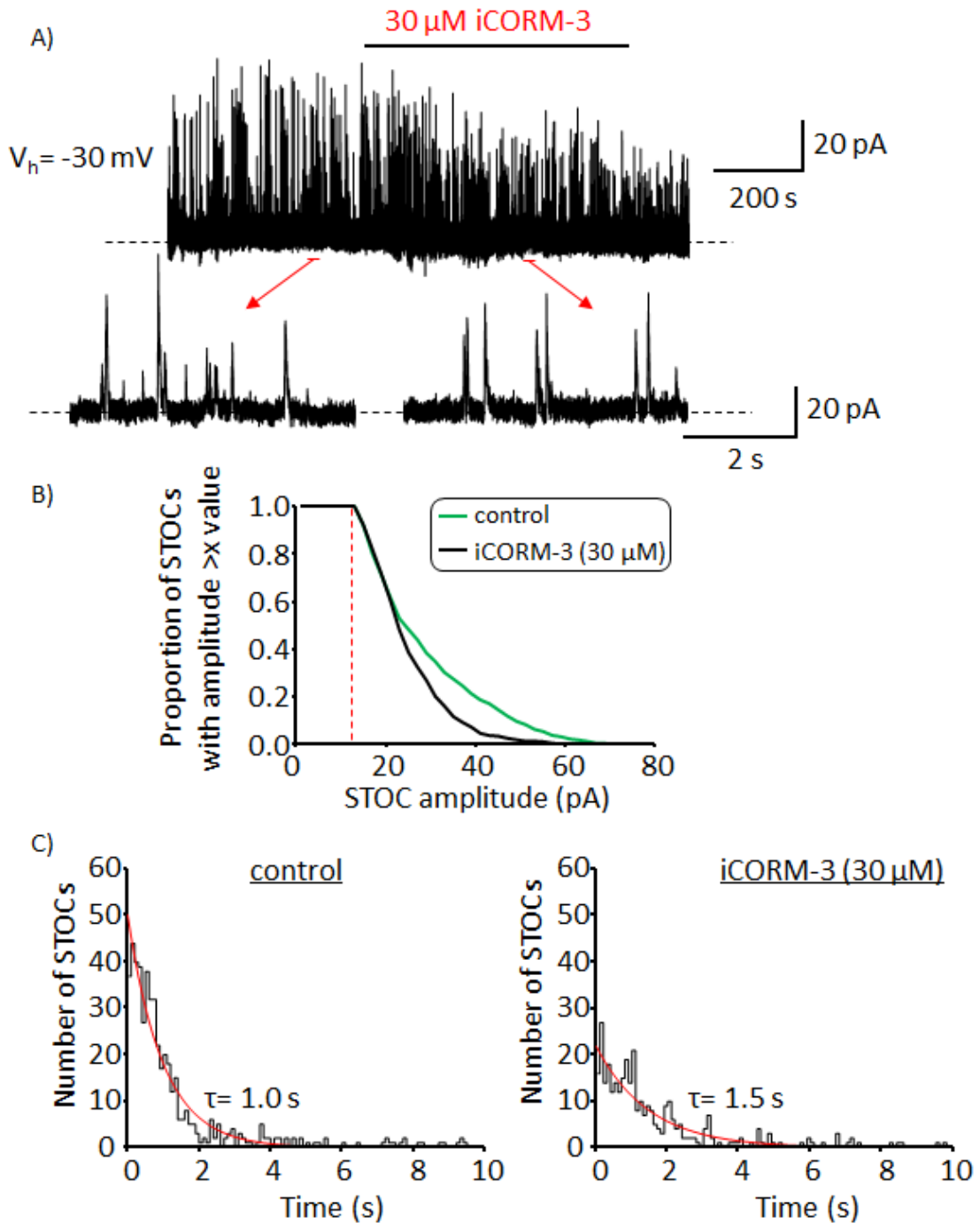


Figure 4.22: Effects of extracellular application of iCORM-3 on STOCs. A) Example traces show the effects of extracellular iCORM-3 (30 μM) on STOCs. STOCs were analysed 4 minutes after iCORM-3 application. B) Cumulative histograms, generated from trace A (above), show STOC amplitude in the presence and absence (control) of iCORM-3 (30 μM). C) STOC frequency distribution in control condition (recording duration = 669 s, no. of STOCs detected = 504) and in iCORM-3 (30 μM) (recording duration = 600 s, no. of STOCs detected = 337). Perforated patch was used for recording. V_m was held at -30 mV.

4.5.3 Summary of the effects of CO on STOCs

Extracellular application of CO gas (100 μ M) and CORM-3 (30 μ M) enhanced STOC frequency but had no effect on STOC amplitude. The mean relative change in STOC frequency (compared to control) that was induced by CORM-3 (30 μ M) was higher than the effect of CO gas (100 μ M), 132.5 ± 48.3 % increase and 49.8 ± 12.3 % increase, respectively. Nevertheless, the results from unpaired t-test indicated that the difference in CORM-3 and CO gas effects was not significant.

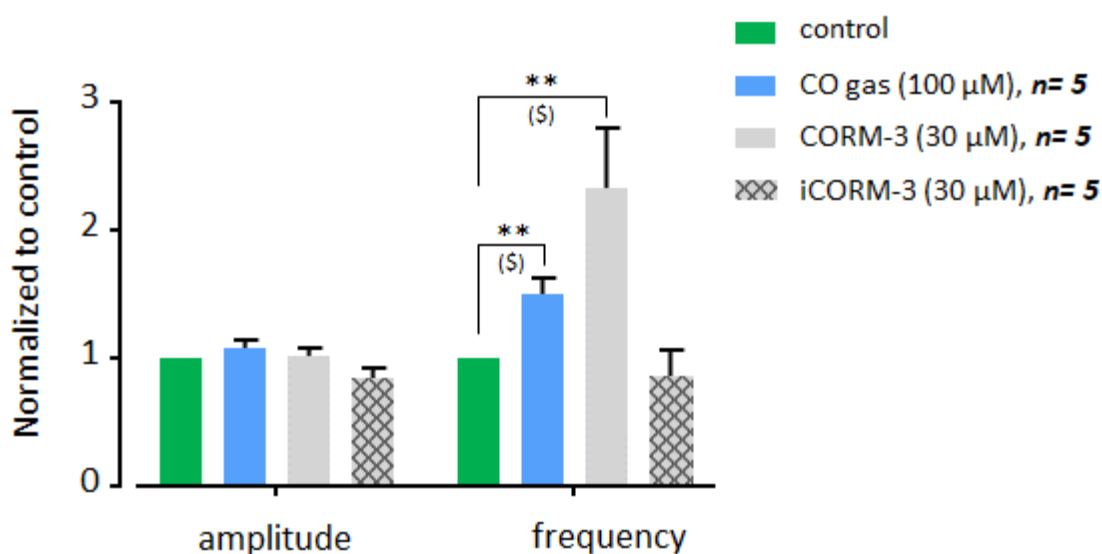


Figure 4.23: Summary of the effects of CO on STOCs. CO was applied to intact cells via CO gas and CORM-3 solutions. Perforated patch was used for all recordings. Ratio paired (\$) and unpaired t-tests were performed on raw data, as appropriate. Only significant results are indicated, ** $p \leq 0.01$.

4.5.4 Extracellular CORM-3 application had no effect on STOC amplitude and frequency in ZnPP-IX pre-treated cells

Jaggar *et al.* (2002) and I (see sections 4.5.1 and 4.5.2 above) have reported that exogenous CO enhanced STOC frequency. Nevertheless, I also decided to test for the possibility that endogenous CO production may have masked the effects of exogenous CO. This was achieved by pre-treating cells with ZnPP-IX, to inhibit HO activity, prior to extracellular application of CO. Although, CO gas and CORM-3 both enhanced STOC

frequency in this study, I decided to perform these experiments with CORM-3 since it was easier and safer to use.

Cells were pre-incubated with ZnPP-IX (10 μ M) for 21 ± 3 minutes, after which excess ZnPP-IX was washed off by perfusing cells with control solution for ~ 5 minutes. CORM-3 (30 μ M) was subsequently applied for 10 minutes and washed off for 5 minutes. Extracellular application of CORM-3 (30 μ M) did not change mean relative STOC amplitude, 91.0 ± 6.4 %, from 38.0 ± 4.92 pA to 35.8 ± 6.6 pA ($p > 0.05$, $n = 7$; Figures 4.24 & 4.25). Mean relative STOC frequency was also not significantly altered, 111.5 ± 18.9 %, from 0.32 ± 0.12 Hz to 0.36 ± 0.14 Hz ($p > 0.05$, $n = 7$; Figures 4.24 & 4.25).

Notably, the one-way ANOVA tests performed on the amplitude and frequency data obtained from recordings made during CORM-3 (30 μ M) application to ZnPP-IX pre-treated and untreated cells was not significant ($p > 0.05$, $n = 5$ in untreated cells and $n = 7$ in ZnPP-IX pre-treated cells; Figure 4.25). The data for untreated cells were those from previous experiment also performed under similar recording conditions as illustrated in Figure 4.21.

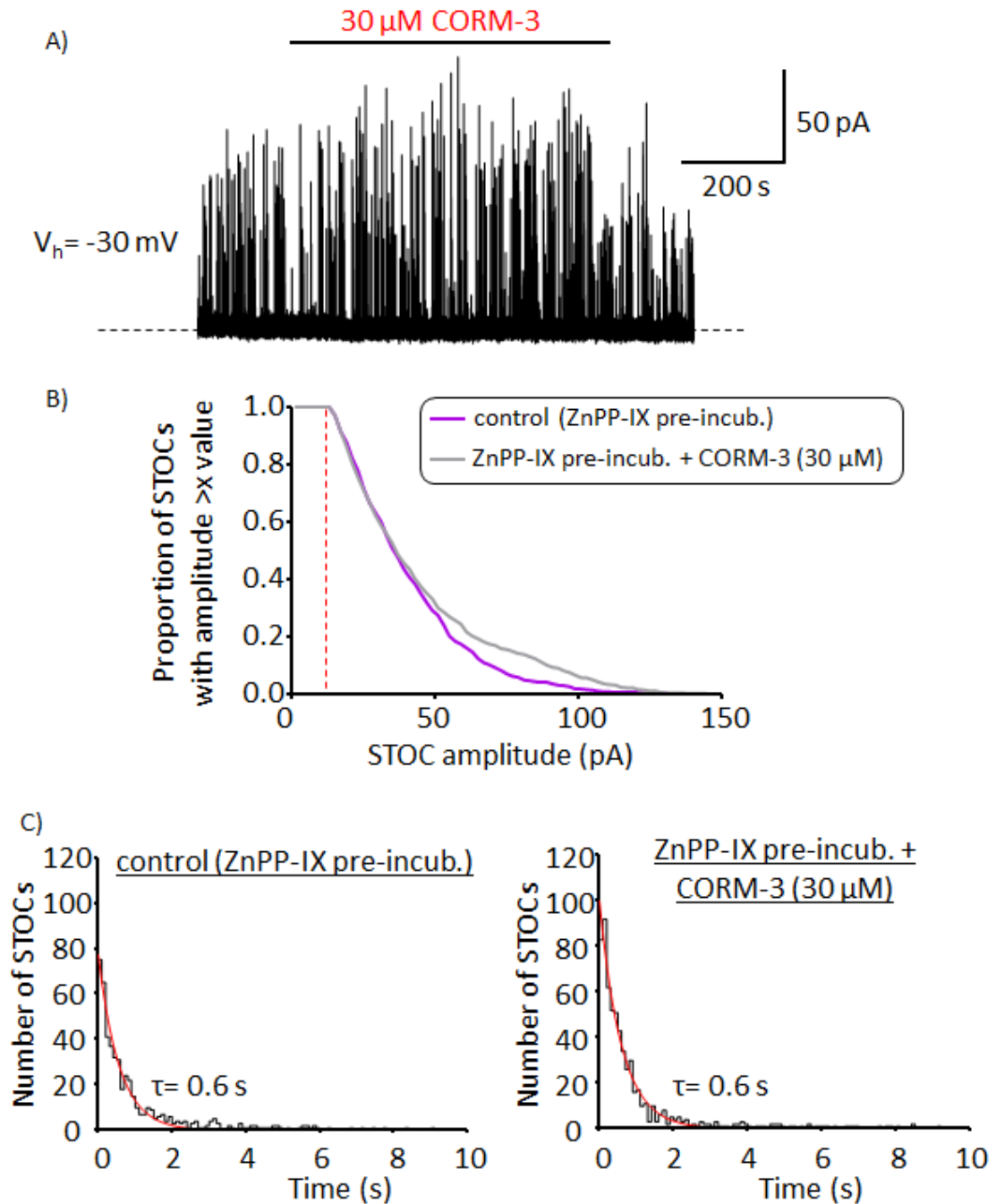


Figure 4.24: Effects CORM-3 on STOCs following cell pre-treatment with ZnPP-IX. A) Example trace shows the effects of extracellular CORM-3 ($30 \mu\text{M}$) on STOCs after cell pre-treatment with ZnPP-IX ($10 \mu\text{M}$) for 20 minutes. STOCs were analysed 4 minutes after CORM-3 application. B) Cumulative histograms, generated from trace A (above), show STOC amplitude before and after CORM-3 ($30 \mu\text{M}$) addition to ZnPP-IX pre-treated cell. C) STOC frequency distribution after ZnPP-IX pre-treatment (recording duration= 671 s, no. of STOCs detected= 520) and during CORM-3 ($30 \mu\text{M}$) application to ZnPP-IX pre-treated cell (recording duration= 632 s, no. of STOCs detected= 643). Perforated patch was used for recording. V_m was held at -30 mV.

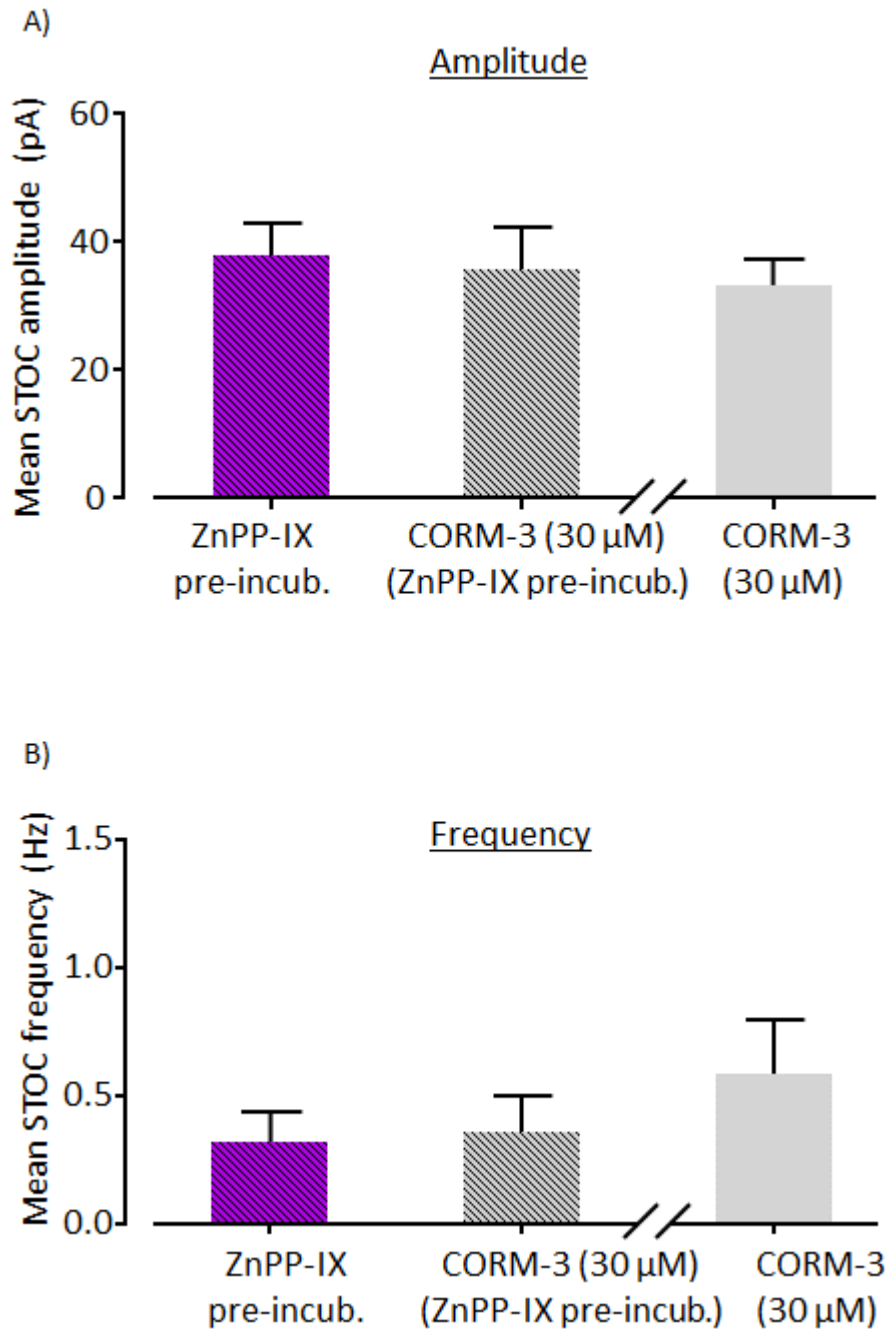


Figure 4.25: Comparison between the effects of CORM-3 on STOCs in the presence and absence of ZnPP-IX. Histograms show effects of CORM-3 (30 μ M) on A) STOC amplitude and B) STOC frequency in ZnPP-IX (10 μ M) pre-incubated cells. Comparison was made with data from untreated cells (shown after the break on the x-axes), see Figure 4.21. Error bars show SEM, $n=5$ (untreated cells) and $n=7$ (ZnPP-IX pre-treated cells). Ratio paired t-tests and one-way ANOVA were performed on amplitude and frequency data, as appropriate. Results were non-significant as $p > 0.05$. Perforated patches were used for all recordings.

4.6 Effects of haem and CO on STOCs after caveolae disruption

Caveolae are flask-shaped membrane invaginations which optimize interaction between signalling molecules, as they serve as signalling microdomains (Anderson, 1993). Specialised proteins called caveolins exist within caveolae which stabilise caveolar structure and are also involved in cell signalling (Rothberg *et al.*, 1992; Oka *et al.*, 1997; Feron *et al.*, 1998; Okamoto *et al.*, 1998). There are 3 known isoforms of caveolins; caveolin-1, -2 and -3 (Cohen *et al.*, 2004). The expression of caveolin-1 and -3 has been confirmed in arterial SMCs (Segal *et al.*, 1999).

Cholesterol extraction and immunocytochemical assays have been used to support the localization of BK_{Ca} channels in SMC caveolae via associations with caveolin-1 and 2 (Babiychuk *et al.*, 2004; Brainard *et al.*, 2005). NOS and HO have also been shown to be localised to caveolae in endothelial cells by caveolin-1, with the caveolin-1 association decreasing enzymatic activity (Feron *et al.*, 1996; Garcia-Cardena *et al.*, 1996; Ju *et al.*, 1997; Kim, 2004). Furthermore, colocalization between HO and BK_{Ca} channels has been demonstrated (Williams *et al.*, 2004). Therefore, it was hypothesised that haem and CO signalling to BK_{Ca} channels could be confined to signalling microdomains. This was investigated via caveolae disruption.

A variety of methods have been employed to examine caveolae signalling. These include; targeting specific caveolins with small interference RNA (siRNA), inclusion of caveolin scaffolding domain (CSD) peptide, using caveolin knockout-mice and depletion of membrane cholesterol with methyl β -cyclodextrin (m β CD) pre-treatment of cells. The m β CD pre-treatment was used in this study because it is relatively easy and inexpensive. Cholesterol is essential for the stabilization of caveolar structure due to its interaction with caveolins (Murata *et al.*, 1995). Thus, it is unsurprising that cholesterol depletion has been shown to disrupt caveolar signalling (Parpal *et al.*, 2001; Dreja *et al.*, 2002; Shmygol *et al.*, 2007).

Evidence compiled from several studies suggest that the concentration of m β CD and incubation times influence the level of cholesterol depletion, with high (≥ 10 mM) m β CD and relatively long (≥ 30 minutes) incubation times suitable for depletion from low and high density membrane fractions (Zidovetzki & Levitan, 2007). Considering this, my experiments were performed by pre-incubating cells at room temperature (22°C to

24°C) with either 1 mM m β CD for 60 minutes or 5 mM m β CD for 20 minutes. These conditions maintained a reasonably high cell survival rate. Furthermore, following m β CD pre-treatment, cells were superfused with bath solution for ~ 7 minutes prior to haem or CORM-3 application. This served as a control to examine the effects of m β CD pre-treatment on STOCs prior to haem or CORM-3 addition.

4.6.1 STOC amplitude was reduced in m β CD pre-treated cells

The effects of m β CD pre-treatment on STOCs was examined over time using perforated patches. STOC amplitudes and frequency were compared with STOCs recorded under similar conditions in untreated cells.

STOC amplitude and frequency from both study groups (m β CD untreated and treated cells) were analysed in sections of 5 minutes from the onset of bath superfusion. STOC amplitude was significantly lower in m β CD pre-treated cells compared with untreated cells (Figure 4.26). However, there was no significant difference between STOC frequency in m β CD treated and untreated cells (Figure 4.26).

A previous study performed using ruptured whole-cell recording of rat uterine myocytes observed that pre-incubation of the cells with m β CD reduced voltage-pulse induced whole-cell BK_{Ca} currents (Shmygol *et al.*, 2007). The results from this study is in line with my report, as STOC amplitude was lower in the m β CD pre-treated cells compared with untreated cells.

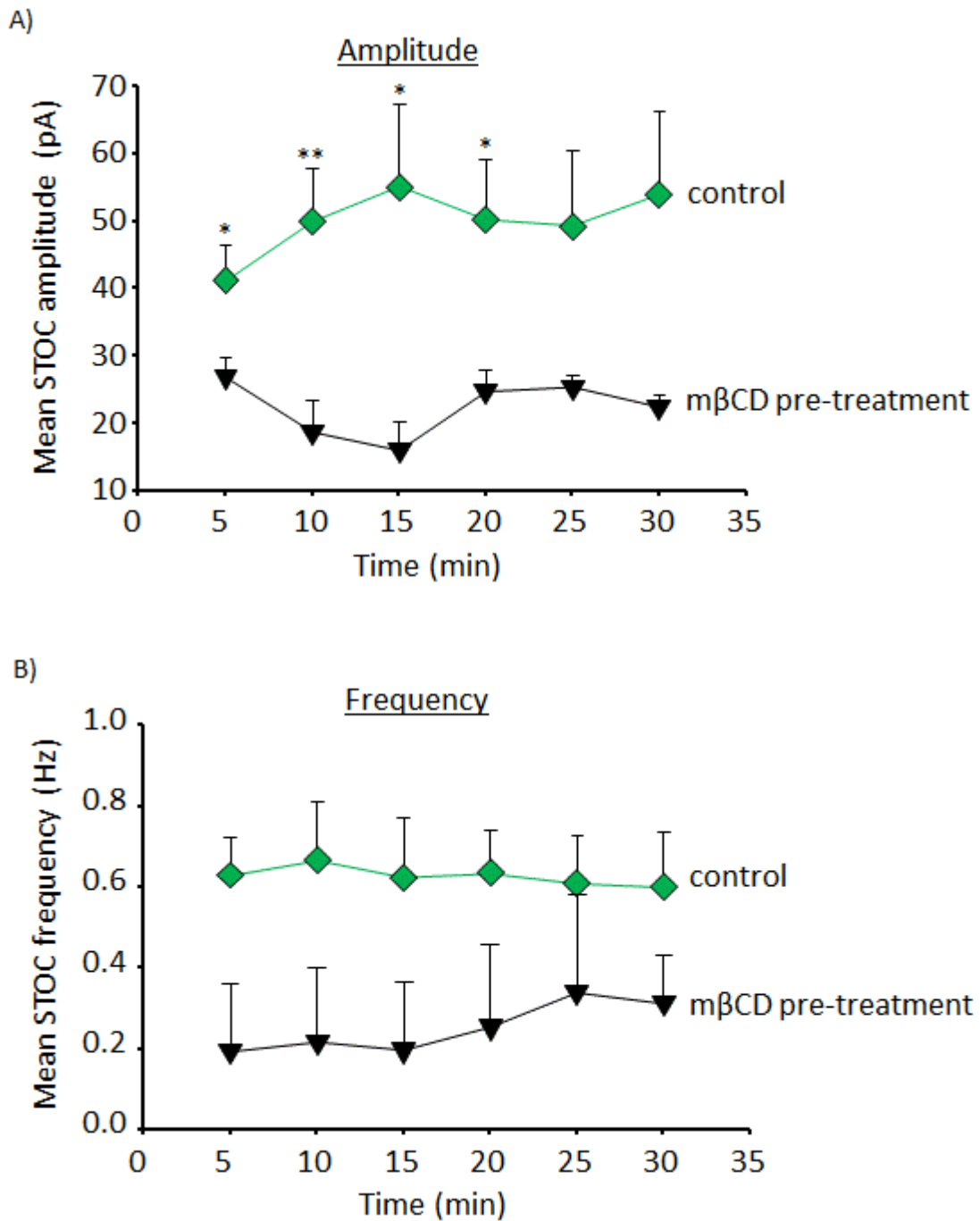


Figure 4.26: Effects of mβCD (1 to 5 mM) pre-treatment of cells on STOCs. Cells were pre-incubated in either 1 mM mβCD for 60 minutes or 5 mM mβCD for 20 minutes. A) STOC amplitude and B) STOC frequency of cells with and without (control) mβCD pre-treatment. Traces were analysed in sections of 5 minutes. Unpaired t-test was performed on raw data, * $p \leq 0.05$, ** $p \leq 0.01$. Non-significant results, with $p > 0.05$, are not indicated. Error bars show SEM, $n = 3$ (mβCD pre-treatment) and $n = 4$ (control). Perforated patch was used for recordings. V_m was held at -30 mV.

4.6.2 External haem enhanced STOC frequency in m β CD pre-treated cells but had no effect on STOC amplitude

Next, the effects of extracellular haem application on STOCs recorded from m β CD pre-treated cells was examined. This was done to investigate whether the modulatory effects of haem on STOCs was confined to signalling microdomains.

Cells were pre-incubated in m β CD (5 mM) for \sim 20 minutes, prior to superfusion with control solution for \sim 5 minutes. Extracellular haem (5 μ M) was then applied and washed off after \sim 7 minutes. Extracellular haem application did not change STOC amplitude in m β CD pre-treated cells as mean STOC amplitudes were 20.3 ± 0.5 pA and 22.0 ± 1.2 pA in the absence and presence of haem respectively ($p > 0.05$, $n = 4$; Figures 4.27 & 4.28). However, haem application to m β CD pre-treated cells increased mean relative STOC frequency to 487.1 ± 154.2 % of the initial frequency that was recorded in the m β CD pre-treated cells, from 0.10 ± 0.02 Hz to 0.60 ± 0.33 Hz ($p < 0.01$, $n = 4$; Figures 4.27 & 4.28)

In addition, one-way ANOVA with Tukey multiple comparisons test were performed on the STOC data obtained from the m β CD experiments and results from haem application to untreated cells (obtained from Figure 4.10). The results of this test indicate that extracellular haem application significantly enhanced STOC amplitude in untreated cells compared with m β CD pre-treated cells ($p \leq 0.05$, $n = 4$; Figures 4.28). However, there was no significant difference between the effects of haem on STOC frequency recorded in untreated and m β CD pre-treated cells ($p > 0.05$, $n = 4$; Figures 4.28).

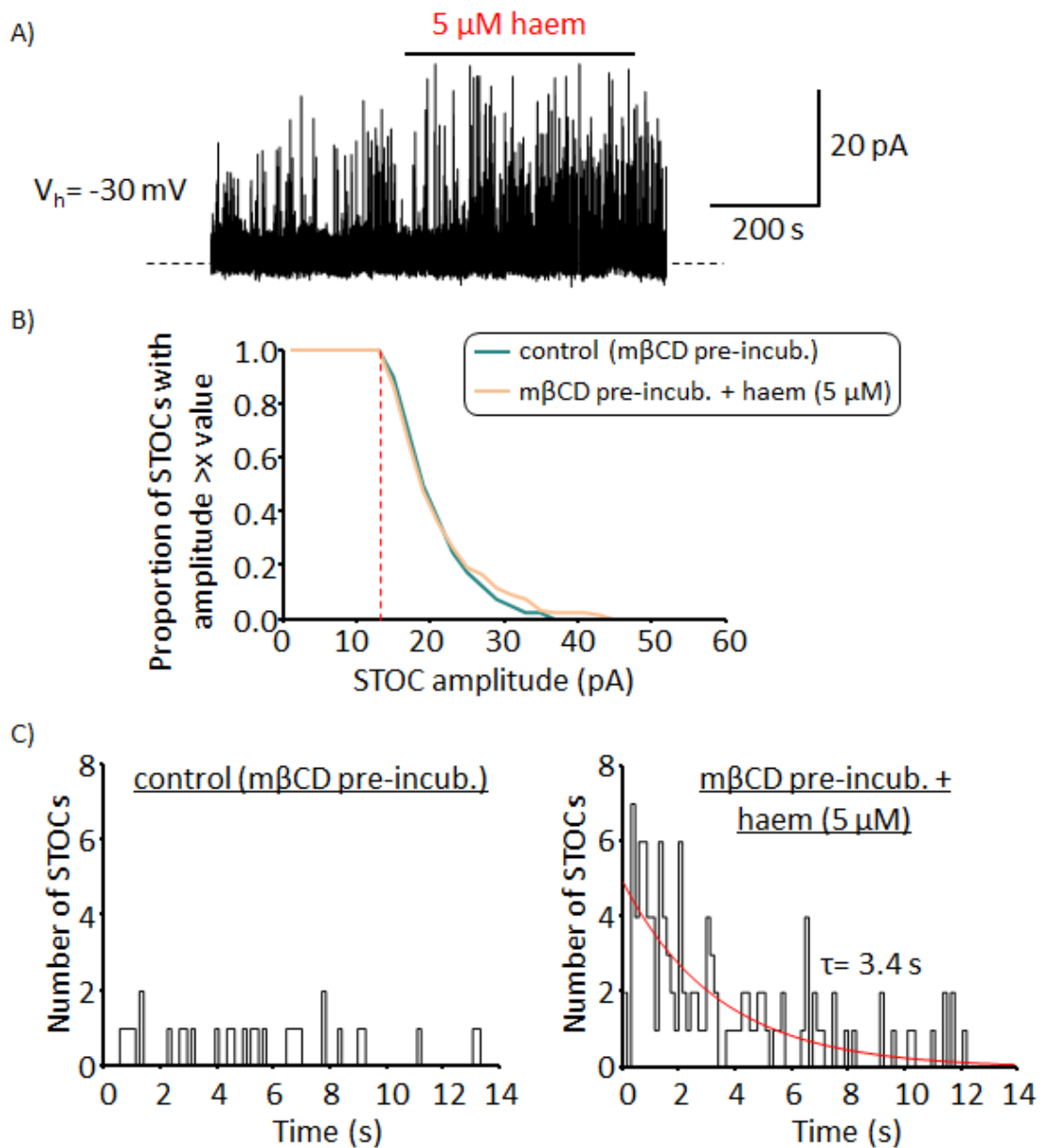


Figure 4.27: Effects of haem on STOCs after cell pre-treatment with mβCD. A) Example trace shows the effects of extracellular haem ($5 \mu\text{M}$) on STOCs following cell pre-treatment with mβCD (5 mM) for 25 minutes. STOCs were analysed 4 minutes after haem application. B) Cumulative histograms generated from trace A (above) show STOC amplitude before and after haem superfusion on mβCD pre-treated cell. C) STOC frequency distribution after mβCD pre-treatment (recording duration = 547 s, no. of STOCs detected = 40), and during haem application on mβCD pre-treated cell (recording duration = 419 s, no. of STOCs detected = 120). Graph for STOC frequency in mβCD pre-treated cells (before haem application) was not fitted due to the low number of STOCs detected. Perforated patch was used for recording. V_m was held at -30 mV.

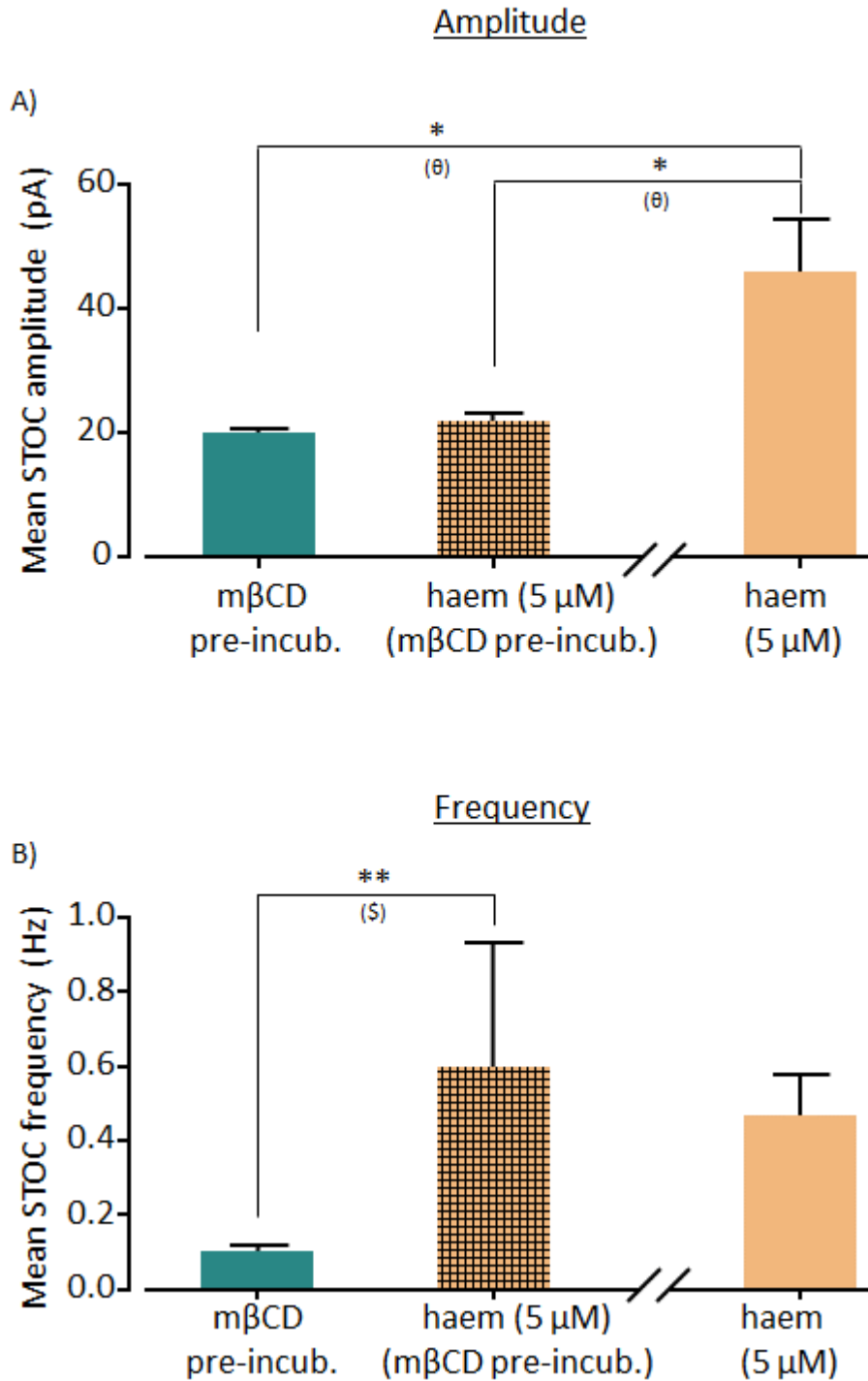


Figure 4.28: Comparison between the effects of haem on STOCs recorded from mβCD pre-treated and untreated cells. Histograms show the effects of haem (5 μM) on A) STOC amplitude and B) STOC frequency in mβCD (5 mM) pre-treated and untreated cells. Comparison was made with data from untreated cells (represented after the break on the x-axes) from Figure 4.10. Error bars show SEM, n= 4. Ratio paired t-tests (\$) and one-way ANOVA with Tukey's multiple comparisons test (θ) was performed on amplitude and frequency data. The lines indicate where a significant difference occurs, * p≤ 0.05 and ** p≤ 0.01. All recordings were performed using perforated patches.

4.6.3 Extracellular application of CORM-3 did not affect STOC amplitude or frequency in m β CD pre-treated cells

A previous study reported colocalization of HO and BK_{Ca} channels in heterologous cells (Williams *et al.*, 2004). Such interaction could enhance the modulatory effect of endogenous CO on BK_{Ca} channels. This assumes that haem degradation by HO could create a localised increase in CO production. To confirm whether the modulatory effects of CO on STOCs required intact microdomain signalling, extracellular CO was applied to m β CD pre-treated cells.

Control recording was generated by perfusing the m β CD pre-treated cells with control solution for ~ 5 minutes prior to extracellular application of CORM-3. Extracellular application of CORM-3 had no significant effect on mean STOC amplitude, as the respective values in control and in CORM-3 were 23.3 ± 5.8 pA and 21.2 ± 4.1 pA ($p > 0.05$, $n = 5$; Figures 4.29 & 4.31). Mean STOC frequency was also unaltered from 0.22 ± 0.05 Hz, in control, to 0.21 ± 0.11 Hz, in the presence of CORM-3 ($p > 0.05$, $n = 5$; Figures 4.29 & 4.31). Furthermore, extracellular application of iCORM-3 (30 μ M) to m β CD pre-treated cells produced no significant effect on mean STOC amplitude, from 35.8 ± 8.9 pA in control conditions, to 36.1 ± 7.5 pA during iCORM-3 superfusion ($p > 0.05$, $n = 3$; Figures 4.30 & 4.31). There was also no change in mean STOC frequency, from 0.31 ± 0.06 Hz in control, to 0.37 ± 0.04 Hz in the presence of iCORM-3 ($p > 0.05$, $n = 3$; Figures 4.30 & 4.31).

One-way ANOVA tests were performed with the STOC data obtained from m β CD experiments (with CORM-3 and iCORM-3) and data obtained from CORM-3 application to untreated cells. The results showed that there was no significant difference between STOC amplitude and frequency recorded during CORM-3/iCORM-3 application to m β CD pre-treated and untreated cells ($p > 0.05$, $n = 3$ for iCORM-3 application to m β CD treated, $n = 5$ for CORM-3 application to m β CD treated, and $n = 6$ for CORM-3 application to untreated cells; Figure 4.31). The data for untreated cells were obtained from previous experiments performed with CORM-3 application (see section 4.5.2 above).

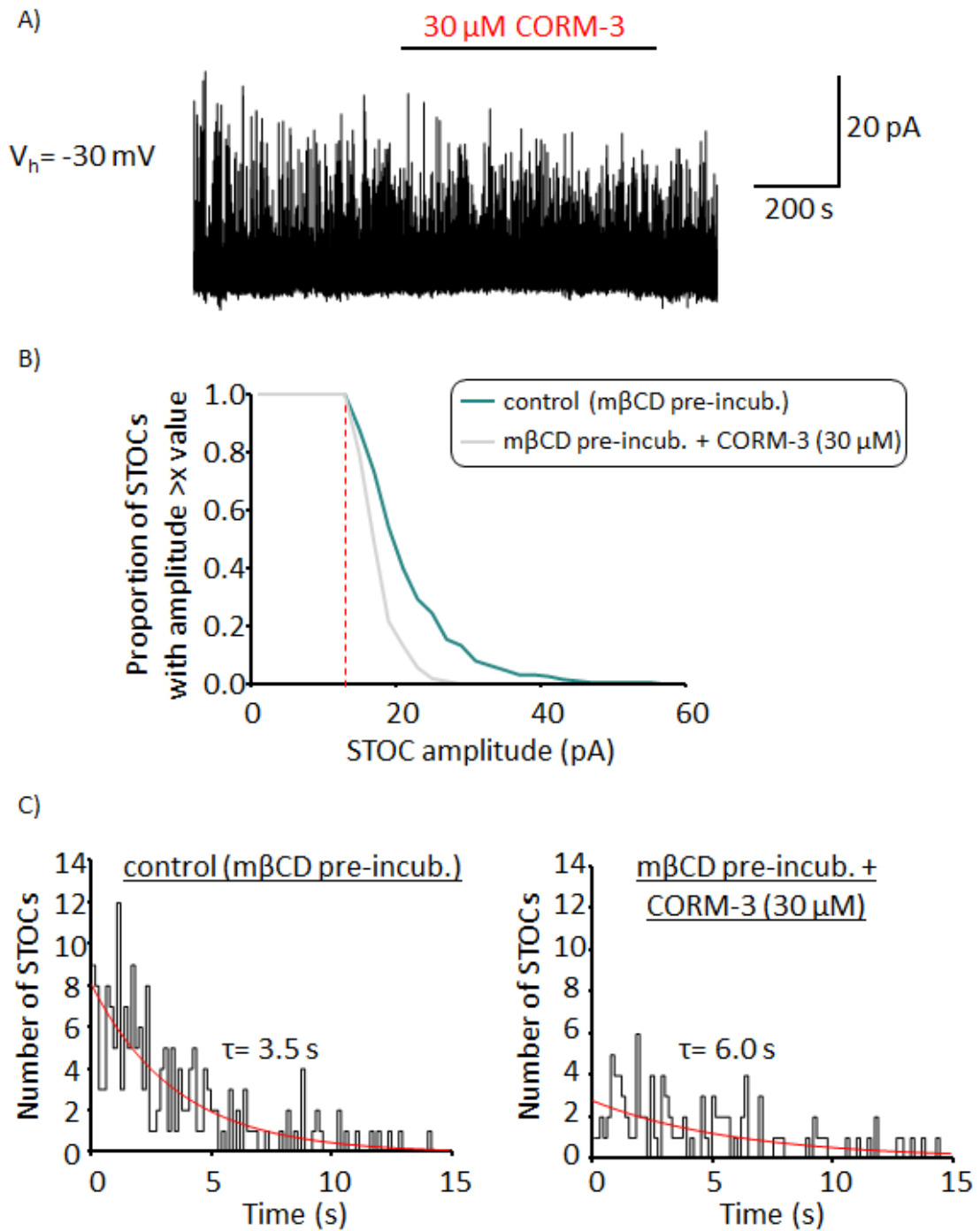


Figure 4.29: Effects of CORM-3 on STOCs after cell pre-treatment with m β CD. A) Example trace shows the effects of extracellular CORM-3 (30 μ M) on STOCs following cell pre-treatment with m β CD (1 mM) for 65 min. STOCs were analysed 4 minutes after CORM-3 application. B) Cumulative histograms, generated from trace A (above), show STOC amplitude before and after CORM-3 superfusion on m β CD pre-treated cell. C) STOC frequency distribution after m β CD (5 mM) pre-treatment (recording duration= 668 s, no. of STOCs detected= 188) and during CORM-3 (30 μ M) application to m β CD pre-treated cell (recording duration= 595 s, no. of STOCs detected= 106). Perforated patch was used for recording. V_m was held at -30 mV.

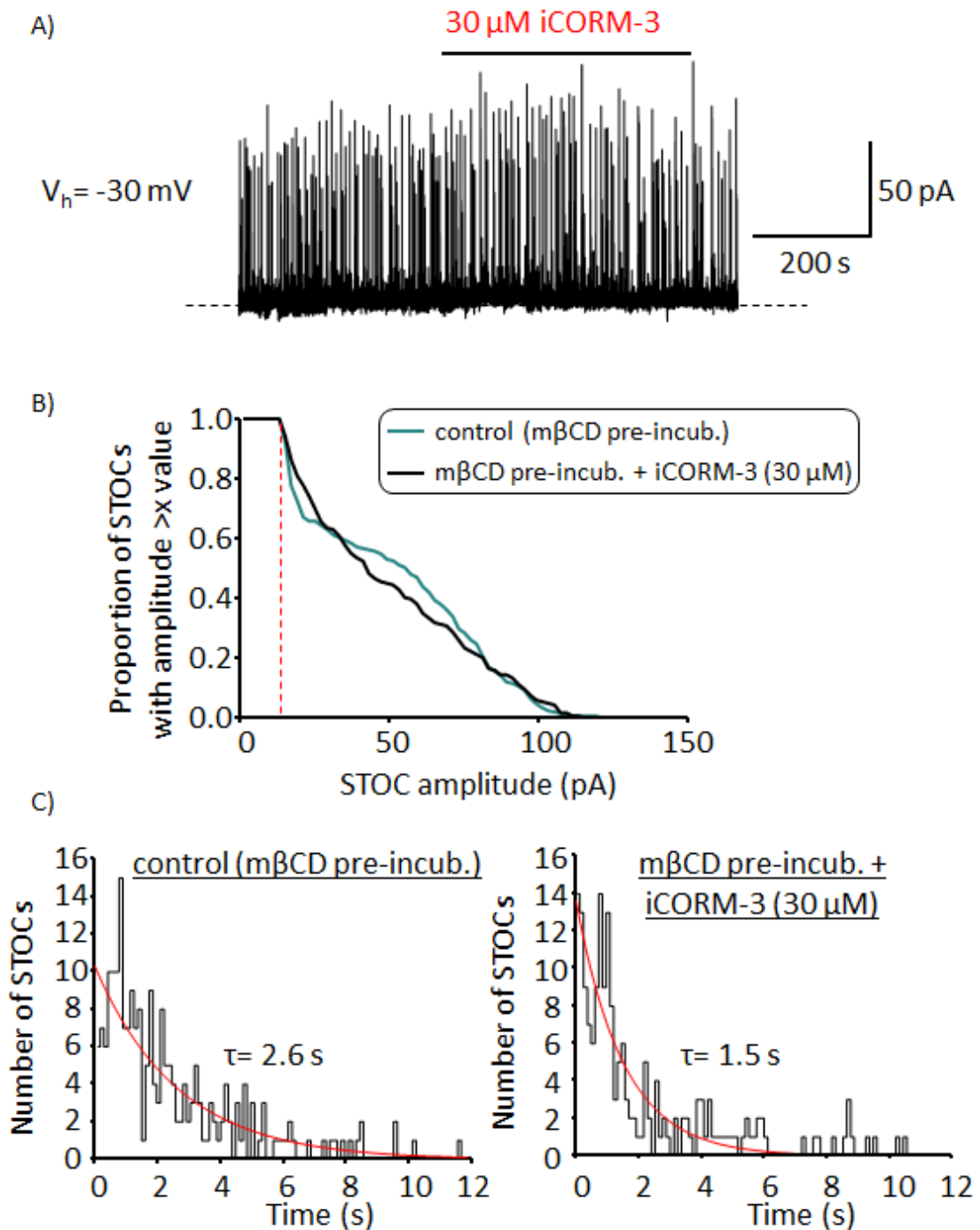


Figure 4.30: Effects of iCORM-3 on STOCs after cell pre-treatment with mβCD. A) Example trace shows the effects of extracellular iCORM-3 (30 μM) on STOCs following cell pre-treatment with mβCD (5 mM) for 20 minutes. STOCs were analysed 4 minutes after iCORM-3 application. B) Cumulative histograms, generated from trace A (above), show STOC amplitude before and after iCORM-3 superfusion on mβCD pre-treated cell. C) STOC frequency distribution after mβCD pre-treatment (recording duration= 539 s, no. of STOCs detected= 220) and during iCORM-3 (30 μM) application on mβCD pre-treated cell (recording duration= 423 s, no. of STOCs detected= 189). Perforated patch was used for recording. V_m was held at -30 mV.

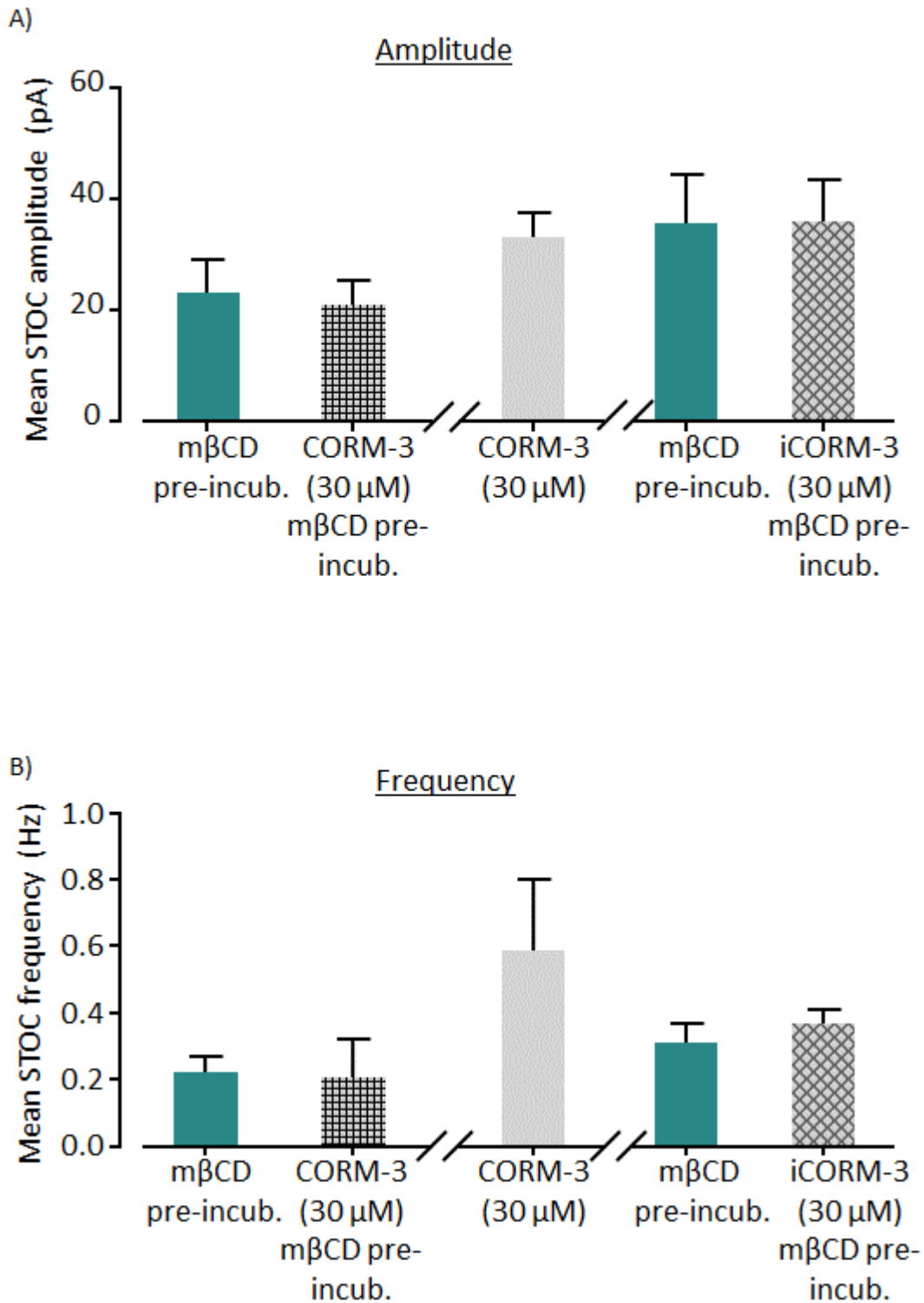


Figure 4.31: Comparison between the effects of CORM-3/iCORM-3 on STOCs recorded from mβCD pre-treated and untreated cells. Histograms show the effects of CORM-3 (30 μM) and iCORM-3 (30 μM) on A) STOC amplitude and B) STOC frequency in mβCD (1 & 5 mM) pre-treated cells. Comparison was made with data from cells without mβCD pre-incubation as illustrated in Figure 4.21 (shown after the first break on the x-axes). Error bars show SEM, n = 3 to 6. Ratio paired t-tests and one-way ANOVA test were non-significant as $p > 0.05$. All recordings were performed using perforated patches.

4.7 Extracellular application of haem did not influence Ca²⁺ spark frequency

In my experiments I found that extracellular haem (5 μM) application alone increased STOC amplitude only. However, an increase in STOC frequency was observed if haem was applied to cells pre-treated with either ZnPP-IX or m β CD. It is assumed that intracellular haem concentration will be high in ZnPP-IX pre-treated cells due to the inhibition of HO activity. However, it is uncertain whether caveolar disruption in m β CD pre-treated cells could itself affect intracellular haem concentration.

STOC frequency is dependent on Ca²⁺ spark frequency. In the presence of HLL, a HO substrate, there was 1.4-fold increase in the Ca²⁺ spark frequency recorded from cerebral arteriole SMCs (Jaggar *et al.*, 2002). It was proposed that CO, the degradation product, was responsible for the increase in Ca²⁺ spark frequency. In addition, Jaggar *et al.* (2002) suggested that CO enhanced STOC frequency by increasing the coupling between Ca²⁺ sparks and BK_{Ca} channel activation. However, these experiments were performed with HLL and not haem. Therefore, this study investigates the effects of haem on Ca²⁺ spark frequency recorded in mesenteric artery SMCs.

Freshly isolated cells were prepared for imaging by loading them with Fluo-4 AM (10 μM) and wortmannin (10 μM) for 40 minutes, as detailed in the Methods section 2.8.1. The bath solution used for cell incubation contained 5 mM K⁺. Control recordings were obtained by imaging several cells within the same petri dish at a rate of 10 frames s⁻¹. Haem (5 μM) was then added by pipette to the same dish that was used for the control. Different cells were then imaged, although not necessarily the ones that were imaged during the control recording. This is because haem application with a pipette inevitably dislodged cells.

Subsequent analysis of the changes in intracellular Ca²⁺ levels with time, using the WinFluor software, displayed the Ca²⁺ sparks and waves as sharp spikes and broad peaks, respectively. Ca²⁺ sparks and waves were observed in both control and haem (5 μM) superfused cells, as shown in Figures 4.32 & 4.33, respectively. Quantitative analysis of the data was performed using the Tracan software, as explained in the Methods section 2.8.2. The results showed that there was no significant difference between Ca²⁺ spark frequency recorded in control and haem-treated cells, 6.90 ± 0.46 Hz and $7.36 \pm$

1.36 Hz, respectively ($p > 0.05$, $n = 5$; Figure 4.34). This contrasts with reports from Jaggar *et al.* (2002) study, where application of HLL to porcine cerebral arteriole SMCs slightly increased Ca^{2+} spark frequency with no observable effects on Ca^{2+} spark amplitude.

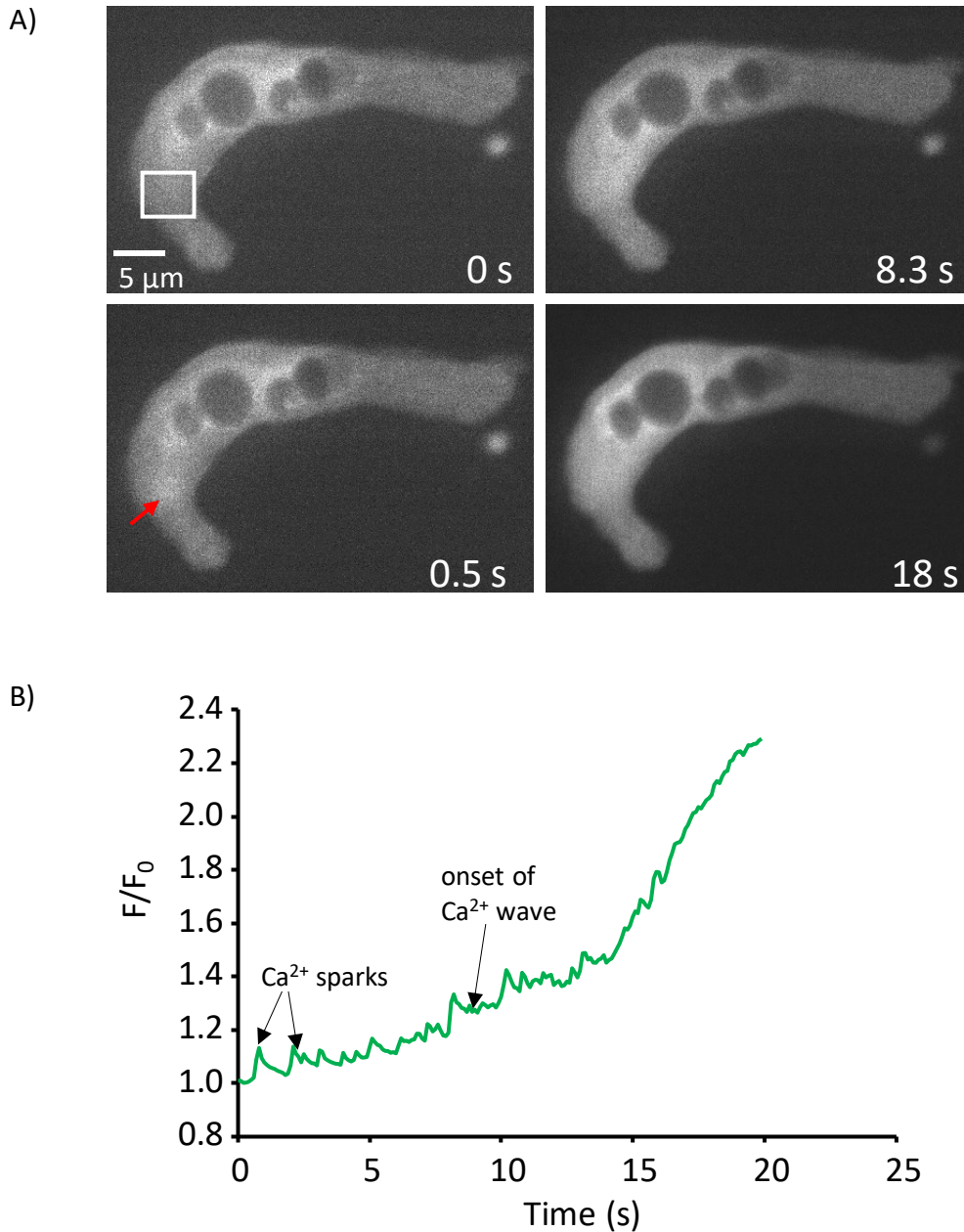


Figure 4.32: Observation of Ca^{2+} sparks in a SMC under control (haem-free) conditions. Cells were pre-incubated with wortmannin ($10 \mu\text{M}$) and fluo-4AM ($10 \mu\text{M}$) for 40 minutes at room temperature. Wortmannin was used to reduce cell contraction to improve image quality. Images were acquired at 10 frames s^{-1} (100 ms exposure) with 200 images captured per cell. A) Example cell imaged at different time points, at resting V_m . Red arrow indicates the primary Ca^{2+} spark site and the white square shows the region of interest used for analysis. B) Graph shows changes in intracellular fluorescence over time from cell shown in A) above. $[\text{Ca}^{2+}]_o = 1 \text{ mM}$; $[\text{K}^+]_o = 5 \text{ mM}$.

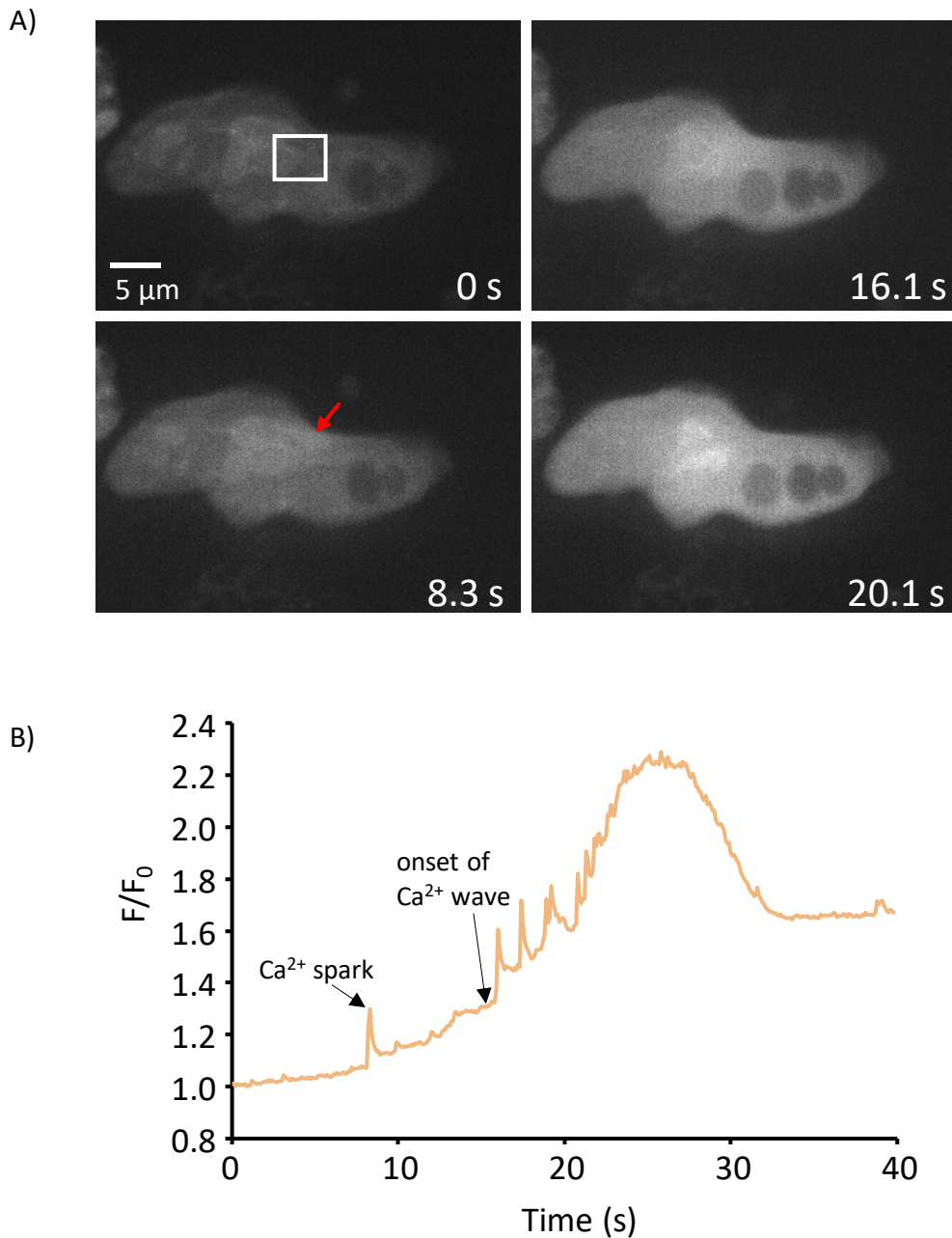


Figure 4.33: Observation of Ca^{2+} sparks in the presence of extracellular haem ($5 \mu\text{M}$). Cells were pre-incubated with wortmannin ($10 \mu\text{M}$) and fluo-4AM ($10 \mu\text{M}$) for 40 minutes at room temperature. Images were acquired at 10 frames s^{-1} (100 ms exposure) with 400 images per cell. A) Example cell imaged at different time points after 4 min of extracellular haem ($5 \mu\text{M}$) application, at resting V_m . Red arrow indicates the primary Ca^{2+} spark site and the white square shows the region of interest used for analysis. B) Graph showing changes in intracellular fluorescence over time after extracellular application of haem ($5 \mu\text{M}$) to cell, in A) above. $[\text{Ca}^{2+}]_o = 1 \text{ mM}$; $[\text{K}^+]_o = 5 \text{ mM}$.

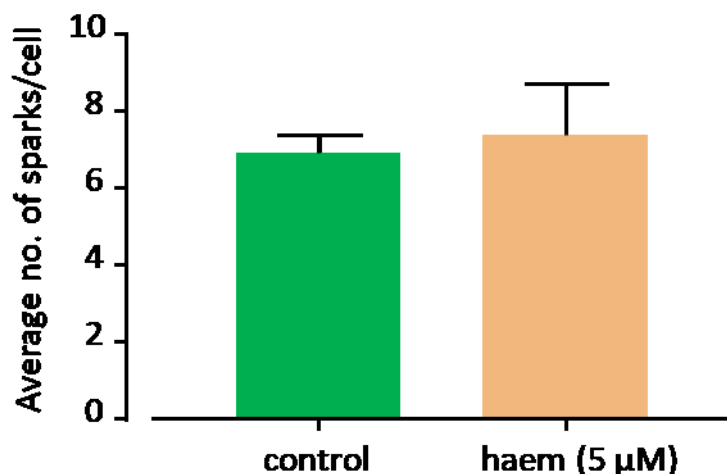


Figure 4.34: Effects of haem (5 μM) on Ca²⁺ spark frequency in mesenteric artery SMCs. Histograms show Ca²⁺ spark frequency before and after extracellular haem (5 μM) application. Ratio paired t-test was performed, results were statistically non-significant as $p > 0.05$. Error bars show SEM, $n = 5$. All recordings were made at resting V_m .

4.8 Effects of haem localization on STOCs

So far, haem has been administered extracellularly based on the hypothesis that its lipophilic nature enables it to enter cells, although haem carriers also exist but relatively little is known about them. However, during haemolytic diseases, the increase in extracellular haem concentration can also enhance intracellular haem concentrations, $[\text{haem}]_i$, due to the ability of haem to traverse the lipid membrane. Therefore, the effects of direct intracellular haem application as well as simultaneous intracellular and extracellular haem application on STOCs was examined.

4.8.1 Intracellular haem application had no modulatory effect on STOCs

Haem (5 μM) was applied intracellularly by adding it to the pipette solution of ruptured patches. Therefore, recordings were made immediately after membrane rupture, whilst perfusing cells with control solution for ~ 15 minutes. Control experiments, in haem-free conditions, were performed separately using the normal pipette solution (see Table 2.2 in Methods chapter) whilst also perfusing cells with control solution for ~ 15 minutes.

Surprisingly, the current traces observed during intracellular haem application and control experiments were similar (Figures 4.35 & 4.36). STOC amplitude and frequency from both set of experiments were analysed in blocks of 3 minutes from the onset of the recording. No significant difference was detected between the stability of STOCs observed during recordings with haem in the pipette solution and under control conditions (Figure 4.37).

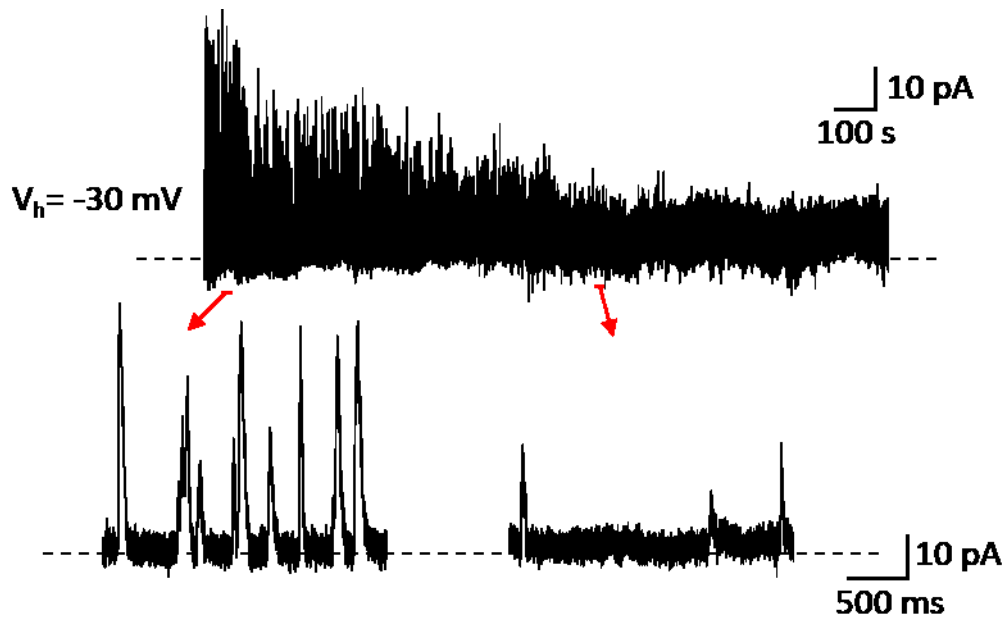


Figure 4.35: Recording of STOCs in the absence of haem. Example traces show STOCs recorded under control (haem-free) conditions. Ruptured patch was used for recording. Pipette solution contained ATP (1 mM). V_m was held at -30 mV. $[Ca^{2+}]_i = 100$ nM; $[K^+]_i = 140$ mM; $[K^+]_o = 5$ mM.

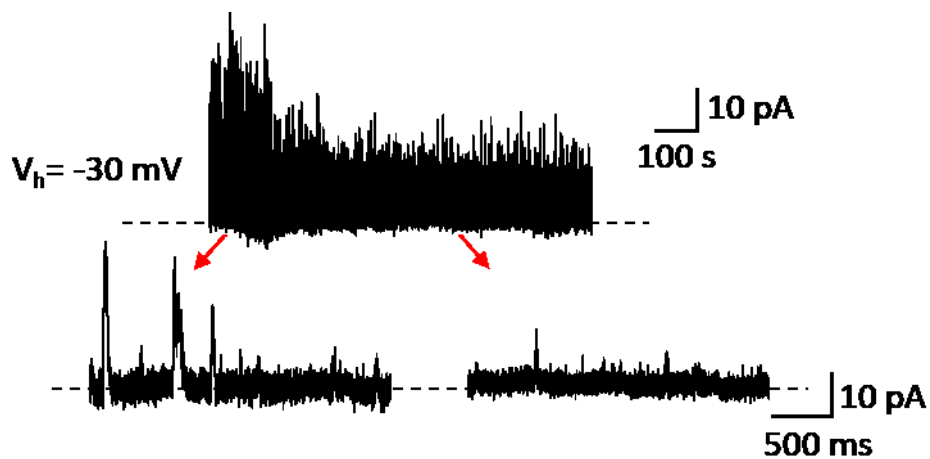


Figure 4.36: Effects of intracellular haem (added via the pipette solution) on STOCs. Example traces show STOCs recorded with haem (5 μ M) in the pipette solution. Ruptured patch was used for recording. Pipette solution also contained ATP (1 mM). V_m was held at -30 mV. $[Ca^{2+}]_i = 100$ nM; $[K^+]_i = 140$ mM; $[K^+]_o = 5$ mM.

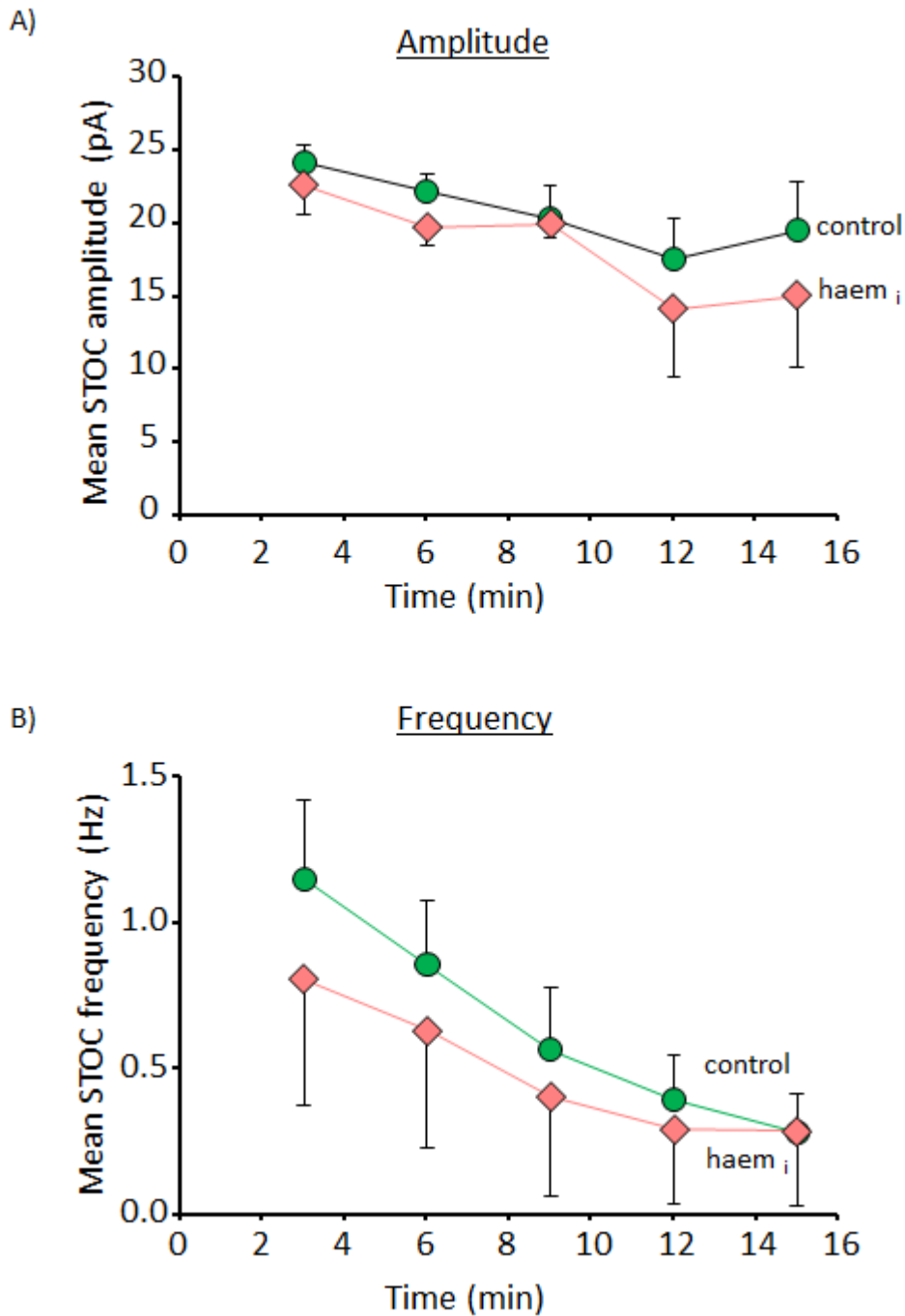


Figure 4.37: Comparison of STOCs under control conditions and in the presence of intracellular haem (haem_i). A) STOC amplitude and B) STOC frequency in control (haem-free) conditions and in the presence of intracellular haem (5 μ M) applied via the pipette solution. Analysis was performed in blocks of 3 minutes from the onset of the recording. Ruptured patch was used for all recordings. V_m was held at -30 mV. Unpaired t-test was performed on STOC amplitude and frequency data, results were non-significant as $p > 0.05$. Error bars show SEM, $n = 6$ (for haem_i) and $n = 11$ (for control).

4.8.2 Simultaneous intracellular and extracellular haem application enhanced STOC frequency but not STOC amplitude

In inside-out patch experiments, intracellular haem application inhibited single BK_{Ca} channel activity (see section 3.3 in chapter 3). Considering this result, it was surprising that intracellular haem, added via the pipette solution, had no effect on STOCs. Notably, extracellular haem application under similar experimental conditions (using ruptured patches) also had no effect on STOCs whereas extracellular haem applied to whole-cell perforated patches enhanced STOC amplitude (see section 4.3.1 above). I decided to measure STOCs in the presence of both intracellular and extracellular haem to determine whether haem might influence STOCs differently under such condition. Experiments were performed using ruptured patches so that haem could be present in the bath and pipette solutions at the same time. Haem (5 μ M) was used because this concentration was previously used to investigate the effects of extracellular or intracellular haem on STOCs (see sections 4.3.1 and 4.8.1 above).

In the presence of both intracellular and extracellular haem, the rundown of STOC amplitudes observed previously in the presence of intracellular haem only (shown in Figure 4.36) was absent (see Figure 4.38). However, statistical analysis of the results revealed that there was no significant difference between the mean STOC amplitude measured in intracellular haem only and in the presence of intracellular and extracellular haem; 19.5 ± 0.4 pA and 20.4 ± 0.7 pA, respectively ($p > 0.05$, $n = 4$; Figure 4.39). In contrast, in the presence of intracellular and extracellular haem, mean relative STOC frequency was increased to 232.1 ± 26.8 % of the measurements made in only intracellular haem, from 0.31 ± 0.08 Hz to 0.70 ± 0.20 Hz ($p \leq 0.01$, $n = 4$; Figure 4.39). It should be noted that the results from 3 patches were excluded from analysis because, even though there was barely any change in their STOC amplitude, they were regarded as outliers as a decrease, no change and 9-fold increase in STOC frequency were observed in those patches.

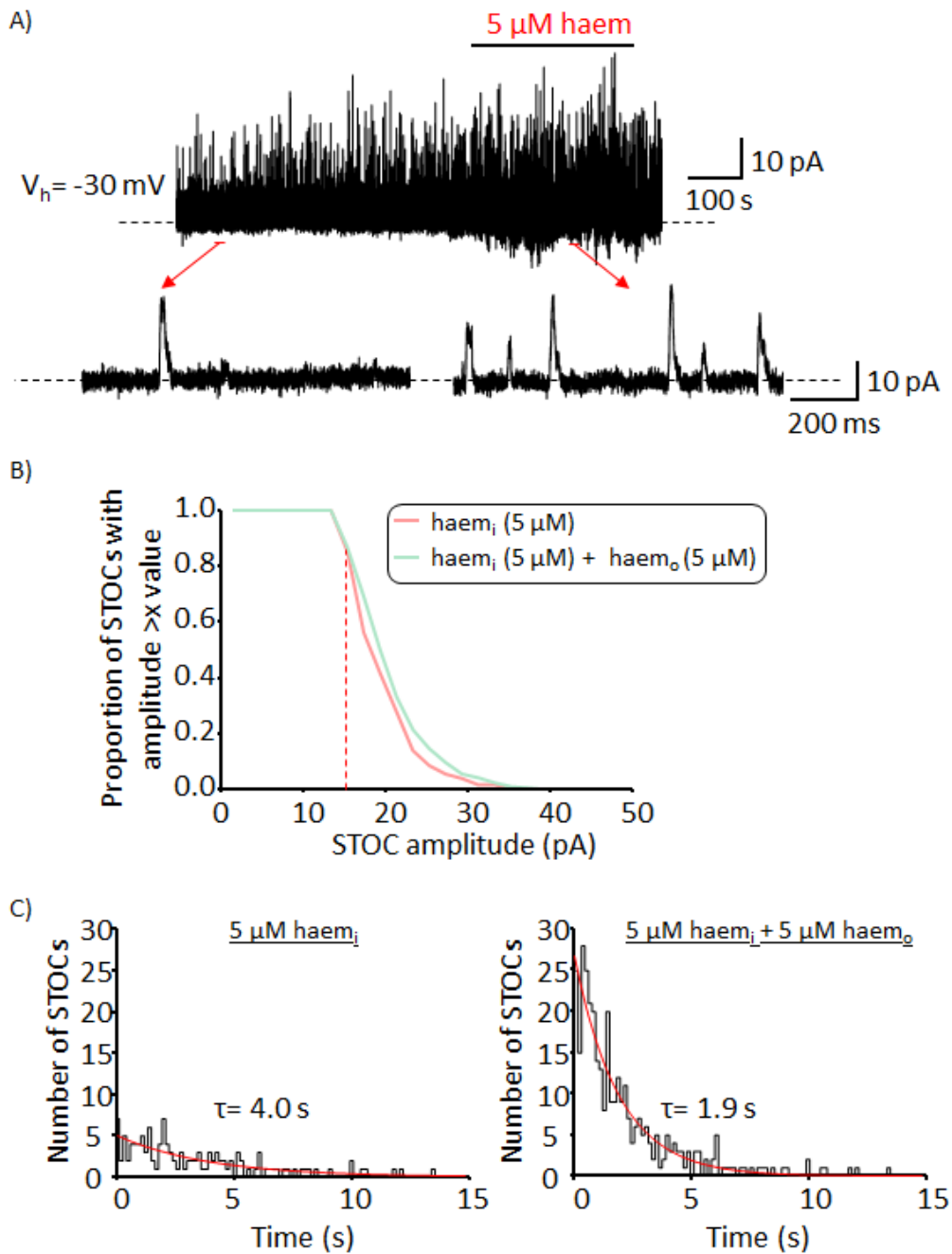


Figure 4.38: Effects of simultaneous application of intracellular and extracellular haem on STOCs. Ruptured patch was used for the recording, thus haem (5 μM) was present in the pipette solution throughout the recording. A) Example traces show STOCs in the presence of intracellular haem (5 μM) and in intracellular + extracellular haem (5 μM). B) Cumulative histograms, generated from trace A (above), show STOC amplitude in intracellular haem (5 μM), haem_i, and in intracellular haem (5 μM) + extracellular haem (5 μM), haem_i + o. C) STOC frequency distribution in intracellular haem (5 μM) (recording duration= 545 s, no. of STOCs detected= 132) and in intracellular + extracellular haem (5 μM) application (recording duration= 304 s, no. of STOCs detected= 223). Pipette solution contained ATP (1 mM) and haem (5 μM). V_m was held at -30 mV. $[\text{Ca}^{2+}]_i = 100 \text{ nM}$; $[\text{K}^+]_i = 140 \text{ mM}$; $[\text{K}^+]_o = 5 \text{ mM}$.

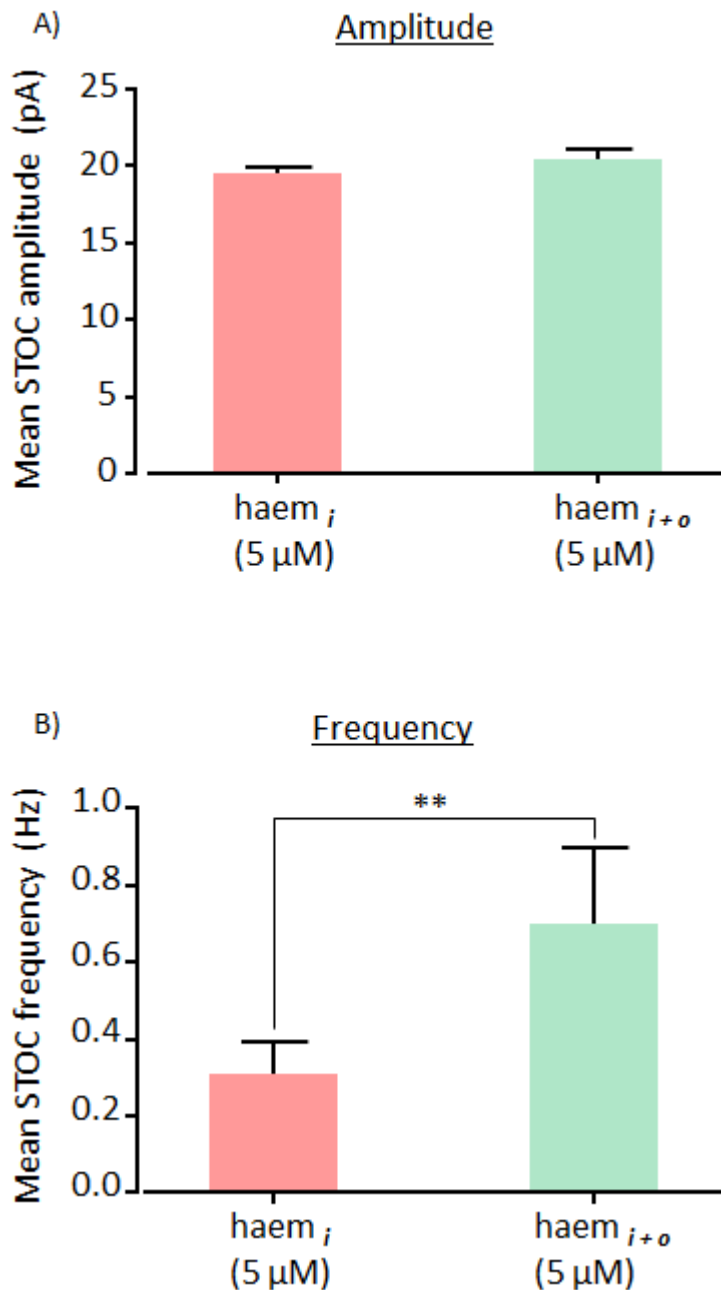


Figure 4.39: Effects of intracellular haem (haem_i) versus extracellular and intracellular haem (haem_{i+o}) on STOCs. Ruptured patch technique was used for all recordings. Haem (5 μM) was applied intracellularly via the pipette solution. After 7 minutes of recording in the presence of intracellular haem, cells were superfused with extracellular haem (5 μM). The histograms show A) mean STOC amplitude and B) mean STOC frequency in intracellular haem (5 μM) and during intracellular haem (5 μM) and extracellular haem (5 μM) application. Ratio paired t-test was performed, using raw data ** p ≤ 0.01. The results for STOC amplitude was not significant as p > 0.05. Error bars show SEM, n = 4.

| Haem/CO application | Experiment | Patch technique | Results | |
|---------------------|--|-----------------|-----------------------|-----------------------|
| | | | <i>STOC amplitude</i> | <i>STOC frequency</i> |
| ext. | Haem (5 μ M) | P | ↑ (4) | ns (4) |
| ext. | Haem (0.1 μ M) | P | ns (6) | ↑ (6) |
| ext. | Haem (30 μ M) | P | ns (4) | ↑ (4) |
| ext. | CO gas (100 μ M) | P | ns (5) | ↑ (5) |
| ext. | CORM-3 (30 μ M) | P | ns (5) | ↑ (5) |
| ext. | ZnPP-IX (10 μ M) | P | ns (4) | ns (4) |
| ext. | ZnPP-IX pre-incub. + Haem (5 μ M) | P | ↑ (4) | ↑ (4) |
| ext. | ZnPP-IX pre-incub. + CORM-3 (30 μ M) | P | ns (7) | ns (7) |
| ext. | m β CD pre-incub. + Haem (5 μ M) | P | ns (4) | ↑ (4) |
| ext. | m β CD pre-incub. + CORM-3 (30 μ M) | P | ns (5) | ns (5) |
| ext. | Haem (5 μ M) | R | ns (4) | ns (4) |
| int. | Haem (5 μ M) | R | ns (6) | ns (6) |
| ext. + int. | Haem (5 μ M) | R | ns (4) | ↑ (4) |

Table 4.1: Summary of the effects of haem and CO on STOCs under different experimental conditions. P and R represent perforated and ruptured patch techniques, respectively. The arrow indicates an incremental response whilst ‘ns’ represents non-significant result. The numbers within the brackets show the number of experimental repeats. Haem and CO were applied extracellularly (ext.) and intracellularly (int.).

4.9 Discussion

4.9.1 Characterisation of STOCs

Earlier studies performed with Cd^{2+} and Ca^{2+} -free solutions showed that STOCs are initiated by Ca^{2+} released from intracellular Ca^{2+} stores (Benham *et al.*, 1986). Extracellular $[\text{Ca}^{2+}]_o$ was also shown to be crucial for the replenishment of Ca^{2+} stores, as STOCs were soon abolished during recordings in Ca^{2+} -free solutions (Buryi *et al.*, 1994). Thus, the increase in STOC frequency observed in 1 mM $[\text{Ca}^{2+}]_o$ compared with 0.1 mM $[\text{Ca}^{2+}]_o$ might have resulted from an increase in Ca^{2+} spark frequency due to a larger SR Ca^{2+} load. However, the increase in STOC amplitude that was observed following a reduction in $[\text{Ca}^{2+}]_o$ from 1 mM to 0.1 mM was unexpected. One possibility is that the loss of surface charge screening due to lowered Ca^{2+} caused a negative shift in the voltage-activation parameters of the BK_{Ca} channels, which would result in a larger activation of BK_{Ca} channels at a given voltage (Mahieu *et al.*, 2010). Nevertheless, the sample number for the assay needs to be increased to statistically test the difference between the effects of 1 mM and 0.1 mM $[\text{Ca}^{2+}]_o$ on STOC amplitude and frequency .

Furthermore, STOC inhibition by TEA^+ and penitrem A confirm that STOCs result from the opening of BK_{Ca} channels, whereas the ryanodine and caffeine-mediated STOC abolition show that Ca^{2+} sparks are crucial for STOC generation.

4.9.2 Effects of haem on STOCs

To the best of my knowledge, this is the first study to examine the effects of extracellular haem application on STOCs. It is unclear why 100 nM and 30 μM haem evoked a different response (increase in STOC frequency) to 5 μM haem (see Table 4.1). Performing future experiments with a wide range of haem concentrations could be useful for investigating whether the modulatory effect of haem on STOCs is concentration-dependent. Such information could provide an insight into how changes in extracellular haem concentrations during health and disease could influence vascular contractility.

The stimulatory effect of extracellular haem application on STOC amplitude was unexpected due to the inhibitory effect of intracellular haem on single BK_{Ca} channel

activity recorded in inside-out patches. Furthermore, the haem-mediated stimulatory effect on STOC amplitude but not STOC frequency contrasts with reports from Jaggar *et al.* (2002) which showed that extracellular application of HLL, another HO substrate, increased STOC amplitude and frequency in arteriole SMCs. This discrepancy may arise from the fact that HLL is a different molecule to haem, even though both can be degraded by HO to CO. Also, it is unclear why STOC frequency was higher in ruptured patches compared with perforated patches, as the cytosolic dialysis in ruptured patches was expected to reduce STOC amplitude and frequency. However, the fact that haem (5 μM) application only increased STOC amplitude in perforated patches but not ruptured patches, suggests that some key intracellular components are required for the modulatory effect of haem on STOC amplitude. Nevertheless, my outside-out patch results (see chapter 5) suggest this may not necessarily be so.

My findings also suggest that the modulatory effect of haem on STOCs is not overly dependent on V_m . This is because extracellular haem (5 μM) application at -30 mV and -50 mV produced similar increases in STOC amplitude with no significant effect on STOC frequency.

4.9.3 Effects of haem on STOCs after inhibition of endogenous CO production via cell pre-incubation with ZnPP-IX

In the study by Jaggar *et al.* (2002) it was proposed that elevation of endogenous CO via extracellular application of a HO substrate enhanced STOC amplitude and frequency. Thus, in the present study, the low STOC amplitude and frequency observed in ZnPP-IX pre-treated cells compared with untreated cells could be attributed to a reduction of single BK_{Ca} channel activity due to low endogenous CO concentration.

The increase in both STOC amplitude and frequency observed during extracellular haem (5 μM) application to ZnPP-IX pre-treated cells (Table 4.1), assuming complete inhibition of HO, suggests that haem produces a CO-independent effect on BK_{Ca} channel activity. Furthermore, there was no difference between the effects of haem on ZnPP-IX pre-treated cells and untreated cells; which further suggests that the modulatory effect of haem on STOCs occurs independently of endogenous CO. However, the discrepancy between my results and that of Wang *et al.* (2013), where the hemin-mediated

stimulatory effect on cortical collecting duct BK_{Ca} channels was abolished by tin mesoporphyrin, SnMP, could result from the difference in cell types used in both studies. ZnPP-IX has reportedly been used in several studies for HO inhibition and assays have been developed to examine HO activity, which involve measuring the amount of CO or bilirubin released (Vreman & Stevenson, 1988; Vera *et al.*, 2007; Mullebner *et al.*, 2015). Such assays could be used in future to check the amount of HO inhibition in my experimental conditions.

4.9.4 Effects of extracellular CO on STOCs

The stimulatory effect of CO on STOC frequency was consistent with results presented by Jaggar *et al.* (2002), where CO gas was shown to enhance STOC frequency, but also STOC amplitude, in cerebral arteriole SMCs. It is unclear why both CO gas and CORM-3 did not enhance STOC amplitude in my study (see Table 4.1). This discrepancy could be due to the cells used, as Jaggar *et al.* (2002) used cerebral arterioles SMCs whereas mesenteric artery SMCs were used in the present study. It could be argued that Jaggar *et al.* (2002) performed their recording at a holding V_m of -40 mV and I have recorded STOCs at -30 mV, but the voltage change from -40 mV to -30 mV produces a negligible change in channel Popen. Furthermore, the stimulatory effects of CO on single BK_{Ca} channel activity has been proposed to be voltage-independent, because CO still modulated channel activity at very negative voltages, in the absence of Ca²⁺ (Hou *et al.*, 2008a). CO has also been shown to enhance single BK_{Ca} channel activity at a range of depolarised potentials up to +100 mV (Williams *et al.*, 2008). Therefore, it is unlikely that the discrepancy between both studies is due to a voltage-dependent effect of CO. Previous studies reported that CO enhanced the Ca²⁺ sensitivity of BK_{Ca} channels expressed in SMCs (Wang *et al.*, 1997b; Xi *et al.*, 2004). In line with this, CO has been proposed to mediate stimulatory effects on STOCs by enhancing the coupling of Ca²⁺ sparks to BK_{Ca} channel opening (Jaggar *et al.*, 2002). Although, such coupling was not investigated in the present study, it could account for the stimulatory effect of CO on STOC frequency.

Furthermore, the application of exogenous CO after inhibition of endogenous CO was expected to still produce stimulatory effects on STOCs, since Jaggar *et al.* (2002) and I showed that exogenous CO application enhanced STOC frequency. Thus, a possible explanation for the absence of CO-mediated stimulatory effect on ZnPP-IX pre-treated cells is that ZnPP-IX binds to BK_{Ca} channels thereby preventing the interaction of CO with the channel. This assumes that CO cannot interact with the Zn²⁺ centre of ZnPP-IX, only the central Fe²⁺ atom of haem-bound to the channel or Fe²⁺ if it is in metalloclusters within the C-terminal domain of the channel. A CO-independent effect of haem is also consistent with the lack of effect of exogenous CO application to ZnPP-IX pre-treated cells; since HO-inhibition in ZnPP-IX pre-treated cells is expected to increase [haem].

ZnPP-IX at concentrations $\geq 0.5 \mu\text{M}$ have been proposed to mediate non-selective effects including inhibition of sGC and NOS activity (Ignarro *et al.*, 1984; Luo & Vincent, 1994; Meffert *et al.*, 1994). CO activates sGC activity and has been proposed to indirectly activate BK_{Ca} channels via the sGC/cGMP pathway (Brune *et al.*, 1990; Furchgott & Jothianandan, 1991; Verma *et al.*, 1993; Morita *et al.*, 1997; Dong *et al.*, 2007). CO can also indirectly enhance sGC activity via NOS activation, with NO activating sGC with a higher potency than CO (Stone & Marletta, 1994; Barkoudah *et al.*, 2004). Thus, it can be argued that the non-selective effects of ZnPP-IX may have contributed to the lack of effect of CO in ZnPP-IX pre-treated cells. Furthermore, a background level of cGMP was proposed to be required for the vasodilatory effect of CO (Barkoudah *et al.*, 2004). Nevertheless, inhibition of sGC activity with ODQ (1H-[1,2,4]oxadiazolo[4,3-a]quinoxalin-1-one) did not abolish the stimulatory effects of CO on whole-cell BK_{Ca} currents (Xi *et al.*, 2004).

In conclusion, my results suggest that the modulatory effect of CO on STOCs might occur via the same signalling mechanism as haem but upstream or downstream of it. This is because extracellular CO application only influenced STOC frequency whereas extracellular haem application only influenced STOC amplitude.

4.9.5 Effects of haem and CO on STOCs after caveolae disruption via cell pre-incubation with m β CD

Caveolae disruption with m β CD pre-treatment would promote the re-distribution of BK_{Ca} channels in the plasma membrane. Furthermore, the SR has been reported to exist close to caveolae (Lohn *et al.*, 2000; Lee *et al.*, 2002; Sweeney *et al.*, 2006). This allows RyRs to exist close to caveolae, thereby allowing Ca²⁺ entry via caveolar LTCCs to act as the trigger for RyR activation, resulting in Ca²⁺ sparks. Caveolar disruption has been reported to decrease Ca²⁺ spark frequency possibly via an increase in the diffusion distance required for Ca²⁺ to reach the RyRs (Lohn *et al.*, 2000). Considering this, the low STOC amplitude observed in m β CD pre-treated cells could result from a reduction in; a) the coupling of Ca²⁺ sparks to BK_{Ca} channel activity, b) the number of BK_{Ca} channels located close to Ca²⁺ spark sites or c) the [Ca²⁺]_i in the immediate vicinity of BK_{Ca} channels. However, based on these assumptions, it is unclear why STOC frequency was not significantly reduced in m β CD pre-treated cells. Perhaps, this could have been influenced by the large variation between cells, indicated by the large error bars.

The abolition of the stimulatory effect of haem on STOC amplitude in m β CD treated cells suggests that haem signalling to BK_{Ca} channels require caveolae (see Table 4.1). This agrees with evidence presented by Williams *et al.* (2004) which showed colocalization of HO and recombinant BK_{Ca} channels. Furthermore, it has previously been proposed that the interaction of cholesterol with membrane lipids can alter the physical properties of the lipid bilayer, leading to modifications in channel protein conformation and function (Bukiya *et al.*, 2011; Dopico *et al.*, 2012). Therefore, it is possible that the modulatory effect of haem on STOC amplitude was abolished in m β CD pre-treated cells because of an alteration in the channel conformation which prevented haem binding. However, the profound increase in STOC frequency during extracellular haem application to m β CD pre-treated cells was unexpected, as extracellular haem application previously did not alter STOC frequency in m β CD untreated cells.

Based on the assumption that HO-mediated haem degradation within caveolae could increase local CO concentration, the abolition of CO-mediated stimulatory effect on STOC frequency in m β CD treated cells was expected (Table 4.1). Thus, my results suggest that the modulatory effect of CO on BK_{Ca} channels may need intact caveolae. Notably,

exogenous CO application to the m β CD treated cells did not restore the effects of CO on STOC frequency. This is unsurprising since m β CD pre-treatment could have disrupted Ca²⁺ spark frequency and Jaggar *et al.* (2002) reported that CO mediates its effect by increasing the coupling between Ca²⁺ spark frequency and BK_{Ca} channel activation.

4.9.6 Haem and Ca²⁺ spark frequency

Ca²⁺ spark frequency can be influenced by several factors including membrane depolarization and SR Ca²⁺ load (Jaggar *et al.*, 1998; Wellman *et al.*, 2001; Cheranov & Jaggar, 2002). To the best of my knowledge, this is the first study to investigate the effects of extracellular haem application on Ca²⁺ spark frequency in SMCs.

The lack of effect of haem on Ca²⁺ spark frequency was expected since extracellular haem had no effect on STOC frequency. Thus, the Ca²⁺ imaging study results agrees with my electrophysiology data. It would also be useful to extend the imaging study to examine Ca²⁺ spark frequency during haem (5 μ M) application to ZnPP-IX and m β CD pre-treated cells. Furthermore, since my imaging study was performed at resting V_m rather than at -30 mV, which was used for patch clamp recordings, it is unclear whether haem would influence Ca²⁺ spark frequency at -30 mV. In addition, it would have been useful to examine whether haem alters the Ca²⁺ concentration released during each Ca²⁺ spark, but due to the use of a non-ratiometric fluorescent indicator, the amount of Ca²⁺ released during each Ca²⁺ spark event could not be quantified.

4.9.7 Effects of the location of haem application on STOCs

The current rundown observed during ruptured patch recordings was expected because cytosolic dialysis via the pipette solution results in loss of key intracellular factors involved in the modulation of BK_{Ca} channel activity.

Since intracellular haem application inhibited the activity of BK_{Ca} channels in inside-out patches (see section 3.3 in chapter 3), intracellular haem application to intact cells was expected to significantly inhibit STOCs. Surprisingly, there were no significant differences in STOC amplitude or frequency between control cells and those recorded with haem in the pipette (see Table 4.1). The lack of effect could be because any haem-

mediated changes in STOCs might have been masked by the current rundown induced by cytosolic dialysis. It is also possible that haem diffusion to all areas of the cell was restricted. Additional assays, such as a fluorescence imaging study with fluorescence-based sensors for haem could be useful for confirming the rate of haem diffusion into cells. Other techniques have also been proposed for the quantification of intracellular haem including the use of hemoprotein peroxidase reporters and heme-specific single domain antibodies (sdAbs) (Yuan *et al.*, 2016; Gouveia *et al.*, 2017).

Interestingly, current rundown was absent in the presence of both intracellular and extracellular haem, instead an increase in STOC frequency was observed (see Table 4.1). The reason for this is unclear.

**Chapter 5 THE EFFECTS OF HAEM AND CO ON VOLTAGE
PULSE-INDUCED BK_{Ca} CURRENTS**

5.1 Introduction

Based on the inhibitory effect of intracellular haem on BK_{Ca} channel activity in inside-out patches (see section 3.3.1 in chapter 3), the stimulatory effects of haem on STOC amplitude was unexpected. In addition, since the effects of haem on STOCs was further enhanced in ZnPP-IX pre-treated cells, where CO production should be negligible, it was hypothesised that haem directly influenced whole-cell BK_{Ca} channel activity. Therefore, in this chapter, the direct effects of haem on whole-cell BK_{Ca} channel activity was investigated by inhibiting Ca²⁺ sparks, to allow the recording of whole-cell BK_{Ca} currents in the absence of STOCs. Thus, BK_{Ca} channels were activated using voltage pulses. The effects of CO on whole-cell BK_{Ca} currents was also investigated.

Ruptured patches were used for this whole-cell experiments because it enabled addition of ryanodine (10 µM) to the cytosol via the pipette solution. Therefore, on entering the whole-cell configuration STOCs were inhibited due to the action of ryanodine, as previously shown in section 4.2.4.1, chapter 4. This allowed pulsed BK_{Ca} currents to be studied in isolation, without contamination from STOCs. Once STOCs were inhibited, control recordings were made by perfusing cells with control solution whilst administering voltage pulses from - 20 mV to + 60 mV. The holding potential at + 60 mV lasted for 200 ms, and mean current was measured between 120 ms and 190 ms of the + 60 mV step. Furthermore, since K_v channels are mostly inactivated by sustained depolarisation, the holding potential of - 20 mV minimised contamination from K_v currents (Nelson & Quayle, 1995; Standen & Quayle, 1998). Also, instantaneous currents were excluded from the analysis as illustrated by the dashed lines on the current traces. Ensemble averages of 50 sweeps were measured. In addition, to account for variability in cell size, current density (calculated by normalizing the actual current size to cell capacitance) was used for analysis.

The effects of haem and CO on BK_{Ca} channels in outside-out patches was also investigated. This was useful for examining the modulation of single BK_{Ca} channel activity by extracellular haem and CO. In addition, unlike the whole-cell patch

configuration, the outside-out patch technique allows the investigation of extracellular haem and CO effects with less complication from intracellular signalling pathways.

5.2 Characterisation of voltage pulsed BK_{Ca} currents using BK_{Ca} channel blockers

5.2.1 Pulsed currents were inhibited by external TEA⁺

To confirm that the current measured at + 60 mV results from the opening of BK_{Ca} channels, experiments were repeated in the presence of 3 mM TEA⁺ because at this concentration, TEA⁺ is a relatively selective BK_{Ca} channel blocker (Nelson & Quayle, 1995). This is evident from the inhibition of STOCs in the presence of TEA⁺ (3 mM), see section 4.2.3.1 in chapter 4. This experiment was only performed once because the effects of TEA⁺ on BK_{Ca} channel activity is well-known.

Within 45 s to 344 s after membrane rupture STOCs were abolished due to the presence of ryanodine in the pipette solution; once STOCs were absent current recording commenced. Voltage pulses from - 20 mV to + 60 mV were given every 2 s during exposure to control solution for ~ 3 minutes. After perfusing the control solution, external TEA⁺ (3 mM) was applied for 5 minutes while continuing to apply voltage pulses. TEA reduced mean current measured at + 60 mV by 85.7 %, from 56 pA to 8 pA (Figure 5.1). Similar results have been reported from studies performed on intact cells isolated from human mesenteric and rabbit cerebral arteries, where TEA⁺ inhibited pulsed outward currents measured at + 80 mV and + 50 mV respectively (Smirnov & Aaronson, 1992b; Robertson & Nelson, 1994).

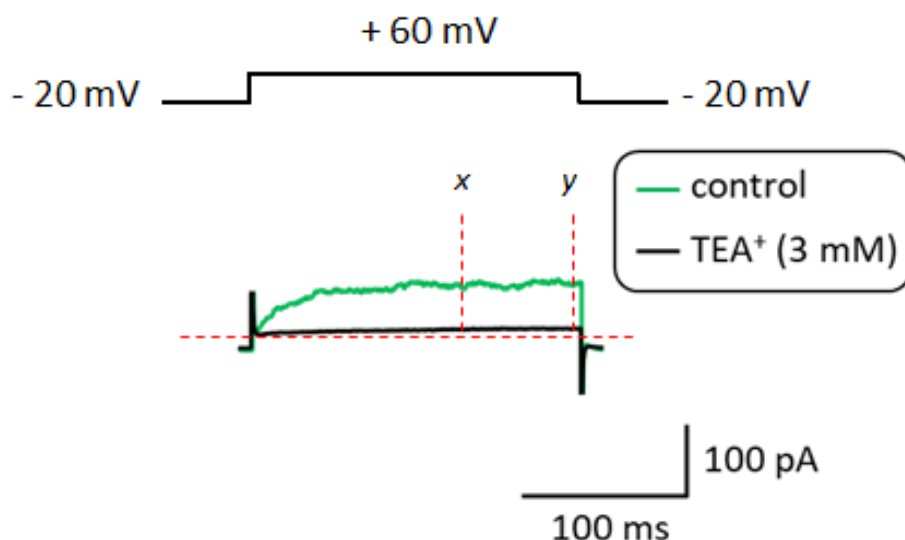


Figure 5.1: Effects of extracellular TEA⁺ application on voltage pulsed whole-cell currents. Recordings were performed using the ruptured patch technique. STOCs were inhibited via addition of ryanodine (10 μ M) to the pipette solution. Currents were induced with voltage pulses from -20 mV to +60 mV, the voltage step at +60 mV lasted for 200 ms. Traces represent average current from 50 sweeps. The effect of external TEA⁺ (3 mM) after 5 minutes of superfusion is shown. Mean current between x and y was measured and analysed in this and subsequent recordings as detailed in Methods section 2.6.2.2. [ATP]_i = 1 mM; [Ca²⁺]_i = 100 nM (achieved with 1 mM EGTA in pipette solution); [K⁺]_i = 140 mM; [K⁺]_o = 5 mM.

5.2.2 Extracellular application of the selective BK_{Ca} channel blocker, penitrem A, inhibited voltage pulsed currents

The specific BK_{Ca} channel blocker, penitrem A, was also used to further confirm the identity of the current induced by pulses to +60 mV. Experiments were performed with 100 nM penitrem A since this concentration blocked STOCs (see section 4.2.3.2 in chapter 4) and has also been shown to block pulsed BK_{Ca} currents (Cotton *et al.*, 1997; Rainbow *et al.*, 2011). As with the TEA⁺ experiment (section 5.2.1 above), the penitrem A experiment was only performed once in this study because the effects of penitrem A on pulsed BK_{Ca} current is also well-known.

Extracellular application of penitrem A (100 nM) for 10 minutes resulted in over 90 % inhibition of current, from 510 pA to 50 pA (Figure 5.2). My result is consistent with earlier reports from voltage pulsed whole-cell experiments performed on sheep mesenteric artery SMCs, where penitrem A (100 nM) was shown to produce ~ 90 % inhibition of outward current measured at +30 mV (Cotton *et al.*, 1997). Also, a study

performed on cultured SMCs showed that penitrem A (1 μM) inhibited voltage pulsed whole-cell BK_{Ca} currents recorded at + 100 mV (Asano *et al.*, 2010).

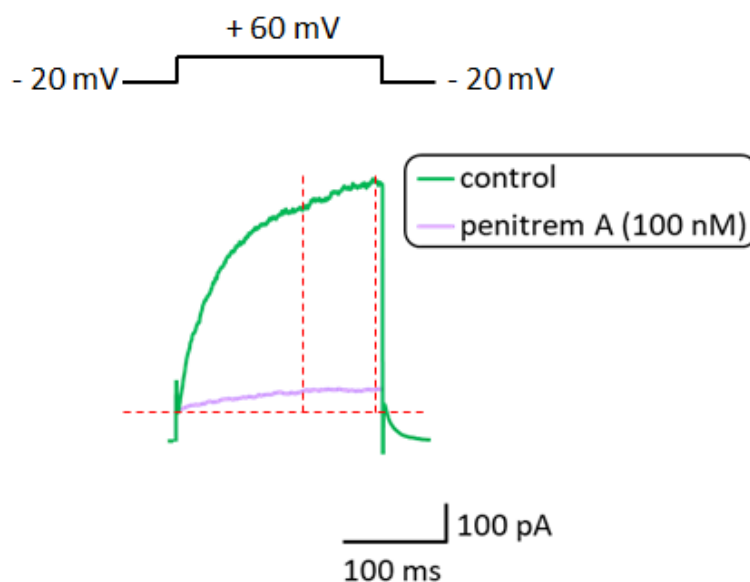


Figure 5.2: Effects of extracellular application of penitrem A on voltage pulsed whole-cell currents. The ruptured patch technique was used for recordings. STOCs were inhibited via addition of ryanodine (10 μM) to the pipette solution. Currents were induced by voltage pulses from - 20 mV to + 60 mV. Traces represent the average current from 50 sweeps. The effects of penitrem A (100 nM) was measured 10 minutes after its application. $[\text{ATP}]_i = 1\text{mM}$; $[\text{Ca}^{2+}]_i = 100\text{ nM}$; $[\text{K}^+]_i = 140\text{ mM}$; $[\text{K}^+]_o = 5\text{ mM}$.

5.2.3 Investigation of the stability of pulsed BK_{Ca} current over time

Having established (using BK_{Ca} channel blockers) that the voltage pulsed currents were mainly BK_{Ca} currents, the next step was to examine the stability of the current over time to enable the design of experimental protocols where complications arising from current rundown are minimised.

Experiments were performed, after STOC abolition, by continuously perfusing cells with control solution for 27 minutes whilst administering voltage pulses from - 20 mV to + 60 mV. Currents were analysed in blocks of 3 minutes (average of 115 sweeps) and, as shown in Figure 5.3, current generally ran down. Therefore, considering the current run down and time constraint on cell viability, control current was always measured after 5

minutes from the onset of the recordings (following STOC inhibition) made with haem and the other reagents, as shown in Figure 5.4A.

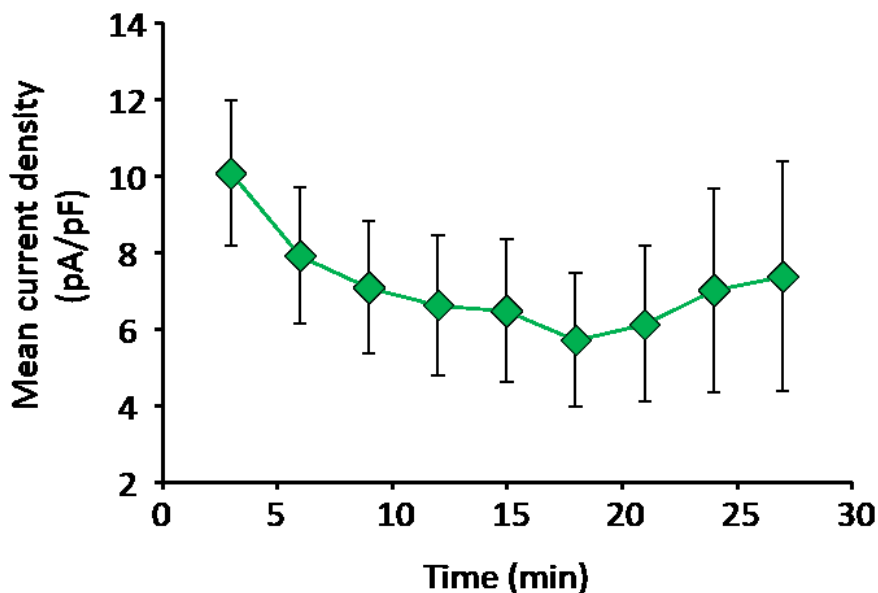


Figure 5.3: Stability of voltage pulsed whole-cell BK_{Ca} currents measured using the ruptured patch technique. Addition of ryanodine ($10 \mu\text{M}$) to the pipette solution inhibited STOCs. Voltage pulses were administered from -20 mV to $+60 \text{ mV}$ whilst continuously perfusing cells with control solution for 27 minutes. Time 0 represents the onset of recording, after STOC abolition. Current was analysed in blocks of 3 minutes. Error bars show SEM, $n = 7$. $[\text{ATP}]_i = 1 \text{ mM}$; $[\text{Ca}^{2+}]_i = 100 \text{ nM}$; $[\text{K}^+]_i = 140 \text{ mM}$; $[\text{K}^+]_o = 5 \text{ mM}$.

5.3 Effects of haem on voltage pulsed BK_{Ca} currents

5.3.1 Extracellular haem application enhanced pulsed currents

A possible reason for the stimulatory effect of haem on STOC amplitude is a haem-induced increase in Ca^{2+} spark amplitude. Therefore, the effects of haem on whole-cell BK_{Ca} current was examined after Ca^{2+} sparks were inhibited by including ryanodine (in the pipette solution). The same haem concentration used for my STOC experiments, $5 \mu\text{M}$, was also used for this assay.

After gaining whole-cell configuration, STOCs were abolished by ryanodine contained in the pipette solution. Voltage steps from -20 to $+60 \text{ mV}$ were administered at 0.5 Hz .

Control solution was superfused for ~ 5 minutes followed by a 7-minute application of haem (5 μ M), wash was rarely performed. Haem increased mean relative BK_{Ca} current to 208.5 ± 26.6 % of control, from 10.9 ± 3.0 pA/pF to 19.2 ± 4.2 pA/pF (n= 10, p< 0.001; Figure 5.4).

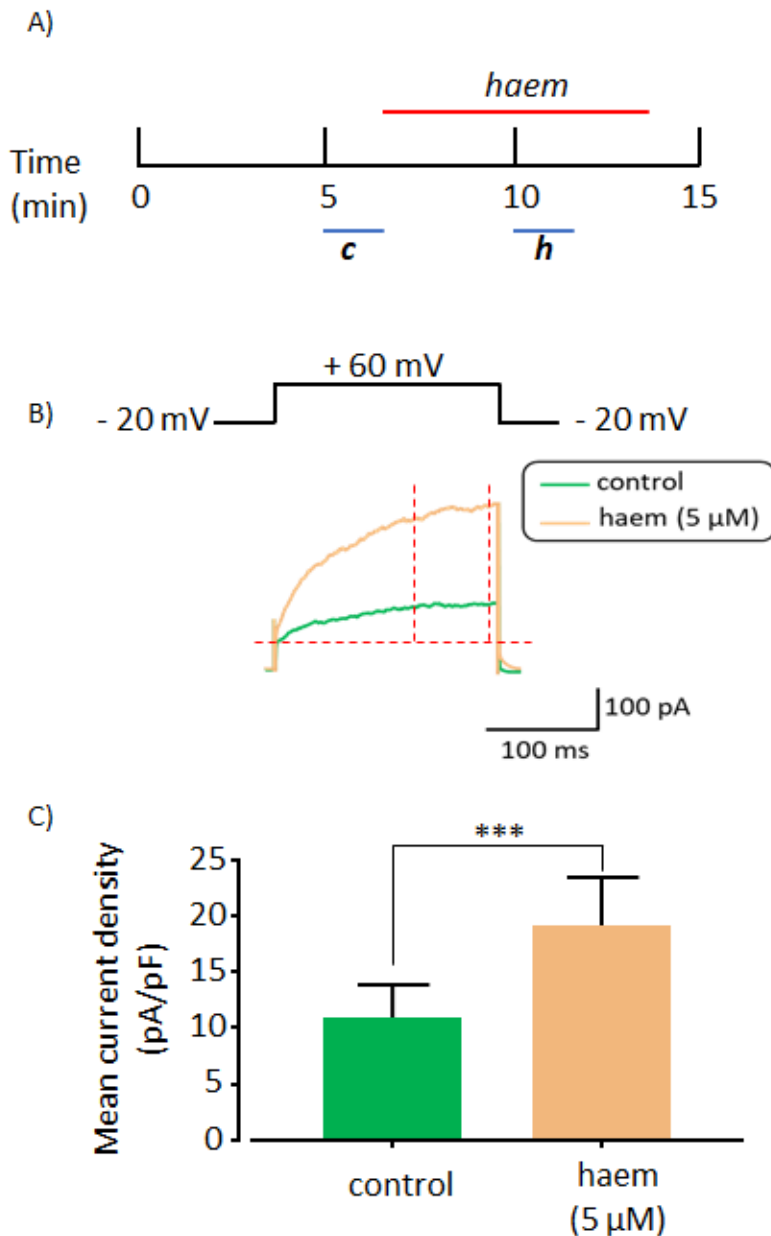


Figure 5.4: Effects of extracellular haem application on pulsed whole-cell BK_{Ca} current. The ruptured patch technique was used for recordings. Addition of ryanodine (10 μ M) to the pipette solution inhibited STOCs. Voltage pulses were administered from - 20 mV to + 60 mV. A) Shows the experimental design based on results from Figure 5.3. The red line indicates the duration of haem application. The blue lines indicate the time points at which control (c) and haem (h) effects were measured. Experiments were typically designed to last for \sim 15 minutes. Time 0 indicates the onset of the recording, after STOC inhibition. B) Example traces show average BK_{Ca} current from 50 sweeps, before (control) and after 7 minutes of extracellular haem (5 μ M) application. C) Histograms show mean BK_{Ca} current density in the absence (control) and presence of haem (5 μ M). Ratio paired t-test was used for statistical analysis, *** $p \leq 0.001$. Error bars show SEM, $n = 10$. $[ATP]_i = 1$ mM; $[Ca^{2+}]_i = 100$ nM; $[K^+]_i = 140$ mM; $[K^+]_o = 5$ mM.

To further examine whether the stimulatory effect of haem stabilized with time, separate experiments were performed where haem was continuously applied to cells for 10 minutes. Analysis of the recordings after the first 5 minutes showed that haem had increased mean relative current to 352.5 ± 104.8 % of control, from 11.9 ± 4.4 pA/pF to 35.9 ± 17.6 pA/pF ($n=6$, $p < 0.05$; Figure 5.5). Interestingly, after 10 minutes of haem application, control current had further increased to 661.8 ± 163.5 %, from 11.9 ± 4.4 pA/pF to 67.9 ± 30.6 pA/pF ($n=6$, $p < 0.01$; Figure 5.5). Therefore, 10 minutes of haem application produced a further 109.2 ± 28.3 % increase in the current that was measured after 5 minutes of haem application, from 35.9 ± 17.6 pA/pF to 67.9 ± 30.6 pA/pF ($n=6$, $p < 0.01$; Figure 5.5).

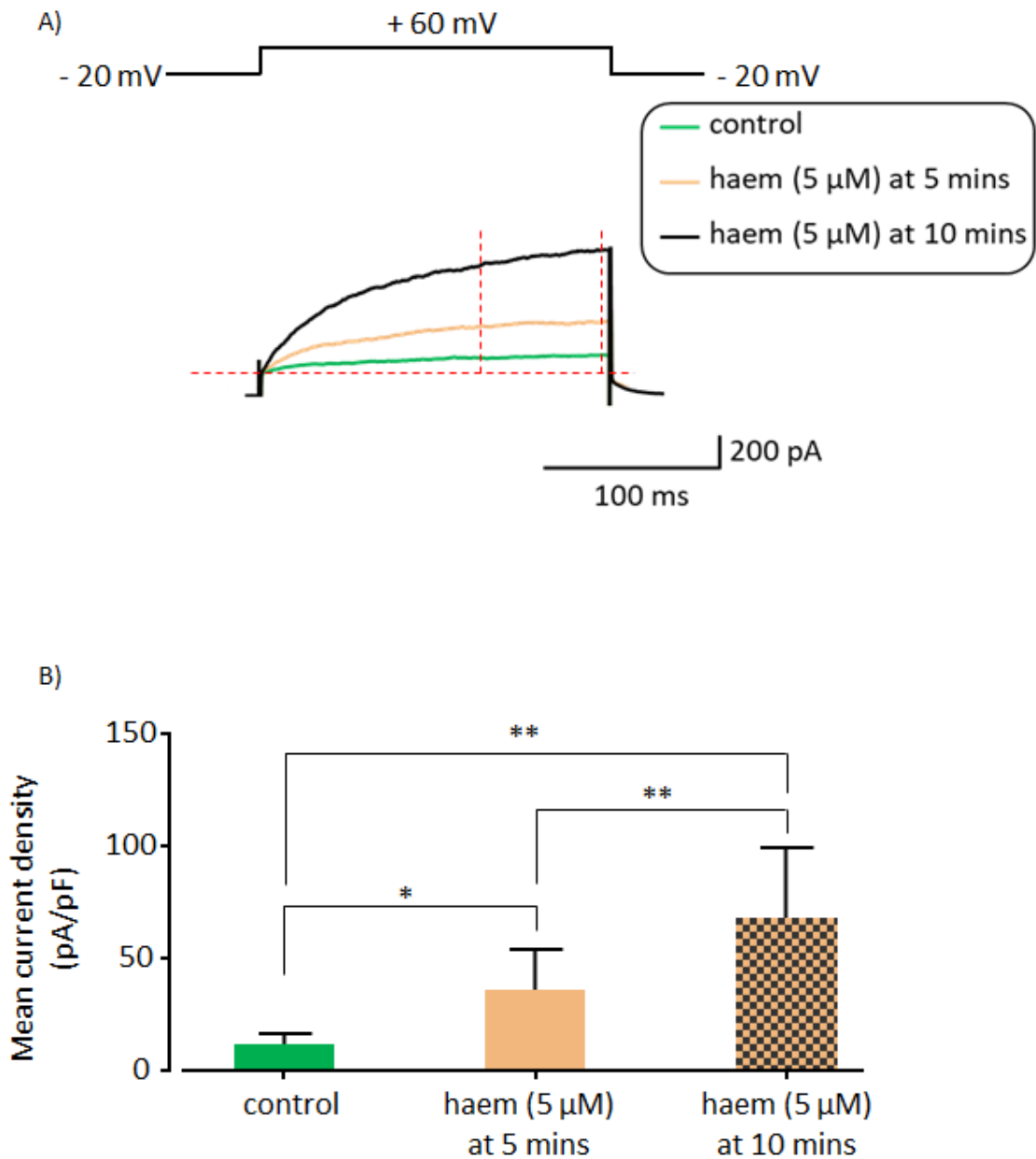


Figure 5.5: Effects of prolonged extracellular haem application on pulsed whole-cell BK_{Ca} current. Recordings were performed using the ruptured patch technique. Addition of ryanodine (10 μM) to the pipette solution inhibited STOCs. Voltage pulses were administered from -20 to +60 mV. A) Example traces show average BK_{Ca} current (from 50 sweeps) before (control) and after 5 and 10 minutes of extracellular haem (5 μM) application. B) Histograms show mean BK_{Ca} current density in the absence (control) and presence of haem (5 μM), 5 and 10 minutes after application. Statistical analysis was performed with ratio paired t-test, * p ≤ 0.05 and ** p ≤ 0.01. Error bars show SEM, n = 6. [ATP]_i = 1 mM; [Ca²⁺]_i = 100 nM; [K⁺]_i = 140 mM; [K⁺]_o = 5 mM.

5.3.2 The stimulatory effect of haem on pulsed currents was inhibited during co-application with penitrem A

To confirm that the increased current in the presence of haem resulted from the opening of BK_{Ca} channels, the sensitivity of this current to penitrem A was assessed.

Haem (5 μ M) was superfused for 5 minutes prior to co-application with penitrem A (100 nM) for an extra 15 minutes. As expected, extracellular haem (5 μ M) application increased mean relative BK_{Ca} current, to 258.5 ± 42.3 % of control, from 6.7 ± 1.2 pA/pF to 16.8 ± 4.1 pA/pF ($n=5$, $p < 0.05$; Figure 5.6). Subsequent co-application with penitrem A (100 nM) inhibited the stimulatory effect of haem by 84.4 ± 2.3 %, from 16.8 ± 4.1 pA/pF to 2.1 ± 0.6 pA/pF ($n=4$, $p < 0.001$; Figure 5.6).

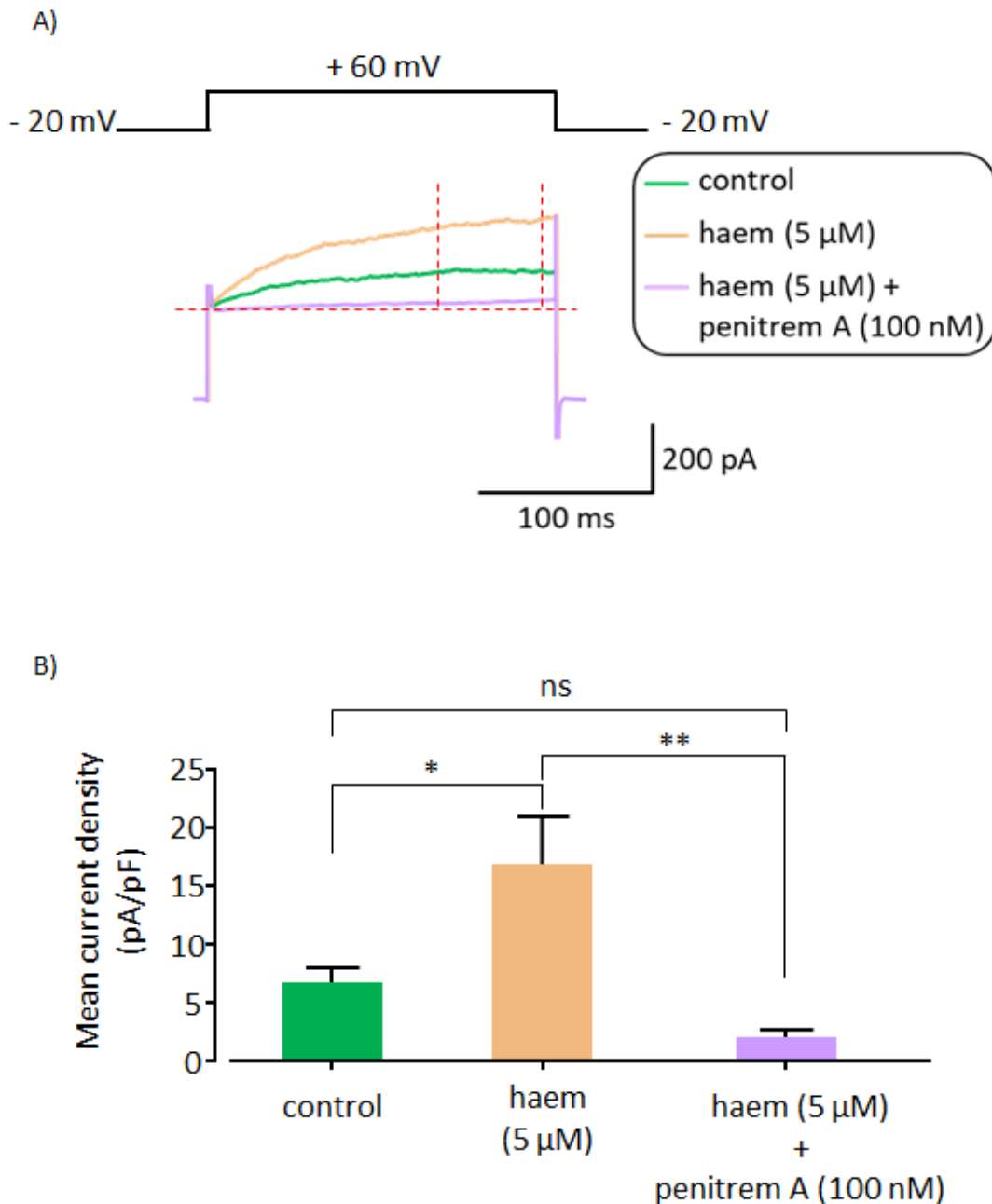


Figure 5.6: Effects of extracellular haem application on pulsed whole-cell current in the presence of a BK_{Ca} channel blocker. Recordings were made using the ruptured patch technique. STOCs were inhibited by ryanodine (10 μM) in the pipette solution. Voltage pulses were administered from -20 mV to +60 mV. A) Example traces show BK_{Ca} current in control, after initial 5 minutes of haem (5 μM) application and subsequent 15 minutes of haem (5 μM) + penitrem A (100 nM) application. Traces represent average current from 50 sweeps. B) Histograms show effects of haem (5 μM) on BK_{Ca} current in the presence and absence of penitrem A (100 nM). One-way ANOVA and Tukey's multiple comparisons test were used for statistical analysis, * $p \leq 0.05$, ** $p \leq 0.01$ and ns $p > 0.05$. Error bars show SEM, $n = 4$ (haem + penitrem A) and 5 (control and haem). $[\text{ATP}]_{\text{i}} = 1 \text{ mM}$; $[\text{Ca}^{2+}]_{\text{i}} = 100 \text{ nM}$; $[\text{K}^{+}]_{\text{i}} = 140 \text{ mM}$; $[\text{K}^{+}]_{\text{o}} = 5 \text{ mM}$.

5.4 Investigation of the mechanism of haem-mediated stimulation of voltage pulsed BK_{Ca} currents

The stimulatory effect of haem on voltage pulsed BK_{Ca} currents was consistent with the increase in STOC amplitude observed in the presence of extracellular haem. It was hypothesised that endogenous CO or Ca²⁺ entry via LTCCs could be involved in the haem-mediated stimulatory effect on pulsed current. These hypotheses were investigated using ZnPP-IX and cadmium (Cd²⁺) which block HO and LTCC activity, respectively.

5.4.1 Is Ca²⁺ entry via L-type Ca²⁺ channels involved in the stimulatory effect of haem on pulsed BK_{Ca} current

Depolarisation of V_m beyond -40 mV has been shown to elicit slowly decaying Ca²⁺ currents which peak around +10 mV and reverse between +40 mV to +60 mV (Cohen & Lederer, 1987; Smirnov & Aaronson, 1992a). These sustained Ca²⁺ currents, referred to as “Ca²⁺ window currents”, result from incomplete inactivation of VGCCs at positive voltages (Shorofsky & January, 1992). Since cells were administered voltage pulses from -20 to +60 mV and Ca²⁺ entry would mainly occur at -20 mV (where the Ca²⁺ window current is close to maximal), it was hypothesised that the modulatory effect of haem on pulsed BK_{Ca} currents could be influenced by Ca²⁺ window currents.

5.4.1.1 Extracellular application of Cd²⁺ inhibited pulsed BK_{Ca} current

Cd²⁺ is a highly potent Ca²⁺ channel blocker which competitively inhibits Ca²⁺ entry into Ca²⁺ channels by blocking the channel pore (Nelson, 1986; Lansman *et al.*, 1986; Rosenberg *et al.*, 1988). Consistent with this, external Cd²⁺ was reported to reduce the mean open time (mot) of single Ca²⁺ channels (Huang *et al.*, 1989). Thus, the aim of this experiment was to use Cd²⁺ to test the hypothesis that Ca²⁺ entry via VGCC was involved in the haem-mediated stimulatory effect on voltage pulsed BK_{Ca} current. Nevertheless, before performing haem with Cd²⁺ experiment, it was important to first examine whether Cd²⁺ mediated direct effects on pulsed BK_{Ca} current. Experiments were performed using 100 μM Cd²⁺ because this concentration has been shown to be sufficient for producing complete block of Ca²⁺ currents (Sun *et al.*, 2003).

External application of Cd²⁺ (100 μM) for ~5 minutes decreased mean relative current by 40.6 ± 5.1 %, from 10.2 ± 5.4 pA/pF to 5.9 ± 3.1 pA/pF (n = 4, p < 0.01; Figure 5.7). The

inhibitory effect of Cd^{2+} on BK_{Ca} currents was not surprising because Ca^{2+} influx via VGCC can induce BK_{Ca} channel activation. My results are also consistent with earlier reports where $100 \mu\text{M}$ external Cd^{2+} was shown to block whole-cell voltage pulsed BK_{Ca} currents recorded from neurons (Sun *et al.*, 2003).

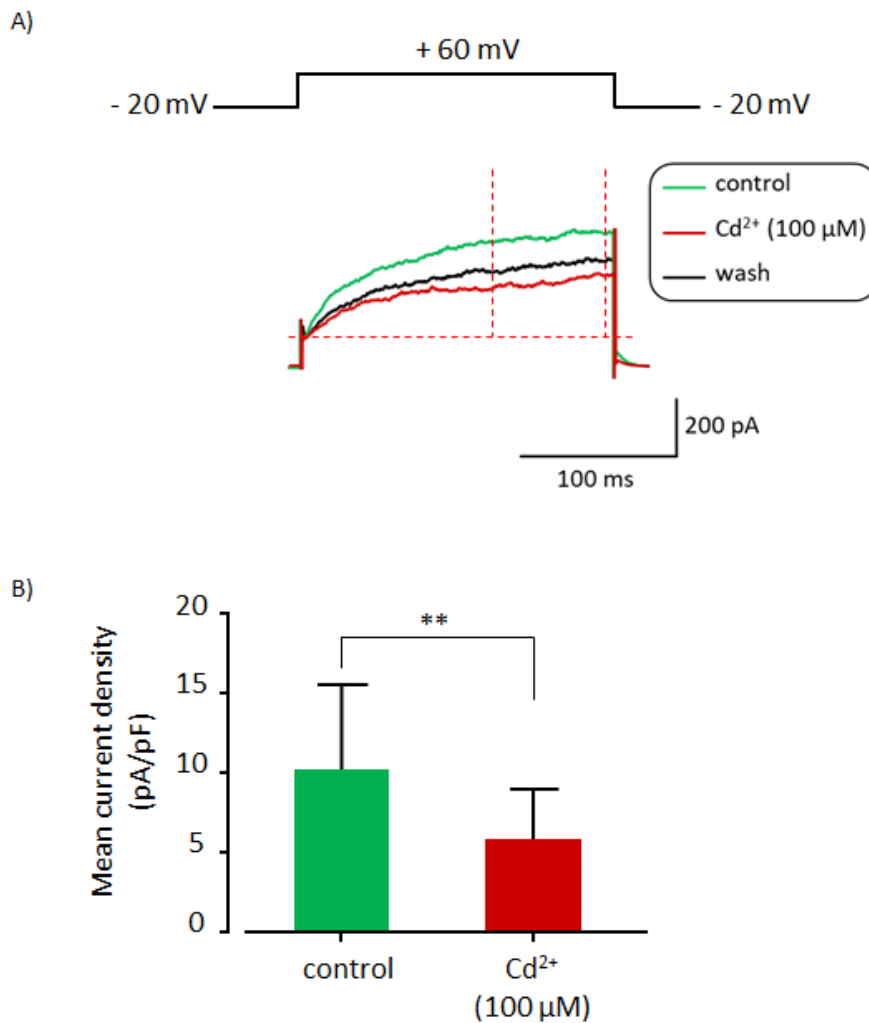


Figure 5.7: Effects of extracellular application of Cd^{2+} on pulsed whole-cell BK_{Ca} current. The ruptured patch technique was used for recordings. STOCs were inhibited by ryanodine ($10 \mu\text{M}$) in the pipette solution. Voltage pulses were administered from -20 mV to $+60 \text{ mV}$. A) Example traces show BK_{Ca} current before (control) and after 5 minutes of Cd^{2+} ($5 \mu\text{M}$) application. Traces represent average current from 50 sweeps. B) Histograms show mean BK_{Ca} current in the presence and absence of Cd^{2+} ($100 \mu\text{M}$). Statistical analysis was performed using ratio paired t-test, ** $p \leq 0.01$. Error bars show SEM, $n = 4$. $[\text{ATP}]_i = 1 \text{ mM}$; $[\text{Ca}^{2+}]_i = 100 \text{ nM}$; $[\text{K}^+]_i = 140 \text{ mM}$; $[\text{K}^+]_o = 5 \text{ mM}$.

5.4.1.2 The stimulatory effect of extracellular haem on pulsed BK_{Ca} currents was not abolished during co-application with Cd²⁺

Having established the effects of Cd²⁺ on pulsed BK_{Ca} current, the involvement of Ca²⁺ entry via L-type Ca²⁺ channels in the haem modulatory effect on BK_{Ca} currents was investigated by simultaneously applying haem and Cd²⁺.

Extracellular haem was applied for 5 minutes followed by another 5 minutes of co-application with Cd²⁺ (100 μM). The results showed that extracellular haem (5 μM) application increased mean relative BK_{Ca} current to 162.1 ± 10.9 % of control, from 17.6 ± 5.5 pA/pF to 27.0 ± 8.0 pA/pF (n= 4, p< 0.01; Figure 5.8). Subsequent co-application of haem (5 μM) with Cd²⁺ (100 μM) increased mean relative current to 311.8 ± 61.6 % of control, from 17.6 ± 5.5 pA/pF to 48.5 ± 16.3 pA/pF (n= 4, p< 0.05; Figure 5.8). The mean current densities recorded during haem superfusion and during haem and Cd²⁺ co-application was 27.0 ± 8.0 pA/pF and 48.5 ± 16.3 pA/pF respectively. Although this shows that there was a mean relative change of 94.6 ± 38.7 % in the current recorded during haem and Cd²⁺ co-application and haem only application, statistical analysis indicate that the difference was not significant. Notably, during prolonged haem application (for 10 minutes) the initial increase in current observed after 5 minutes of haem application was also further enhanced by 109.2 ± 28.3 % (see Figure 5.5).

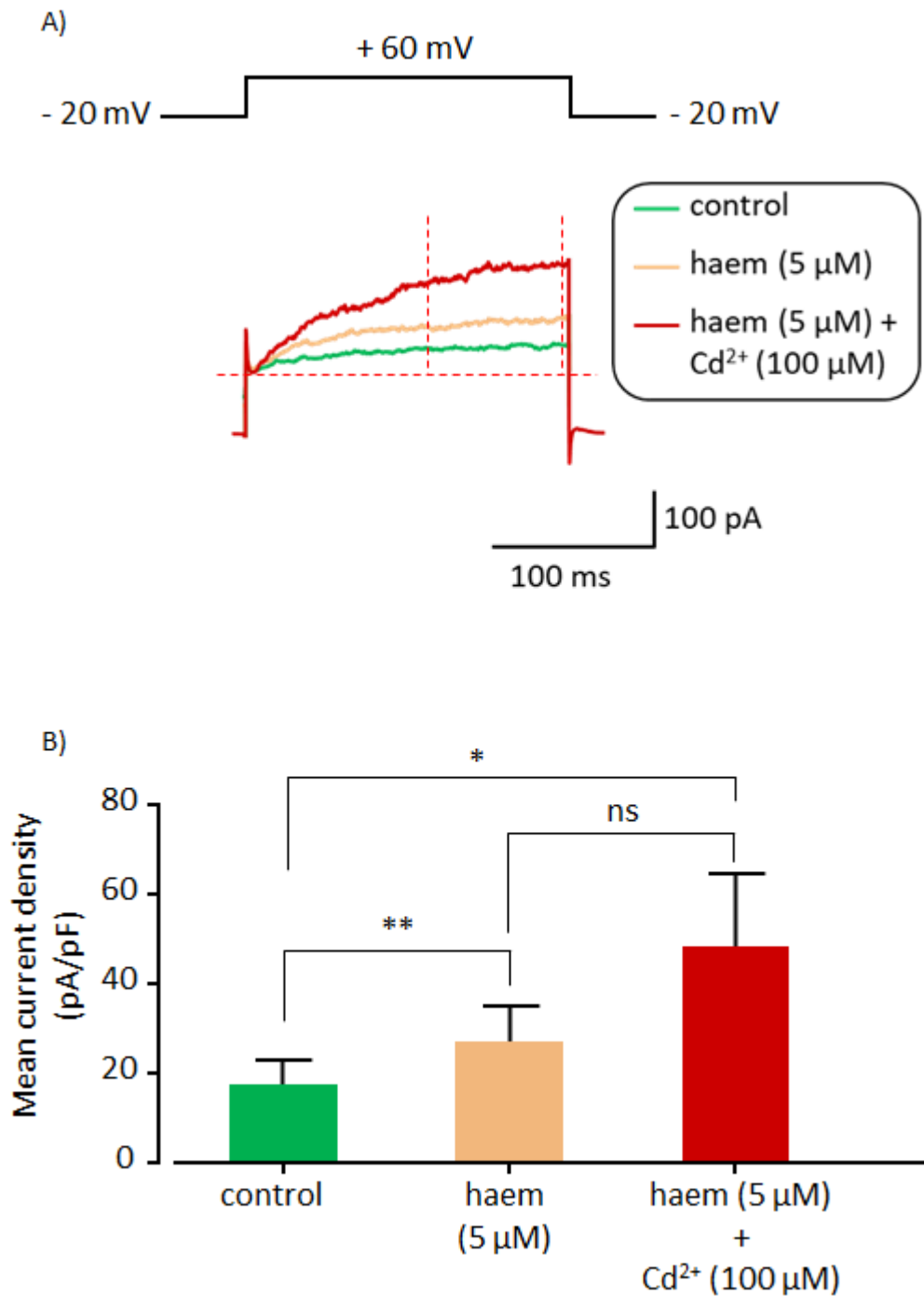


Figure 5.8: Effects of extracellular haem application on pulsed whole-cell BK_{Ca} current in the presence of the L-type Ca²⁺ channel blocker, Cd²⁺. The ruptured patch technique was used with ryanodine (10 μM) in the pipette solution. Voltage pulses were administered from -20 mV to +60 mV. A) Example traces show BK_{Ca} current under control conditions, 5 minutes after haem (5 μM) application and 5 minutes after subsequent haem (5 μM) + Cd²⁺ (100 μM) co-application. Traces represent average current from 50 sweeps. B) Histograms show mean BK_{Ca} current density in the presence of haem (5 μM) and haem (5 μM) + Cd²⁺ (100 μM). Ratio paired t-test results are shown, * p ≤ 0.05, ** p ≤ 0.01 and ns p > 0.05. Error bars show SEM, n = 4. [ATP]_i = 1 mM; [Ca²⁺]_i = 100 nM; [K⁺]_i = 140 mM; [K⁺]_o = 5 mM.

5.4.2 Is endogenous CO involved in the stimulatory effect of haem on voltage pulsed BK_{Ca} current

Free intracellular haem is degraded to CO by HO enzymes. It is therefore possible that endogenous CO, produced from haem degradation, could have contributed to the stimulatory effect of haem on pulsed BK_{Ca} current. This hypothesis was investigated using the non-selective HO inhibitor, ZnPP-IX.

5.4.2.1 Voltage pulse-induced BK_{Ca} current was unaltered by extracellular application of ZnPP-IX

Firstly, it was important to investigate whether ZnPP-IX produced direct effects on BK_{Ca} currents. To maintain consistency with my STOC studies, experiments were performed with 10 μM ZnPP-IX.

A 7-minute extracellular application of ZnPP-IX (10 μM) produced a relative change of $16.1 \pm 0.3\%$ in mean BK_{Ca} current, from 4.8 ± 0.7 pA/pF to 5.9 ± 1.9 pA/pF ($n = 6$, $p > 0.05$; Figure 5.9). However, statistical analysis showed that this effect was not significant. Thus, the results are consistent with those observed from my STOCs studies, as extracellular application of ZnPP-IX (10 μM) also had no effect on STOCs (see section 4.4.1 in chapter 4).

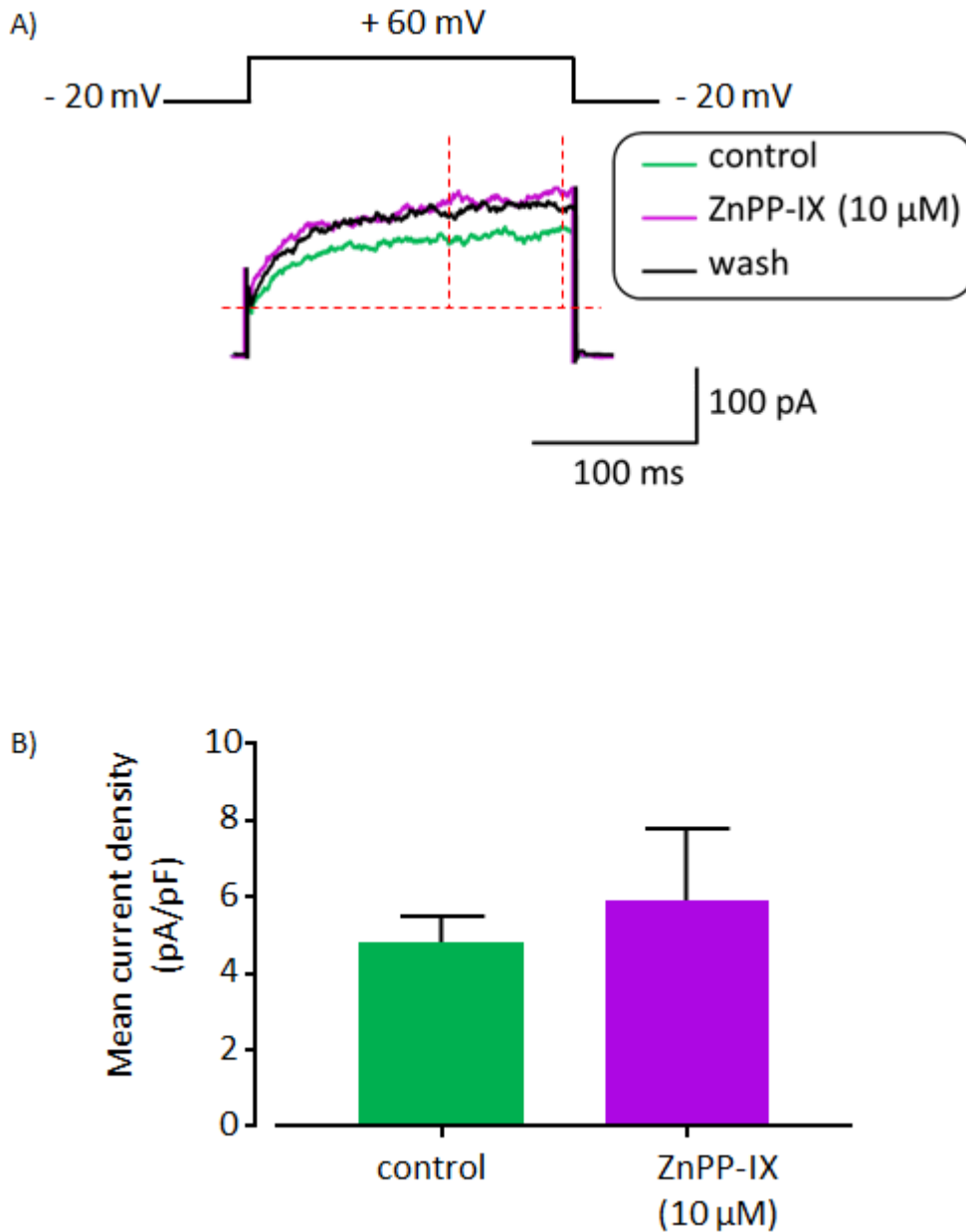


Figure 5.9: Effects of extracellular application of ZnPP-IX on pulsed whole-cell BK_{Ca} current. Recordings were performed using the ruptured patch technique. STOCs were inhibited by ryanodine (10 μM) in the pipette solution. Voltage pulses were administered from -20 mV to +60 mV. A) Example traces show BK_{Ca} current before (control) and after 7 minutes of ZnPP-IX (10 μM) application. Traces represent average current from 50 sweeps. B) Histograms show mean BK_{Ca} current density in the presence and absence (control) of ZnPP-IX (10 μM). Ratio paired t-test was performed, results were non-significant as $p > 0.05$. Error bars show SEM, $n = 6$. $[ATP]_i = 1$ mM; $[Ca^{2+}]_i = 100$ nM; $[K^+]_i = 140$ mM; $[K^+]_o = 5$ mM.

5.4.2.2 Voltage pulsed BK_{Ca} current was higher in ZnPP-IX pre-treated cells compared with untreated cells

The direct application of ZnPP-IX to cells for 7 minutes had little effect on BK_{Ca} current; however, to ensure that HO was blocked in the following experiments it was necessary to pre-treat cells with ZnPP-IX. Thus, the next step was to examine the effects of ZnPP-IX pre-treatment on the stability of BK_{Ca} current over time.

Cells were pre-incubated with ZnPP-IX (10 μ M) for 10 minutes before membrane rupture. After STOC inhibition, cells were continuously superfused with control solution for 18 minutes whilst administering voltage steps from -20 mV to +60 mV. Current density was then analysed in blocks of 3 minutes, comprising of 115 sweeps of the voltage pulse.

The results were compared with those from untreated cells under similar experimental conditions (see Figure 5.3). The unpaired t-test results showed that BK_{Ca} current was higher in ZnPP-IX pre-treated cells compared with untreated cells (n= 4 for ZnPP-IX treated cells, and n= 7 for untreated cells, p< 0.05; Figure 5.10).

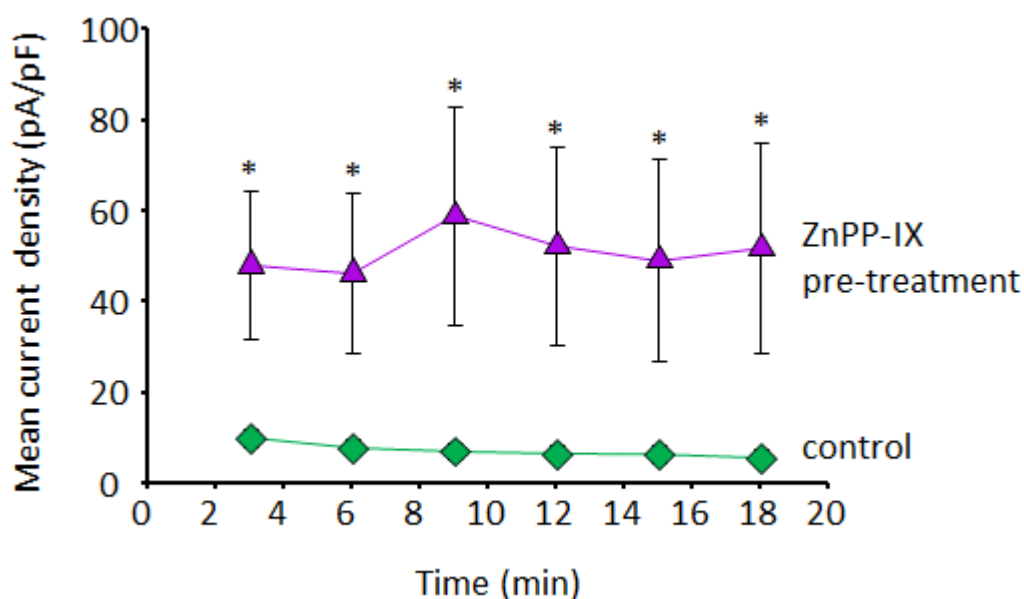


Figure 5.10: Comparison between BK_{Ca} current density in ZnPP-IX pre-treated and untreated (control) cells. Cells were pre-treated with ZnPP-IX (10 μ M) for 10 minutes. Cell membrane was ruptured and STOCs were inhibited by ryanodine (10 μ M) application via the pipette solution. Voltage pulses were administered from -20 mV to +60 mV. Data for untreated cells were obtained from Figure 5.3 (error bars are within the symbols). Unpaired t-test was performed, *p \leq 0.05. Error bars show SEM, n= 4 (for ZnPP-IX pre-treatment) and n= 7 (control). [ATP]_i = 1 mM; [Ca²⁺]_i = 100 nM; [K⁺]_i = 140 mM; [K⁺]_o = 5 mM.

5.4.2.3 Extracellular application of haem enhanced pulsed BK_{Ca} current in ZnPP-IX pre-treated cells

Based on the assumption that the stimulatory effect of extracellular haem was mediated via endogenous CO, cells were pre-treated with ZnPP-IX (to inhibit endogenous CO production) prior to extracellular haem application.

Cells were pre-incubated with ZnPP-IX (10 μ M) for \sim 10 minutes prior to membrane rupture. The results indicate that haem increased BK_{Ca} current even in the presence of this HO blocker. A paired t-test showed that haem (5 μ M) application to the ZnPP-IX pre-treated cells increased mean relative BK_{Ca} current to 142.7 ± 13.7 % of control, from 53.5 ± 6.9 pA/pF to 72.3 ± 5.1 pA/pF ($n= 6$, $p < 0.05$; Figure 5.11). One-way ANOVA with Tukey's multiple comparisons tests also showed that mean current density in ZnPP-IX pre-treated cells (which had not been superfused with haem), was higher than the haem-mediated stimulatory effect observed in untreated cells, 53.5 ± 6.9 pA/pF and 19.2 ± 4.2 pA/pF respectively, ($n= 6$ for ZnPP-IX pre-treated cells, and $n= 10$ for untreated cells, $p < 0.001$; Figure 5.11). In addition, the stimulatory effect of haem on ZnPP-IX pre-treated cells was also higher than its effect on untreated cells, 72.3 ± 5.1 pA/pF and 19.2 ± 4.2 pA/pF respectively, ($n= 6$ for ZnPP-IX pre-treated cells, and $n= 10$ for untreated cells, $p < 0.0001$; Figure 5.11). These comparisons were made with data from untreated cells shown in Figure 5.4.

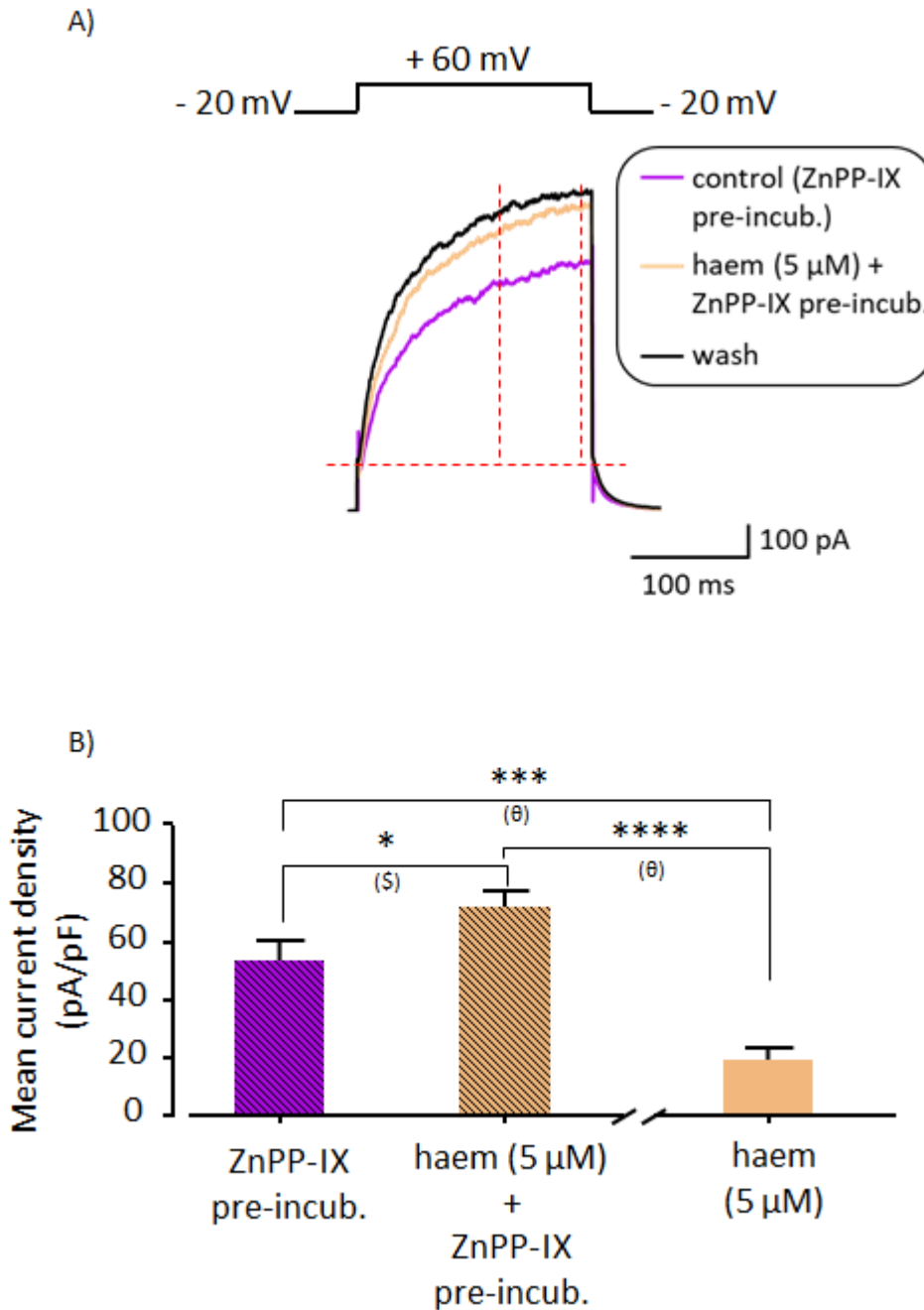


Figure 5.11: Effects of extracellular haem application on pulsed whole-cell BK_{Ca} current recorded from ZnPP-IX pre-treated cells. Cell pre-treatment with ZnPP-IX lasted for 10 minutes and the ruptured patch technique was used for recording. STOCs were inhibited by ryanodine (10 μ M) in the pipette solution. Voltage pulses were administered from -20 mV to +60 mV. A) Example traces show BK_{Ca} current before and after addition of haem (5 μ M) to ZnPP-IX (10 μ M) pre-treated cell. Traces represent average current from 50 sweeps. B) Histograms show mean BK_{Ca} current density in the presence and absence of haem in ZnPP-IX (10 μ M) pre-treated cells. Results were compared with effects of haem (5 μ M) application on untreated cells obtained from Figure 5.4 (shown after the break in x-axis). Ratio paired t-test (\$) and one-way ANOVA with Tukey's multiple comparisons test (θ) was performed, * $p \leq 0.05$, *** $p \leq 0.001$ and **** $p \leq 0.0001$. Error bars show SEM, $n = 6$ (ZnPP-IX pre-treatment) and $n = 10$ (haem, untreated cells). $[ATP]_i = 1$ mM; $[Ca^{2+}]_i = 100$ nM; $[K^+]_i = 140$ mM; $[K^+]_o = 5$ mM.

5.5 Effects of CO on voltage pulsed BK_{Ca} current

There is little knowledge about the effects of CO on whole-cell BK_{Ca} currents, as most studies have been performed using excised patches. Furthermore, since my inside-out patch data showed that CORM-3 activated channel activity in 300 nM Ca²⁺ with a less pronounced effect in 3 μM Ca²⁺, it is plausible to hypothesize that the lack of effect of CO on STOC amplitude (see section 4.5 in chapter 4) could have resulted from a maximal activation of BK_{Ca} channels by the Ca²⁺ released from Ca²⁺ sparks. Therefore, pulsed recordings where Ca²⁺ levels are expected to be low, due to inhibition of Ca²⁺ sparks via ryanodine application in the pipette solution, should be useful for elucidating the effects of CO on whole-cell BK_{Ca} currents.

5.5.1 Extracellular application of CO gas or CORM-3 did not produce significant effects on pulsed BK_{Ca} current

The lack of effect of ZnPP-IX (10 μM) superfusion on pulsed BK_{Ca} currents in section 5.4.2.1 above suggest that endogenous CO does not modulate whole-cell BK_{Ca} currents under these conditions. This was unexpected considering that I (see section 3.4.2 in chapter 3) and others (Wang & Wu, 1997; Wang *et al.*, 1997b; Williams *et al.*, 2004; Jaggar *et al.*, 2005) have shown that intracellular application of CO to inside-out patches enhances single BK_{Ca} channel activity. Nevertheless, the effect of exogenous CO application on voltage pulsed whole-cell BK_{Ca} currents was examined due to the limited information about it.

My results showed that extracellular superfusion of CORM-3 for 5 minutes did not significantly alter mean relative BK_{Ca} currents; 92.3 ± 17.1 %, from 20.4 ± 14.3 pA/pF to 17.0 ± 10.7 pA/pF ($n = 5$, $p > 0.05$; Figure 5.12). Surprisingly, prolonged CORM-3 application (for 10 minutes) also produced no significant change in control current; 83.7 ± 18.7 %, from 20.4 ± 14.3 pA/pF to 17.2 ± 11.2 pA/pF ($n = 5$, $p > 0.05$; Figure 5.12). This was unexpected because I assumed that similar to results seen with haem application for 10 minutes (see Figure 5.5), prolonged CO application could increase pulsed BK_{Ca} currents.

As expected, extracellular application of iCORM-3 (30 μM), for 5 minutes, did not affect mean relative BK_{Ca} current either; 104.5 ± 16.5 %, from 3.5 ± 0.5 pA/pF to 3.7 ± 0.8 pA/pF ($n = 6$, $p > 0.05$; Figure 5.13).

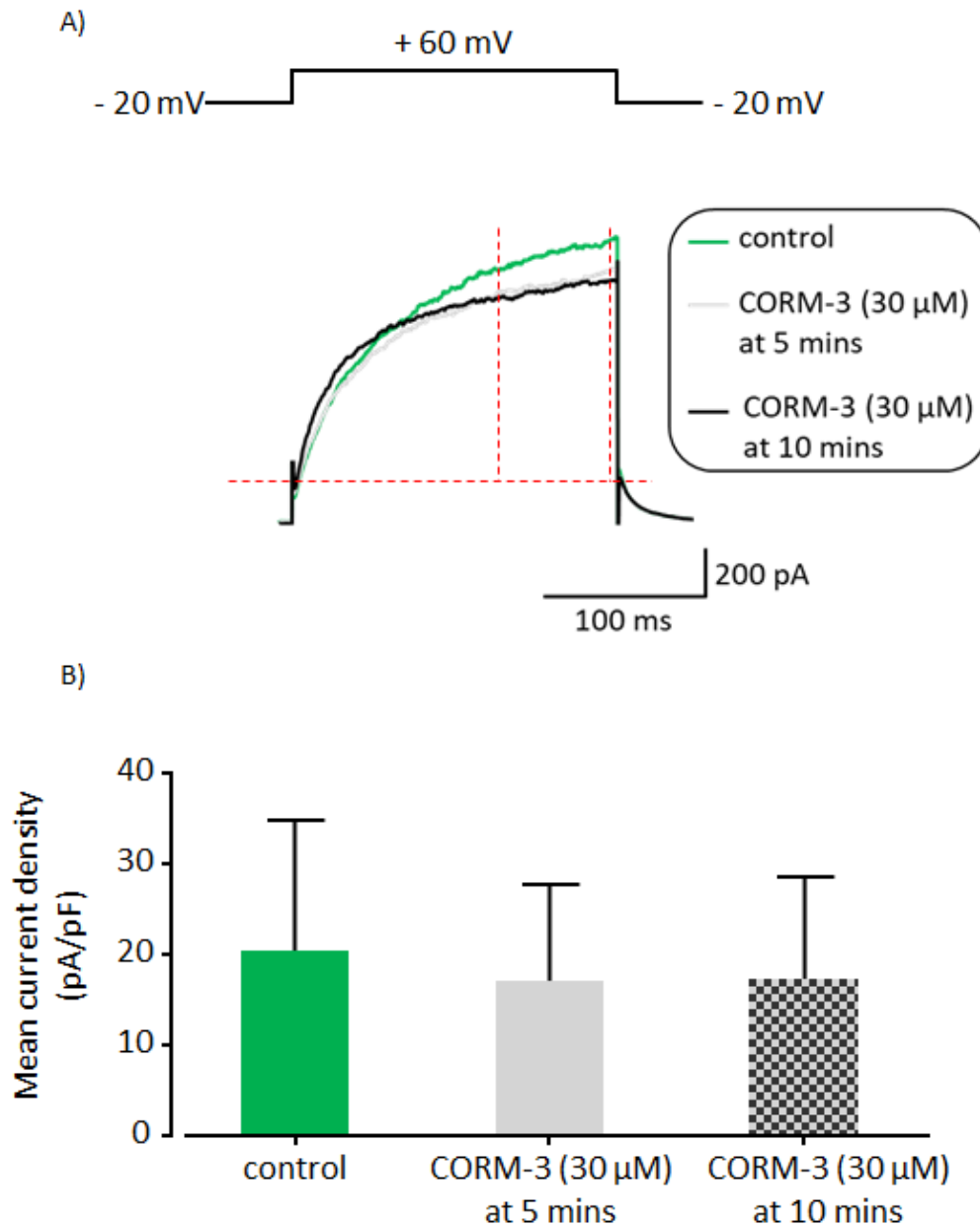


Figure 5.12: Effects of extracellular application of CORM-3 on pulsed whole-cell BK_{Ca} currents. The ruptured patch technique was used for recording. STOCs were inhibited by ryanodine (10 μM) in the pipette solution. Voltage pulses were administered from -20 mV to +60 mV. A) Example traces show BK_{Ca} currents under control conditions and after 5- and 10-minutes application of CORM-3 (30 μM). B) Histograms show mean BK_{Ca} current density in the absence (control) and presence of CORM-3. One-way ANOVA and ratio paired t-tests were performed but the results were non-significant, as $p > 0.05$. Error bars show SEM, $n = 5$. $[ATP]_i = 1$ mM; $[Ca^{2+}]_i = 100$ nM; $[K^+]_i = 140$ mM; $[K^+]_o = 5$ mM.

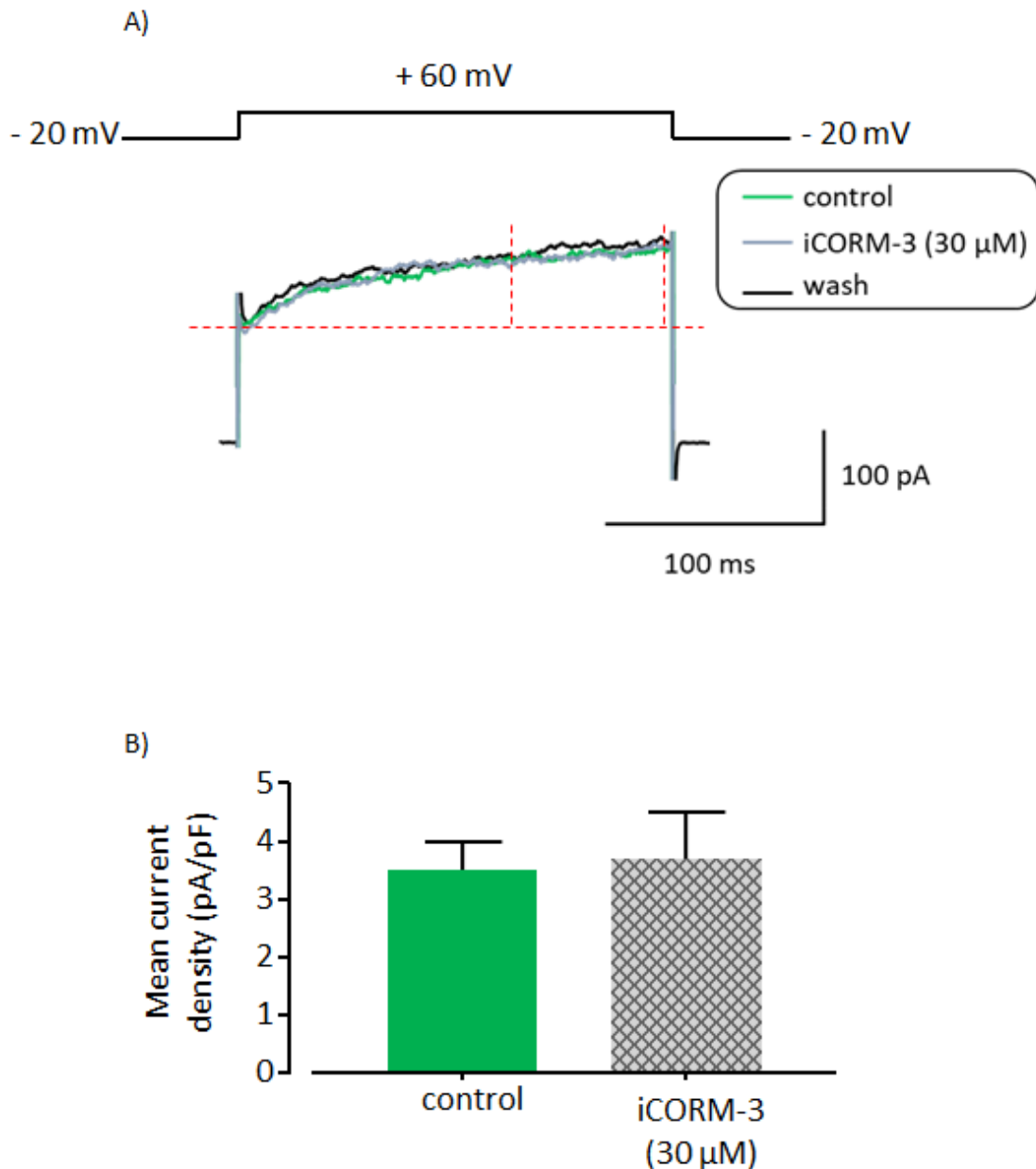


Figure 5.13: Effects of extracellular application of iCORM-3 on pulsed whole-cell BK_{Ca} currents. Recordings were performed using the ruptured patch technique. STOCs were inhibited by ryanodine (10 μM) in the pipette solution. Voltage pulses were administered from -20 mV to +60 mV. A) Example traces show BK_{Ca} currents under control conditions and after 5 minutes of iCORM-3 (30 μM) application. B) Histograms show mean BK_{Ca} current density in the absence (control) and presence of iCORM-3. Results from ratio paired t-test was non-significant as $p > 0.05$. Error bars show SEM, $n = 6$. $[ATP]_i = 1$ mM; $[Ca^{2+}]_i = 100$ nM; $[K^+]_i = 140$ mM; $[K^+]_o = 5$ mM.

The lack of effect of CORM-3 application on the BK_{Ca} current was unexpected because CORM-3 had activated single BK_{Ca} channels in inside-out patches (see section 3.4.2 in chapter 3). I had also hypothesised that CO released from CORM-3 would diffuse across the plasma membrane to interact with ferrous haem that was already bound to the intracellular side of the BK_{Ca} channels expressed in the intact cells.

Therefore, experiments were repeated using CO gas (30 μ M) solution. However, 5 minutes application of CO gas was also without effect on mean relative BK_{Ca} current; 75.1 ± 10.6 %, from 5.9 ± 1.8 pA/pF to 4.2 ± 1.1 pA/pF ($n=6$, $p > 0.05$; Figure 5.14). Even after 10 mins of CO gas application, there was still no significant change in mean relative current; 71.0 ± 9.1 %, from 5.9 ± 1.8 to 3.9 ± 1.2 ($n=6$, $p > 0.05$; Figure 5.14). These results also contrast with a previous report where CO gas application to rat tail artery SMCs increased whole-cell BK_{Ca} currents at a depolarising potential of 0 mV (Wang *et al.*, 1997b).

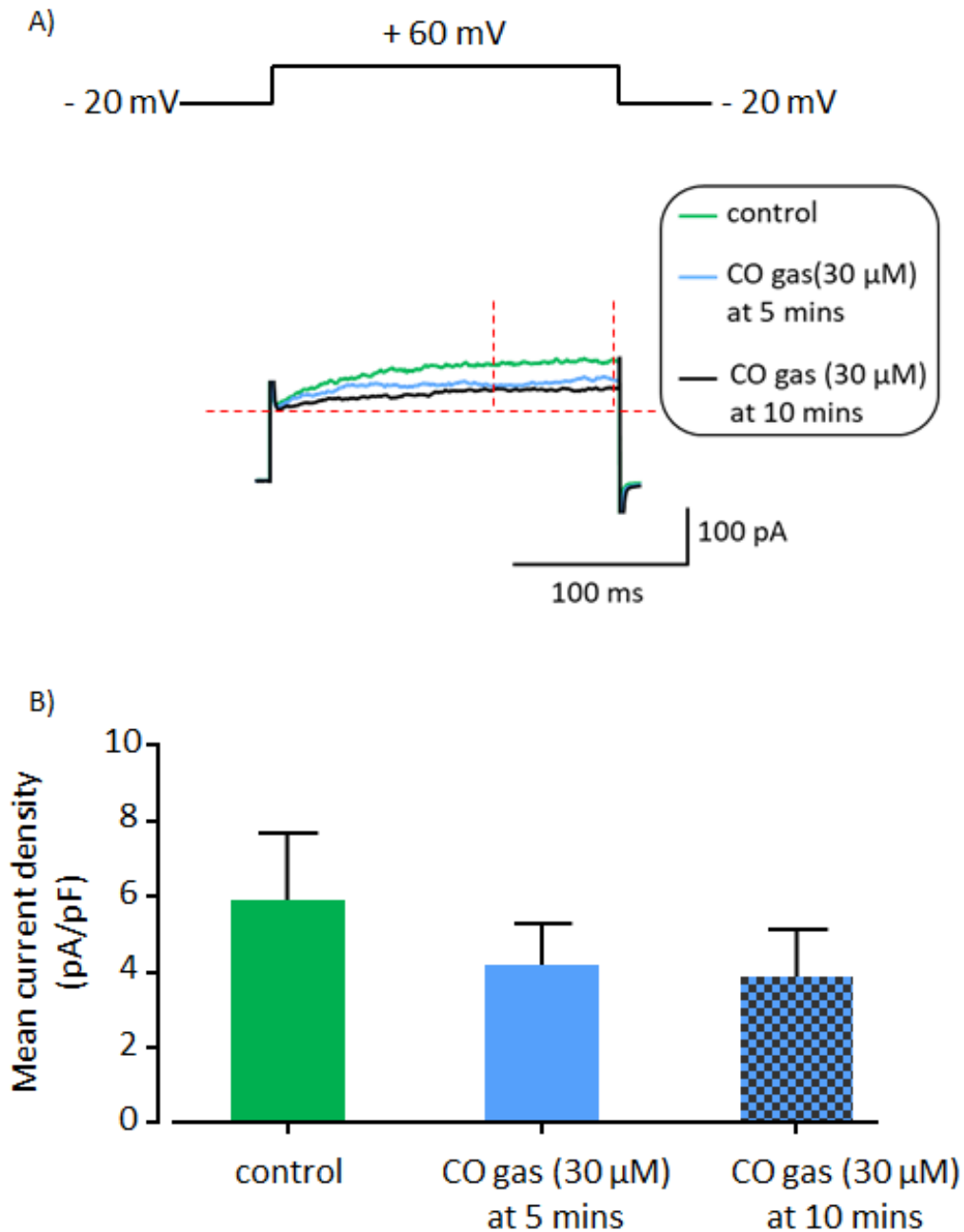


Figure 5.14: Effects of extracellular application of CO gas on pulsed whole-cell BK_{Ca} currents. The ruptured patch technique was used for recording. STOCs were inhibited by ryanodine (10 μM) in the pipette solution. Voltage pulses were administered from -20 mV to +60 mV. A) Example traces show BK_{Ca} currents under control conditions and after 5- and 10-minutes application of CO gas (30 μM). B) Histograms show mean BK_{Ca} current density in the absence (control) and presence of CO gas. Results from one-way ANOVA and ratio paired t-tests were not significant as $p > 0.05$. Error bars show SEM, $n = 6$. $[ATP]_i = 1$ mM; $[Ca^{2+}]_i = 100$ nM; $[K^+]_i = 140$ mM; $[K^+]_o = 5$ mM.

5.5.2 Does intracellular Ca^{2+} concentration, $[\text{Ca}^{2+}]_i$, modulate the effect of CO on pulsed BK_{Ca} currents

So far, the pulsed recordings have been performed in 100 nM $[\text{Ca}^{2+}]_i$. However, my results from inside-out patch study showed that the effects of CORM-3 on BK_{Ca} channel activity was only significant in 300 nM $[\text{Ca}^{2+}]_i$.

Therefore, the influence of $[\text{Ca}^{2+}]_i$ levels on the modulatory effect of CO on pulsed whole-cell BK_{Ca} current was examined by raising $[\text{Ca}^{2+}]_i$ to 300 nM. This was achieved using the fast Ca^{2+} chelator, 1,2-bis(o-aminophenoxy) ethane-N, N, N', N'-tetraacetic acid, commonly known as BAPTA. Chelation of $[\text{Ca}^{2+}]_i$ to 300 nM was performed with BAPTA rather than EGTA due to the faster rate of Ca^{2+} binding by BAPTA (Tsien, 1980).

BAPTA was introduced into the cytosol via the pipette solution. Experiments were performed with 10 mM BAPTA because this concentration has been shown to reduce basal and stimulated $[\text{Ca}^{2+}]_i$ in vascular SMCs (Smirnov & Aaronson, 1992b). The amount of CaCl_2 required to have free $[\text{Ca}^{2+}]_i$ of 300 nM, after chelation by BAPTA (10 mM), was calculated using the Webmaxc Standard Calculator (<http://web.stanford.edu/~cpatton/webmaxcS.htm>). Furthermore, the addition of BAPTA to the pipette solution, replaced the use of both EGTA and ryanodine. This is because BAPTA was sufficient for STOC inhibition as it can also chelate the Ca^{2+} released during Ca^{2+} sparks.

5.5.2.1 Investigation of the stability of whole-cell voltage pulsed BK_{Ca} current in higher $[\text{Ca}^{2+}]_i$, 300 nM

The plan was to record whole-cell BK_{Ca} currents from cells in which free $[\text{Ca}^{2+}]_i$ had been chelated to 300 nM, using BAPTA (10 mM); this concentration of BAPTA should also abolish STOCs.

BAPTA (10 mM) was added to the pipette solution so that on entering the whole-cell configuration it was introduced into the cytosol. STOCs were inhibited shortly after membrane rupture. Recordings were then made by continuously perfusing cells with control solution for 27 minutes. Analysis of current density was performed in blocks of 3 minutes as described earlier in section 5.2.3 above. These results were compared with those from experiments performed under similar conditions but with EGTA (1 mM) and ryanodine (10 μM) in the pipette solution (obtained from Figure 5.3). Surprisingly,

pulsed current recorded in the presence of BAPTA seemed lower than current recorded in the presence of EGTA. This was unexpected because the high $[Ca^{2+}]_i$ of 300 nM achieved in the presence of BAPTA was expected to further increase BK_{Ca} channel activation, thereby resulting in higher BK_{Ca} current density. Interestingly, the results from unpaired t-test performed between both sets of results (EGTA versus BAPTA chelation) was not significant ($n=7$ for EGTA, and $n=5$ for BAPTA, $p>0.05$; Figure 5.15).

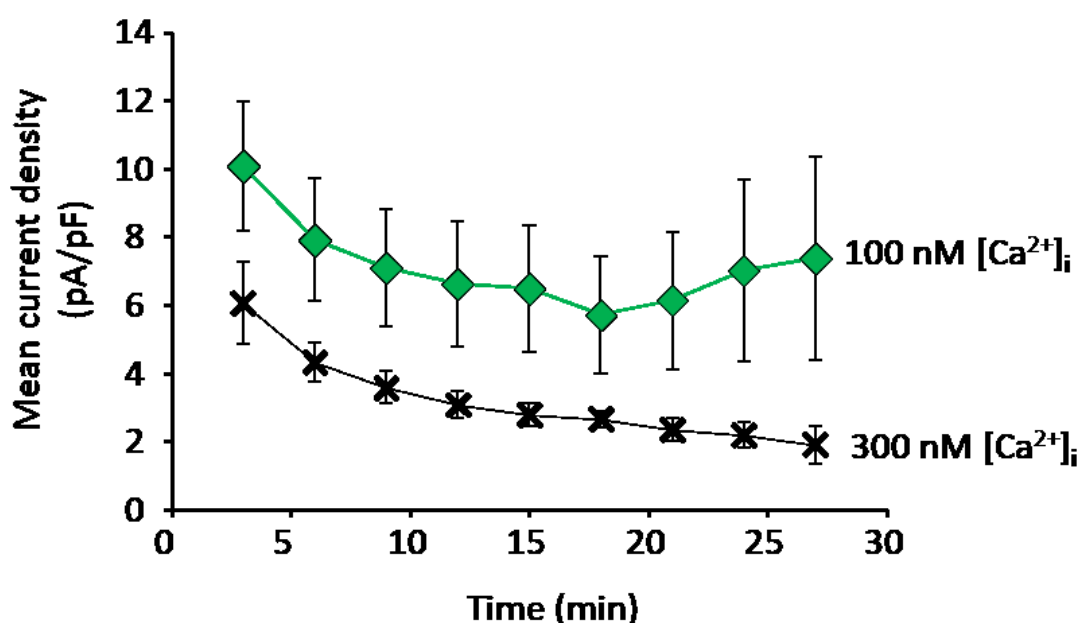


Figure 5.15: Comparison between the stability of BK_{Ca} currents in different $[Ca^{2+}]_i$. Recordings were performed using the ruptured patch technique. Voltage pulses were administered to cells from -20 mV to $+60$ mV. Mean BK_{Ca} current was measured in 100 nM free $[Ca^{2+}]_i$, where Ca^{2+} chelation and STOC inhibition were achieved with EGTA (1 mM) and ryanodine in the pipette solution respectively. Current density was separately measured in 300 nM free $[Ca^{2+}]_i$, where both chelation and STOC inhibition were achieved with BAPTA (10 mM) in the pipette solution. Unpaired t-test was performed, results were not significant with $p>0.05$. Error bars show SEM, $n=5$ (for 300 nM $[Ca^{2+}]_i$) and $n=7$ (for 100 nM $[Ca^{2+}]_i$). $[ATP]_i = 1$ mM; $[K^+]_i = 140$ mM; $[K^+]_o = 5$ mM.

It was surprising that current looked smaller in the presence of BAPTA, even though $[Ca^{2+}]_i$ was meant to be higher (at 300 nM), than in cells exposed to EGTA. Therefore, regardless of the non-significant results from the statistical test performed on current

density measured in the presence of EGTA and BAPTA, I decided to closely examine single BK_{Ca} channel current amplitude in the presence of BAPTA (10 mM) and EGTA (1 mM).

These experiments were performed using outside-out patches, with either BAPTA or EGTA contained in the pipette solution. Recordings were made at V_m of +60 mV whilst perfusing the extracellular side of the channels with control solution. The results showed that mean current amplitude in the presence of BAPTA and EGTA was 7.8 ± 0.5 pA and 15.3 ± 1.0 pA, respectively ($n=3$ for BAPTA, and $n=5$ for EGTA, $p < 0.01$; Figure 5.16). The block of BK_{Ca} currents by BAPTA is consistent with observations from earlier studies, where ≥ 1 mM BAPTA was reported to reduce but not completely abolish BK_{Ca} currents (Smirnov & Aaronson, 1992b; Avdonin *et al.*, 2003). The proposed mechanism of action of BAPTA is a fast voltage-dependent block of BK_{Ca} channels (Avdonin *et al.*, 2003).

So far, I (see section 3.4.2 in chapter 3) and others (Wang & Wu, 1997; Wang *et al.*, 1997b; Williams *et al.*, 2004; Jaggar *et al.*, 2005) have shown that CO increases BK_{Ca} channel Popen with no effect on single channel current. Therefore, although BAPTA reduced single BK_{Ca} channel current, this would be unlikely to alter any effect CO might have on the channel's Popen.

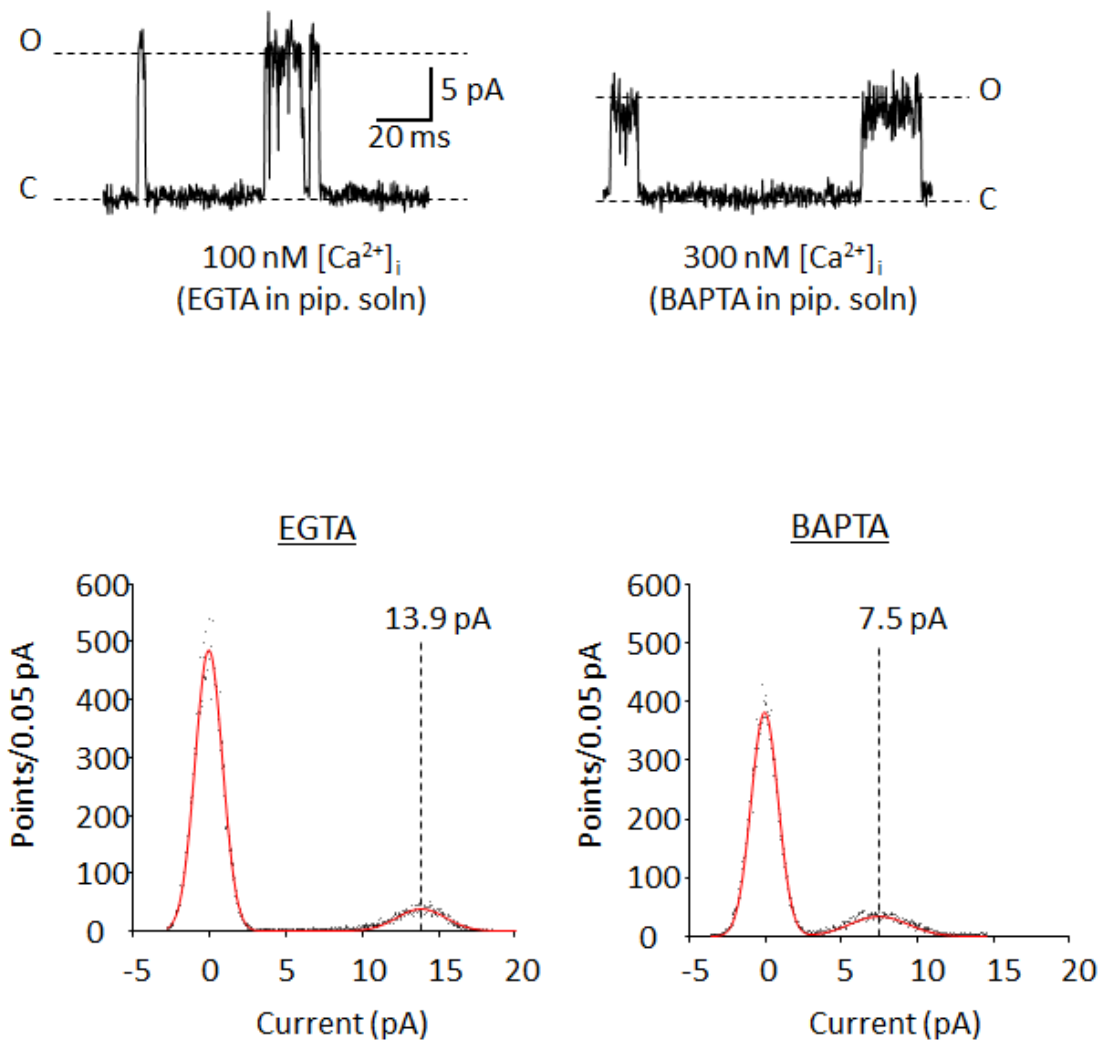


Figure 5.16: Effects of Ca²⁺ chelators on single BK_{Ca} channel activity. A) Example traces show single BK_{Ca} channel activity in 100 nM and 300 nM [Ca²⁺]_i. Both [Ca²⁺]_i were achieved by addition of EGTA (1 mM) and BAPTA (10 mM) in pipette solution, respectively. Open and closed channel levels are indicated by 'O' and 'C', respectively. B) Amplitude histograms of traces shown in A (above). Mean unitary current was reduced from 13.9 pA in the presence of EGTA to 7.5 pA in the presence of BAPTA. Recordings were performed with the outside-out patch configuration. Membrane potential was held at +60 mV. [ATP]_i = 1 mM; [K⁺]_i = 140 mM; [K⁺]_o = 5 mM.

5.5.2.2 Extracellular application of CO gas or CORM-3 in 300 nM $[Ca^{2+}]_i$ had no significant effect on pulsed BK_{Ca} current

Based on the results that CORM-3 increased BK_{Ca} channel activity in inside out patches exposed to 300 nM Ca^{2+} (see section 3.4.2 in chapter 3), CO was expected to enhance voltage pulsed whole-cell BK_{Ca} current measured with 300 nM $[Ca^{2+}]_i$ in the pipette.

Contrary to my expectations, extracellular application of CORM-3 for 5 minutes still did not produce a significant change in mean relative BK_{Ca} current in 300 nM $[Ca^{2+}]_i$; $97.4 \pm 4.6 \%$, from 7.9 ± 1.9 pA/pF to 7.7 ± 1.9 pA/pF ($n=5$, $p > 0.05$; Figure 5.17). A further 10 minutes of CORM-3 application also did not produce any change in mean relative current; $90.0 \pm 8.7 \%$, from 7.9 ± 1.9 pA/pF to 6.9 ± 1.7 pA/pF ($n=5$, $p > 0.05$; Figure 5.17). These results contrast with observations from my single channel studies where intracellular application of CORM-3 (30 μ M) in 300 nM $[Ca^{2+}]_i$ increased single BK_{Ca} channel Popen to $643 \pm 191\%$ of control (see section 3.4.2 in chapter 3).

Furthermore, 5 minutes application of CO gas (30 μ M) solution in a separate experiment also produced no change in mean relative current; $100.6 \pm 11.6 \%$, from 4.4 ± 0.4 pA/pF to 4.4 ± 0.7 pA/pF ($n=4$, $p > 0.05$; Figure 5.18). Prolonged application of CO gas for 10 minutes still did not affect mean relative current; $77.9 \pm 8.2 \%$, from 4.4 ± 0.4 pA/pF to 3.3 ± 0.5 pA/pF ($n=4$ for control, and $n=3$ for 10 minutes CORM-3 application, $p > 0.05$; Figure 5.18).

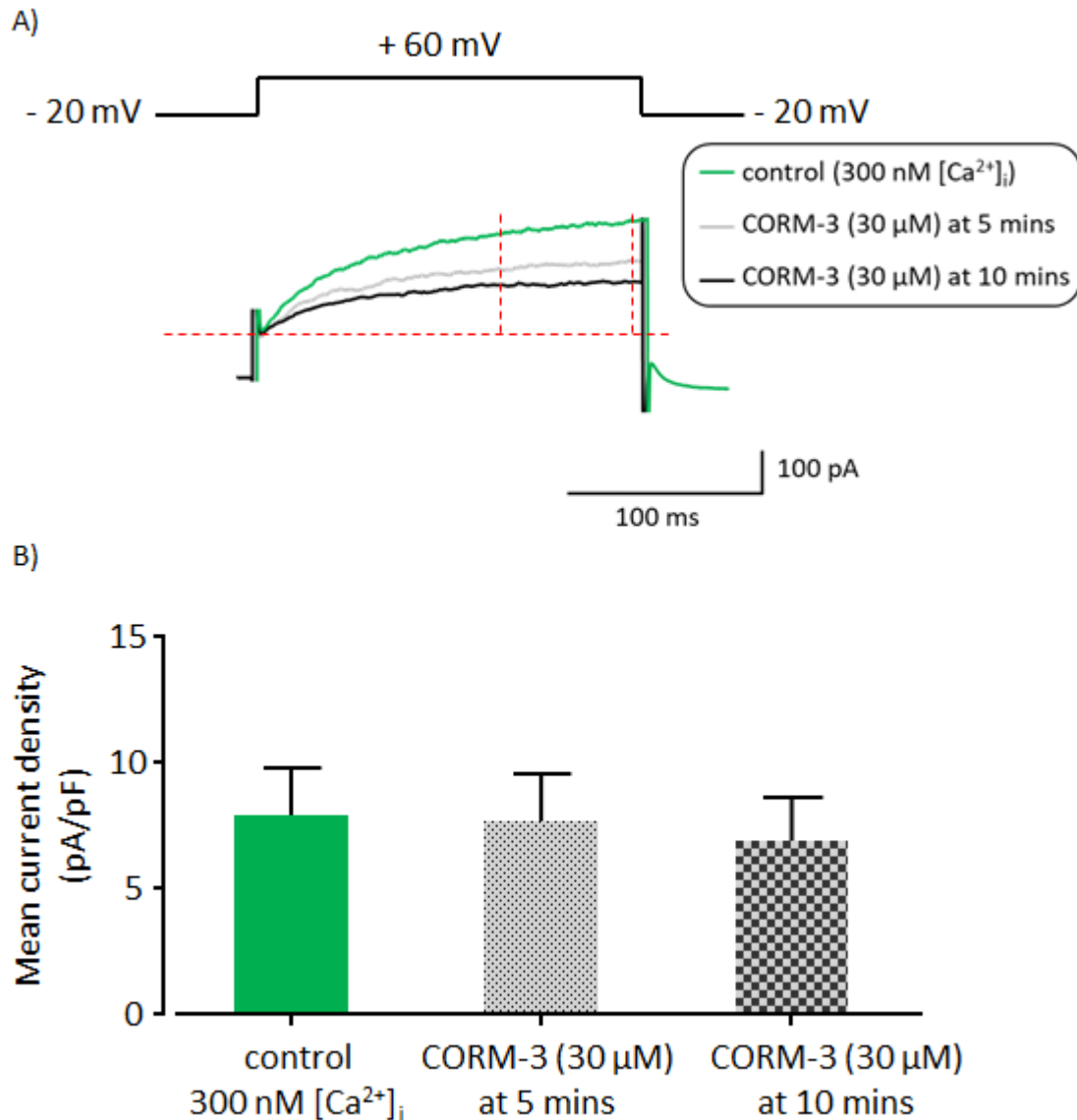


Figure 5.17: Effects of extracellular CORM-3 application on pulsed whole-cell BK_{Ca} currents in 300 nM $[Ca^{2+}]_i$. The ruptured patch technique was used for recordings. STOC inhibition and chelation of free $[Ca^{2+}]_i$ to 300 nM was achieved by addition of BAPTA (10 mM) to the pipette solution. Voltage pulses were administered from -20 mV to +60 mV. A) Example traces show BK_{Ca} current under control conditions and after 5 and 10 minutes of CORM-3 (30 μ M) application. B) Histograms show mean BK_{Ca} current in the presence and absence of CORM-3. One-way ANOVA and ratio paired t-tests were performed as appropriate, results were not significant as $p > 0.05$. Error bars show SEM, $n = 5$. $[ATP]_i = 1$ mM; $[K^+]_i = 140$ mM; $[K^+]_o = 5$ mM.

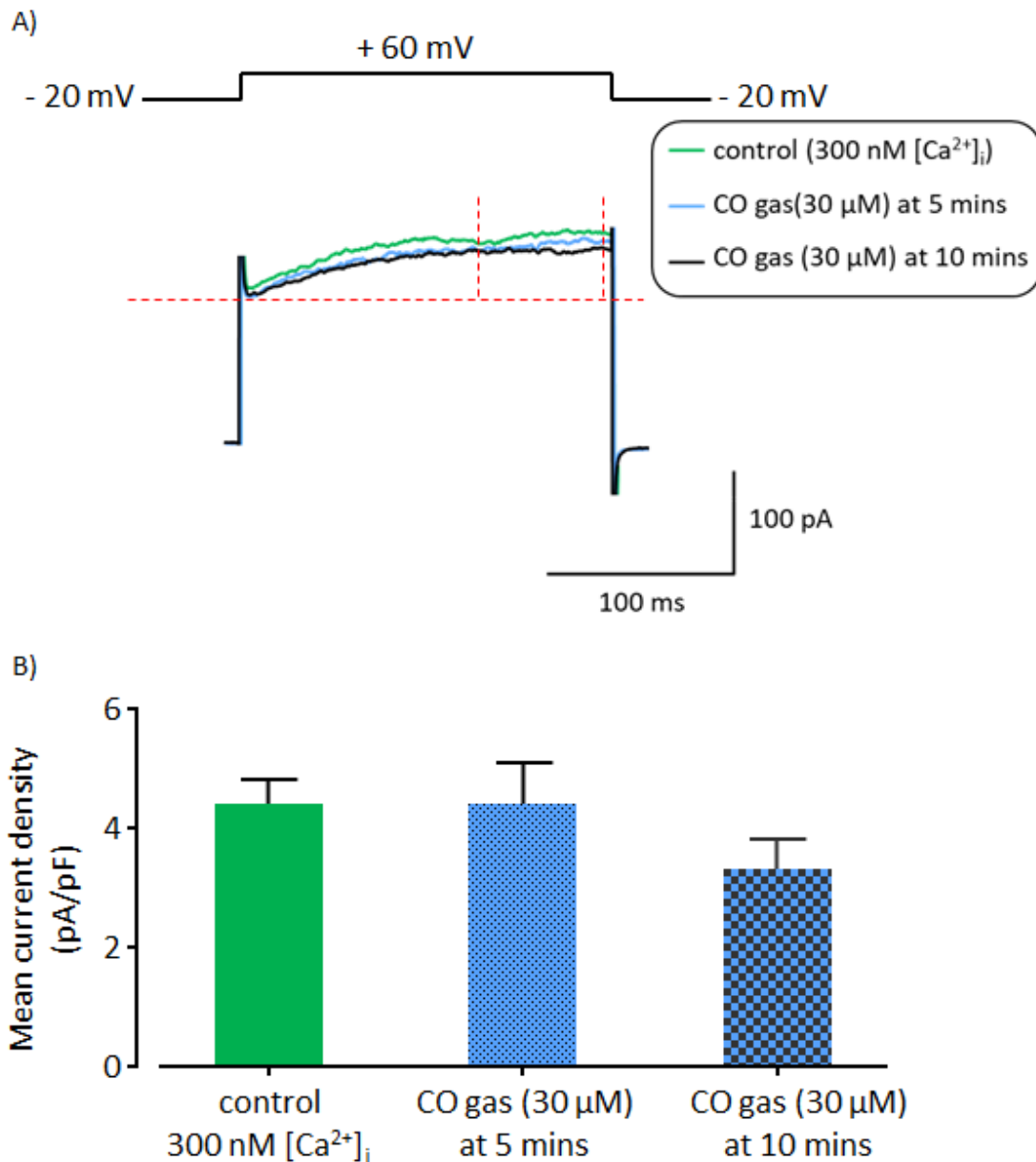


Figure 5.18: Effects of extracellular CO gas application on pulsed whole-cell BK_{Ca} currents in 300 nM $[Ca^{2+}]_i$. The ruptured patch technique was used for recordings. STOC inhibition and chelation of free $[Ca^{2+}]_i$ to 300 nM was achieved by addition of BAPTA (10 mM) to the pipette solution. Voltage pulses were administered from -20 mV to +60 mV. A) Example traces show BK_{Ca} current under control conditions and after 5 and 10 minutes of CO gas (30 μ M) application. B) Histograms show mean BK_{Ca} current density in the presence and absence of CO gas. One-way ANOVA and ratio paired t-tests were performed as appropriate, results were not significant as $p > 0.05$. Error bars show SEM, $n = 4$ (at 5 mins) and 3 (at 10 mins). $[ATP]_i = 1$ mM; $[K^+]_i = 140$ mM; $[K^+]_o = 5$ mM.

5.6 Effects of extracellular haem or CO application on single BK_{Ca} channels in outside-out patches

During certain haemolytic diseases such as haemorrhagic stroke, extracellular haem concentration, [haem]_o can increase. Taking this into consideration, my experiments have been designed to exploit the lipophilic nature of haem by raising [haem]_i via extracellular haem superfusion, even though haem carriers can also exist on the plasma membrane.

Extracellular haem application enhanced STOC amplitude and pulsed BK_{Ca} currents, but contrary to the expectation that this was produced by the BK_{Ca} channel activator, CO (generated from HO-mediated haem degradation), the stimulatory effect of haem persisted in the presence of ZnPP-IX, a HO inhibitor. Therefore, it was hypothesised that BK_{Ca} channel activity could be directly modulated by extracellular haem. This assumption was investigated further using outside-out patches. In addition, CO has been reported to enhance the activity of BK_{Ca} channels in outside-out patches by interacting with extracellular histidine residues (Wang & Wu, 1997). Therefore, the effects of extracellular CO on single BK_{Ca} channel activity was also examined under the present experimental conditions.

Outside-out patches were isolated as detailed in Methods section 2.4.5.1.2. BK_{Ca} channels in the excised patches were activated by administering voltage pulses from -20 mV to +60 mV with the step at +60 mV lasting for 200 ms or 300 ms. The BK_{Ca} currents used for analysis were always measured at +60 mV.

5.6.1 Extracellular haem application enhanced single BK_{Ca} channel activity in outside-out patches

The aim of these experiments was to investigate whether extracellular haem would enhance the activity of BK_{Ca} channels in the absence of much of the intracellular signalling pathways present under whole-cell conditions. The same concentration of haem used for my whole-cell studies, 5 μM, was also used for the outside-out patch study.

After patch excision, voltage pulses from - 20 mV to + 60 mV were applied whilst perfusing the patch with control solution for ~ 5 minutes. Extracellular haem (5 μ M) was then applied for 5 minutes and washed off with control solution for another 5 minutes. Extracellular haem (5 μ M) application produced a mean relative change of 208.4 ± 65.8 % in channel Popen under control conditions, from 0.03 ± 0.01 to 0.08 ± 0.03 ($n= 10$, $p < 0.001$; Figure 5.19). The stimulatory effect of haem was reversed ~ 3 minutes into the wash stage. Notably, extracellular haem (5 μ M) application also increased voltage pulsed whole-cell BK_{Ca} currents to 208.5 ± 26.6 % (see Figure 5.4).

The outside-out patch results contrast with reports from Tang *et al.* (2003), where extracellular haem (125 nM) application was reported to have no effect on the activity of recombinant BK_{Ca} channels in outside-out patches.

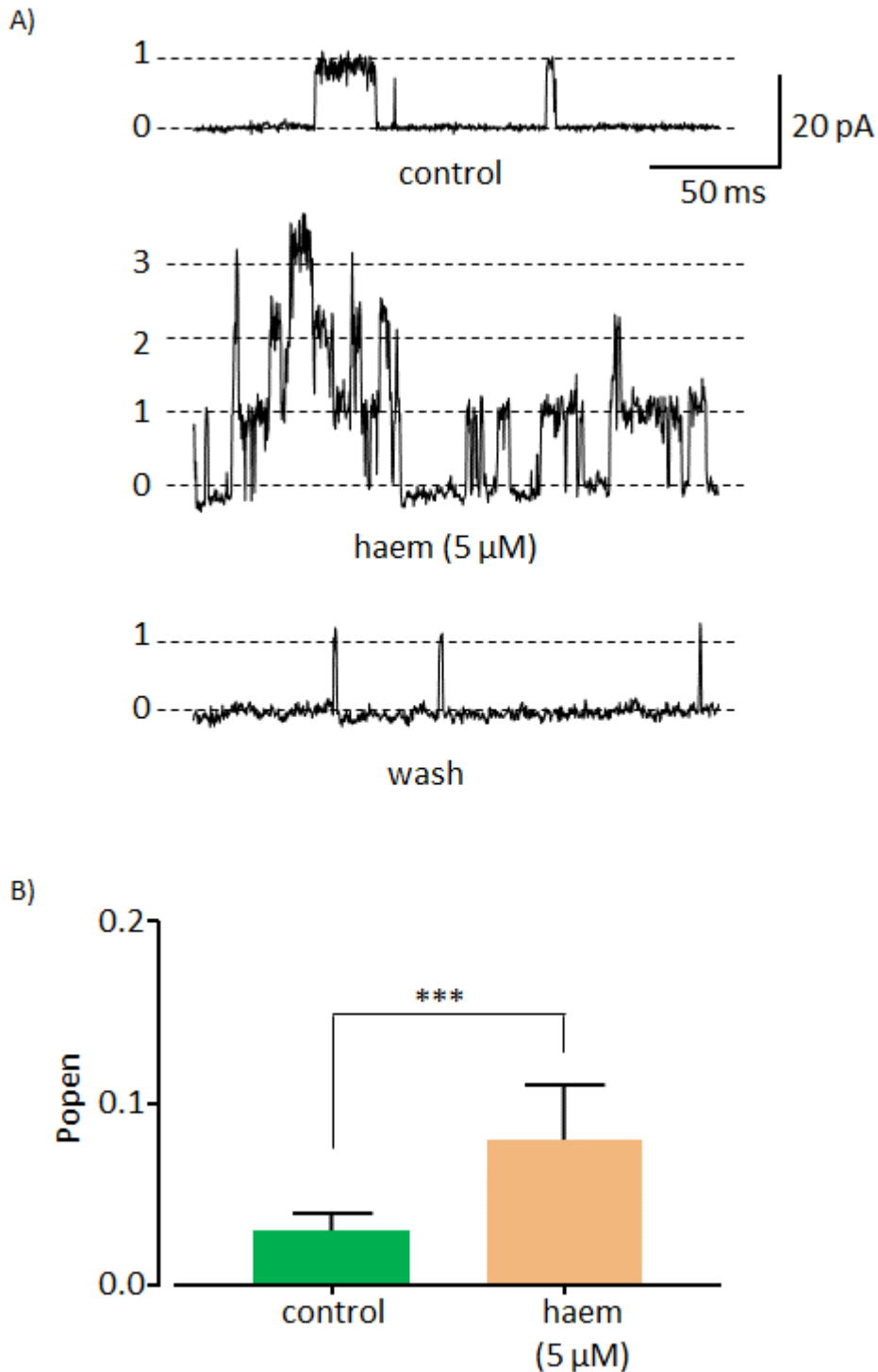


Figure 5.19: Effects of extracellular haem application on single BK_{Ca} channel activity. A) Example traces show channel activity in the presence and absence of extracellular haem (5 μ M). B) Histograms show mean channel Popen in the presence and absence of extracellular haem (5 μ M). Ratio paired t-test was performed, *** $p \leq 0.001$. Error bars show SEM, $n = 10$. The outside-out patch configuration was used for recordings. Membrane potential was held at +60 mV. $[ATP]_i = 1$ mM; $[K^+]_i = 140$ mM; $[K^+]_o = 5$ mM.

5.6.1.1 The stimulatory effect of extracellular haem on single BK_{Ca} channel activity was abolished in the presence a BK_{Ca} channel blocker, penitrem A

To further confirm that the current recorded in the presence of haem resulted from BK_{Ca} channel activation, experiments were performed with the specific BK_{Ca} channel blocker, penitrem A.

Membrane patches were initially superfused with control solution for ~ 5 minutes prior to haem (5 µM) application for another 5 minutes. Haem application produced a mean relative change of 187.0 ± 63.0 % in channel Popen, from 0.05 ± 0.02 to 0.11 ± 0.08 (n= 3, $p \leq 0.05$; Figure 5.20), but subsequent co-application of haem (5 µM) with penitrem A (100 nM) for an extra 5 minutes completely abolished channel activity (Figure 5.20).

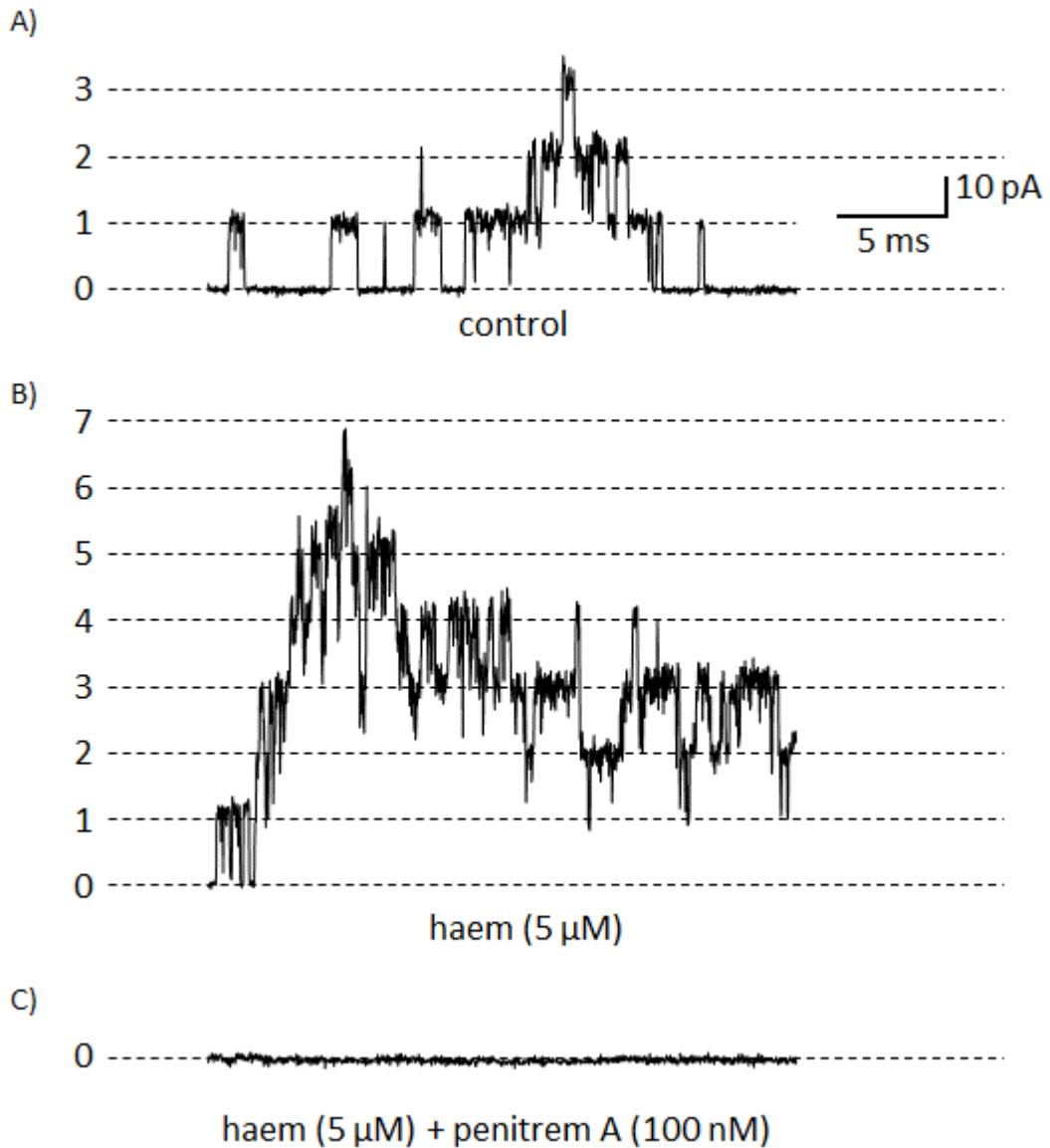


Figure 5.20: Effects of extracellular haem application on single BK_{Ca} channel activity in the presence of the BK_{Ca} channel blocker, penitrem A. The outside-out patch configuration was used for recordings with membrane potential held at +60 mV. Example traces show channel activity in A) control B) haem (5 μ M), 5 minutes after its application and C) haem (5 μ M) + penitrem A (100 nM), 5 minutes after their co-application. $[ATP]_i = 1$ mM; $[K^+]_i = 140$ mM; $[K^+]_o = 5$ mM.

5.6.2 Extracellular CO gas application did not alter single BK_{Ca} channel activity in outside-out patches

The mechanism by which CO influences BK_{Ca} channel activity is still unclear. It has been speculated that CO activates BK_{Ca} channels by interacting with key amino acid residues on the extracellular side of the channel (Wang & Wu, 1997). Although extracellular application of CO in the present study enhanced STOC frequency, it had no effect on STOC amplitude or voltage pulsed BK_{Ca} current. Nevertheless, the effects of extracellular CO gas on single BK_{Ca} channel activity was examined. Experiments were performed with 30 μ M CO gas because the same concentration was used for my whole-cell studies.

Extracellular application of CO gas for \sim 5 minutes produced no significant change in mean relative single BK_{Ca} channel activity; 106.1 ± 12.8 %, from 0.19 ± 0.17 to 0.18 ± 0.16 ($n= 5$, $p > 0.05$; Figure 5.21). These results contrasts with previous reports where extracellular application of CO gas (30 μ M) to BK_{Ca} channels in outside-out patches, isolated from rat tail artery SMCs, reversibly enhanced channel activity (Wang & Wu, 1997).

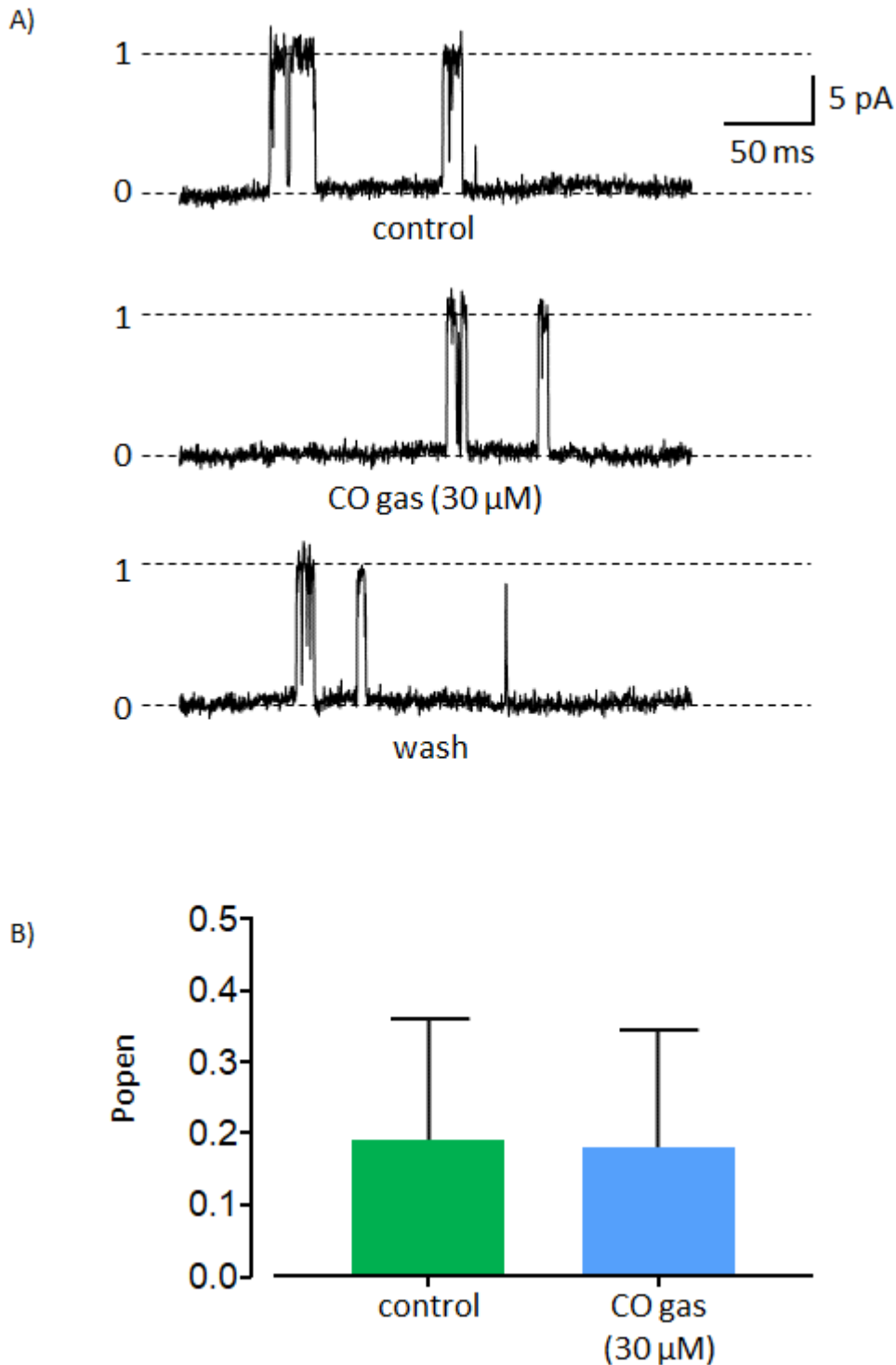


Figure 5.21: Effects of extracellular CO gas application on single BK_{Ca} channel activity. Recordings were performed with the outside-out patch configuration. Membrane potential was held at +60 mV. A) Example traces show channel activity in the presence and absence of extracellular CO gas (30 μM). B) Histograms show mean channel Popen in the presence and absence (control) of CO gas (30 μM). Ratio paired t-test was used for statistical analysis, results were non-significant as $p > 0.05$. Error bars show SEM, $n = 5$. $[\text{ATP}]_i = 1 \text{ mM}$; $[\text{K}^+]_i = 140 \text{ mM}$; $[\text{K}^+]_o = 5 \text{ mM}$.

5.6.3 Extracellular application of CORM-3 had no effect on single BK_{Ca} channels in outside-out patches

Extracellular application of CORM-3 also enhanced STOC frequency, although, it had no significant effect on both STOC amplitude and voltage pulsed BK_{Ca} currents. Nevertheless, the effects of extracellular CORM-3 application on the activity of BK_{Ca} channels in outside-out patches was also examined.

Extracellular superfusion of CORM-3 (30 μ M) also did not produce a significant change in channel activity, from 0.17 ± 0.12 to 0.17 ± 0.12 ($n = 7$, $p > 0.05$; Figure 5.22). This result is consistent with the lack of effect of CO gas (30 μ M) on channel activity, shown in Figure 5.21.

Experiments were also repeated with iCORM-3 (30 μ M). As expected, extracellular application of iCORM-3 (30 μ M) did not significantly change channel activity, from 0.27 ± 0.13 to 0.24 ± 0.16 ($n = 5$, $p > 0.05$; Figure 5.23).

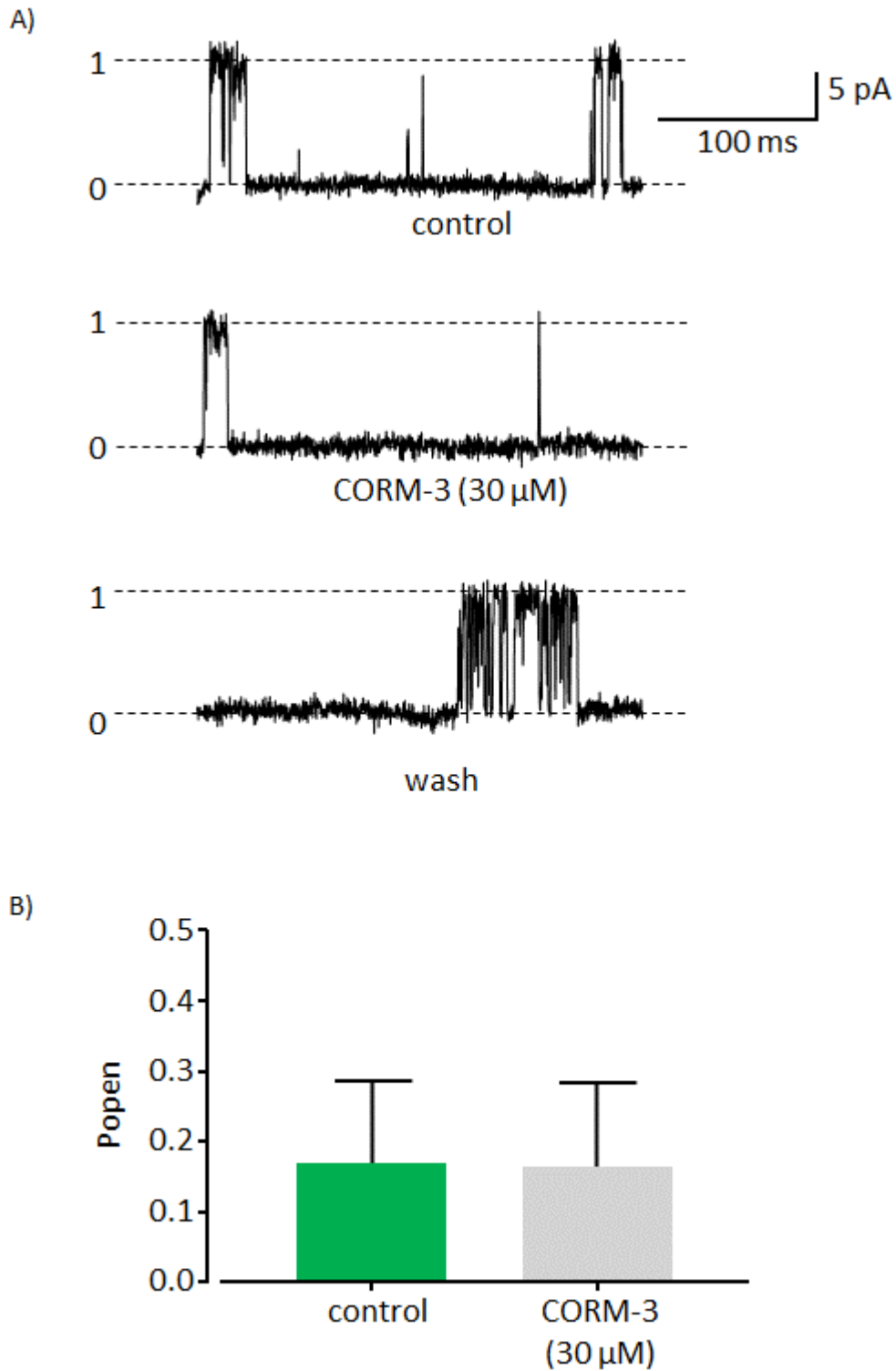


Figure 5.22: Effects of extracellular CORM-3 application on single BK_{Ca} channel activity. Recordings were performed with the outside-out patch configuration. Membrane potential was held at +60 mV. A) Example traces showing channel activity in the presence and absence of extracellular CORM-3 (30 μ M). B) Histograms show mean channel Popen in the presence and absence of CORM-3 (30 μ M). Statistical analysis was performed using ratio paired t-test, results were not significant as $p > 0.05$. Error bars show SEM, $n = 7$. $[ATP]_i = 1$ mM; $[K^+]_i = 140$ mM; $[K^+]_o = 5$ mM.

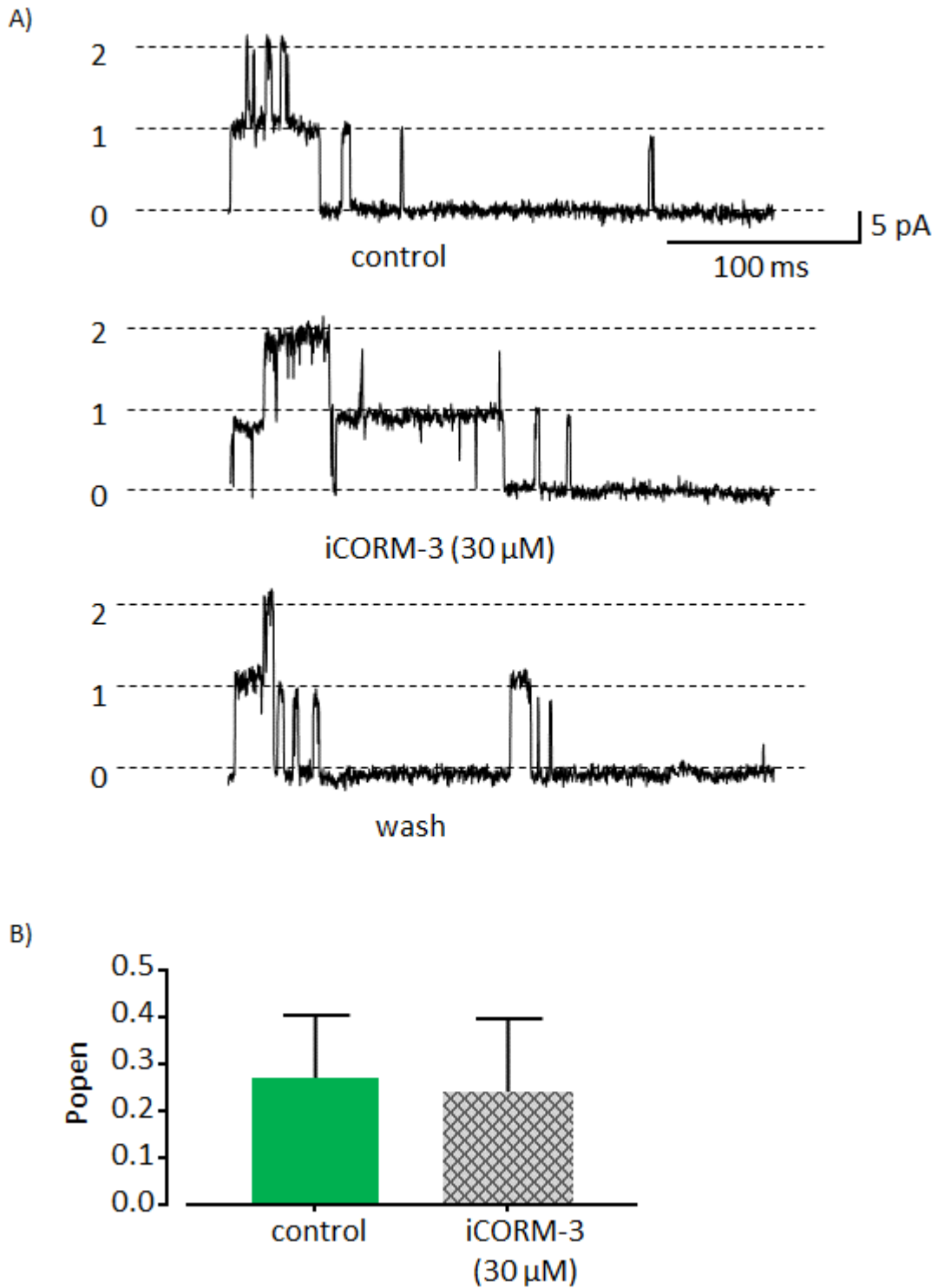


Figure 5.23: Effects of extracellular iCORM-3 application on single BK_{Ca} channel activity. Recordings were performed with the outside-out patch configuration. Membrane potential was held at +60 mV. A) Example traces show channel activity in the presence and absence of extracellular iCORM-3 (30 μ M). B) Histograms show mean channel Popen in the presence and absence of iCORM-3 (30 μ M). Ratio paired t-test was used for statistical analysis, results were non-significant as $p > 0.05$. Error bars show SEM, $n = 5$. $[ATP]_i = 1$ mM; $[K^+]_i = 140$ mM; $[K^+]_o = 5$ mM.

| Haem/CO application | Experiment | Results | |
|---------------------|--|----------------------------------|--------------------|
| | | <i>Whole-cell</i> | <i>Outside-out</i> |
| | | mean current density (pA/pF) | Popen |
| ext. | Haem (5 μM) | ↑ (10) | ↑ (10) |
| ext. | Cd^{2+} (100 μM) | ↓ (4) | - |
| ext. | Haem (5 μM) + Cd^{2+} (100 μM) | ↑ (4) | - |
| ext. | ZnPP-IX (10 μM) | ns (6) | - |
| ext. | ZnPP-IX pre-incub. + Haem (5 μM) | ↑ (6) | - |
| ext. | CO gas (30 μM) | ns (6) | ns (5) |
| ext. | CORM-3 (30 μM) | ns (5) | ns (7) |
| ext. | CO gas (30 μM) in 300 nM $[Ca^{2+}]_i$ | ns (4) | - |
| ext. | CORM-3 (30 μM) in 300 nM $[Ca^{2+}]_i$ | ns (5) | - |

Table 5.1: Summary of the effects of haem and CO on voltage pulsed whole-cell BK_{Ca} currents under the different experimental conditions. The upward and downward arrows indicate increase and decrease in mean current, respectively. The numbers within the brackets show the number of experimental repeats.

5.7 Discussion

5.7.1 Characterisation of voltage pulsed BK_{Ca} currents

The inhibition of the voltage pulse-induced current by TEA⁺ (3 mM) and penitrem A (100 nM) indicate that the currents primarily result from the opening of BK_{Ca} channels. This is consistent with the fact that STOCs were also inhibited by a similar concentration of both drugs (see section 4.2.3 in chapter 4). Furthermore, the inhibitory effects of TEA⁺ and penitrem A on the pulsed current agrees with earlier reports, where external TEA⁺ (with $K_d = 0.85$ mM) and penitrem A (100 nM) reduced whole-cell pulsed BK_{Ca} currents produced by channels expressed in native SMCs (Smirnov & Aaronson, 1992b; Rainbow *et al.*, 2011). Furthermore, the residual currents observed after TEA⁺ and penitrem A-mediated inhibition could be residual non-specific cation currents or K_v currents that were not fully inactivated.

5.7.2 Effects of haem on voltage pulsed BK_{Ca} currents

The increase in voltage pulsed whole-cell BK_{Ca} current during extracellular haem application is consistent with the increase in STOC amplitude induced by extracellular haem application. Furthermore, the reduction of the haem-mediated stimulatory effect in the presence of penitrem A confirms that haem does enhance voltage pulsed whole-cell BK_{Ca} current, rather than activating another current. Interestingly, the stimulatory effects of haem on pulsed BK_{Ca} current did not saturate even after 10 minutes of haem application.

It has been shown that endogenous CO production, via HO activity, enhanced BK_{Ca} channel activity (Jaggar *et al.*, 2002). Therefore, the involvement of endogenous CO in the stimulatory effects observed in the presence of haem was investigated by pre-treating cells with the HO inhibitor, ZnPP-IX. Interestingly, BK_{Ca} current amplitude was higher in ZnPP-IX pre-treated cells (which are assumed to have less endogenous CO because of HO inhibition) compared with untreated cells. The mechanism behind the large current size in ZnPP-IX pre-treated cells is unclear; however, ZnPP-IX has been reported to induce non-specific effects including inhibition of guanylate cyclase activity and Ca²⁺ currents (Ignarro *et al.*, 1984; Linden *et al.*, 1993).

Notably, extracellular application of haem to ZnPP-IX pre-treated cells also enhanced pulsed BK_{Ca} currents (see Table 5.1). This suggests that haem activation of BK_{Ca} current occurs via a CO independent mechanism, but this contradicts the hypothesis put forward by Jaggar *et al.* (2005), where haem was proposed to confer CO sensitivity to BK_{Ca} channels. In addition, my results are in contrast with previous report where 20 µM of tin mesoporphyrin (SnMP), another HO inhibitor, was shown to reduce the stimulatory effect of hemin (40 µM) on whole-cell BK_{Ca} currents recorded from cultured human endothelial cells (Dong *et al.*, 2007). This discrepancy suggests that the involvement of CO in the haem-mediated stimulatory effect on BK_{Ca} channel activity could be subunit-specific; as β1 subunits have been reported to be unexpressed in endothelial BK_{Ca} channels (Papassotiriou *et al.*, 2000). Nevertheless, as mentioned in the previous chapter, the inhibitory effect of ZnPP-IX on HO activity needs to be validated.

A possible haem-induced increase in LTCC activity was investigated using Cd²⁺ to block LTCC (Nelson, 1986; Lansman *et al.*, 1986; Rosenberg *et al.*, 1988). Application of Cd²⁺ reduced BK_{Ca} channel activity (see Table 5.1); this is not surprising as Ca²⁺ entry through LTCC while holding at -20 mV would increase intracellular Ca²⁺ thereby increasing BK_{Ca} channel activation. However, even in the presence of Cd²⁺ the stimulatory effect of haem was still observed (see Table 5.1), suggesting that haem did not increase BK_{Ca} current because of an increase in LTCC activity. Furthermore, haem application in the absence of Cd²⁺ but under otherwise comparable conditions (prolonged haem application for 10 minutes) increased BK_{Ca} currents to a similar size.

5.7.3 Effects of CO on voltage pulsed BK_{Ca} currents

The inability of exogenous CO to enhance pulsed BK_{Ca} currents reflects the lack of effect of CO on STOC amplitude in the present study (see sections 4.5 in chapter 4). However, the reason behind the lack of effect of both extracellular CO gas and CORM-3 application on pulsed BK_{Ca} currents (see Table 5.1) is unclear. Intracellular CORM-3 application enhanced single BK_{Ca} channel activity in inside-out patches, in 300 nM [Ca²⁺]_i (see section 3.4.2 in chapter 3), thus, it was surprising that CO had no significant effect on pulsed whole-cell BK_{Ca} currents in similar [Ca²⁺]_i.

It could be hypothesised that the use of ruptured patches for the whole-cell experiment created an oxidised environment such that CO was unable to activate pulsed whole-cell BK_{Ca} currents because it cannot interact with ferric or oxidised haem. This assumption is based on the spectrophotometry and electrophysiology results presented by Jaggar *et al.* (2005) which showed that the redox state of haem is essential for CO-haem interaction. However, Hou *et al.* (2008) showed that CO enhanced recombinant BK_{Ca} channel activity even after cell pre-treatment with H₂O₂, which suggested that CO did not require reduced haem to mediate its effects. In addition, the data from my inside-out patch experiments agrees with the haem-independent effect of CO since CORM-3 enhanced single BK_{Ca} channel activity without simultaneous haem superfusion. Also, the inside-out patch experiments are performed under more aerobic environments compared with the usual reducing environment of the cytoplasm.

In conclusion, my results contrasts with the well-known stimulatory effect of CO on BK_{Ca} channel activity (Wang *et al.*, 1997b; Wang & Wu, 1997; Jaggar *et al.*, 2005; Dubuis *et al.*, 2005; Williams *et al.*, 2008; Hou *et al.*, 2008a; Telezhkin *et al.*, 2011), since under my experimental conditions CO had little effect on pulsed whole-cell BK_{Ca} currents. Additional experiments are still required for further elucidation of the role of CO in the regulation of whole-cell BK_{Ca} channel activity.

5.7.4 Effects of extracellular application of haem or CO on single BK_{Ca} channels in outside-out patches

Tang *et al.* (2003) reported that extracellular haem (125 nM) application to outside-out patches had no effect on BK_{Ca} channel activity. Therefore, the stimulatory effect of extracellular haem on single BK_{Ca} channel activity observed in this study was unexpected. The discrepancy between both studies could result from the fact that Tang *et al.* (2003) performed his study with only 125 nM haem and on recombinant cells, but I have applied a higher concentration, 5 µM, of haem on native cells. Interestingly, extracellular application of haem (5 µM) increased single channel activity (in outside-out patches) and voltage pulsed whole-cell BK_{Ca} currents to similar levels, ~ 200 %. This suggests either that intracellular components might not be necessary in the stimulatory

effect of haem on pulsed BK_{Ca} currents, or that the necessary signalling components are present within isolated patches.

The modulatory effect of external haem on BK_{Ca} channel activity could occur via direct and/or indirect mechanisms. The direct mechanism assumes that haem can bind to unknown extracellular binding sites on BK_{Ca} channels or a binding site accessible from the plasma membrane. Such interaction between haem and BK_{Ca} channels might have induced a channel conformation that favours the open configuration. In addition, the reversibility of the stimulatory effect of haem suggests that such interaction between haem and the channel is weak. On the other hand, intercalation of haem in the plasma membrane has been reported to catalyse lipid peroxidation which could result in membrane disruption (Khan & Quigley, 2011). Therefore, the indirect mechanism could involve membrane impairment induced by haem intercalation into the plasma membrane which alters BK_{Ca} channel conformation. It is also possible that haem could indirectly regulate BK_{Ca} channel activity by binding to an unknown intermediary protein already associated with the BK_{Ca} channel.

Extracellular application of CO gas to native BK_{Ca} channels in outside-out patches has been shown to enhance channel activity (Wang & Wu, 1997). Thus, the lack of effect of extracellular CO gas and CORM-3 application on single BK_{Ca} channel activity in this study was unexpected. Nevertheless, the proposed mechanism by Wang & Wu (1997) that extracellular CO gas activates single BK_{Ca} channel activity by binding to extracellular histidine residues is implausible. This is because there is no experimental evidence or chemical mechanism to support the direct interaction of CO gas with amino acids (Leffler *et al.*, 2011). However, the reason for the lack of effect of CO on the activity of BK_{Ca} channels in outside-out patches is unclear.

Chapter 6 GENERAL DISCUSSION

6.1 The biological context of my study

Haemolytic diseases such as malaria and sickle cell anaemia are characterised by severe haemolysis which encourages haem release from haemoglobin (Belcher *et al.*, 2010; Sawicki *et al.*, 2015). During such pathological conditions, tissues can be exposed to up to 20 μM of free haem (Arruda *et al.*, 2004). Prolonged haemolysis elevates HO-1 levels in animal models and patients (Wagener *et al.*, 2001; Nath *et al.*, 2001; Belcher *et al.*, 2006). Nevertheless, saturated levels of haem can reduce the effectiveness of the HO system resulting in toxic effects like oxidative stress, haemolysis and inflammation (Belcher *et al.*, 2010; Sawicki *et al.*, 2015). Haem and its degradation products have also been speculated to be involved in the vasospasm that occurs during some haemolytic diseases (Osaka, 1977; Heros *et al.*, 1983). The mechanism behind the vasospasm is still not clearly understood. However, it is known that haem and its degradation products affect a range of ion channels which are involved in regulating arterial SMC membrane potential.

BK_{Ca} channels, which are involved in the regulation of vascular tone, possess a highly conserved cytochrome c haem binding sequence motif, CXXCH (Tang *et al.*, 2003). Thus, BK_{Ca} channels have been classified as hemoproteins because haem was shown to interact with the channels and alter their activity (Yi *et al.*, 2010; Riddle & Walker, 2012). The current understanding of how haem regulates BK_{Ca} channel activity is minimal. This study contributes to existing knowledge by focusing on the effects of haem on native BK_{Ca} channels expressed in arterial SMCs using both excised patch and whole-cell recordings.

6.2 Intracellular acidic pH slows the rate of haem-mediated channel inhibition without affecting its potency

Changes in intracellular pH can be induced by changes in cell metabolism, partial pressure of carbon monoxide (pCO₂) and extracellular pH (Smith *et al.*, 1998). In addition, hypoxia induces intracellular acidosis and has also been suggested to promote an increase in intracellular haem concentration (Mitsufuji *et al.*, 1995; Dore, 2002). The

effects of intracellular acidosis on arteries has been controversial. Some studies report vasoconstriction (Aalkjaer & Cragoe, 1988; Krampetz & Rhoades, 1991; Nagesetty & Paul, 1994; Matthews *et al.*, 1992), whilst others show vasodilation (Austin & Wray, 1993; Nagesetty & Paul, 1994; Hayabuchi *et al.*, 1998). It has been speculated that regional and species difference as well as the duration of intracellular acidification may account for the discrepancy (Smith *et al.*, 1998).

The almost complete inhibition of BK_{Ca} channels in inside-out patches by 100 nM haem seen in this study is similar to the 95 % inhibition reported by Jaggar *et al.* (2005) with 100 nM haem applied to rat cerebral artery BK_{Ca} channels. So far, the proposed mechanism of the haem-mediated inhibition involves haem binding to the CXXCH motif in the C-terminal domain of the channel. This interaction is believed to reduce the coupling strength between the channel gate and the voltage sensing domain (Horrigan *et al.*, 2005). The results from my pH experiments could indicate that protonation of haem and/or the imidazole side chain of histidine residues expressed in the channel protein, including His616 in the CXXCH motifs, altered the interaction of haem with the BK_{Ca} channels. Nevertheless, the inhibitory effect of haem seemed unaffected by such channel/haem modification, as haem produced 99.8 % and 99.6 % inhibition of channel activity at pH 6.7 and 7.2, respectively. Thus, even though the rate of haem-mediated inhibition of BK_{Ca} channel activity was slower at pH 6.7, the overall inhibition was similar to that at pH 7.2. Interestingly, heme loss from myoglobin at acidic pH, pH 5 (37 °C), was reported to be faster than that at pH 7 (37 °C) (Hargrove *et al.*, 1996). Histidine protonation under acidic pH, which could disrupt the interaction between the histidine imidazole side chain and haem iron, was indicated to be involved in the pH dependence of haem loss.

6.3 Externally applied haem enhanced STOC amplitude and voltage pulsed whole-cell BK_{Ca} currents via a CO-independent mechanism

My results and those of others showed that intracellular CO application to BK_{Ca} channels in inside-out patches enhanced their activity (Wang *et al.*, 1997b; Wang & Wu, 1997; Wu *et al.*, 2002; Jaggar *et al.*, 2005). Also, the findings from Jaggar *et al.* (2005) study

indicated that CO binding to reduced haem reversed the inhibitory effect of haem on single BK_{Ca} channel activity. Furthermore, Jaggar *et al.* (2005) proposed that the mechanism of CO action involves a reduction in the inhibitory interaction of haem with BK_{Ca} channel, thereby promoting an open configuration of the channel which increases the channel's Ca²⁺ sensitivity. However, the details of this mechanism seem unclear.

Unlike reports from Jaggar *et al.* (2002), where exogenous CO gas application enhanced both STOC amplitude and frequency, in this study external application of CO gas and CORM-3 only enhanced STOC frequency. Based on these results, I assumed that endogenous CO could also activate STOCs partly by interacting with haem bound to BK_{Ca} channels and that this may account for the stimulatory effect of haem on STOCs in my study. Therefore, the plan was to inhibit endogenous CO production by pre-incubating cells with ZnPP-IX, a HO inhibitor. Interestingly, STOC amplitude and frequency were lower in ZnPP-IX pre-treated cells compared with untreated cells. In contrast, voltage pulsed BK_{Ca} current density was higher in ZnPP-IX pre-treated cells compared with untreated cells. The reason behind the discrepancy between the STOC and voltage pulsed current results is unclear, perhaps the differences in recording conditions might be an important factor.

Nevertheless, extracellular application of haem to ZnPP-IX pre-treated cells, which are expected to have low endogenous CO levels due to HO inhibition, enhanced both voltage pulsed BK_{Ca} currents and STOC amplitude and frequency. This indicates that haem can activate STOCs via a CO-independent mechanism. This conclusion is corroborated by my findings from the outside-out patch experiments, where extracellular haem application (without CO) enhanced single BK_{Ca} channel activity.

Therefore, since CO enhanced STOC frequency only and haem enhanced only STOC amplitude, my results suggest that both molecules influence whole-cell BK_{Ca} channel activity, possibly via different signalling pathways.

6.4 The stimulatory effects of haem on whole-cell BK_{Ca} channel activity does not require Ca²⁺ sparks

Since HO-induced CO production did not appear to be involved in the stimulation of BK_{Ca} currents by haem, the involvement of other factors was investigated. For instance, it was hypothesized that haem modulated STOCs by altering Ca²⁺ spark frequency. However, my imaging data showed that this was not the case, because haem did not significantly change Ca²⁺ spark frequency. Information about whether the Ca²⁺ load released during each spark was altered by haem or not, could not be obtained due to the use of Fluo-4, a non-ratiometric fluorescent indicator. Nevertheless, the stimulatory effect of haem on pulsed BK_{Ca} currents following Ca²⁺ spark inhibition, by including ryanodine in the pipette, further indicates that the modulatory effects of haem on whole-cell BK_{Ca} channel activity occurs independently of Ca²⁺ sparks.

Interestingly, the effect of haem on pulsed current was almost twice its effect on STOC amplitude. The difference could have resulted from the fact that during STOC recordings the large increase in local [Ca²⁺]_i around BK_{Ca} channels, due to Ca²⁺ sparks, increased channel P_{open} close to maximum; thus, the effects of haem on STOC amplitude was limited by the already high channel P_{open}. In contrast, the absence of Ca²⁺ sparks during the recording of pulsed BK_{Ca} current could have resulted in sub-maximal channel P_{open}, such that the presence of haem induced a larger change in channel P_{open}. Notably, Ca²⁺ entry via the LTCC did not appear to be involved in the stimulatory effect of haem on pulsed BK_{Ca} current. This is because the stimulatory effect of haem on pulsed BK_{Ca} currents remained unaffected in the presence of the LTCC blocker, cadmium (Cd²⁺).

6.5 Haem signalling to BK_{Ca} channels could occur within but not be limited to caveolae

Williams *et al.* (2004) reported, using fluorescence microscopy and western blot analysis, that recombinant BK_{Ca} channels co-localized with HO-2. This suggests that BK_{Ca} channel activity may be tightly regulated by a localised pool of CO.

In this study, the abolition of the stimulatory effect of CO on STOC frequency after caveolar disruption with mβCD was expected. This is because caveolae disruption could

have increased the distance between RyRs and LTCCs, previously located in the caveolae, which serve as a trigger for RyR activation (Lohn *et al.*, 2000). This would have resulted in a reduction in Ca^{2+} spark frequency such that an increased coupling of Ca^{2+} spark to BK_{Ca} channel activation by CO could be reduced.

Interestingly, extracellular haem application had no effect on STOC amplitude in $\text{m}\beta\text{CD}$ pre-treated cells but STOC frequency was enhanced. It is unclear how haem increased STOC frequency in the $\text{m}\beta\text{CD}$ pre-treated cells. Nevertheless, the removal of the stimulatory effects of haem and CO on STOC amplitude and frequency respectively, after $\text{m}\beta\text{CD}$ treatment, suggest that haem and CO signalling to BK_{Ca} channels may require caveolae. These results would need to be consolidated with additional studies performed using either small interference RNA (siRNA) targeting specific caveolins or caveolin scaffolding domain (CSD) peptide.

6.6 The location of haem application might influence its effect on whole-cell BK_{Ca} channel activity

Whole-cell studies were mostly performed by applying haem extracellularly. This is because haem was expected to traverse the plasma membrane due to its lipophilic nature. However, it is possible that extracellular haem directly stimulates BK_{Ca} channels. This is corroborated by the increase in channel activity seen in outside-out patches exposed to similar amount of haem. Interestingly, the reversal of the haem-mediated stimulatory effect (which occurs within about 3 minutes of washing) in outside-out patches contrast with the persistence of the stimulatory effect of haem on STOC amplitude (after several minutes of washing). This difference could arise from haem accumulation in intact cells.

On the other hand, intracellular application of haem to intact cells (via the pipette solution) surprisingly had no effect on STOCs. It could be argued that the lack of effect from intracellular haem application resulted from the fact that most of the haem was bound to cytoplasmic proteins, thus, the amount of haem that interacted with the BK_{Ca} channels was low. The results could have also been influenced by a slow diffusion rate of haem from the pipette solution to the cytosol.

Interestingly, there was no current rundown when haem was concurrently present in the pipette and bath solutions. Also, STOC frequency but not STOC amplitude was increased under such condition. The mechanism behind these observations is unclear.

6.7 Limitations of this study

There are several caveats in the present study; For instance, the cell is a complex environment with different enzymes and signalling cascades working together to maintain cell physiology. Hence, data interpretation needs to be made with caution. Furthermore, ZnPP-IX has been described as a potent HO inhibitor, but its effects are non-specific (Grundemar & Ny, 1997; Labbe *et al.*, 1999). Thus, further experiments may be required to confirm the extent of HO inhibition by ZnPP-IX. Another limitation is that intracellular haem was not visualised. Thus, it is unknown whether the lack of channel activity in some isolated patches resulted from haem bound to BK_{Ca} channels at the time of membrane patch excision or not. Although vesicular patches or absence of BK_{Ca} channels in the excised patches could also be responsible for such occurrence.

Furthermore, lack of appropriate equipment restricted the simultaneous performance of imaging and electrophysiology assays. Thus, the effects of haem on STOCs and Ca²⁺ spark frequency could not be monitored at the same time. Also, since HO-1 and HO-2 were found to be expressed in the mesenteric artery of Wistar-Kyoto rats, the current study assumed that both enzymes were expressed in the SMCs that were used (Ndisang *et al.*, 2002). However, it can be argued that Ndisang *et al.* (2002) used vessels that had been frozen and homogenized them without denuding their endothelium, thus it is impossible to establish whether the enzymes were derived from endothelial or SMCs. It is also possible that enzymatic expression might vary between frozen and freshly isolated cells. Thus, it would have been useful to confirm the expression of HO-1 and HO-2 in the current study using western blotting and/or RT-qPCR. This was not done due to time constraints.

| Experiment | Results | | | | |
|-----------------------------|-------------------|--------------------|-------------------|------------------|------------------------------|
| | <i>Inside-out</i> | <i>Outside-out</i> | <i>Whole-cell</i> | | |
| | Popen | | STOC | | mean current density (pA/pF) |
| | | | <i>amplitude</i> | <i>frequency</i> | |
| Haem | ↓ | ↑ | ↑ | no change | ↑ |
| CO gas | no change | no change | no change | ↑ | no change |
| CORM-3 | ↑ | no change | no change | ↑ | no change |
| ZnPP-IX pre-incub. + Haem | - | - | ↑ | ↑ | ↑ |
| ZnPP-IX pre-incub. + CORM-3 | - | - | no change | no change | - |
| mβCD pre-incub. + Haem | - | - | no change | ↑ | - |
| mβCD pre-incub. + CORM-3 | - | - | no change | no change | - |

Table 6.1: Summary of the key findings from this study. The effects of haem and CO on single and whole-cell BK_{Ca} channel activity were examined using excised patch (inside-out and outside-out) and whole-cell patch (ruptured and perforated) recordings. The upward and downward arrows respectively indicate an increase and decrease in mean current or channel Popen, as appropriate.

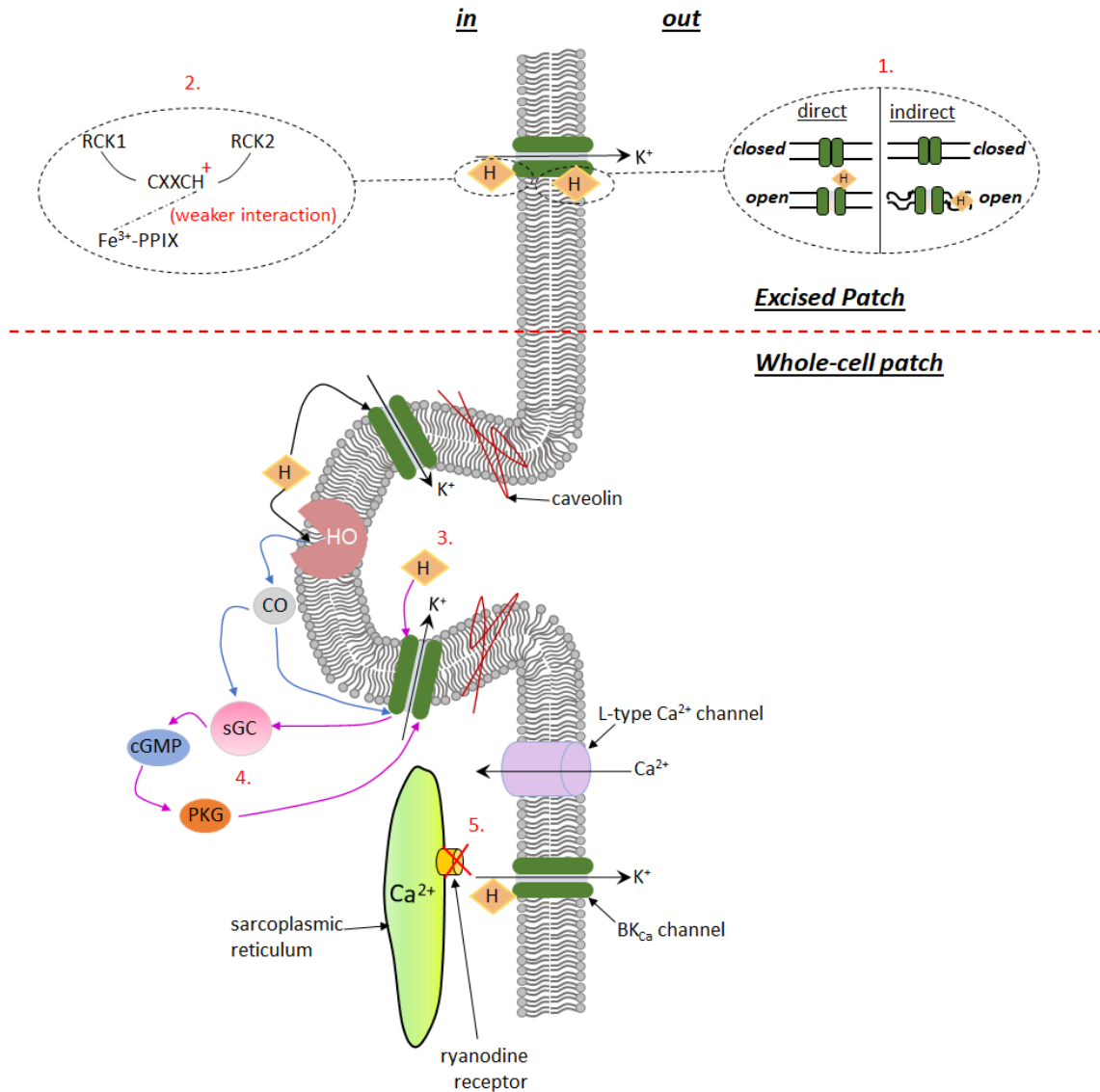


Figure 6.1: Schematic diagram showing the proposed mechanisms of action of haem on SMC BK_{Ca} channel activity, based on results from the present study. 1) The stimulatory effect of extracellular haem might occur via a direct mechanism (involving haem binding directly to extracellular amino acid residues) or an indirect mechanism (resulting from membrane impairment induced by haem insertion into the membrane which alters channel conformation). 2) At low intracellular pH, protonation of H616 in the CXXCH motif, located in the CTD of BK_{Ca} channels, might alter haem binding, thus increasing the time course of haem inhibition of channel activity. 3) Haem signalling could occur within caveolae, where haem and CO might independently regulate BK_{Ca} channel activity. 4) The stimulatory effect of haem on STOCs could involve intracellular components. This might include the sGC/cGMP signalling cascade; not investigated in the present study. 5) The stimulatory effects of haem on whole-cell BK_{Ca} channel activity occurs independent of Ca^{2+} sparks.

6.8 Future work

To the best of my knowledge, this is the first study to examine the effects of haem on STOCs. I have also tried to investigate the mechanism of haem-mediated activation of STOCs, but clearly more work is required. Some future experiments that could be useful for improving our understanding of haem regulation of whole-cell BK_{Ca} channel activity are discussed below.

6.8.1 Mutagenesis studies could be used to further confirm the number and location of haem binding sites on BK_{Ca} channels

It is generally accepted that haem binds to the CXXCH motif in the cytosolic terminal domain of the channel. However, the number of haem binding sites on BK_{Ca} channels is unknown. My results from the extracellular application of haem to outside-out patches suggest that BK_{Ca} channels could also have an extracellular haem binding site. Therefore, mutagenesis studies, with channel expression in a stable cell line such as HEK293, could be useful for investigating other potential haem binding sites that may exist on BK_{Ca} channels.

6.8.2 Inhibition of haem synthesis can be used to investigate the modulatory effect of endogenous haem on STOCs.

The stimulatory effect of haem on STOCs was an interesting find, considering that haem application to BK_{Ca} channels expressed in inside-out patches produced inhibition. It was also surprising that the stimulatory effect of haem was enhanced in the presence of the HO inhibitor, ZnPP-IX. This suggested that haem rather than CO was responsible for the stimulatory effect. Therefore, the effects of haem could be further confirmed by inhibiting haem synthesis using succinyl acetone (SA); an inhibitor of the second enzyme in the haem biosynthesis pathway, δ -aminolevulinic acid dehydratase (ALAD) (Ebert *et al.*, 1979).

6.8.3 Investigate whether the stimulatory effects of haem might have occurred via cGMP-dependent and -independent mechanisms

Extracellular application of haem or haem analogs has been reported to produce vasodilation in *in vitro* and *in vivo* studies (Levere *et al.*, 1990; Martasek *et al.*, 1991; Wang *et al.*, 1997a; Ndisang *et al.*, 2002; Wang *et al.*, 2006b), although vasoconstriction has also been reported (Joerk *et al.*, 2014). However, these studies overlooked the possibility that haem could be responsible for the vasodilation, as they suggested that the vasodilatory effects observed in the presence of haem occur via upregulation of HO-1 expression and activity and an increase in sGC expression (Levere *et al.*, 1990; Martasek *et al.*, 1991; Wang *et al.*, 1997a; Ndisang *et al.*, 2002; Wang *et al.*, 2006b; Li *et al.*, 2011; Joerk *et al.*, 2014).

An earlier study showed that haem increased cGMP levels in rat aortic SMCs (Christodoulides *et al.*, 1995). Thus, it is plausible to speculate that in the present study the sGC/cGMP pathway could have been involved in the haem-mediated stimulatory effect on STOC amplitude. This is consistent with the fact that the stimulatory effect of haem on STOC amplitude was absent in ruptured patches, where cGMP levels could have been low due to cytosolic dialysis. Nevertheless, it can be argued that the effects of haem occurred independent of the sGC/cGMP pathway, because haem also enhanced pulsed whole-cell BK_{Ca} currents (recorded using ruptured patches) and in outside-out patch recordings. Thus, it can be speculated that the effects of haem on whole-cell BK_{Ca} currents could partly occur via cGMP-dependent and -independent mechanisms. This can be investigated using blockers of sGC and PKG, such as ODQ, 1H-[1,2,4]oxadiazolo[4,3-a]quinoxalin-1-one, and KT5822 respectively.

6.8.4 Investigate whether intracellular pH influences the effects of haem on whole-cell BK_{Ca} channel activity

The effects of intracellular pH on haem interaction with BK_{Ca} channels was examined using inside-out patches. Due to time constraints, the pH experiments were not repeated on intact cells. It would be useful to examine whether changing intracellular pH alters the effects of haem on STOCs. This could be achieved by using the appropriate compounds to change and monitor intracellular pH. For instance, ammonium chloride

can be used for both alkalinisation and acidification (Cardelli *et al.*, 1989; Vonrecklinghausen *et al.*, 1992). The changes in intracellular pH can be monitored using fluorescent pH indicators like BCECF-AM.

6.8.5 Investigate whether haem, CO and NO interact to regulate whole-cell BK_{Ca} channel activity

The HO/CO system can interact with the nitric oxide synthase/nitric oxide (NOS/NO) system. This is because CO has been shown to reduce NOS expression and activate or inactivate NOS (Turcanu *et al.*, 1998; Thorup *et al.*, 1999; Meyer *et al.*, 2015; Yang *et al.*, 2016). These effects allow CO to modulate NO signalling. Conversely, NO reportedly increases HO-1 expression but downregulates HO-2 activity (Durante *et al.*, 1997; Datta & Lianos, 1999; Ding *et al.*, 1999). Therefore, NO can also influence CO production and signalling. Notably, CO and NO can signal via similar pathways, as CO binds to Fe²⁺ and NO interacts with both Fe²⁺ and Fe³⁺ (Boczkowski *et al.*, 2006). However, the association constant of NO with Fe²⁺-haem is higher than that of CO, but CO has a lower dissociation constant compared with NO or O₂ (Gibson *et al.*, 1986; Wu & Wang, 2005). Thus, it is speculated that CO could displace NO from Fe²⁺-haem proteins (Wu & Wang, 2005).

NO has been shown to enhance native BK_{Ca} channel activity in excised patches and intact cells (Bolotina *et al.*, 1994; Mistry & Garland, 1998; Lang *et al.*, 2000; Wu *et al.*, 2002). To the best of my knowledge the effects of NO on STOCs has not been documented. Therefore, it would be useful to examine; (1) the effects of NO on STOCs in the presence and absence of haem (2) possible interaction between CO and NO signalling to BK_{Ca} channels (3) the effects of cellular redox state on CO and NO signalling.

6.9 Conclusion

In conclusion, the findings presented here highlight the importance of haem as an endogenous signalling molecule which can influence BK_{Ca} channel activity via multiple mechanisms, as summarised in Figure 6.1. In addition, my results suggest that haem may act as a feedback regulator to reduce the vasospasm that occurs during haemolytic diseases.

Nevertheless, additional work is still required to fully elucidate the mechanism of action of haem on BK_{Ca} channel activity. Information gained from further studies could improve our understanding of the changes in vascular tone that occur during haemolytic diseases, thereby encouraging the design of novel and effective therapeutic strategies.

REFERENCES

- AALKJAER, C. & CRAGOE, E. J., JR., 1988. Intracellular pH regulation in resting and contracting segments of rat mesenteric resistance vessels. *J Physiol*, 402, 391-410.
- ABRAHAM, N. G. & KAPPAS, A., 2008. Pharmacological and clinical aspects of heme oxygenase. *Pharmacol Rev*, 60, 79-127.
- AGGARWAL, S. K. & MACKINNON, R., 1996. Contribution of the S4 segment to gating charge in the Shaker K⁺ channel. *Neuron*, 16, 1169-77.
- AGUILAR-BRYAN, L. & BRYAN, J., 1999. Molecular biology of adenosine triphosphate-sensitive potassium channels. *Endocr Rev*, 20, 101-35.
- AIDLEY, D. J. & STANFIELD, P. R. 1996. *Ion Channels: Molecules in Action*. United Kingdom, Cambridge:University Press, 33-57.
- AIELLO, E. A., CLEMENTCHOMIENNE, O., SONTAG, D. P., WALSH, M. P. & COLE, W. C., 1996. Protein kinase C inhibits delayed rectifier K⁺ current in rabbit vascular smooth muscle cells. *American Journal of Physiology-Heart and Circulatory Physiology*, 271, H109-H119.
- AIELLO, E. A., MALCOLM, A. T., WALSH, M. P. & COLE, W. C., 1998. beta-adrenoceptor activation and PKA regulate delayed rectifier K⁺ channels of vascular smooth muscle cells. *American Journal of Physiology-Heart and Circulatory Physiology*, 275, H448-H459.
- ALLEN, J. W., DALTRUP, O., STEVENS, J. M. & FERGUSON, S. J., 2003. C-type cytochromes: diverse structures and biogenesis systems pose evolutionary problems. *Philos Trans R Soc Lond B Biol Sci*, 358, 255-66.
- ALSHEHRI, A., BOURGUIGNON, M. P., CLAVREUL, N., BADIER-COMMANDER, C., GOSGNACH, W., SIMONET, S., VAYSETTES-COURCHAY, C., CORDI, A., FABIANI, J. N., VERBEUREN, T. J. & FELETOU, M., 2013. Mechanisms of the vasorelaxing effects of CORM-3, a water-soluble carbon monoxide-releasing molecule: interactions with eNOS. *Naunyn Schmiedebergs Arch Pharmacol*, 386, 185-96.
- AMBERG, G. C. & NAVEDO, M. F., 2013. Calcium dynamics in vascular smooth muscle. *Microcirculation*, 20, 281-9.
- ANDERSON, R. G., 1993. Caveolae: where incoming and outgoing messengers meet. *Proc Natl Acad Sci U S A*, 90, 10909-13.
- ANTONINI, E. & BRUNORI, M. 1971. *Haemoglobin and myoglobin in their reactions with ligands*. Amsterdam:North-Holland publishing company, 19.
- ARNAUDEAU, S., MACREZ-LEPRETRE, N. & MIRONNEAU, J., 1996. Activation of calcium sparks by angiotensin II in vascular myocytes. *Biochem Biophys Res Commun*, 222, 809-15.
- ARRUDA, M. A., ROSSI, A. G., DE FREITAS, M. S., BARJA-FIDALGO, C. & GRACA-SOUZA, A. V., 2004. Heme inhibits human neutrophil apoptosis: involvement of phosphoinositide 3-kinase, MAPK, and NF-kappaB. *J Immunol*, 173, 2023-30.
- ASANO, S., BRATZ, I. N., BERWICK, Z. C., FANCHER, I. S., TUNE, J. D. & DICK, G. M., 2012. Penitrem A as a tool for understanding the role of large conductance Ca(2+)/voltage-sensitive K(+) channels in vascular function. *J Pharmacol Exp Ther*, 342, 453-60.
- ASANO, S., TUNE, J. D. & DICK, G. M., 2010. Bisphenol A activates Maxi-K (K(Ca)1.1) channels in coronary smooth muscle. *Br J Pharmacol*, 160, 160-70.
- ASHER, C., DE VILLIERS, K. A. & EGAN, T. J., 2009. Speciation of Ferri protoporphyrin IX in Aqueous and Mixed Aqueous Solution Is Controlled by Solvent Identity, pH, and Salt Concentration. *Inorganic Chemistry*, 48, 7994-8003.
- ASHIDA, T. & BLAUSTEIN, M. P., 1987. Regulation of cell calcium and contractility in mammalian arterial smooth muscle: the role of sodium-calcium exchange. *J Physiol*, 392, 617-35.

- ATAMNA, H. & GINSBURG, H., 1995. Heme degradation in the presence of glutathione. A proposed mechanism to account for the high levels of non-heme iron found in the membranes of hemoglobinopathic red blood cells. *J Biol Chem*, 270, 24876-83.
- ATKIN, A. J., LYNAM, J. M., MOULTON, B. E., SAWLE, P., MOTTERLINI, R., BOYLE, N. M., PRYCE, M. T. & FAIRLAMB, I. J., 2011. Modification of the deoxy-myoglobin/carbonmonoxy-myoglobin UV-vis assay for reliable determination of CO-release rates from organometallic carbonyl complexes. *Dalton Trans*, 40, 5755-61.
- ATKINSON, N. S., ROBERTSON, G. A. & GANETZKY, B., 1991. A component of calcium-activated potassium channels encoded by the *Drosophila slo* locus. *Science*, 253, 551-5.
- AUGUSTYNEK, B., KUDIN, A. P., BEDNARCZYK, P., SZEWCZYK, A. & KUNZ, W. S., 2014. Hemin inhibits the large conductance potassium channel in brain mitochondria: a putative novel mechanism of neurodegeneration. *Exp Neurol*, 257, 70-5.
- AUSTIN, C. & WRAY, S., 1993. Extracellular pH signals affect rat vascular tone by rapid transduction into intracellular pH changes. *J Physiol*, 466, 1-8.
- AVDONIN, V., TANG, X. D. & HOSHI, T., 2003. Stimulatory action of internal protons on Slo1 BK channels. *Biophys J*, 84, 2969-80.
- BABIYCHUK, E. B., SMITH, R. D., BURDYGA, T., BABIYCHUK, V. S., WRAY, S. & DRAEGER, A., 2004. Membrane cholesterol regulates smooth muscle phasic contraction. *J Membr Biol*, 198, 95-101.
- BAGGALEY, E., MCLARNON, S., DEMETER, I., VARGA, G. & BRUCE, J. I., 2007. Differential regulation of the apical plasma membrane Ca(2+) -ATPase by protein kinase A in parotid acinar cells. *J Biol Chem*, 282, 37678-93.
- BALL, C. J., WILSON, D. P., TURNER, S. P., SAINT, D. A. & BELTRAME, J. F., 2009. Heterogeneity of L- and T-Channels in the Vasculature Rationale for the Efficacy of Combined L- and T-Blockade. *Hypertension*, 53, 654-660.
- BAO, L. & COX, D. H., 2005. Gating and ionic currents reveal how the BKCa channel's Ca²⁺ sensitivity is enhanced by its beta1 subunit. *J Gen Physiol*, 126, 393-412.
- BAO, L., KALDANY, C., HOLMSTRAND, E. C. & COX, D. H., 2004. Mapping the BKCa channel's "Ca²⁺ bowl": Side-chains essential for Ca²⁺ sensing. *Journal of General Physiology*, 123, 475-489.
- BARANANO, D. E., RAO, M., FERRIS, C. D. & SNYDER, S. H., 2002. Biliverdin reductase: a major physiologic cytoprotectant. *Proc Natl Acad Sci U S A*, 99, 16093-8.
- BARKOUDAH, E., JAGGAR, J. H. & LEFFLER, C. W., 2004. The permissive role of endothelial NO in CO-induced cerebrovascular dilation. *Am J Physiol Heart Circ Physiol*, 287, H1459-65.
- BARLOW, R. S. & WHITE, R. E., 1998. Hydrogen peroxide relaxes porcine coronary arteries by stimulating BKCa channel activity. *Am J Physiol*, 275, H1283-9.
- BARRETT, J. N., MAGLEBY, K. L. & PALLOTTA, B. S., 1982. Properties of single calcium-activated potassium channels in cultured rat muscle. *J Physiol*, 331, 211-30.
- BAYGUINOV, O., HAGEN, B., KENYON, J. L. & SANDERS, K. M., 2001. Coupling strength between localized Ca(2+) transients and K(+) channels is regulated by protein kinase C. *Am J Physiol Cell Physiol*, 281, C1512-23.
- BEAN, B. P., STUREK, M., PUGA, A. & HERMSMEYER, K., 1986. Calcium Channels in Muscle-Cells Isolated from Rat Mesenteric-Arteries - Modulation by Dihydropyridine Drugs. *Circulation Research*, 59, 229-235.
- BEHRENS, R., NOLTING, A., REIMANN, F., SCHWARZ, M., WALDSCHUTZ, R. & PONGS, O., 2000. hKCNMB3 and hKCNMB4, cloning and characterization of two members of the large-conductance calcium-activated potassium channel beta subunit family. *FEBS Lett*, 474, 99-106.
- BELCHER, J. D., BECKMAN, J. D., BALLA, G., BALLA, J. & VERCELLOTTI, G., 2010. Heme degradation and vascular injury. *Antioxid Redox Signal*, 12, 233-48.

- BELCHER, J. D., MAHASETH, H., WELCH, T. E., OTTERBEIN, L. E., HEBBEL, R. P. & VERCELLOTTI, G. M., 2006. Heme oxygenase-1 is a modulator of inflammation and vaso-occlusion in transgenic sickle mice. *J Clin Invest*, 116, 808-16.
- BENHAM, C. D., BOLTON, T. B., LANG, R. J. & TAKEWAKI, T., 1985. The mechanism of action of Ba²⁺ and TEA on single Ca²⁺-activated K⁺ -channels in arterial and intestinal smooth muscle cell membranes. *Pflugers Arch*, 403, 120-7.
- BENHAM, C. D., BOLTON, T. B., LANG, R. J. & TAKEWAKI, T., 1986. Calcium-activated potassium channels in single smooth muscle cells of rabbit jejunum and guinea-pig mesenteric artery. *J Physiol*, 371, 45-67.
- BENHAM, C. D., HESS, P. & TSIEN, R. W., 1987. Two types of calcium channels in single smooth muscle cells from rabbit ear artery studied with whole-cell and single-channel recordings. *Circ Res*, 61, 110-6.
- BERMAN, J. M. & AWAYDA, M. S., 2013. Redox artifacts in electrophysiological recordings. *Am J Physiol Cell Physiol*, 304, C604-13.
- BERRA-ROMANI, R., BLAUSTEIN, M. P. & MATTESON, D. R., 2005. TTX-sensitive voltage-gated Na⁺ channels are expressed in mesenteric artery smooth muscle cells. *Am J Physiol Heart Circ Physiol*, 289, H137-45.
- BIAN, S., FAVRE, I. & MOCZYDLOWSKI, E., 2001. Ca²⁺-binding activity of a COOH-terminal fragment of the Drosophila BK channel involved in Ca²⁺-dependent activation. *Proc Natl Acad Sci U S A*, 98, 4776-81.
- BOCZKOWSKI, J., PODEROSO, J. J. & MOTTERLINI, R., 2006. CO-metal interaction: Vital signaling from a lethal gas. *Trends Biochem Sci*, 31, 614-21.
- BOER, J. L., MULROONEY, S. B. & HAUSINGER, R. P., 2014. Nickel-dependent metalloenzymes. *Arch Biochem Biophys*, 544, 142-52.
- BOITTIN, F. X., COUSSIN, F., MOREL, J. L., HALET, G., MACREZ, N. & MIRONNEAU, J., 2000. Ca²⁺ signals mediated by Ins(1,4,5)P₃-gated channels in rat ureteric myocytes. *Biochemical Journal*, 349, 323-332.
- BOLOTINA, V., OMELYANENKO, V., HEYES, B., RYAN, U. & BREGESTOVSKI, P., 1989. Variations of membrane cholesterol alter the kinetics of Ca²⁺(+)-dependent K⁺ channels and membrane fluidity in vascular smooth muscle cells. *Pflugers Arch*, 415, 262-8.
- BOLOTINA, V. M., NAJIBI, S., PALACINO, J. J., PAGANO, P. J. & COHEN, R. A., 1994. Nitric oxide directly activates calcium-dependent potassium channels in vascular smooth muscle. *Nature*, 368, 850-3.
- BOLTON, T. B. & LIM, S. P., 1989. Properties of calcium stores and transient outward currents in single smooth muscle cells of rabbit intestine. *J Physiol*, 409, 385-401.
- BONNETT, R. & IOANNOU, S., 1987. Phototherapy and the chemistry of bilirubin. *Mol Aspects Med*, 9, 457-71.
- BOOTMAN, M. D. & BERRIDGE, M. J., 1996. Subcellular Ca²⁺ signals underlying waves and graded responses in HeLa cells. *Current Biology*, 6, 855-865.
- BORSOOK, H. & KEIGHLEY, G., 1933. Oxidation-Reduction Potential of Ascorbic Acid (Vitamin C). *Proc Natl Acad Sci U S A*, 19, 875-8.
- BOULAY, G., ZHU, X., PEYTON, M., JIANG, M., HURST, R., STEFANI, E. & BIRNBAUMER, L., 1997. Cloning and expression of a novel mammalian homolog of Drosophila transient receptor potential (Trp) involved in calcium entry secondary to activation of receptors coupled by the Gq class of G protein. *J Biol Chem*, 272, 29672-80.
- BOYCOTT, H. E., DALLAS, M. L., ELIES, J., PETTINGER, L., BOYLE, J. P., SCRAGG, J. L., GAMPER, N. & PEERS, C., 2013. Carbon monoxide inhibition of Cav3.2 T-type Ca²⁺ channels reveals tonic modulation by thioredoxin. *FASEB J*, 27, 3395-407.
- BRADLEY, K. K., JAGGAR, J. H., BONEV, A. D., HEPNER, T. J., FLYNN, E. R., NELSON, M. T. & HOROWITZ, B., 1999. Kir2.1 encodes the inward rectifier potassium channel in rat arterial smooth muscle cells. *J Physiol*, 515 (Pt 3), 639-51.

- BRAINARD, A. M., MILLER, A. J., MARTENS, J. R. & ENGLAND, S. K., 2005. Maxi-K channels localize to caveolae in human myometrium: a role for an actin-channel-caveolin complex in the regulation of myometrial smooth muscle K⁺ current. *Am J Physiol Cell Physiol*, 289, C49-57.
- BRAYDEN, J. E. & NELSON, M. T., 1992. Regulation of arterial tone by activation of calcium-dependent potassium channels. *Science*, 256, 532-5.
- BRENNER, R., PEREZ, G. J., BONEV, A. D., ECKMAN, D. M., KOSEK, J. C., WILER, S. W., PATTERSON, A. J., NELSON, M. T. & ALDRICH, R. W., 2000. Vasoregulation by the beta1 subunit of the calcium-activated potassium channel. *Nature*, 407, 870-6.
- BROUARD, S., OTTERBEIN, L. E., ANRATHER, J., TOBIASCH, E., BACH, F. H., CHOI, A. M. & SOARES, M. P., 2000. Carbon monoxide generated by heme oxygenase 1 suppresses endothelial cell apoptosis. *J Exp Med*, 192, 1015-26.
- BRUNE, B., SCHMIDT, K. U. & ULLRICH, V., 1990. Activation of soluble guanylate cyclase by carbon monoxide and inhibition by superoxide anion. *Eur J Biochem*, 192, 683-8.
- BRUNE, B. & ULLRICH, V., 1987. Inhibition of platelet aggregation by carbon monoxide is mediated by activation of guanylate cyclase. *Mol Pharmacol*, 32, 497-504.
- BRYAN, J., 1990. Caldesmon - Fragments, Sequence, and Domain Mapping. *Cell Lineages in Development*, 599, 100-110.
- BUDELLI, G., GENG, Y., BUTLER, A., MAGLEBY, K. L. & SALKOFF, L., 2013. Properties of Slo1 K⁺ channels with and without the gating ring. *Proc Natl Acad Sci U S A*, 110, 16657-62.
- BUKIYA, A. N., VAITHIANATHAN, T., KUNTAMALLAPPANAVAR, G., ASUNCION-CHIN, M. & DOPICO, A. M., 2011. Smooth muscle cholesterol enables BK beta1 subunit-mediated channel inhibition and subsequent vasoconstriction evoked by alcohol. *Arterioscler Thromb Vasc Biol*, 31, 2410-23.
- BULLEY, S. & JAGGAR, J. H., 2014. Cl(-) channels in smooth muscle cells. *Pflugers Arch*, 466, 861-72.
- BURNS, J. A., BUTLER, J. C., MORAN, J. & WHITESIDES, G. M., 1991. Selective Reduction of Disulfides by Tris(2-Carboxyethyl)Phosphine. *Journal of Organic Chemistry*, 56, 2648-2650.
- BURTON, M. J., KAPETANAKI, S. M., CHERNOVA, T., JAMIESON, A. G., DORLET, P., SANTOLINI, J., MOODY, P. C., MITCHESON, J. S., DAVIES, N. W., SCHMID, R., RAVEN, E. L. & STOREY, N. M., 2016. A heme-binding domain controls regulation of ATP-dependent potassium channels. *Proc Natl Acad Sci U S A*.
- BURYI, V. A., GORDIENKO, D. V. & SHUBA, M. F., 1994. 2 Kinds of Spatially Separated Caffeine-Sensitive Calcium Stores in Smooth-Muscle Cells from Guinea-Pig Mesenteric-Artery. *Resistance Arteries*, 71-82.
- BYCHKOV, R., PIEPER, K., RIED, C., MILOSHEVA, M., BYCHKOV, E., LUFT, F. C. & HALLER, H., 1999. Hydrogen peroxide, potassium currents, and membrane potential in human endothelial cells. *Circulation*, 99, 1719-25.
- CALLAMARAS, N. & PARKER, I., 2000. Phasic characteristic of elementary Ca²⁺ release sites underlies quantal responses to IP₃. *Embo Journal*, 19, 3608-3617.
- CAMADRO, J. M. & LABBE, P., 1982. Kinetic-Studies of Ferrochelataze in Yeast - Zinc or Iron as Competing Substrates. *Biochimica Et Biophysica Acta*, 707, 280-288.
- CARDELLI, J. A., RICHARDSON, J. & MIEARS, D., 1989. Role of Acidic Intracellular Compartments in the Biosynthesis of Dictyostelium Lysosomal-Enzymes - the Weak Bases Ammonium-Chloride and Chloroquine Differentially Affect Proteolytic Processing and Sorting. *Journal of Biological Chemistry*, 264, 3454-3463.
- CASTEELS, R., KITAMURA, K., KURIYAMA, H. & SUZUKI, H., 1977. Membrane Properties of Smooth-Muscle Cells of Rabbit Main Pulmonary-Artery. *Journal of Physiology-London*, 271, 41-61.

- CATTERALL, W. A., 2011. Voltage-gated calcium channels. *Cold Spring Harb Perspect Biol*, 3, a003947.
- CATTERALL, W. A., GOLDIN, A. L., WAXMAN, S. G. & INTERNATIONAL UNION OF, P., 2003. International Union of Pharmacology. XXXIX. Compendium of voltage-gated ion channels: sodium channels. *Pharmacol Rev*, 55, 575-8.
- CHAKDER, S., RATHI, S., MA, X. L. & RATTAN, S., 1996. Heme oxygenase inhibitor zinc protoporphyrin IX causes an activation of nitric oxide synthase in the rabbit internal anal sphincter. *J Pharmacol Exp Ther*, 277, 1376-82.
- CHAKRAVARTHI, S., JESSOP, C. E. & BULLEID, N. J., 2006. The role of glutathione in disulphide bond formation and endoplasmic-reticulum-generated oxidative stress. *EMBO Rep*, 7, 271-5.
- CHAVES-FERREIRA, M., ALBUQUERQUE, I. S., MATAK-VINKOVIC, D., COELHO, A. C., CARVALHO, S. M., SARAIVA, L. M., ROMAO, C. C. & BERNARDES, G. J., 2015. Spontaneous CO release from Ru(II)(CO)₂-protein complexes in aqueous solution, cells, and mice. *Angew Chem Int Ed Engl*, 54, 1172-5.
- CHENG, H., LEDERER, W. J. & CANNELL, M. B., 1993. Calcium sparks: elementary events underlying excitation-contraction coupling in heart muscle. *Science*, 262, 740-4.
- CHEONG, A., DEDMAN, A. M. & BEECH, D. J., 2001a. Expression and function of native potassium channel (K-v alpha 1) subunits in terminal arterioles of rabbit. *Journal of Physiology-London*, 534, 691-700.
- CHEONG, A., DEDMAN, A. M., XU, S. Z. & BEECH, D. J., 2001b. K-v alpha 1 channels in murine arterioles: differential cellular expression and regulation of diameter. *American Journal of Physiology-Heart and Circulatory Physiology*, 281, H1057-H1065.
- CHERANOV, S. Y. & JAGGAR, J. H., 2002. Sarcoplasmic reticulum calcium load regulates rat arterial smooth muscle calcium sparks and transient K(Ca) currents. *J Physiol*, 544, 71-84.
- CHIABRANDO, D., MARRO, S., MERCURIO, S., GIORGI, C., PETRILLO, S., VINCHI, F., FIORITO, V., FAGOONEE, S., CAMPOREALE, A., TURCO, E., MERLO, G. R., SILENGO, L., ALTRUDA, F., PINTON, P. & TOLOSANO, E., 2012. The mitochondrial heme exporter FLVCR1b mediates erythroid differentiation. *J Clin Invest*, 122, 4569-79.
- CHIABRANDO, D., VINCHI, F., FIORITO, V., MERCURIO, S. & TOLOSANO, E., 2014. Heme in pathophysiology: a matter of scavenging, metabolism and trafficking across cell membranes. *Front Pharmacol*, 5, 61.
- CHING, L. L., WILLIAMS, A. J. & SITSAPESAN, R., 2000. Evidence for Ca(2+) activation and inactivation sites on the luminal side of the cardiac ryanodine receptor complex. *Circ Res*, 87, 201-6.
- CHOU, A. C. & FITCH, C. D., 1981. Mechanism of hemolysis induced by ferriprotoporphyrin IX. *J Clin Invest*, 68, 672-7.
- CHOWDHURY, S. & CHANDA, B., 2012. Perspectives on: conformational coupling in ion channels: thermodynamics of electromechanical coupling in voltage-gated ion channels. *J Gen Physiol*, 140, 613-23.
- CHRISTODOULIDES, N., DURANTE, W., KROLL, M. H. & SCHAFER, A. I., 1995. Vascular smooth muscle cell heme oxygenases generate guanylyl cyclase-stimulatory carbon monoxide. *Circulation*, 91, 2306-9.
- CHURCH, J., BAXTER, K. A. & MCLARNON, J. G., 1998. pH modulation of Ca²⁺ responses and a Ca²⁺-dependent K⁺ channel in cultured rat hippocampal neurones. *J Physiol*, 511 (Pt 1), 119-32.
- CLARK, J. E., FORESTI, R., GREEN, C. J. & MOTTERLINI, R., 2000. Dynamics of haem oxygenase-1 expression and bilirubin production in cellular protection against oxidative stress. *Biochem J*, 348 Pt 3, 615-9.

- CLARK, J. E., NAUGHTON, P., SHUREY, S., GREEN, C. J., JOHNSON, T. R., MANN, B. E., FORESTI, R. & MOTTERLINI, R., 2003. Cardioprotective actions by a water-soluble carbon monoxide-releasing molecule. *Circ Res*, 93, e2-8.
- CLELAND, W. W., 1964. Dithiothreitol, a New Protective Reagent for Sh Groups. *Biochemistry*, 3, 480-2.
- CLINE, D. J., REDDING, S. E., BROHAWN, S. G., PSATHAS, J. N., SCHNEIDER, J. P. & THORPE, C., 2004. New water-soluble phosphines as reductants of peptide and protein disulfide bonds: reactivity and membrane permeability. *Biochemistry*, 43, 15195-203.
- CODDOU, C., YAN, Z., OBSIL, T., HUIDOBRO-TORO, J. P. & STOJILKOVIC, S. S., 2011. Activation and regulation of purinergic P2X receptor channels. *Pharmacol Rev*, 63, 641-83.
- COHEN, A. W., HNASKO, R., SCHUBERT, W. & LISANTI, M. P., 2004. Role of caveolae and caveolins in health and disease. *Physiol Rev*, 84, 1341-79.
- COHEN, N. M. & LEDERER, W. J., 1987. Calcium Current in Isolated Neonatal Rat Ventricular Myocytes. *Journal of Physiology-London*, 391, 169-191.
- COTTON, K. D., HOLLYWOOD, M. A., MCHALE, N. G. & THORNBURY, K. D., 1997. Outward currents in smooth muscle cells isolated from sheep mesenteric lymphatics. *J Physiol*, 503 (Pt 1), 1-11.
- CRESPO, M. P., TILLEY, L. & KLONIS, N., 2010. Solution behavior of hemein under acidic conditions and implications for its interactions with chloroquine. *J Biol Inorg Chem*, 15, 1009-22.
- CRUSE, I. & MAINES, M. D., 1988. Evidence Suggesting That the 2 Forms of Heme Oxygenase Are Products of Different Genes. *Journal of Biological Chemistry*, 263, 3348-3353.
- CUI, J., COX, D. H. & ALDRICH, R. W., 1997. Intrinsic voltage dependence and Ca²⁺ regulation of mslo large conductance Ca-activated K⁺ channels. *J Gen Physiol*, 109, 647-73.
- CUMMING, R. C., ANDON, N. L., HAYNES, P. A., PARK, M., FISCHER, W. H. & SCHUBERT, D., 2004. Protein disulfide bond formation in the cytoplasm during oxidative stress. *J Biol Chem*, 279, 21749-58.
- DALLAS, M. L., BOYLE, J. P., MILLIGAN, C. J., SAYER, R., KERRIGAN, T. L., MCKINSTY, C., LU, P., MANKOURI, J., HARRIS, M., SCRAGG, J. L., PEARSON, H. A. & PEERS, C., 2011. Carbon monoxide protects against oxidant-induced apoptosis via inhibition of Kv2.1. *FASEB J*, 25, 1519-30.
- DATTA, P. K. & LIANOS, E. A., 1999. Nitric oxide induces heme oxygenase-1 gene expression in mesangial cells. *Kidney International*, 55, 1734-1739.
- DAVIS, M. J., DONOVITZ, J. A. & HOOD, J. D., 1992a. Stretch-Activated Single-Channel and Whole Cell Currents in Vascular Smooth-Muscle Cells. *American Journal of Physiology*, 262, C1083-C1088.
- DAVIS, M. J., MEININGER, G. A. & ZAWIEJA, D. C., 1992b. Stretch-Induced Increases in Intracellular Calcium of Isolated Vascular Smooth-Muscle Cells. *American Journal of Physiology*, 263, H1292-H1299.
- DAWSON, R. M. C., ELLIOT, D. C., ELLIOT, W. H. & JONES, K. M. 1975. *Data for Biochemical Research*. Oxford:Oxford University Press, 230-231.
- DE VILLIERS, K. A., KASCHULA, C. H., EGAN, T. J. & MARQUES, H. M., 2007. Speciation and structure of ferriprotoporphyrin IX in aqueous solution: spectroscopic and diffusion measurements demonstrate dimerization, but not mu-oxo dimer formation. *J Biol Inorg Chem*, 12, 101-17.
- DERGOUSSOVA, E. A., PETRUSHANKO, I. Y., KLIMANOVA, E. A., MITKEVICH, V. A., ZIGANSHIN, R. H., LOPINA, O. D. & MAKAROV, A. A., 2017. Effect of Reduction of Redox Modifications of Cys-Residues in the Na,K-ATPase alpha1-Subunit on Its Activity. *Biomolecules*, 7.
- DESMARD, M., FORESTI, R., MORIN, D., DAGOUASSAT, M., BERDEAUX, A., DENAMUR, E., CROOK, S. H., MANN, B. E., SCAPENS, D., MONTRAVERS, P., BOCZKOWSKI, J. & MOTTERLINI, R., 2012. Differential antibacterial activity against Pseudomonas

- aeruginosa by carbon monoxide-releasing molecules. *Antioxid Redox Signal*, 16, 153-63.
- DICHIARA, T. J. & REINHART, P. H., 1997. Redox modulation of hsl α 1Ca²⁺-activated K⁺ channels. *J Neurosci*, 17, 4942-55.
- DING, Y., MCCOUBREY, W. K., JR. & MAINES, M. D., 1999. Interaction of heme oxygenase-2 with nitric oxide donors. Is the oxygenase an intracellular 'sink' for NO? *Eur J Biochem*, 264, 854-61.
- DOLPHIN, A. C., 2013. The α 2 δ subunits of voltage-gated calcium channels. *Biochim Biophys Acta*, 1828, 1541-9.
- DOMKIN, V. & CHABES, A., 2014. Phosphines are ribonucleotide reductase reductants that act via C-terminal cysteines similar to thioredoxins and glutaredoxins. *Sci Rep*, 4, 5539.
- DONG, D. L., YUE, P., YANG, B. F. & WANG, W. H., 2008. Hydrogen peroxide stimulates the Ca²⁺-activated big-conductance K channels (BK) through cGMP signaling pathway in cultured human endothelial cells. *Cell Physiol Biochem*, 22, 119-26.
- DONG, D. L., ZHANG, Y., LIN, D. H., CHEN, J., PATSCHAN, S., GOLIGORSKY, M. S., NASJLETTI, A., YANG, B. F. & WANG, W. H., 2007. Carbon monoxide stimulates the Ca²⁺-activated big conductance k channels in cultured human endothelial cells. *Hypertension*, 50, 643-51.
- DOPICO, A. M., BUKIYA, A. N. & SINGH, A. K., 2012. Large conductance, calcium- and voltage-gated potassium (BK) channels: regulation by cholesterol. *Pharmacol Ther*, 135, 133-50.
- DORE, S., 2002. Decreased activity of the antioxidant heme oxygenase enzyme: implications in ischemia and in Alzheimer's disease. *Free Radic Biol Med*, 32, 1276-82.
- DOYLE, D. A., MORAIS CABRAL, J., PFUETZNER, R. A., KUO, A., GULBIS, J. M., COHEN, S. L., CHAIT, B. T. & MACKINNON, R., 1998. The structure of the potassium channel: molecular basis of K⁺ conduction and selectivity. *Science*, 280, 69-77.
- DOYLE, L. & ROSS, D. D., 2003. Multidrug resistance mediated by the breast cancer resistance protein BCRP (ABCG2). *Oncogene*, 22, 7340-58.
- DREJA, K., VOLDSTEDLUND, M., VINTEN, J., TRANUM-JENSEN, J., HELLSTRAND, P. & SWARD, K., 2002. Cholesterol depletion disrupts caveolae and differentially impairs agonist-induced arterial contraction. *Arterioscler Thromb Vasc Biol*, 22, 1267-72.
- DRINGEN, R., 2000. Metabolism and functions of glutathione in brain. *Progress in Neurobiology*, 62, 649-671.
- DU, J., CULLEN, J. J. & BUETTNER, G. R., 2012. Ascorbic acid: Chemistry, biology and the treatment of cancer. *Biochimica Et Biophysica Acta-Reviews on Cancer*, 1826, 443-457.
- DUBUIS, E., POTIER, M., WANG, R. & VANDIER, C., 2005. Continuous inhalation of carbon monoxide attenuates hypoxic pulmonary hypertension development presumably through activation of BKCa channels. *Cardiovascular Research*, 65, 751-761.
- DUFFY, S. P., SHING, J., SARAON, P., BERGER, L. C., EIDEN, M. V., WILDE, A. & TAILOR, C. S., 2010. The Fowler Syndrome-Associated Protein FLVCR2 Is an Importer of Heme. *Molecular and Cellular Biology*, 30, 5318-5324.
- DURANTE, W., KROLL, M. H., CHRISTODOULIDES, N., PEYTON, K. J. & SCHAFER, A. I., 1997. Nitric oxide induces heme oxygenase-1 gene expression and carbon monoxide production in vascular smooth muscle cells. *Circulation Research*, 80, 557-564.
- DWORETZKY, S. I., TROJNACKI, J. T. & GRIBKOFF, V. K., 1994. Cloning and expression of a human large-conductance calcium-activated potassium channel. *Brain Res Mol Brain Res*, 27, 189-93.
- EBERT, P. S., HESS, R. A., FRYKHOLM, B. C. & TSCHUDY, D. P., 1979. Succinylacetone, a Potent Inhibitor of Heme-Biosynthesis - Effect on Cell-Growth, Heme Content and Delta-Aminolevulinic-Acid Dehydratase Activity of Malignant Murine Erythroleukemia-Cells. *Biochemical and Biophysical Research Communications*, 88, 1382-1390.

- EDWARDS, F. R. & HIRST, G. D., 1988. Inward rectification in submucosal arterioles of guinea-pig ileum. *J Physiol*, 404, 437-54.
- EDWARDS, F. R., HIRST, G. D. & SILVERBERG, G. D., 1988. Inward rectification in rat cerebral arterioles; involvement of potassium ions in autoregulation. *J Physiol*, 404, 455-66.
- EISENSTEIN, R. S., GARCIA-MAYOL, D., PETTINGELL, W. & MUNRO, H. N., 1991. Regulation of ferritin and heme oxygenase synthesis in rat fibroblasts by different forms of iron. *Proc Natl Acad Sci U S A*, 88, 688-92.
- ELKINS, T., GANETZKY, B. & WU, C. F., 1986. A Drosophila mutation that eliminates a calcium-dependent potassium current. *Proc Natl Acad Sci U S A*, 83, 8415-9.
- ELPHINSTONE, R. E., CONROY, A. L., HAWKES, M., HERMANN, L., NAMASOPO, S., WARREN, H. S., JOHN, C. C., LILES, W. C. & KAIN, K. C., 2016. Alterations in Systemic Extracellular Heme and Hemopexin Are Associated With Adverse Clinical Outcomes in Ugandan Children With Severe Malaria. *J Infect Dis*, 214, 1268-75.
- ENDO, M., 1975. Conditions Required for Calcium-Induced Release of Calcium from Sarcoplasmic-Reticulum. *Proceedings of the Japan Academy*, 51, 467-472.
- ENGLARD, S. & SEIFTER, S., 1986. The Biochemical Functions of Ascorbic-Acid. *Annual Review of Nutrition*, 6, 365-406.
- ENYEDI, A., ELWESS, N. L., FILOTEO, A. G., VERMA, A. K., PASZTY, K. & PENNISTON, J. T., 1997. Protein kinase C phosphorylates the "a" forms of plasma membrane Ca²⁺ pump isoforms 2 and 3 and prevents binding of calmodulin. *J Biol Chem*, 272, 27525-8.
- ENYEDI, A., VERMA, A. K., FILOTEO, A. G. & PENNISTON, J. T., 1996. Protein kinase C activates the plasma membrane Ca²⁺ pump isoform 4b by phosphorylation of an inhibitory region downstream of the calmodulin-binding domain. *J Biol Chem*, 271, 32461-7.
- ENYEDI, A., VORHERR, T., JAMES, P., MCCORMICK, D. J., FILOTEO, A. G., CARAFOLI, E. & PENNISTON, J. T., 1989. The calmodulin binding domain of the plasma membrane Ca²⁺ pump interacts both with calmodulin and with another part of the pump. *J Biol Chem*, 264, 12313-21.
- FAKLER, B., BRANDLE, U., BOND, C., GLOWATZKI, E., KONIG, C., ADELMAN, J. P., ZENNER, H. P. & RUPPERSBERG, J. P., 1994. A structural determinant of differential sensitivity of cloned inward rectifier K⁺ channels to intracellular spermine. *FEBS Lett*, 356, 199-203.
- FAKLER, B., BRANDLE, U., GLOWATZKI, E., WEIDEMANN, S., ZENNER, H. P. & RUPPERSBERG, J. P., 1995. Strong voltage-dependent inward rectification of inward rectifier K⁺ channels is caused by intracellular spermine. *Cell*, 80, 149-54.
- FAY, F. S., 1995. Calcium Sparks in Vascular Smooth-Muscle - Relaxation Regulators. *Science*, 270, 588-589.
- FERON, O., BELHASSEN, L., KOBZIK, L., SMITH, T. W., KELLY, R. A. & MICHEL, T., 1996. Endothelial nitric oxide synthase targeting to caveolae. Specific interactions with caveolin isoforms in cardiac myocytes and endothelial cells. *J Biol Chem*, 271, 22810-4.
- FERON, O., SALDANA, F., MICHEL, J. B. & MICHEL, T., 1998. The endothelial nitric-oxide synthase-caveolin regulatory cycle. *J Biol Chem*, 273, 3125-8.
- FICKER, E., TAGLIALATELA, M., WIBLE, B. A., HENLEY, C. M. & BROWN, A. M., 1994. Spermine and spermidine as gating molecules for inward rectifier K⁺ channels. *Science*, 266, 1068-72.
- FORESTI, R., GREEN, C. J. & MOTTERLINI, R., 2004a. Generation of bile pigments by haem oxygenase: a refined cellular strategy in response to stressful insults. *Biochem Soc Symp*, 177-92.
- FORESTI, R., HAMMAD, J., CLARK, J. E., JOHNSON, T. R., MANN, B. E., FRIEBE, A., GREEN, C. J. & MOTTERLINI, R., 2004b. Vasoactive properties of CORM-3, a novel water-soluble carbon monoxide-releasing molecule. *Br J Pharmacol*, 142, 453-60.

- FORESTI, R., SARATHCHANDRA, P., CLARK, J. E., GREEN, C. J. & MOTTERLINI, R., 1999. Peroxynitrite induces haem oxygenase-1 in vascular endothelial cells: a link to apoptosis. *Biochem J*, 339 (Pt 3), 729-36.
- FORT, A., CORDAILLAT, M., THOLLON, C., SALAZAR, G., MECHALY, I., VILLENEUVE, N., VILAINE, J. P., RICHARD, S. & VIRSOLVY, A., 2009. New insights in the contribution of voltage-gated Na(v) channels to rat aorta contraction. *PLoS One*, 4, e7360.
- FRANCO, R., MOURA, J. J., MOURA, I., LLOYD, S. G., HUYNH, B. H., FORBES, W. S. & FERREIRA, G. C., 1995. Characterization of the iron-binding site in mammalian ferrochelatase by kinetic and Mossbauer methods. *J Biol Chem*, 270, 26352-7.
- FRYDMAN, R. B., TOMARO, M. L., BULDAIN, G., AWRUCH, J., DIAZ, L. & FRYDMAN, B., 1981. Specificity of Heme Oxygenase - a Study with Synthetic Hemins. *Biochemistry*, 20, 5177-5182.
- FUKAO, M., MASON, H. S., BRITTON, F. C., KENYON, J. L., HOROWITZ, B. & KEEF, K. D., 1999. Cyclic GMP-dependent protein kinase activates cloned BKCa channels expressed in mammalian cells by direct phosphorylation at serine 1072. *J Biol Chem*, 274, 10927-35.
- FURCHGOTT, R. F. & JOTHIANANDAN, D., 1991. Endothelium-dependent and -independent vasodilation involving cyclic GMP: relaxation induced by nitric oxide, carbon monoxide and light. *Blood Vessels*, 28, 52-61.
- FURUYAMA, K., KANEKO, K. & VARGAS, P. D., 2007. Heme as a magnificent molecule with multiple missions: heme determines its own fate and governs cellular homeostasis. *Tohoku J Exp Med*, 213, 1-16.
- GALBRAITH, R. A., SASSA, S. & KAPPAS, A., 1985. Heme binding to murine erythroleukemia cells. Evidence for a heme receptor. *J Biol Chem*, 260, 12198-202.
- GANDHI, C. S. & ISACOFF, E. Y., 2002. Molecular models of voltage sensing. *J Gen Physiol*, 120, 455-63.
- GANITKEVICH, V. & ISENBERG, G., 1990. Contribution of two types of calcium channels to membrane conductance of single myocytes from guinea-pig coronary artery. *J Physiol*, 426, 19-42.
- GARCIA-CARDENA, G., FAN, R., STERN, D. F., LIU, J. & SESSA, W. C., 1996. Endothelial nitric oxide synthase is regulated by tyrosine phosphorylation and interacts with caveolin-1. *J Biol Chem*, 271, 27237-40.
- GENG, Y. & MAGLEBY, K. L., 2014. Single-channel kinetics of BK (Slo1) channels. *Front Physiol*, 5, 532.
- GETZ, E. B., XIAO, M., CHAKRABARTY, T., COOKE, R. & SELVIN, P. R., 1999. A comparison between the sulfhydryl reductants tris(2-carboxyethyl)phosphine and dithiothreitol for use in protein biochemistry. *Anal Biochem*, 273, 73-80.
- GIBSON, Q. H., OLSON, J. S., MCKINNIE, R. E. & ROHLFS, R. J., 1986. A kinetic description of ligand binding to sperm whale myoglobin. *J Biol Chem*, 261, 10228-39.
- GIULIVI, C. & CADENAS, E., 1993. The Reaction of Ascorbic-Acid with Different Heme Iron Redox States of Myoglobin - Antioxidant and Prooxidant Aspects. *Febs Letters*, 332, 287-290.
- GIUSTARINI, D., DALLE-DONNE, I., COLOMBO, R., MILZANI, A. & ROSSI, R., 2008. Is ascorbate able to reduce disulfide bridges? A cautionary note. *Nitric Oxide*, 19, 252-8.
- GOLDIN, A. L., 2001. Resurgence of sodium channel research. *Annu Rev Physiol*, 63, 871-94.
- GONZALEZ-PEREZ, V., XIA, X. M. & LINGLE, C. J., 2015. Two classes of regulatory subunits coassemble in the same BK channel and independently regulate gating. *Nat Commun*, 6, 8341.
- GOUVEIA, Z., CARLOS, A. R., YUAN, X., AIRES-DA-SILVA, F., STOCKER, R., MAGHZAL, G. J., LEAL, S. S., GOMES, C. M., TODOROVIC, S., IRANZO, O., RAMOS, S., SANTOS, A. C., HAMZA, I., GONCALVES, J. & SOARES, M. P., 2017. Characterization of plasma labile heme in hemolytic conditions. *FEBS J*, 284, 3278-3301.

- GRACA-SOUZA, A. V., ARRUDA, M. A., DE FREITAS, M. S., BARJA-FIDALGO, C. & OLIVEIRA, P. L., 2002. Neutrophil activation by heme: implications for inflammatory processes. *Blood*, 99, 4160-5.
- GRASBECK, R., KOUVONEN, I., LUNDBERG, M. & TENHUNEN, R., 1979. An intestinal receptor for heme. *Scand J Haematol*, 23, 5-9.
- GRASBECK, R., MAJURI, R., KOUVONEN, I. & TENHUNEN, R., 1982. Spectral and other studies on the intestinal haem receptor of the pig. *Biochim Biophys Acta*, 700, 137-42.
- GRASSIE, M. E., SUTHERLAND, C., ULKE-LEMEE, A., CHAPPELLAZ, M., KISS, E., WALSH, M. P. & MACDONALD, J. A., 2012. Cross-talk between Rho-associated kinase and cyclic nucleotide-dependent kinase signaling pathways in the regulation of smooth muscle myosin light chain phosphatase. *J Biol Chem*, 287, 36356-69.
- GRIMSLEY, G. R., SCHOLTZ, J. M. & PACE, C. N., 2009. A summary of the measured pK values of the ionizable groups in folded proteins. *Protein Sci*, 18, 247-51.
- GRUNDEMAR, L. & NY, L., 1997. Pitfalls using metalloporphyrins in carbon monoxide research. *Trends in Pharmacological Sciences*, 18, 193-195.
- GRUSLOVA, A., SEMENOV, I. & WANG, B., 2012. An extracellular domain of the accessory beta1 subunit is required for modulating BK channel voltage sensor and gate. *J Gen Physiol*, 139, 57-67.
- GUNTER, T. E. & PFEIFFER, D. R., 1990. Mechanisms by which mitochondria transport calcium. *Am J Physiol*, 258, C755-86.
- GUSTAFSSON, F., ANDREASEN, D., SALOMONSSON, M., JENSEN, B. L. & HOLSTEIN-RATHLOU, N., 2001. Conducted vasoconstriction in rat mesenteric arterioles: role for dihydropyridine-insensitive Ca(2+) channels. *Am J Physiol Heart Circ Physiol*, 280, H582-90.
- GUTMAN, G. A., CHANDY, K. G., GRISSMER, S., LAZDUNSKI, M., MCKINNON, D., PARDO, L. A., ROBERTSON, G. A., RUDY, B., SANGUINETTI, M. C., STUHMER, W. & WANG, X., 2005. International Union of Pharmacology. LIII. Nomenclature and molecular relationships of voltage-gated potassium channels. *Pharmacol Rev*, 57, 473-508.
- HA, T. S., HEO, M. S. & PARK, C. S., 2004. Functional effects of auxiliary beta4-subunit on rat large-conductance Ca(2+)-activated K(+) channel. *Biophys J*, 86, 2871-82.
- HALLIWELL, J. V., WHITAKER, M. J. & OGDEN, D. 1994. Using microelectrodes. In: OGDEN, D. (2nd ed.) *Microelectrode Techniques: The Plymouth Workshop Handbook*. United Kingdom, Cambridge: The Company of Biologists Limited, 1-15.
- HAMILTON, J. W., BEMENT, W. J., SINCLAIR, P. R., SINCLAIR, J. F., ALCEDO, J. A. & WETTERHAHN, K. E., 1991. Heme regulates hepatic 5-aminolevulinic synthase mRNA expression by decreasing mRNA half-life and not by altering its rate of transcription. *Arch Biochem Biophys*, 289, 387-92.
- HAN, S. Q., LIU, E. B. & LI, H., 2005. Investigation of the photodecomposition of hemin and trace amount determination of hemin with flow injection chemiluminescence method. *Journal of the Chinese Chemical Society*, 52, 399-404.
- HARGROVE, M. S., WILKINSON, A. J. & OLSON, J. S., 1996. Structural factors governing hemin dissociation from metmyoglobin. *Biochemistry*, 35, 11300-9.
- HARTSHORNE, D. J., ITO, M. & ERDODI, F., 2004. Role of protein phosphatase type 1 in contractile functions: myosin phosphatase. *J Biol Chem*, 279, 37211-4.
- HAYABUCHI, Y., NAKAYA, Y., MATSUOKA, S. & KURODA, Y., 1998. Effect of acidosis on Ca2+-activated K+ channels in cultured porcine coronary artery smooth muscle cells. *Pflugers Arch*, 436, 509-14.
- HAYASHI, S., OMATA, Y., SAKAMOTO, H., HIGASHIMOTO, Y., HARA, T., SAGARA, Y. & NOGUCHI, M., 2004. Characterization of rat heme oxygenase-3 gene. Implication of processed pseudogenes derived from heme oxygenase-2 gene. *Gene*, 336, 241-50.

- HEMRIC, M. E., LU, F. W., SHRAGER, R., CAREY, J. & CHALOVICH, J. M., 1993. Reversal of caldesmon binding to myosin with calcium-calmodulin or by phosphorylating caldesmon. *J Biol Chem*, 268, 15305-11.
- HENSLEY, K., ROBINSON, K. A., GABBITA, S. P., SALSMAN, S. & FLOYD, R. A., 2000. Reactive oxygen species, cell signaling, and cell injury. *Free Radic Biol Med*, 28, 1456-62.
- HEROS, R. C., ZERVAS, N. T. & VARSOS, V., 1983. Cerebral Vasospasm after Subarachnoid Hemorrhage - an Update. *Annals of Neurology*, 14, 599-608.
- HERRMANN, W. A., 1990. 100 Years of Metal-Carbonyls - a Serendipitous Chemical Discovery of Major Scientific and Industrial-Impact. *Journal of Organometallic Chemistry*, 383, 21-44.
- HERRMANNFRANK, A., DARLING, E. & MEISSNER, G., 1991. Functional-Characterization of the Ca²⁺-Gated Ca²⁺ Release Channel of Vascular Smooth-Muscle Sarcoplasmic-Reticulum. *Pflugers Archiv-European Journal of Physiology*, 418, 353-359.
- HIBINO, H., INANOBE, A., FURUTANI, K., MURAKAMI, S., FINDLAY, I. & KURACHI, Y., 2010. Inwardly rectifying potassium channels: their structure, function, and physiological roles. *Physiol Rev*, 90, 291-366.
- HILL-EUBANKS, D. C., WERNER, M. E., HEPPNER, T. J. & NELSON, M. T., 2011. Calcium signaling in smooth muscle. *Cold Spring Harb Perspect Biol*, 3, a004549.
- HIRATA, M., SUEMATSU, E., HASHIMOTO, T., HAMACHI, T. & KOGA, T., 1984. Release of Ca²⁺ from a Non-Mitochondrial Store Site in Peritoneal-Macrophages Treated with Saponin by Inositol 1,4,5-Trisphosphate. *Biochemical Journal*, 223, 229-236.
- HIRST, G. D. & EDWARDS, F. R., 1989. Sympathetic neuroeffector transmission in arteries and arterioles. *Physiol Rev*, 69, 546-604.
- HITE, R. K., TAO, X. & MACKINNON, R., 2017. Structural basis for gating the high-conductance Ca²⁺-activated K⁺ channel. *Nature*, 541, 52-57.
- HO, W. S., DAVIS, A. J., CHADHA, P. S. & GREENWOOD, I. A., 2013. Effective contractile response to voltage-gated Na⁺ channels revealed by a channel activator. *Am J Physiol Cell Physiol*, 304, C739-47.
- HOFMANN, T., OBUKHOV, A. G., SCHAEFER, M., HARTENECK, C., GUDERMANN, T. & SCHULTZ, G., 1999. Direct activation of human TRPC6 and TRPC3 channels by diacylglycerol. *Nature*, 397, 259-63.
- HOGG, R. C., WANG, Q. & LARGE, W. A., 1994. Effects of Cl channel blockers on Ca-activated chloride and potassium currents in smooth muscle cells from rabbit portal vein. *Br J Pharmacol*, 111, 1333-41.
- HOPKINS, P. N., WU, L. L., HUNT, S. C., JAMES, B. C., VINCENT, G. M. & WILLIAMS, R. R., 1996. Higher serum bilirubin is associated with decreased risk for early familial coronary artery disease. *Arterioscler Thromb Vasc Biol*, 16, 250-5.
- HORRIGAN, F. T. & ALDRICH, R. W., 1999. Allosteric voltage gating of potassium channels II. Mslo channel gating charge movement in the absence of Ca(2+). *J Gen Physiol*, 114, 305-36.
- HORRIGAN, F. T. & ALDRICH, R. W., 2002a. Coupling between voltage sensor activation, Ca²⁺(+) binding and channel opening in large conductance (BK) potassium channels (vol 120, pg 267, 2002). *Journal of General Physiology*, 120, 599-599.
- HORRIGAN, F. T. & ALDRICH, R. W., 2002b. Coupling between voltage sensor activation, Ca²⁺ binding and channel opening in large conductance (BK) potassium channels. *J Gen Physiol*, 120, 267-305.
- HORRIGAN, F. T., CUI, J. & ALDRICH, R. W., 1999. Allosteric voltage gating of potassium channels I. Mslo ionic currents in the absence of Ca(2+). *J Gen Physiol*, 114, 277-304.
- HORRIGAN, F. T., HEINEMANN, S. H. & HOSHI, T., 2005. Heme regulates allosteric activation of the Slo1 BK channel. *J Gen Physiol*, 126, 7-21.

- HORRIGAN, F. T. & MA, Z., 2008. Mg²⁺ enhances voltage sensor/gate coupling in BK channels. *J Gen Physiol*, 131, 13-32.
- HOU, S., HEINEMANN, S. H. & HOSHI, T., 2009. Modulation of BKCa channel gating by endogenous signaling molecules. *Physiology (Bethesda)*, 24, 26-35.
- HOU, S., REYNOLDS, M. F., HORRIGAN, F. T., HEINEMANN, S. H. & HOSHI, T., 2006. Reversible binding of heme to proteins in cellular signal transduction. *Acc Chem Res*, 39, 918-24.
- HOU, S., XU, R., HEINEMANN, S. H. & HOSHI, T., 2008a. The RCK1 high-affinity Ca²⁺ sensor confers carbon monoxide sensitivity to Slo1 BK channels. *Proc Natl Acad Sci U S A*, 105, 4039-43.
- HOU, S., XU, R., HEINEMANN, S. H. & HOSHI, T., 2008b. Reciprocal regulation of the Ca²⁺ and H⁺ sensitivity in the SLO1 BK channel conferred by the RCK1 domain. *Nat Struct Mol Biol*, 15, 403-10.
- HUANG, Y., QUAYLE, J. M., WORLEY, J. F., STANDEN, N. B. & NELSON, M. T., 1989. External cadmium and internal calcium block of single calcium channels in smooth muscle cells from rabbit mesenteric artery. *Biophys J*, 56, 1023-8.
- IGNARRO, L. J., BALLOT, B. & WOOD, K. S., 1984. Regulation of soluble guanylate cyclase activity by porphyrins and metalloporphyrins. *J Biol Chem*, 259, 6201-7.
- IINO, M., 1990. Biphasic Ca²⁺ Dependence of Inositol 1,4,5-Trisphosphate-Induced Ca Release in Smooth-Muscle Cells of the Guinea-Pig Taenia Ceci. *Journal of General Physiology*, 95, 1103-1122.
- IINO, M., KASAI, H. & YAMAZAWA, T., 1994. Visualization of Neural Control of Intracellular Ca²⁺ Concentration in Single Vascular Smooth-Muscle Cells in-Situ. *Embo Journal*, 13, 5026-5031.
- IINO, M., KOBAYASHI, T. & ENDO, M., 1988. Use of ryanodine for functional removal of the calcium store in smooth muscle cells of the guinea-pig. *Biochem Biophys Res Commun*, 152, 417-22.
- IMMENSCHUH, S., IWAHARA, S., SATOH, H., NELL, C., KATZ, N. & MULLER-EBERHARD, U., 1995. Expression of the mRNA of heme-binding protein 23 is coordinated with that of heme oxygenase-1 by heme and heavy metals in primary rat hepatocytes and hepatoma cells. *Biochemistry*, 34, 13407-11.
- INUI, M., CHAMBERLAIN, B. K., SAITO, A. & FLEISCHER, S., 1986. The nature of the modulation of Ca²⁺ transport as studied by reconstitution of cardiac sarcoplasmic reticulum. *J Biol Chem*, 261, 1794-800.
- ISHIHARA, K., MITSUIYE, T., NOMA, A. & TAKANO, M., 1989. The Mg²⁺ Block and Intrinsic Gating Underlying Inward Rectification of the K⁺ Current in Guinea-Pig Cardiac Myocytes. *Journal of Physiology-London*, 419, 297-320.
- ISHIKAWA, K., SATO, M. & YOSHIDA, T., 1991. Expression of Rat Heme Oxygenase in Escherichia-Coli as a Catalytically Active, Full-Length Form That Binds to Bacterial-Membranes. *European Journal of Biochemistry*, 202, 161-165.
- ITO, K., SHIMOMURA, E., IWANAGA, T., SHIRAIISHI, M., SHINDO, K., NAKAMURA, J., NAGUMO, H., SETO, M., SASAKI, Y. & TAKUWA, Y., 2003. Essential role of rho kinase in the Ca²⁺ sensitization of prostaglandin F(2alpha)-induced contraction of rabbit aortae. *J Physiol*, 546, 823-36.
- IWAMORI, S., SATO, E., SAIGUSA, D., YOSHINARI, K., ITO, S., SATO, H. & TAKAHASHI, N., 2015. A novel and sensitive assay for heme oxygenase activity. *Am J Physiol Renal Physiol*, 309, F667-71.
- JACKSON, W. F. & BLAIR, K. L., 1998. Characterization and function of Ca(2+)-activated K⁺ channels in arteriolar muscle cells. *Am J Physiol*, 274, H27-34.
- JAGGAR, J. H., LEFFLER, C. W., CHERANOV, S. Y., TCHERANOVA, D., E. S. & CHENG, X., 2002. Carbon monoxide dilates cerebral arterioles by enhancing the coupling of Ca²⁺ sparks to Ca²⁺-activated K⁺ channels. *Circ Res*, 91, 610-7.

- JAGGAR, J. H., LI, A., PARFENOVA, H., LIU, J., UMSTOT, E. S., DOPICO, A. M. & LEFFLER, C. W., 2005. Heme is a carbon monoxide receptor for large-conductance Ca²⁺-activated K⁺ channels. *Circ Res*, 97, 805-12.
- JAGGAR, J. H., PORTER, V. A., LEDERER, W. J. & NELSON, M. T., 2000. Calcium sparks in smooth muscle. *Am J Physiol Cell Physiol*, 278, C235-56.
- JAGGAR, J. H., STEVENSON, A. S. & NELSON, M. T., 1998. Voltage dependence of Ca²⁺ sparks in intact cerebral arteries. *Am J Physiol*, 274, C1755-61.
- JAMES, A. F., OKADA, T. & HORIE, M., 1995. A fast transient outward current in cultured cells from human pulmonary artery smooth muscle. *Am J Physiol*, 268, H2358-65.
- JAMES, P., MAEDA, M., FISCHER, R., VERMA, A. K., KREBS, J., PENNISTON, J. T. & CARAFOLI, E., 1988. Identification and primary structure of a calmodulin binding domain of the Ca²⁺ pump of human erythrocytes. *J Biol Chem*, 263, 2905-10.
- JENSEN, L. J., SALOMONSSON, M., JENSEN, B. L. & HOLSTEIN-RATHLOU, N. H., 2004. Depolarization-induced calcium influx in rat mesenteric small arterioles is mediated exclusively via mibefradil-sensitive calcium channels. *Br J Pharmacol*, 142, 709-18.
- JL, L. L., FU, R. G. & MITCHELL, E. W., 1992. Glutathione and Antioxidant Enzymes in Skeletal-Muscle - Effects of Fiber Type and Exercise Intensity. *Journal of Applied Physiology*, 73, 1854-1859.
- JIANG, Y., LEE, A., CHEN, J., CADENE, M., CHAIT, B. T. & MACKINNON, R., 2002. Crystal structure and mechanism of a calcium-gated potassium channel. *Nature*, 417, 515-22.
- JIANG, Z., WALLNER, M., MEERA, P. & TORO, L., 1999. Human and rodent MaxiK channel beta-subunit genes: cloning and characterization. *Genomics*, 55, 57-67.
- JOERK, A., SEIDEL, R. A., WALTER, S. G., WIEGAND, A., KAHNES, M., KLOPFLEISCH, M., KIRMSE, K., POHNERT, G., WESTERHAUSEN, M., WITTE, O. W. & HOLTTHOFF, K., 2014. Impact of heme and heme degradation products on vascular diameter in mouse visual cortex. *J Am Heart Assoc*, 3.
- JOHNSON, R. A., KOZMA, F. & COLOMBARI, E., 1999. Carbon monoxide: from toxin to endogenous modulator of cardiovascular functions. *Braz J Med Biol Res*, 32, 1-14.
- JOHNSON, T. R., MANN, B. E., TEASDALE, I. P., ADAMS, H., FORESTI, R., GREEN, C. J. & MOTTERLINI, R., 2007. Metal carbonyls as pharmaceuticals? [Ru(CO)₃Cl(glycinate)], a CO-releasing molecule with an extensive aqueous solution chemistry. *Dalton Trans*, 1500-8.
- JONAS, E. A. & KACZMAREK, L. K., 1996. Regulation of potassium channels by protein kinases. *Curr Opin Neurobiol*, 6, 318-23.
- JONKER, J. W., BUITELAAR, M., WAGENAAR, E., VAN DER VALK, M. A., SCHEFFER, G. L., SCHEPER, R. J., PLOSCHE, T., KUIPERS, F., ELFERINK, R. P., ROSING, H., BEIJNEN, J. H. & SCHINKEL, A. H., 2002. The breast cancer resistance protein protects against a major chlorophyll-derived dietary phototoxin and protoporphyria. *Proc Natl Acad Sci U S A*, 99, 15649-54.
- JU, H., ZOU, R., VENEMA, V. J. & VENEMA, R. C., 1997. Direct interaction of endothelial nitric-oxide synthase and caveolin-1 inhibits synthase activity. *J Biol Chem*, 272, 18522-5.
- KAMM, K. E. & STULL, J. T., 1985. The function of myosin and myosin light chain kinase phosphorylation in smooth muscle. *Annu Rev Pharmacol Toxicol*, 25, 593-620.
- KAMM, K. E. & STULL, J. T., 2001. Dedicated myosin light chain kinases with diverse cellular functions. *J Biol Chem*, 276, 4527-30.
- KAPETANAKI, S. M., BURTON, M. J., BASRAN, J., URAGAMI, C., MOODY, P. C. E., MITCHESON, J. S., SCHMID, R., DAVIES, N. W., DORLET, P., VOS, M. H., STOREY, N. M. & RAVEN, E., 2018. A mechanism for CO regulation of ion channels. *Nat Commun*, 9, 907.
- KEEF, K. D., HUME, J. R. & ZHONG, J., 2001. Regulation of cardiac and smooth muscle Ca²⁺ channels (Ca_v1.2a,b) by protein kinases. *Am J Physiol Cell Physiol*, 281, C1743-56.

- KHAN, A. A. & QUIGLEY, J. G., 2011. Control of intracellular heme levels: heme transporters and heme oxygenases. *Biochim Biophys Acta*, 1813, 668-82.
- KHAN, A. A. & QUIGLEY, J. G., 2013. Heme and FLVCR-related transporter families SLC48 and SLC49. *Molecular Aspects of Medicine*, 34, 669-682.
- KIM 2004. Caveolae compartmentalization of heme oxygenase-1 in endothelial cells.
- KINTNER, D. B., ANDERSON, M. K., FITZPATRICK, J. H., JR., SAILOR, K. A. & GILBOE, D. D., 2000. ³¹P-MRS-based determination of brain intracellular and interstitial pH: its application to in vivo H⁺ compartmentation and cellular regulation during hypoxic/ischemic conditions. *Neurochem Res*, 25, 1385-96.
- KITAZAWA, T., ETO, M., WOODSOME, T. P. & BRAUTIGAN, D. L., 2000. Agonists trigger G protein-mediated activation of the CPI-17 inhibitor phosphoprotein of myosin light chain phosphatase to enhance vascular smooth muscle contractility. *J Biol Chem*, 275, 9897-900.
- KLOCKNER, U., 1993. Intracellular calcium ions activate a low-conductance chloride channel in smooth-muscle cells isolated from human mesenteric artery. *Pflugers Arch*, 424, 231-7.
- KNAUS, H. G., GARCIA-CALVO, M., KACZOROWSKI, G. J. & GARCIA, M. L., 1994a. Subunit composition of the high conductance calcium-activated potassium channel from smooth muscle, a representative of the mSlo and slowpoke family of potassium channels. *J Biol Chem*, 269, 3921-4.
- KNAUS, H. G., GARCIALALVO, M., KACZOROWSKI, G. J. & GARCIA, M. L., 1994b. Subunit Composition of the High-Conductance Calcium-Activated Potassium Channel from Smooth-Muscle, a Representative of the Mslo and Slowpoke Family of Potassium Channels. *Journal of Biological Chemistry*, 269, 3921-3924.
- KNAUS, H. G., MCMANUS, O. B., LEE, S. H., SCHMALHOFER, W. A., GARCIA-CALVO, M., HELMS, L. M., SANCHEZ, M., GIANGIACOMO, K., REUBEN, J. P., SMITH, A. B., 3RD & ET AL., 1994c. Tremorgenic indole alkaloids potently inhibit smooth muscle high-conductance calcium-activated potassium channels. *Biochemistry*, 33, 5819-28.
- KNOT, H. J. & NELSON, M. T., 1998. Regulation of arterial diameter and wall [Ca²⁺] in cerebral arteries of rat by membrane potential and intravascular pressure. *J Physiol*, 508 (Pt 1), 199-209.
- KOMORI, S. & BOLTON, T. B., 1989. Actions of guanine nucleotides and cyclic nucleotides on calcium stores in single patch-clamped smooth muscle cells from rabbit portal vein. *Br J Pharmacol*, 97, 973-82.
- KRAMPETZ, I. K. & RHOADES, R. A., 1991. Intracellular pH: effect on pulmonary arterial smooth muscle. *Am J Physiol*, 260, L516-21.
- KRANC, K. R., PYNE, G. J., TAO, L., CLARIDGE, T. D., HARRIS, D. A., CADOUX-HUDSON, T. A., TURNBULL, J. J., SCHOFIELD, C. J. & CLARK, J. F., 2000. Oxidative degradation of bilirubin produces vasoactive compounds. *Eur J Biochem*, 267, 7094-101.
- KRANIAS, E. G., 1985. Regulation of Ca²⁺ Transport by Cyclic 3',5'-Amp-Dependent and Calcium-Calmodulin-Dependent Phosphorylation of Cardiac Sarcoplasmic-Reticulum. *Biochimica Et Biophysica Acta*, 844, 193-199.
- KUBO, Y., BALDWIN, T. J., JAN, Y. N. & JAN, L. Y., 1993. Primary structure and functional expression of a mouse inward rectifier potassium channel. *Nature*, 362, 127-33.
- KUMAR, S. & BANDYOPADHYAY, U., 2005. Free heme toxicity and its detoxification systems in human. *Toxicol Lett*, 157, 175-88.
- KUME, H., HALL, I. P., WASHABAU, R. J., TAKAGI, K. & KOTLIKOFF, M. I., 1994. Beta-adrenergic agonists regulate K_{Ca} channels in airway smooth muscle by cAMP-dependent and -independent mechanisms. *J Clin Invest*, 93, 371-9.
- KUME, H., TAKAGI, K., SATAKE, T., TOKUNO, H. & TOMITA, T., 1990. Effects of intracellular pH on calcium-activated potassium channels in rabbit tracheal smooth muscle. *J Physiol*, 424, 445-57.

- KUME, H., TAKAI, A., TOKUNO, H. & TOMITA, T., 1989. Regulation of Ca²⁺-dependent K⁺-channel activity in tracheal myocytes by phosphorylation. *Nature*, 341, 152-4.
- KUTER, D., STRELTSOV, V., DAVYDOVA, N., VENTER, G. A., NAIDOO, K. J. & EGAN, T. J., 2014. Molecular Structures and Solvation of Free Monomeric and Dimeric Ferriheme in Aqueous Solution: Insights from Molecular Dynamics Simulations and Extended X-ray Absorption Fine Structure Spectroscopy. *Inorganic Chemistry*, 53, 10811-10824.
- KUTTY, R. K. & MAINES, M. D., 1981. Purification and characterization of biliverdin reductase from rat liver. *J Biol Chem*, 256, 3956-62.
- KUTTY, R. K. & MAINES, M. D., 1984. Hepatic heme metabolism: possible role of biliverdin in the regulation of heme oxygenase activity. *Biochem Biophys Res Commun*, 122, 40-6.
- KWAK, J. Y., TAKESHIGE, K., CHEUNG, B. S. & MINAKAMI, S., 1991. Bilirubin inhibits the activation of superoxide-producing NADPH oxidase in a neutrophil cell-free system. *Biochim Biophys Acta*, 1076, 369-73.
- KYLE, B. D. & BRAUN, A. P., 2014. The regulation of BK channel activity by pre- and post-translational modifications. *Front Physiol*, 5, 316.
- KYLE, B. D., HURST, S., SWAYZE, R. D., SHENG, J. & BRAUN, A. P., 2013. Specific phosphorylation sites underlie the stimulation of a large conductance, Ca²⁺-activated K⁺ channel by cGMP-dependent protein kinase. *FASEB J*, 27, 2027-38.
- LABBE, R. F., VREMAN, H. J. & STEVENSON, D. K., 1999. Zinc protoporphyrin: A metabolite with a mission. *Clin Chem*, 45, 2060-72.
- LAFTAH, A. H., LATUNDE-DADA, G. O., FAKIH, S., HIDER, R. C., SIMPSON, R. J. & MCKIE, A. T., 2009. Haem and folate transport by proton-coupled folate transporter/haem carrier protein 1 (SLC46A1). *Br J Nutr*, 101, 1150-6.
- LAMB, F. S., VOLK, K. A. & SHIBATA, E. F., 1994. Calcium-activated chloride current in rabbit coronary artery myocytes. *Circ Res*, 75, 742-50.
- LANDINO, L. M., KOUMAS, M. T., MASON, C. E. & ALSTON, J. A., 2006. Ascorbic acid reduction of microtubule protein disulfides and its relevance to protein S-nitrosylation assays. *Biochem Biophys Res Commun*, 340, 347-52.
- LANG, R. J., HARVEY, J. R., MCPHEE, G. J. & KLEMM, M. F., 2000. Nitric oxide and thiol reagent modulation of Ca²⁺-activated K⁺ (BKCa) channels in myocytes of the guinea-pig taenia caeci. *J Physiol*, 525 Pt 2, 363-76.
- LANGTON, P. D., NELSON, M. T., HUANG, Y. & STANDEN, N. B., 1991. Block of calcium-activated potassium channels in mammalian arterial myocytes by tetraethylammonium ions. *Am J Physiol*, 260, H927-34.
- LANSMAN, J. B., HESS, P. & TSIEN, R. W., 1986. Blockade of current through single calcium channels by Cd²⁺, Mg²⁺, and Ca²⁺. Voltage and concentration dependence of calcium entry into the pore. *J Gen Physiol*, 88, 321-47.
- LARGE, W. A. & WANG, Q., 1996. Characteristics and physiological role of the Ca²⁺-activated Cl⁻ conductance in smooth muscle. *American Journal of Physiology-Cell Physiology*, 271, C435-C454.
- LATUNDE-DADA, G. O., SIMPSON, R. J. & MCKIE, A. T., 2006. Recent advances in mammalian haem transport. *Trends Biochem Sci*, 31, 182-8.
- LEE, C. H., POBURKO, D., KUO, K. H., SEOW, C. Y. & VAN BREEMEN, C., 2002. Ca²⁺ oscillations, gradients, and homeostasis in vascular smooth muscle. *Am J Physiol Heart Circ Physiol*, 282, H1571-83.
- LEFFLER, C. W., PARFENOVA, H. & JAGGAR, J. H., 2011. Carbon monoxide as an endogenous vascular modulator. *Am J Physiol Heart Circ Physiol*, 301, H1-H11.
- LEICHER, T., BAHRING, R., ISBRANDT, D. & PONGS, O., 1998. Coexpression of the KCNA3B gene product with Kv1.5 leads to a novel A-type potassium channel. *J Biol Chem*, 273, 35095-101.

- LEMON, B. J. & PETERS, J. W., 1999. Binding of exogenously added carbon monoxide at the active site of the iron-only hydrogenase (Cpl) from *Clostridium pasteurianum*. *Biochemistry*, 38, 12969-73.
- LEVERE, R. D., MARTASEK, P., ESCALANTE, B., SCHWARTZMAN, M. L. & ABRAHAM, N. G., 1990. Effect of heme arginate administration on blood pressure in spontaneously hypertensive rats. *J Clin Invest*, 86, 213-9.
- LI VOLTI, G., IENTILE, R., ABRAHAM, N. G., VANELLA, A., CANNAVO, G., MAZZA, F., CURRO, M., RACITI, G., AVOLA, R. & CAMPISI, A., 2004. Immunocytochemical localization and expression of heme oxygenase-1 in primary astroglial cell cultures during differentiation: effect of glutamate. *Biochemical and Biophysical Research Communications*, 315, 517-524.
- LI, Z., WANG, Y. & VANHOUTTE, P. M., 2011. Upregulation of heme oxygenase 1 by hemin impairs endothelium-dependent contractions in the aorta of the spontaneously hypertensive rat. *Hypertension*, 58, 926-34.
- LIGHT, W. R., 3RD & OLSON, J. S., 1990. Transmembrane movement of heme. *J Biol Chem*, 265, 15623-31.
- LIM, I., GIBBONS, S. J., LYFORD, G. L., MILLER, S. M., STREGE, P. R., SARR, M. G., CHATTERJEE, S., SZURSZEWSKI, J. H., SHAH, V. H. & FARRUGIA, G., 2005. Carbon monoxide activates human intestinal smooth muscle L-type Ca²⁺ channels through a nitric oxide-dependent mechanism. *Am J Physiol Gastrointest Liver Physiol*, 288, G7-14.
- LIN, D. H., STERLING, H., LEREA, K. M., GIEBISCH, G. & WANG, W. H., 2002. Protein kinase C (PKC)-induced phosphorylation of ROMK1 is essential for the surface expression of ROMK1 channels. *Journal of Biological Chemistry*, 277, 44278-44284.
- LINDEN, D. J., NARASIMHAN, K. & GURFEL, D., 1993. Protoporphyrins modulate voltage-gated Ca current in AtT-20 pituitary cells. *J Neurophysiol*, 70, 2673-7.
- LING, S. Z., WORONUK, G., SY, L., LEV, S. & BRAUN, A. P., 2000. Enhanced activity of a large conductance, calcium-sensitive K⁺ channel in the presence of Src tyrosine kinase. *Journal of Biological Chemistry*, 275, 30683-30689.
- LINKE, K. & JAKOB, U., 2003. Not every disulfide lasts forever: disulfide bond formation as a redox switch. *Antioxid Redox Signal*, 5, 425-34.
- LIYOU, J., KIM, M. L., HEO, W. D., JONES, J. T., MYERS, J. W., FERRELL, J. E. & MEYER, T., 2005. STIM is a Ca²⁺ sensor essential for Ca²⁺-store-depletion-triggered Ca²⁺ influx. *Current Biology*, 15, 1235-1241.
- LIPPIAT, J. D. 2008. Whole-Cell Recording Using the Perforated Patch Clamp Technique. In: LIPPIAT, J. D. *Potassium Channels: Methods and Protocols*. United Kingdom: Humana Press Inc., 141-149.
- LIPPIAT, J. D., STANDEN, N. B., HARROW, I. D., PHILLIPS, S. C. & DAVIES, N. W., 2003. Properties of BK(Ca) channels formed by bicistronic expression of hSloalpha and beta1-4 subunits in HEK293 cells. *J Membr Biol*, 192, 141-8.
- LIU, B., GAN, L., SUN, X., ZHU, Y., TONG, Z., XU, H. & YANG, X., 2009. Enhancement of BK(Ca) channel activity induced by hydrogen peroxide: involvement of lipid phosphatase activity of PTEN. *Biochim Biophys Acta*, 1788, 2174-82.
- LIU, H., MOCZYDLOWSKI, E. & HADDAD, G. G., 1999. O₂ deprivation inhibits Ca²⁺-activated K⁺ channels via cytosolic factors in mice neocortical neurons. *J Clin Invest*, 104, 577-88.
- LIU, P., O'MARA, B. W., WARRACK, B. M., WU, W., HUANG, Y., ZHANG, Y., ZHAO, R., LIN, M., ACKERMAN, M. S., HOCKNELL, P. K., CHEN, G., TAO, L., RIEBLE, S., WANG, J., WANG-IVERSON, D. B., TYMIAK, A. A., GRACE, M. J. & RUSSELL, R. J., 2010. A tris (2-carboxyethyl) phosphine (TCEP) related cleavage on cysteine-containing proteins. *J Am Soc Mass Spectrom*, 21, 837-44.

- LIU, S. C., ZHAI, S. & PALEK, J., 1988. Detection of heme release during hemoglobin S denaturation. *Blood*, 71, 1755-8.
- LOHN, M., FURSTENAU, M., SAGACH, V., ELGER, M., SCHULZE, W., LUFT, F. C., HALLER, H. & GOLLASCH, M., 2000. Ignition of calcium sparks in arterial and cardiac muscle through caveolae. *Circ Res*, 87, 1034-9.
- LOIRAND, G., MIRONNEAU, C., MIRONNEAU, J. & PACAUD, P., 1989. Two types of calcium currents in single smooth muscle cells from rat portal vein. *J Physiol*, 412, 333-49.
- LONG, S. B., CAMPBELL, E. B. & MACKINNON, R., 2005. Voltage sensor of Kv1.2: structural basis of electromechanical coupling. *Science*, 309, 903-8.
- LOPATIN, A. N., MAKHINA, E. N. & NICHOLS, C. G., 1994. Potassium channel block by cytoplasmic polyamines as the mechanism of intrinsic rectification. *Nature*, 372, 366-9.
- LU, Z., KLEM, A. M. & RAMU, Y., 2002. Coupling between voltage sensors and activation gate in voltage-gated K⁺ channels. *J Gen Physiol*, 120, 663-76.
- LUIK, R. M., WU, M. M., BUCHANAN, J. & LEWIS, R. S., 2006. The elementary unit of store-operated Ca²⁺ entry: local activation of CRAC channels by STIM1 at ER-plasma membrane junctions. *Journal of Cell Biology*, 174, 815-825.
- LUNDBALD, R. L. 2014. *Chemical Reagents for Protein Modification*. USA, North Carolina: CRC press.
- LUO, D. & VINCENT, S. R., 1994. Metalloporphyrins inhibit nitric oxide-dependent cGMP formation in vivo. *Eur J Pharmacol*, 267, 263-7.
- MA, N., DING, X., DOI, M., IZUMI, N. & SEMBA, R., 2004. Cellular and subcellular localization of heme oxygenase-2 in monkey retina. *J Neurocytol*, 33, 407-15.
- MA, Z., LOU, X. J. & HERRIGAN, F. T., 2006. Role of charged residues in the S1-S4 voltage sensor of BK channels. *J Gen Physiol*, 127, 309-28.
- MAHER, P., 2005. The effects of stress and aging on glutathione metabolism. *Ageing Res Rev*, 4, 288-314.
- MAHIEU, F., JANSSENS, A., GEES, M., TALAVERA, K., NILIUS, B. & VOETS, T., 2010. Modulation of the cold-activated cation channel TRPM8 by surface charge screening. *J Physiol*, 588, 315-24.
- MAINES, M. D., 1988. Heme oxygenase: function, multiplicity, regulatory mechanisms, and clinical applications. *FASEB J*, 2, 2557-68.
- MAINES, M. D., 1997. The heme oxygenase system: a regulator of second messenger gases. *Annu Rev Pharmacol Toxicol*, 37, 517-54.
- MAINES, M. D., TRAKSHEL, G. M. & KUTTY, R. K., 1986. Characterization of two constitutive forms of rat liver microsomal heme oxygenase. Only one molecular species of the enzyme is inducible. *J Biol Chem*, 261, 411-9.
- MAJURI, R., 1989. Heme-binding plasma membrane proteins of K562 erythroleukemia cells: adsorption to heme-microbeads, isolation with affinity chromatography. *Eur J Haematol*, 43, 220-5.
- MANN, B. E. & MOTTERLINI, R., 2007. CO and NO in medicine. *Chemical Communications*, 4197-4208.
- MARBAN, E., YAMAGISHI, T. & TOMASELLI, G. F., 1998. Structure and function of voltage-gated sodium channels. *J Physiol*, 508 (Pt 3), 647-57.
- MARCELLI, A., JELOVICA BADOVINAC, I., ORLIC, N., SALVI, P. R. & GELLINI, C., 2013. Excited-state absorption and ultrafast relaxation dynamics of protoporphyrin IX and hemein. *Photochem Photobiol Sci*, 12, 348-55.
- MARTASEK, P., SCHWARTZMAN, M. L., GOODMAN, A. I., SOLANGI, K. B., LEVERE, R. D. & ABRAHAM, N. G., 1991. Heme and L-arginine regulation of blood pressure in spontaneous hypertensive rats. *J Am Soc Nephrol*, 2, 1078-84.
- MATSUDA, H., SAIGUSA, A. & IRISAWA, H., 1987. Ohmic conductance through the inwardly rectifying K channel and blocking by internal Mg²⁺. *Nature*, 325, 156-9.

- MATTHEWS, J. G., GRAVES, J. E. & POSTON, L., 1992. Relationships between Phi and Tension in Isolated Rat Mesenteric Resistance Arteries. *Journal of Vascular Research*, 29, 330-340.
- MAYHEW, S. G., 1978. The redox potential of dithionite and SO₂ from equilibrium reactions with flavodoxins, methyl viologen and hydrogen plus hydrogenase. *Eur J Biochem*, 85, 535-47.
- MCCOUBREY, W. K., HUANG, T. J. & MAINES, M. D., 1997a. Heme oxygenase-2 is a hemoprotein and binds heme through heme regulatory motifs that are not involved in heme catalysis. *Journal of Biological Chemistry*, 272, 12568-12574.
- MCCOUBREY, W. K., JR., HUANG, T. J. & MAINES, M. D., 1997b. Isolation and characterization of a cDNA from the rat brain that encodes hemoprotein heme oxygenase-3. *Eur J Biochem*, 247, 725-32.
- MCLEAN, S., MANN, B. E. & POOLE, R. K., 2012. Sulfite species enhance carbon monoxide release from CO-releasing molecules: implications for the deoxymyoglobin assay of activity. *Anal Biochem*, 427, 36-40.
- MCMANUS, O. B., HELMS, L. M., PALLANCK, L., GANETZKY, B., SWANSON, R. & LEONARD, R. J., 1995. Functional role of the beta subunit of high conductance calcium-activated potassium channels. *Neuron*, 14, 645-50.
- MCMANUS, O. B. & MAGLEBY, K. L., 1991. Accounting for the Ca²⁺-dependent kinetics of single large-conductance Ca²⁺-activated K⁺ channels in rat skeletal muscle. *J Physiol*, 443, 739-77.
- MEERA, P., ANWER, K., MONGA, M., OBERTI, C., STEFANI, E., TORO, L. & SANBORN, B. M., 1995. Relaxin stimulates myometrial calcium-activated potassium channel activity via protein kinase A. *Am J Physiol*, 269, C312-7.
- MEERA, P., WALLNER, M. & TORO, L., 2000. A neuronal beta subunit (KCNMB4) makes the large conductance, voltage- and Ca²⁺-activated K⁺ channel resistant to charybdotoxin and iberiotoxin. *Proc Natl Acad Sci U S A*, 97, 5562-7.
- MEFFERT, M. K., HALEY, J. E., SCHUMAN, E. M., SCHULMAN, H. & MADISON, D. V., 1994. Inhibition of hippocampal heme oxygenase, nitric oxide synthase, and long-term potentiation by metalloporphyrins. *Neuron*, 13, 1225-33.
- MEGURO, K., IIDA, H., TAKANO, H., MORITA, T., SATA, M., NAGAI, R. & NAKAJIMA, T., 2009. Function and role of voltage-gated sodium channel NaV1.7 expressed in aortic smooth muscle cells. *Am J Physiol Heart Circ Physiol*, 296, H211-9.
- MEISSNER, G., 1986. Ryanodine activation and inhibition of the Ca²⁺ release channel of sarcoplasmic reticulum. *J Biol Chem*, 261, 6300-6.
- MEYER, G., ANDRE, L., KLEINDIENST, A., SINGH, F., TANGUY, S., RICHARD, S., OBERT, P., BOUCHER, F., JOVER, B., CAZORLA, O. & REBOUL, C., 2015. Carbon monoxide increases inducible NOS expression that mediates CO-induced myocardial damage during ischemia-reperfusion. *American Journal of Physiology-Heart and Circulatory Physiology*, 308, H759-H767.
- MILNER, R. E., FAMULSKI, K. S. & MICHALAK, M., 1992. Calcium binding proteins in the sarcoplasmic/endoplasmic reticulum of muscle and nonmuscle cells. *Mol Cell Biochem*, 112, 1-13.
- MINAMI, K., FUKUZAWA, K. & NAKAYA, Y., 1993. Protein kinase C inhibits the Ca²⁺-activated K⁺ channel of cultured porcine coronary artery smooth muscle cells. *Biochem Biophys Res Commun*, 190, 263-9.
- MISTRY, D. K. & GARLAND, C. J., 1998. Nitric oxide (NO)-induced activation of large conductance Ca²⁺-dependent K⁺ channels (BK(Ca)) in smooth muscle cells isolated from the rat mesenteric artery. *Br J Pharmacol*, 124, 1131-40.
- MITSUFUJI, N., YOSHIOKA, H., TOMINAGA, M., OKANO, S., NISHIKI, T. & SAWADA, T., 1995. Intracellular alkalosis during hypoxia in newborn mouse brain in the presence of

- systemic acidosis: a phosphorus magnetic resonance spectroscopic study. *Brain Dev*, 17, 256-60.
- MORITA, T., MITSIALIS, S. A., KOIKE, H., LIU, Y. & KOUREMBANAS, S., 1997. Carbon monoxide controls the proliferation of hypoxic vascular smooth muscle cells. *J Biol Chem*, 272, 32804-9.
- MORITA, T., PERRELLA, M. A., LEE, M. E. & KOUREMBANAS, S., 1995. Smooth muscle cell-derived carbon monoxide is a regulator of vascular cGMP. *Proc Natl Acad Sci U S A*, 92, 1475-9.
- MORROW, J. P., ZAKHAROV, S. I., LIU, G., YANG, L., SOK, A. J. & MARX, S. O., 2006. Defining the BK channel domains required for beta1-subunit modulation. *Proc Natl Acad Sci U S A*, 103, 5096-101.
- MOTTERLINI, R., CLARK, J. E., FORESTI, R., SARATHCHANDRA, P., MANN, B. E. & GREEN, C. J., 2002. Carbon monoxide-releasing molecules: characterization of biochemical and vascular activities. *Circ Res*, 90, E17-24.
- MOTTERLINI, R., HAAS, B. & FORESTI, R., 2012. Emerging concepts on the anti-inflammatory actions of carbon monoxide-releasing molecules (CO-RMs). *Med Gas Res*, 2, 28.
- MOTTERLINI, R., MANN, B. E., JOHNSON, T. R., CLARK, J. E., FORESTI, R. & GREEN, C. J., 2003. Bioactivity and pharmacological actions of carbon monoxide-releasing molecules. *Curr Pharm Des*, 9, 2525-39.
- MULLEBNER, A., MOLDZIO, R., REDL, H., KOZLOV, A. V. & DUVIGNEAU, J. C., 2015. Heme Degradation by Heme Oxygenase Protects Mitochondria but Induces ER Stress via Formed Bilirubin. *Biomolecules*, 5, 679-701.
- MULLER-EBERHARD, U. & VINCENT, S. H., 1985. Concepts of heme distribution within hepatocytes. *Biochem Pharmacol*, 34, 719-25.
- MURATA, M., PERANEN, J., SCHREINER, R., WIELAND, F., KURZCHALIA, T. V. & SIMONS, K., 1995. VIP21/caveolin is a cholesterol-binding protein. *Proc Natl Acad Sci U S A*, 92, 10339-43.
- MURPHY, R. A., 1982. Myosin phosphorylation and crossbridge regulation in arterial smooth muscle. State-of-the-art review. *Hypertension*, 4, 3-7.
- NAGESETTY, R. & PAUL, R. J., 1994. Effects of Ph(I) on Isometric Force and [Ca²⁺](I) in Porcine Coronary-Artery Smooth-Muscle. *Circulation Research*, 75, 990-998.
- NARA, M., DHULIPALA, P. D., JI, G. J., KAMASANI, U. R., WANG, Y. X., MATALON, S. & KOTLIKOFF, M. I., 2000. Guanylyl cyclase stimulatory coupling to K(Ca) channels. *Am J Physiol Cell Physiol*, 279, C1938-45.
- NARA, M., DHULIPALA, P. D., WANG, Y. X. & KOTLIKOFF, M. I., 1998. Reconstitution of beta-adrenergic modulation of large conductance, calcium-activated potassium (maxi-K) channels in *Xenopus* oocytes. Identification of the camp-dependent protein kinase phosphorylation site. *J Biol Chem*, 273, 14920-4.
- NATH, K. A., GRANDE, J. P., HAGGARD, J. J., CROATT, A. J., KATUSIC, Z. S., SOLOVEY, A. & HEBBEL, R. P., 2001. Oxidative stress and induction of heme oxygenase-1 in the kidney in sickle cell disease. *Am J Pathol*, 158, 893-903.
- NDISANG, J. F., ZHAO, W. & WANG, R., 2002. Selective regulation of blood pressure by heme oxygenase-1 in hypertension. *Hypertension*, 40, 315-21.
- NEILD, T. O. & KEEF, K., 1985. Measurements of the membrane potential of arterial smooth muscle in anesthetized animals and its relationship to changes in artery diameter. *Microvasc Res*, 30, 19-28.
- NELSON, M. T., 1986. Interactions of Divalent-Cations with Single Calcium Channels from Rat-Brain Synaptosomes. *Journal of General Physiology*, 87, 201-222.
- NELSON, M. T., CHENG, H., RUBART, M., SANTANA, L. F., BONEV, A. D., KNOT, H. J. & LEDERER, W. J., 1995. Relaxation of arterial smooth muscle by calcium sparks. *Science*, 270, 633-7.

- NELSON, M. T., CONWAY, M. A., KNOT, H. J. & BRAYDEN, J. E., 1997. Chloride channel blockers inhibit myogenic tone in rat cerebral arteries. *Journal of Physiology-London*, 502, 259-264.
- NELSON, M. T., PATLAK, J. B., WORLEY, J. F. & STANDEN, N. B., 1990. Calcium channels, potassium channels, and voltage dependence of arterial smooth muscle tone. *Am J Physiol*, 259, C3-18.
- NELSON, M. T. & QUAYLE, J. M., 1995. Physiological roles and properties of potassium channels in arterial smooth muscle. *Am J Physiol*, 268, C799-822.
- NELSON, T. E. & NELSON, K. E., 1990. Intra- and extraluminal sarcoplasmic reticulum membrane regulatory sites for Ca²⁺-induced Ca²⁺ release. *FEBS Lett*, 263, 292-4.
- NEUZIL, J. & STOCKER, R., 1993. Bilirubin attenuates radical-mediated damage to serum albumin. *FEBS Lett*, 331, 281-4.
- NEWTON, C. L., MIGNERY, G. A. & SUDHOF, T. C., 1994. Co-expression in vertebrate tissues and cell lines of multiple inositol 1,4,5-trisphosphate (InsP₃) receptors with distinct affinities for InsP₃. *J Biol Chem*, 269, 28613-9.
- NGUYEN, X. N. & DENNERY, P. A., 2002. Nuclear translocation of heme oxygenase-1 and heme oxygenase-2 proteins: A novel signaling pathway. *Pediatric Research*, 51, 55a-55a.
- NICHOLS, C. G., 2006. KATP channels as molecular sensors of cellular metabolism. *Nature*, 440, 470-6.
- NICOLET, Y., CAVAZZA, C. & FONTECILLA-CAMPS, J. C., 2002. Fe-only hydrogenases: structure, function and evolution. *J Inorg Biochem*, 91, 1-8.
- NIEVES-CINTRON, M., AMBERG, G. C., NAVEDO, M. F., MOLKENTIN, J. D. & SANTANA, L. F., 2008. The control of Ca²⁺ influx and NFATc3 signaling in arterial smooth muscle during hypertension. *Proc Natl Acad Sci U S A*, 105, 15623-8.
- NIRO, N., KOGA, Y. & IKEBE, M., 2003. Agonist-induced changes in the phosphorylation of the myosin-binding subunit of myosin light chain phosphatase and CPI17, two regulatory factors of myosin light chain phosphatase, in smooth muscle. *Biochem J*, 369, 117-28.
- NIU, X. W. & MAGLEBY, K. L., 2002. Stepwise contribution of each subunit to the cooperative activation of BK channels by Ca²⁺. *Proceedings of the National Academy of Sciences of the United States of America*, 99, 11441-11446.
- NOWIS, D., BUGAJSKI, M., WINIARSKA, M., BIL, J., SZOKALSKA, A., SALWA, P., ISSAT, T., WAS, H., JOZKOWICZ, A., DULAK, J., STOKLOSA, T. & GOLAB, J., 2008. Zinc protoporphyrin IX, a heme oxygenase-1 inhibitor, demonstrates potent antitumor effects but is unable to potentiate antitumor effects of chemotherapeutics in mice. *BMC Cancer*, 8, 197.
- OHYA, Y., KITAMURA, K. & KURIYAMA, H., 1987. Cellular calcium regulates outward currents in rabbit intestinal smooth muscle cell. *Am J Physiol*, 252, C401-10.
- OKA, N., YAMAMOTO, M., SCHWENCKE, C., KAWABE, J., EBINA, T., OHNO, S., COUET, J., LISANTI, M. P. & ISHIKAWA, Y., 1997. Caveolin interaction with protein kinase C. Isoenzyme-dependent regulation of kinase activity by the caveolin scaffolding domain peptide. *J Biol Chem*, 272, 33416-21.
- OKABE, K., KITAMURA, K. & KURIYAMA, H., 1988. The existence of a highly tetrodotoxin sensitive Na channel in freshly dispersed smooth muscle cells of the rabbit main pulmonary artery. *Pflugers Arch*, 411, 423-8.
- OKAMOTO, T., SCHLEGEL, A., SCHERER, P. E. & LISANTI, M. P., 1998. Caveolins, a family of scaffolding proteins for organizing "preassembled signaling complexes" at the plasma membrane. *J Biol Chem*, 273, 5419-22.
- OLSON, J. S., FOLEY, E. W., MAILLETT, D. H. & PASTER, E. V., 2003. Measurement of rate constants for reactions of O₂, CO, and NO with hemoglobin. *Methods Mol Med*, 82, 65-91.
- ORIO, P. & LATORRE, R., 2005. Differential effects of beta 1 and beta 2 subunits on BK channel activity. *J Gen Physiol*, 125, 395-411.

- ORIO, P., ROJAS, P., FERREIRA, G. & LATORRE, R., 2002. New disguises for an old channel: MaxiK channel beta-subunits. *News Physiol Sci*, 17, 156-61.
- OSAKA, K., 1977. Prolonged vasospasm produced by the breakdown products of erythrocytes. *J Neurosurg*, 47, 403-11.
- OTTERBEIN, L. E., BACH, F. H., ALAM, J., SOARES, M., TAO LU, H., WYSK, M., DAVIS, R. J., FLAVELL, R. A. & CHOI, A. M., 2000. Carbon monoxide has anti-inflammatory effects involving the mitogen-activated protein kinase pathway. *Nat Med*, 6, 422-8.
- PACAUD, P., LOIRAND, G., GREGOIRE, G., MIRONNEAU, C. & MIRONNEAU, J., 1992. Calcium-dependence of the calcium-activated chloride current in smooth muscle cells of rat portal vein. *Pflugers Arch*, 421, 125-30.
- PALLANCK, L. & GANETZKY, B., 1994. Cloning and characterization of human and mouse homologs of the *Drosophila* calcium-activated potassium channel gene, slowpoke. *Hum Mol Genet*, 3, 1239-43.
- PALLOTTA, B. S., MAGLEBY, K. L. & BARRETT, J. N., 1981. Single channel recordings of Ca²⁺-activated K⁺ currents in rat muscle cell culture. *Nature*, 293, 471-4.
- PAO, S. S., PAULSEN, I. T. & SAIER, M. H., JR., 1998. Major facilitator superfamily. *Microbiol Mol Biol Rev*, 62, 1-34.
- PAPASSOTIRIOU, J., KOHLER, R., PRENEN, J., KRAUSE, H., AKBAR, M., EGGERMONT, J., PAUL, M., DISTLER, A., NILIUS, B. & HOYER, J., 2000. Endothelial K(+) channel lacks the Ca(2+) sensitivity-regulating beta subunit. *FASEB J*, 14, 885-94.
- PAREKH, A. B. & PUTNEY, J. W., 2005. Store-operated calcium channels. *Physiological Reviews*, 85, 757-810.
- PARPAL, S., KARLSSON, M., THORN, H. & STRALFORS, P., 2001. Cholesterol depletion disrupts caveolae and insulin receptor signaling for metabolic control via insulin receptor substrate-1, but not for mitogen-activated protein kinase control. *J Biol Chem*, 276, 9670-8.
- PATCHELL, V. B., VOROTNIKOV, A. V., GAO, Y., LOW, D. G., EVANS, J. S., FATTOUM, A., EL-MEZGUELDI, M., MARSTON, S. B. & LEVINE, B. A., 2002. Phosphorylation of the minimal inhibitory region at the C-terminus of caldesmon alters its structural and actin binding properties. *Biochim Biophys Acta*, 1596, 121-30.
- PEERS, C., BOYLE, J. P., SCRAGG, J. L., DALLAS, M. L., AL-OWAIS, M. M., HETTIARACHICHI, N. T., ELIES, J., JOHNSON, E., GAMPER, N. & STEELE, D. S., 2015. Diverse mechanisms underlying the regulation of ion channels by carbon monoxide. *Br J Pharmacol*, 172, 1546-56.
- PEERS, C. & GREEN, F. K., 1991. Inhibition of Ca(2+)-activated K⁺ currents by intracellular acidosis in isolated type I cells of the neonatal rat carotid body. *J Physiol*, 437, 589-602.
- PENG, W., HOIDAL, J. R. & FARRUKH, I. S., 1996. Regulation of Ca²⁺-activated K⁺ channels in pulmonary vascular smooth muscle cells: Role of nitric oxide. *Journal of Applied Physiology*, 81, 1264-1272.
- PENNER, R., 1995. A Practical Guide to Patch Clamping. In: SAKMANN, B. & NEHER, E. (2nd ed.) *Single-Channel Recording*. New York: Plenum Press, 3-28.
- PEREZ, G. J., BONEV, A. D. & NELSON, M. T., 2001. Micromolar Ca(2+) from sparks activates Ca(2+)-sensitive K(+) channels in rat cerebral artery smooth muscle. *Am J Physiol Cell Physiol*, 281, C1769-75.
- PEREZ, G. J., BONEV, A. D., PATLAK, J. B. & NELSON, M. T., 1999. Functional coupling of ryanodine receptors to KCa channels in smooth muscle cells from rat cerebral arteries. *J Gen Physiol*, 113, 229-38.
- PESSAH, I. N. & ZIMANYI, I., 1991. Characterization of multiple [3H]ryanodine binding sites on the Ca²⁺ release channel of sarcoplasmic reticulum from skeletal and cardiac muscle: evidence for a sequential mechanism in ryanodine action. *Mol Pharmacol*, 39, 679-89.

- PLATOSHYN, O., REMILLARD, C. V., FANTOZZI, I., SISON, T. & YUAN, J. X., 2005. Identification of functional voltage-gated Na⁺ channels in cultured human pulmonary artery smooth muscle cells. *Pflugers Arch*, 451, 380-387.
- PONKA, P., 1999. Cell biology of heme. *American Journal of the Medical Sciences*, 318, 241-256.
- QIU, A., JANSEN, M., SAKARIS, A., MIN, S. H., CHATTOPADHYAY, S., TSAI, E., SANDOVAL, C., ZHAO, R., AKABAS, M. H. & GOLDMAN, I. D., 2006. Identification of an intestinal folate transporter and the molecular basis for hereditary folate malabsorption. *Cell*, 127, 917-28.
- QUAYLE, J. M., BONEV, A. D., BRAYDEN, J. E. & NELSON, M. T., 1994. Calcitonin gene-related peptide activated ATP-sensitive K⁺ currents in rabbit arterial smooth muscle via protein kinase A. *J Physiol*, 475, 9-13.
- QUAYLE, J. M., MCCARRON, J. G., BRAYDEN, J. E. & NELSON, M. T., 1993. Inward rectifier K⁺ currents in smooth muscle cells from rat resistance-sized cerebral arteries. *Am J Physiol*, 265, C1363-70.
- QUAYLE, J. M., NELSON, M. T. & STANDEN, N. B., 1997. ATP-sensitive and inwardly rectifying potassium channels in smooth muscle. *Physiol Rev*, 77, 1165-232.
- QUAYLE, J. M. & STANDEN, N. B., 1994. KATP channels in vascular smooth muscle. *Cardiovasc Res*, 28, 797-804.
- QUIGLEY, J. G., BURNS, C. C., ANDERSON, M. M., LYNCH, E. D., SABO, K. M., OVERBAUGH, J. & ABKOWITZ, J. L., 2000. Cloning of the cellular receptor for feline leukemia virus subgroup C (FeLV-C), a retrovirus that induces red cell aplasia. *Blood*, 95, 1093-9.
- QUIGLEY, J. G., YANG, Z., WORTHINGTON, M. T., PHILLIPS, J. D., SABO, K. M., SABATH, D. E., BERG, C. L., SASSA, S., WOOD, B. L. & ABKOWITZ, J. L., 2004. Identification of a human heme exporter that is essential for erythropoiesis. *Cell*, 118, 757-66.
- QUINN, K. V., GIBLIN, J. P. & TINKER, A., 2004. Multisite phosphorylation mechanism for protein kinase A activation of the smooth muscle ATP-sensitive K⁺ channel. *Circ Res*, 94, 1359-66.
- RAE, J., COOPER, K., GATES, P. & WATSKY, M., 1991. Low access resistance perforated patch recordings using amphotericin B. *J Neurosci Methods*, 37, 15-26.
- RAEYMAEKERS, L., VERBIST, J., WUYTACK, F., PLESSERS, L. & CASTEELS, R., 1993. Expression of Ca²⁺ binding proteins of the sarcoplasmic reticulum of striated muscle in the endoplasmic reticulum of pig smooth muscles. *Cell Calcium*, 14, 581-9.
- RAGSDALE, S. W. & YI, L., 2011. Thiol/Disulfide redox switches in the regulation of heme binding to proteins. *Antioxid Redox Signal*, 14, 1039-47.
- RAINBOW, R., PARKER, A. & DAVIES, N., 2011. Protein kinase C-independent inhibition of arterial smooth muscle K⁺ channels by a diacylglycerol analogue. *Br J Pharmacol*, 163, 845-56.
- RAJAGOPAL, A., RAO, A. U., AMIGO, J., TIAN, M., UPADHYAY, S. K., HALL, C., UHM, S., MATHEW, M. K., FLEMING, M. D., PAW, B. H., KRAUSE, M. & HAMZA, I., 2008. Haem homeostasis is regulated by the conserved and concerted functions of HRG-1 proteins. *Nature*, 453, 1127-31.
- RAJAGOPALAN, S., KURZ, S., MUNZEL, T., TARPEY, M., FREEMAN, B. A., GRIENGLING, K. K. & HARRISON, D. G., 1996. Angiotensin II-mediated hypertension in the rat increases vascular superoxide production via membrane NADH/NADPH oxidase activation. Contribution to alterations of vasomotor tone. *J Clin Invest*, 97, 1916-23.
- RIDDLE, M. A. & WALKER, B. R., 2012. Regulation of endothelial BK channels by heme oxygenase-derived carbon monoxide and caveolin-1. *American Journal of Physiology-Cell Physiology*, 303, C92-C101.

- ROBERTSON, B. E. & NELSON, M. T., 1994. Aminopyridine inhibition and voltage dependence of K⁺ currents in smooth muscle cells from cerebral arteries. *Am J Physiol*, 267, C1589-97.
- ROBERTSON, B. E., SCHUBERT, R., HESCHELER, J. & NELSON, M. T., 1993. cGMP-dependent protein kinase activates Ca-activated K channels in cerebral artery smooth muscle cells. *Am J Physiol*, 265, C299-303.
- ROBINSON, S. R., DANG, T. N., DRINGEN, R. & BISHOP, G. M., 2009. Hemin toxicity: a preventable source of brain damage following hemorrhagic stroke. *Redox Rep*, 14, 228-35.
- ROMAO, C. C., BLATTLER, W. A., SEIXAS, J. D. & BERNARDES, G. J., 2012. Developing drug molecules for therapy with carbon monoxide. *Chem Soc Rev*, 41, 3571-83.
- ROSENBERG, R. L., HESS, P. & TSIEN, R. W., 1988. Cardiac Calcium Channels in Planar Lipid Bilayers - L-Type Channels and Calcium-Permeable Channels Open at Negative Membrane-Potentials. *Journal of General Physiology*, 92, 27-54.
- ROST, J. & RAPOPORT, S., 1964. Reduction-Potential of Glutathione. *Nature*, 201, 185.
- ROTHBERG, K. G., HEUSER, J. E., DONZELL, W. C., YING, Y. S., GLENNEY, J. R. & ANDERSON, R. G., 1992. Caveolin, a protein component of caveolae membrane coats. *Cell*, 68, 673-82.
- ROUSSEAU, E., SMITH, J. S. & MEISSNER, G., 1987. Ryanodine Modifies Conductance and Gating Behavior of Single Ca²⁺ Release Channel. *American Journal of Physiology*, 253, C364-C368.
- RYTER, S. W., ALAM, J. & CHOI, A. M. K., 2006. Heme oxygenase-1/carbon monoxide: From basic science to therapeutic applications. *Physiological Reviews*, 86, 583-650.
- SAHOO, N., GORADIA, N., OHLENSCHLAGER, O., SCHONHERR, R., FRIEDRICH, M., PLASS, W., KAPPL, R., HOSHI, T. & HEINEMANN, S. H., 2013. Heme impairs the ball-and-chain inactivation of potassium channels. *Proc Natl Acad Sci U S A*, 110, E4036-44.
- SALEH, S., YEUNG, S. Y., PRESTWICH, S., PUCOVSKY, V. & GREENWOOD, I., 2005. Electrophysiological and molecular identification of voltage-gated sodium channels in murine vascular myocytes. *J Physiol*, 568, 155-69.
- SALKOFF, L., BUTLER, A., FERREIRA, G., SANTI, C. & WEI, A., 2006. High-conductance potassium channels of the SLO family. *Nat Rev Neurosci*, 7, 921-31.
- SAMAHA, F. F., HEINEMAN, F. W., INCE, C., FLEMING, J. & BALABAN, R. S., 1992. ATP-sensitive potassium channel is essential to maintain basal coronary vascular tone in vivo. *Am J Physiol*, 262, C1220-7.
- SANDERS, K. M., 2001. Invited review: mechanisms of calcium handling in smooth muscles. *J Appl Physiol (1985)*, 91, 1438-49.
- SANO, K., NAKAMURA, H. & MATSUO, T., 1985. Mode of inhibitory action of bilirubin on protein kinase C. *Pediatr Res*, 19, 587-90.
- SANTANA, L. F., NAVEDO, M. F., AMBERG, G. C., NIEVES-CINTRON, M., VOTAW, V. S. & UFRET-VINCENY, C. A., 2008. Calcium sparklets in arterial smooth muscle. *Clin Exp Pharmacol Physiol*, 35, 1121-6.
- SANTARINO, I. B., OLIVEIRA, S. C. B. & OLIVEIRA-BRETT, A. M., 2012. Protein reducing agents dithiothreitol and tris(2-carboxyethyl)phosphine anodic oxidation. *Electrochemistry Communications*, 23, 114-117.
- SARANTOPOULOS, C. 2007. Patch-Clamp Analysis: Advanced Techniques. In: WALZ, W. (2nd ed.) *Perforated Patch-Clamp Techniques*. USA, New Jersey: Humana Press Inc., 253 – 293.
- SASSA, S., 2006. Biological implications of heme metabolism. *Journal of Clinical Biochemistry and Nutrition*, 38, 138-155.
- SAUNDERS, H. M. & FARLEY, J. M., 1991. Spontaneous transient outward currents and Ca(++)-activated K⁺ channels in swine tracheal smooth muscle cells. *J Pharmacol Exp Ther*, 257, 1114-20.

- SAWAMURA, T., TANAKA, T., ISHIGE, H., IIZUKA, M., MURAYAMA, Y., OTSUJI, E., OHKUBO, A., OGIURA, S. & YUASA, H., 2015. The Effect of Coatings on the Affinity of Lanthanide Nanoparticles to MKN45 and HeLa Cancer Cells and Improvement in Photodynamic Therapy Efficiency. *Int J Mol Sci*, 16, 22415-24.
- SAWICKI, K. T., CHANG, H. C. & ARDEHALI, H., 2015. Role of heme in cardiovascular physiology and disease. *J Am Heart Assoc*, 4, e001138.
- SCAPAGNINI, G., D'AGATA, V., CALABRESE, V., PASCALE, A., COLOMBRITA, C., ALKON, D. & CAVALLARO, S., 2002. Gene expression profiles of heme oxygenase isoforms in the rat brain. *Brain Res*, 954, 51-9.
- SCHAER, C. A., VALLELIAN, F., IMHOF, A., SCHOEDON, G. & SCHAER, D. J., 2008. Heme carrier protein (HCP-1) spatially interacts with the CD163 hemoglobin uptake pathway and is a target of inflammatory macrophage activation. *J Leukoc Biol*, 83, 325-33.
- SCHATZSCHNEIDER, U., 2015. Novel lead structures and activation mechanisms for CO-releasing molecules (CORMs). *Br J Pharmacol*, 172, 1638-50.
- SCHREIBER, M. & SALKOFF, L., 1997. A novel calcium-sensing domain in the BK channel. *Biophys J*, 73, 1355-63.
- SCHUBERT, R. & NELSON, M. T., 2001. Protein kinases: tuners of the BKCa channel in smooth muscle. *Trends in Pharmacological Sciences*, 22, 505-512.
- SCHUBERT, R., NOACK, T. & SEREBRYAKOV, V. N., 1999. Protein kinase C reduces the KCa current of rat tail artery smooth muscle cells. *Am J Physiol*, 276, C648-58.
- SCRAGG, J. L., DALLAS, M. L., WILKINSON, J. A., VARADI, G. & PEERS, C., 2008. Carbon monoxide inhibits L-type Ca²⁺ channels via redox modulation of key cysteine residues by mitochondrial reactive oxygen species. *J Biol Chem*, 283, 24412-9.
- SEDLAK, T. W. & SNYDER, S. H., 2004. Bilirubin benefits: Cellular protection by a biliverdin reductase antioxidant cycle. *Pediatrics*, 113, 1776-1782.
- SEGAL, S. S., BRETT, S. E. & SESSA, W. C., 1999. Codistribution of NOS and caveolin throughout peripheral vasculature and skeletal muscle of hamsters. *Am J Physiol*, 277, H1167-77.
- SERFASS, L. & BURSTYN, J. N., 1998. Effect of heme oxygenase inhibitors on soluble guanylyl cyclase activity. *Arch Biochem Biophys*, 359, 8-16.
- SETOGUCHI, M., OHYA, Y., ABE, I. & FUJISHIMA, M., 1997. Stretch-activated whole-cell currents in smooth muscle cells from mesenteric resistance artery of guinea-pig. *Journal of Physiology-London*, 501, 343-353.
- SEWING, S., ROEPER, J. & PONGS, O., 1996. Kv beta 1 subunit binding specific for shaker-related potassium channel alpha subunits. *Neuron*, 16, 455-63.
- SHAYEGHI, M., LATUNDE-DADA, G. O., OAKHILL, J. S., LAFTAH, A. H., TAKEUCHI, K., HALLIDAY, N., KHAN, Y., WARLEY, A., MCCANN, F. E., HIDER, R. C., FRAZER, D. M., ANDERSON, G. J., VULPE, C. D., SIMPSON, R. J. & MCKIE, A. T., 2005. Identification of an intestinal heme transporter. *Cell*, 122, 789-801.
- SHEN, K. Z., LAGRUTTA, A., DAVIES, N. W., STANDEN, N. B., ADELMAN, J. P. & NORTH, R. A., 1994. Tetraethylammonium block of Slowpoke calcium-activated potassium channels expressed in *Xenopus* oocytes: evidence for tetrameric channel formation. *Pflugers Arch*, 426, 440-5.
- SHI, J. & CUI, J., 2001. Intracellular Mg²⁺ enhances the function of BK-type Ca²⁺-activated K⁺ channels. *J Gen Physiol*, 118, 589-606.
- SHI, J. Y., KRISHNAMOORTHY, G., YANG, Y. W., HU, L., CHATURVEDI, N., HARILAL, D., QIN, J. & CUI, J. M., 2002. Mechanism of magnesium activation of calcium-activated potassium channels. *Nature*, 418, 876-880.
- SHIBAHARA, S., MULLER, R., TAGUCHI, H. & YOSHIDA, T., 1985. Cloning and expression of cDNA for rat heme oxygenase. *Proc Natl Acad Sci U S A*, 82, 7865-9.

- SHIN, H. M., JE, H. D., GALLANT, C., TAO, T. C., HARTSHORNE, D. J., ITO, M. & MORGAN, K. G., 2002. Differential association and localization of myosin phosphatase subunits during agonist-induced signal transduction in smooth muscle. *Circ Res*, 90, 546-53.
- SHMYGOL, A., NOBLE, K. & WRAY, S., 2007. Depletion of membrane cholesterol eliminates the Ca²⁺-activated component of outward potassium current and decreases membrane capacitance in rat uterine myocytes. *J Physiol*, 581, 445-56.
- SHOROFSKY, S. R. & JANUARY, C. T., 1992. L- and T-type Ca²⁺ channels in canine cardiac Purkinje cells. Single-channel demonstration of L-type Ca²⁺ window current. *Circ Res*, 70, 456-64.
- SIEGMAN, M. J., BUTLER, T. M., MOOERS, S. U. & DAVIES, R. E., 1976. Calcium-dependent resistance to stretch and stress relaxation in resting smooth muscles. *Am J Physiol*, 231, 1501-8.
- SIGWORTH, F. J. 1995. Electronic Design of the Patch Clamp. In: SAKMANN, B. & NEHER, E. (2nd ed.) *Single-Channel Recording*. New York: Plenum Press, 95-126.
- SIGWORTH, F. J. & SINE, S. M., 1987. Data transformations for improved display and fitting of single-channel dwell time histograms. *Biophys J*, 52, 1047-54.
- SINGER, J. J. & WALSH, J. V., 1984. Large conductance Ca-activated K channels in smooth muscle cell membrane: reduction in unitary currents due to internal Na ions. *Biophys J*, 45, 68-70.
- SINGH, A. K., MCMILLAN, J., BUKIYA, A. N., BURTON, B., PARRILL, A. L. & DOPICO, A. M., 2012. Multiple cholesterol recognition/interaction amino acid consensus (CRAC) motifs in cytosolic C tail of Slo1 subunit determine cholesterol sensitivity of Ca²⁺- and voltage-gated K⁺ (BK) channels. *J Biol Chem*, 287, 20509-21.
- SMIRNOV, S. V. & AARONSON, P. I., 1992a. Ca²⁺ currents in single myocytes from human mesenteric arteries: evidence for a physiological role of L-type channels. *J Physiol*, 457, 455-75.
- SMIRNOV, S. V. & AARONSON, P. I., 1992b. Ca²⁺-Activated and Voltage-Gated K⁺ Currents in Smooth-Muscle Cells Isolated from Human Mesenteric-Arteries. *Journal of Physiology-London*, 457, 431-454.
- SMITH, A. G., RAVEN, E. L. & CHERNOVA, T., 2011a. The regulatory role of heme in neurons. *Metallomics*, 3, 955-62.
- SMITH, G. L., AUSTIN, C., CRICHTON, C. & WRAY, S., 1998. A review of the actions and control of intracellular pH in vascular smooth muscle. *Cardiovasc Res*, 38, 316-31.
- SMITH, H., MANN, B. E., MOTTERLINI, R. & POOLE, R. K., 2011b. The carbon monoxide-releasing molecule, CORM-3 (Ru(CO)(3)Cl(glycinate)), targets respiration and oxidases in *Campylobacter jejuni*, generating hydrogen peroxide. *IUBMB Life*, 63, 363-71.
- SOBOLOFF, J., SPASSOVA, M., XU, W., HE, L. P., CUESTA, N. & GILL, D. L., 2005. Role of endogenous TRPC6 channels in Ca²⁺ signal generation in A7r5 smooth muscle cells. *Journal of Biological Chemistry*, 280, 39786-39794.
- SOBUE, K., MORIMOTO, K., INUI, M., KANDA, K. & KAKIUCHI, S., 1982. Control of Actin-Myosin Interaction of Gizzard Smooth-Muscle by Calmodulin-Linked and Caldesmon-Linked Flip-Flop Mechanism. *Biomedical Research-Tokyo*, 3, 188-196.
- SOH, H., JUNG, W., UHM, D. Y. & CHUNG, S., 2001. Modulation of large conductance calcium-activated potassium channels from rat hippocampal neurons by glutathione. *Neurosci Lett*, 298, 115-8.
- SONG, R., NING, W., LIU, F., AMEREDES, B. T., CALHOUN, W. J., OTTERBEIN, L. E. & CHOI, A. M., 2003. Regulation of IL-1 β -induced GM-CSF production in human airway smooth muscle cells by carbon monoxide. *Am J Physiol Lung Cell Mol Physiol*, 284, L50-6.
- SONO, M., DAWSON, J. H. & HAGER, L. P., 1984. The Generation of a Hyperporphyrin Spectrum Upon Thiol Binding to Ferric Chloroperoxidase - Further Evidence of Endogenous Thiolate Ligation to the Ferric Enzyme. *Journal of Biological Chemistry*, 259, 3209-3216.

- SOTO, M. A., GONZALEZ, C., LISSI, E., VERGARA, C. & LATORRE, R., 2002. Ca²⁺-activated K⁺ channel inhibition by reactive oxygen species. *Am J Physiol Cell Physiol*, 282, C461-71.
- STANDEN, N. B. & QUAYLE, J. M., 1998. K⁺ channel modulation in arterial smooth muscle. *Acta Physiol Scand*, 164, 549-57.
- STANDEN, N. B., QUAYLE, J. M., DAVIES, N. W., BRAYDEN, J. E., HUANG, Y. & NELSON, M. T., 1989. Hyperpolarizing vasodilators activate ATP-sensitive K⁺ channels in arterial smooth muscle. *Science*, 245, 177-80.
- STEFANI, E., OTTOLIA, M., NOCETI, F., OLCESE, R., WALLNER, M., LATORRE, R. & TORO, L., 1997. Voltage-controlled gating in a large conductance Ca²⁺-sensitive K⁺ channel (hsl_o). *Proc Natl Acad Sci U S A*, 94, 5427-31.
- STOCKER, R., GLAZER, A. N. & AMES, B. N., 1987a. Antioxidant activity of albumin-bound bilirubin. *Proc Natl Acad Sci U S A*, 84, 5918-22.
- STOCKER, R., YAMAMOTO, Y., MCDONAGH, A. F., GLAZER, A. N. & AMES, B. N., 1987b. Bilirubin is an antioxidant of possible physiological importance. *Science*, 235, 1043-6.
- STONE, J. R. & MARLETTA, M. A., 1994. Soluble guanylate cyclase from bovine lung: activation with nitric oxide and carbon monoxide and spectral characterization of the ferrous and ferric states. *Biochemistry*, 33, 5636-40.
- STRAUB, K. L., BENZ, M. & SCHINK, B., 2001. Iron metabolism in anoxic environments at near neutral pH. *FEMS Microbiol Ecol*, 34, 181-186.
- STULL, J. T., LIN, P. J., KRUEGER, J. K., TREWHELLA, J. & ZHI, G., 1998. Myosin light chain kinase: functional domains and structural motifs. *Acta Physiol Scand*, 164, 471-82.
- SUN, X., GU, X. Q. & HADDAD, G. G., 2003. Calcium influx via L- and N-type calcium channels activates a transient large-conductance Ca²⁺-activated K⁺ current in mouse neocortical pyramidal neurons. *J Neurosci*, 23, 3639-48.
- SUZUKI, T. & WANG, J. H., 1986. Stimulation of bovine cardiac sarcoplasmic reticulum Ca²⁺ pump and blocking of phospholamban phosphorylation and dephosphorylation by a phospholamban monoclonal antibody. *J Biol Chem*, 261, 7018-23.
- SWEENEY, M., JONES, C. J., GREENWOOD, S. L., BAKER, P. N. & TAGGART, M. J., 2006. Ultrastructural features of smooth muscle and endothelial cells of isolated isobaric human placental and maternal arteries. *Placenta*, 27, 635-47.
- TADA, M., INUI, M., YAMADA, M., KADOMA, M., KUZUYA, T., ABE, H. & KAKIUCHI, S., 1983. Effects of Phospholamban Phosphorylation Catalyzed by Adenosine 3'-5'-Monophosphate-Dependent and Calmodulin-Dependent Protein-Kinases on Calcium-Transport ATPase of Cardiac Sarcoplasmic-Reticulum. *Journal of Molecular and Cellular Cardiology*, 15, 335-346.
- TADA, M., KIRCHBERGER, M. A., REPKE, D. I. & KATZ, A. M., 1974. The stimulation of calcium transport in cardiac sarcoplasmic reticulum by adenosine 3':5'-monophosphate-dependent protein kinase. *J Biol Chem*, 249, 6174-80.
- TAGUCHI, K., KANEKO, K. & KUBO, T., 2000. Protein kinase C modulates Ca²⁺-activated K⁺ channels in cultured rat mesenteric artery smooth muscle cells. *Biol Pharm Bull*, 23, 1450-4.
- TAILOR, C. S., WILLET, B. J. & KABAT, D., 1999. A putative cell surface receptor for anemia-inducing feline leukemia virus subgroup C is a member of a transporter superfamily. *J Virol*, 73, 6500-5.
- TALUKDER, G. & ALDRICH, R. W., 2000. Complex voltage-dependent behavior of single unliganded calcium-sensitive potassium channels. *Biophys J*, 78, 761-72.
- TANG, Q. Y., ZHANG, Z., MENG, X. Y., CUI, M. & LOGOTHETIS, D. E., 2014. Structural determinants of phosphatidylinositol 4,5-bisphosphate (PIP₂) regulation of BK channel activity through the RCK1 Ca²⁺ coordination site. *J Biol Chem*, 289, 18860-72.

- TANG, X. D., GARCIA, M. L., HEINEMANN, S. H. & HOSHI, T., 2004. Reactive oxygen species impair Slo1 BK channel function by altering cysteine-mediated calcium sensing. *Nat Struct Mol Biol*, 11, 171-8.
- TANG, X. D., XU, R., REYNOLDS, M. F., GARCIA, M. L., HEINEMANN, S. H. & HOSHI, T., 2003. Haem can bind to and inhibit mammalian calcium-dependent Slo1 BK channels. *Nature*, 425, 531-5.
- TAO, X., HITE, R. K. & MACKINNON, R., 2017. Cryo-EM structure of the open high-conductance Ca²⁺-activated K⁺ channel. *Nature*, 541, 46-51.
- TASKER, P. N., MICHELANGELI, F. & NIXON, G. F., 1999. Expression and distribution of the type 1 and type 3 inositol 1,4, 5-trisphosphate receptor in developing vascular smooth muscle. *Circ Res*, 84, 536-42.
- TELEZHKIN, V., BRAZIER, S. P., MEARS, R., MULLER, C. T., RICCARDI, D. & KEMP, P. J., 2011. Cysteine residue 911 in C-terminal tail of human BK(Ca) α channel subunit is crucial for its activation by carbon monoxide. *Pflugers Arch*, 461, 665-75.
- TENHUNEN, R., 1972. Enzymatic Degradation of Heme. *Seminars in Hematology*, 9, 19-&.
- TENHUNEN, R., GRASBECK, R., KOUVONEN, I. & LUNDBERG, M., 1980. An intestinal receptor for heme: its parital characterization. *Int J Biochem*, 12, 713-6.
- TENHUNEN, R., MARVER, H. S. & SCHMID, R., 1969. Microsomal heme oxygenase. Characterization of the enzyme. *J Biol Chem*, 244, 6388-94.
- THOMAS, D., LIPP, P., BERRIDGE, M. J. & BOOTMAN, M. D., 1998. Hormone-evoked elementary Ca²⁺ signals are not stereotypic, but reflect activation of different size channel clusters and variable recruitment of channels within a cluster. *Journal of Biological Chemistry*, 273, 27130-27136.
- THORUP, C., JONES, C. L., GROSS, S. S., MOORE, L. C. & GOLIGORSKY, M. S., 1999. Carbon monoxide induces vasodilation and nitric oxide release but suppresses endothelial NOS. *Am J Physiol*, 277, F882-9.
- TOGANE, Y., MORITA, T., SUEMATSU, M., ISHIMURA, Y., YAMAZAKI, J. I. & KATAYAMA, S., 2000. Protective roles of endogenous carbon monoxide in neointimal development elicited by arterial injury. *Am J Physiol Heart Circ Physiol*, 278, H623-32.
- TORO, L., WALLNER, M., MEERA, P. & TANAKA, Y., 1998. Maxi-K(Ca), a Unique Member of the Voltage-Gated K Channel Superfamily. *News Physiol Sci*, 13, 112-117.
- TRAKSHEL, G. M., KUTTY, R. K. & MAINES, M. D., 1986. Purification and characterization of the major constitutive form of testicular heme oxygenase. The noninducible isoform. *J Biol Chem*, 261, 11131-7.
- TRISTANI-FIROUZI, M., CHEN, J. & SANGUINETTI, M. C., 2002. Interactions between S4-S5 linker and S6 transmembrane domain modulate gating of HERG K⁺ channels. *J Biol Chem*, 277, 18994-9000.
- TSAI, K. L., WANG, S. M., CHEN, C. C., FONG, T. H. & WU, M. L., 1997. Mechanism of oxidative stress-induced intracellular acidosis in rat cerebellar astrocytes and C6 glioma cells. *J Physiol*, 502 (Pt 1), 161-74.
- TSIEN, R. Y., 1980. New calcium indicators and buffers with high selectivity against magnesium and protons: design, synthesis, and properties of prototype structures. *Biochemistry*, 19, 2396-404.
- TURCANU, V., DHOUB, M. & POINDRON, P., 1998. Nitric oxide synthase inhibition by haem oxygenase decreases macrophage nitric-oxide-dependent cytotoxicity: a negative feedback mechanism for the regulation of nitric oxide production. *Research in Immunology*, 149, 741-744.
- TZANAVARAS, P. D., MITANI, C., ANTHEMIDIS, A. & THEMELIS, D. G., 2012. On-line cleavage of disulfide bonds by soluble and immobilized tris-(2-carboxyethyl)phosphine using sequential injection analysis. *Talanta*, 96, 21-5.

- UEBELE, V. N., LAGRUTTA, A., WADE, T., FIGUEROA, D. J., LIU, Y., MCKENNA, E., AUSTIN, C. P., BENNETT, P. B. & SWANSON, R., 2000. Cloning and functional expression of two families of beta-subunits of the large conductance calcium-activated K⁺ channel. *J Biol Chem*, 275, 23211-8.
- UEMURA, K., ADACHI-AKAHANE, S., SHINTANI-ISHIDA, K. & YOSHIDA, K., 2005. Carbon monoxide protects cardiomyogenic cells against ischemic death through L-type Ca²⁺ channel inhibition. *Biochem Biophys Res Commun*, 334, 661-8.
- VAGHEFI, N., GUILLOCHON, D., BUREAU, F., NEUVILLE, D., LEBRUN, F., ARHAN, P. & BOUGLE, D., 2000. The effect of cysteine and 2,4-dinitrophenol on heme and nonheme absorption in a rat intestinal model. *J Nutr Biochem*, 11, 562-567.
- VAITHIANATHAN, T., BUKIYA, A., LIU, J., LIU, P., ASUNCION-CHIN, M., FAN, Z. & DOPICO, A., 2008. Direct regulation of BK channels by phosphatidylinositol 4,5-bisphosphate as a novel signaling pathway. *J Gen Physiol*, 132, 13-28.
- VALKO, M., MORRIS, H. & CRONIN, M. T., 2005. Metals, toxicity and oxidative stress. *Curr Med Chem*, 12, 1161-208.
- VAN DEN AKKER, J., VANBAVEL, E., VAN GEEL, R., MATLUNG, H. L., GUVENC TUNA, B., JANSSEN, G. M., VAN VELEN, P. A., BOELEN, W. C., DE MEY, J. G. & BAKKER, E. N., 2011. The redox state of transglutaminase 2 controls arterial remodeling. *PLoS One*, 6, e23067.
- VERA, T., KELSEN, S., YANES, L. L., RECKELHOFF, J. F. & STEC, D. E., 2007. HO-1 induction lowers blood pressure and superoxide production in the renal medulla of angiotensin II hypertensive mice. *Am J Physiol Regul Integr Comp Physiol*, 292, R1472-8.
- VERGARA, C., LATORRE, R., MARRION, N. V. & ADELMAN, J. P., 1998. Calcium-activated potassium channels. *Curr Opin Neurobiol*, 8, 321-9.
- VERMA, A., HIRSCH, D. J., GLATT, C. E., RONNETT, G. V. & SNYDER, S. H., 1993. Carbon monoxide: a putative neural messenger. *Science*, 259, 381-4.
- VINCHI, F., INGOGLIA, G., CHIABRANDO, D., MERCURIO, S., TURCO, E., SILENGO, L., ALTRUDA, F. & TOLOSANO, E., 2014. Heme exporter FLVCR1a regulates heme synthesis and degradation and controls activity of cytochromes P450. *Gastroenterology*, 146, 1325-38.
- VONRECKLINGHAUSEN, I. R., KINNE, R. K. H. & JANS, A. W. H., 1992. Ammonium Chloride-Induced Acidification in Renal Talh Sve.1 Cells Monitored by P-31-Nmr. *Biochimica Et Biophysica Acta*, 1136, 129-135.
- VREMAN, H. J., EKSTRAND, B. C. & STEVENSON, D. K., 1993. Selection of metalloporphyrin heme oxygenase inhibitors based on potency and photoreactivity. *Pediatr Res*, 33, 195-200.
- VREMAN, H. J. & STEVENSON, D. K., 1988. Heme oxygenase activity as measured by carbon monoxide production. *Anal Biochem*, 168, 31-8.
- VREMAN, H. J., WONG, R. J. & STEVENSON, D. K., 2011. Quantitating carbon monoxide production from heme by vascular plant preparations in vitro. *Plant Physiol Biochem*, 49, 61-8.
- WAGENER, F. A., ABRAHAM, N. G., VAN KOOYK, Y., DE WITTE, T. & FIGDOR, C. G., 2001. Heme-induced cell adhesion in the pathogenesis of sickle-cell disease and inflammation. *Trends Pharmacol Sci*, 22, 52-4.
- WAGENER, F. A., VOLK, H. D., WILLIS, D., ABRAHAM, N. G., SOARES, M. P., ADEMA, G. J. & FIGDOR, C. G., 2003. Different faces of the heme-heme oxygenase system in inflammation. *Pharmacol Rev*, 55, 551-71.
- WALLNER, M., MEERA, P. & TORO, L., 1999. Molecular basis of fast inactivation in voltage and Ca²⁺-activated K⁺ channels: a transmembrane beta-subunit homolog. *Proc Natl Acad Sci U S A*, 96, 4137-42.

- WANG, B. & BRENNER, R., 2006. An S6 mutation in BK channels reveals beta1 subunit effects on intrinsic and voltage-dependent gating. *J Gen Physiol*, 128, 731-44.
- WANG, B., ROTHBERG, B. S. & BRENNER, R., 2006a. Mechanism of beta4 subunit modulation of BK channels. *J Gen Physiol*, 127, 449-65.
- WANG, C. L. A., WANG, L. W. C., XU, S., LU, R. C., SAAVEDRAALANIS, V. & BRYAN, J., 1991. Localization of the Calmodulin-Binding and the Actin-Binding Sites of Caldesmon. *Journal of Biological Chemistry*, 266, 9166-9172.
- WANG, G., 2017. Mechanistic insight into the heme-independent interplay between iron and carbon monoxide in CFTR and Slo1 BKCa channels. *Metallomics*, 9, 634-645.
- WANG, R., SHAMLOUL, R., WANG, X., MENG, Q. & WU, L., 2006b. Sustained normalization of high blood pressure in spontaneously hypertensive rats by implanted hemin pump. *Hypertension*, 48, 685-92.
- WANG, R., WANG, Z. & WU, L., 1997a. Carbon monoxide-induced vasorelaxation and the underlying mechanisms. *Br J Pharmacol*, 121, 927-34.
- WANG, R. & WU, L., 1997. The chemical modification of KCa channels by carbon monoxide in vascular smooth muscle cells. *J Biol Chem*, 272, 8222-6.
- WANG, R., WU, L. & WANG, Z., 1997b. The direct effect of carbon monoxide on KCa channels in vascular smooth muscle cells. *Pflugers Arch*, 434, 285-91.
- WANG, S., PUBLICOVER, S. & GU, Y., 2009. An oxygen-sensitive mechanism in regulation of epithelial sodium channel. *Proc Natl Acad Sci U S A*, 106, 2957-62.
- WANG, Y. W., DING, J. P., XIA, X. M. & LINGLE, C. J., 2002. Consequences of the stoichiometry of Slo1 alpha and auxiliary beta subunits on functional properties of large-conductance Ca²⁺-activated K⁺ channels. *Journal of Neuroscience*, 22, 1550-1561.
- WANG, Z., YUE, P., LIN, D. H. & WANG, W. H., 2013. Carbon monoxide stimulates Ca²⁺ - dependent big-conductance K channels in the cortical collecting duct. *Am J Physiol Renal Physiol*, 304, F543-52.
- WEISS, S. & DASCAL, N., 2015. Molecular Aspects of Modulation of L-type Calcium Channels by Protein Kinase C. *Curr Mol Pharmacol*, 8, 43-53.
- WELLMAN, G. C., SANTANA, L. F., BONEV, A. D. & NELSON, M. T., 2001. Role of phospholamban in the modulation of arterial Ca(2+) sparks and Ca(2+)-activated K(+) channels by cAMP. *Am J Physiol Cell Physiol*, 281, C1029-37.
- WHITE, C., YUAN, X., SCHMIDT, P. J., BRESCIANI, E., SAMUEL, T. K., CAMPAGNA, D., HALL, C., BISHOP, K., CALICCHIO, M. L., LAPIERRE, A., WARD, D. M., LIU, P., FLEMING, M. D. & HAMZA, I., 2013. HRG1 is essential for heme transport from the phagolysosome of macrophages during erythrophagocytosis. *Cell Metab*, 17, 261-70.
- WILLIAMS, S. E., BRAZIER, S. P., BABAN, N., TELEZHKIN, V., MULLER, C. T., RICCARDI, D. & KEMP, P. J., 2008. A structural motif in the C-terminal tail of slo1 confers carbon monoxide sensitivity to human BK Ca channels. *Pflugers Arch*, 456, 561-72.
- WILLIAMS, S. E., WOOTTON, P., MASON, H. S., BOULD, J., ILES, D. E., RICCARDI, D., PEERS, C. & KEMP, P. J., 2004. Hemoxygenase-2 is an oxygen sensor for a calcium-sensitive potassium channel. *Science*, 306, 2093-7.
- WINDER, S. J., ALLEN, B. G., FRASER, E. D., KANG, H. M., KARGACIN, G. J. & WALSH, M. P., 1993. Calponin Phosphorylation In vitro and in Intact Muscle. *Biophysical Journal*, 64, A31-A31.
- WINDER, S. J. & WALSH, M. P., 1990. Smooth muscle calponin. Inhibition of actomyosin MgATPase and regulation by phosphorylation. *J Biol Chem*, 265, 10148-55.
- WINTHER, J. R. & THORPE, C., 2014. Quantification of thiols and disulfides. *Biochim Biophys Acta*, 1840, 838-46.
- WONG, R. J., VREMAN, H. J., SCHULZ, S., KALISH, F. S., PIERCE, N. W. & STEVENSON, D. K., 2011. In vitro inhibition of heme oxygenase isoenzymes by metalloporphyrins. *Journal of Perinatology*, 31, S35-S41.

- WOOD, B. R., LANGFORD, S. J., COOKE, B. M., LIM, J., GLENISTER, F. K., DURISKA, M., UNTHANK, J. K. & MCNAUGHTON, D., 2004. Resonance Raman spectroscopy reveals new insight into the electronic structure of beta-hematin and malaria pigment. *J Am Chem Soc*, 126, 9233-9.
- WORTHINGTON, M. T., COHN, S. M., MILLER, S. K., LUO, R. Q. & BERG, C. L., 2001. Characterization of a human plasma membrane heme transporter in intestinal and hepatocyte cell lines. *Am J Physiol Gastrointest Liver Physiol*, 280, G1172-7.
- WU, L., CAO, K., LU, Y. & WANG, R., 2002. Different mechanisms underlying the stimulation of K(Ca) channels by nitric oxide and carbon monoxide. *J Clin Invest*, 110, 691-700.
- WU, L. & WANG, R., 2005. Carbon monoxide: endogenous production, physiological functions, and pharmacological applications. *Pharmacol Rev*, 57, 585-630.
- WU, R. S. & MARX, S. O., 2010. The BK potassium channel in the vascular smooth muscle and kidney: alpha- and beta-subunits. *Kidney Int*, 78, 963-74.
- XI, Q., TCHERANOVA, D., PARFENOVA, H., HOROWITZ, B., LEFFLER, C. W. & JAGGAR, J. H., 2004. Carbon monoxide activates KCa channels in newborn arteriole smooth muscle cells by increasing apparent Ca²⁺ sensitivity of alpha-subunits. *Am J Physiol Heart Circ Physiol*, 286, H610-8.
- XIA, X. M., ZENG, X. H. & LINGLE, C. J., 2002. Multiple regulatory sites in large-conductance calcium-activated potassium channels. *Nature*, 418, 880-884.
- YAMADA, M. & KURACHI, Y., 1995. Spermine gates inward-rectifying muscarinic but not ATP-sensitive K⁺ channels in rabbit atrial myocytes. Intracellular substance-mediated mechanism of inward rectification. *J Biol Chem*, 270, 9289-94.
- YAMAMOTO, M., HAYASHI, N. & KIKUCHI, G., 1982. Evidence for the transcriptional inhibition by heme of the synthesis of delta-aminolevulinic synthase in rat liver. *Biochem Biophys Res Commun*, 105, 985-90.
- YAMAMOTO, M., HAYASHI, N. & KIKUCHI, G., 1983. Translational inhibition by heme of the synthesis of hepatic delta-aminolevulinic synthase in a cell-free system. *Biochem Biophys Res Commun*, 115, 225-31.
- YAMAUCHI, K., HAYASHI, N. & KIKUCHI, G., 1980. Translocation of delta-aminolevulinic synthase from the cytosol to the mitochondria and its regulation by heme in the rat liver. *J Biol Chem*, 255, 1746-51.
- YAMAZAKI, J., DUAN, D., JANIAC, R., KUENZLI, K., HOROWITZ, B. & HUME, J. R., 1998. Functional and molecular expression of volume-regulated chloride channels in canine vascular smooth muscle cells. *Journal of Physiology-London*, 507, 729-736.
- YAN, J. S. & ALDRICH, R. W., 2010. LRRC26 auxiliary protein allows BK channel activation at resting voltage without calcium. *Nature*, 466, 513-U15.
- YAN, J. S. & ALDRICH, R. W., 2012. BK potassium channel modulation by leucine-rich repeat-containing proteins. *Proceedings of the National Academy of Sciences of the United States of America*, 109, 7917-7922.
- YANG, H., HU, L., SHI, J., DELALOYE, K., HERRIGAN, F. T. & CUI, J., 2007. Mg²⁺ mediates interaction between the voltage sensor and cytosolic domain to activate BK channels. *Proc Natl Acad Sci U S A*, 104, 18270-5.
- YANG, H., ZHANG, G. & CUI, J., 2015. BK channels: multiple sensors, one activation gate. *Front Physiol*, 6, 29.
- YANG, H. H., SHI, J. Y., ZHANG, G. H., YANG, J. Q., DELALOYE, K. L. & CUI, J. M., 2008. Activation of Slo1 BK channels by Mg²⁺ coordinated between the voltage sensor and RCK1 domains. *Nature Structural & Molecular Biology*, 15, 1152-1159.
- YANG, J., JAN, Y. N. & JAN, L. Y., 1995. Determination of the subunit stoichiometry of an inwardly rectifying potassium channel. *Neuron*, 15, 1441-7.

- YANG, J. Q., YANG, H. H., SUN, X. H., DELALOYE, K., YANG, X., MOLLER, A., SHI, J. Y. & CUI, J. M., 2013. Interaction between residues in the Mg²⁺-binding site regulates BK channel activation. *Journal of General Physiology*, 141, 217-228.
- YANG, P. M., HUANG, Y. T., ZHANG, Y. Q., HSIEH, C. W. & WUNG, B. S., 2016. Carbon monoxide releasing molecule induces endothelial nitric oxide synthase activation through a calcium and phosphatidylinositol 3-kinase/Akt mechanism. *Vascular Pharmacology*, 87, 209-218.
- YAO, Y. & PARKER, I., 1994. Ca²⁺ Influx Modulation of Temporal and Spatial Patterns of Inositol Trisphosphate-Mediated Ca²⁺ Liberation in *Xenopus*-Oocytes. *Journal of Physiology-London*, 476, 17-28.
- YATANI, A., SEIDEL, C. L., ALLEN, J. & BROWN, A. M., 1987. Whole-cell and single-channel calcium currents of isolated smooth muscle cells from saphenous vein. *Circ Res*, 60, 523-33.
- YI, L., MORGAN, J. T. & RAGSDALE, S. W., 2010. Identification of a thiol/disulfide redox switch in the human BK channel that controls its affinity for heme and CO. *J Biol Chem*, 285, 20117-27.
- YI, L. & RAGSDALE, S. W., 2007. Evidence that the heme regulatory motifs in heme oxygenase-2 serve as a thiol/disulfide redox switch regulating heme binding. *J Biol Chem*, 282, 21056-67.
- YOSHIDA, T., BIRO, P., COHEN, T., MULLER, R. M. & SHIBAHARA, S., 1988. Human heme oxygenase cDNA and induction of its mRNA by hemin. *Eur J Biochem*, 171, 457-61.
- YOSHINAGA, T., SASSA, S. & KAPPAS, A., 1982. Purification and properties of bovine spleen heme oxygenase. Amino acid composition and sites of action of inhibitors of heme oxidation. *J Biol Chem*, 257, 7778-85.
- YU, W., XU, J. & LI, M., 1996. NAB domain is essential for the subunit assembly of both alpha-alpha and alpha-beta complexes of shaker-like potassium channels. *Neuron*, 16, 441-53.
- YUAN, L., LIN, W., TAN, L., ZHENG, K. & HUANG, W., 2013. Lighting up carbon monoxide: fluorescent probes for monitoring CO in living cells. *Angew Chem Int Ed Engl*, 52, 1628-30.
- YUAN, P., LEONETTI, M. D., PICO, A. R., HSIUNG, Y. & MACKINNON, R., 2010. Structure of the human BK channel Ca²⁺-activation apparatus at 3.0 Å resolution. *Science*, 329, 182-6.
- YUAN, X., RIETZSCHEL, N., KWON, H., WALTER NUNO, A. B., HANNA, D. A., PHILLIPS, J. D., RAVEN, E. L., REDDI, A. R. & HAMZA, I., 2016. Regulation of intracellular heme trafficking revealed by subcellular reporters. *Proc Natl Acad Sci U S A*, 113, E5144-52.
- YUAN, X. J., 1997. Role of calcium-activated chloride current in regulating pulmonary vasomotor tone. *Am J Physiol*, 272, L959-68.
- YUAN, X. J., PROTCHENKO, O., PHILPOTT, C. C. & HAMZA, I., 2012. Topologically Conserved Residues Direct Heme Transport in HRG-1-related Proteins. *Journal of Biological Chemistry*, 287, 4914-4924.
- YUASA, H., INOUE, K. & HAYASHI, Y., 2009. Molecular and functional characteristics of proton-coupled folate transporter. *J Pharm Sci*, 98, 1608-16.
- YUSAF, S. P., WRAY, D. & SIVAPRASADARAO, A., 1996. Measurement of the movement of the S4 segment during the activation of a voltage-gated potassium channel. *Pflugers Arch*, 433, 91-7.
- ZAKHARY, R., GAINE, S. P., DINERMAN, J. L., RUAT, M., FLAVAHAN, N. A. & SNYDER, S. H., 1996. Heme oxygenase 2: endothelial and neuronal localization and role in endothelium-dependent relaxation. *Proc Natl Acad Sci U S A*, 93, 795-8.
- ZENG, X. H., XIA, X. M. & LINGLE, C. J., 2003. Redox-sensitive extracellular gates formed by auxiliary beta subunits of calcium-activated potassium channels. *Nat Struct Biol*, 10, 448-54.

- ZHANG, G., GENG, Y., JIN, Y., SHI, J., MCFARLAND, K., MAGLEBY, K. L., SALKOFF, L. & CUI, J., 2017. Deletion of cytosolic gating ring decreases gate and voltage sensor coupling in BK channels. *J Gen Physiol*, 149, 373-387.
- ZHANG, S. Y. L., YU, Y., ROOS, J., KOZAK, J. A., DEERINCK, T. J., ELLISMAN, M. H., STAUDERMAN, K. A. & CAHALAN, M. D., 2005. STIM1 is a Ca²⁺ sensor that activates CRAC channels and migrates from the Ca²⁺ store to the plasma membrane. *Nature*, 437, 902-905.
- ZHANG, X., SOLARO, C. R. & LINGLE, C. J., 2001. Allosteric regulation of BK channel gating by Ca²⁺ and Mg²⁺ through a nonselective, low affinity divalent cation site. *J Gen Physiol*, 118, 607-36.
- ZHOU, X. B., RUTH, P., SCHLOSSMANN, J., HOFMANN, F. & KORTH, M., 1996. Protein phosphatase 2A is essential for the activation of Ca²⁺-activated K⁺ currents by cGMP-dependent protein kinase in tracheal smooth muscle and Chinese hamster ovary cells. *J Biol Chem*, 271, 19760-7.
- ZIDOVETZKI, R. & LEVITAN, I., 2007. Use of cyclodextrins to manipulate plasma membrane cholesterol content: evidence, misconceptions and control strategies. *Biochim Biophys Acta*, 1768, 1311-24.
- ZUCCHI, R. & RONCATESTONI, S., 1997. The sarcoplasmic reticulum Ca²⁺ channel/ryanodine receptor: Modulation by endogenous effectors, drugs and disease states. *Pharmacological Reviews*, 49, 1-51.

